THE UNIVERSITY LIBRARY

PROTECTION OF AUTHOR'S COPYRIGHT

Transition Metal Complexes of Pyrazine-Based Bis-Terdentate Diamide Ligands

Julia Hausmann

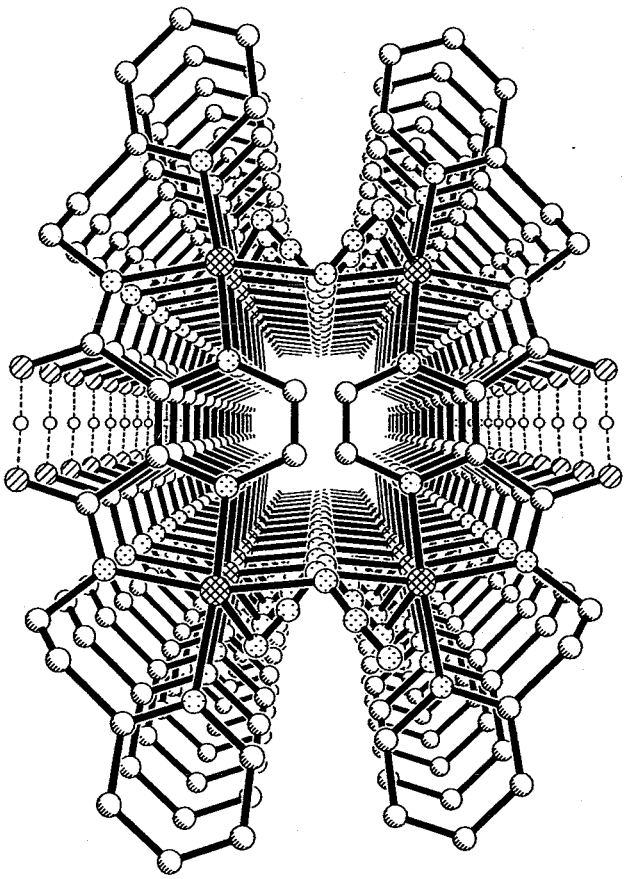

A thesis submitted for the degree of

Doctor of Philosophy

at the University of Otago,

Dunedin, New Zealand

February 2004

This thesis is dedicated to

my family and to my friends.

"Inventions reached their limit a long time ago, and I see no hope for further development."

Sextus Julius Frontinus
(1st century AD, Roman soldier and author,
governor of Britain)

The work presented in this thesis was carried out over the period June 2001–February 2004 in the Department of Chemistry of the University of Otago under the supervision of Assoc. Prof. Sally Brooker (primary supervisor), Dr. Eng Wui Tan (co-supervisor) and Prof. Brian H. Robinson (co-supervisor). Parts of the content of this thesis have been published:

"Self-Assembly of Di- and Tetranuclear Copper(II) Complexes of Two homologous Bis-Terdentate Diamide Ligands"

J. Hausmann, S. Brooker, *Poster No. 29*, Conference of the Inorganic Chemistry Division of the Royal Australian Chemical institute (IC-03), University of Melbourne, Australia, 02–06 February **2003**.

"Control of molecular architecture by the degree of deprotonation: self-assembled di- and tetranuclear copper(II) complexes of *N,N'*-bis(2-pyridylmethyl)pyrazine-2,3-dicarboxamide"

J. Hausmann, G. B. Jameson, S. Brooker, *Chem. Commun.* **2003**, 2992–2993.

ABSTRACT

The four symmetrical, closely related pyrazine-based bis-terdentate diamide ligands *N,N'*-bis(2-pyridylmethyl)pyrazine-2,3-dicarboxamide (H_2L^{M1}), *N,N'*-bis[2-(2-pyridyl)ethyl]pyrazine-2,3-dicarboxamide (H_2L^{M2}), *N,N'*-bis(2-pyridylmethyl)-pyrazine-2,5-dicarboxamide (H_2L^{S1}) and *N,N'*-bis[2-(2-pyridyl)ethyl]pyrazine-2,5-dicarboxamide (H_2L^{S2}) have been synthesised and characterised. Their coordination chemistry towards first row transition metal ion has been investigated.

Several dinuclear copper(II) complexes of $(HL^{M1})^-$, $(HL^{M2})^-$, $(L^{S1})^{2-}$ and $(L^{S2})^{2-}$ have been obtained, of which six were structurally characterised, namely $[Cu^{II}_2(HL^{M1})(MeCN)_4](BF_4)_3 \cdot MeCN$, $[Cu^{II}_2(L^{S1})(H_2O)_2(MeCN)_2](BF_4)_2 \cdot H_2O$, $[Cu^{II}_2(L^{S1})(H_2O)_4](SiF_6) \cdot 0.5\ H_2O$, $\{[Cu^{II}_2(L^{S1})(H_2O)_2(SiF_6)] \cdot 4\ H_2O\}_\infty$, $[Cu^{II}_2(L^{S2})(H_2O)_2(MeCN)_2](BF_4)_2$ and $[Cu^{II}_2(L^{S2})(H_2O)_4(BF_4)_2] \cdot 2\ H_2O$. Curiously, only one complex of $(L^{S2})^{2-}$ contained six-coordinate copper(II) ions, whereas all other structures contained five-coordinate copper(II) ions. The preparation of the dinuclear copper(II) complexes $[Cu^{II}_2(L^{S1})(H_2O)_4](SiF_6) \cdot 0.5\ H_2O$ and $\{[Cu^{II}_2(L^{S1})(H_2O)_2(SiF_6)] \cdot 4\ H_2O\}_\infty$ was carried out in water, employing $Cu(BF_4)_2$, which resulted in the formation of SiF_6^{2-} ions, by hydrolysis of the BF_4^- anions and attack of the resulting HF onto the glassware.

Under identical reaction conditions, two structurally very different complexes have been obtained with the homologous ligands H_2L^{M1} and H_2L^{M2}, namely the dimeric dinuclear copper(II) complex $[Cu^{II}_2(H_2L^{M1})_2(MeCN)_2](BF_4)_4$ of a zwitterionic form of H_2L^{M1} and the square-like tetranuclear copper(II) complex $[Cu^{II}_4(H_2L^{M2})_2(HL^{M2})_2](BF_4)_6 \cdot 3\ MeCN \cdot 0.5\ H_2O$ incorporating $(HL^{M2})^-$ and a zwitterionic form of H_2L^{M2}.

The conversion of the dimeric dinuclear copper(II) complex of H_2L^{M1} into a [2 × 2] grid-type structure of $(HL^{M1})^-$ in solution with base was monitored by UV/VIS spectroscopy. The [2 × 2] grid-type complex $[Cu^{II}_4(HL^{M1})_4](BF_4)_4 \cdot 3.5\ MeCN$ of $(HL^{M1})^-$ has been structurally characterised. The related square-like tetranuclear copper(II)

complex of $(HL^{M2})^-$ $[Cu^{II}_4(HL^{M2})_4](BF_4)_4$ has also been obtained and structurally characterised by X-ray crystallography.

Furthermore, the nickel(II) [2 × 2] grid $[Ni^{II}_4(HL^{M2})_4](BF_4)_4 \cdot 10$ MeCN and the cobalt(III) [2 × 2] grid $[Co^{III}_4(L^{S2})_4](BF_4)_4 \cdot 12.75$ MeCN have been obtained and structurally characterised. A nickel(II) [2 × 2] grid-type complex of $(HL^{M1})^-$ was also obtained, but not structurally characterised.

Two mononuclear cobalt(III) complexes of zwitterionc forms of H_2L^{M1} and H_2L^{M2} have been obtained. The H_2L^{M2} containing complex $[Co^{III}(H_2L^{M2})_2](BF_4)_3 \cdot 2$ EtOH has been structurally characterised.

Azido bridged copper(II) complexes of $(HL^{M1})^-$ and $(HL^{M2})^-$ have been prepared. The dimeric tetranuclear $\mu_{(1,1)}$-azido bridged complex $[Cu^{II}_4(HL^{M1})_2(\mu_{(1,1)}\text{-}N_3)_2(N_3)_3(MeCN)_2](BF_4)_2 \cdot$ MeCN of $(HL^{M1})^-$ and the $\mu_{(1,3)}$-azido bridged polymeric chain compound $\{[Cu^{II}_2(HL^{M2})(\mu_{(1,3)}\text{-}N_3)_2](BF_4) \cdot MeCN\}_\infty$ of $(HL^{M2})^-$ have been structurally characterised.

IR, UV/VIS spectroscopic, cyclic voltammetric and magnetic studies have been carried out on several of the complexes mentioned above. The results are presented in this thesis.

ACKNOWLEDGEMENTS

I would like to thank Mette and Henrik Kjaergaard for welcoming us in their home and for introducing us to the Danish community of Dunedin. They were all amazingly caring. I especially would like to express my gratitude to Betty and Kurt Gramstrup and their entire family. Betty and Kurt were a very important hold for me during my time in Dunedin. I am very grateful for their friendship, their amazing kindness and their unlimited help. Unfortunately, Kurt is no longer with us, I still think of him and his unbelievably good heart every day.

During my time in Otago I met a few dear friends to whom I would like to express my gratitude:

Thanks Ian Hewitt, Simon Iremonger, Tom Mulder and Tanya Ronson for their friendship and for sharing drinks and BBQs with me. I especially apreciated the friendship of Karl Bailey and the weekends we spent in Twizel. Many thanks to Daryl Braid and Marie Simpson for managing to raise my spirit everyday anew. I also want to thank my fellow PhD students Yanhua Lan and Rongqing Li for their companionship and friendship. Our German postdocs Udo Beckmann, Wolfgang Mohr, Carsten Brandt and Markus Weitzer certainly made sure I wouldn't forget my mother tongue. Unfortunately, it didn't quite work out and now I speak neither German nor English... Thanks to Carsten for accepting us as flatmates. Allan Blackman's outbursts of laughter certainly made me feel welcome in Otago. I am very grateful for his friendship and moral support, not to speak of the brilliant music that nobody else seems to appreciate. I want to thank Lyall Hanton for proof-reading this manuscript, for trying to improve my English, for being around and the good guy he is. For always sticking around till the bitter end, but also for reading parts of this manuscript and for giving me helpful lectures on "English for beginners", I thank Paul Addison. Paula Caradoc-Davies also deserves my gratitude as I could always count on her kindness. It is good to have happy people around you! Jim

McQuillan's crib in Albert Town was a very important haven and gave me the opportunity to refuel and get a bit of sun. I am very grateful to him for letting us make use of his lovely house.

Many people within the University of Otago deserve my gratitude. Unfortunately, it would fill pages to thank them all individually. But I especially would like to mention Marianne Dick and Bob McAllister who measured over 250 elemental analyses for me!! I would also like to mention our tea lady Heather Hannagan and her unforgettable scones and sandwiches which surely saved me from starving.

Without the love and support of my fiancé Marco Klingele none of this would have been possible. I am grateful for him being by my side. I am also very grateful to my family who have always supported me unconditionally. And of course I am deeply grateful to all my good friends that I had to leave behind in Germany, for not forgetting me and for showing me what true friendship means.

Here, I especially would like to thank my German friends Thorsten Fritz and Gabriel Siedle who helped me get hold of some exotic papers and offered their help with drawing some of the figures.

I would like to say thank you to Prof. Keith S. Murray and Dr. Boujemaa Moubaraki for contributing to this work by measuring and interpreting the magnetic data presented in this thesis. I would also like to thank them for welcoming us in Melbourne. I owe Prof. Geoffrey B. Jameson my gratitude as he helped refining some of the crystal structures and introduced me to the "SQUEEZE" program. Prof. Keith A. Hunter is thanked for helping me with the pK_a titrations of the ligands and for analysing the data. I thank Assoc. Prof. Sally Brooker for reading the manuscript. This work was supported by the Postgraduate Scholarship of the University of Otago.

TABLE OF CONTENTS

ABBREVIATIONS

Ac	acetyl group
AcOH	acetic acid
aq	Aqueous
ax	axial
bipy	2,2′-bipyridine
Bu	butyl group
calcd.	calculated
cf.	confer
conc.	concentrated
cyclen	1,4,7,10-tetraazacylcododecane
d	doublet
DABCO	1,4-diaza-[2,2,2]-bicyclo octane
DCM	dichloromethane
dd	doubled doublet
ddd	doubly doubled doublet
DIBAL	diisobutyl aluminium hydride
dien	diethylenetriamine
DMF	*N,N'*-dimethylformamide
dt	doubled triplet
eq	equatorial
eq.	equivalent
ESI	electrospray ionisation
Et	ethyl group
EtOH	ethanol
hfac	hexafluoropentane-2,4-dioneate
IR	infrared
L	ligand
M	metal centre
m	multiplet
Mp.	melting point
Me	methyl group
MeCN	acetonitrile
MeOH	methanol
MS	mass spectrometry
NEt_3	triethylamine
NMR	nuclear magnetic resonance
Ph	phenyl group
pd	pyridazine ring
pdH^+	pyridazinium monocation
pm	pyrimidine ring

pmH^+	pyrimidinium monocation
PPh_3	triphenylphosphane
p-TSA	*para*-toluene sulfonic acid
py	pyridine ring
pyH^+	pyridinium cation
pz	pyrazine ring
pzH^+	pyrazinium monocation
R	substituent
RT	room temperature
s	singlet
solv	solvent
t	triplet
TBAP	tetrabutyl ammonium hexafluorophosphate
THF	tetrahydrofuran
TLC	thin layer chromatography
TMS	tetramethylsilane
UV/VIS	ultraviolet/visible
viz	*N*-vinylimidazole

1. Introduction

1.1. *General aspects of pyrazine*[1-6]

Aromatic six-membered heterocycles that contain two, three, or four ring nitrogen atoms are named systematically as diazines, triazines and tetrazines, respectively. The three diazines are stable, colourless compounds, which are soluble in water. They have the recognized trivial names pyridazine (for 1,2-diazine), pyrimidine (for 1,3-diazine) and pyrazine (for 1,4-diazine) (Figure 1.1.1).

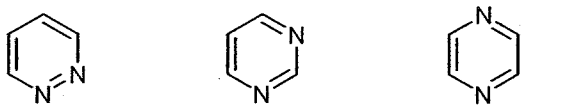

pyridazine 1,2-diazine | pyrimidine 1,3-diazine | pyrazine 1,4-diazine

Figure 1.1.1. The three diazines.

Pyrazine and its derivatives usually sublime readily and in general they possess a narcotic odour and nutty, roasted or earthy flavour tonalities. The pyrazine nucleus is planar with D_{2h} symmetry. It may be considered a resonance hybrid of which two of the contributing forms are analogous to those of benzene (Figure 1.1.2, **i** and **ii**). However, the high electronegativity of the nitrogen atom probably leads to significant additional contributions of resonance structures such as **iii** in Figure 1.1.2.

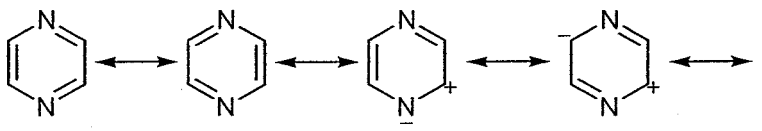

i ii iii iv

Figure 1.1.2. Resonance structures of pyrazine.

The pyrazines are aromatic compounds as well as tertiary amines, and their properties closely resemble those of the pyridines. However, the diazines in general are much weaker bases than pyridine (pyH^+: $pK_a = 5.23$),[7] presumably because of the destabilizing effects, both inductive and mesomeric, of the second ring nitrogen on the protocations. Why the basicity drops along the series pyridazine (pdH^+: $pK_a = 2.3$), pyrimidine (pmH^+: $pK_a = 1.3$), pyrazine (pzH^+: $pK_a = 0.6$), is not understood.

Over the years numerous studies of metal complexes of pyrazine have been described.[8-12] Despite its low basicity pyrazine can function as a bridging bidentate ligand, giving rise for instance, to dimers[13-23] like the famous mixed-valent Creutz-Taube ion $[(NH_3)_5Ru\text{-}pz\text{-}Ru(NH_3)_5]^{5+}$ **(I)**,[24,25] or $[(ClO_4)_2(dien)Cu^{II}\text{-}pz\text{-}Cu^{II}(dien)(ClO_4)_2]$ (dien = diethylenetriamine),[26] linear strands[27-32] like $[Cu^{II}(hfac)_2pz]_\infty$ (hfac = hexafluoropentane-2,4-dionate) **(II)**[33] or $[Cu^{II}(NO_3)_2pz]_\infty$,[34] 2D sheet-like structures[35-39] like $[Co^{II}pz_2(NCS)_2]_\infty$ **(III)**[40,41], $[Fe^{II}pz_2(SCN)_2]_\infty$[42] or $\{RuCl_2pz_4Ag](NO_3)\}_\infty$ (Figure 1.1.3).[43] Discrete polynuclear complexes, like triangles[16,44] or squares,[45] *e.g.* the mixed-valent "Creutz-Taube" square $[(cyclen)_4Ru_4pz_4]^{9+}$ **(IV)** (cyclen = 1,4,7,10-tetraazacylcododecane),[46] or polymeric 3D structures like $\{[Agpz_3](SbF_6)\}_\infty$[47] or $\{[Agpz_3](BF_4)\}_\infty$ have been reported.[48] In some of these compounds it has been shown that in spite of the length of the bridge, pyrazine can support significant spin-spin and electronic interactions between metal ions.

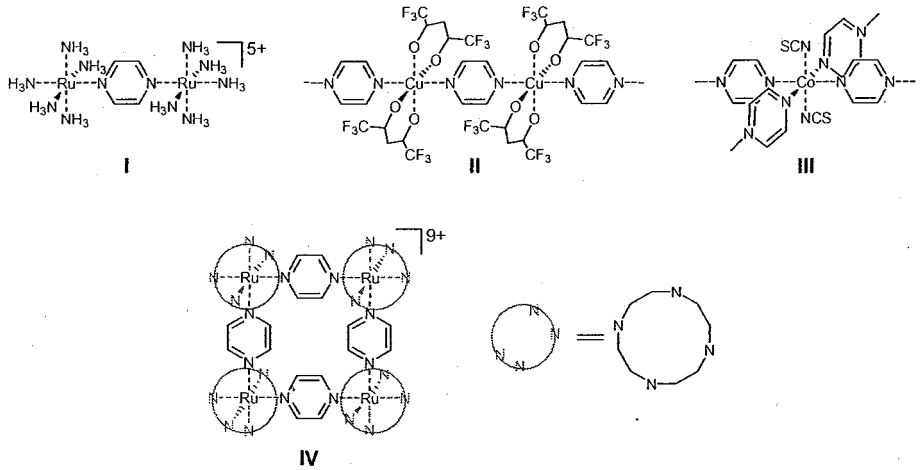

Figure 1.1.3. Some pyrazine bridged complexes: **I**: Creutz-Taube ion $[(NH_3)_5Ru\text{-}pz\text{-}Ru(NH_3)_5]^{5+}$[24,25]; **II**: $[Cu^{II}(hfac)_2pz]_\infty$[33]; **III**: $[Co^{II}pz_2(NCS)_2]_\infty$;[40,41] **IV**: "Creutz-Taube" square $[(cyclen)_4Ru_4pz_4]^{9+}$.[34]

For studies of how the structural factors involving the bridging pyrazine units affect the magnetic and electronic interaction properties of the resulting complexes, simple systems such as dinuclear species, are desirable. To date a variety of simple dinuclear complexes have been synthesised and structurally characterised, obtained from pyrazine derivatives which have coordinating substituents,[12,49-51] by the addition of bulky coligands,[52] or both.[53]

1.2. *Supramolecular chemistry*[54-74]

From the press release of The Royal Swedish Academy of Sciences: The 1987 Nobel Prize in Chemistry (14 October 1987)

"In 1987 the Nobel Prize in Chemistry has been awarded to **Donald J. Cram**, USA, **Jean-Marie Lehn**, France, and **Charles J. Pedersen**, USA, for their development and application of molecules with highly selective structurespecific interaction, *i.e.* molecules that can "recognize" each other and choose with which other molecules they will form complexes. The laureates have been rewarded for synthesising organic compounds of low molecular weight and with very special properties. The molecules in these compounds are designed principally to bind cations (positive ions), but also anions (negative ions) and neutral-molecules, in a specific and selective manner. The three researchers have studied chemical and physical properties of these complexes and have elucidated the factors that determine the ability of the molecules to recognize each other and fit into one another like a key fits a lock. Molecules have been produced that mimic the mode of action of enzymes. The laureates' research has been of great importance for developments within coordination chemistry, organic synthesis, analytical chemistry and bioorganic and bioinorganic chemistry, and has thus laid the foundation for the active interdisciplinary area of research within chemistry that has now come to be termed host-guest chemistry or supramolecular chemistry."[75]

1.2.1. *Background*

In general *supramolecular chemistry* is defined as the chemistry beyond the molecule as it is based on intermolecular interactions. It is specified as the chemistry of the intermolecular bond, exactly as molecular chemistry is that of the covalent bond.

Self-organized systems are capable of spontaneously generating a well-defined supramolecular architecture by *self-assembly* from their components under a well-defined set of conditions.

The selective binding of a substrate by a molecular receptor to form a supermolecule involves *molecular recognition,* which rests on the *molecular information* stored in the interacting partners.

It is universally recognised that self-organized processes play a primordial role in biological systems, where well-defined supramolecular structures form spontaneously, *via* self-assembly, from simple molecular building blocks.[76] Each complementary building block thus contains precise information to generate solely the correct final supramolecular structure within all possible structures. Molecular interactions form the basis of biological processes such as recognition, reaction, regulation, transport, catalysis, *etc.* Examples of molecular recognition and self-organized systems can be found anywhere in biology *e.g.* substrate binding to a receptor protein, enzymatic reactions, intermolecular reading, translation and transcription of the genetic code, cellular recognition, proteins that spontaneously form their predetermined secondary, tertiary and quaternary structures, spontaneous formation of the double helix of nucleic acids.

As early as 1955, Fraenkel-Conrat and Williams demonstrated that for example the tobacco mosaic virus, after complete dissociation into its components, could be reconstituted *in vitro* leading to the reconstruction of the intact virus.[76,77]

Self-assembly offers considerable advantages over the stepwise bond formation in the construction of large supramolecular assemblies, crucial for the development and distribution of living organisms:

(*i*): The synthesis of large assemblies *via* the *simultaneous* assembly of predetermined building blocks requires significantly fewer steps than the comparable covalent synthesis.

(*ii*): Since noncovalent interactions are usually established very rapidly, the formation of the final product is *fast* and *facile*.

(*iii*): As there exists an equilibrium between the components and the final products, the system continues to self-rearrange until the assembly has become *defect free*.

(*iv*): The synthesis of supramolecular species in biological systems often employs multiple copies of a single subunit. This strategy is *economical* in terms of genetic material, as one single short nucleic acid sequence can code for a very large protein.

Several types of self-assembly processes have been identified,[57] and three of them will be described in the following.

(*i*): The *strict* or *thermodynamic self-assembly* is characterised by the existence of a rapid, reversible thermodynamic equilibrium between the starting materials and the products at all times and for all steps. As the equilibrium is reversible, the process is self-correcting. A thermodynamic self-assembly process in general should generate one product which is substantially more stable than any of its competitors.

(*ii*): The *irreversible self-assembly* involves a cascade of irreversible reactions which are kinetically guided down a particular pathway. In this kind of process there is no capacity for self-correction and every bond must be formed correctly the first time. The products of each step are kinetically stable.

(*iii*): The *self-assembly following a precursor modification* usually involves self-assembly after the precursor building blocks have been modified. This, in chemistry,

rather rare type of self-assembly is mentioned at this point, as the term will be used later on.

1.2.2. *Metallosupramolecular chemistry*

In general supramolecular self-assembled species in biology are constructed by means of different kinds of non-covalent binding interactions, such as electrostatic, hydrophobic, hydrophilic, π-π stacking, dipolar, van der Waals forces or hydrogen bonding. However, chemistry is not limited to systems similar to those found in nature but is free to create novel species and to invent novel processes. One approach of modern supramolecular chemistry for the formation of supramolecular species *via* spontaneous self-assembly of precursor building blocks is the use of metal ions and dative bonding *via* coordination, the so-called *metallosupramolecular chemistry*. Metal-ligand bonding offers advantages, compared to the weak electrostatic, π-π-stacking or hydrogen bonding, having a greater directionality. Benefits are also given by the great range of transition metals and an almost unlimited variety of ligands available as building blocks. The typical energies of 40–120 kJ mol^{-1} per metal-ligand interaction are in between the ranges of strong covalent bonds and weak interactions of biological systems. This is beneficial for the design of supramolecular assemblies, as compared to biological systems fewer interactions are necessary to stabilise the structure, but self-correction processes still remain possible.

For the metal mediated self-assembly, Stang and co-workers[68] assigned four commonalities:

(*i*): Self-assembling units are held together by coordinative interactions.

(*ii*): The assembling of subunits into larger aggregates is selective, *i.e.* the subunits bind cooperatively to form the most stable aggregate.

(*iii*): The aggregates can be recognized by their properties that differ from those of the individual components

(*iv*): The aggregates are discrete rather than infinite.

In 1997 Lehn[78] and Stoddart[79] have suggested independently that the structural complexity in synthetic self-assembled systems can be compared to that of biological systems, *e.g.* the levels of organisation of a protein (Figure 1.2.1). As a natural protein, a synthetic self-assembled architecture has a *primary structure* (1°) (Lehn), *i.e.* is build by *tectons* or *building blocks* (Stoddart). The organisation of the building blocks, like a twist in a helicate as present in a protein, is characterised by Lehn as the *secondary structure* (2°), by Stoddart as a *supermolecule*. A *tertiary structure* (3°) (Lehn) or *supramolecular array* (Stoddart) is formed where secondary structural elements or supermolecules are arranged relative to each other, *e.g.* in a circular helicate. Finally, when separate molecules with tertiary structures or supramolecular arrays are connected to each other, forming a fourth level of structural organisation, a *quaternary structure* (Lehn) or a *macroscopic conglomerate* (Stoddart) is formed.

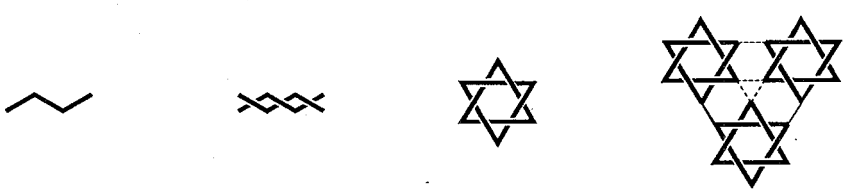

	Starting material	Helicate	Circular helicate	Interconnected circular helicates
Level of organisation	first	second	third	fourth
Stoddart	Primary molecules (tectons)	Supermolecule	Supramolecular array	Macroscopic conglomerate
Lehn	Primary structure (1°)	Secondary structure (2°)	Tertiary structure (3°)	Quarternary structure (4°)

Figure 1.2.1. Supramolecular hierarchy.

In recent years the number of metal mediated synthetic self-assembled species has multiplied and a great variety of assemblies of diverse structures and shapes have been synthesised.

1.2.3. *Thermodynamic factors*

As mentioned above, in self-assembly processes of a metallacycle coordination bonds must form between the donor and acceptor elements involved and bonds formed must be kinetically labile to allow self-correction. Most importantly, the desired assembly must be thermodynamically favourable over competing structures. Generally one can say that cyclic structures are preferred over linear ones for enthalpic reasons, as the number of bonds per subunit is greater in a cyclic than in a linear structure. For example a triangle with three linear and three angular units contains six coordinate bonds (one per subunit) while its acyclic equivalent contains only five bonds (0.83 bonds per subunit). Even on polymerisation the acceptor sites at each end of the polymer will always remain uncoordinated, so that if cyclisation is impossible, it is likely that the polymer will grow until its precipitation as a kinetic product occurs. The ideal number of bonds formed per subunit, however, can only be achieved if cyclisation occurs.

According to Le Chatelier's law, a pertubation to a dynamic equilibrium results in a readjustment of the equilibrium to minimise the effect. Thus, dilution of a solution containing an equilibrium mixture of cyclic oligomers results in a shift of the equilibrium to increase the total number of species. As a result, small cycles are favoured at low concentrations whereas large cycles predominate in high concentrations.

1.2.4. *Latticed motifs*

Latticed motifs include grid-, rack- and ladder-type structures as well as 2D coordination networks. A characteristic common to all latticed motifs is that they incorporate exclusively orthogonal or near-orthogonal binding, *i.e.* they form

coordination bonds at alternating right angles to each other. The orthogonal bonding is generally achieved by the coordination of tetrahedral or octahedral metal ions in combination with rigid linear polybidentate or polyterdentate chelating sites, respectively (Figure 1.2.2).

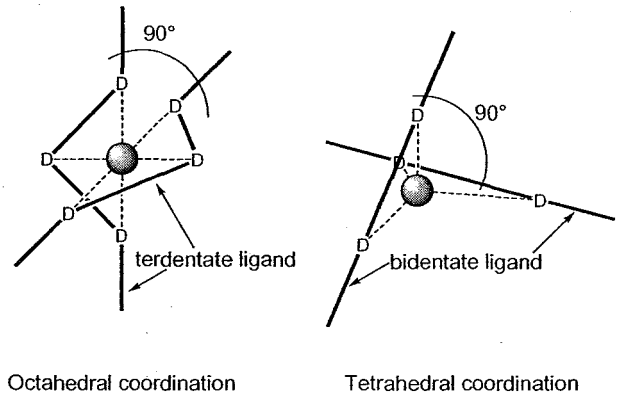

Figure 1.2.2. Octahedral and tetrahedral coordination leading to orthogonal ligand strands.

Grid-type complexes

A grid-type complex is usually based on a single ligand species featuring a linear repeating array of bi- or terdentate chelating units. The nuclearity of the resulting grid therefore depends on the polytopic nature of the ligand. Grid compounds are described using the nomenclature [n × n′]G, *i.e.* ligands with n and n′ binding sites combine with (n × n′) metal ions to form a grid complex that contains (n + n′) ligands and (n × n′) metal ions. To date a variety of different grid-type complexes have been reported but at this point only a few selected examples will be presented.

Pyridazine-based grid compounds

Tetrahedral metal ions such as silver(I) or copper(I) have been most widely employed for grid formation, and as early as 1992 the first tetranuclear [2 × 2] grid compound $[Cu^{I}_{4}(\mathbf{V})_4](CF_3SO_3)_4$, employing the rigid pyridazine-based bis-bidentate ligand 3,6-di(2-pyridyl)pyridazine (**V**), was crystallographically characterised by Youinou and co-workers (Figure 1.2.3).[80] Following the strategy of pyridazine-based ligands, the first [3 × 3] grid-type structure employing **VI** and nine tetrahedral silver(I) ions was published in 1994 by Lehn and co-workers (Figure 1.2.3).[81] Since then several grid-type structures of tetrahedral metal ions have been published employing pyridazine-[82,83] but also bipyridine[84] or phenanthroline[85] derivatives like **VII** or **VIII** (Figure 1.2.3).

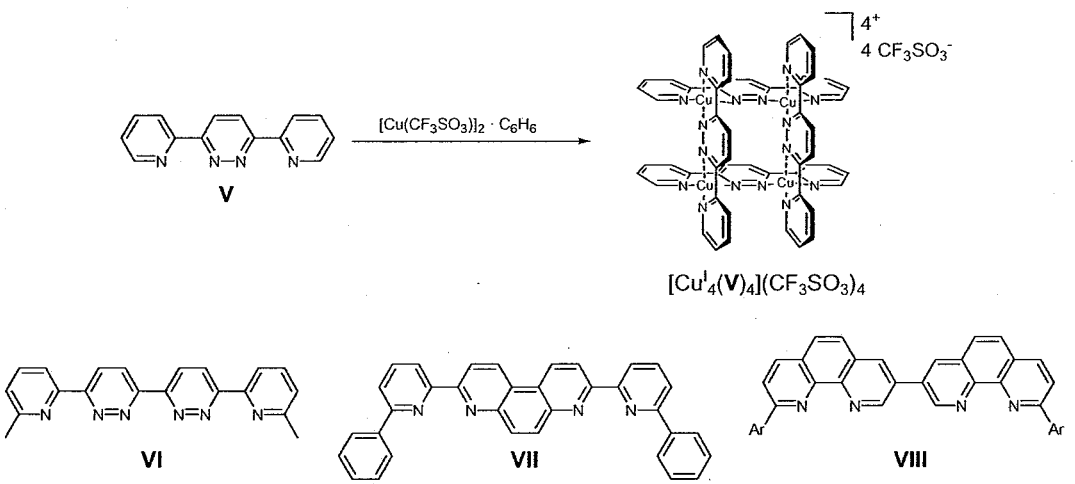

Figure 1.2.3. Formation of a tetranuclear grid, incorporating Cu(I) and **V**; the tris-bidentate ligand **VI** and the bis-bidentate ligands **VII** and **VIII**.

Pyrimidine-based grid compounds

For the formation of grid compounds that incorporate octahedral rather than tetrahedral metal ions, the use of poly-terdentate, rather than poly-bidentate ligands is required. Several grid-type complexes employing pyrimidine-based poly-terdentate ligands have been characterised, especially by Lehn and co-workers[86-96] but also by other groups.[97-100] Following this strategy [4 × 4] grid-type complexes, incorporating eight tris-terdentate ligands (**IX**[94] or **X**[100] in Figure 1.2.4)

and 16 lead(II) ions, have been synthesised. Employing the hybrid bidentate-terdentate pyrimidine-based ligand **XI**, a [2 × 2] nickel(II) grid has been synthesised where the two nickel(II) ions coordinated to the bidentate binding pockets of two ligand molecules complete their distorted octahedral coordination spheres by a dimethyl sulfoxide and a water coligand each. An even higher level of organisation was achieved by Lehn and co-workers,[91] who employed a bis-terdentate ligand with fitted complementary hydrogen bonding subunits (**XII**), and achieved the formation of infinite chains of grids.

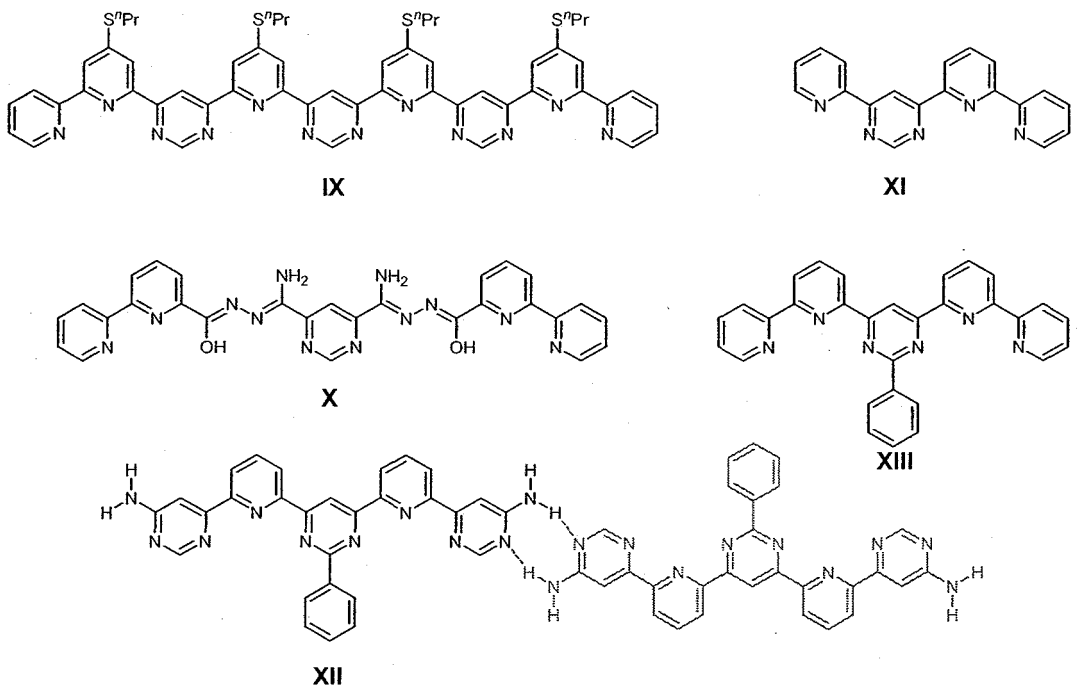

Figure 1.2.4. Pyrimidine-based ligands **IX**, **X**, **XI**, **XII** and **XIII**.

With the employment of the relatively simple pyrimidine-based bis-terdentate ligand **XIII** (Figure 1.2.4) and cobalt(II) ions, Lehn and co-workers[89] isolated the grid-type complex $[Co^{II}_4(\mathbf{XIII})_4](BF_4)_8$. This complex was described as a multilevel molecular electronic species, from cyclovoltammetric studies at –20 °C, which showed ten well-resolved, completely reversible reduction steps. Using the same bis-terdentate pyrimidine-based ligand **XIII**, another very interesting [2 × 2] complex incorporating iron(II) was formed.[90] In this tetranuclear complex $[Fe^{II}_4(\mathbf{XIII})_4](ClO_4)_8$ a spin crossover could be triggered by temperature, light or pressure. This complex

thus presented the first tetranuclear grid-like compound, generated by self-assembly, with spin transition properties and the first triply switchable system. Later further [2 × 2] iron(II) complexes incorporating derivatives of **XIII** were synthesised and characterised, some of which exhibited temperature triggered spin transitions.[95]

Pyrazine-based grid compounds

In striking contrast to the variety of pyridazine and pyrimidine-based grid-type complexes, only one report describing pyrazine-based grid complexes has been published so far. In 2001, von Zelewsky and co-workers[101] employed the pyrazine-based ligands **XIV** and **XV** in grid formation and obtained the chiral [2 × 2] zinc(II) complexes $[Zn^{II}_4(\mathbf{XIV})_4](PF_6)_8$ and $[Zn^{II}_4(\mathbf{XV})_4](PF_6)_8$ (Figure 1.2.5).

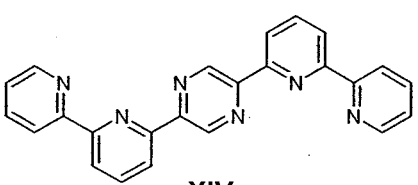

XIV

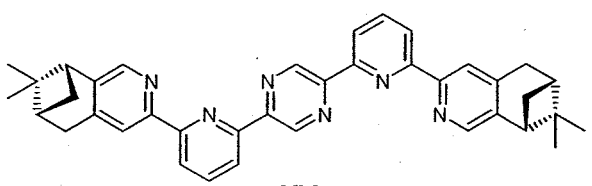

XV

Figure 1.2.5. The pyrazine-based ligands **XIV** and **XV**.

Other ligands

The common feature of the ligands described so far (with the exception of **X**) is the symmetrical built-up and the repeating linear array of similar, if not identical, polydentate binding pockets. The hydrazide-based tris-terdentate ligand **XVI** used by Thompson and co-workers[102-104] does not have a repeating linear array but features two N_2O binding pockets on the periphery and one NO_2 binding pocket in the middle (Figure 1.2.6). Using this ligand for [3 × 3] grid formation, the resulting nonanuclear complex featured three different coordination environments for the metal ions: N_4O_2 in each corner, N_3O_3 on the sides and N_2O_4 in the middle.

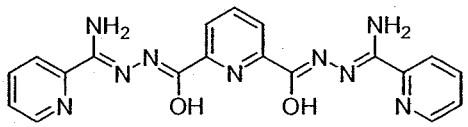

XVI

Figure 1.2.6. The tris-terdentate ligand **XVI**, featuring two N_2O and one NO_2 terdentate binding pocket.

Other examples of non-diazine-based ligands used for grid formation are the alkoxy-based bis-terdentate ligand **XVII**,[105] the phenoxy-based ligand **XVIII**[106] and the terpyridine-based ligand **XIX** (Figure 1.2.7). Using the thiocarbazone-based ligand **XX** and iron(III) chloride, Chun-Ying and co-workers[107] obtained a mixed-valent grid complex $[Fe^{II}_3Fe^{III}(XX)_2(HXX)_2][Fe^{III}Cl_4]_3$ (Figure 1.2.7).

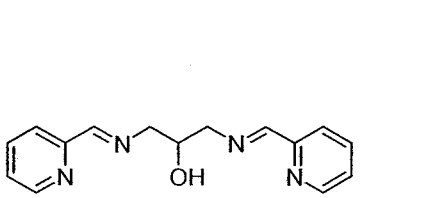

XVII

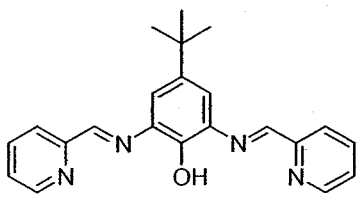

XVIII

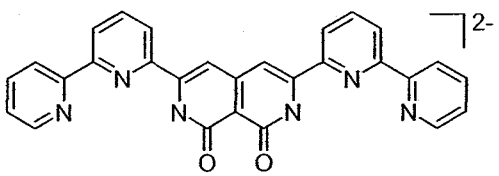

XIX

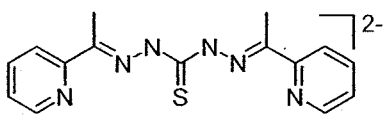

XX

Figure 1.2.7. The bis-terdentate ligands **XVII**, **XVIII**, **XIX** and **XX**.

2. Results and Discussion

2.1. *The diamide ligands H_2L^{M1} and H_2L^{M2}*

The homologous symmetrical diamide ligands *N,N'*-bis(2-pyridylmethyl)-pyrazine-2,3-dicarboxamide (H_2L^{M1}) and *N,N'*-bis[2-(2-pyridyl)ethyl]pyrazine-2,3-dicarboxamide (H_2L^{M2})[108,109] (Figure 2.1.1) both feature two potentially chelating terdentate binding sites. These cavities are made up of a pyridine containing ligand arm connected by an amide function to the central bridging pyrazine unit. Only in the deprotonated state can the amide containing binding pockets of the ligands be employed in N_3 terdentate metal chelating coordination, because in the neutral ligand, the chelating unit will act either as an NO dinucleating binding pocket or simply as an N or O monodentate donor.

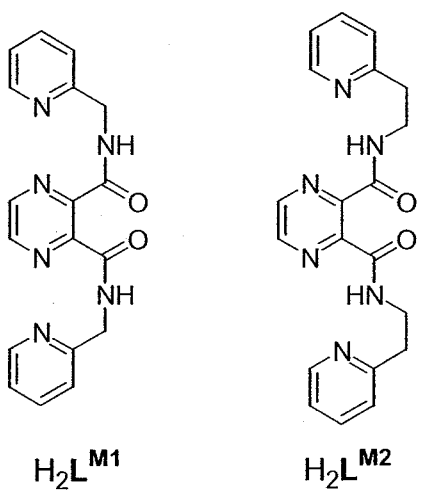

H_2L^{M1} H_2L^{M2}

Figure 2.1.1. The symmetrical diamide ligands H_2L^{M1} and H_2L^{M2}.

The only difference between the two homologous ligands H_2L^{M1} and H_2L^{M2} is a single methylene link between each of the amide and pyridine units. Both ligands derive from 2,3-substituted pyrazine which gives rise to an M-shaped appearance of the ligand backbone as drawn, hence the capital M in the ligand abbreviations. A methylene link consists of one, an ethylene link of two carbon atoms, therefore the use of the superscripts 1 and 2. In combination this results in their respective abbreviations, H_2L^{M1} and H_2L^{M2}. The slight difference between the ligand frameworks can be expected to lead to pronounced differences in the coordination chemistry as complexation reactions employing H_2L^{M1} will lead to two five-membered chelate rings while complexation reactions with H_2L^{M2} will lead to one five- and one six-membered chelate ring per terdentate unit.[110,111]

Synthesis of H_2L^{M1} and H_2L^{M2}

The common ligand precursor, dimethyl pyrazine-2,3-dicarboxylate (**3**), was synthesised from commercially available quinoxaline (**1**) in a one-pot two-step procedure giving pure diester **3**. The first step consisted of the oxidative degradation of the benzene ring with potassium permanganate to obtain pyrazine-2,3-dicarboxylic acid (**2**) (Scheme 2.1.1). [112-114] Efforts to isolate pure **2** resulted in huge losses of product, so instead the subsequent esterification with thionyl chloride in methanol was carried out without isolation of the intermediate pyrazine-2,3-dicarboxylic acid (**2**). In this way excellent yields of 90 % of the pure diester **3** could be obtained directly from quinoxaline.

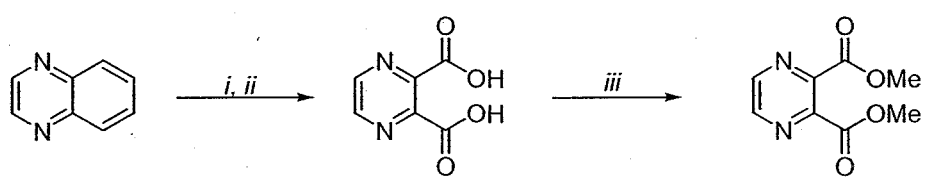

1 **2** **3**

Scheme 2.1.1. Synthesis of **3**. Reagents and conditions: (*i*) $KMnO_4$, H_2O, 80–90 °C; (*ii*) conc. HCl, H_2O, RT; (*iii*) $SOCl_2$, MeOH, reflux.

The symmetrical bis-terdentate diamide ligands *N,N'*-bis(2-pyridylmethyl)-pyrazine-2,3-dicarboxamide (H_2L^{M1}) and *N,N'*-bis[2-(2-pyridyl)ethyl]pyrazine-2,3-dicarboxamide (H_2L^{M2})[108,109] were obtained by reacting diester **3** with 2-(aminomethyl)pyridine (**4**) or 2-(2-aminoethyl)pyridine (**5**) in a molar ratio of 1:2, respectively, in an open flask allowing the methanol formed in the reaction to evaporate (Scheme 2.1.2). Thus, essentially pure H_2L^{M1} that could be used for subsequent complexations, was obtained in 90–96 % yield after redissolving the crude product in dichloromethane, filtration of the insoluble material and evaporation of the filtrate under reduced pressure. Analytically pure H_2L^{M2} was obtained in 80–83 % yield by redissolving the crude product in dichloromethane/acetone (2:1), reduction of the volume to a third under reduced pressure and filtration of the colourless microcrystalline precipitate which resulted. Both compounds proved to be well soluble in all common polar solvents like *N,N*-dimethylformamide, acetonitrile, acetone, alcohols, water, as well as in dichloromethane, chloroform, *etc.*

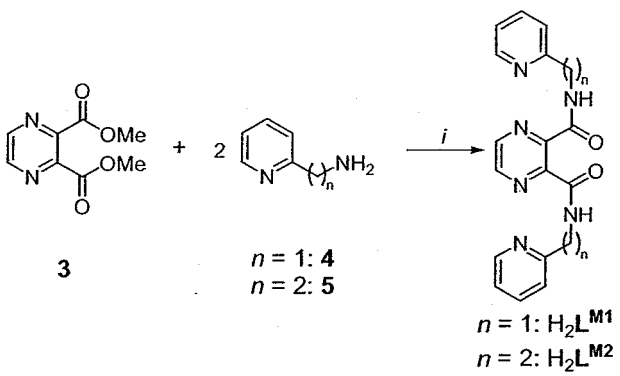

Scheme 2.1.2. Synthesis of H_2L^{M1} and H_2L^{M2}. Reagents and conditions: (*i*) MeOH, 80–90 °C, open flask.

IR spectroscopic studies on H_2L^{M1} and H_2L^{M2}

Owing to the apparent symmetry of the ligands H_2L^{M1} and H_2L^{M2} their IR spectra were expected to show only one band for the N-H and C=O stretching (ν_{NH} and ν_{CO}), as well as for the N-H bending vibration (δ_{NH}), respectively. In reality, the IR spectra of both compounds (Figure 2.1.2 and Figure 2.1.3) showed two absorption bands for ν_{CO} and δ_{NH}, respectively, as listed in Table 2.1.1.

Table 2.1.1. IR absorption bands of the amide functions of the ligands $H_2\mathbf{L}^{M1}$ and $H_2\mathbf{L}^{M2}$.

Ligand	ν_{CO} / cm^{-1}	δ_{NH} / cm^{-1}
H_2L^{M1}	1690	1533
	1655	1514
H_2L^{M2}	1674	1541
	1651	1509

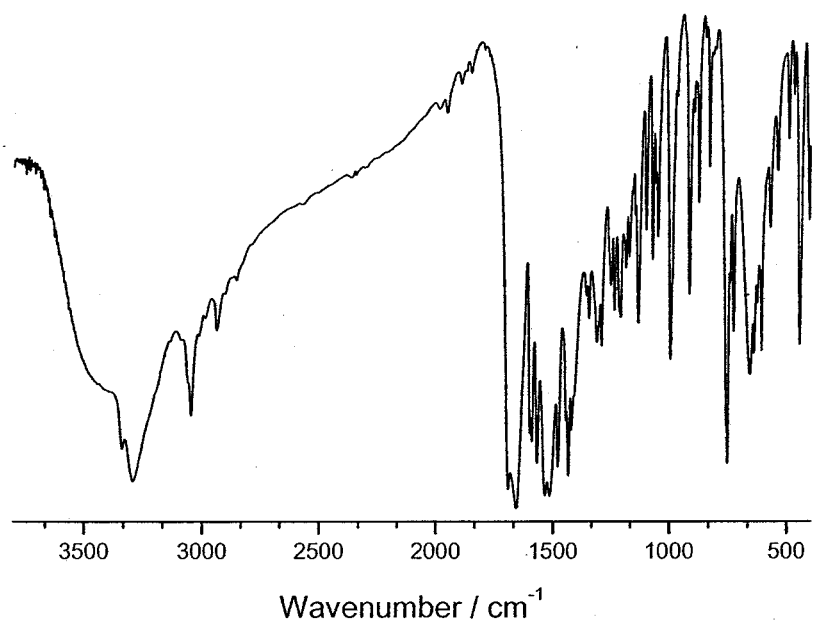

Figure 2.1.2. IR spectrum (KBr) of $H_2\mathbf{L}^{M1}$.

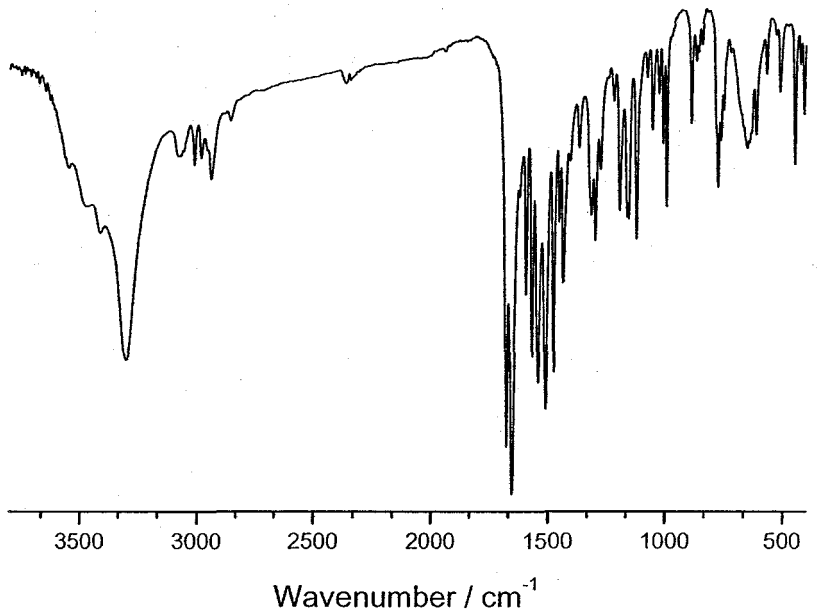

Figure 2.1.3. IR spectrum (KBr) of $H_2\mathbf{L}^{M2}$.

This unexpected result led to the postulation of tautomeric equilibria, as shown in Figure 2.1.4, which were believed to exist for both of the diamide ligands $H_2\mathbf{L}^{M1}$ and $H_2\mathbf{L}^{M2}$.

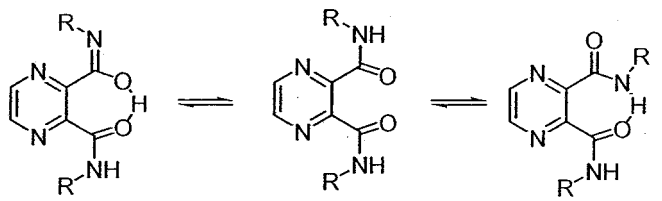

Figure 2.1.4. Schematic formulation of the equilibria expected for $H_2\mathbf{L}^{M1}$ and $H_2\mathbf{L}^{M2}$.

Asymmetrical amide functions have also been observed by IR in similar compounds incorporating 4,5-disubstituted imidazole instead of 2,3-disubstituted pyrazine.[115]

pK_a studies on H_2L^{M1} and H_2L^{M2}

The acid dissociation constants of the two amide ligands H_2L^{M1} and H_2L^{M2} were measured by potentiometric titration with standard alkali solution using established methods.[116] The method involved back titration of an aqueous solution containing known amounts of the ligand and standard aqueous hydrochloric acid with standard aqueous sodium hydroxide. The hydrochloric acid was added to allow calibration of the glass electrode in terms of solution pH. Titrations were conducted in a constant ionic medium of 0.1 M sodium perchlorate to control variations in activity coefficients. Each ligand was titrated in duplicate, with each titration comprising approximately 50 data points. The results were analysed using a non-linear least squares method which obtained the best fit of the titration data to a proton balance model for the ligand (Section 5.6). In this case, it was assumed that each neutral ligand molecule contained two pyridine-N groups capable of accepting protons and a third functional group (amide) capable of losing a proton.

The results obtained from the non-linear fitting procedure are presented in Table 2.1.2. The table shows the computed first, second and third pK_a values in each case for the two ligands H_2L^{M1} and H_2L^{M2}.

Table 2.1.2. pK_a values for $H_2\mathbf{L}^{\mathbf{M1}}$ and $H_2\mathbf{L}^{\mathbf{M2}}$.

	H_2L^{M1} (#1/#2)	H_2L^{M1} (average)	H_2L^{M2} (#1/#2)	H_2L^{M2} (average)
pK_1	4.58/4.21	4.4	5.74/4.84	5.3
pK_2	5.22/5.13	5.2	5.76/5.53	5.6
pK_3	12.9/13.2	13.1	14.0/14.4	14.2

For H_2L^{M1}, the agreement between the two replicate titrations was quite good for all pK_a values, while for H_2L^{M2} the agreement between the replicates was less good for pK_1. The general magnitude of the pK_1 and pK_2 values for both ligands was consistent with the dissociation of isolated pyridinium protons, *e.g.* pK_a = 5.23 for the pyridinium ion (at zero ionic strength).[7] In the presence of the 0.1 M sodium perchlorate electrolyte, the conditional pK_a for pyridinium protons is expected to be

slightly lower.[7] The much higher pK_3 values were likely to be linked to the dissociation of an amide proton. However, it is important to note that it is difficult to obtain accurate pK_a at values greater than about 12 in aqueous. Furthermore it is worthwhile noting that since the method of potentiometric titration is based on thermodynamics, it is not possible to deduce structural information about the likely functional groups on the basis of these results alone. Compared to the pK_a values of mono-amide compounds, which usually range from 16–19 (*e.g.* $pK_{a(benzamide)} > 19$, $pK_{a(acetanilide)} = 17.6$, $pK_{a(benzanilide)} = 16.5$),[117] the pK_3 values of around 13 and 14 for the first amide group of H_2L^{M1} and H_2L^{M2}, respectively, were still remarkably low. This result provided further confidence in the equilibria formulated in Figure 2.1.4 and similar equilibria with charge delocalisation were proposed to occur for the monodeprotonated ligands $(HL^{M1})^-$ and $(HL^{M2})^-$ (Figure 2.1.5).

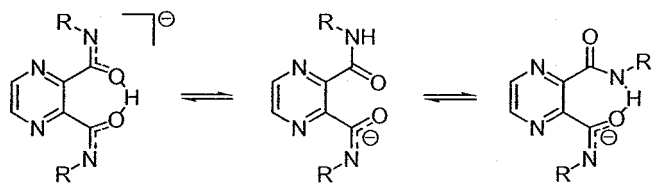

Figure 2.1.5. Schematic formulation of the equilibria expected for the monodeprotonated ligands $(HL^{M1})^-$ and $(HL^{M2})^-$.

NMR spectroscopic studies on H_2L^{M1} and H_2L^{M2}

The aromatic regions of the ^1H NMR spectra of both H_2L^{M1} (Figure 2.1.6, Figure 5.1.1) and H_2L^{M2} (Figure 2.1.7, Figure 5.1.2) showed six signals. Four of these signals, at 8.46 (ddd), 7.60 (dt), 7.35 (d) and 7.13 (ddd) ppm for H_2L^{M1} and at 8.51 (ddd), 7.61 (dt), 7.34 (td) and 7.13 (ddd) ppm for H_2L^{M2}, could be assigned to the protons of the pyridine rings and showed the typical coupling patterns of 2-substituted pyridines.[118] The singlet at the chemical shift of 8.58 ppm in both spectra belonged to the pyrazine protons and lay in the expected region of

8.5–9.0 ppm.[1,6] The signal belonging to the amide protons could be identified as a broad triplet at 8.23 ppm for $H_2\mathbf{L}^{M1}$ and at 7.83 ppm for $H_2\mathbf{L}^{M2}$.

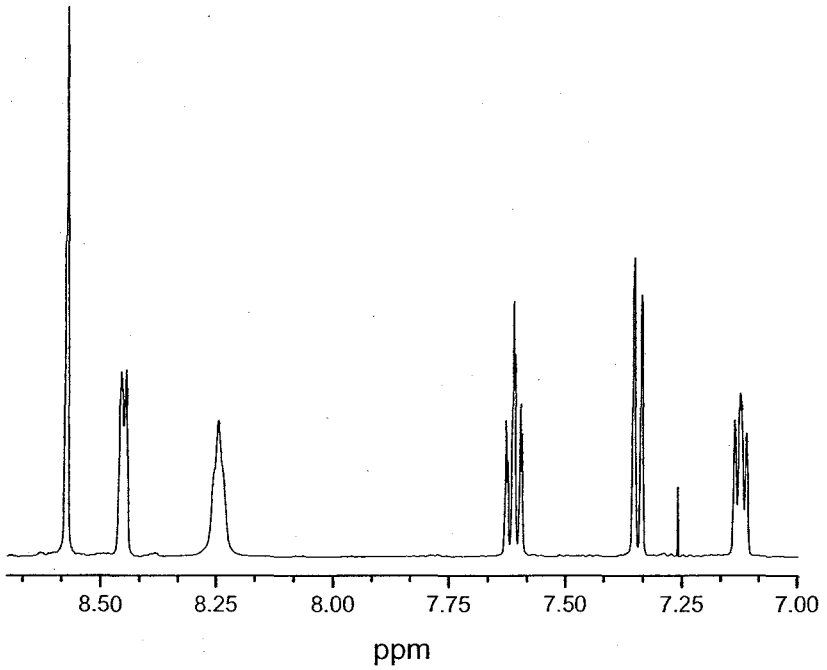

Figure 2.1.6. Aromatic region of the ^{1}H NMR spectrum ($CDCl_3$) of $H_2\mathbf{L}^{M1}$.

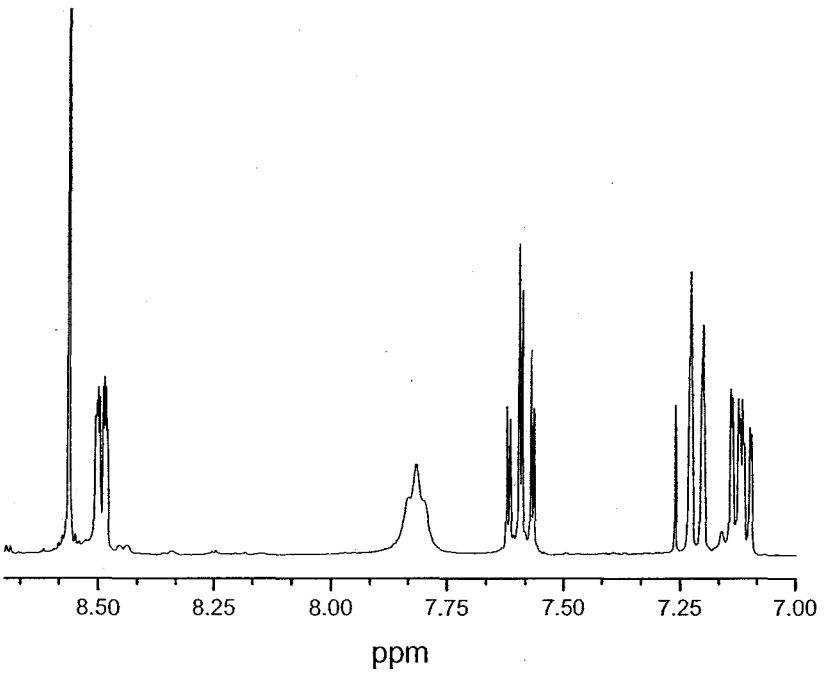

Figure 2.1.7. Aromatic region of the ^{1}H NMR spectrum ($CDCl_3$) of $H_2\mathbf{L}^{M2}$.

The ^{13}C NMR spectra of the ligands H_2L^{M1} and H_2L^{M2} showed all of the expected signals (Figures 5.1.3 and 5.1.4, Appendix). Comparing the two spectra, none of the corresponding signals suffered any remarkable shifts. However, the signals belonging to the 3-*py* (122.0 and 123.6 ppm, respectively) and the 5-*py* (122.3 and 121.6 ppm, respectively) carbon atoms of H_2L^{M1} and H_2L^{M2} were switched in their relative order.

Cyclic voltammetric studies on H_2L^{M1} and H_2L^{M2}

Both ligands proved to be redox innocent in the range of around 2 V to –2 V in acetonitrile. However, on further lowering the reduction potential, an irreversible reduction wave occurred at E_{pc} = –2.10 V and –2.16 V relative to the Fc^+/Fc redox couple for H_2L^{M1} and H_2L^{M2}, respectively (Figure 2.1.8).

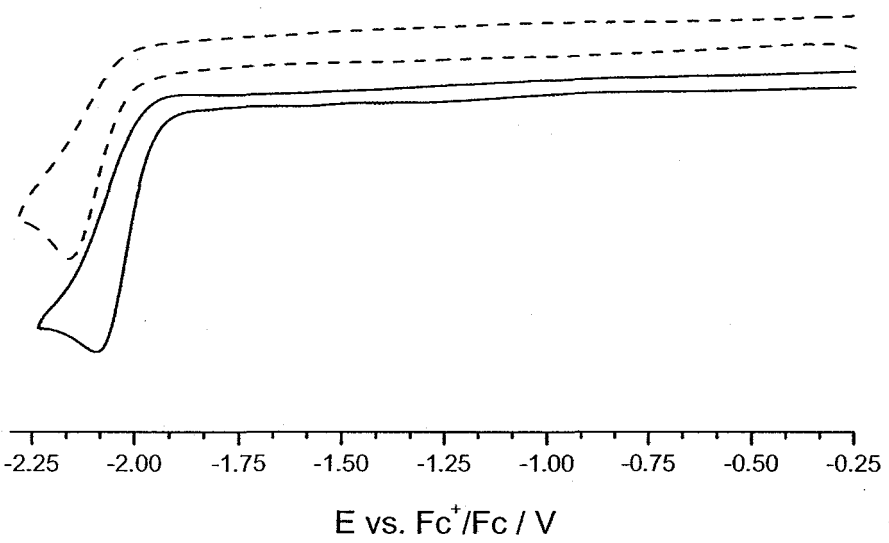

Figure 2.1.8. Cyclic voltammograms (1 mM, 0.1 M TBAP, MeCN, scan rate: 50 mV s^{-1}) of $H_2\mathbf{L^{M1}}$ (solid line) and $H_2\mathbf{L^{M2}}$ (dashed line).

Single crystal X-ray structural analysis of H_2L^{M2}

Single crystals of H_2L^{M2} were obtained by recrystallisation from acetone. The molecular structure shows H_2L^{M2} to be a true diamide ligand with protonated amide N atoms (Figure 2.1.9). No evidence of the other tautomers from the equilibria formulated in Figure 2.1.4 is present. However, both N-H amide protons are involved in different intermolecular hydrogen bonds, involving one pyridine nitrogen and one carbonyl oxygen atom from two symmetry generated neighbouring ligands (Figure 2.1.9, Figure 2.1.10). The carbonyl oxygen involving N(5)···O(2B) hydrogen bonding distance of 2.825(3) Å is significantly shorter than the pyridine nitrogen involving N(2)···N(3A) hydrogen bonding distance of 3.165(3) Å.

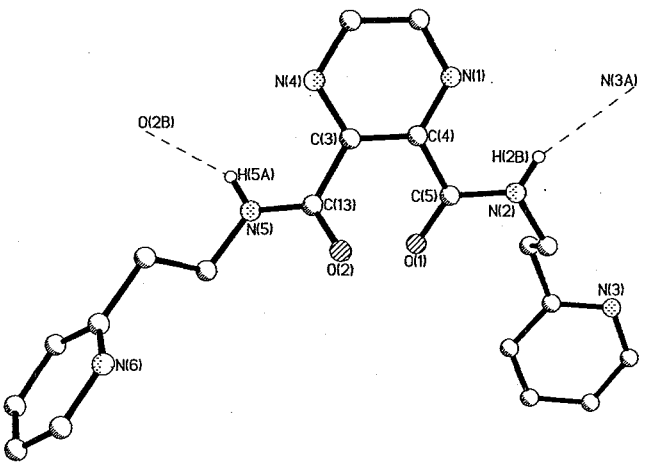

Figure 2.1.9. Molecular structure of H_2L^{M2}. Hydrogen atoms except H(2B) and H(5A) have been omitted for clarity. Selected distances (Å) and angles (°): C(5)-O(1) 1.235(3), C(13)-O(2) 1.241(3), C(5)-N(2) 1.345(3), C(13)-N(5) 1.335(4), N(2)···N(3A) 3.165(3), N(5)···O(2B) 2.825(3); C(3)-C(13)-N(5) 116.0(3), C(4)-C(5)-N(2) 116.9(2). Symmetry operations used to generate equivalent atoms: A = -x-2, -y+1, -z-1; B = x+1, y, z.

Possibly due to sterical reasons, the amide functions are not coplanar with each other and with the pyrazine ring; instead the mean planes defined by the amide functions [O(1)-C(5)-N(2)-H(2B) and O(2)-C(13)-N(5)-H(5A)] form angles of 17.4° and 50.0° to the pyrazine ring, respectively.

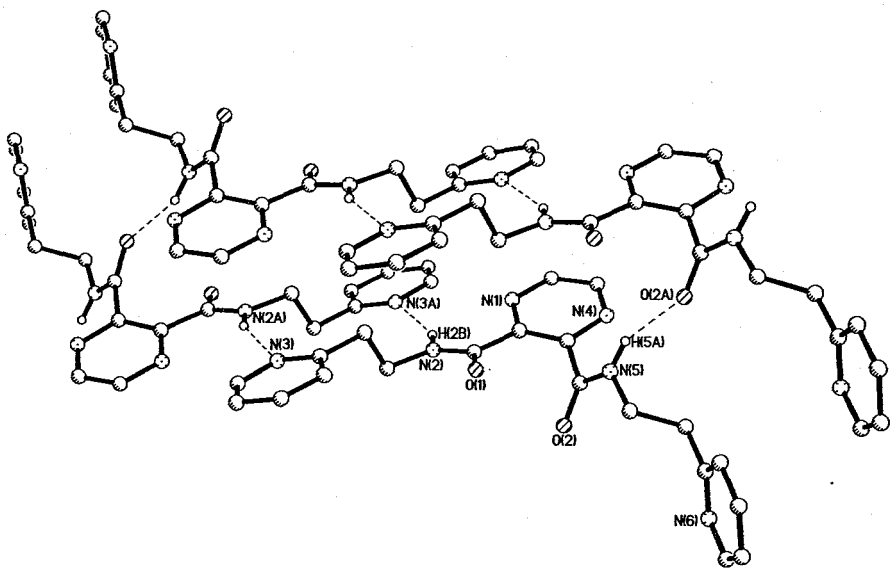

Figure 2.1.10. Section of the polymeric network of the crystal structure of $H_2\mathbf{L}^{M2}$. Hydrogen atoms, except amide hydrogen atoms, are omitted for clarity.

Note: Just prior to submission of this thesis the X-ray crystal structure of $H_2\mathbf{L}^{M1}$ was reported by Cati and Stoeckli-Evans.[119]

2.2. *Coordination of the ligands H_2L^{M1} and H_2L^{M2}, employing a 1:2 molar ratio of ligand to metal(II) ions*

On metal coordination the homologous ligands $H_2\mathbf{L}^{M1}$ and $H_2\mathbf{L}^{M2}$ were expected to function as chelating ligands, encapsulating the metal ions in their terdentate binding pockets. As metal coordination to amide nitrogen atoms requires the

deprotonation of the respective amide functions,[120,121] dinuclear complexes of H_2L^{M1} and H_2L^{M2} were initially expected to employ the doubly deprotonated ligands $(L^{M1})^{2-}$ and $(L^{M2})^{2-}$, respectively.

2.2.1. *Copper(II) tetrafluoroborate tetrahydrate*

Complexations

Metalation of H_2L^{M1} with copper(II) tetrafluoroborate tetrahydrate in neutral acetonitrile solution, employing a molar ratio of ligand to metal(II) salt of 1:2, and subsequent precipitation with toluene gave a deep navy blue complex in 70–80 % yield. Elemental analyses suggested that the complex could be formulated as $[Cu^{II}_2(HL^{M1})(MeCN)_{4-x}(H_2O)_x](BF_4)_3$, giving the best fit with $x = 2$ (**6**) (Scheme 2.2.1). The compound proved to be readily soluble in most common polar solvents, like alcohols, acetonitrile, *N,N*-dimethylformamide, water, acetone, *etc.* but was insoluble in *e.g.* chloroform or dichloromethane. The conductivity measurement in acetonitrile solution [Λ_m(MeCN) = 378 mol^{-1} cm^2 Ω^{-1}], in accordance to the proposed formulation, indicated a 1:3 ratio of complex cation to tetrafluoroborate counter ion, supporting the formulation of the ligand as a mono anionic species $(HL^{M1})^-$.

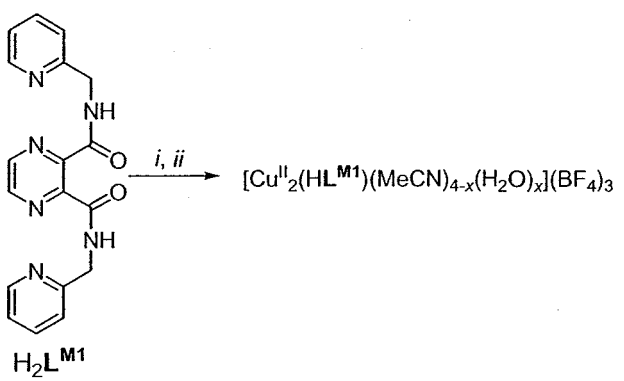

Scheme 2.2.1. Synthesis of **6**. Reagents and conditions: (*i*) 2 eq. $Cu(BF_4)_2 \cdot 4\ H_2O$, MeCN, RT; (*ii*) toluene (precipitation).

The positive ion electrospray mass spectrum of **6** in acetonitrile (Figure 5.2.1, Appendix) had the most intense peaks at m/z = 410.0, 256.5, 226.0 and 205.5. Based on isotopic patterns the peaks were assigned to the species $[Cu^{II}(HL^{M1})]^+$, $[Cu^{II}_2(L^{M1})(MeCN)]^{2+}$, $[Cu^{II}(H_2L^{M1})(MeCN)]^{2+}$ and $[Cu^{II}(H_2L^{M1})]^{2+}$, respectively, giving further evidence in support of the dinuclearity of **6**. Furthermore a smaller peak at m/z = 277.0 was assigned to the dinuclear species $[Cu^{II}_2(L^{M1})(MeCN)_2]^{2+}$.

A similar complex of the higher ligand homologue $(HL^{M2})^-$, such as $[Cu^{II}_2(HL^{M2})(MeCN)_{4-x}(H_2O)_x]_4(BF_4)_3$, could not be isolated following the synthetic approach described above.

IR spectroscopic studies on $[Cu^{II}_2(HL^{M1})(MeCN)_2(H_2O)_2](BF_4)_3$ (6)

The IR spectrum of **6** showed no clear δ_{NH} absorption band, so both nitrogen amide atoms were expected to be deprotonated (Figure 2.2.1). Furthermore only one ν_{CO} absorption band at $\tilde{\upsilon}$ = 1609 cm^{-1} was present, suggesting that, in contrast to the free ligand, the amide functions of **6** were equivalent (see Table 2.2.1). The preparation of a KBr pellet of **6** resulted in a colour change from dark navy blue to grass green, which possibly indicated a coligand exchange with the bromide ions.

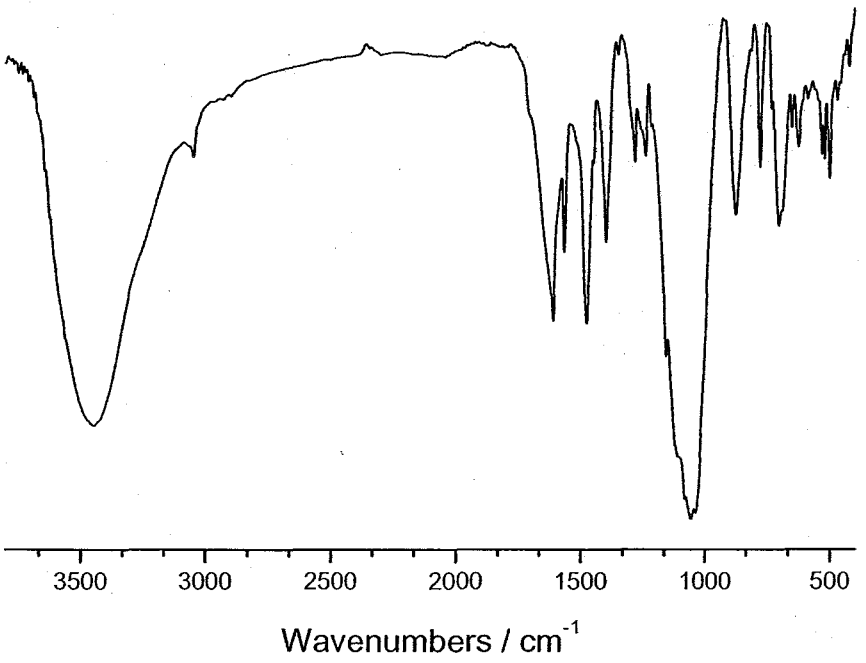

Figure 2.2.1. IR spectrum (KBr) of $[Cu^{II}_2(HL^{M1})(MeCN)_2(H_2O)_2](BF_4)_3$ (**6**).

Conclusions

According to the results from elemental analyses, the empirical formula of compound **6** comprised of two copper(II) ions, one singly deprotonated diamide ligand, four neutral coligands and three tetrafluoroborate counter ions. Also the conductivity measurement was in accordance with **6** being a 3:1 electrolyte. As the IR spectrum had indicated that both amide nitrogen atoms were deprotonated, but the dinuclear complex cation apparently still held three positive charges, the existence of one shifted, retained former N-H amide proton was suggested. As all of the nitrogen atoms of the ligand were expected to be involved in metal coordination and could therefore not easily be protonated with the retained proton, it was suggested that the retention of the former N-H amide proton was achieved by protonation of a carbonyl oxygen atom. The expected equivalence of the amide functions, as well as the retention of only one proton, could only be achieved by the two carbonyl atoms

sharing the proton in a symmetrical O···H···O hydrogen bond as shown in Figure 2.2.2.

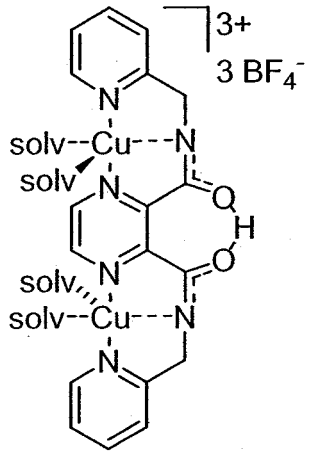

Figure 2.2.2. Proposed formulation of $[Cu^{II}_2(HL^{M1})(solv)_4](BF_4)_3$ (**6**) (solv = MeCN or H_2O), with emphasis on the existence and location of one retained former amide proton.

This motif is not unprecedented in the literature, as in 1974 Fleischer and co-workers suggested a similar feature for the polymeric complex $[Cu^{II}_2(HL^{M2})(Cl)_3]_\infty$ of the higher ligand homologue (H_2L^{M2}).[122]

Single X-ray structural analysis of $[Cu^{II}_2(HL^{M1})(MeCN)_4](BF_4)_3 \cdot MeCN$ (6b · MeCN)

By vapour diffusion of diethyl ether into a solution of **6** in acetonitrile single crystals of $[Cu^{II}_2(HL^{M1})(MeCN)_4](BF_4)_3 \cdot MeCN$ (**6b** · MeCN) suitable for X-ray crystal structure determination were obtained (Figure 2.2.3). Although the data obtained were of poor quality with a final *R*1 value of only 0.16, the overall connectivity of the molecular structure of the compound was clear.

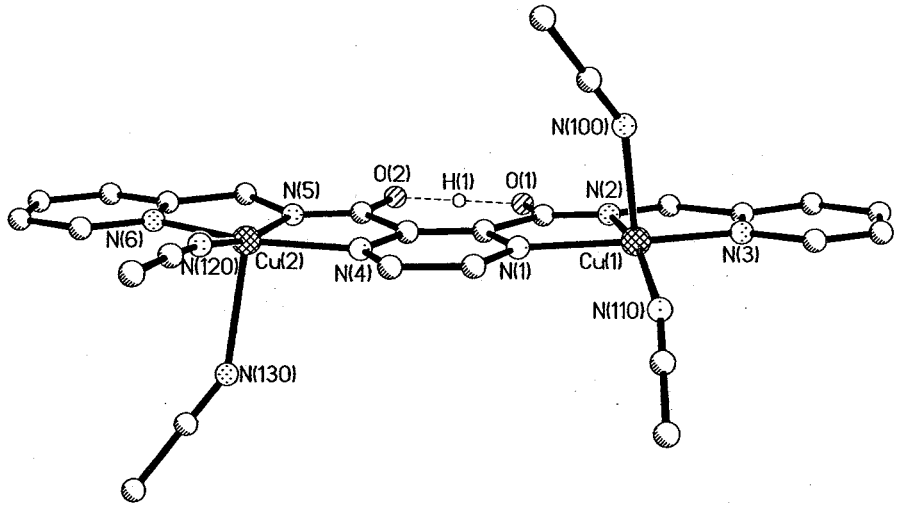

Figure 2.2.3. Molecular structure of $[Cu^{II}_2(HL^{M1})(MeCN)_4]^{3+}$, the cation of complex **6b** · MeCN. Hydrogen atoms, except H(1), have been omitted for clarity. Selected distances (Å) and angles (°): Cu(1)-N(1) 2.02(1), Cu(1)-N(2) 1.93(1), Cu(1)-N(3) 1.95(1), Cu(1)-N(100) 2.33(1), Cu(1)-N(110) 1.98(1), Cu(2)-N(4) 2.04(1), Cu(2)-N(5) 1.94(1), Cu(2)-N(6) 1.99(1), Cu(2)-N(120) 1.97(1), Cu(2)-N(130) 2.36(1), Cu(1)···Cu(2) 6.745(5), O(1)···O(2) 2.41(1); N(1)-Cu(1)-N(2) 80.3(4), N(1)-Cu(1)-N(3) 163.0(5), N(1)-Cu(1)-N(100) 85.4(5), N(1)-Cu(1)-N(110) 96.3(5), N(2)-Cu(1)-N(3) 82.9(5), N(2)-Cu(1)-N(100) 107.7(5), N(2)-Cu(1)-N(110) 160.4(5), N(3)-Cu(1)-N(100) 102.4(5), N(3)-Cu(1)-N(110) 98.6(5), N(100)-Cu(1)-N(110) 91.1(5), N(4)-Cu(2)-N(5) 80.5(4), N(4)-Cu(2)-N(6) 161.9(5), N(4)-Cu(2)-N(120) 96.8(5), N(4)-Cu(2)-N(130) 94.4(5), N(5)-Cu(2)-N(6) 81.4(5), N(5)-Cu(2)-N(120) 167.4(5), N(5)-Cu(2)-N(130) 105.6(5), N(6)-Cu(2)-N(120) 100.4(5), N(6)-Cu(2)-N(130) 92.2(5), N(120)-Cu(2)-N(130) 86.8(5).

As expected, the two copper(II) ions are coordinated by one monodeprotonated ligand $(HL^{M1})^-$. The coordination geometries around the copper(II) ions are best described as N_5 distorted square pyramidal. Both amide functions of the ligand are N-metalated and therefore deprotonated. All six nitrogen donors of the ligand function as equatorial donor atoms encapsulating the two copper(II) ions in the two terdentate binding sites. In both cases the fourth equatorial, as well as the axial, coordination position is occupied by nitrogen donors from acetonitrile coligands. As expected the average Cu^{II}-N_{ax} distance of 2.35 Å is significantly longer than the average Cu^{II}-N_{eq} distance of 1.98 Å. Also it has been found that the average Cu^{II}-N_{amide} bond length of 1.94 Å is significantly shorter than the average Cu^{II}-N_{pz} bond length of 2.03 Å. In related complexes of *N*-(2-picolyl)picolinamide (HL^{N1}),[123] *N*-(2-pyridylethyl)picolinamide (HL^{N2}),[124] *N*-(bis(2-pyridyl)methyl)pyridine-2-carboxamide (HL^{N11})[125] and *N*-(1,2-bis(2-pyridyl)ethyl)pyridine-2-carboxamide

(HL^{N12}) [126] (Figure 2.2.4) a similar tendency of longer Cu^{II}-$N_{heterocycle}$ than Cu^{II}-N_{amide} distances has been observed.

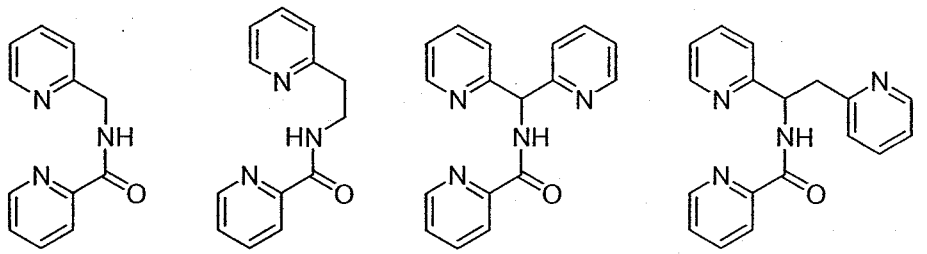

Figure 2.2.4. The related ligands *N*-(2-picolyl)picolinamide (HL^{N1}),[123] *N*-(2-pyridylethyl)picolinamide (HL^{N2}),[124] *N*-(bis(2-pyridyl)methyl)pyridine-2-carboxamide (HL^{N11})[125] and *N*-(1,2-bis(2-pyridyl)ethyl)pyridine-2-carboxamide (HL^{N12}).[126]

The degree of trigonality τ is given by β–α/60 (Figure 2.2.5), where $\tau = 0$ for a perfect square pyramid and $\tau = 1$ for a perfect trigonal bipyramid. The angles β and α are defined as the two largest L-M-L angles of the coordination sphere.[127] For compound **6b** · MeCN τ, and therefore the distortion of the square pyramid, is very small, with $\tau_{(1)} = 0.04$ and $\tau_{(2)} = 0.09$ for Cu(1) and Cu(2), respectively.

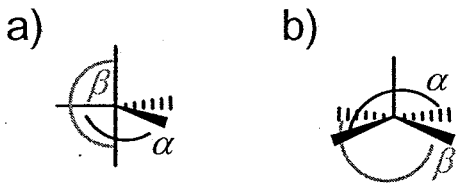

Figure 2.2.5. Degree of trigonality $\tau = \beta$–α/60, shown on the examples of a) a distorted trigonal bipyramid and b) a distorted square pyramid.[127]

Nevertheless, the copper(II) ions are pulled 0.146(7) Å for Cu(1) and 0.220(7) Å for Cu(2) out of the N_4 plane in the direction of the axial donor atom. The two copper(II) ions are bridged by the pyrazine ring of the ligand and are separated by 6.745(5) Å. As shown in Figure 2.2.3, a retained former amide proton H(1), is believed to be centred in a symmetrical O···H···O hydrogen bond, between the two amide oxygen atoms of the ligand (see Section 3.4.2). This feature makes the two amide groups close to coplanar to each other (with an angle of 7.0°) and to the pyrazine ring (with angles

of around 4.1 and 3.0°). The O···O distance of the resulting seven-membered ring is 2.41(1) Å. As mentioned before, Fleischer and co-workers described in 1974 a similar albeit polymeric complex of the higher ligand homologue $(HL^{M2})^-$, $[Cu^{II}_2(HL^{M2})(Cl_3)]_\infty$.[122]

UV/VIS spectroscopic studies on $[Cu^{II}_2(HL^{M1})(MeCN)_4](BF_4)_3 \cdot MeCN$ (6b · MeCN)

The UV/VIS spectrum of **6b** · MeCN in acetonitrile solution showed a broad weak asymmetrical absorption peak at λ_{max} = 616 nm (ε = 322 M^{-1} cm^{-1}) and a relatively sharp intense absorption peak at λ_{max} = 254 nm (ε = 26100 M^{-1} cm^{-1}) (Figure 2.2.6).

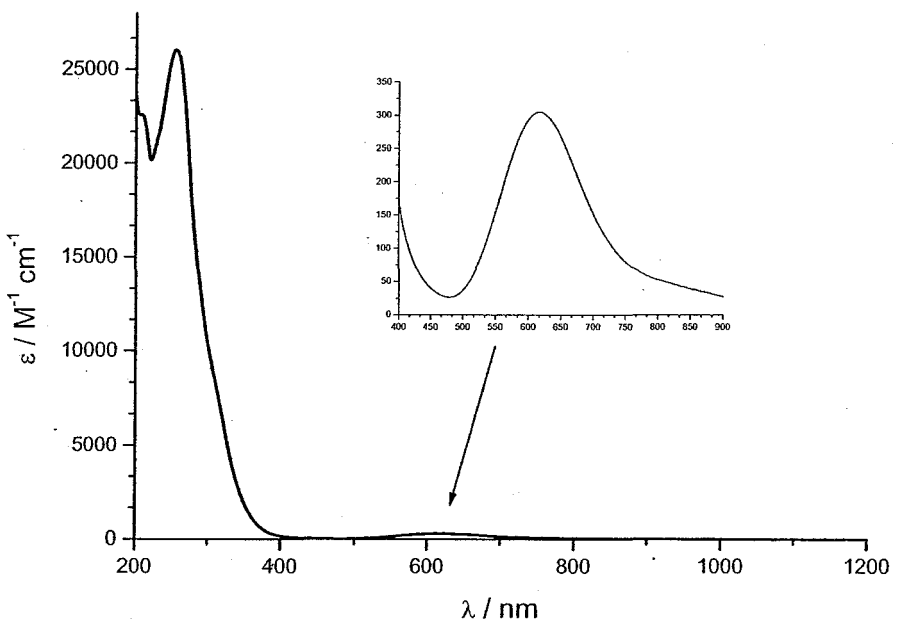

Figure 2.2.6. UV/VIS spectra [MeCN, 1 mM (inset) and 0.1 mM (main)] of $[Cu^{II}_2(HL^{M1})(MeCN)_4](BF_4)_3 \cdot MeCN$ (**6b** · MeCN).

The absorption band at λ_{max} = 616 nm ($\tilde{\nu}$ = 16230 cm^{-1}) was assigned to the overlapping absorption bands of the *d-d* transitions.[128-130] Owing to the higher energy ($\tilde{\nu}$ = 39370 cm^{-1}) and the high molar extinction coefficient, the absorption band at λ_{max} = 254 nm might be a charge transfer absorption band.[130]

Cyclic voltammetric studies on $[Cu^{II}_2(HL^{M1})(MeCN)_4](BF_4)_3 \cdot MeCN$ (6b · MeCN)

The cyclic voltammogram of **6b** · MeCN in acetonitrile solution showed two metal-centred irreversible one-electron reduction waves, occurring at $E_{pc} = -0.33$ V for $[Cu^{II}Cu^{II}] \rightarrow [Cu^{II}Cu^{I}]$ and at $E_{pc} = -0.76$ V for $[Cu^{II}Cu^{I}] \rightarrow [Cu^{I}Cu^{I}]$, relative to the Fc^+/Fc redox couple (Figure 2.2.7). Controlled potential coulometry at $E = -0.40$ V confirmed that the first process corresponded a one-electron reduction of the initial $[Cu^{II}Cu^{II}]$ complex. Taking into account the symmetrical coordination environment of the two metal centres, the two reduction waves were remarkably well separated ($\Delta E_{pc} = 0.43$ V), suggesting an electronic interaction of the two metal centres.[131] For instance only one quasi-reversible two-electron reduction peak was found for the square pyramidal dinuclear copper(II) complexes $[Cu^{II}_2L^{S11}Cl_2](ClO_4)_2$ and $[Cu^{II}_2L^{S22}Cl_2](ClO_4)_2$ of the related ligand pair 2,5-bis[*N*,*N*-bis(2′-pyridylmethyl)-aminomethyl]pyrazine (L^{S11}) and 2,5-bis[*N*,*N*-bis(2′-pyridylethyl)aminomethyl]-pyrazine (L^{S22}), (Figure 2.2.8).[12,51] At lower potentials a plating process ($E_{pc} = -1.10$ V) with associated stripping peak ($E_{pa} = -0.45$ V) was observed for **6b** · MeCN.

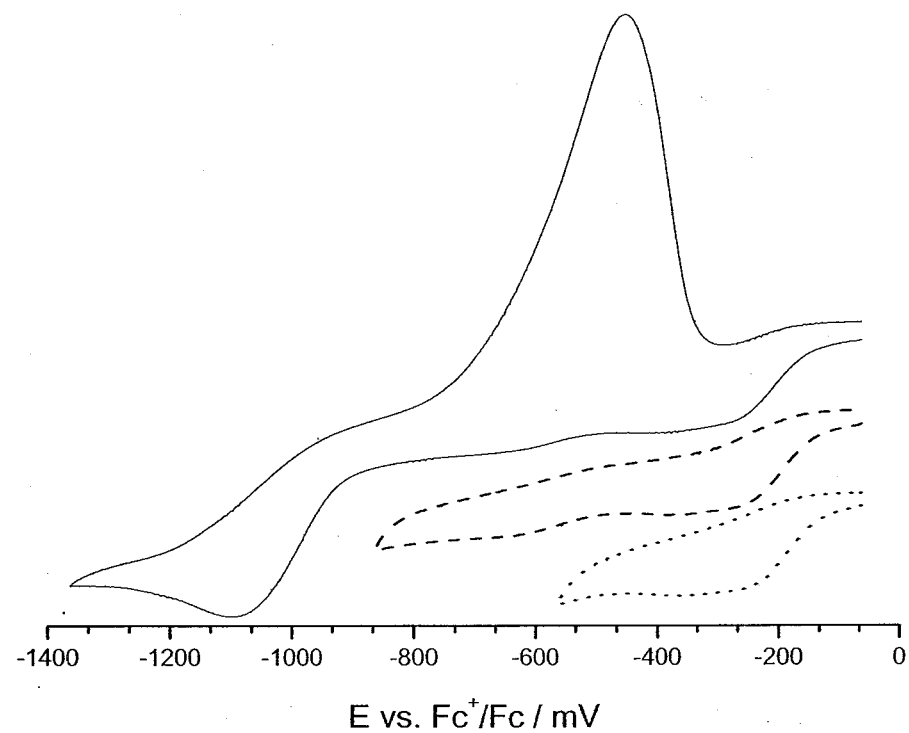

Figure 2.2.7. Cyclic voltammograms (1 mM, 0.1 M TBAP, MeCN, scan rate: 50 mV s^{-1}) of $[Cu^{II}_2(HL^{M1})(MeCN)_4](BF_4)_3 \cdot MeCN$ (**6b** · MeCN).

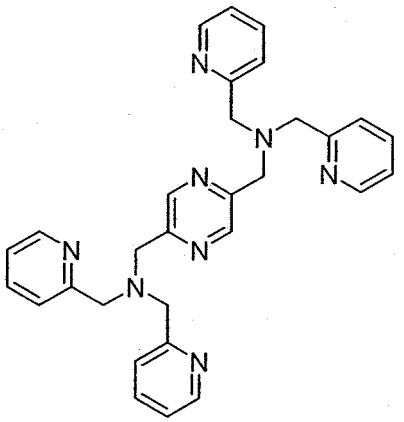

L^{S11}

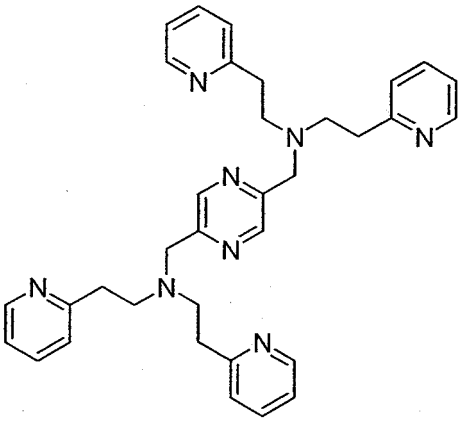

L^{S22}

Figure 2.2.8. The related homologous ligands 2,5-bis[*N*,*N*-bis(2'-pyridyl-methyl)aminomethyl]pyrazine ($\mathbf{L^{S11}}$) and 2,5-bis[*N*,*N*-bis(2'-pyridylethyl)-aminomethyl]pyrazine ($\mathbf{L^{S22}}$).[12,51]

Magnetic studies on $[Cu^{II}_2(HL^{M1})(MeCN)_4](BF_4)_3 \cdot MeCN$ (6b · MeCN)

In the majority of pyrazine bridged copper(II) complexes studied in the literature the magnetic interaction is weak and of antiferromagnetic character, and there has been a debate on whether the exchange takes place through a σ- or a π-type exchange pathway. [11,34,132-134] Hatfield and co-workers have studied the magnetic properties of two polymeric pyrazine bridged copper(II) complexes $[Cu^{II}(hfac)_2(pz)]_\infty$[33,135] and $[Cu^{II}(NO_3)_2(pz)]_\infty$[34] (Figure 2.2.9).

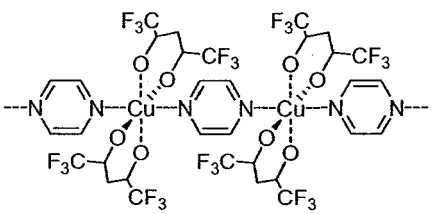

$[Cu^{II}(hfac)_2(pz)]_\infty$

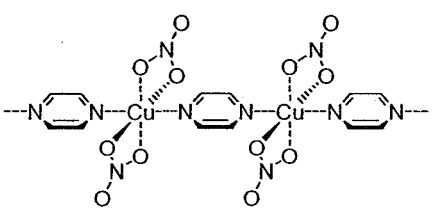

$[Cu^{II}(NO_3)_2(pz)]_\infty$

Figure 2.2.9. The polymeric pyrazine bridged copper(II) complexes $[Cu^{II}(hfac)_2(pz)]_\infty$[33,135] and $[Cu^{II}(NO_3)_2(pz)]_\infty$.[34]

The linear chain structure of $[Cu^{II}(hfac)_2(pz)]_\infty$ is built up of square planar $Cu^{II}(hfac)_2$ units bridged in the axial direction by pyrazine rings.[135] No exchange interaction

was observed, which was attributed to the fact that the plane of the pyrazine bridge lies in the *xz* plane of the $Cu^{II}(hfac)_2$ unit.[33] As the copper(II) ground state is $d_{x^2-y^2}$ there is no effective π-orbital pathway available on the pyrazine (Figure 2.2.10). On the other hand, in complex $[Cu^{II}(NO_3)_2(pz)]_\infty$ the pyrazine rings are canted some 50° out of the copper(II) *xy* plane (Figure 2.2.10).[34] This allows for $d_{x^2-y^2}$–$\pi(b_{1g})$ and d_{xy}–$\pi(b_{2g})$ overlap which was interpreted to lead to a π-orbital pathway for the pyrazine superexchange interactions. Accordingly an antiferromagnetic interaction was noted for $[Cu^{II}(NO_3)_2(pz)]_\infty$ ($J = -7.4$ cm^{-1}).

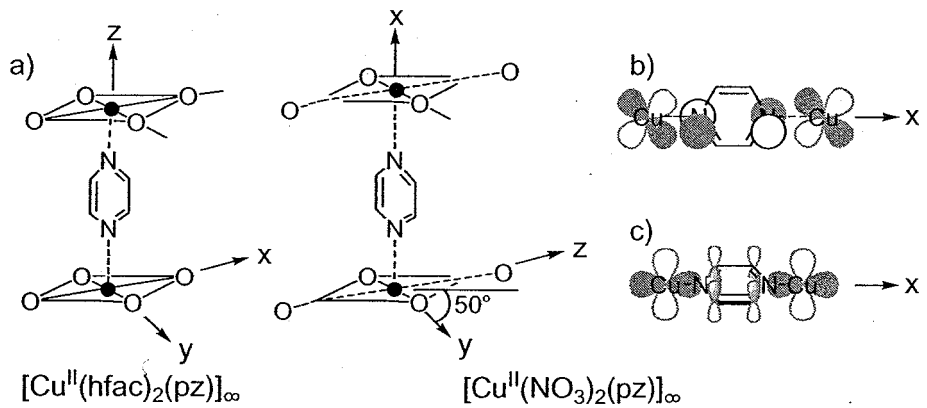

Figure 2.2.10. Environment about the copper(II) ion in $[Cu^{II}(hfac)_2(pz)]_\infty$ and $[Cu^{II}(NO_3)_2(pz)]_\infty$, a) indicating the relative position of the pyrazine ring plane; b) and c) Symmetry allowed possibilities for *d-π* overlap in $[Cu^{II}(NO_3)_2(pz)]_\infty$; b) d_{xy} -$\pi(b_{2g})$; c) $d_{x^2-y^2}$ –$\pi(b_{1g})$ (HOMO).

In 1975 Hoffmann and co-workers concluded that pyrazine bridges are very effective in supporting antiferromagnetic interactions *via* a σ-type pathway.[134] The two nitrogen electron lone pairs on the pyrazine interact *via* empty and occupied σ levels to produce an appreciable splitting in the lone pair energy levels. It was suggested that this through-bond coupling provides an effective σ-type exchange pathway (Figure 2.2.11.). Dinuclear copper(II) complexes thus should be constructed in a way that the copper(II) ions have their unpaired electrons in σ-type orbitals interacting directly with the nitrogen lone-pair orbitals of pyrazine.

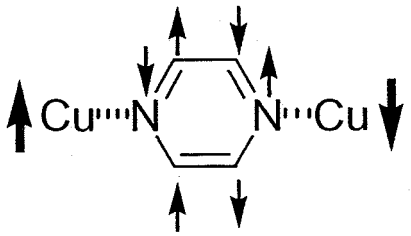

Figure 2.2.11. σ-type exchange pathway through the bridging pyrazine unit, resulting in antiferromagnetic spin coupling of the copper(II) centres.[136]

In summary, on one hand in the π-type pathway, the dihedral angle between the coordination plane of the copper(II) atoms and the plane of the pyrazine ring will be such that the larger the angle, the greater the orbital overlap, and the larger the antiferromagnetic interaction. On the other hand, in the σ-type pathway, the antiferromagnetic interaction will be independent of the dihedral angle.

The magnetic orbitals for square planar coordinated copper(II) ions ($d_{x^2-y^2}$) lie in the equatorial plane pointing straight at the donor atoms. Similarly, the $d_{x^2-y^2}$ orbitals of the copper(II) ions in the square pyramidal dinuclear complex $[Cu^{II}_2(HL^{M1})(MeCN)_4](BF_4)_3 \cdot MeCN$ (**6b** · MeCN), were expected to be coplanar with the mean plane of the bridging pyrazine ring and were therefore expected to have a good overlap with the σ orbitals of the N atoms. Therefore an antiferromagnetic spin coupling of the copper(II) centres was expected through the σ-type exchange pathway, although in general pyrazine is not expected to have strong spin coupling transfer abilities.[40,137,138]

Figure 2.2.12 shows the temperature dependence of the effective magnetic moment (μ_{eff}). Figure 2.2.13 shows the temperature dependence of the molar magnetic susceptibility (χ_m), per copper(II) ion. At higher temperatures the temperature dependence of the effective magnetic moment showed Curie-like behaviour. At very low temperatures, a dramatic decrease of the effective magnetic moment was observed, suggesting weak antiferromagnetic spin coupling. The molar magnetic susceptibility (χ_m) increased with lower temperatures and showed a maximum at 9.5 K (0.022 $cm^3\ mol^{-1}$) before decreasing very rapidly at very low temperatures.

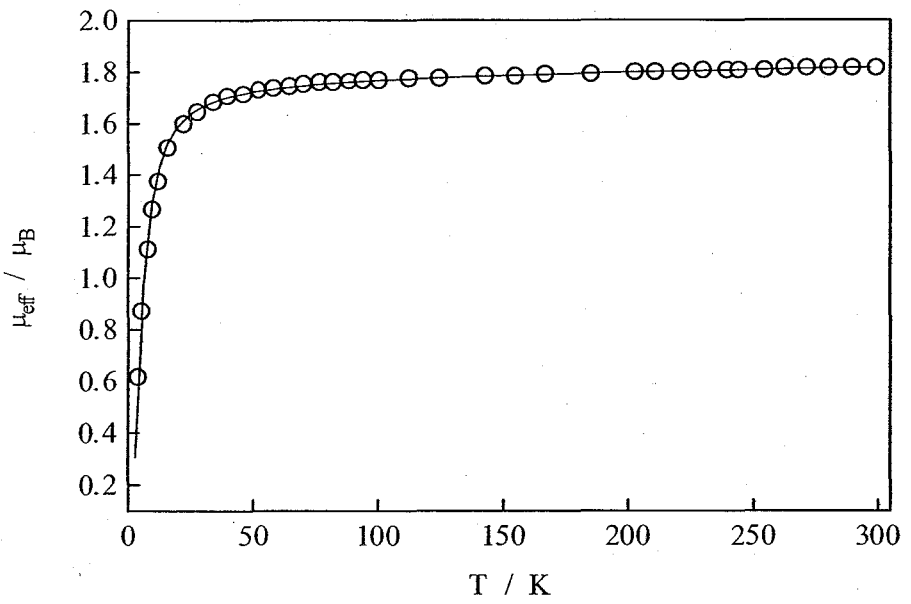

Figure 2.2.12. Thermal variation of the magnetic moment μ_{eff} (∘∘) of $[Cu^{II}_2(HL^{M1})(MeCN)_4](BF_4)_3 \cdot MeCN$ (**6b** · MeCN). The solid line represents the best fit.

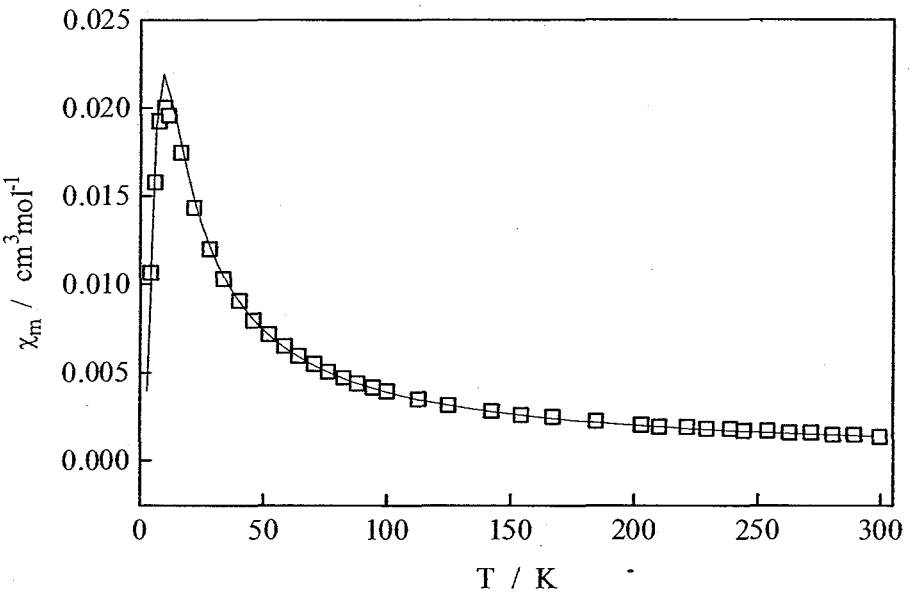

Figure 2.2.13. Thermal variation of the molar susceptibility χ_m (▫▫) of $[Cu^{II}_2(HL^{M1})(MeCN)_4](BF_4)_3 \cdot MeCN$ (**6b** · MeCN). The solid line represents the best fit.

The best fits for the dinuclear complex (**6b** · MeCN) (solid lines in Figures 2.2.12 and 2.2.13) were obtained with the parameters $g = 2.06$, $TIP = 60 \times 10^{-6}$ cm^3 mol^{-1} and $J = -5.1$ cm^{-1} representing a weak antiferromagnetic interaction, but still relatively large for pyrazine bridged copper(II) complexes.[9-11,34,132] The effective magnetic

moment per copper(II) ion at room temperature was $\mu_{eff} = 1.8\ \mu_B$, as expected for weakly coupled copper(II) d^9 ions. In the related complex $[Cu^{II}_2(HL^{M2})(Cl)_3]_\infty$, Fleischer and co-workers also found an antiferromagnetic interaction between the two metal centres, with a decreasing magnetic moment with decreasing temperatures below 12 K.[122]

2.2.2. *Copper(II) perchlorate hexahydrate*

Complexations of H_2L^{M1} and H_2L^{M2} with copper(II) salts other then copper(II) tetrafluoroborate tetrahydrate were carried out in the hope of better accessibility and/or increased crystallisation properties of the resulting compounds (Scheme 2.2.2).

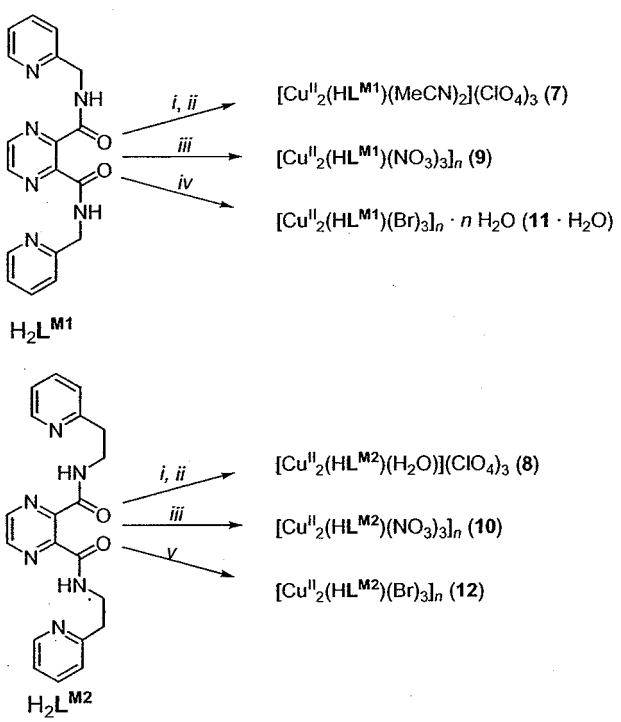

Scheme 2.2.2. Synthesis of **7**–**12**. Reagents and conditions: (*i*) $Cu(ClO_4)_2 \cdot 6\ H_2O$, MeCN, RT; (*ii*) Et_2O (vapour-diffusion); (*iii*) $Cu(NO_3)_2 \cdot 3\ H_2O$, MeCN, RT; (*iv*) $CuBr_2$, H_2O, RT (*v*) $CuBr_2$, MeCN, RT.

Complexations

The reactions of H_2L^{M1} and H_2L^{M2} with copper(II) perchlorate hexahydrate were carried out in acetonitrile solution with a 1:2 molar ratio of ligand to copper(II) salt. Subsequent vapour diffusion of diethyl ether into the reaction mixtures gave a dark navy blue compound in around 60 % and a dark sky blue compound in around 70 % yield, respectively, both in form of a feathery crystalline material. Elemental analyses suggested that the complexes could be formulated as $[Cu^{II}_2(HL^{M1})(MeCN)_2](ClO_4)_3$ (**7**) and $[Cu^{II}_2(HL^{M2})(H_2O)](ClO_4)_3$ (**8**), respectively. Both compounds proved to be readily soluble in all common polar solvents. The conductivity measurement of **8** in acetonitrile solution [Λ_m(MeCN) = 328 mol^{-1} cm^2 Ω^{-1}] was in accordance with the proposed formulation and indicated a 1:3 ratio of complex cation to perchlorate counter ion. Unfortunately the positive ion electrospray mass spectrum of **8** in acetonitrile gave only weak evidence supporting the formulation as a dinuclear species. The most intense peaks at m/z = 377.1, 189.1 and 147.1 were assigned to the charged ligand species $(H_3L^{M2})^+$, $(H_4L^{M2})^{2+}$ and the mononuclear complex fragment $[Cu^I(H_2L^{M2})]^{3+}$, respectively. The very low intensity peaks at m/z = 599.0, 538.0, 499.1, 477.1, 474.0 and 439.0 were assigned to the dinuclear complex fragments $\{[Cu^{II}_2(L^{M2})](ClO_4)\}^+$ and $[Cu^I_2(HL^{M2})(H_2O)_2]^+$ and the mononuclear complex fragments $[Cu^I(H_2L^{M2})(H_2O)(MeCN)]^+$, $[Cu^{II}(HL^{M2})(MeCN)]^+$, $[Cu^{II}(HL^{M2})(H_2O)_2]^+$ and $[Cu^I(H_2L^{M2})]^+$, respectively.

Unfortunately none of the recrystallisation attempts afforded crystals suitable for an X-ray crystal structure determination, so that the exact copper(II) coordination environments in **7** and **8** remain unknown.

IR spectroscopic studies on $[Cu^{II}_2(HL^{M1})(MeCN)_2](ClO_4)_3$ (7) and $[Cu^{II}_2(HL^{M2})(H_2O)](ClO_4)_3$ (8)

The IR spectra of $[Cu^{II}_2(HL^{M1})(MeCN)_2](ClO_4)_3$ (7) and $[Cu^{II}_2(HL^{M2})(H_2O)](ClO_4)_3$ (8) proved to be very similar to each other and to the spectrum of the corresponding tetrafluoroborate compound $[Cu^{II}_2(HL^{M1})(MeCN)_2(H_2O)_2](BF_4)_3$ (6) (Figures 5.3.1 and 5.3.2, Appendix; Table 2.2.1). Two absorption bands at $\tilde{\upsilon}$ = 1116 and 626 cm^{-1} for 7 and at $\tilde{\upsilon}$ = 1118 and 626 cm^{-1} for 8 were assigned to vibration modes of the perchlorate group, confirming the presence of perchlorate ions.[139-141] However, a change of colour from dark navy or sky blue, respectively, to grass green indicated a coligand exchange on preparation of the KBr pellets. Similar, although much broader, absorption bands were found for the perchlorate vibration modes around $\tilde{\upsilon}$ = 1000–1200 cm^{-1}, in the IR spectra of $[Cu^{II}_2(HL^{M1})(MeCN)_2](ClO_4)_3$ (7) and $[Cu^{II}_2(HL^{M2})(H_2O)](ClO_4)_3$ (8) taken from Nujol mulls. In principle, it is difficult to distinguish between coordinated and ionic perchlorate ions on the basis of IR spectroscopy alone as the only IR-active bands in the spectrum of an uncoordinated perchlorate ion are the T_2 modes found in the regions near $\tilde{\upsilon}$ = 1100 and 620 cm^{-1}. However, a splitting of the band around $\tilde{\upsilon}$ = 1100 cm^{-1} and the presence of a band near $\tilde{\upsilon}$ = 650 cm^{-1} in the spectrum, might indicate a distortion of the T_d symmetry (to C_{3v} for unidentate and C_{2v} for bidentate coordinated perchlorato groups) and suggest some kind of interaction of the perchlorate groups.[139,140,142] Unfortunately, in the spectra of 7 and 8, the region around $\tilde{\upsilon}$ = 650 cm^{-1} was obscured by absorption bands of the ligands $(HL^{M1})^-$ and $(HL^{M2})^-$, so an unambiguous conclusion as to the nature of the perchlorate ions could not be made.

UV/VIS spectroscopic studies on $[Cu^{II}_2(HL^{M2})(H_2O)](ClO_4)_3$ (8)

The UV/VIS spectrum of $[Cu^{II}_2(HL^{M2})(H_2O)](ClO_4)_3$ (**8**) in acetonitrile solution compared very well to the spectrum of the corresponding tetrafluoroborate complex $[Cu^{II}_2(HL^{M1})(MeCN)_4](BF_4)_3 \cdot MeCN$ (**6b** · MeCN) of the lower ligand homologue $(HL^{M1})^-$ and showed an asymmetrical broad weak absorption band at λ_{max} = 623 nm (ε = 190 M^{-1} cm^{-1}) and a relatively sharp intense absorption peak at λ_{max} = 259 nm (ε = 32400 M^{-1} cm^{-1}). The band of the overlapping *d-d* absorptions of **8** (λ_{max} = 623 nm, $\tilde{\upsilon}$ = 16050 cm^{-1}) occurred at nearly the same energy as that of the corresponding band of **6b** · MeCN (λ_{max} = 616 nm, $\tilde{\upsilon}$ = 16230 cm^{-1}). It was therefore suggested that in acetonitrile solution both complexes experienced the same coordination environment, leading to the formulation of $[Cu^{II}_2(HL^{M2})(MeCN)_4]^{3+}$ for the complex cation of **8** in acetonitrile solution (Figure 2.2.14).

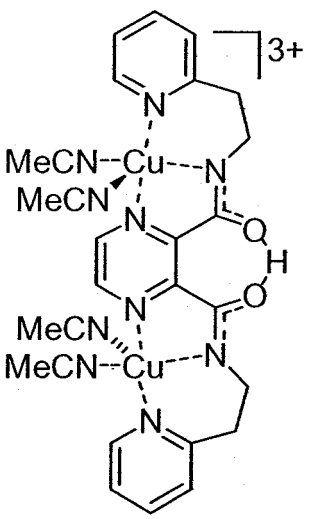

Figure 2.2.14. Assumed structure of $[Cu^{II}_2(HL^{M2})(MeCN)_4]^{3+}$, the complex cation of **8**, in acetonitrile solution.

It is noteworthy that the molar extinction coefficient ε of **8** was about half the value of the complex **6b** · MeCN of the lower ligand homologue (Figure 2.4.13).

Cyclic volatmmetric studies on $[Cu^{II}_2(HL^{M2})(H_2O)](ClO_4)_3$ (8)

The cyclic voltammogram of **8** in acetonitrile proved to be very similar to the cyclic voltammogram of $[Cu^{II}_2(HL^{M1})(MeCN)_4](BF_4)_3 \cdot MeCN$ (**6b** · MeCN) of the lower ligand homologue and showed two irreversible metal-centred reduction processes (E_{pc} = –0.26 and –0.49 V, relative to the Fc^+/Fc redox couple) and a plating process (E_{pc} = –0.99 V) with an associated stripping peak (E_{pa} = –0.61 V) (Figure 2.2.15).

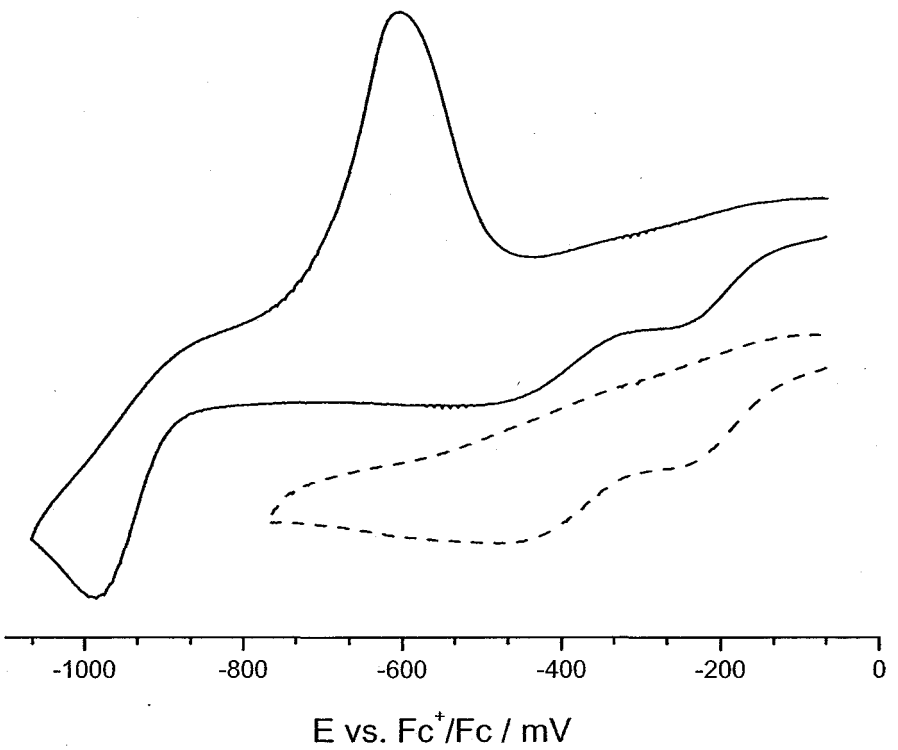

Figure 2.2.15. Cyclic voltammograms (1 mM, 0.1 M TBAP, MeCN, scan rate: 50 mV s^{-1}) of $[Cu^{II}_2(HL^{M2})(H_2O)](ClO_4)_3$ (**8**).

Compared to **6b** · MeCN, the supposed reduction of the $[Cu^{II}Cu^{II}]$ species to the mixed valent $[Cu^{II}Cu^{I}]$ species in **8** (E_{pc} = –0.26 V) occurred with a shift of $\Delta E_{(8,6b)}$ = 0.07 V to less negative potentials. The subsequent supposed reduction to the $[Cu^{I}Cu^{I}]$ species (E_{pc} = –0.49 V) occurred with a greater shift of $\Delta E_{(8,6b)}$ = 0.27 V to less negative potentials (Figure 2.2.16, Table 2.4.1). These observations were explained by the greater flexibility of the ligand H_2L^{M2} with its ethylene linkers, making the

complex more capable of modifying its coordination geometry as the copper(II) ions were reduced. Therefore the complex **8** of the higher ligand homologue was reduced more easily than the related complex **6b** · MeCN of the lower ligand homologue. This tendency was observed earlier in the dicopper(II) complexes of the related ligand pair $\mathbf{L}^{S11}$ and $\mathbf{L}^{S22}$ (Figure 2.2.8).[12,51] Compared to **6b** · MeCN, the separation of the reduction waves in **8**, stated with only $\Delta E_{pc} = 0.23$ V, a less dramatic stabilisation of the mixed valent state.

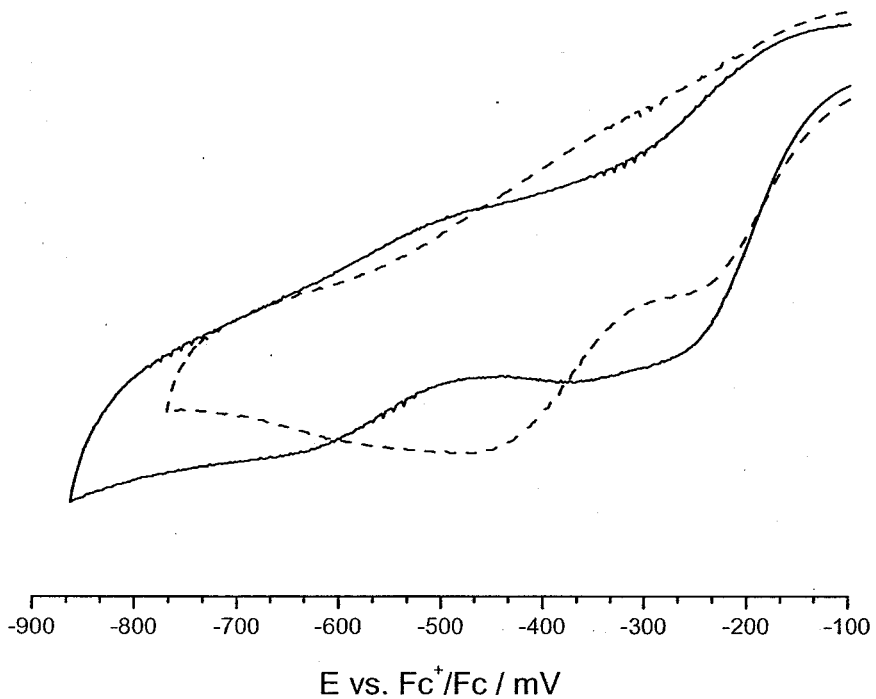

Figure 2.2.16. Comparison of the cyclic voltammograms (1 mM, 0.1 M TBAP, MeCN, scan rate 50 mV s^{-1}) of $[Cu^{II}_2(H\mathbf{L}^{M1})(MeCN)_4](BF_4)_3$ · MeCN (**6b** · MeCN) (solid line) and $[Cu^{II}_2(H\mathbf{L}^{M2})(H_2O)](ClO_4)_3$ (**8**) (dashed line).

2.2.3. *Copper(II) nitrate trihydrate*

Complexations

The metalations of H_2L^{M1} and H_2L^{M2} with a 1:2 molar ratio of ligand to copper(II) nitrate trihydrate were carried out in acetonitrile solution. In contrast to the previous metalations carried out with the corresponding tetrafluoroborate or perchlorate salts, a microcrystalline turquoise solid precipitated in both cases, after complete addition of the copper(II) nitrate salt, in around 60 % yield (Scheme 2.2.2). Results from elemental analyses were consistent with the formulation of $[Cu^{II}_2(HL^{M1})(NO_3)_3]_n$ (**9**) and $[Cu^{II}_2(HL^{M2})(NO_3)_3]_n$ (**10**). Both compounds **9** and **10** were readily soluble only in water, slightly soluble in *N,N*-dimethylformamide and insoluble or slightly soluble in alcohols, acetonitrile, acetone *etc.* The positive ion electrospray mass spectrum of $[Cu^{II}_2(HL^{M2})(NO_3)_3]_n$ (**10**) in acetonitrile was very similar to the spectrum of the corresponding perchlorate complex **8** but showed no evidence of a dinuclear species.

Unfortunately none of the recrystallisation attempts afforded single crystals, so that the exact copper(II) coordination environments in **9** and **10** remain unknown. Owing to the drastic colour differences of the nitrate compounds **9** and **10**, compared to the tetrafluoroborate complex **6** or the perchlorate complexes **7** and **8** the nitrate ions in both cases were expected to be involved in the metal coordination. Owing to the drastic solubility difference of the compounds **9** and **10** compared to **6**, **7** or **8** and because of the instant formation of microcrystalline precipitates on complexation the nitrato coordination could be expected to lead to a similar polymeric network like that found for the complex $[Cu^{II}_2(HL^{M2})(Cl)_3]_\infty$ of Fleischer and co-workers.[122]

IR spectroscopic studies on $[Cu^{II}_2(HL^{M1})(NO_3)_3]_n$ (9) and $[Cu^{II}_2(HL^{M2})(NO_3)_3]_n$ (10)

The IR spectra of the compounds **9** and **10** (Figures 5.3.3 and 5.3.4, Appendix) were relatively similar to each other and compared well to the corresponding spectra of $[Cu^{II}_2(HL^{M1})(MeCN)_2(H_2O)_2](BF_4)_3$ (**6**), $[Cu^{II}_2(HL^{M1})(MeCN)_2](ClO_4)_3$ (**7**) and $[Cu^{II}_2(HL^{M2})(H_2O)](ClO_4)_3$ (**8**) (see Table 2.2.1). In both cases, only one absorption band at $\tilde{\upsilon}$ = 1384 cm^{-1} could be clearly assigned to the vibration modes of the nitrate groups, so no information about the coordination status of the nitrate groups could be obtained from the IR spectra alone.[140,141]

UV/VIS spectroscopic studies on $[Cu^{II}_2(HL^{M1})(NO_3)_3]_n$ (9) and $[Cu^{II}_2(HL^{M2})(NO_3)_3]_n$ (10)

The UV/VIS spectrum of $[Cu^{II}_2(HL^{M1})(NO_3)_3]_n$ (**9**) in acetonitrile solution showed a shoulder at λ = 247 nm (ε = 23100 M^{-1} cm^{-1}) and an asymmetrical weak broad absorption band at λ_{max} = 649 nm (ε = 252 M^{-1} cm^{-1}) (Figure 2.2.17). The corresponding spectrum of $[Cu^{II}_2(HL^{M2})(NO_3)_3]_n$ (**10**) showed a sharp band at λ_{max} = 257 nm (ε = 28400 M^{-1} cm^{-1}) and a weak broad asymmetrical absorption band at λ_{max} = 645 nm (ε = 176 M^{-1} cm^{-1}) (Figure 5.4.1, Appendix). The absorption bands at λ_{max} = 649 nm ($\tilde{\upsilon}$ = 15410 cm^{-1}) and λ_{max} = 645 nm ($\tilde{\upsilon}$ = 15500 cm^{-1}) were assigned as absorption band of the overlapping *d-d* transitions of the copper(II) ions.

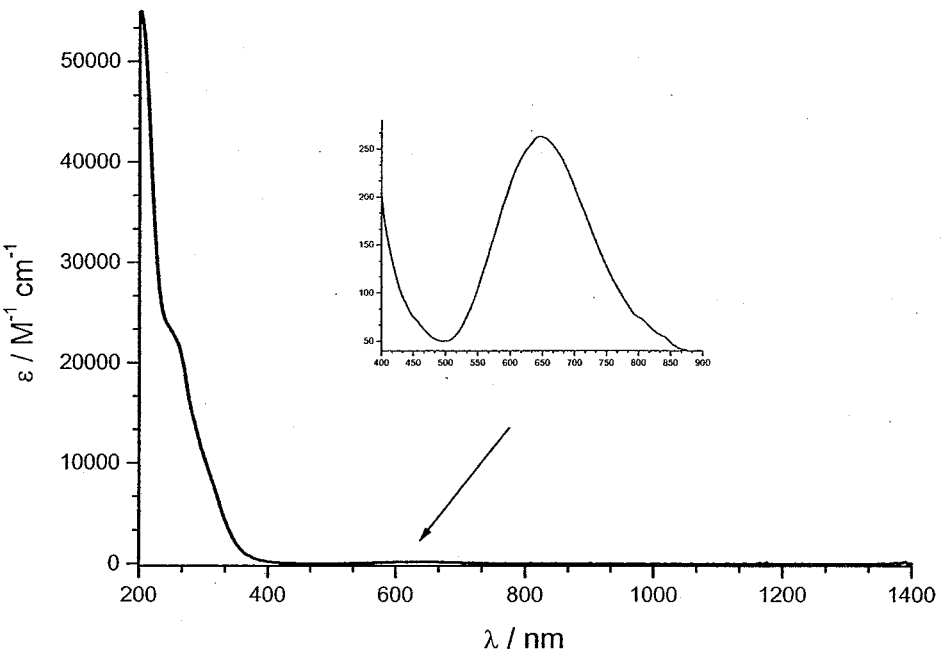

Figure 2.2.17. UV/VIS spectra [MeCN, 0.25 (inset) and 0.025 (main) mM] of $[Cu^{II}_2(HL^{M1})(NO_3)_3]$ (**9**).

Compared to the corresponding spectrum of the tetrafluoroborate complex $[Cu^{II}_2(HL^{M1})(MeCN)_4](BF_4)_3 \cdot MeCN$ (**6b** · MeCN) of the lower ligand homologue the absorption band of the nitrate complex **9** of the lower ligand homologue experienced a shift of $\Delta E_{(9,6b)} = 826$ cm^{-1} to lower energy. Comparing the respective bands of the corresponding complex pair $[Cu^{II}_2(HL^{M2})(H_2O)](ClO_4)_3$ (**8**) and **10** of the higher ligand homologue, the shift was $\Delta E_{(10,8)} = 547$ cm^{-1} to lower energy. Both results indicated a weaker ligand field for the copper(II) ions in the nitrato complexes **9** and **10**, as would be expected for a coligand exchange from acetonitrile to the weaker nitrate ion (Figure 2.2.18 and Figure 2.2.19).

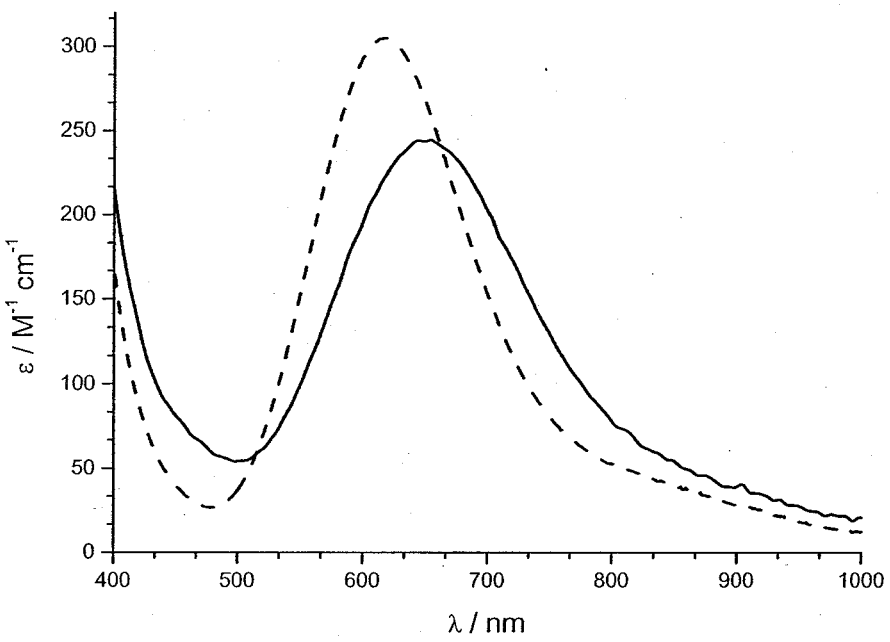

Figure 2.2.18. Comparison of the UV/VIS spectra of $[Cu^{II}_2(HL^{M1})(NO_3)_3]$ (**9**) (solid line, MeCN, 0.25 mM) and $[Cu^{II}_2(HL^{M1})(MeCN)_4](BF_4)_3 \cdot MeCN$ (**6b** · MeCN) (dashed line, MeCN, 1 mM) in the region of 400–1000 nm.

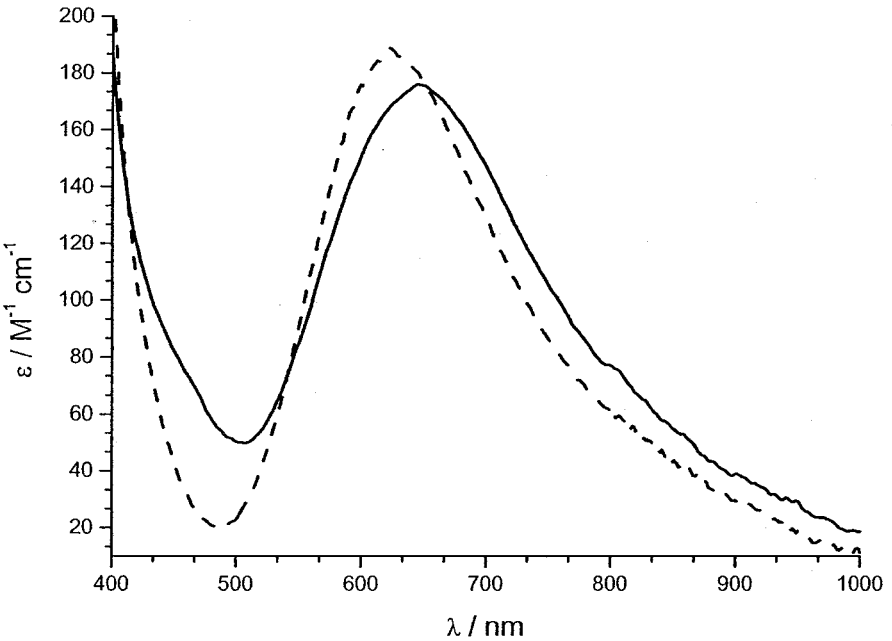

Figure 2.2.19. Comparison of the UV/VIS spectra of $[Cu^{II}_2(HL^{M2})(NO_3)_3]$ (**10**) (solid line, MeCN, 0.25 mM) and $[Cu^{II}_2(HL^{M2})(H_2O)](ClO_4)_3$ (**8**) (dashed line, MeCN, 1 mM) in the region of 400–1000 nm.

2.2.4. *Copper(II) bromide*

Complexations

The reaction of H_2L^{M2} with copper(II) bromide was carried out at room temperature in acetonitrile solution, employing a molar ratio of ligand to copper(II) salt of 1:2 (Scheme 2.2.2). Similar to the preparation of the nitrate complex $[Cu^{II}_2(HL^{M2})(NO_3)_3]$ (**10**), a grass green compound precipitated readily, after complete addition of the copper(II) salt, in around 70 % yield. The elemental analysis was in accordance with the formulation of $[Cu^{II}_2(HL^{M2})(Br)_3]_n$ (**12**).

The reaction of H_2L^{M1} under otherwise identical conditions, led to the formation of an undefined grass green precipitate. Instead, the formation of a grass green complex, which according to microanalysis was formulated as $[Cu^{II}_2(HL^{M1})(Br)_3]_n \cdot n\ H_2O$ (**11** · H_2O), was achieved by changing the reaction solvent to water, employing the same molar ratio as for **12** (Scheme 2.2.2). The solid **11** · H_2O precipitated in around 40 % yield from the bottle green reaction solution after 18 hours of stirring at room temperature.

The positive ion electrospray mass spectrum of **12** in acetonitrile showed two peaks at m/z = 1203.5 and 1060.7, which were assigned to the tetranuclear complex fragments $[Cu^{II}_4(HL^{M2})(L^{M2})(MeCN)(Br)_2]^+$ and $[Cu^{II}_4(HL^{M2})(L^{M2})(MeCN)(H_2O)]^+$, respectively, giving evidence of the polymeric nature of the compound (Figure 5.2.2, Appendix). Furthermore the peaks at m/z = 660.6, 581.7 and 452.1 were assigned to the dinuclear complex fragments $[Cu^{II}_2(HL^{M2})(Br)_2]^+$, $[Cu^{II}_2(L^{M2})(Br)]^+$ and $[Cu^{II}_2(HL^{M2})(MeCN)]^+$, respectively, demonstrating the dinuclearity of the subunit. Additionally, peaks at m/z = 519.9, 439.0 and 377.1 were assigned to the monomeric complex fragments $[Cu^{II}(HL^{M2})(MeCN)_2]^+$ and $[Cu^{II}(H_2L^{M2})]^+$ and the protonated ligand species $(H_3L^{M2})^+$, respectively.

As both complexes **11** · H_2O and **12** were readily formed on complexation and were practically insoluble in all common solvents, in both cases the bromide ions were expected to bridge the dinuclear cores leading to polymeric stair-like structure, as was found by Fleischer and co-workers for the chloride-bridged complex $[Cu^{II}_2(HL^{M2})(Cl)_3]_\infty$.[122] The complexes were therefore tentatively formulated as $\{[Cu^{II}_2(HL^{M1})(Br)_3] \cdot H_2O\}_\infty$ (**11** · H_2O) and $[Cu^{II}_2(HL^{M2})(Br)_3]_\infty$ (**12**). Figure 2.2.20 shows a fragment of the assumed polymeric stair-like structure of both compounds, for the example of the $(HL^{M1})^-$-containing complex **11** · H_2O.

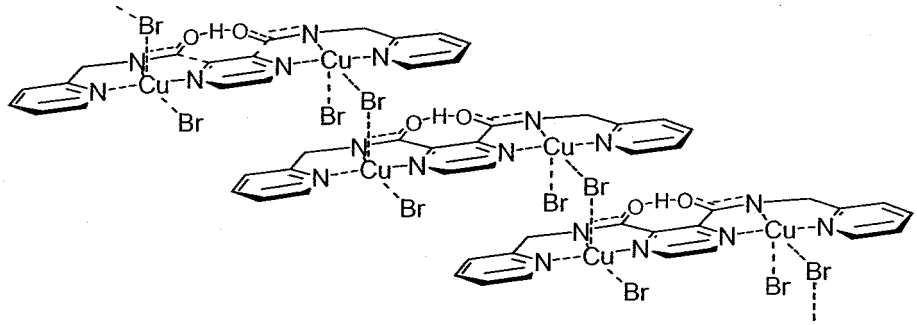

Figure 2.2.20. Fragment of the assumed polymeric stair-like structure of $\{[Cu^{II}_2(HL^{M1})(Br)_3] \cdot H_2O\}_\infty$ (**11** · H_2O).

IR spectroscopic studies on $\{[Cu^{II}_2(HL^{M1})(Br)_3] \cdot H_2O\}_\infty$ (11 · H_2O) and $[Cu^{II}_2(HL^{M2})(Br)_3]_\infty$ (12)

The IR spectra of the two bromide compounds **11** · H_2O and **12** (Figures 5.3.5 and 5.3.6, Appendix) compared well to each other and to the spectra of the corresponding tetrafluoroborate-, perchlorate- and nitrate complexes **6**, **7**, **8**, **9** and **10**. In Table 2.2.1 are summarized the ν_{CO} absorption bands of the complexes mentioned above.

Table 2.2.1. Comparison of the ν_{CO} vibration bands in the IR spectra of the dinuclear complexes **6–12**.

Complex	νCO vibration / cm^{-1}
$[Cu^{II}_2(HL^{M1})(MeCN)_2(H_2O)_2](BF_4)_3$ (**6**)	1609
$[Cu^{II}_2(HL^{M1})(MeCN)_2](ClO_4)_3$ (**7**)	1608
$[Cu^{II}_2(HL^{M1})(NO_3)_3]_n$ (**9**)	1609
$\{[Cu^{II}_2(HL^{M1})(Br)_3] \cdot H_2O\}_\infty$ (**11** · H_2O)	1608
$[Cu^{II}_2(HL^{M2})(H_2O)](ClO_4)_3$ (**8**)	1605
$[Cu^{II}_2(HL^{M2})(NO_3)_3]_n$ (**10**)	1609
$[Cu^{II}_2(HL^{M2})(Br)_3]_\infty$ (**12**)	1604

Note: Just prior to submission of this thesis the X-ray crystal structure and the magnetic properties of $[Cu^{II}_2(HL^{M1})(Cl)_3(H_2O)] \cdot H_2O$ were reported by Cati, Stoeckli-Evans and co-workers.[143]

2.2.5. *Metal(II) ions other than copper(II)*

Reactions employing metal(II) ions other than copper(II) with the homologous bis-terdentate ligands H_2L^{M1} or H_2L^{M2} in a molar ratio of 2:1, respectively, were carried out in the hope of improved crystallisation properties, and to allow comparisons of the resulting compounds. Of the divalent first row transition metals, copper(II) is suggested to have the strongest tendency to promote amide deprotonation.[121] The additional use of base was expected to facilitate amide deprotonation and therefore metal coordination of metal(II) ions other than copper(II).

Complexations with iron(II) and H_2L^{M1} or H_2L^{M2}

In acetonitrile solution, the reaction of H_2L^{M1} with iron(II) tetrafluoroborate hexahydrate employing a molar ratio of 1:2 led to the formation of a very dark deep blue-black solution from which, after several hours of stirring at room temperature, a very fine inhomogeneous dark blue-black solid of unknown composition precipitated. Addition of base did not alter the reaction outcome.

Under identical reaction conditions, without the use of base, the employment of H_2L^{M2} led to the formation of a rust brown inhomogeneous amorphous solid. A charcoal-like solid of unknown composition was formed with the addition of triethylamine under otherwise identical conditions.

Complexations with cobalt(II) and H_2L^{M1} or H_2L^{M2}

The reaction of H_2L^{M1} and cobalt(II) tetrafluoroborate hexahydrate in a molar ratio of 1:2 without the addition of base led, after several hours of stirring in acetonitrile solution, to the formation of a very small amount of a very fine dark brown precipitate of unknown composition. The vapour diffusion of diethyl ether into the strawberry red reaction filtrate resulted in an unidentified orange precipitate. Under otherwise identical reaction conditions the addition of triethylamine as base led to the quantitative precipitation of a very fine dark brown solid. The IR spectra of all compounds isolated showed intense absorption peaks at $\tilde{\upsilon} = 1734$ cm^{-1} suggesting that decomposition of the ligand had occurred. In all cases, recrystallisation attempts failed to give single crystals of a size suitable for X-ray crystal structure determination.

The employment of a molar ratio of 1:2 of the higher ligand homologue H_2L^{M2} and cobalt(II) tetrafluoroborate hexahydrate in acetonitrile solution gave a strawberry red solution, from which, after vapour diffusion of diethyl ether into the solution, an

inhomogeneous red-to-brown solid of unknown composition was isolated. The addition of triethylamine under otherwise identical reaction conditions led to the isolation of an orange-red solid of unknown composition. Elemental analysis suggested the compound to be dinuclear. The IR spectrum showed no evidence of disintegration of the ligand. Recrystallisation attempts failed to give single crystals of a size suitable for X-ray crystal structure determination.

Complexations with nickel(II) and H_2L^{M1} or H_2L^{M2}

The employment of a molar ratio of 1:2 of H_2L^{M1} and nickel(II) tetrafluoroborate hexahydrate in acetonitrile solution led, after vapour diffusion of diethyl ether into the reaction mixture, to the formation of a pale beige amorphous solid. Elemental analysis suggested a molar ratio of 1:1 of nickel(II) to ligand. The addition of triethylamine or 1,4-diaza-[2,2,2]-bicyclo octane (DABCO) as base did not have any effect on the reaction outcome. In *N,N*-dimethylformamide solution under otherwise identical reaction conditions, the beige reaction solution was darkened to dark red-brown on the addition of sodium hydroxide as base. Vapour diffusion of diethyl ether into the reaction solution led to the formation of dark red-brown crystals of a molar ratio of nickel(II) to ligand of 1:1 (see Section 2.5.2).

The employment of a molar ratio of 1:2 of the higher ligand homologue H_2L^{M2} and nickel(II) tetrafluoroborate hexahydrate in acetonitrile solution resulted in a beige solution. The addition of triethylamine as base resulted in the darkening of the solution to red-brown. By vapour diffusion of diethyl ether into the reaction solution dark red-brown crystals of a molar ratio of nickel(II) to ligand of 1:1 were obtained (see Section 2.5.2).

The employment of nickel(II) acetate tetrahydrate and H_2L^{M1} in a 2:1 molar ratio, in *N,N*-dimethylformamide solution, led with the addition of sodium hydroxide as base, and after vapour diffusion of diethyl ether into the reaction mixture to the

formation of a beige solid. The IR spectrum of the compound showed two ν_{CO} vibration bands at $\tilde{\nu}$ = 1695 and 1593 cm^{-1}. According to elemental analysis the compound was tentatively formulated as $[Ni^{II}_2(HL^{M1})(OAc)(OH)_2]$ or $[Ni^{II}_2(L^{M1})(OAc)(OH)_3]$.

2.2.6. *Summary*

The successful isolation of the complex $[Cu^{II}_2(HL^{M1})(MeCN)_4](BF_4)_3 \cdot MeCN$ (**6b** · MeCN) and its perchlorate, nitrate and bromide derivatives (**7**, **9** and **11** · H_2O), and of their $(HL^{M2})^-$-containing derivatives (**8**, **10** and **12**) demonstrated that both homologous diamide ligands H_2L^{M1} and H_2L^{M2} form dinuclear copper(II) complexes. The molecular structure of **6b** · MeCN showed that the ligand acted as a bis-terdentate chelate with two N-deprotonated amide functions. The resulting dinuclear core still retained one former N-H amide proton, presumably situated in a symmetrical O···H···O hydrogen bond between the carbonyl oxygen atoms, resulting in a seven-membered ring. Thus the dinuclear cores of **6**–**12** could be described as $[Cu^{II}_2(HL^{M1})]^{3+}$ and $[Cu^{II}_2(HL^{M2})]^{3+}$ with an overall charge of +3 (Figure 2.2.21).

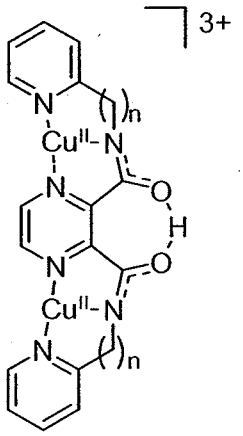

Figure 2.2.21. Schematic drawing of the dinuclear cores $[Cu^{II}_2(HL^{M1})]^{3+}$ (n = 1) and $[Cu^{II}_2(HL^{M2})]^{3+}$ (n = 2), emphasising the position of the retained former N-H amide proton and the resulting seven-membered ring.

The complexes **6b** · MeCN and **8** proved to be redox active and showed two well-separated irreversible metal-centred reduction waves, respectively. The two reduction waves of complex **8** of the more flexible higher ligand homologue H_2L^{M2} occurred closer together but both at less negative potentials, compared to **6b** · MeCN. Complex **6b** · MeCN showed weak antiferromagnetic coupling and was believed to be an example of a complex with pyrazine bridged metal centres showing spin coupling through a σ-type exchange pathway.

Attempts to employ metal salts other than copper(II) salts were unsuccessful and no discrete coordination compound could be isolated and unambiguously characterised.

2.3. *Dinuclear complexes as building blocks*

As shown in Section 2.2, the copper(II) ions of the dinuclear complex $[Cu^{II}_2(HL^{M1})(MeCN)_4](BF_4)_3$ · MeCN (**6b** · MeCN) have a distorted square pyramidal coordination environment. Two labile acetonitrile coligands occupy an equatorial and the axial coordination site of each copper(II) ion, forming an angle of around 90° to each other. By controlled coligand exchange with appropriate rigid bridging ligands the $[Cu^{II}_2(HL^{M1})]^{3+}$ core of the complex **6b** · MeCN may function as a parent compound or building block in subsequent self-assembly processes leading to polynuclear species, like those shown in the examples in Figure 2.3.1.

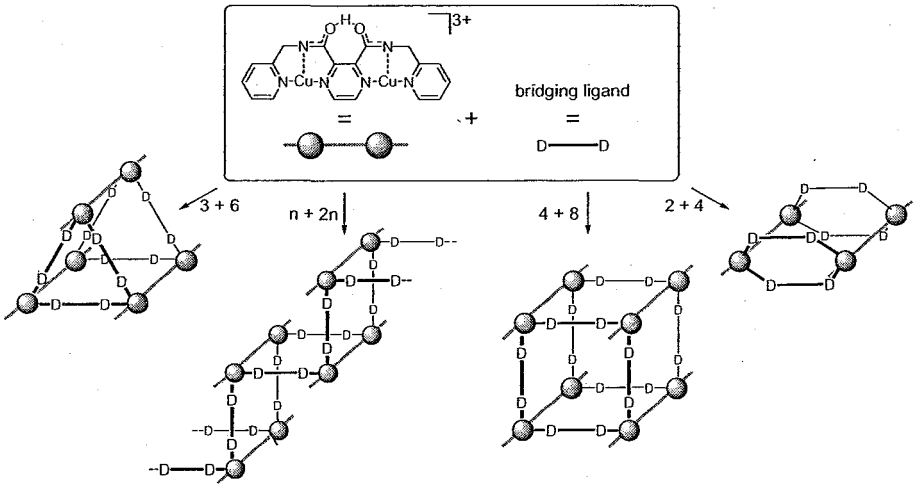

Figure 2.3.1. Formation of polynuclear species formed through bridging dinuclear building blocks with rigid coligands: (2 + 4): cyclic dimer; (3 + 6): prism; (4 + 8): cube; (*n* + 2*n*): polymeric zigzag chain.

The same ability was expected for the dinuclear $[Cu^{II}_2(HL^{M2})]^{3+}$ core of the higher ligand homologue.

2.3.1. *Neutral bridging ligands*

The treatment of a dark navy blue solution of $[Cu^{II}_2(HL^{M1})(MeCN)_2(H_2O)_2](BF_4)_3$ (**6**) in acetonitrile with the neutral linear bidentate ligands pyrazine or 4,4'-bipyridine (Figure 2.3.2) in a 1:2 molar ratio, respectively, led after several hours of stirring at room temperature to the formation of an inhomogeneous brown-green precipitate of unknown composition. In both cases, purification attempts proved to be unsuccessful.

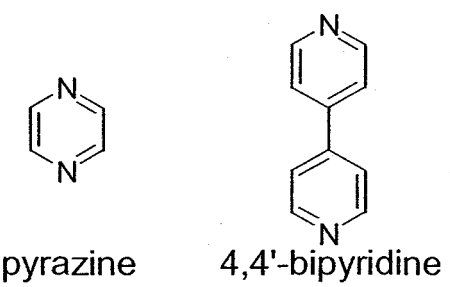

Figure 2.3.2. The neutral bidentate linear bridging ligands pyrazine and 4,4'-bipyridine.

2.3.2. *Thiocyanato ligand*

Complexations

The treatment of a dark navy blue acetonitrile solution of **6** with potassium thiocyanate in a molar ratio of 1:2 resulted, after stirring for several hours at room temperature, in a green solution from which a grass green solid precipitated. Elemental analysis revealed unexpectedly low mass percentages of carbon (around 18 %) and hydrogen (around 0.7 %), indicating the possible disintegration of the parent complex core $[Cu^{II}_2(HL^{M1})]^{3+}$. By vapour diffusion of diethyl ether into the solvate, turquoise feathery crystals could be isolated. Elemental analysis suggested a formulation of $[Cu^{II}_2(HL^{M1})(SCN)_2(solv)_x]_n(BF_4)_n$ (**13**), giving the best fit with $x = 2$, solv = H_2O.

No information about the possible polynuclear nature of compound **13** could be obtained from the positive ion electrospray mass spectrum, which gave evidence of mononuclear fragments only. Various recrystallisation attempts from acetonitrile, ethanol or mixed solvent solutions by slow evaporation, vapour diffusion of diethyl ether or by layering with toluene failed to give single crystals of acceptable size so that the structure of the compound **13** remains unknown.

The treatment of the *in situ* prepared parent complex cation $[Cu^{II}_2(HL^{M2})]^{3+}$ of the higher ligand homologue with potassium thiocyanate in a molar ratio of 1:2 led to a deep olive-green solution, from which after several hours of stirring a grass green solid precipitated in quantitative yield. The compound proved to be readily soluble in *N*,*N*-dimethylformamide only and was insoluble in other common polar solvents like water, ethanol, acetonitrile, *etc.* The elemental analysis of the compound revealed a relatively low mass percentage for carbon (around 20 %) and hydrogen (around 1 %), compared to a relatively high mass percentage of sulfur (around 9–10 %), suggesting the disintegration of the parent complex cation $[Cu^{II}_2(HL^{M2})]^{3+}$.

IR spectroscopic studies

The IR spectrum of **13** showed a single absorption band at $\tilde{\upsilon}$ = 2094 cm^{-1} for the ν_{CN} stretching vibration of the thiocyanate group (Figure 2.3.3). N-coordinated or isothiocyanato complexes usually show a band near or below $\tilde{\upsilon}$ = 2050 cm^{-1} for the ν_{CN} stretching vibration, whereas S-coordinated or thiocyanato complexes usually show this band around $\tilde{\upsilon}$ = 2100 cm^{-1} and thiocyanato ligands in the M–NCS–M bridging fashion are expected to show this band at above $\tilde{\upsilon}$ = 2100 cm^{-1}.[141,144] However, other coordination modes of the thiocyanato group are known.[145,146] In general, first row transition metals are expected to form isothiocyanato rather then thiocyanato complexes, therefore coordinating to the N donor of the thiocyanato coligand. In compound **13**, the ν_{CN} stretching vibration occurred at higher wavenumbers than expected for isothiocyanato complexes and therefore the thiocyanato coligand was expected to possibly be S-coordinated or M-SCN-M bridging. The latter could result in a di- or polymeric coordination compound. Unfortunately, the bands for the ν_{CS} stretching vibration (expected at $\tilde{\upsilon}$ = 860–780 cm^{-1} for N-coordinated and at $\tilde{\upsilon}$ = 720–690 cm^{-1} for S-coordinated thiocyanato ligands) and for the δ_{NCS} bending vibration (expected as a single sharp band at around $\tilde{\upsilon}$ = 480 cm^{-1} for N-coordinated and as several bands of low intensity at around $\tilde{\upsilon}$ = 420 cm^{-1} for S-coordinated thiocyanato ligands) of complex **13** were obscured by strong absorption bands of the parent core $[Cu^{II}_2(HL^{M1})]^{3+}$.[141,144] Therefore no further information about the coordination modes of the thiocyanato coligands could be obtained. The characteristic absorption band of the parent compound **6** (ν_{CO}: $\tilde{\upsilon}$ = 1610 cm^{-1}) and a strong absorption band belonging to the tetrafluoroborate ions could be identified in the IR spectrum of **13**.

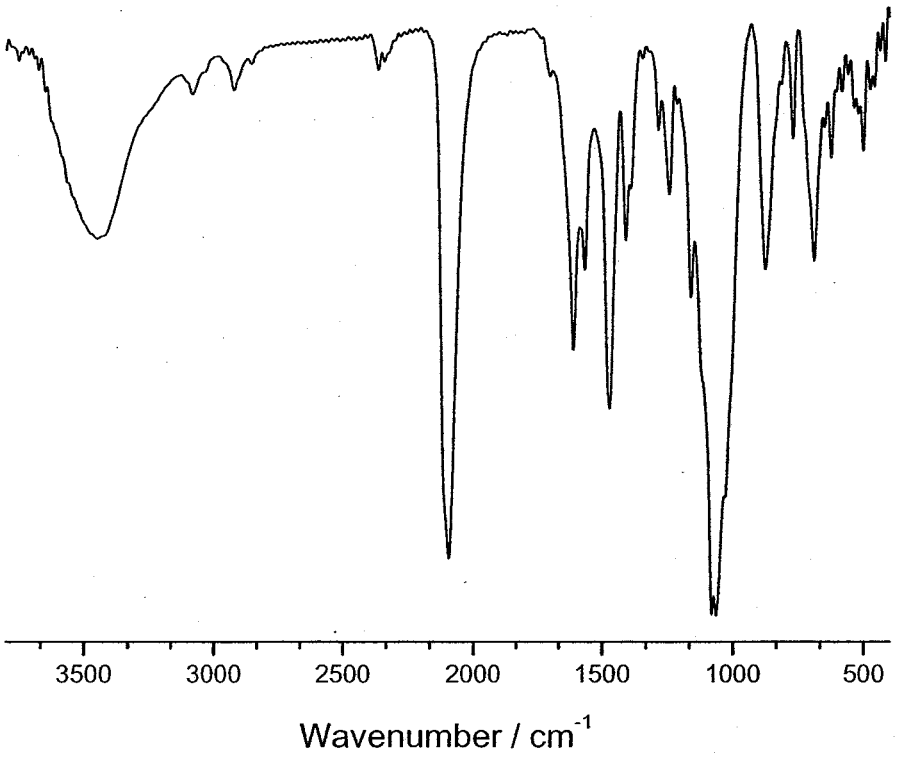

Figure 2.3.3. IR spectrum (KBr) of $[Cu^{II}_2(HL^{M1})(SCN)_2(H_2O)_2]_n(BF_4)_n$ (**13**).

The IR spectrum of the grass green compound obtained from the higher homologue parent complex cation $[Cu^{II}_2(HL^{M2})]^{3+}$, revealed one sharp intense band at $\tilde{\upsilon}$ = 2101 cm^{-1} for the ν_{CN} stretching vibration of the thiocyanato ligand. Absorption bands of the ligand $(HL^{M2})^-$ appeared with a relatively low intensity and atypical additional carbonyl absorptions were present around $\tilde{\upsilon}$ = 1700 cm^{-1}, further supporting the proposal that the parent core had decomposed. A very strong absorption multiplet at $\tilde{\upsilon}$ = 1160–1032 cm^{-1} was assigned to stretching vibrations of the tetrafluoroborate ions.

2.3.3. *Azido ligand*

The azide anion is a versatile ligand that can coordinate to metal centres in a variety of ways (Figure 2.3.4). In the terminal coordination mode a) the azido group is bound to one metal centre, usually forming an angle of 120–130° between the metal and the linear azido ligand.[147-159] However, a very unusual example of linear coordination was reported in 1996 by Mautner and Goher.[160] The azido ligand is also well known as bridging ligand, commonly bridging two metal centres in either the $\mu_{(1,1)}$- or end-on b)[147,149,151-153,155-166] or the $\mu_{(1,3)}$- or end-to-end bridge c).[148,151,153,156,159,161,163,165] Both possibilities are well represented in the literature. Examples of linear end-to-end azido coordination have been published.[167-169] Occasionally, the azido ligand may bridge three metal centres in an asymmetrical fashion as a $\mu_{3(1,1,1)}$- d) or $\mu_{3(1,1,3)}$-bridge e).[152,154,164,170-172] Furthermore two examples of a $\mu_{4(1,1,1,1)}$-bridging mode f) have been reported in 2001 by Escuer, Perlepes and co-workers.[173,174] It is not unusual for the azido ligand to occur in the same complex in various different coordination modes.

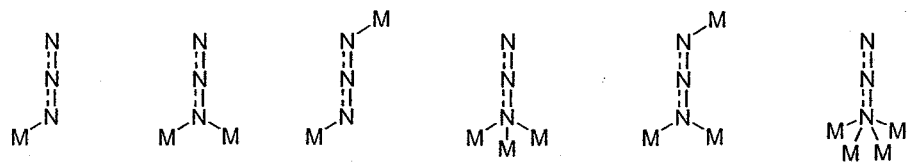

Figure 2.3.4. Coordination modes of the azido ligand.

In bis-azido bridged five coordinate complexes with Cu^{II}-N_{azide} bonds in equatorial positions, ferromagnetic interactions have been observed in double end-on bridged complexes (Figure 2.3.5, a).[161,162,175]

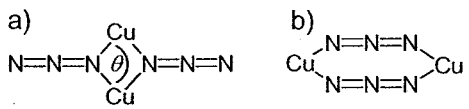

Figure 2.3.5. a) double end-on azido bridge; b) double end-to-end azido bridge.

The accidental orthogonality between the two copper(II) magnetic orbitals accounts for the ferromagnetic coupling through the end-on azido bridge. The magnetic coupling is therefore strongly dependent on the value of the angle θ at the bridging nitrogen atom of the Cu^{II}-N_{azide}-Cu^{II} unit (Figure 2.3.5). The larger this angle, the weaker the ferromagnetic coupling.[161,162] Antiferromagnetic coupling is predicted at $\theta > 108°$.[155,162] In Cu^{II}-$_{eq}N(N_2)_{ax}$-Cu^{II} type complexes, the coupling is usually very small as the magnetic orbital describing the single electron is mainly of an x^2–y^2 type, lying in the basal plane of the copper(II) atoms and therefore having only a small contribution on the axis perpendicular to the basal plane.[176] In double end-to-end bridged complexes antiferromagnetic coupling has generally been observed (Figure 2.3.5, b).[162,177-179]

Reactions with $[Cu^{II}_2(HL^{M1})(MeCN)_2(H_2O)_2](BF_4)_3$ (6)

The treatment of a dark navy blue solution of the dinuclear complex $[Cu^{II}_2(HL^{M1})(MeCN)_2(H_2O)_2](BF_4)_3$ (**6**) in acetonitrile with solid sodium azide resulted, after several hours of stirring at room temperature, in a dark bottle green solution. The employment of a molar ratio of **6** to sodium azide of 1:2 and the slow evaporation of the solvent led to the formation of a dark bottle green crystalline material in around 25 % yield (Scheme 2.3.1). Elemental analysis suggested a formulation of $[Cu^{II}_2(HL^{M1})(N_3)_2]_n(BF_4)_n$ (**14**). The compound was readily soluble in *N,N*-dimethylformamide, slightly soluble in acetonitrile but insoluble in most other common polar solvents like water or ethanol.

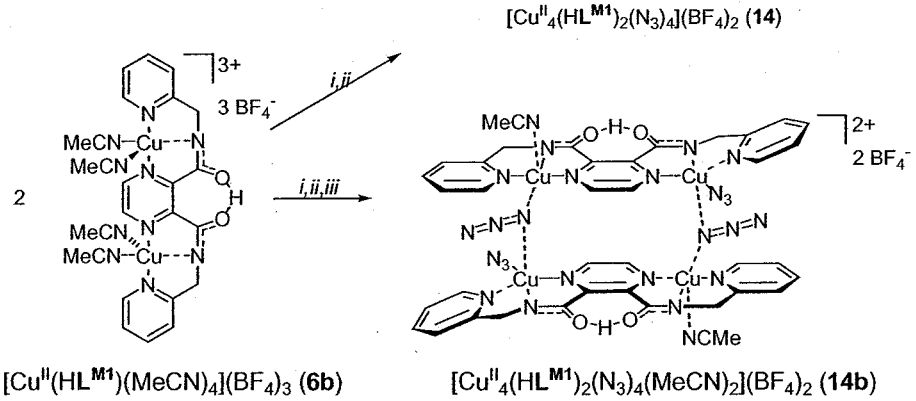

Scheme 2.3.1. Synthesis of **14**. Reagents and conditions: (*i*) 2 eq. NaN_3, MeCN, RT; (*ii*) slow evaporation; (*iii*) Et_2O (vapour diffusion).

Dark bottle green crystals of $[Cu^{II}_4(HL^{M1})_2(N_3)_4(MeCN)_2](BF_4)_2 \cdot MeCN$ (**14b** · MeCN) were obtained by vapour diffusion of diethyl ether into the bottle green filtrate (Scheme 2.3.1). The positive ion electrospray mass spectrum of **14b** · MeCN in acetonitrile showed peaks at *m/z* = 277.2 and 256.7 that were assigned to the dinuclear complex fragments $[Cu^{II}_2(L^{M1})(MeCN)_2]^{2+}$ and $[Cu^{II}_2(L^{M1})(MeCN)]^{2+}$, respectively. Furthermore peaks at *m/z* = 410.0, 226.3, 214.3 and 205.8 were assigned to the mononuclear complex fragments $[Cu^{II}(HL^{M1})]^+$, $[Cu^{II}(H_2L^{M1})(MeCN)]^{2+}$, $[Cu^{II}(H_2L^{M1})(H_2O)]^{2+}$ and $[Cu^{II}(H_2L^{M1})]^{2+}$, respectively. No assignment could be made for three peaks occurring at *m/z* = 562.7, 517.8 and 456.0.

The employment of a molar ratio of the dinuclear parent complex $[Cu^{II}_2(HL^{M1})(MeCN)_2(H_2O)_2](BF_4)_3$ (**6**) and sodium azide in a molar ratio of 1:1 and slow evaporation of the acetonitrile solvent did not lead to the formation of a solid compound. The vapour diffusion of diethyl ether into the dark bottle green reaction solution, resulted in an inhomogeneous amorphous grass green solid of unknown composition.

Increasing the molar ratio of sodium azide and parent compound $[Cu^{II}_2(HL^{M1})(MeCN)_2(H_2O)_2](BF_4)_3$ (**6**) to 3:1 or 4:1 led, after several hours of stirring at room temperature, to the formation of grass green precipitates in quantitative yields. Elemental analyses suggested that both products might have a composition of $[Cu^{II}_2(L^{M1})(N_3)_2]_n$ (**15**), employing fully deprotonated ligand $(L^{M1})^{2-}$. It was therefore

suggested that in employing excess azide ions they acted as a base ($pK_b = 9.08$)[180] and deprotonated the former amide proton of the $(HL^{M1})^-$ core rather than coordinated as an additional coligand to the copper(II) ions. Similar results were obtained from a molar ratio of sodium azide to parent compound **6** of 2:1 in the presence of triethylamine or lithium hydroxide as base. Complex **15** proved to be insoluble in all common solvents like water, ethanol, acetonitrile, acetone, *N,N*-dimethylformamide, dimethylsulfoxide, nitromethane, dichloromethane, *etc.* Unfortunately crystallisation attempts by slow evaporation of the mother liquor or by diffusion of solutions containing the reaction components respectively, failed to succeed.

IR spectroscopic studies on $[Cu^{II}_2(HL^{M1})(N_3)_2]_n(BF_4)_n$ (14) and $[Cu^{II}_2(L^{M1})(N_3)_2]_n$ (15)

Both compounds **14** and **14b** · MeCN proved to have identical IR spectra and were expected to exhibit very similar or identical molecular structures. So the following discussion will be concentrated on the IR spectrum of **14** (Figure 2.3.6). The IR spectrum of **14** showed the ν_{CO} vibration band at $\tilde{\upsilon} = 1610$ cm^{-1}, which compared well to the position of the corresponding band of the parent compound $[Cu^{II}_2(HL^{M1})(MeCN)_2(H_2O)_2](BF_4)_3$ (**6**) (see Table 2.3.1).

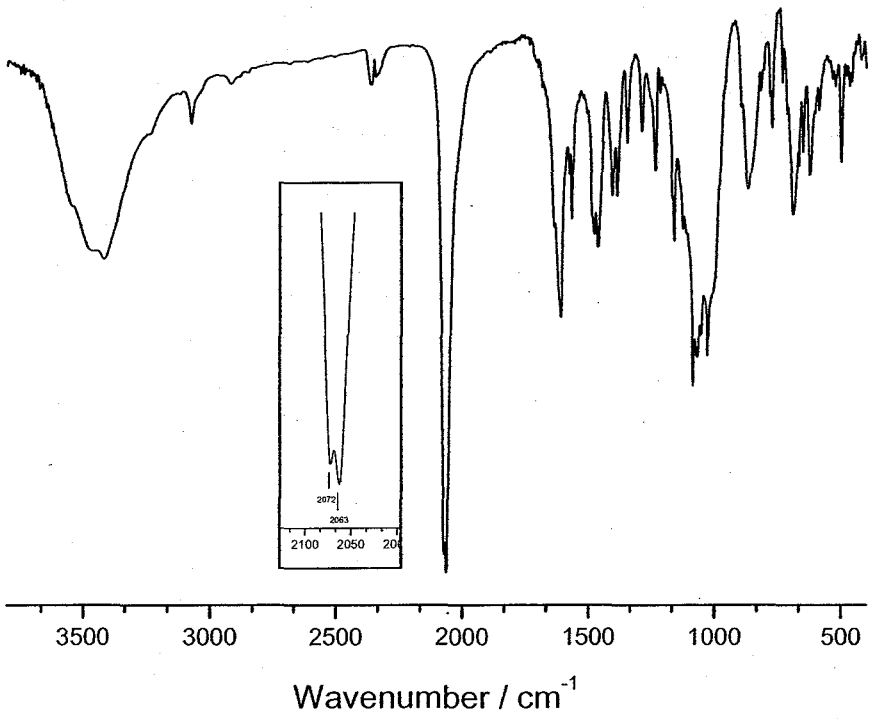

Figure 2.3.6. IR spectrum (KBr) of $[Cu^{II}_2(HL^{M1})(N_3)_2]_n(BF_4)_n$ (**14**).

The coordination mode of azido ligands is in theory identifiable from the absorption bands of the three characteristic vibrational modes ν_{as}, ν_s and δ. The antisymmetric stretching vibration (ν_{as}) is the most important one and the absorption band usually appears in the region above $\tilde{\upsilon}$ = 2000 cm^{-1}, typically between 2000 and 2100 cm^{-1},[168] as a very intense sharp peak. It has been found that the energy of ν_{as} is generally shifted to higher values by increasing the difference Δd between the two N-N-distances in the azido ion.[150] The absorption band due to the symmetric stretching vibration (ν_s) is usually of medium to weak intensity and only IR active in the case of a terminal or a $\mu_{(1,1)}$-bridging mode of the azido ligand. This absorption band usually occurs in the region at about $\tilde{\upsilon}$ = 1300 cm^{-1}. The absorption due to the bending vibration (δ) is of very weak intensity and usually occurs in the region around $\tilde{\upsilon}$ = 500–700 cm^{-1} and has less diagnostic value.[141,150,162]

In the IR spectrum of **14** two sharp very strong absorption bands at $\tilde{\upsilon}$ = 2072 and 2063 cm^{-1} were assigned to ν_{as} vibrations, suggesting the possible existence of two different azido coordination modes (Figure 2.3.6, Table 2.3.2). Unfortunately, the ν_s

and δ bands of the azido ligands could not be assigned, due to strong absorptions of the dinuclear parent core $[Cu^{II}_2(HL^{M1})]^{3+}$ in the relevant regions.

The IR spectrum of the presumably fully deprotonated compound $[Cu^{II}_2(\mathbf{L}^{M1})(N_3)_2]_n$ (**15**) showed only one ν_{as} band for the vibration of the azide group at $\tilde{\upsilon}$ = 2054 cm^{-1} and the absence of tetrafluoroborate counter ions (Figure 5.3.7, Appendix). The absorption band of the ν_{CO} vibration occurred at the unusually high wavenumber of $\tilde{\upsilon}$ = 1633 cm^{-1}.

Single crystal X-ray structural analysis of $[Cu^{II}_4(HL^{M1})_2(\mu_{(1,1)}\text{-}N_3)_2(N_3)_2(MeCN)_2](BF_4)_2 \cdot MeCN$ (14b · MeCN)

The X-ray crystal structure determination carried out on single crystals obtained by vapour diffusion of diethyl ether into the bottle green filtrate, after removal of the microcrystalline solid **14**, revealed the dimeric tetranuclear nature of the centro-symmetric compound **14b** · MeCN. The dimeric complex cation is formed by two antiparallel orientated dinuclear $[Cu^{II}_2(HL^{M1})]^{3+}$ cores, connected by two end-on azido bridges (Figure 2.3.7).

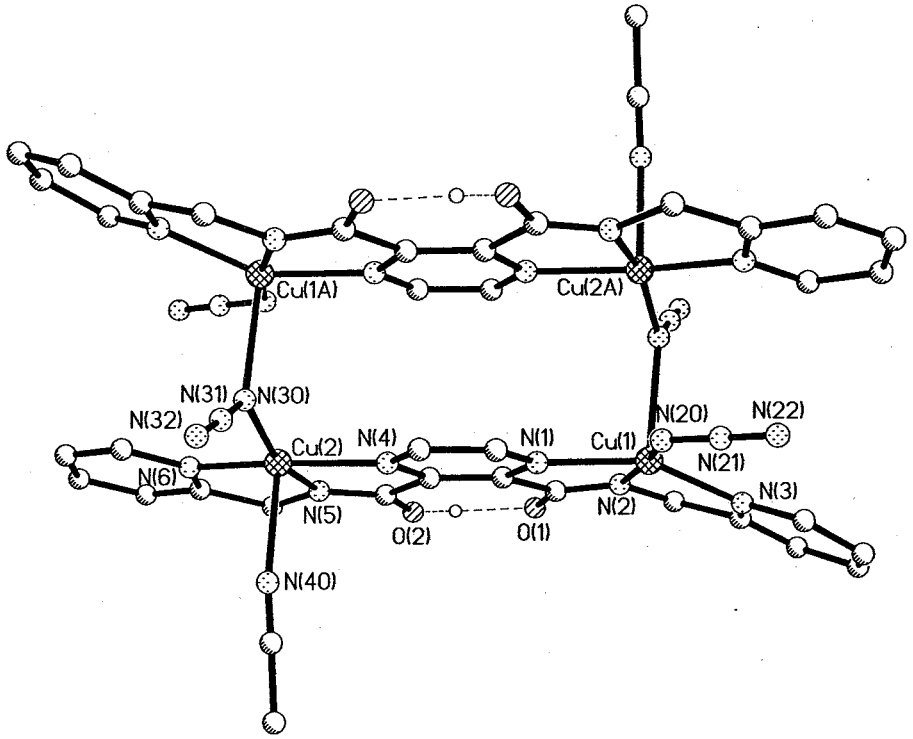

Figure 2.3.7. Molecular structure of $[Cu^{II}_4(HL^{M1})_2(\mu_{(1,1)}\text{-}N_3)_2(N_3)_2(MeCN)_2]^{2+}$, the cation of complex **14b** · MeCN. Hydrogen atoms, except H(12) and H(12A), have been omitted for clarity. Selected distances (Å) and angles (°): Cu(1)-N(1) 2.057(3), Cu(1)-N(2) 1.933(3), Cu(1)-N(3) 1.998(4), Cu(1)-N(30A) 2.321(4), Cu(1)-N(20) 1.942(3), Cu(2)-N(4) 2.053(3), Cu(2)-N(5) 1.929(3), Cu(2)-N(6) 1.991(4), CU(2)-N(30) 1.961(3), Cu(2)-N(40) 2.348(4), N(30)-N(31) 1.196(5), N(31)-N(32) 1.154(6), N(20)-N(21) 1.199(5), N(31)-N(32) 1.154(6), Cu(1)···Cu(2) 6.828(1), Cu(1)···(Cu2A) 3.579(1), Cu(1)···Cu(1A) 7.849(1), O(1)···O(2) 2.419(3); N(1)-Cu(1)-N(2) 78.8(1), N(1)-Cu(1)-N(3) 152.6(1), N(1)-Cu(1)-N(30A) 96.6(1), N(1)-Cu(1)-N(20) 90.9(1), N(2)-Cu(1)-N(3) 82.4(1), N(2)-Cu(1)-N(30A) 94.4(1), N(2)-Cu(1)-N(20) 169.3(2), N(3)-Cu(1)-N(30A) 104.6(1), N(3)-Cu(1)-N(20) 106.2(2), N(20)-Cu(1)-N(30A) 89.8(2), N(4)-Cu(2)-N(5) 79.1(1), N(4)-Cu(2)-N(6) 161.0(1), N(4)-Cu(2)-N(30) 96.5(2), N(4)-Cu(2)-N(40) 88.5(1), N(5)-Cu(2)-N(6) 82.1(2), N(5)-Cu(2)-N(30) 161.3(2), N(5)-Cu(2)-N(40) 97.3(2), N(6)-Cu(2)-N(30) 100.3(2), N(6)-Cu(2)-N(40) 96.9(2), N(30)-Cu(2)-N(40) 100.8(2), Cu(1)-N(30A)-Cu(2A) 113.1(2), Cu(1)-N(20)-N(21) 129.7(3). Symmetry operations used to generate equivalent atoms: A = -x+2,-y+2, -z+1.

The copper(II) ions of **14b** · MeCN are in distorted N_5 square pyramidal coordination spheres. As was found in the parent complex $[Cu^{II}_2(HL^{M1})(MeCN)_4](BF_4)_3$ · MeCN (**6b** · MeCN), three equatorial coordination positions of each copper(II) ion are occupied by one terdentate binding pocket of a monodeprotonated ligand $(HL^{M1})^-$. The two copper(II) ions of the subunit are bridged by the pyrazine unit and are separated by 6.828(1) Å, which is around 0.08 Å greater than in the parent compound **6b** · MeCN. The corresponding Cu^{II}-N_{ligand} distances of **14b** · MeCN and **6b** · MeCN

are similar. In **14b** · MeCN the degree of trigonality and therefore the distortion from the square pyramid is greater for Cu(1) ($\tau_{(1)}$ = 0.28) than for Cu(2) ($\tau_{(2)}$ = 0.01). The angle formed by the ring planes of the pyridine with the pyrazine is also greater for Cu(1) (23.3(2)°) than for Cu(2) (7.9(3)°). As found in **6b** · MeCN, one former amide proton per ligand of **14b** · MeCN remains in a O···H···O hydrogen bond between the amide carbonyl oxygen atoms (see Section 3.4.3). The O···O separation in the seven-membered ring (2.419(3) Å) is similar to the corresponding distance in **6b** · MeCN (2.41(1) Å). As was expected from the IR analysis, two types of azido coligands coexist in the structure of **14b** · MeCN: a terminal azido group which occupies the free equatorial coordination site of one copper(II) ion [Cu(1), in Figure 2.3.7] and an end-on $\mu_{(1,1)}$-azido group which occupies the axial position of that copper(II) ion, and at the same time bridges to the free equatorial coordination site of the other copper(II) ion [Cu(2A), in Figure 2.3.7] of the symmetry generated $[Cu^{II}_2(HL^{M1})]^{3+}$ core. The end-on coordinated azido group of compound **14b** · MeCN forms an Cu^{II}-N-N_2 angle of 129.7(3)° with Cu(1). The $\mu_{(1,1)}$-azido bridge is not symmetrical, but a shorter equatorial [Cu(2A)-N(30A): 1.961(3) Å] and a longer axial [Cu(1)-N(30A): 2.321(4) Å] Cu^{II}-N bond is observed. A relatively large Cu^{II}-N-Cu^{II} angle of 113.1(2)° is observed.[147,157,158,161,163,164] The Cu^{II}···Cu^{II} distance of the azido bridged ions is 3.579(1) Å. The remaining axial coordination site of the copper(II) ion [Cu(2), Cu(2A)] with the equatorial azido-bridge coordination is completed by an acetonitrile coligand. The complex can therefore more precisely be formulated as $[Cu^{II}_4(HL^{M1})_2(\mu_{(1,1)}\text{-}N_3)_2(N_3)_2(MeCN)_2](BF_4)_2$ (**14b**).

UV/VIS spectroscopic studies on

$[Cu^{II}_4(HL^{M1})_2(\mu_{(1,1)}\text{-}N_3)_2(N_3)_2(MeCN)_2](BF_4)_2$ · MeCN (14b · MeCN)

The UV/VIS spectrum of **14b** · MeCN in acetonitrile solution showed a very intense band at λ_{max} = 384 nm (ε = 11500 M^{-1} cm^{-1}, $\tilde{\upsilon}$ = 26040 cm^{-1}), which so far was

unique for the azido derivative of the dinuclear $[Cu^{II}_2(HL^{M1})]^{3+}$ core (Figure. 2.3.8). Furthermore a very broad less intense band was found at λ_{max} = 640 nm (ε = 1130 M^{-1} cm^{-1}, $\tilde{\upsilon}$ = 15630 cm^{-1}) that was assigned to the overlapping bands of the *d-d* transitions of the copper(II) ions. Compared to the corresponding band of the parent complex $[Cu^{II}_2(HL^{M1})(MeCN)_4](BF_4)_3 \cdot MeCN$ (**6b** · MeCN) (λ_{max} = 616 nm) a shift of ~600 cm^{-1} to lower energy occurred, indicating a weaker ligand field for the copper(II) ions which would be expected for a coligand exchange from acetonitrile to the weaker azido ligand. Accordingly it was suggested that in acetonitrile solution the azido ligands remained coordinated to the dinuclear core.

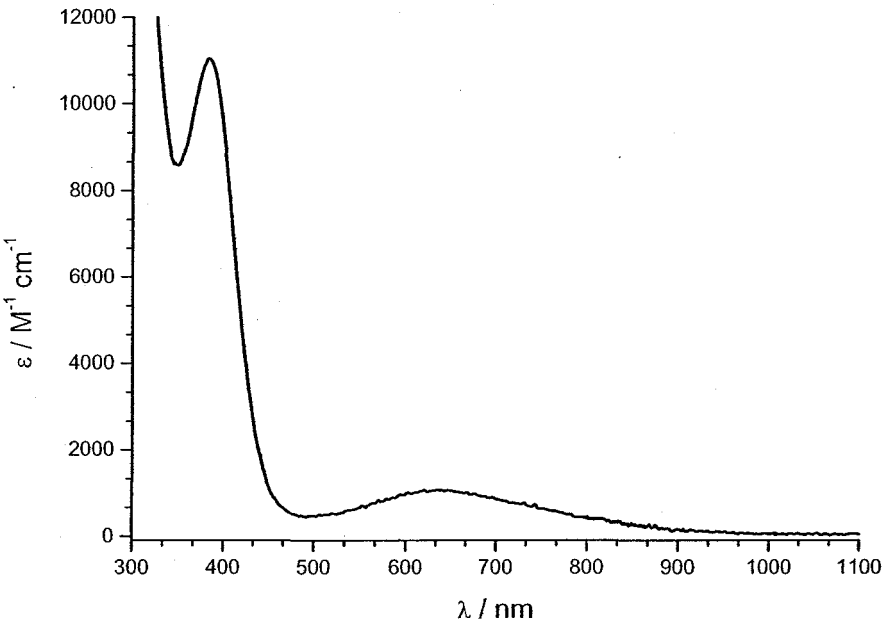

Figure 2.3.8. UV/VIS spectrum [MeCN, 0.025 mM] of $[Cu^{II}_4(HL^{M1})_2(\mu_{(1,1)}\text{-}N_3)_2(N_3)_2(MeCN)_2](BF_4)_2 \cdot MeCN$ (**14b** · MeCN).

The result of the conductivity measurement in *N,N*-dimethylformamide solution [Λ_m(DMF) = 136 mol^{-1} cm^2 Ω^{-1}], was in good agreement with this statement as it indicated that **14b** · MeCN was a 2:1 electrolyte and that azido ligands remained coordinated in *N,N*-dimethylformamide solution. Remarkably, the extinction coefficient per dinuclear core has increased by a factor of around two, comparing **14b** · MeCN with **6b** · MeCN.

Cyclic voltammetric studies on $[Cu^{II}_4(HL^{M1})_2(\mu_{(1,1)}\text{-}N_3)_2(N_3)_2(MeCN)_2](BF_4)_2 \cdot MeCN$ (14b · MeCN)

The cyclic voltammogram of $[Cu^{II}_4(HL^{M1})_2(\mu_{(1,1)}\text{-}N_3)_2(N_3)_2(MeCN)_2](BF_4)_2 \cdot MeCN$ (**14b** · MeCN) in acetonitrile solution, similarly to the cyclic voltammogram of the parent compound $[Cu^{II}_2(HL^{M1})(MeCN)_4](BF_4)_3 \cdot MeCN$ (**6b** · MeCN), showed two irreversible metal centered presumably one-electron reduction waves (Figure 2.3.9).

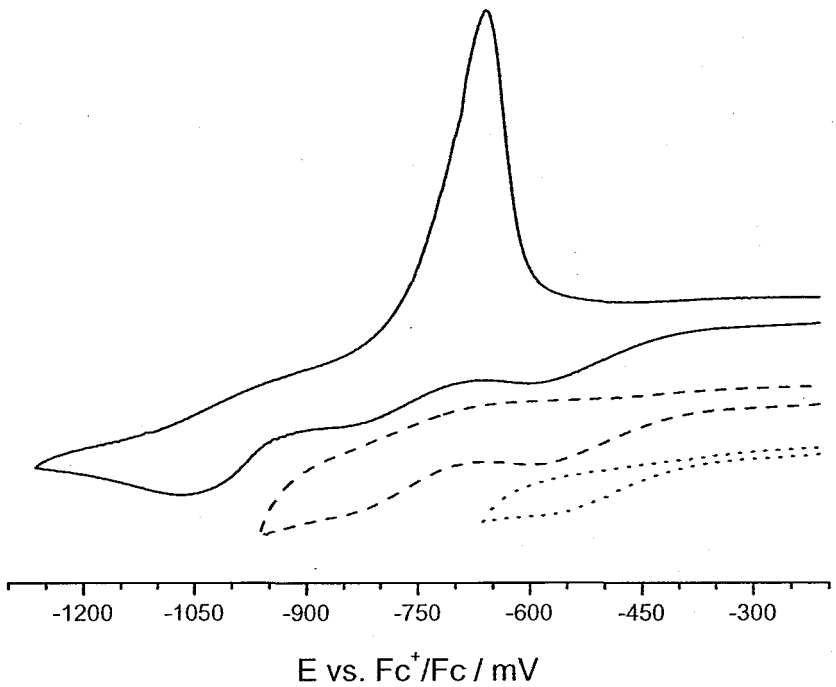

Figure 2.3.9. Cyclic voltammograms (1 mM, 0.1 M TBAP, MeCN, scan rate: 50 mV s^{-1}) of $[Cu^{II}_4(HL^{M1})_2(\mu_{(1,1)}\text{-}N_3)_2(N_3)_2(MeCN)_2](BF_4)_2 \cdot MeCN$ (**14b** · MeCN).

The reduction wave for the presumed $[Cu^{II}Cu^{II}] \rightarrow [Cu^{II}Cu^{I}]$ process of **14b** · MeCN occurred at $E_{pc} = -0.61$ V relative to the Fc^+/Fc redox couple. Compared to the parent compound **6b** · MeCN the reduction wave was significantly shifted to more negative potentials ($\Delta E_{(14b,6b)} = 0.28$ V), thus indicating that **14b** · MeCN was harder to reduce than its parent compound **6b** · MeCN (Figure 2.3.10). The subsequent reduction of the presumed $[Cu^{II}Cu^{I}] \rightarrow [Cu^{I}Cu^{I}]$ process, compared to the parent compound **6b** · MeCN, experienced only a small shift to more negative potentials ($\Delta E_{(14b,6b)} = 0.09$ V) and occurred at $E_{pc} = -0.85$ V. The separation of the two reduction

waves (ΔE_{pc} = 0.24 V) of **14b** · MeCN had therefore decreased by 0.19 V, compared to the parent compound **6b** · MeCN. At lower potentials (E_{pc} = –1.07 V) a plating process with associated stripping peak (E_{pa} = –0.66 V) was observed in the cyclic voltammogram of **14b** · MeCN.

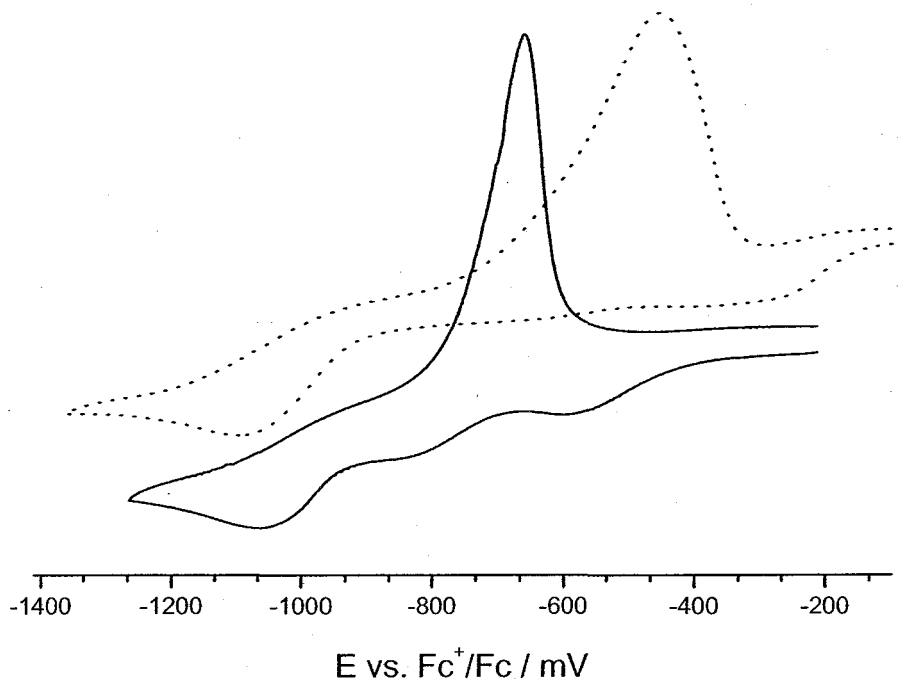

Figure 2.3.10. Comparison of the cyclic voltammograms (1 mM, 0.1 M TBAP, MeCN, scan rate: 50 mV s^{-1}) of $[Cu^{II}_4(HL^{M1})_2(\mu_{(1,1)}\text{-}N_3)_2(N_3)_2(MeCN)_2](BF_4)_2$ · MeCN (**14b** · MeCN) (solid line) and $[Cu^{II}_2(HL^{M1})(MeCN)_4](BF_4)_3$ · MeCN (**6b** · MeCN) (dotted line).

Magnetic studies on $[Cu^{II}_4(HL^{M1})_2(\mu_{(1,1)}\text{-}N_3)_2(N_3)_2(MeCN)_2](BF_4)_2$ · MeCN (**14b** · MeCN)

Figures 2.3.11 and 2.3.12 show the temperature dependence of the effective magnetic moment (μ_{eff}) and of the molar magnetic susceptibility (χ_m) of **14b** · MeCN, per copper(II) ion, respectively.

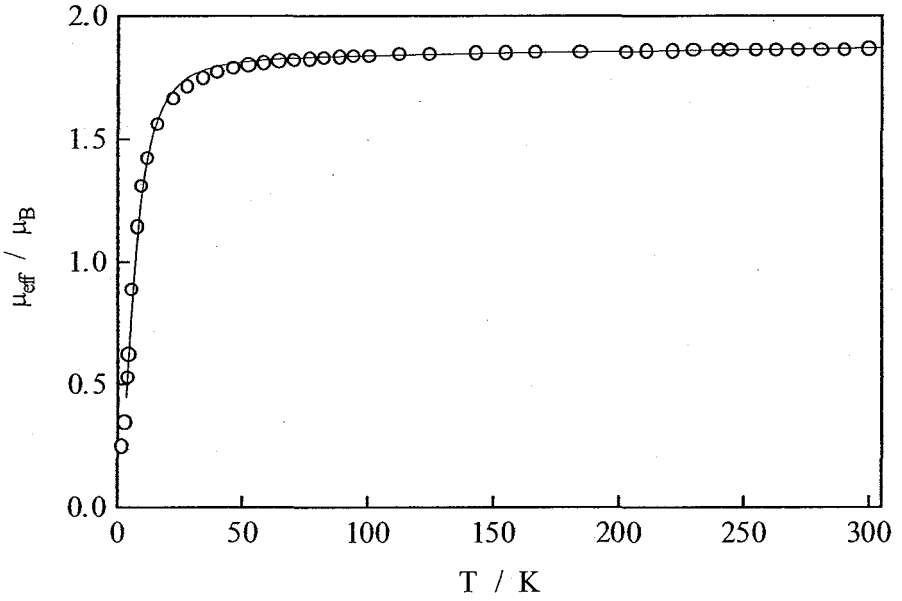

Figure 2.3.11. Thermal variation of the magnetic moment μ_{eff} (◦◦) of $[Cu^{II}_4(HL^{M1})_2(\mu_{(1,1)}\text{-}N_3)_2(N_3)_2(MeCN)_2](BF_4)_2 \cdot MeCN$ (**14b** · MeCN). The solid line represents the best fit.

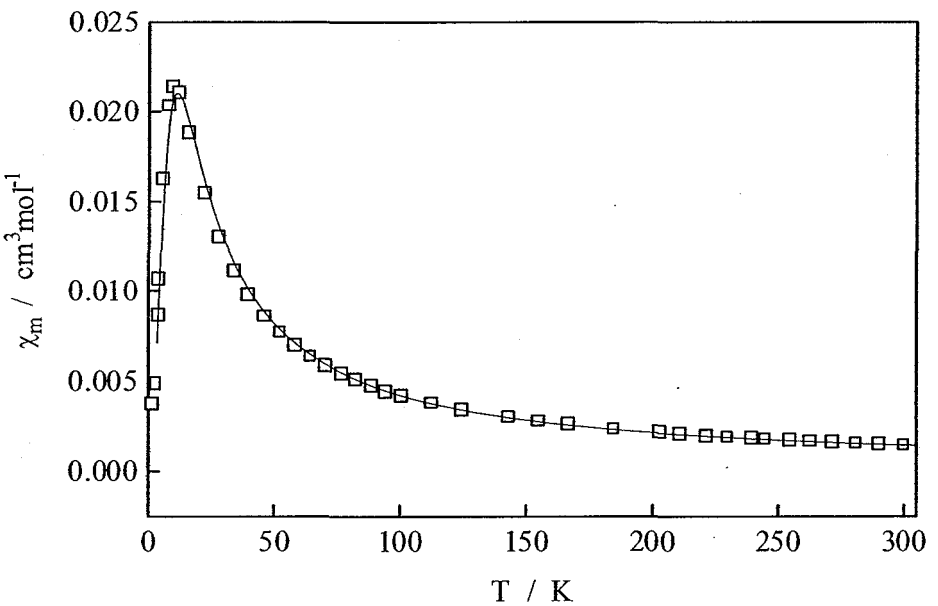

Figure 2.3.12. Thermal variation of the molar susceptibility χ_m (▫▫) of $[Cu^{II}_4(HL^{M1})_2(\mu_{(1,1)}\text{-}N_3)_2(N_3)_2(MeCN)_2](BF_4)_2 \cdot MeCN$ (**14b** · MeCN). The solid line represents the best fit.

At higher temperatures the temperature dependence of μ_{eff} showed Curie-like behaviour while at lower temperature a dramatic decrease of the effective magnetic moment was observed. The corresponding χ_m values increased with lower

temperatures and showed a maximum at around 17 K before decreasing very rapidly at lower temperatures due to antiferromagnetic coupling.

A tetranuclear model using two exchange pathways was employed (Figure 2.3.13, $J_{12} = J_{34} = 0$).[181] The best fits for **14b** · MeCN (solid lines in Figures 2.3.11 and 2.3.12) were obtained introducing two parameters: $J_{13} = J_{24} = -6.4$ cm^{-1}, assigned to an antiferromagnetic coupling through the pyrazine ring and $J_{14} = J_{23} = +7.4$ cm^{-1}, assigned to an ferromagnetic interaction, presumably through the end-on azido bridge. The following parameters $g = 2.05$ and $TIP = 60 \times 10^{-6}$ cm^3 mol^{-1} were calculated, with 1.4 % of monomeric impurities. If the J_{14} was set to zero the fit was much poorer.

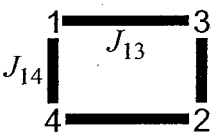

Figure 2.3.13. Tetrameric arrangement of copper(II) centres.

Reactions with $[Cu^{II}_2(HL^{M2})]^{3+}$

The employment of a molar ratio of 1:2 of the *in situ* prepared complex core $[Cu^{II}_2(HL^{M2})]^{3+}$ to sodium azide in acetonitrile solution, led to a deep bottle green solution from which, after several hours of stirring at room temperature, a deep grass green microcrystalline solid was isolated in around 10 % yield. Elemental analysis suggested that the complex could be formulated as $[Cu^{II}_2(HL^{M2})(N_3)_2]_n(BF_4)_n \cdot 2n\ H_2O$ (**16** · 2 H_2O). After the addition of ethanol to the remaining dark bottle green solution, leading to a ratio of ethanol to acetonitrile of 1:2, and by slow evaporation of the resulting solution in air, bottle green crystals were isolated in around 35 % yield (Scheme 2.3.2). Based on the results of elemental analyses the compound was formulated as $[Cu^{II}_2(HL^{M2})(N_3)_2]_n(BF_4)_n$ (**16b**). Both compounds **16** · 2 H_2O and **16b** were readily soluble only in acetonitrile and *N,N*-dimethylformamide. Unfortunately

the positive ion electrospray mass spectrum of **16b** in acetonitrile did not show any evidence of di- or higher nuclearity. The most intense peaks at m/z = 377.1, 189.1 and 147.1 were assigned to the protonated ligand species $(H_3L^{M2})^+$ and $(H_4L^{M2})^{2+}$ and to the mononuclear complex fragment $[Cu^{I}(H_4L^{M2})]^{3+}$, respectively. Conductivity measurements for both compounds [Λ_m(MeCN) = 153 mol^{-1} cm^2 Ω^{-1} for **16** · 2 H_2O and Λ_m(MeCN) = 129 mol^{-1} cm^2 Ω^{-1} for **16b** per ligand, respectively] suggested that no dissociation of the azido ligands occurred in acetonitrile solution.

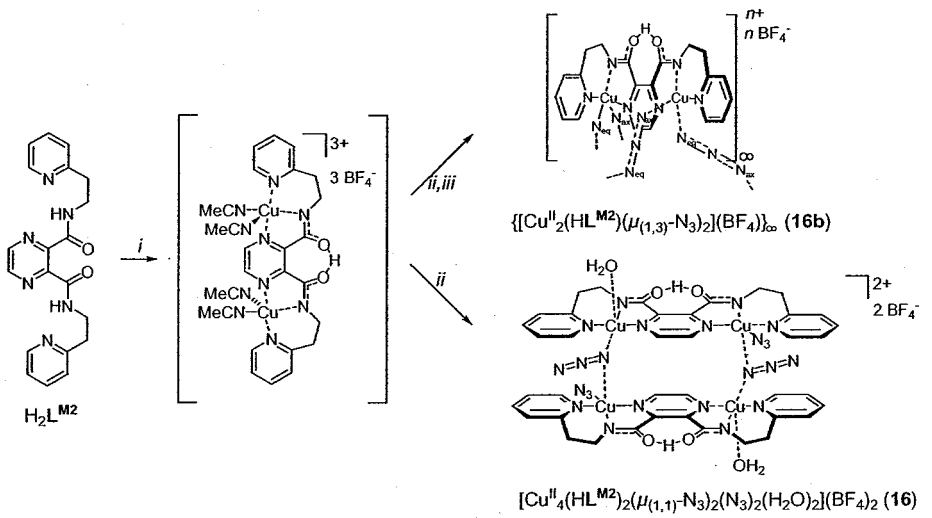

Scheme 2.3.2. Synthesis of **16** and **16b**. Reagents and conditions: (*i*) 2 eq. $Cu(BF_4)_2$ · 4 H_2O, MeCN, RT; (*ii*) 2 eq. NaN_3, MeCN, filtration; (*iii*) filtrate, EtOH, slow evaporation.

The employment of a molar ratio of the *in situ* prepared parent complex cation $[Cu^{II}_2(HL^{M2})]^{3+}$ and sodium azide in a molar ratio of 1:1 and slow evaporation of the acetonitrile solvent did not lead to the formation of a solid compound. The diethyl ether diffusion into the dark bottle green reaction solution led to the oiling out of a dark bottle green sticky syrup and no discrete compound could be isolated.

IR spectroscopic studies on $[Cu^{II}_2(HL^{M2})(N_3)_2]_n(BF_4)_n \cdot 2n\ H_2O$ (16 · 2 H_2O) and $\{[Cu^{II}_2(HL^{M2})(N_3)_2]_n(BF_4)_n$ (16b)

The IR spectra of **16** · 2 H_2O and **16b** compared well with the spectrum of the perchlorate parent complex $[Cu^{II}_2(HL^{M2})(H_2O)](ClO_4)_3$ (**8**) (Figures 2.3.14 and 2.3.15, Table 2.3.1). The ν_{CO} vibration bands were located at $\tilde{\upsilon}$ = 1606 and 1607 cm^{-1} in the IR spectra of **16** · 2 H_2O and **16b**, respectively.

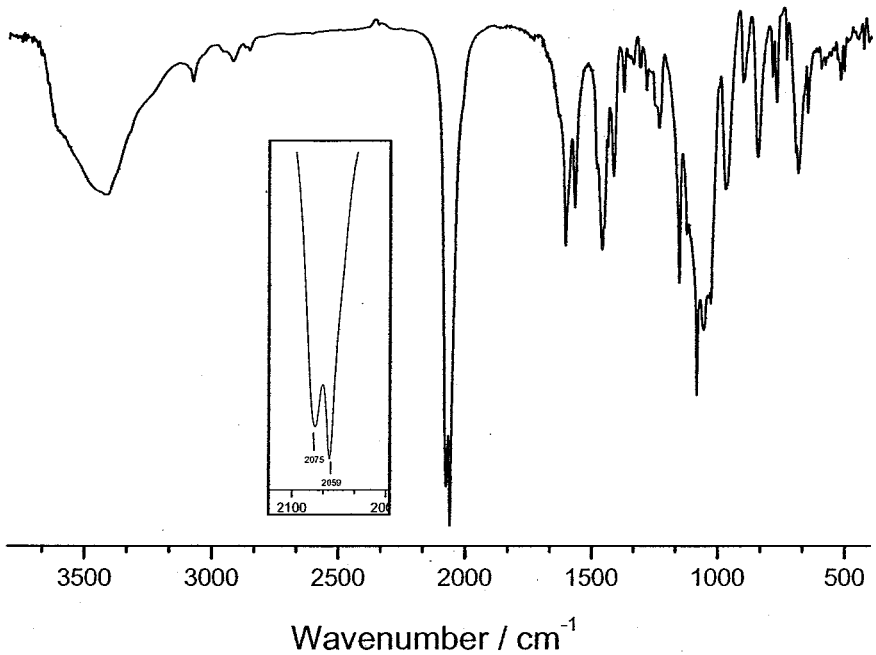

Figure 2.3.14. IR spectrum (KBr) of $[Cu^{II}_2(HL^{M2})(N_3)_2]_n(BF_4)_n \cdot 2n\ H_2O$ (**16** · 2 H_2O).

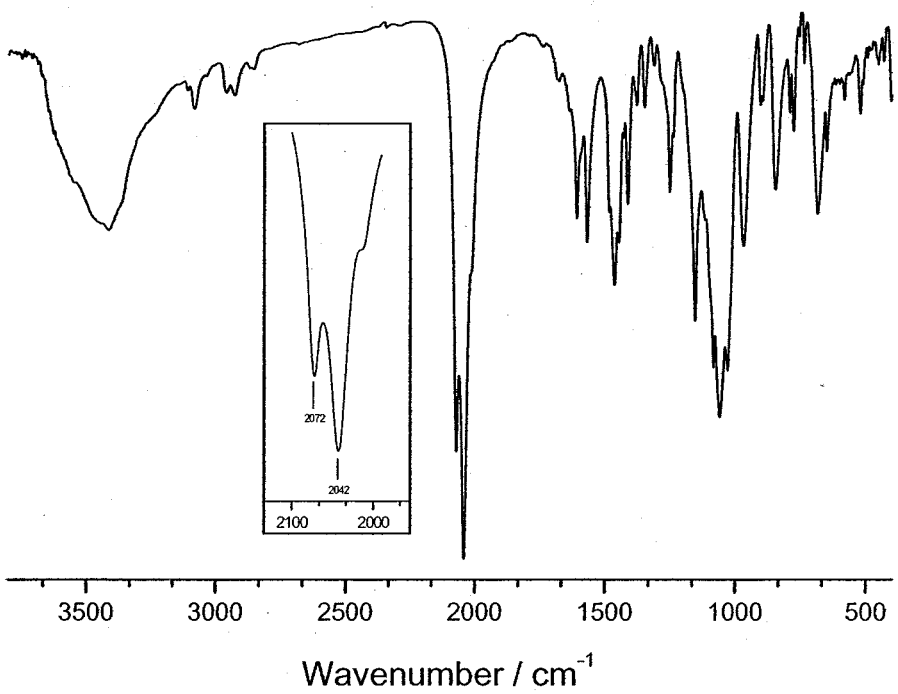

Figure 2.3.15. IR spectrum (KBr) of $[Cu^{II}_2(HL^{M2})(N_3)_2]_n(BF_4)_n$ (**16b**).

Table 2.3.1. Comparison of the ν_{CO} vibration bands in the IR spectra of the parent complexes **6** and **8** and their azido derivatives **14**, **14b**, **16** · 2 H_2O and **16b**.

Complex	ν_{CO} vibration / cm^{-1}
$[Cu^{II}_2(HL^{M1})(MeCN)_2(H_2O)_2](BF_4)_3$ (**6**)	1609
$[Cu^{II}_2(HL^{M1})(N_3)_2]_n(BF_4)_n$ (**14**)	1610
$[Cu^{II}_4(HL^{M1})_2(N_3)_4(MeCN)_2](BF_4)_2 \cdot MeCN$ (**14b** · MeCN)	1610
$[Cu^{II}_2(HL^{M2})(H_2O)](ClO_4)_3 \cdot H_2O$ (**8**)	1605
$[Cu^{II}_2(HL^{M2})(N_3)_2]_n(BF_4)_n \cdot 2n\ H_2O$ (**16** · 2 H_2O)	1606
$[Cu^{II}_2(HL^{M2})(N_3)_2]_n(BF_4)_n$ (**16b**)	1607

The IR spectrum of **16** · 2 H_2O also proved to be very similar to the IR spectrum of the azido complex $[Cu^{II}_4(HL^{M1})(\mu_{(1,1)}\text{-}N_3)_2(N_3)_2(MeCN)_2](BF_4)_2 \cdot MeCN$ (**14b** · MeCN) of the lower ligand homologue (see Table 2.3.2). Two sharp very strong absorption bands at $\tilde{\upsilon}$ = 2075 and 2059 cm^{-1} were assigned to the ν_{as} vibrations of the azido coligands. These bands appeared unchanged when the IR spectrum was taken in a Nujol mull. It was therefore suggested that both compounds **16** · 2 H_2O and **14b** · MeCN contained azido coligands in similar coordination modes. The azido ν_{as} vibrations of

compound **16b** also gave two sharp very strong absorption peaks at $\tilde{\nu}$ = 2072 and 2042 cm^{-1}, regardless of whether the IR spectrum was taken as a KBr pellet or in a Nujol mull. Compared to the IR spectra of **14b** · MeCN and **16** · 2 H_2O, the ν_{as} absorption band of **16b** at higher wavenumbers experienced no shift within experimental error (see Table 2.3.2). A shift of $\Delta\tilde{\nu}_{(16b,14b)}$ = 17 cm^{-1} compared to **14b** · MeCN, and of $\Delta\tilde{\nu}_{(16b,16)}$ = 21 cm^{-1} compared to **16** · 2 H_2O, was observed for the absorption peak occurring at lower wavenumbers ($\tilde{\nu}$ = 2042 cm^{-1}). The responsible azido coordination mode was therefore expected to possibly result in slightly more equal N-N azido distances, possibly through an end-to-end rather than an end-on or a terminal coordination mode. Caution must be exercised however, as this suggestion was based on results of an IR spectroscopic analysis of the ν_{as} vibration alone. Unfortunately in both cases **16** · 2 H_2O and **16b** the ν_s and δ bands of the azido ligands could not be identified, due to the strong absorptions of the dinuclear parent core $[Cu^{II}_2(HL^{M2})]^{3+}$ in the relevant regions.

Owing to the similarities of the IR spectra of **16** · 2 H_2O and **14b** · MeCN, a possible formulation of $[Cu^{II}_4(HL^{M2})_2(\mu_{(1,1)}\text{-}N_3)_2(N_3)_2(H_2O)_2](BF_4)_2$ · 2 H_2O was suggested for the spontaneously formed microcrystalline compound **16** · 2 H_2O, as indicated in Scheme 2.3.2.

Table 2.3.2. Comparison of the IR bands of the ν_{as} vibrations of the azido groups of the compounds **14**, **14b**, **16** · 2 H_2O and **16b** · MeCN.

Complex	ν_{as} vibration (1) / cm^{-1}	ν_{as} vibration (2) / cm^{-1}
$[Cu^{II}_2(HL^{M1})(N_3)_2]_n(BF_4)_n$ (**14**)	2072	2063
$[Cu^{II}_4(HL^{M1})_2(\mu_{(1,1)}\text{-}N_3)_2(N_3)_2(MeCN)_2](BF_4)_2$ · MeCN (**14b** · MeCN)	2072	2063
$[Cu^{II}_4(HL^{M2})_2(\mu_{(1,1)}\text{-}N_3)_2(N_3)_2(H_2O)_2](BF_4)_2$ · 2 H_2O (**16** · 2 H_2O)	2075	2059
$[Cu^{II}_2(HL^{M2})(N_3)_2]_n(BF_4)_n$ (**16b**)	2072	2042

Single crystal X-ray structural analysis of {[Cu^{II}_2(HL^{M2})($\mu_{(1,3)}$-N_3)$_2$](BF$_4$) · MeCN}$_\infty$ (16b · MeCN)

Single crystals of **16b** · MeCN were obtained by slow evaporation of the reaction filtrate containing two portions of acetonitrile to one portion of ethanol. The subsequent X-ray crystal structure determination revealed the polymeric zigzag-like chain structure of compound **16b** · MeCN, which can be formulated more precisely as {[Cu^{II}_2(HL^{M2})($\mu_{(1,3)}$-N_3)$_2$](BF$_4$) · MeCN}$_\infty$ (**16b** · MeCN) (Figure 2.3.16).

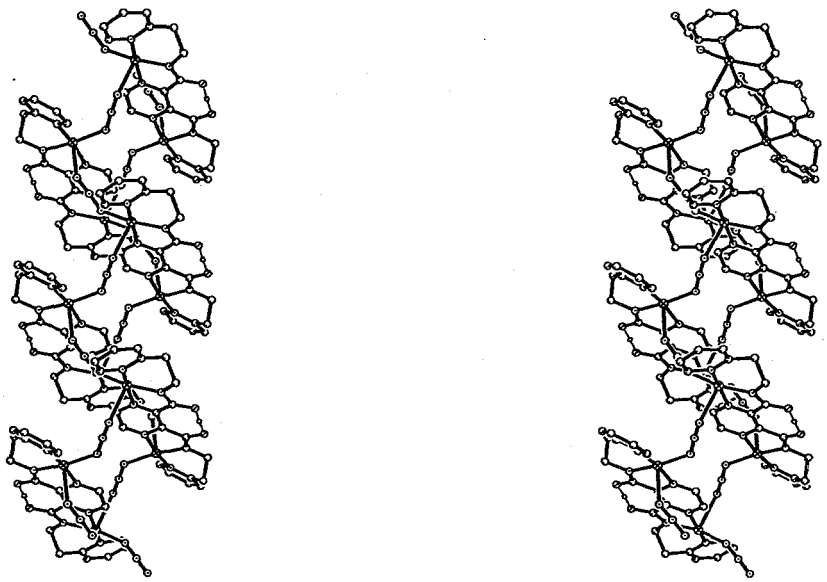

Figure 2.3.16. Stereo picture of a section of the polymeric zigzag-like chain structure of the complex cation of **16b** · MeCN. Hydrogen atoms, not involved in hydrogen bonds, have been omitted for clarity.

The structure consists of C_2-symmetrical dinuclear [Cu^{II}_2(HL^{M2})]$^{3+}$ subunits, which are bridged by end-to-end coordinated azido ligands, forming a polymeric zigzag chain. Unexpectedly, referring to the two bands of ν_{as} stretching vibrations found in the IR spectrum of the compound, only one type of azido coligand can be identified: the end-to-end or $\mu_{(1,3)}$-bridging type. As expected all nitrogen atoms of the monodeprotonated ligands (HL^{M2})$^-$ act as metal coordinating donors. As found in the dinuclear complex [Cu^{II}_2(HL^{M1})(MeCN)$_4$](BF$_4$)$_3$ · MeCN (**6b** · MeCN) and in the azido bridged tetranuclear complex [Cu^{II}_4(HL^{M1})$_2$($\mu_{1,1}$-N_3)$_2$(N_3)$_2$(MeCN)$_2$](BF$_4$)$_2$ · MeCN (**14b** · MeCN) of the lower ligand homologue, respectively, the ligand of **16b** · MeCN

retains one former N-H amide proton (on a special position) in a symmetrical O···H···O hydrogen bond between the two amide carbonyl oxygen atoms (Figure 2.3.17, see Section 3.4.4). The coordination environment around the copper(II) ion is best described as N_5 distorted square pyramidal, with three of the equatorial positions being occupied by the ligand donors of a terdentate binding pocket. The Cu^{II}-N_{ligand} bond distances thus compare well to the respective distances of the related complex **14b** · MeCN of the lower ligand homologue. The $Cu^{II}\cdots Cu^{II}$ distance within the dinuclear core is 6.763(3) Å, which compares well to the corresponding distance in **14b** · MeCN.

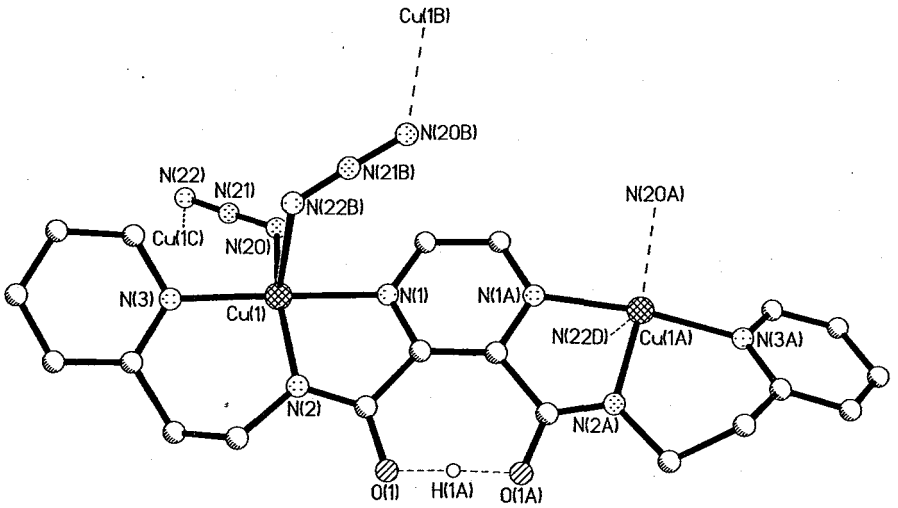

Figure 2.3.17. Molecular subunit $[Cu^{II}_2(HL^{M2})(\mu_{(1,3)}\text{-}N_3)_2]^+$ of the zigzag-like chain structure of the complex cation of **16b** · MeCN emphasising the coordination environment about Cu(1). Hydrogen atoms except H(1A) have been omitted for clarity. Selected distances (Å) and angles (°): Cu(1)-N(1) 2.030(2), Cu(1)-N(2) 1.953(2), Cu(1)-N(3) 2.002(2), Cu(1)-N(20) 1.973(2), Cu(1)-N(22B) 2.433(2), N(20)-N(21) 1.188(3), N(21)-N(22) 1.160(3), Cu(1)···Cu(1A) 6.763(3), Cu(1)···Cu(1B) 5.733(3), O(1)···O(1A) 2.390(3); N(1)-Cu(1)-N(2) 80.05(8), N(1)-Cu(1)-N(3) 171.19(8), N(1)-Cu(1)-N(20) 91.15(8), N(1)-Cu(1)-N(22B) 83.44(7), N(2)-Cu(1)-N(3) 94.29(9), N(2)-Cu(1)-N(20) 161.90(9), N(2)-Cu(1)-N(22B) 99.66(8), N(3)-Cu(1)-N(20) 96.10(9), N(3)-Cu(1)-N(22B) 90.94(8), N(20)-Cu(1)-N(22B) 95.0(1), Cu(1)-N(20)-N(21) 126.9(2), Cu(1)-N(22B)-N(21B) 123.3(2). Symmetry operations used to generate equivalent atoms: A = −x, +y, −0.5−z; B = +x, −y, z−0.5; C = +x, −y, 0.5+z.

The remaining equatorial coordination position is occupied by a $\mu_{(1,3)}$-bridging azido coligand, which at the same time occupies the axial coordination position of a

symmetry generated copper(II) ion (Figure 2.3.17). The degree of trigonality ($\tau = 0.15$) lies in between that observed for the two independent copper(II) centres of **14b** · MeCN ($\tau_{(1)} = 0.28$, $\tau_{(2)} = 0.01$). The apical and the equatorial Cu^{II}-N_{azide} bond distances are significantly different, giving a shorter Cu^{II}-N_{eq} equatorial bond length of 1.973(2) Å and a longer Cu^{II}-N_{ax} apical bond length of 2.433(2) Å. Both of these distances are slightly longer than in the related compound **14b** · MeCN of the lower ligand homologue. The angles formed by Cu^{II}-N-N_2 are 126.9(2)° and 123.2(2)°, respectively, resulting in a Cu^{II}-N···N-Cu^{II} torsion angle of 112.2°. The pyridine ring mean plane forms a relatively large angle of 29.7(1)° with the pyrazine ring mean plane.

UV/VIS spectroscopic studies on $\{[Cu^{II}_2(HL^{M2})(\mu_{(1,3)}\text{-}N_3)_2](BF_4) \cdot MeCN\}_\infty$ (16b · MeCN)

As the UV/VIS spectra of **16** · 2 H_2O and **16b** · MeCN in acetonitrile solution proved to be identical the following discussion is based on the spectrum obtained from **16b** · MeCN (Figure 2.3.18).

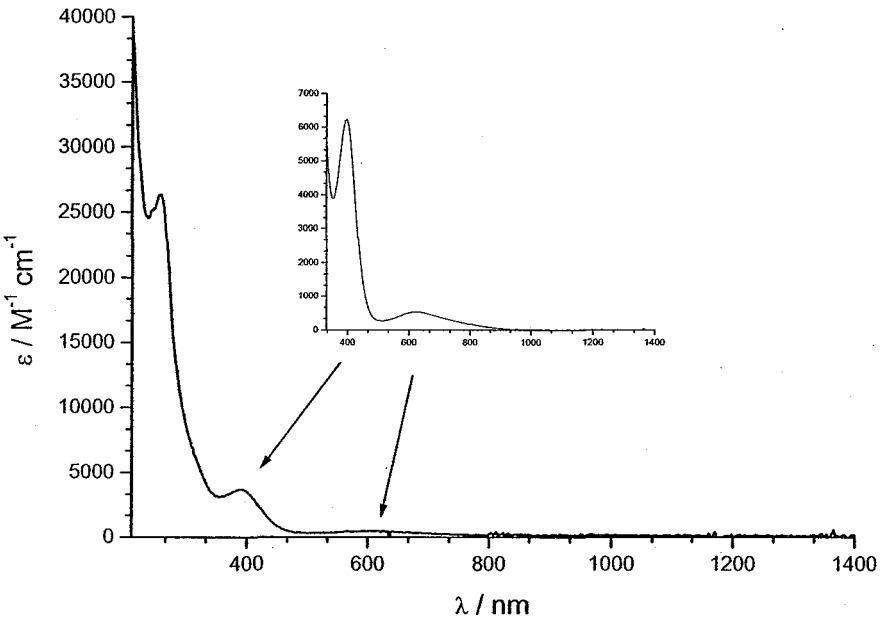

Figure 2.3.18. UV/VIS spectra [MeCN, 0.1 mM (inset) and 0.01 mM (main)] of $\{[Cu^{II}_2(HL^{M2})(\mu_{(1,3)}\text{-}N_3)_2](BF_4) \cdot MeCN\}_\infty$ (**16b** · MeCN).

Unlike the UV/VIS spectrum of the related compound $[Cu^{II}_4(HL^{M1})_2(\mu_{(1,1)}\text{-}N_3)_2(N_3)_2(MeCN)_2](BF_4)_2 \cdot MeCN$ (**14b** · MeCN) of the lower ligand homologue, the UV/VIS spectrum of **16b** · MeCN in acetonitrile solution showed a very intense absorption peak at λ_{max} = 257 nm (ε = 26000 M^{-1} cm^{-1}, $\bar{\upsilon}$ = 38910 cm^{-1}). Similar to the UV/VIS spectrum of **14b** · MeCN an intense band, which was characteristic for the azido derivatives described so far, was observed at λ_{max} = 396 nm (ε = 6260 M^{-1} cm^{-1}, $\bar{\upsilon}$ = 25250 cm^{-1}). Compared to the spectrum of **14b** · MeCN (λ_{max} = 384 nm) a shift of ~790 cm^{-1} to lower energy had occurred. Furthermore a very broad less intense band, assigned to the overlapping *d-d* transitions of the copper(II) ions, was present at λ_{max} = 625 nm (ε = 588 M^{-1} cm^{-1}, $\bar{\upsilon}$ = 16000 cm^{-1}). Compared to the corresponding band of the related complex **14b** · MeCN (λ_{max} = 640 nm) this band experienced a shift of ~370 cm^{-1} to higher energy (Figure 2.3.19). As was observed for the complex pair **14b** · MeCN and $[Cu^{II}_2(HL^{M1})(MeCN)_2(H_2O)_2](BF_4)_3$ (**6**) of the lower ligand homologue the extinction coefficient per dinuclear core of the complex **16b** · MeCN has increased by a factor of around two relative to its parent complex $[Cu^{II}_2(HL^{M2})(H_2O)](ClO_4)_3$ (**8**).

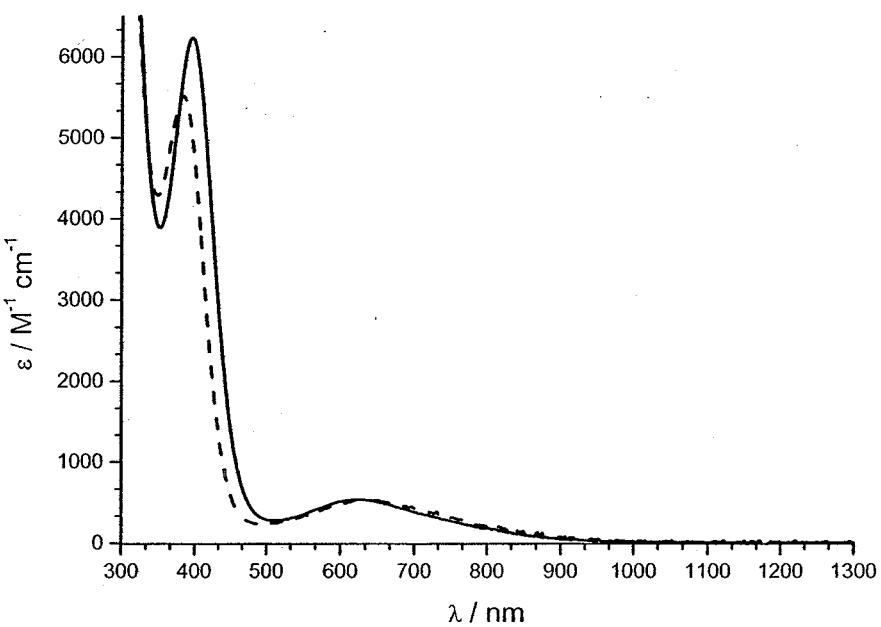

Figure 2.3.19. Comparison of the UV/VIS spectra (ε per dinuclear core) of $\{[Cu^{II}_2(HL^{M2})(\mu_{(1,3)}\text{-}N_3)_2](BF_4) \cdot MeCN\}_\infty$ (**16b** · MeCN) [MeCN, 0.01 mM, solid line] and $[Cu^{II}_4(HL^{M1})_2(\mu_{(1,1)}\text{-}N_3)_2(N_3)_2(MeCN)_2](BF_4)_2 \cdot MeCN$ (**14b** · MeCN) [MeCN, 0.025 mM, dashed line].

Cyclic voltammetric studies on $\{[Cu^{II}_2(HL^{M2})(\mu_{(1,3)}\text{-}N_3)_2](BF_4) \cdot MeCN\}_\infty$ (16b · MeCN)

As expected, the cyclic voltammogram of $\{[Cu^{II}_2(HL^{M2})(\mu_{(1,3)}\text{-}N_3)_2](BF_4) \cdot MeCN\}_\infty$ (**16b** · MeCN) in acetonitrile solution showed two irreversible metal centered one-electron reduction waves (Figure 2.3.20). At lower potentials (E_{pc} = –1.02 V) a plating process with associated stripping peak (E_{pa} = –0.55 V) was observed.

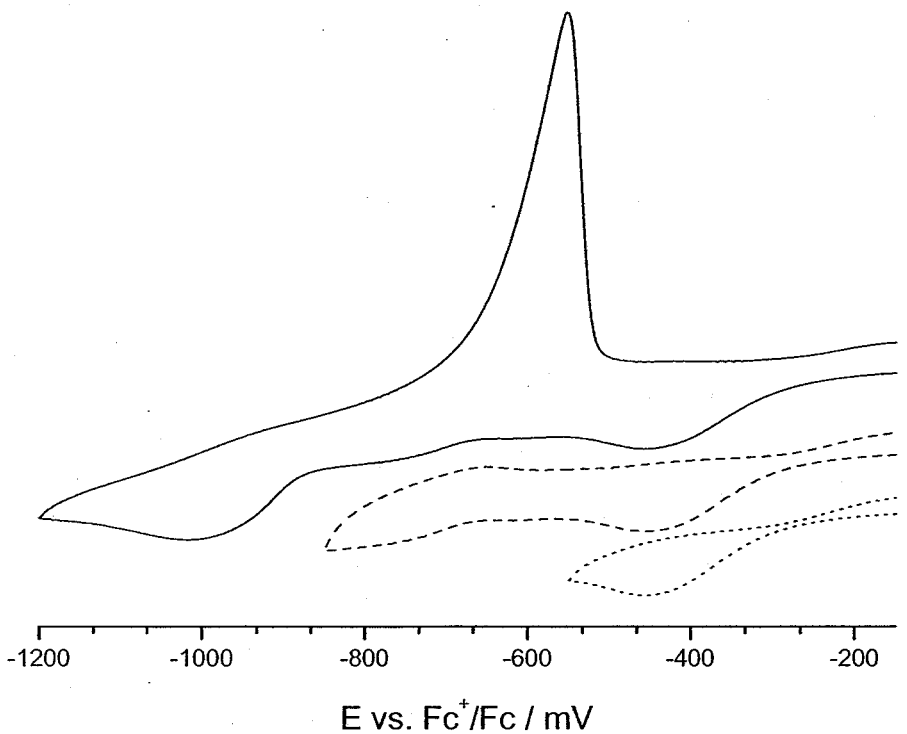

Figure 2.3.20. Cyclic voltammograms (1 mM, 0.1 M TBAP, MeCN, scan rate: 50 mV s^{-1}) of $\{[Cu^{II}_2(HL^{M2})(\mu_{(1,3)}\text{-}N_3)_2](BF_4) \cdot MeCN\}_\infty$ (**16b** · MeCN).

The first reduction wave of **16b** · MeCN, associated with the reduction $[Cu^{II}Cu^{II}] \rightarrow [Cu^{II}Cu^{I}]$, occurred at E_{pc} = –0.45 V relative to the Fc^+/Fc redox couple. Controlled potential coulometry at E = –0.50 V confirmed that the first process corresponded a one-electron reduction of the initial copper(II) complex. Compared to the cyclic voltammogram of the related perchlorate parent compound $[Cu^{II}_2(HL^{M2})(H_2O)](ClO_4)_3$ (**8**) a shift of ΔE_{pc} = 0.19 V to more negative potential was observed (Figure 2.3.21), a tendency that has been observed earlier for the related complex pair $[Cu^{II}_4(HL^{M1})(\mu_{(1,1)}\text{-}N_3)_2(N_3)_2(MeCN)_2](BF_4)_2 \cdot MeCN$ (**14b** · MeCN) and $[Cu^{II}_2(HL^{M1})(MeCN)_4](BF_4)_3 \cdot MeCN$ (**6b** · MeCN) of the lower ligand homologue.

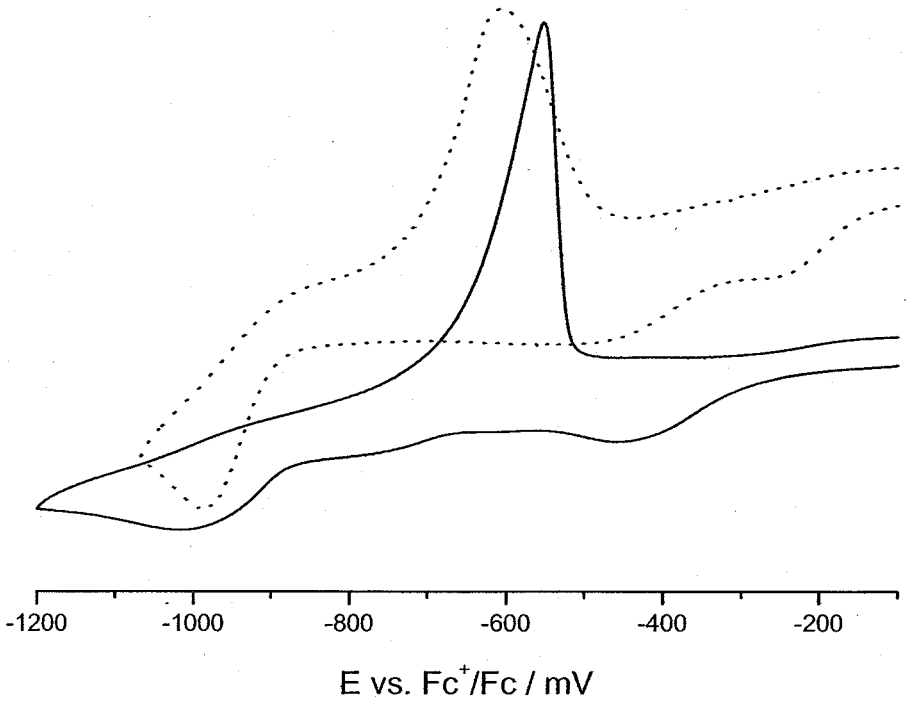

Figure 2.3.21. Comparison of the cyclic voltammograms (1 mM, 0.1 M, MeCN, scan rate: 50 mV s^{-1}) of $\{[Cu^{II}_2(HL^{M2})_2(\mu_{(1,3)}\text{-}N_3)_2](BF_4) \cdot MeCN\}_\infty$ (**16b** · MeCN) (solid line) and $[Cu^{II}_2(HL^{M2})(H_2O)](ClO_4)_3$ (**8**) (dotted line).

The second reduction wave, presumably associated with the process $[Cu^{II}Cu^{I}] \rightarrow [Cu^{I}Cu^{I}]$, occurred at E_{pc} = –0.79 V. Relative to the related perchlorate parent compound **8** the reduction wave was significantly shifted to more negative potential ($\Delta E_{pc(8,16b)}$ = 0.30 V). The resulting separation of the two reduction waves of **16b** · MeCN thus increased by 0.11 V to ΔE_{pc} = 0.34 V. This is different to the observations made for the related pair of complexes **6b** · MeCN and **14b** · MeCN of the lower ligand homologue, where the separation of the reduction waves decreased by 0.19 V.

2.3.4. *Terephthalato ligand*

The treatment of a dark navy blue solution of the parent complex $[Cu^{II}_2(HL^{M1})(MeCN)_2(H_2O)_2](BF_4)_3$ (**6**) in acetonitrile solution, containing around 1 % of water, with solid disodium terephthalate in a molar ratio of 1:1 led, after several hours of stirring at room temperature, to the formation of a dark sky blue microcrystalline solid in almost quantitative yield. The compound was insoluble in all common solvents. Elemental analysis suggested a formulation of $[Cu^{II}_2(HL^{M1})(O_4C_8H_4)]_n(BF_4)_n \cdot 4n\ H_2O$. The IR spectrum of the compound showed two sharp ν_{CO} vibration absorption bands at $\tilde{\upsilon}$ = 1683 cm^{-1} and at $\tilde{\upsilon}$ = 1636 cm^{-1}, which were assigned to the terephthalato- and ligand amide carbonyl groups, respectively (Figure 5.3.8, Appendix). A weak absorption band for stretching vibrations of the tetrafluoroborate counter ions was observed at $\tilde{\upsilon}$ = 1083 cm^{-1}. The presence of a single ν_{CO} vibration absorption band for the terephthalato coligand, suggested that the two carbonyl functions were equivalent, presumably both being coordinated. Two possible structures (n = 2 and ∞) of the compound are implied in Figure 2.3.22. The compound was tentatively formulated as $[Cu^{II}_2(HL^{M1})(O_4C_8H_4)(H_2O)_2]_n(BF_4)_n \cdot 2n\ H_2O$ (**17** · 2 H_2O). Unfortunately, crystallisation attempts by diffusion of solutions containing the two building blocks respectively, failed to succeed.

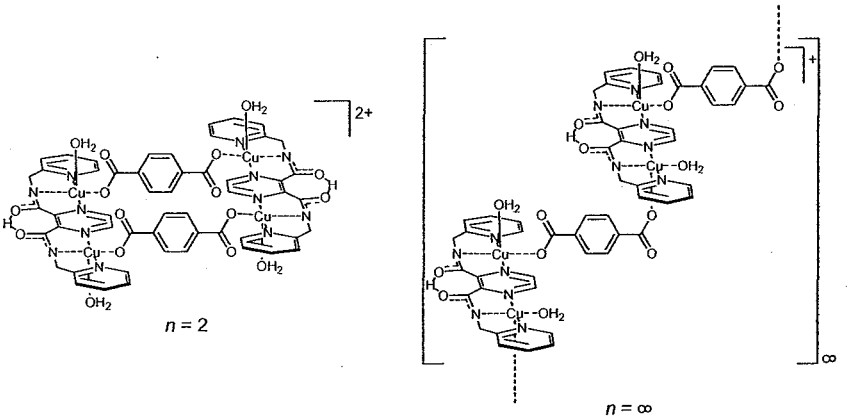

Figure 2.3.22. Possible structures of the complex cation of $[Cu^{II}_2(HL^{M1})(O_4C_8H_4)(H_2O)_2]_n(BF_4)_n \cdot 2n\ H_2O$ (**17** · 2 H_2O), n = 2: $[Cu^{II}_4(HL^{M1})_2(O_4C_8H_4)_2(H_2O)_4](BF_4)_2 \cdot 4\ H_2O$; n = ∞: $[Cu^{II}_2(HL^{M1})(O_4C_8H_4)(H_2O)_2](BF_4) \cdot 2\ H_2O]_\infty$.

The treatment of the dark navy blue solution of the *in situ* prepared parent complex core $[Cu^{II}_2(HL^{M2})]^{3+}$ of the higher ligand homologue in water with disodium terephthalate led, after several hours of stirring at room temperature, to the formation of a colourless precipitate. Elemental and IR analyses suggested the compound to be free terephthalic acid. Slow evaporation of the very intense dark blue coloured filtrate did not lead to the formation of a discrete compound.

2.3.5. *Summary*

It has been shown that the rigid dinuclear complex fragments $[Cu^{II}_2(HL^{M1})]^{3+}$ and $[Cu^{II}_2(HL^{M2})]^{3+}$, in combination with suitable bridging coligands, are capable of functioning as parent cores in self-assembly processes. The two azido bridged compounds $[Cu^{II}_4(HL^{M1})(\mu_{(1,1)}\text{-}N_3)_2(N_3)_2(MeCN)_2](BF_4)_2 \cdot MeCN$ (**14b** · MeCN), incorporating terminal and end-on coordinated azido coligands, and $\{[Cu^{II}_2(HL^{M2})(\mu_{(1,3)}\text{-}N_3)_2](BF_4) \cdot MeCN\}_\infty$ (**16b** · MeCN), incorporating end-to-end bridging azido coligands, have been structurally characterised.

2.4. *Coordination of the ligands H_2L^{M1} and H_2L^{M2}, employing a 1:1 molar ratio of ligand to metal(II) ions*

As discussed earlier, the ligands H_2L^{M1} and H_2L^{M2} each exhibit two identical terdentate binding units in a repeating linear array (Figure 2.1.1). Therefore the employment of metal(II) ions, predisposed to an octahedral coordination environment, in a molar ratio of 1:1 might be expected to lead to [2 × 2] grid-like arrangements as shown in Figure 2.4.1.

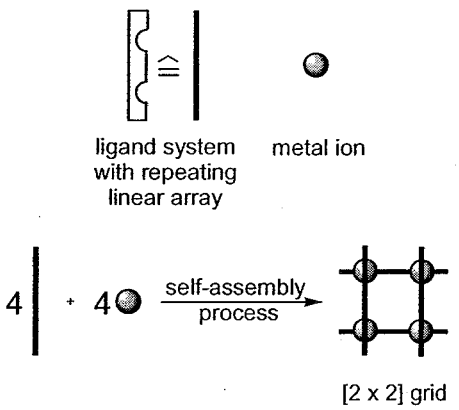

Figure 2.4.1. Formation of a [2 × 2] grid-like arrangement, employing a molar ratio of linear ligand to metal ion of 1:1.

As metalation of the diamide nitrogen donors of H_2L^{M1} and H_2L^{M2} leads to their deprotonation,[120,121] the formation of tetranuclear [2 × 2] grid-type species of metal(II) ions was initially expected to lead to neutral compounds of the deprotonated ligands $(L^{M1})^{2-}$ and $(L^{M2})^{2-}$ (Scheme 2.4.1, a), respectively.

a)
$$4\ H_2L^{M1} + 4\ M^{II} \longrightarrow [M^{II}L^{M1}]_4{}^0$$
$$4\ H_2L^{M2} + 4\ M^{II} \longrightarrow [M^{II}L^{M2}]_4{}^0$$

b)
$$4\ H_2L^{M1} + 4\ M^{II} \longrightarrow [M^{II}(HL^{M1})]_4{}^{4+}$$
$$4\ H_2L^{M2} + 4\ M^{II} \longrightarrow [M^{II}(HL^{M2})]_4{}^{4+}$$

Scheme 2.4.1. Formation of [2 × 2] grid-type complexes resulting in a) neutral or b) quadruply positively charged tetranuclear species.

In the Sections 2.2 and 2.3 it has been shown that both ligands H_2L^{M1} and H_2L^{M2} are indeed capable of coordinating metal(II) ions in both terdentate binding pockets. However, it has been found that although in doing so both amide nitrogen atoms are deprotonated, the ligands each still retain one former N-H amide proton centred in an O···H···O hydrogen bond between the two amide oxygen atoms, as shown in Figure 2.2.21. When incorporated in the [2 × 2] grid assembly this feature was expected to result in quadruply positively charged, rather than neutral, species (Figure 2.4.1, b).

2.4.1. *Copper(II) tetrafluoroborate tetrahydrate*

Complexation with H_2L^{M1}

A deep navy blue acetonitrile solution was obtained by the reaction of H_2L^{M1} and copper(II) tetrafluoroborate tetrahydrate in a molar ratio of 1:1. By vapour diffusion of diethyl ether into the reaction mixture a deep navy blue crystalline solid (**18**) could be isolated in around 70 % yield (Scheme 2.4.2). The compound was readily soluble in all common polar solvents like alcohols, acetonitrile, water, *N,N*-dimethylformamide but insoluble in *e.g.* dichloromethane.

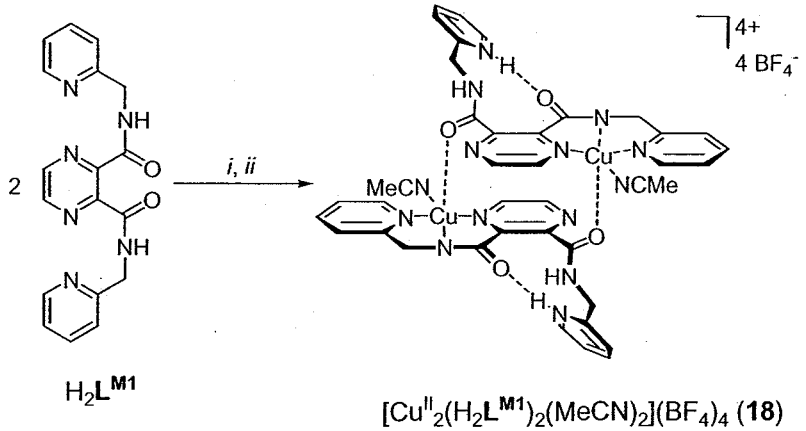

H_2L^{M1} $[Cu^{II}_2(H_2L^{M1})_2(MeCN)_2](BF_4)_4$ (**18**)

Scheme 2.4.2. Synthesis of **18**. Reagents and conditions: (*i*) 1 eq. $Cu(BF_4)_2 \cdot 4\ H_2O$, MeCN, RT; (*ii*) Et_2O (vapour diffusion).

The elemental analysis suggested a rather unexpected formulation of $[Cu^{II}(H_2L^{M1})(MeCN)]_n(BF_4)_{2n}$ (**18**), suggesting that no ligand deprotonation had occurred at all. This was not in accordance with either of the two possible expected [2 × 2] grid-type structures: neither the neutral $[Cu^{II}_4(L^{M1})_4]^0$ species nor the quadruply positively charged $[Cu^{II}_4(HL^{M1})_4]^{4+}$ species (Scheme 2.4.1). However, conductivity measurements in acetonitrile solution [Λ_m(MeCN) = 288 mol^{-1} cm^2 Ω^{-1} per ligand] were in accordance with the proposed 1:2 molar ratio of copper(II) complex to tetrafluoroborate counter ions. The positive ion electrospray mass spectrum of **18** in acetonitrile provided no evidence of polynuclear species, but peaks at *m/z* = 538.1, 410.1 and 226.1 were assigned to the mononuclear complex fragments $\{[Cu^{II}(HL^{M1})(MeCN)](BF_4)\}^+$, $[Cu^{II}(HL^{M1})]^+$ and $[Cu^{II}(H_2L^{M1})(MeCN)]^{2+}$, respectively. Further peaks at *m/z* = 349.2 and 175.1 were assigned to the protonated ligand species $(H_3L^{M1})^+$ and $(H_4L^{M1})^{2+}$.

IR spectroscopic studies on $[Cu^{II}(H_2L^{M1})(MeCN)]_n(BF_4)_{2n}$ (18)

As observed for the dinuclear complex $[Cu^{II}_2(HL^{M1})(MeCN)_2(H_2O)_2](BF_4)_3$ (**6**) the preparation of the KBr pellet for IR analysis of **18** resulted in a colour change from dark navy blue to grass green, which possibly indicated a coligand exchange with the bromide ions. The IR spectrum of **18** showed a series of broad strong absorption bands in the region $\tilde{\upsilon}$ = 3100–2700 cm^{-1}, which was so far unprecedented for complexes of either diamide ligand (Figure 2.4.2). In the region $\tilde{\upsilon}$ = 1700–1600 cm^{-1}, three very strong sharp absorption bands at $\tilde{\upsilon}$ = 1668, 1644 and 1618 cm^{-1} were identified.

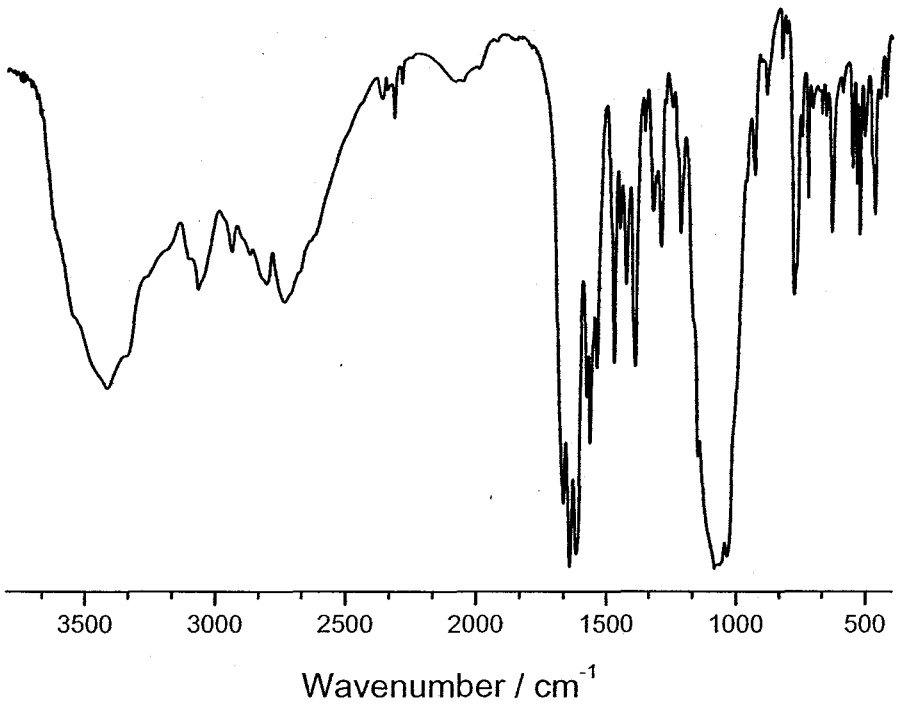

Figure 2.4.2. IR spectrum (KBr) of $[Cu^{II}(H_2\mathbf{L}^{M1})(MeCN)]_n(BF_4)_{2n}$ (**18**).

By analogy with the IR spectra of H_2L^{M1} and H_2L^{M2} the band at $\tilde{\upsilon}$ = 1668 cm^{-1} was tentatively assigned as ν_{CO} absorption band of a neutral amide group. The two bands at $\tilde{\upsilon}$ = 1644 and 1618 cm^{-1} were accordingly assigned as a split band of ν_{CO} vibrations of a metalated amide group. A strong sharp absorption peak at $\tilde{\upsilon}$ = 1539 cm^{-1} was tentatively assigned as δ_{NH} absorption band. The occurrence of a split band for the ν_{CO} vibrations of a metalated amide group, along with the occurrence of a ν_{CO} and δ_{NH} absorption band of a neutral amide group respectively, suggested that the two amide functions of the ligand were probably not equivalent, but that one of the amide nitrogen donors was still protonated and not involved in metal coordination, whereas the other amide function was possibly N-metalated and involved in metal chelation. The expected presence of tetrafluoroborate counter ions was confirmed with a broad split absorption wave at $\tilde{\upsilon}$ = 1083 cm^{-1}.

UV/VIS spectroscopic studies on $[Cu^{II}(H_2L^{M1})(MeCN)]_n(BF_4)_{2n}$ (18)

The UV/VIS spectrum of $[Cu^{II}(H_2L^{M1})(MeCN)]_n(BF_4)_{2n}$ **18** in acetonitrile solution (Figure 2.4.3) proved to be very similar to the spectrum of the related compound $[Cu^{II}_2(H_2L^{M1})(MeCN)_4](BF_4)_3 \cdot MeCN$ (**6b** · MeCN). It showed a broad weak absorption peak at λ_{max} = 600 nm (ε = 150 M^{-1} cm^{-1} per ligand; $\tilde{\upsilon}$ = 16667 cm^{-1}) which was assigned to the overlapping absorption bands of the copper(II) *d-d* transitions (Figure 2.2.7). Furthermore a relatively sharp intense absorption peak at λ_{max} = 262 nm (ε = 24800 M^{-1} cm^{-1} per ligand, $\tilde{\upsilon}$ = 38168 cm^{-1}) was observed.

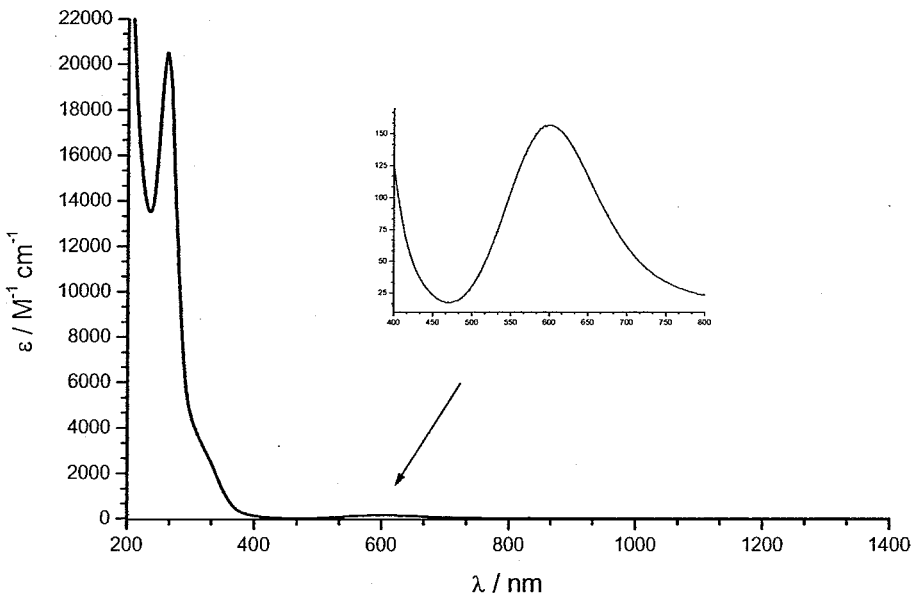

Figure 2.4.3. UV/VIS spectra [MeCN, 1 mM per ligand (inset) and 0.1 mM per ligand (main)] of $[Cu^{II}(H_2\mathbf{L^{M1}})(MeCN)]_n(BF_4)_{2n}$ (**18**).

On comparing the UV/VIS spectra of **6b** · MeCN and **18** it is noteworthy that the molar extinction coefficient per ligand of the copper(II) *d-d* transition was almost exactly halved for the 1:1 complex **18**, and that the values for λ_{max} for both compounds were very similar. It was therefore suggested that in acetonitrile solution the copper(II) ions of both complexes were in similar coordination environments. The proposed structures of compound **18** in acetonitrile solution possibly existed in equilibrium, as shown in Figure 2.4.4.

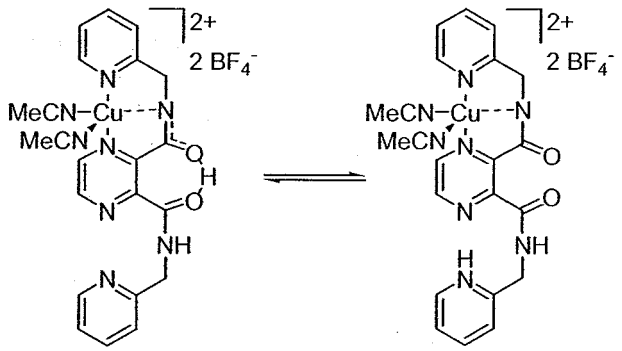

Figure 2.4.4. Proposed equilibrium structures of the mononuclear complex cation $[Cu^{II}(H_2\mathbf{L}^{M1})(MeCN)_2]^{2+}$ of **18** in acetonitrile solution.

Single crystal X-ray structural analysis of $[Cu^{II}_2(H_2L^{M1})_2(MeCN)_2](BF_4)_4$ (18)

Single crystals of **18** were obtained by the vapour diffusion of diethyl ether into an acetonitrile solution of the compound. The X-ray crystal structure determination revealed compound **18** to be a centrosymmetric dimeric ($[Cu^{II}(H_2L^{M1})(MeCN)]_n(BF_4)_{2n}$, n = 2) complex of a zwitterionic form of the ligand H_2L^{M1}. The compound can more precisely be formulated as $[Cu^{II}_2(H_2L^{M1})_2(MeCN)_2](BF_4)_4$ (**18**) (Figure 2.4.5).

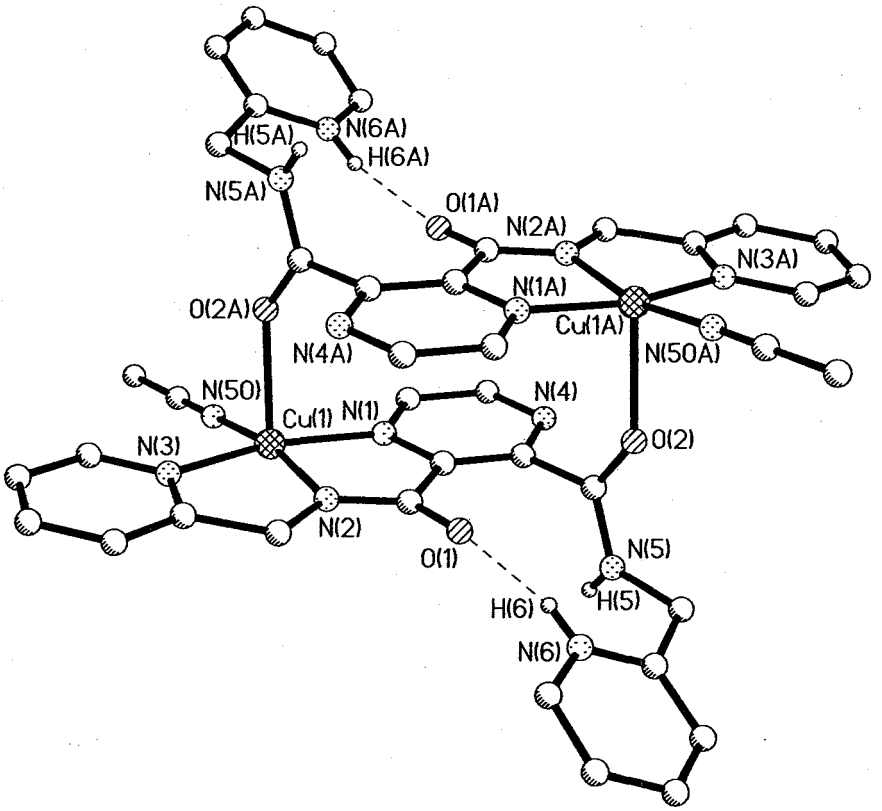

Figure 2.4.5. Molecular structure of $[Cu^{II}_2(H_2\mathbf{L}^{M1})_2(MeCN)_2]^{4+}$, the cation of complex **18**. Hydrogen atoms, except H(5), H(5A), H(6) and H(6A) have been omitted for clarity. Selected distances (Å) and angles (°): Cu(1)-N(1) 2.044(2), Cu(1)-N(2) 1.913(2), Cu(1)-N(3) 2.017(2), Cu(1)-N(50) 1.979(2), Cu(1)-O(2A) 2.270(1), N(6)···O(1) 2.657(3), Cu(1)···Cu(1A) 6.547(3); N(1)-Cu(1)-N(2) 81.08(6), N(1)-Cu(1)-N(3) 162.85(6), N(1)-Cu(1)-N(50) 98.90(7), N(1)-Cu(1)-O(2A) 92.22(6), N(2)-Cu(1)-N(3) 81.82(7), N(2)-Cu(1)-N(50) 165.93(7), N(2)-Cu(1)-O(2A) 106.16(6), N(3)-Cu(1)-N(50) 97.39(7), N(3)-Cu(1)-O(2A) 93.70(6), N(50)-Cu(1)-O(2A) 87.91(6). Symmetry operations used to generate equivalent atoms: A = -x+2, -y+2, -z+1.

The coordination environment around the copper(II) ion in the mononuclear $[Cu^{II}(H_2\mathbf{L}^{M1})(MeCN)]^{2+}$ core is best described as a distorted square pyramid with N_4O coordination. The distortion of the square pyramid is very small as given by the degree of trigonality $\tau = 0.05$,[127] which compares well to the small distortion of the square pyramids around the copper(II) ions of the dinuclear complex **6b** · MeCN ($\tau_{(1)} = 0.04$; $\tau_{(2)} = 0.09$). The ligand in **18** acts as hybrid terdentate-monodentate N_3-O chelate. The N_3-terdentate ligand half occupies three equatorial coordination sites, the fourth being occupied by an acetonitrile coligand. The symmetry generated O-monodentate ligand part occupies the axial coordination position, thereby forming the dimeric cation. The N_3-terdentate half of the ligand is extremely flat, with the

greatest deviation from the mean plane defined by the coordinated pyridine ring, the pyrazine ring, the carbonyl group and the methylene linker being only 0.037 Å for N(2). In contrast the O-monodentate ligand half is very twisted and the O-coordinated amide group is almost perpendicular (91.5°) to the mean plane of the terdentate ligand half. As has been found in related copper(II) complexes of HL^{N1},[123] HL^{N2},[124] HL^{N11}[125] or HL^{N12} (Figure 2.2.4),[126] the Cu^{II}-N_{amide} bond distance of **18** (1.913(2) Å) is significantly shorter than the Cu^{II}-N_{pz} bond length (2.044(2) Å) or the Cu^{II}-N_{py} bond length (2.017(2) Å). The copper(II) ion is pulled out of the N_4 mean plane by 0.150 Å in direction of the axial coordination site.[182] The Cu-O-C angle is 137.2(1)°. The amide group of the N_3-terdentate ligand half is deprotonated but the ligand retains the former N-H amide proton on the uncoordinated pyridine nitrogen atom of the O-monodentate ligand half. The shifting of an amide proton on complexation to a "free" pyridine moiety of the ligand is a feature that has been observed earlier *e.g.* by Kinoshita and co-workers in a copper(II) complex of the related ligand *N,N'*-bis[*S*-1-(2-pyridyl)-ethyl]pyridine-2,6-dicarboxamide.[183] In complex **18** the shifted proton is involved in an N-H···O hydrogen bond, from the pyridinium of the O-monodentate ligand half to the amide carbonyl oxygen atom of the deprotonated amide group of the N_3-terdentate ligand half of the same ligand. The protonated pyridine ring forms an angle of 30.1(1)° with the plane of the pyrazine ring. The other, O-coordinated amide function is still N-protonated and its proton is involved in an N-H···F hydrogen bond to a tetrafluoroborate counter ion. Only one of the pyrazine nitrogen donors is coordinated, so the pyrazine ring does not function as a Cu^{II}···Cu^{II} bridging moiety. The copper(II) ions of the dimeric unit are separated by 6.547(3) Å.

Cyclic voltammetric studies on $[Cu^{II}_2(H_2L^{M1})_2(MeCN)_2](BF_4)_4$ (18)

The cyclic voltammogram of **18** in acetonitrile solution showed only one metal-centred irreversible one-electron reduction wave at $E_{pc} = -0.51$ V, relative to the Fc^+/Fc redox couple (Figure 2.4.6). Controlled potential coulometry at $E = -0.50$ V confirmed that the first process corresponded a $[Cu^{II}] \rightarrow [Cu^{I}]$ one-electron reduction of the initial monomeric copper(II) complex (Figure 2.4.4).

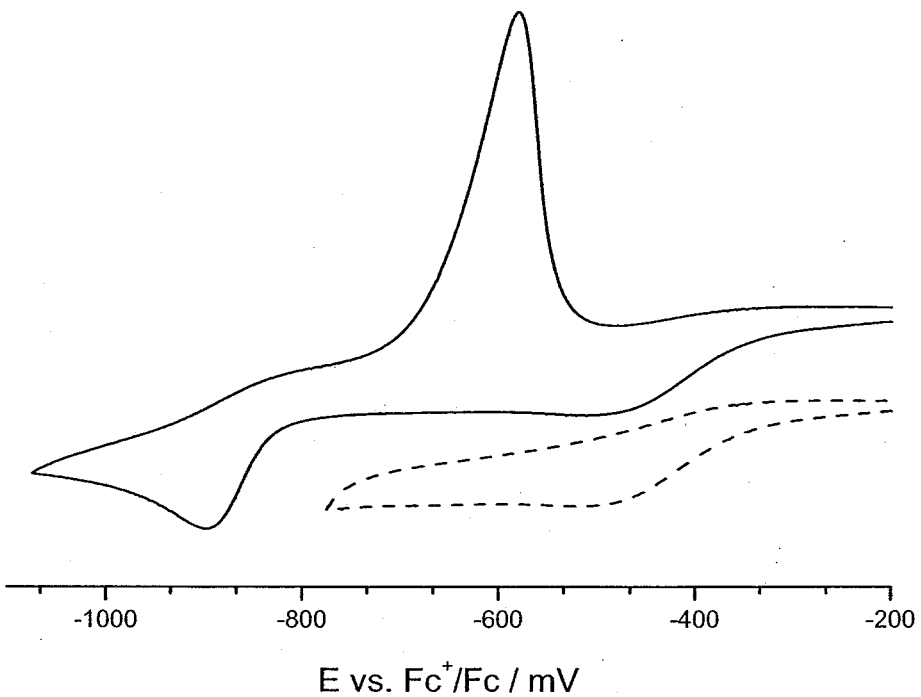

Figure 2.4.6. Cyclic voltammograms (1 mM, 0.1 M TBAP, MeCN, scan rate: 50 mV s^{-1}) of $[Cu^{II}_2(H_2\mathbf{L^{M1}})_2(MeCN)_2](BF_4)_4$ (**18**).

Compared to the two reduction waves of **6b** · MeCN ($E_{pc(6b)} = -0.33$ V and –0.76 V) the single reduction wave of **18** occurred in between those values. A shift of $\Delta E_{pc(6b,18)} = 0.18$ V to more negative potential compared to the first, and a shift of $\Delta E_{pc(6b,18)} = 0.25$ V to more positive potential compared to the second reduction process of **6b** · MeCN was observed. A plating process ($E_{pc} = -0.90$ V) with associated stripping peak ($E_{pa} = -0.58$ V) was observed in the cyclic voltammogram of **18** (Figure 2.4.7).

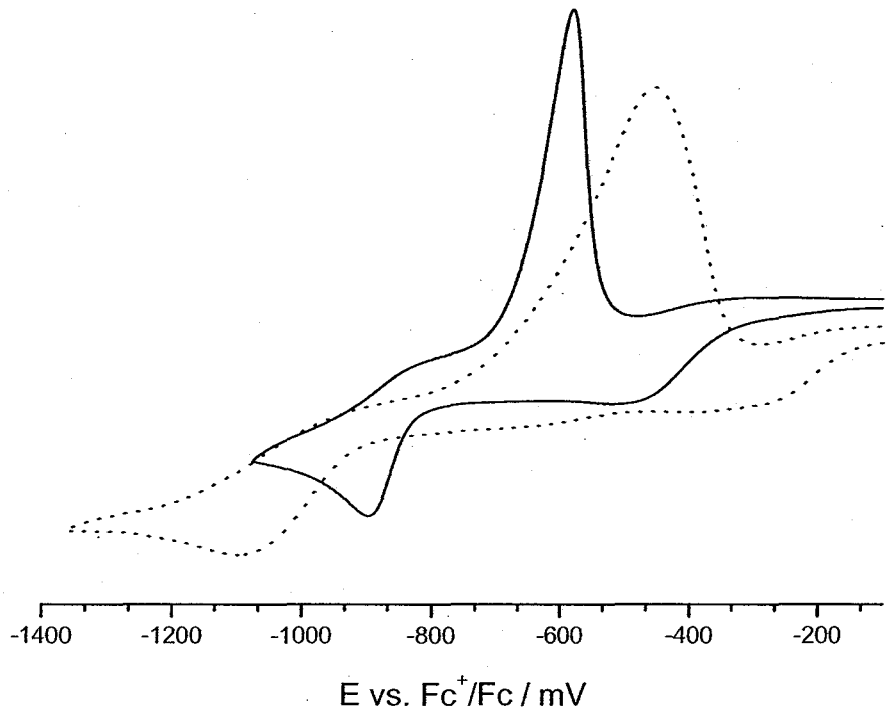

Figure 2.4.7. Comparison of the cyclic voltammograms (1 mM, 0.1 M TBAP, MeCN, scan rate: 50 mV s^{-1}) of the dimeric complex $[Cu^{II}_2(H_2\mathbf{L}^{\mathbf{M1}})_2(MeCN)_2](BF_4)_4$ (**18**) (solid line) and the dinuclear complex $[Cu^{II}_2(H\mathbf{L}^{\mathbf{M1}})(MeCN)_4](BF_4)_3 \cdot MeCN$ (**6b** · MeCN) (dotted line).

Magnetic studies on $[Cu^{II}_2(H_2L^{M1})_2(MeCN)_2](BF_4)_4$ (18)

The plots of the magnetic moment (μ_{eff}) per Cu^{II}_2 as well as of the reciprocal molar magnetic susceptibility (χ_m^{-1}) versus the temperature (T) for the dimeric complex **18** are given in Figure 2.4.8. In the temperature range of 3–297 K the magnetic moment (μ_{eff} of 2.65 μ_B per Cu^{II}_2) proved to be independent of the temperature. As expected for such a structure with essentially non-bridged copper(II) ions the magnetic behaviour obeyed the Curie law in that temperature range, showing that no spin coupling was occuring. The Curie and the Weiss constants were found to be $C = 0.84$ cm^3 K mol^{-1} and $\theta = 0.00$ K.

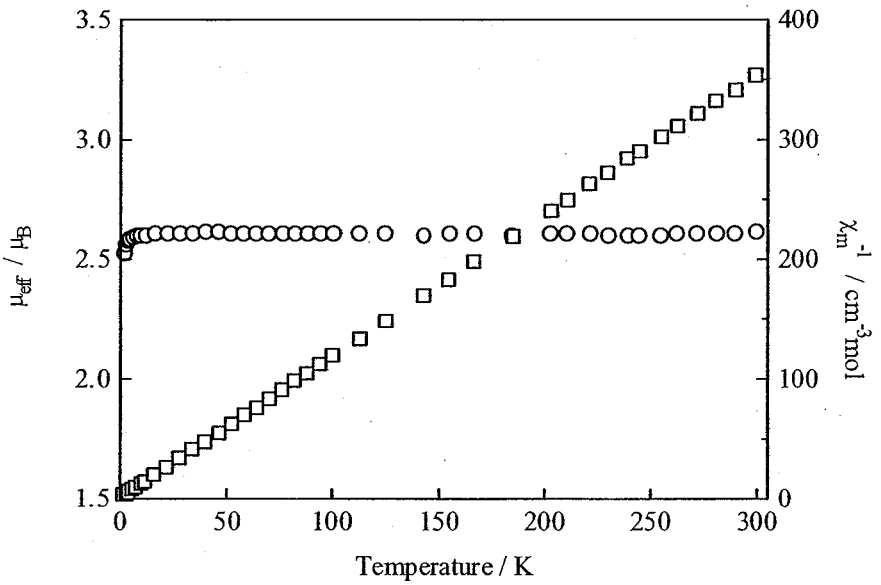

Figure 2.4.8. Thermal variation of the magnetic moment μ_{eff} (◦◦) per Cu^{II}_2 and the reciprocal molar susceptibility χ_m^{-1} (▫▫) of $[Cu^{II}_2(H_2\mathbf{L^{M1}})_2(MeCN)_2](BF_4)_4$ (**18**).

Note: Just prior to submission of this thesis the X-ray crystal structure of the structurally related complex $[Cu^{II}_2(H_2L^{M1})_2(OSO_3)_2]$ was reported by Cati and Stoeckli-Evans.[184]

Complexation with H_2L^{M2}

To compare the complexation behaviour of the two homologous ligands H_2L^{M1} and H_2L^{M2}, the reaction employing H_2L^{M2} was carried out under otherwise identical conditions, to those employed for the preparation of **18**. From the resulting dark turquoise reaction solution a turquoise-green feathery crystalline material was obtained by the vapour diffusion of diethyl ether into this solution. Compound **19** was thus isolated in around 85 % yield (Scheme 2.4.3).

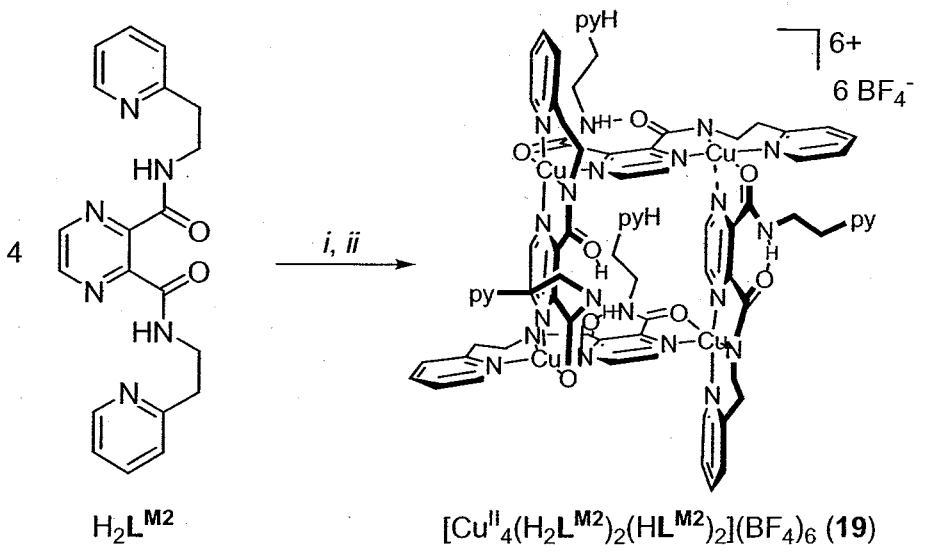

H_2L^{M2} $[Cu^{II}_4(H_2L^{M2})_2(HL^{M2})_2](BF_4)_6$ (**19**)

Scheme 2.4.3. Synthesis of **19**. Reagents and conditions: (*i*) 1 eq. $Cu(BF_4)_2 \cdot 4\ H_2O$, MeCN, RT; (*ii*) Et_2O (vapour diffusion).

The compound proved to be readily soluble in all common polar solvents like alcohols, acetonitrile, water and *N*,*N*-dimethylformamide. Elemental analysis suggested a rather unexpected ratio of copper(II) complex to tetrafluoroborate of 2:3. The compound was preliminary formulated as $[Cu^{II}_2(H_2L^{M2})(HL^{M2})]_n(BF_4)_{3n} \cdot 2n\ H_2O$ (**19** $\cdot$ $2n$ H_2O). The result of the conductivity measurement in acetonitrile solution [$\Lambda_m = 192\ mol^{-1}\ cm^2\ \Omega^{-1}$, per ligand] suggested that **19** might be a 1:1.5 electrolyte (per ligand), which fitted well with the preliminary formulation. Unfortunately, the positive ion electrospray mass spectrum of **19** in acetonitrile did not help to clarify the nature or composition of the compound and only three peaks at m/z = 439.2, 377.3 and 189.1 could be assigned. The only copper containing peak at m/z = 439.2 was assigned to the complex fragment $[Cu^{I}(H_2L^{M2})]^+$, the other two peaks derived from the protonated ligand species $(H_3L^{M2})^+$ and $(H_4L^{M2})^{2+}$.

IR spectroscopic studies on $[Cu^{II}_2(H_2L^{M2})(HL^{M2})]_n(BF_4)_{3n} \cdot 2n\ H_2O$ (19 $\cdot$ $2n$ H_2O)

In contrast to the preparation of the KBr pellet of the related compound $[Cu^{II}_2(H_2L^{M1})_2(MeCN)_2](BF_4)_4$ **18** of the lower ligand homologue, the preparation of the KBr pellet of **19** did not result in a colour change. The IR spectrum of **19**, in the region

around $\tilde{\upsilon}$ = 1700–1600 cm^{-1}, showed a very strong sharp split band at $\tilde{\upsilon}$ = 1636 and 1607 cm^{-1} which was assigned to the ν_{CO} vibration of metalated amide groups in two different environments (Figure 2.4.9). A second very strong split band was observed at $\tilde{\upsilon}$ = 1569 and 1542 cm^{-1}. As for **18**, but with lower intensity, broad absorption bands were observed in the region of $\tilde{\upsilon}$ = 3100–2700 cm^{-1}. A very broad absorption multiplet was observed at $\tilde{\upsilon}$ = 1080–1030 cm^{-1} and was ascribed to stretching vibrations of the tetrafluoroborate counter ions.

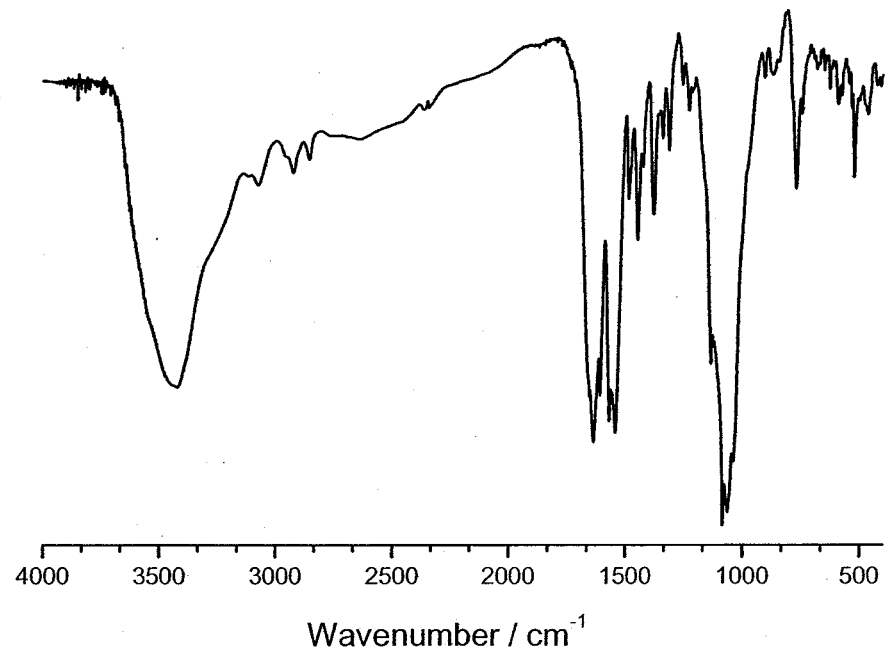

Figure 2.4.9. IR spectrum (KBr) of $[Cu^{II}_2(H_2\mathbf{L}^{M2})(H\mathbf{L}^{M2})]_n(BF_4)_{3n} \cdot 2n\ H_2O$ (**19** · $2n\ H_2O$).

Summarising these observations, it was suggested that both amide groups of the ligand were involved in metal coordination, but probably not in similar coordination motifs.

Single crystal X-ray structural analysis of

$[Cu^{II}_4(H_2L^{M2})_2(HL^{M2})_2](BF_4)_6 \cdot 3\ MeCN \cdot 0.5\ H_2O$ ($19 \cdot 3\ MeCN \cdot 0.5\ H_2O$)

Single crystals of **19** · 3 MeCN · 0.5 H_2O suitable for X-ray crystal structure determination were obtained by vapour diffusion of diethyl ether into a dilute solution (1 mg ml^{-1}) of the compound in acetonitrile (Figure 2.4.10). The compound could accordingly be formulated as $[Cu^{II}_4(H_2L^{M2})_2(HL^{M2})_2](BF_4)_6 \cdot 3\ MeCN \cdot 0.5\ H_2O$ (**19** · 3 MeCN · 0.5 H_2O). With the assumption that the primarily isolated compound **19** · 2*n* H_2O shared the same overall molecular structure this compound was retrospectively formulated as $[Cu^{II}_4(H_2L^{M2})_2(HL^{M2})_2](BF_4)_6 \cdot 4\ H_2O$ (**19** · 4 H_2O).

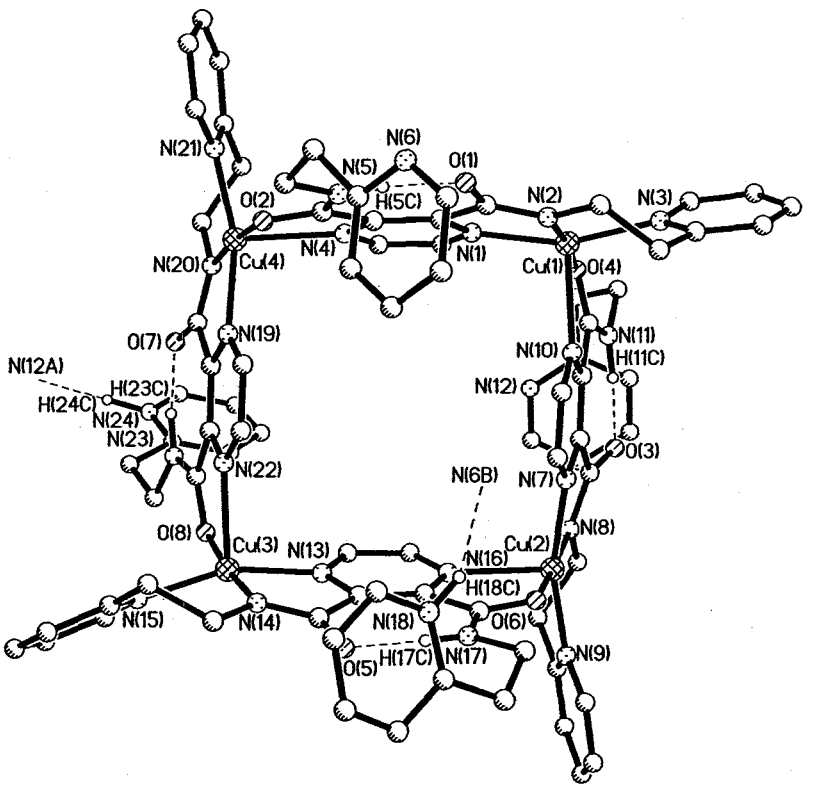

Figure 2.4.10. Molecular structure of $[Cu^{II}_4(H_2\mathbf{L}^{M2})_2(H\mathbf{L}^{M2})_2]^{6+}$, the cation of complex **19** · 3 MeCN · 0.5 H_2O. Hydrogen atoms, except H(5C), H(11C), H(17C), H(23C), H(18C) and H(24C) have been omitted for clarity. Selected distances (Å) and angles (°): Cu(1)-N(1) 2.032(5), Cu(1)-N(2) 1.914(5), Cu(1)-N(3) 2.004(5), Cu(1)-O(4) 1.958(4), Cu(1)-N(10) 2.316(5), Cu(1)···Cu(2) 7.051(1), Cu(2)···Cu(3) 6.997(1), Cu(3)···Cu(4) 7.009(1), Cu(4)···Cu(1) 7.037(1), Cu(1)···Cu(3) 9.953(1), Cu(2)···Cu(4) 9.847(1), N(5)···O(1) 2.576(5), N(11)···O(3) 2.561(5), N(17)···O(5) 2.547(5), N(23)···O(7) 2.557(5), N(18C)···N(6A) 2.703(5), N(24C)···N(12B) 2.732(5); N(1)-Cu(1)-N(2) 80.6(2), N(1)-Cu(1)-N(3) 160.2(2), N(1)-Cu(1)-O(4) 93.5(2), N(1)-Cu(1)-N(10) 99. 6(2), N(2)-Cu(1)-N(3) 94.2(2), N(2)-Cu(1)-O(4) 174.0(2), N(2)-Cu(1)-N(10) 105.2(2), N(3)-Cu(1)-O(4) 91.8(2), N(3)-Cu(1)-N(10) 100.3(2), O(4)-Cu(1)-N(10) 74.3(2). Symmetry operations used to generate equivalent atoms: A = −x+1, −y+1, −z; B = −x+1, −y+1, −z+1.

As found for the related dimeric compound $[Cu^{II}_2(H_2L^{M1})_2(MeCN)_2](BF_4)_4$ (**18**) of the lower ligand homologue, the copper(II) ions of the tetrameric complex **19** · 3 MeCN · 0.5 H_2O adopt a distorted square pyramidal N_4O coordination environment. In the tetranuclear subunit of **19** · 3 MeCN · 0.5 H_2O each ligand functions as a hybrid terdentate-bidentate N_3-NO chelate. The donor atoms of the N_3-terdentate half thus occupy three equatorial positions of a copper(II) ion. Unlike in the related complex **18** of the lower ligand homologue the coordinated pyridines are not roughly coplanar with the corresponding pyrazine rings but form an average canting angle of 31.4°. To complete the distorted square pyramidal coordination, the fourth equatorial and the axial coordination positions of each copper(II) ion are occupied by the amide oxygen and the pyrazine nitrogen atom, belonging to the NO-bidentate half of the ligand. The two chelate planes are close to perpendicular to each other. In this way the square-like arrangement of the tetrameric unit is formed. In all four distorted square pyramids the copper(II) ions are pulled out of the base towards the axial pyrazine ligand [Cu(1): 0.165 Å, Cu(2): 0.162 Å, Cu(3): 0.157 Å, Cu(4): 0.127 Å]. The degree of trigonality, with an average of $\tau_{av} = 0.20$, ranges from $\tau_{min} = 0.14$ to $\tau_{max} = 0.26$.[127] These values are significantly higher, compared to the related compound **18** ($\tau = 0.05$). Unlike in compound **18** of the lower ligand homologue, neighbouring copper(II) ions of compound **19** · 3 MeCN · 0.5 H_2O are bridged through a ligand pyrazine ring, which occupies the axial coordination site of one, and an equatorial coordination site of the other copper(II) ion, respectively. Thereby two shorter [Cu(2)···Cu(3) 6.997(1) Å and Cu(3)···Cu(4) 7.009(1) Å] and two longer [Cu(1)···Cu(2) 7.051(1) Å and Cu(1)···Cu(4) 7.037(1) Å] Cu^{II}···Cu^{II} distances are observed. Hence, the average Cu^{II}···Cu^{II} distance is 7.02 Å and is significantly longer than the respective Cu^{II}···Cu^{II} distances of the complexes $[Cu^{II}_2(HL^{M1})(MeCN)_4](BF_4)_3$ · MeCN (**6b** · MeCN) (6.745(5) Å), $[Cu^{II}_4(HL^{M1})_2(\mu_{(1,1)}\text{-}N_3)_2(N_3)_2(MeCN)_2](BF_4)_2$ · MeCN (**14b** · MeCN) (6.828(1) Å) and $\{[Cu^{II}_2(HL^{M2})(\mu_{(1,3)}\text{-}N_3)_2](BF_4)$ · MeCN$\}_\infty$ (**16b** · MeCN) (6.763(3) Å) described so far. Relative to the Cu^{II}_4 mean plane, the copper(II) ions of **19** · 3 MeCN · 0.5 H_2O are

shifted by ca. 0.28 Å in an up-down-up-down fashion leading to a small tetrahedral distortion of the Cu^{II}_4 square.

The O-coordinated amide group of the NO-bidentate ligand half is still N-protonated and the proton is involved in an N-H···O hydrogen bond to the oxygen atom of the N-metalated amide group of the N_3-terdentate half of the same ligand (see Section 3.4.6). The N···O distances in the consequent seven-membered rings range from 2.547–2.576 Å. Both amide groups in these rings are reasonably coplanar with the corresponding pyrazine ring. The greatest shifts out of planes are 0.21(1) Å for O(1), 0.406(9) Å for O(4), 0.232(9) Å for O(6) and 0.246(9) Å for O(8). The amide group of the N-metalated function is deprotonated but in the tetrameric complex, two of the four ligands retain a former N-H amide proton by relocating it to the nitrogen atom of the free pyridine of the NO-bidentate ligand half. This feature also has been observed in the molecular structure of the related dimeric complex **18** of the lower ligand homologue and in other related systems.[183] In the tetranuclear subunit of **19** · 3 MeCN · 0.5 H_2O, the two relocated protons are involved in intermolecular N-H···N hydrogen bonds to the two unprotonated pyridine nitrogen atoms of a neighbouring tetranuclear subunit, respectively. Thus a polymeric chain structure of tetranuclear subunits is formed (Figure 2.4.11).

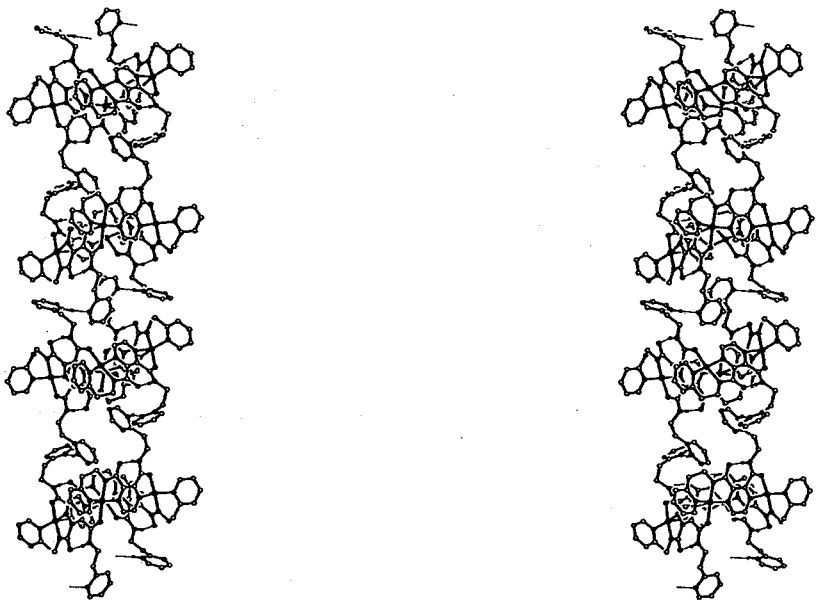

Figure 2.4.11. Stereo picture of a section of the crystal structure of complex **19** · 3 MeCN · 0.5 H_2O. Hydrogen atoms not involved in hydrogen bonds and solvent molecules have been omitted for clarity.

UV/VIS spectroscopic studies on $[Cu^{II}_4(H_2L^{M2})_2(HL^{M2})_2](BF_4)_6 \cdot 4\ H_2O$ (19 · 4 H_2O)

The UV/VIS spectrum of **19** · 4 H_2O showed a broad weak absorption band at λ_{max} = 622 nm (ε = 434 M^{-1} cm^{-1}; $\tilde{\upsilon}$ = 16077 cm^{-1}), with a distinct shoulder to lower energy, which was assigned to the overlapping absorption bands of the copper(II) *d-d* transitions. Furthermore a relatively sharp intense absorption band at λ_{max} = 262 nm (ε = 87300 M^{-1} cm^{-1}, $\tilde{\upsilon}$ = 38168 cm^{-1}) was observed (Figure 2.4.12).

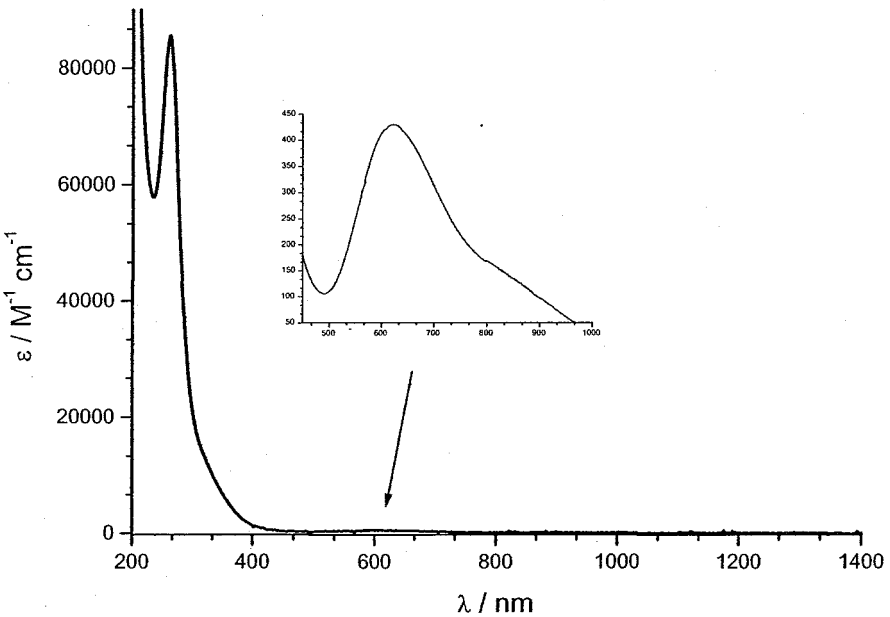

Figure 2.4.12. UV/VIS spectra [MeCN, 0.5 mM (inset) and 0.005 mM (main)] of $[Cu^{II}_4(H_2\mathbf{L^{M2}})_2(H\mathbf{L^{M2}})_2](BF_4)_6 \cdot 4\ H_2O$ (**19** · 4 H_2O).

A comparison of the UV/VIS spectra [ε per copper(II) ion] of the two complexes **8** and **19** · 4 H_2O of the higher ligand homologue and the two complexes **6b** · MeCN and **18** of the lower ligand homologue is shown in Figure 2.4.13.

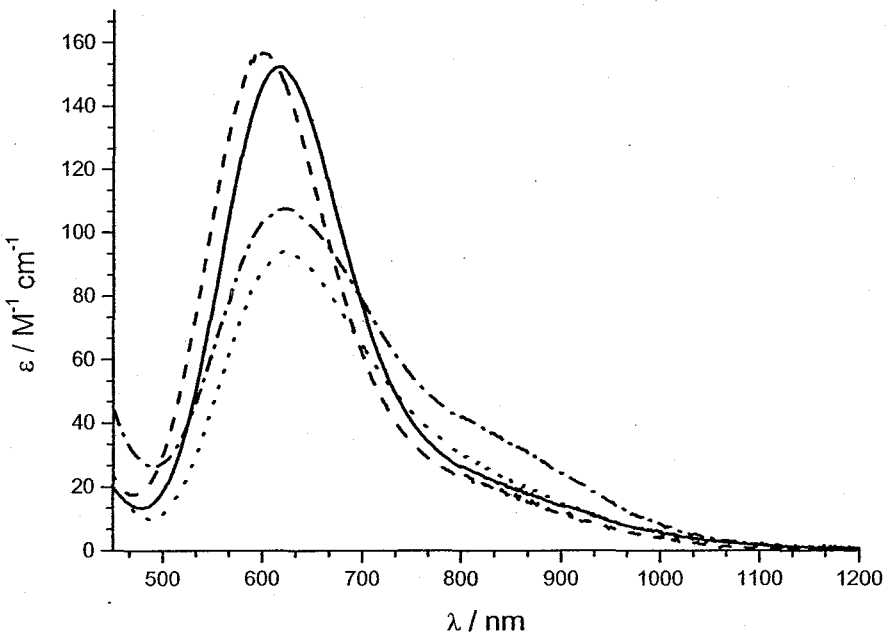

Figure 2.4.13. Comparison of the UV/VIS spectra (per copper(II) ion) of $[Cu^{II}_2(HL^{M1})(MeCN)_4](BF_4)_3 \cdot MeCN$ (**6b** · MeCN) [MeCN, 1 mM, solid line], $[Cu^{II}_2(H_2L^{M1})_2(MeCN)_2](BF_4)_4$ (**18**) [MeCN, 1 mM, dashed line], $[Cu^{II}_2(HL^{M2})(H_2O)](ClO_4)_3$ (**8**) [MeCN, 1 mM, dotted line] and $[Cu^{II}_4(H_2L^{M2})_2(HL^{M2})_2](BF_4)_6 \cdot 4\ H_2O$ (**19** · 4 H_2O) [MeCN, 0.125 mM dash-dotted line] in the region of the *d-d* transition.

The energies of the *d-d* transition bands were a little higher for the complexes of the lower ligand homologue [**6b** · MeCN ($\tilde{\nu}$ = 16230 cm^{-1}) and **18** ($\tilde{\nu}$ = 16667 cm^{-1})] than for the complexes of the higher ligand homologue [**8** ($\tilde{\nu}$ = 16050 cm^{-1}) and **19** · 4 H_2O ($\tilde{\nu}$ = 16077 cm^{-1})]. However, the energies of all four complexes were still very similar. It was therefore suggested that all of these complexes adopted similar coordination environments in acetonitrile solution and that the tetranuclear compound **19** · 4 H_2O underwent dissociation. This assumption was also supported by the positive ion electrospray mass spectrum that showed only evidence of mononuclear complex fragments. It is noteworthy that the intensity of the molar extinction coefficients per copper(II) ion were lower for the complexes **8** (ε = 95 M^{-1} cm^{-1}) and **19** · 4 H_2O (ε = 109 M^{-1} cm^{-1}) of the higher ligand homologue, than for the complexes **6b** · MeCN (ε = 161 M^{-1} cm^{-1}) and **18** (ε = 150 M^{-1} cm^{-1}) of the lower ligand homologue.

Cyclic voltammetric studies on $[Cu^{II}_4(H_2L^{M2})_2(HL^{M2})_2](BF_4)_6 \cdot 4\ H_2O$ ($19 \cdot 4\ H_2O$)

The cyclic voltammogram of **19** · 4 H_2O in acetonitrile solution unexpectedly showed two irreversible reduction waves, occurring at E_{pc} = –0.42 and –0.69 V, relative to the Fc^+/Fc redox couple (Figure 2.4.14).

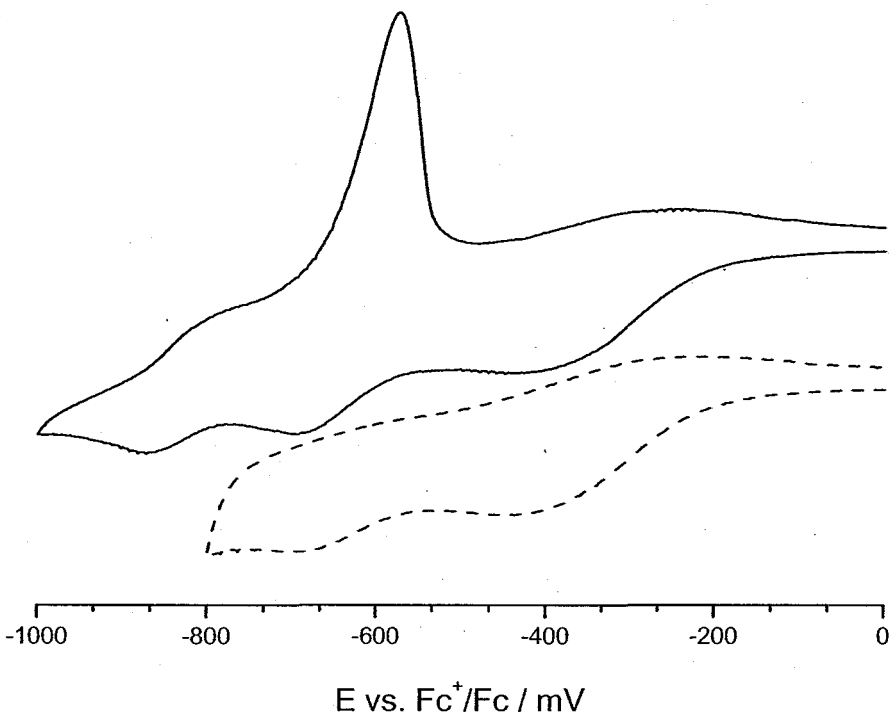

Figure 2.4.14. Cyclic voltammograms (0.25 mM, 0.1 M TBAP, scan rate: 50 mV s^{-1}) of $[Cu^{II}_4(H_2\mathbf{L}^{M2})_2(H\mathbf{L}^{M2})_2](BF_4)_6 \cdot 4\ H_2O$ (**19** · 4 H_2O) in acetonitrile solution.

By comparison with the cyclic voltammogram of the dimeric complex $[Cu^{II}_2(H_2\mathbf{L}^{M1})_2(MeCN)_2](BF_4)_4$ (**18**), which was believed to dissociate in solution and showed only one reduction wave, it appeared that the tetrameric complex cation of **19** suffered only partial dissociation in acetonitrile solution, although the results of the UV/VIS and positive ion electrospray analyses suggested otherwise. This apparent stability difference between the two related compounds **18** and **19** · 4 H_2O was probably due to the different bridging modes assumed by the ligands, *i.e.* by the different ways the mononuclear subunits were connected with each other. In the former complex **18**, the subunits were linked by only one axially coordinated amide carbonyl oxygen, which in solution was expected to be rather labile, whereas in the

latter complex **19** · 4 H_2O the subunits were linked through two donor atoms, involving Cu^{II}-pz-Cu^{II} bridges which were probably more stable to dissociation. Compared to the dinuclear complex $[Cu^{II}_2(HL^{M2})(H_2O)](ClO_4)_3$ (**8**) of the same ligand the first reduction peak in the cyclic voltammogram of **19** · 4 H_2O occurred with a shift of $\Delta E_{pc(19,8)}$ = 0.16 V, and the second reduction wave with a shift of $\Delta E_{pc(19,8)}$ = 0.20 V to more negative potentials, respectively (see Table 2.4.1). The separation of the two reduction waves (ΔE_{pc} = 0.27 V) of **19** · 4 H_2O compared well to the separation ($\Delta E_{pc(8)}$ = 0.23 V) of the dinuclear complex **8** of the same ligand. At lower potentials (E_{pc} = –0.87 V) a plating process with associated stripping peak (E_{pa} = –0.57 V) was observed in the cyclic voltammogram of **19** · 4 H_2O (Figure 2.4.14). This overall shift of around 0.2 V to more negative potentials, comparing the reduction processes of **19** · 4 H_2O and **8**, was probably due to the more rigid coordination environment of the former complex **19** · 4 H_2O, disfavouring the reduction of copper(II) to copper(I).

Table 2.4.1. Comparison of E_{pc} of the reduction processes of **6b** · MeCN, **8**, **18** and **19** · 4 H_2O in acetonitrile solution.

Complex	E_{pc}(1) / V	E_{pc}(2) / V	ΔE_{pc}(1,2) / V
$[Cu^{II}_2(HL^{M1})(MeCN)_4](BF_4)_3$ · MeCN (**6b** · MeCN)	–0.33	–0.76	0.43
$[Cu^{II}_2(HL^{M2})(H_2O)](ClO_4)_3$ (**8**)	–0.26	–0.49	0.23
$[Cu^{II}_2(H_2L^{M1})_2(MeCN)_2](BF_4)_4$ (**18**)	–0.51		—
$[Cu^{II}_4(H_2L^{M2})_2(HL^{M2})_2](BF_4)_6$ · 4 H_2O (**19** · 4 H_2O)	–0.42	–0.69	0.27

Magnetic studies on $[Cu^{II}_4(H_2L^{M2})_2(HL^{M2})_2](BF_4)_6 \cdot 4\ H_2O$ (19 · 4 H_2O)

The plots of μ_{eff} per copper(II) ion and of χ_m versus the temperature (T) for the tetranuclear complex $[Cu^{II}_4(H_2L^{M2})_2(HL^{M2})_2](BF_4)_6 \cdot 4\ H_2O$ (**19** · 4 H_2O) are shown in Figure 2.4.15 and Figure 2.4.16.

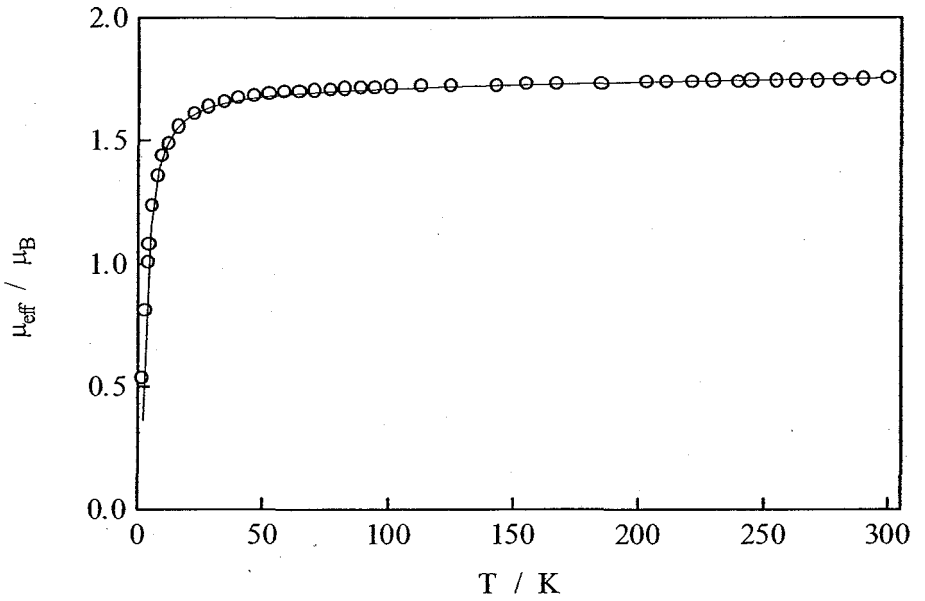

Figure 2.4.15. Thermal variation of the magnetic moment μ_{eff} (∘∘) of $[Cu^{II}_4(H_2\mathbf{L}^{\mathbf{M2}})_2(H\mathbf{L}^{\mathbf{M2}})_2](BF_4)_6 \cdot 4\ H_2O$ (**19** · 4 H_2O). The solid line represents the best fit.

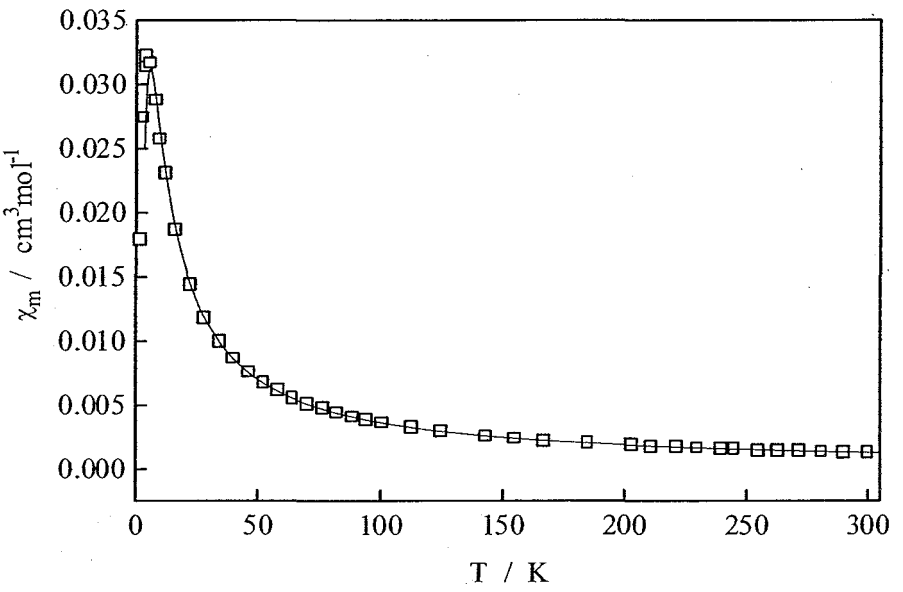

Figure 2.4.16. Thermal variation of the molar susceptibility χ_m (▫▫) of $[Cu^{II}_4(H_2\mathbf{L}^{\mathbf{M2}})_2(H\mathbf{L}^{\mathbf{M2}})_2](BF_4)_6 \cdot 4\ H_2O$ (**19** · 4 H_2O). The solid line represents the best fit.

The magnetic measurement of **19** · 4 H_2O obeyed the Curie-Weiss law above 20 K. Below that temperature the value of χ_m increased with decreasing temperature, reaching a maximum at 5.5 K (0.031 $cm^3\ mol^{-1}$). Consequently the values of μ_{eff} (1.25 μ_B at 300 K) decreased rapidly, when the temperature was lowered below 50 K, indicating the presence of antiferromagnetic interactions. The best fits (solid lines in Figure 2.4.15 and Figure 2.4.16) for **19** · 4 H_2O were obtained introducing two small and slightly different coupling constants as in **14b** · MeCN. The coupling constants $J_{13} = J_{24}$ and $J_{14} = J_{23}$ (Figure 2.3.13) of **19** · 4 H_2O were calculated to –1.90 and –2.36 cm^{-1}, respectively. The values of g = 1.99, monomeric impurity = 0.1 % and $TIP = 65 \times 10^{-6}\ cm^3\ mol^{-1}$ (per Cu^{II}) were calculated.

2.4.2. *Metal(II) ions other than copper(II)*

Complexations employing the two homologous ligands H_2L^{M1} or H_2L^{M2} and metal(II) ions other than copper(II) in a 1:1 molar ratio, respectively, have been carried out with the purpose of comparing the resulting complexes with each other and with the related copper(II) derivatives $[Cu^{II}_2(H_2L^{M1})_2(MeCN)_2](BF_4)_4$ (**18**) and $[Cu^{II}_4(H_2L^{M2})_2(HL^{M2})_2](BF_4)_6 \cdot 4\ H_2O$ (**19** · 4 H_2O).

Complexations with manganese(II) and H_2L^{M1} or H_2L^{M2}

Complexations employing H_2L^{M1} or H_2L^{M2} and manganese(II) perchlorate hexahydrate or manganese(II) chloride in a molar ratio of 1:1, respectively, have been carried out in acetonitrile and in ethanol solution. In all cases only inhomogeneous pale solids of unknown compositions could be isolated. Further attempts to isolate pure samples were unsuccessful.

Complexation with iron(II) and H_2L^{M1}

The employment of iron(II) tetrafluoroborate hexahydrate and the lower ligand homologue H_2L^{M1} in a molar ratio of 1:1 in acetonitrile resulted in a very dark deep purple solution. By vapour diffusion of diethyl ether into the reaction solution, a dark blue solid was isolated in around 60 % yield (**20**) (Scheme 2.4.4). Elemental analysis of the compound suggested a 1:1:2 molar ratio of iron ions to ligand to tetrafluoroborate, leading to the preliminary formulation of $[Fe^{II}(H_2L^{M1})(MeCN)]_n(BF_4)_{2n}$ (**20**). Conductivity measurements in acetonitrile solution [Λ_m = 281 mol^{-1} cm^2 Ω^{-1} per ligand] fitted well with the expected values for a 2:1 electrolyte.

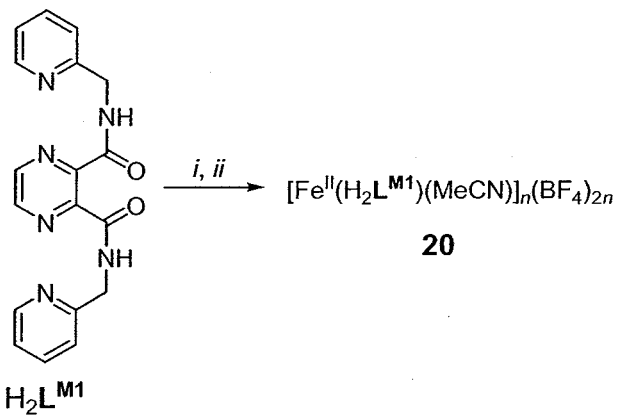

Scheme 2.4.4. Synthesis of **20**. Reagents and conditions: (*i*) 1 eq. $Fe(BF_4)_2 \cdot 6\ H_2O$, MeCN, RT; (*ii*) Et_2O (vapour diffusion).

The positive ion electrospray mass spectrum of **20** in acetonitrile showed the most intense peak at m/z = 349.1 which was assigned to the protonated ligand species $(H_2L^{M1})^+$. A relatively weak peak at m/z = 750.0 was assigned to the complex fragment $[Fe^{III}(HL^{M1})_2]^+$. Unfortunately no evidence of higher nuclearity fragments was present.

The IR spectrum of the compound showed a split band at $\tilde{\upsilon}$ = 1636 and 1616 cm^{-1}, which was assigned to the ν_{CO} vibrations of two amide groups in different coordination environments (Figure 5.3.9, Appendix). These bands appeared at similar wavenumbers than the corresponding bands of **19** · 4 H_2O.

The UV/VIS spectrum of **20** in acetonitrile solution showed a number of very intense absorption bands in the range of λ = 200–1000 nm, probably due to charge transfer absorptions (Figure 5.4.2, Appendix).

Unfortunately no meaningful ^{1}H NMR spectrum could be obtained, due to very broad absorption peaks, probably caused by a paramagnetic contaminant.

Cyclic voltammetric studies of **20** in acetonitrile solution showed two metal-centred quasi-reversible oxidation processes at $E_{1/2}$ = –0.02 V (ΔE = 0.09 V) and $E_{1/2}$ = +0.33 V (ΔE = 0.18 V), relative to the Fc^+/Fc redox couple, probably associated with oxidation processes iron(II) → iron(III), respectively (Figure 2.4.17).[185]

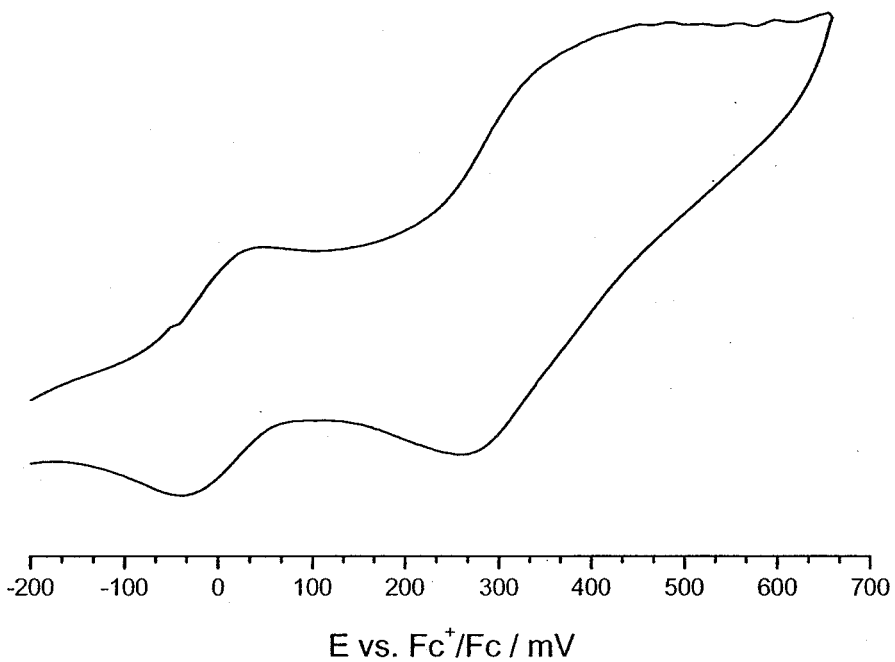

Figure 2.4.17. Cyclic voltammogram (1 mM, 0.1 M TBAP, MeCN, scan rate: 200 mV s^{-1}) of $[Fe^{II}(H_2\mathbf{L}^{\mathbf{M1}})(MeCN)]_n(BF_4)_{2n}$ (**20**).

It is worthwhile emphasising that the first oxidation wave occurred with a relatively large difference of ΔE = 0.35 V to the second oxidation process, so that the potentially polynuclear complex **20** could possibly exist in a mixed valent Fe^{II}/Fe^{III} state. One broad irreversible reduction wave (possibly two poorly resolved reduction processes) at a quite low potential of around E_{pc} = –1.18 V was observed (Figure 5.5.1, Appendix).

Summarising, it was proposed that compound **20** was not mononuclear but of di- or higher nuclearity. Unfortunately, all attempts at recrystallisation, for example the vapour diffusion of diethyl ether into a solution of **20** in acetonitrile, the slow evaporation of the solvent, or the layering of the solution with toluene, were unsuccessful, so that no further information regarding the molecular structure of the compound could be gained.

Complexation with iron(II) and H_2L^{M2}

The employment of the higher ligand homologue H_2L^{M2} under otherwise identical reaction conditions, led to a very deep purple solution from which, after vapour diffusion of diethyl ether into the solution, an inhomogeneous sticky rust brown solid of unknown composition was isolated. The layering of the reaction mixture with toluene, also led to the formation of an inhomogeneous sticky solid of unknown formulation. Further attempts of isolating homogeneous material were unsuccessful.

Complexation with cobalt(II) and H_2L^{M1}

The reaction of H_2L^{M1} and cobalt(II) tetrafluoroborate hexahydrate in a molar ratio of 1:1 in acetonitrile solution led, after several hours of stirring at room temperature, to a dark red-brown suspension. By filtration an amorphous red-brown solid was isolated in around 35 % yield. Elemental analysis of the compound suggested a 1:2:3 molar ratio of cobalt ions to ligand to tetrafluoroborate counter ion. This result led to the assumption that the initially employed cobalt(II) ions, in the course of the complexation, had been oxidised to cobalt(III) ions in air. The compound was preliminary formulated as $[Co^{III}(H_2L^{M1})_2](BF_4)_3$ (**21**). Accordingly the

employment of a molar ratio of H_2L^{M1} to cobalt(II) tetrafluoroborate hexahydrate of 2:1 under otherwise identical reaction conditions led to the formation of $[Co^{III}(H_2L^{M1})_2](BF_4)_3 \cdot 4\ H_2O$ (**21** · 4 H_2O) in around 50 % yield (Scheme 2.4.5). The conductivity measurement in acetonitrile solution [Λ_m(MeCN) = 391 $mol^{-1}\ cm^2\ \Omega^{-1}$] fitted well for a 3:1 electrolyte.

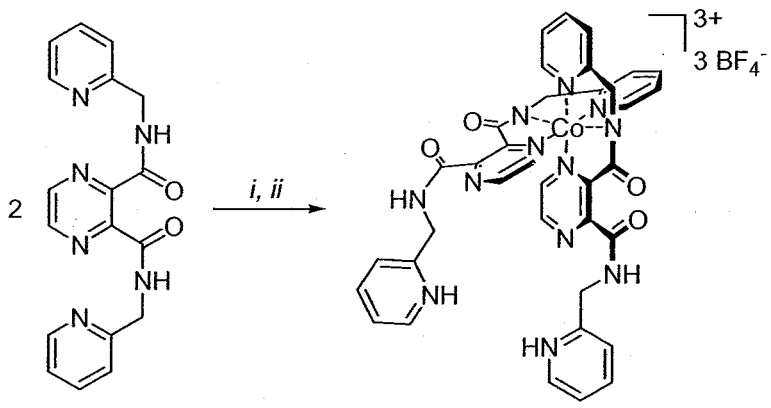

H_2L^{M1} $[Co^{III}(H_2L^{M1})_2](BF_4)_3$ (**21**)

Scheme 2.4.5. Synthesis of **21**. Reagents and conditions: (*i*) ½ eq. $Co(BF_4)_2 \cdot 6\ H_2O$, MeCN, RT; (*ii*) filtration.

The positive ion electrospray mass spectrum of **21** · 4 H_2O in acetonitrile showed the most intense peaks at *m/z* = 928.7, 840.7, 753.1 and 377.1 (Figure 5.2.3, Appendix). The first three peaks were assigned to the complex fragments $\{[Co^{III}(H_2L^{M1})_2](BF_4)_2\}^+$, $\{[Co^{III}(H_2L^{M1})(HL^{M1})](BF_4)\}^+$ and $[Co^{III}(HL^{M1})_2]^+$, respectively, and revealed the stepwise loss of tetrafluoroborate counter ions, thus corroborating the suggested composition of **21**.

Unfortunately, crystallisation attempts failed to give crystals of a size suitable for X-ray crystal structure determination, so that no final conclusion of the molecular structure concerning the compound could be made.

IR spectroscopic studies on $[Co^{III}(H_2L^{M1})_2](BF_4)_3 \cdot 4\ H_2O$ ($21 \cdot 4\ H_2O$)

The IR spectrum of the presumed cobalt(III) complex **21** · 4 H_2O showed three sharp absorption bands in the region of around $\tilde{\upsilon}$ = 1700–1600 cm^{-1} (Figure 2.4.18), similar to the IR spectrum of the related copper(II) complex **18**. By analogy, the band at $\tilde{\upsilon}$ = 1678 cm^{-1} was tentatively assigned as ν_{CO} absorption band of a neutral amide group. The two bands at $\tilde{\upsilon}$ = 1644 and 1614 cm^{-1} were accordingly assigned as a split band of ν_{CO} vibrations of a metalated amide group. It was therefore suggested that the amide groups of the ligands were not equivalent and that not all amide groups in **21** · 4 H_2O were deprotonated, *i.e.* that at least one N-protonated amide group was present in the structure. This result further supported the assumption made in Scheme 2.4.5. As in the IR spectrum of **18**, a series of broad strong absorption bands in the region $\tilde{\upsilon}$ = 3100–2700 cm^{-1} was observed in the IR spectrum of **21** · 4 H_2O. It was noted that a small peak at $\tilde{\upsilon}$ = 1734 cm^{-1}, most likely due to ν_{CO} vibrations of a carboxylic aicd, indicated partial degradation of the ligand.

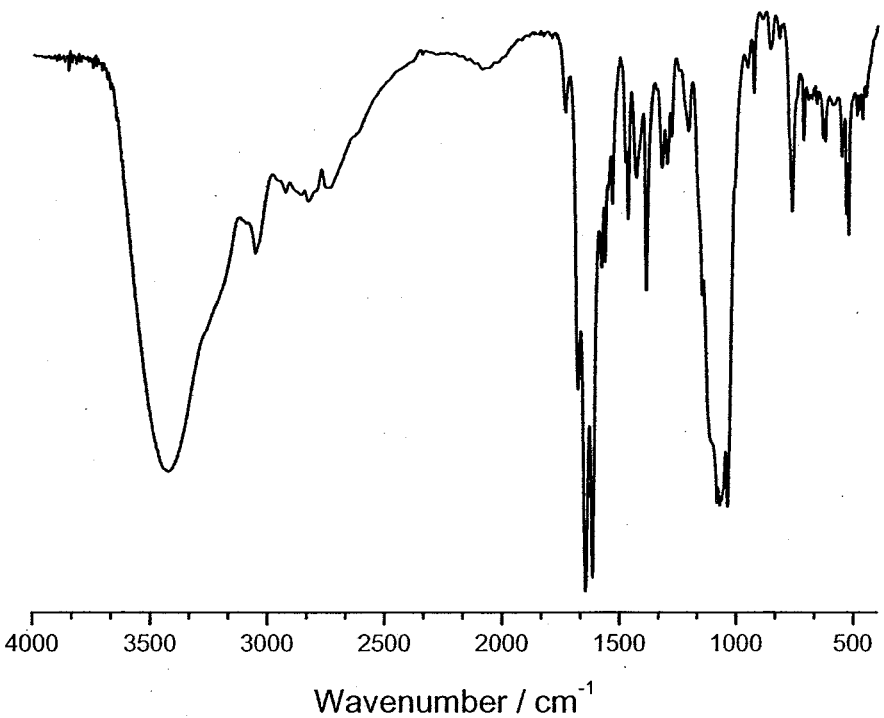

Figure 2.4.18. IR spectrum (KBr) of $[Co^{III}(H_2\mathbf{L^{M1}})_2](BF_4)_3 \cdot 4\ H_2O$ (**21** · 4 H_2O).

NMR spectroscopic studies on $[Co^{III}(H_2L^{M1})_2](BF_4)_3 \cdot 4\ H_2O$ (21 · 4 H_2O)

As the cobalt(III) ions of $[Co^{III}(H_2L^{M1})_2](BF_4)_3 \cdot 4\ H_2O$ (**21** · 4 H_2O) were expected to exist in a diamagnetic ground state, NMR spectroscopic studies were carried out. Figure 2.4.19 shows the aromatic region of the ^1H NMR spectrum obtained for **21** · 4 H_2O in d^7-DMF. The spectrum was very complex and most peaks could not unambiguously be assigned. However it was observed that a splitting and distinct broadening occurred for the signals of the pyrazine protons (9.13 and 8.88 ppm), compared to the spectrum of the free ligand H_2L^{M1}. Furthermore the integration of the peak originating from the amide proton (7.78 ppm) corresponded to one proton per ligand only. These observations further corroborated the asymmetrical coordination as would be expected for **21** · 4 H_2O with a structure as shown in Scheme 2.4.5.

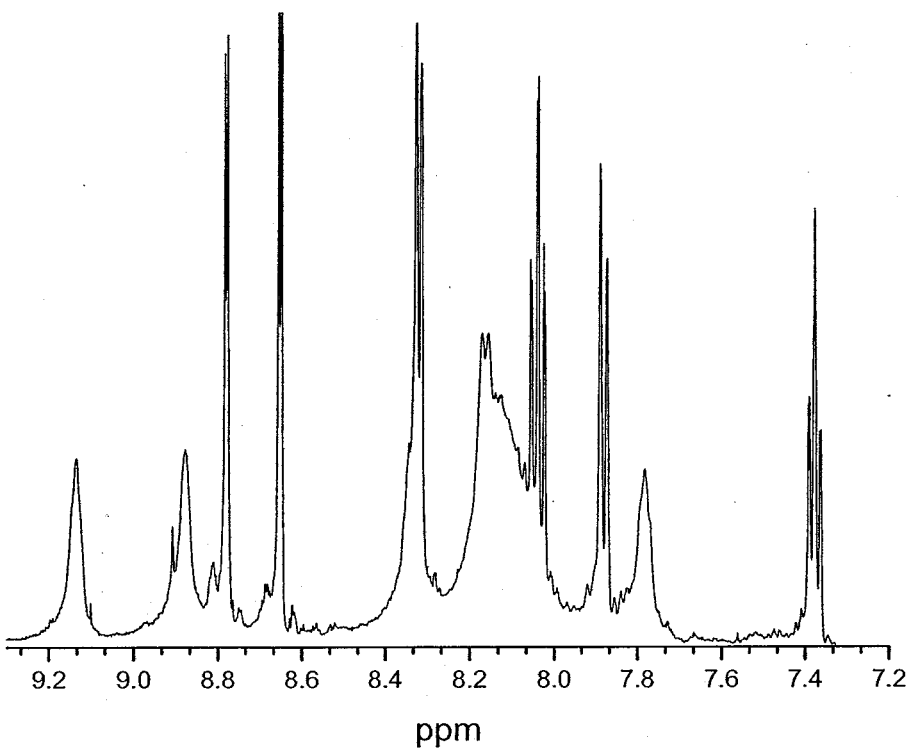

Figure 2.4.19. Aromatic region of the ^1H NMR spectrum (d^7-DMF) of $[Co^{III}(H_2\mathbf{L^{M1}})_2](BF_4)_3 \cdot 4\ H_2O$ (**21** · 4 H_2O).

Cyclic voltammetric studies on $[Co^{III}(H_2L^{M1})_2](BF_4)_3 \cdot 4\ H_2O$ (21 · 4 H_2O)

The cyclic voltammogram of the compound showed one irreversible metal-centred reduction wave at E_{pc} = –0.60 V, relative to the Fc^+/Fc redox couple, presumably associated with the reduction $[Co^{III}] \rightarrow [Co^{II}]$ (Figure 5.5.2, Appendix). At lower potentials a second very broad partially reversible reduction wave at E_{pc} = –1.38 V was observed.

Note: Just prior to submission of this thesis the X-ray crystal structure of the complex $[Co^{III}(H_2L^{M1})_2](ClO_4)_3 \cdot 3.5$ MeCN was reported by Cati and Stoeckli-Evans.[186]

Complexation with cobalt(II) and H_2L^{M2}

The reaction of the higher ligand homologue H_2L^{M2} and cobalt(II) tetrafluoroborate hexahydrate in acetonitrile, employing a 1:1 molar ratio, led to a dark brick red solution. By addition of ethanol and slow evaporation of the resulting solution, huge brick red crystals could be isolated. Elemental analysis of the compound, by analogy with **21** · 4 H_2O of the lower ligand homologue, suggested a 2:1:3 molar ratio of ligand to cobalt to tetrafluoroborate counter ion. As for **21** · 4 H_2O this led to the assumption that the initially employed cobalt(II) ions, in the course of the complexation, had been oxidised to cobalt(III) ions in air. Thereupon the reaction of H_2L^{M2} and cobalt(II) tetrafluoroborate hexahydrate was carried out employing a 2:1 molar ratio in acetonitrile solution (Scheme 2.4.6). Following this procedure, the complex $[Co^{III}(H_2L^{M2})_2](BF_4)_3 \cdot EtOH$ (**22** · EtOH) was isolated by slow evaporation of a solution containing one part of acetonitrile and four parts of ethanol as a dark brick red crystalline solid in around 65 % yield. Conductivity measurements in acetonitrile [Λ_m = 356 $mol^{-1}\ cm^2\ \Omega^{-1}$] fitted well for the expected 3:1 electrolyte. The positive ion electrospray mass spectrum in acetonitrile showed the most intense peak at

m/z = 809.1 which was assigned to the complex fragment $[Co^{III}(HL^{M2})_2]^+$ and further substantiated the nature of the assumed complex structure as is shown in Scheme 2.4.6.

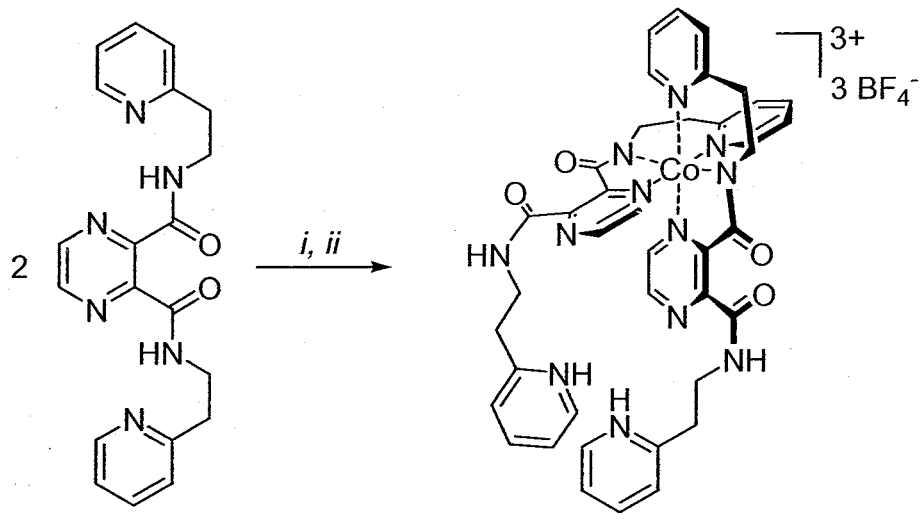

H_2L^{M2} $[Co^{III}(H_2L^{M2})_2](BF_4)_3$ (**22**)

Scheme 2.4.6. Synthesis of **22**. Reagents and conditions: (*i*) ½ eq. $Co(BF_4)_2 \cdot 6\ H_2O$, MeCN/EtOH (1:4), RT; (*ii*) slow evaporation.

IR spectroscopic studies on $[Co^{III}(H_2L^{M2})_2](BF_4)_3 \cdot EtOH$ (22 · EtOH)

As was observed in the IR spectrum of the dimeric copper(II) compound **18** and the mononuclear cobalt(III) complex **21** · 4 H_2O of the lower ligand homologue and of **19** · 4 H_2O of the higher ligand homologue, the IR spectrum of **22** · EtOH showed very broad absorption bands in the region around $\tilde{\upsilon}$ = 3100 to 2700 cm^{-1} (Figure 2.4.20). Two very broad absorption bands were observed at $\tilde{\upsilon}$ = 1652 and 1559 cm^{-1}.

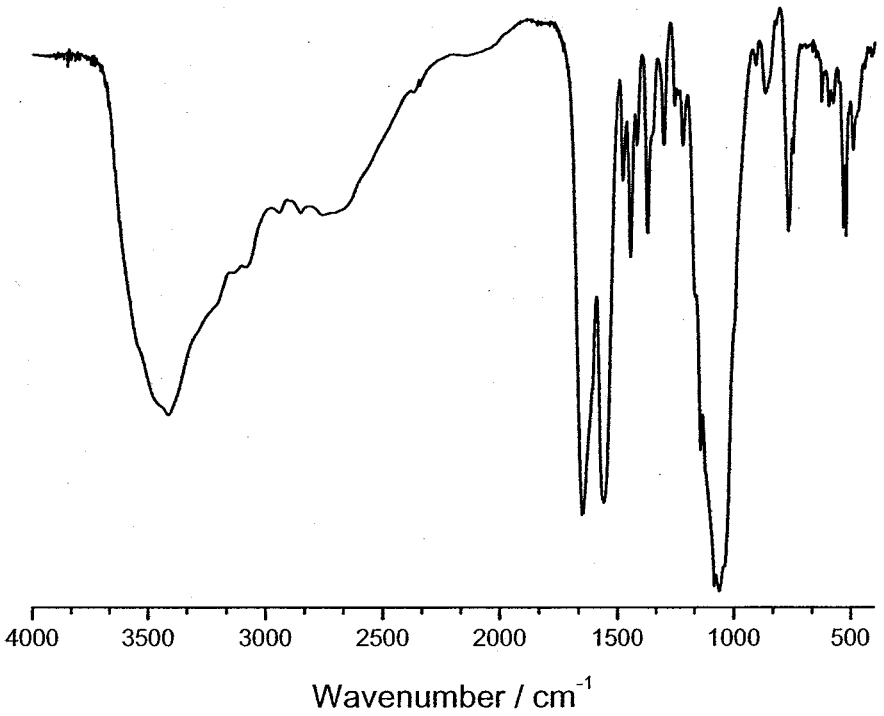

Figure 2.4.20. IR spectrum (KBr) of $[Co^{III}(H_2\mathbf{L}^{M2})_2](BF_4)_3 \cdot EtOH$ (**22** · EtOH).

Given the breadth of these bands and by comparison to the spectra of the free ligand $H_2\mathbf{L}^{M2}$ and the related complexes $[Cu^{II}(HL^{M2})(H_2O)](ClO_4)_3$ (**8**) and $[Cu^{II}_4(H_2L^{M2})_2(HL^{M2})_2](BF_4)_6 \cdot 4\ H_2O$ (**19** · 4 H_2O), the band at $\tilde{\upsilon}$ = 1652 cm^{-1} was assigned to overlapping ν_{CO} absorptions. It was suggested that, as was observed for the related dinuclear copper(II) complex **18** and the cobalt(III) complex **21** · 4 H_2O of the lower ligand homologue and the tetranuclear complex **19** · 4 H_2O of the higher ligand homologue, the amide groups in **22** · EtOH were not equivalent, and that one amide group was possibly still N-protonated and non-coordinating, as shown in Scheme 2.4.6.

Single crystal X-ray structural analysis of $[Co^{III}(H_2L^{M2})_2](BF_4)_3 \cdot 2$ EtOH (22 · 2 EtOH)

Single crystals of $[Co^{III}(H_2L^{M2})_2](BF_4)_3 \cdot 2$ EtOH (**22** · 2 EtOH) were obtained by slow evaporation of a reaction solution, containing one part of acetonitrile and four

parts of ethanol. The X-ray crystal structure determination confirmed the 2:1:3 molar ratio of ligand to cobalt(III) to tetrafluoroborate counter ions (Figure 2.4.21).

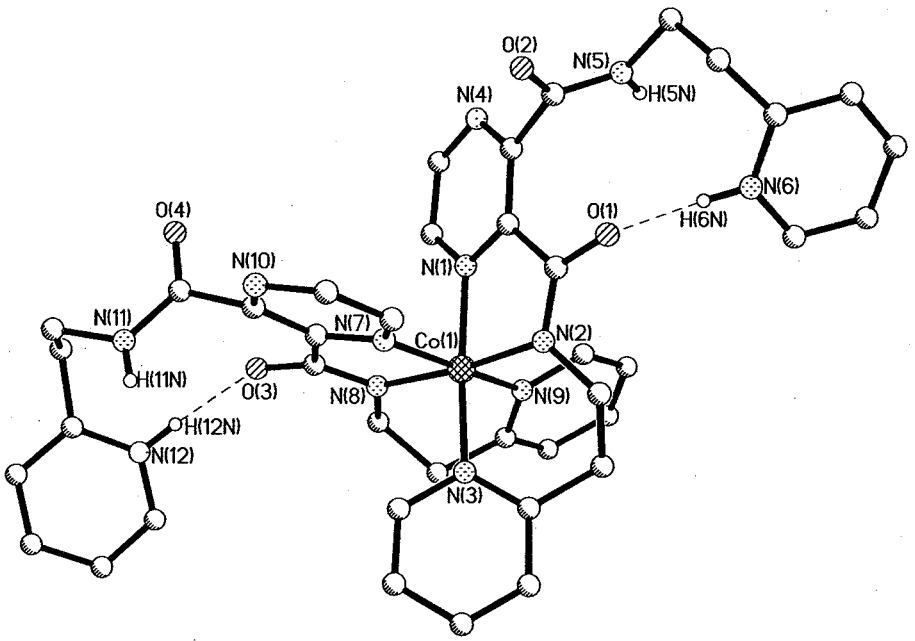

Figure 2.4.21. Molecular structure of $[Co^{III}(H_2\mathbf{L}^{M2})_2]^{3+}$, the complex cation of complex **22** · 2 EtOH. Hydrogen atoms not involved in hydrogen bonds have been omitted for clarity. Selected distances (Å) and angles (°): Co(1)-N(1) 1.956(2), Co(1)-N(2) 1.924(2), Co(1)-N(3) 1.983(2), Co(1)-N(7) 1.972(2), Co(1)-N(8) 1.931(2), Co(1)-N(9) 1.980(2), O(1)···N(6) 2.678(2), O(3)···N(12) 2.729(2); N(1)-Co(1)-N(2) 82.0(1), N(1)-Co(1)-N(3) 171.0(1), N(1)-Co(1)-N(7) 86.0(1), N(1)-Co(1)-N(8) 93.7(1), N(1)-Co(1)-N(9) 89.6(1), N(2)-Co(1)-N(3) 89.7(1), N(2)-Co(1)-N(7) 93.6(1), N(2)-Co(1)-N(8) 173.7(1), N(2)-Co(1)-N(9) 93.5(1), N(3)-Co(1)-N(7) 91.9(1), N(3)-Co(1)-N(8) 94.2(1), N(3)-Co(1)-N(9) 94.5(1), N(7)-Co(1)-N(8) 81.5(1), N(7)-Co(1)-N(9) 171.1(1), N(8)-Co(1)-N(9) 91.1(1).

As previously data implied, the cobalt ion in **22** · 2 EtOH, coordinated by two amide N atoms, has been oxidised in air from cobalt(II) to cobalt(III). The cobalt(III) ion adopts a distorted N_6 octahedral coordination environment, built up from two terdentate binding pockets of two ligands $H_2\mathbf{L}^{M2}$, acting as mono-terdentate ligands. The mean planes of the two meridionally coordinating terdentate binding pockets N(1)-N(2)-N(3) and N(7)-N(8)-N(9) are arranged perpendicularly, with an angle of 89.9°. The resulting structure thus can be described as a "corner-type" precursor complex, as it defines one corner of a square and contains a substitutionally inert cobalt(III) centre. Thus a stepwise, controlled build up of a heterodimetallic [2 × 2]

grid-type complex appears possible with the use of a second type of metal ion (see Scheme 2.11.2).[187]

As was observed for the related dimeric copper(II) complex **18** of the lower ligand homologue, in the mononuclear cobalt(III) complex **22** · 2 EtOH both ligands exist in a neutral zwitterionic form where only one half of the ligand is coordinating in a N_3-terdentate fashion. However, unlike in **18**, the coordination environment around the metal ion in **22** · 2 EtOH is completed by a second N_3-terdentate chelate from a second ligand. As was observed for the copper(II) complex **18** of the lower ligand homologue, the average Co^{III}-N_{amide} distance (1.93 Å) in **22** · 2 EtOH is shorter than the average Co^{III}-N_{py} distances (1.96 Å) or the average Co^{III}-N_{pz} distance (1.98 Å), which results in a compression of the octahedron along the N_{amide}-Co^{III}-N_{amide} axis. The Co^{III}-N_{ligand} distances of **22** · 2 EtOH are around 0.02–0.05 Å longer than in a related $[Co^{III}(\mathbf{L}^{N1})_2]^+$ complex.[188] The planes of the pyrazine rings of **22** · 2 EtOH are not coplanar with the planes of the respective coordinated pyridine rings, but form an average angle of 51.7°. The amide groups involved in cobalt(III) coordination are deprotonated but as observed in the related dinuclear copper(II) complex **18**, the former N-H amide protons have relocated to the pyridine nitrogen atoms of the uncoordinated ligand halves, respectively. There each former N-H amide proton is involved in a strong N-H···O hydrogen bond to the amide oxygen atom of the coordinating deprotonated amide group of the same ligand [N(6)···O(1) 2.678(2) Å, N(12)···O(3) 2.729(2) Å]. The uncoordinated amide groups of the two ligands are still N-protonated, and with an average angle of 82.8°, are almost perpendicular to the respective pyrazine mean ring planes. These N-H amide protons are involved in N-H···F hydrogen bonds to tetrafluoroborate counter ions [N(5)···F(21): 2.996(2) Å, N(11)···F(21A): 3.167(2) Å, N(11)···F(24A): 3.023(2) Å].

UV/VIS spectroscopic studies on $[Co^{III}(H_2L^{M2})_2](BF_4)_3 \cdot EtOH$ (22 · EtOH)

With the exception of some fluoride complexes, six coordinate complexes of cobalt(III) are invariably low spin with the diamagnetic ground state term $^1A_{1g}$. Hence, in the absence of obscuring charge transfer absorptions the two *d-d* transitions to the $^1T_{1g}$ and $^1T_{2g}$ states can be observed (Figure 2.4.22).[130]

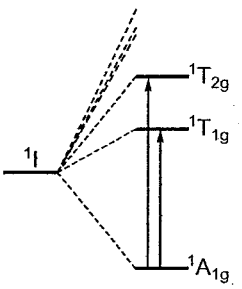

Figure 2.4.22. Partial term splitting diagram for low spin d^6 ions in an octahedral crystal field.

The UV/VIS spectrum of **22** · EtOH showed a very strong absorption band at $\lambda_{max} = 263$ nm ($\varepsilon = 29800$ M^{-1} cm^{-1}, $\tilde{\upsilon} = 38023$ cm^{-1}). This band showed a very weak but distinct shoulder, which was assigned as a *d-d* transition (Figure 2.4.23).

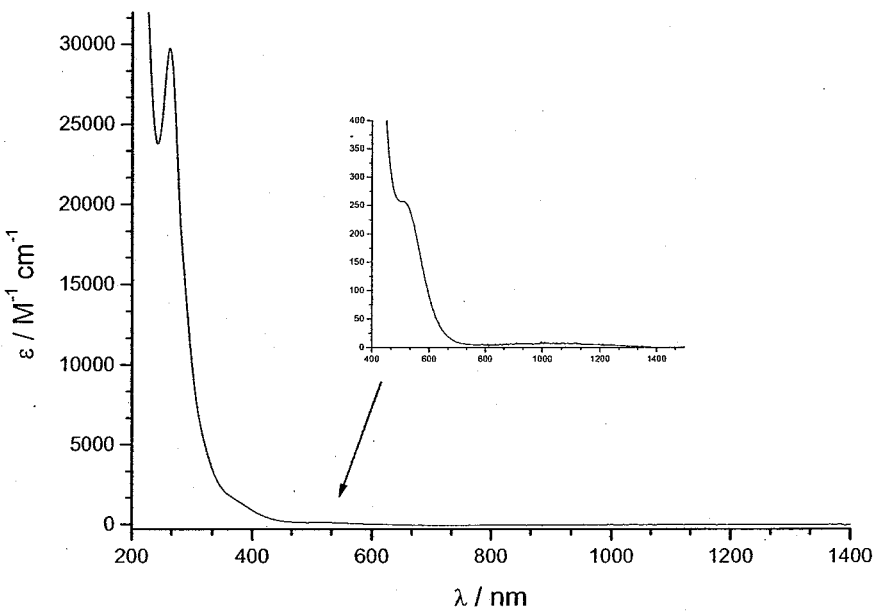

Figure 2.4.23. UV/VIS spectra [MeCN, 1 mM (inset) and 0.1 mM (main)] of $[Co^{III}(H_2\mathbf{L}^{\mathbf{M2}})_2](BF_4)_3 \cdot EtOH$ (**22** · EtOH).

The shoulder (λ_{max} = 510 nm, ε = 257 M^{-1} cm^{-1}, $\tilde{\upsilon}$ = 19608 cm^{-1}) was tentatively assigned to the absorption band of the lower energy transmission $^1A_{1g} \rightarrow {}^1T_{1g}$ and occurred in between the corresponding bands found for the complexes $[Co^{III}(NH_3)_6]^{3+}$ ($\tilde{\upsilon}$ = 21200 cm^{-1}) and $[Co^{III}(H_2O)_6]^{3+}$ ($\tilde{\upsilon}$ = 16500 cm^{-1}).[130]

NMR spectroscopic studies on $[Co^{III}(H_2L^{M2})_2](BF_4)_3 \cdot EtOH$ (22 · EtOH)

As stated earlier, the cobalt(III) ion of the complex $[Co^{III}(H_2L^{M2})_2](BF_4)_3 \cdot EtOH$ (**22** · EtOH) was expected to exist in a low spin ground state, hence being diamagnetic and readily analysable by NMR spectroscopy. Figure 2.4.24 shows the aromatic region of the ^1H NMR spectrum obtained for **22** · EtOH in d^3-MeCN. Compared to the spectrum of the free ligand H_2L^{M2} (Figure 2.1.7), a splitting had occurred for nearly all of the signals. Two distinct singlets at 8.68 and 8.56 ppm were observed for the two inequivalent pyrazine protons. As expected a distinct triplet for the amide proton was observed at 7.87 ppm, with an integration corresponding to one proton per ligand.

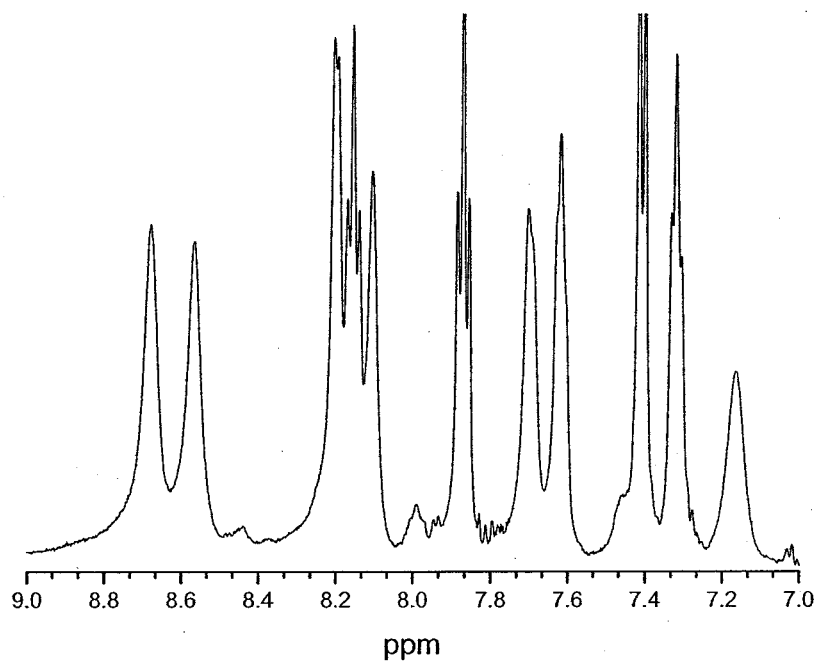

Figure 2.4.24. Aromatic region of the ^1H NMR spectrum (d^3-MeCN) of $[Co^{III}(H_2\mathbf{L^{M2}})_2](BF_4)_3 \cdot EtOH$ (**22** · EtOH).

Cyclic voltammetric studies on $[Co^{III}(H_2L^{M2})_2](BF_4)_3 \cdot EtOH$ (22 · EtOH)

The cyclic voltammogram of **22** · EtOH in acetonitrile showed one irreversible metal-centred reduction wave at E_{pc} = –0.44 V, presumably associated with the reduction $[Co^{III}] \rightarrow [Co^{II}]$, relative to the Fc^+/Fc redox couple (Figure 2.4.25). The obvious similarity to the cyclic voltammogram of the related cobalt(III) complex **21** · 4 H_2O of the lower ligand homologue, with a shift of $\Delta E_{(22,21)}$ = 0.24 V to a more positive potential, was not unexpected as both compounds were believed to have homologous structures.

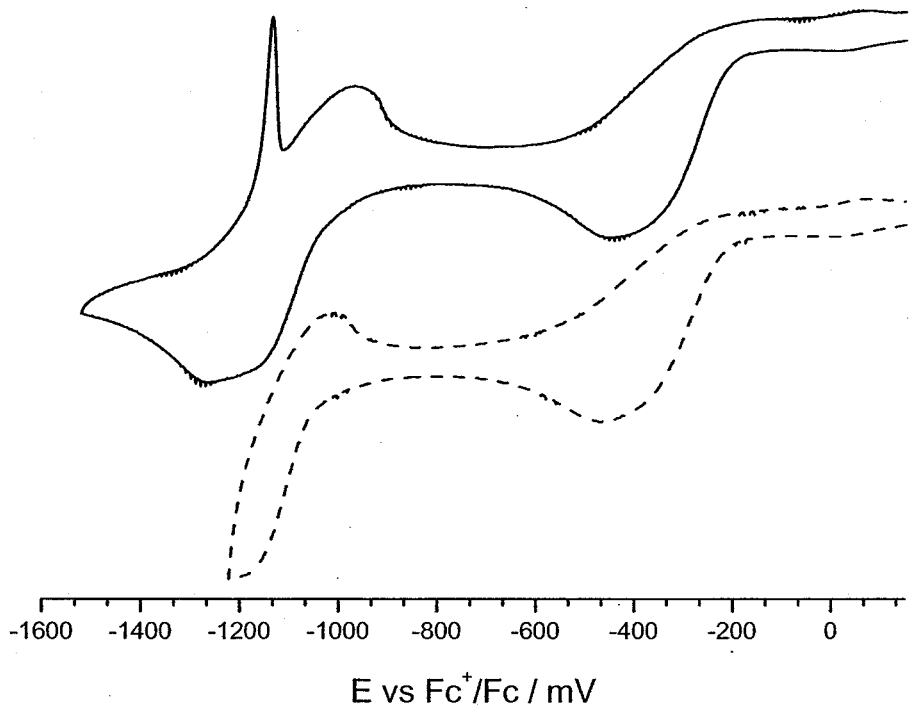

Figure 2.4.25. Cyclic voltammograms (MeCN, scan rate: 50 mV s^{-1}) of $[Co^{III}(H_2\mathbf{L^{M2}})_2](BF_4)_3 \cdot EtOH$ (**22** · EtOH).

At lower potentials a partially reversible reduction wave was noted in the cyclic voltammogram of **22** · EtOH. The reduction appeared at $E_{1/2}$ = –1.10 V (ΔE = 0.25 V), with a shift of ΔE = 0.28 V to more a positive potential, compared to the related complex **21** · 4 H_2O of the lower ligand homologue. The major difference in the cyclic voltammograms of the complexes **22** · EtOH and **21** · 4 H_2O of the two homologous ligands was that in the cyclic voltammogram of **22** · EtOH a stripping peak appeared

at E_{pa} = –1.14 V on lowering the potential below around E_{pc} = –1.27 V before returning, experiencing an increase in its intensity on lowering the return voltage or the scan rate.

Complexations with nickel(II) and H_2L^{M1} or H_2L^{M2}

The reactions of H_2L^{M1} or H_2L^{M2} and nickel(II) tetrafluoroborate hexahydrate in acetonitrile or ethanol solution employing a 1:1 molar ratio, led to the precipitation of pale beige inhomogeneous solids of unknown compositions. Further attempts at isolating pure samples were unsuccessful. Attempts at recrystallisation from acetonitrile, ethanol or mixed solvent systems, by vapour diffusion of diethyl ether, layering with toluene, or slow evaporation, failed to give single crystals.

Complexations with zinc(II) and H_2L^{M1} or H_2L^{M2}

The employment of H_2L^{M1} or H_2L^{M2} and zinc(II) tetrafluoroborate hydrate in a molar ratio of ligand to metal of 1:1 in acetonitrile solution failed to give defined coordination compounds. Instead, in both cases a sticky solid was isolated, which was believed to be the respective ligands.

2.4.3. Summary

The molecular structures of the dimeric copper(II) complex **18**, the tetrameric copper(II) complex **19** · 3 MeCN · 0.5 H_2O and the monomeric cobalt(III) complex **22** · 2 EtOH have been presented. Thus it has been shown that even in complexes involving an amide nitrogen donor atom, the ligands H_2L^{M1} and H_2L^{M2} can exist in a

neutral state. In these complexes the ligands have been found to exist in zwitterionic forms, where the former N-H amide proton has relocated to a free pyridine nitrogen atom of the same ligand, leading to a complex fragment as indicated in Figure 2.4.26.

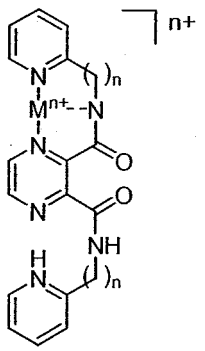

Figure 2.4.26. Zwitterionic fragment of complexes involving only one terdentate binding pocket.

The homologous ligands H_2L^{M1} and H_2L^{M2} have been found to reflect a variety of coordination modes. In Section 2.2.1 bis-terdentate binding was observed in **6b** · MeCN of the lower ligand homologue. The dimeric complex **18** employed H_2L^{M1} as hybrid N_3-O terdentate-mondentate ligand whereas the related complex **19** · 3 MeCN 0.5 H_2O utilised the higher ligand homologue H_2L^{M2} as hybrid N_3-NO terdentate-bidentate ligand (Section 2.4.1).

Apart from copper(II) both ligands have been found to be able to coordinate as N_3-terdenate chelates to cobalt ions, bringing about the air oxidation of the initially employed cobalt(II) to cobalt(III). In **22** · 2 EtOH the ligand was utilised as N_3 mono-terdentate ligand. To complete the preferred octahedral coordination sphere of the cobalt(III) a second N_3-terdentate ligand was bound, forming a 90° angle to the former N_3-chelate plane, leading to a precursor "corner-type' complex.

2.5. *Coordination of the ligands H_2L^{M1} and H_2L^{M2}, employing a 1:1:1 molar ratio of ligand to metal(II) ions to base*

In Section 2.4 it has been shown that reactions employing H_2L^{M1} or H_2L^{M2} and metal(II) salts in a 1:1 molar ratio did not lead to the complete deprotonation of the ligands. Thus it has been shown that coordination of a copper(II) or a cobalt(III) ion into one N_3-terdentate binding pocket of the ligands H_2L^{M1} or H_2L^{M2} resulted in the deprotonation of the respective amide group and in the relocation of the former N-H amide proton to the pyridine nitrogen of the other ligand half. This led to the effective blockage of the latter ligand half as an N_3-terdentate binding site. It was therefore suggested that the formation of grid-type complexes of the kind $[M^{II}_4(HL^{M1})_4]^{4+}$ and $[M^{II}_4(HL^{M2})_4]^{4+}$, with N_6 coordinated metal(II) ions, could only be formed by deliberate *in situ* deprotonation of the respective ligands or by deprotonation of respective precursor complexes, like $[Cu^{II}_2(H_2L^{M1})_2(MeCN)_2](BF_4)_4$ (**18**) or $[Cu^{II}_4(H_2L^{M2})_2(HL^{M2})_2](BF_4)_6$ (**19**), in solution.

2.5.1. *Copper(II) salts*

Complexation with H_2L^{M1} and copper(II) tetrafluoroborate tetrahydrate

The addition of one equivalent of triethylamine to a dark navy blue reaction mixture, obtained using a 1:1 molar ratio of H_2L^{M1} and copper(II) tetrafluoroborate tetrahydrate in acetonitrile, resulted in a drastic colour change to grass green

(Figure 2.5.1). The same colour change was observed on addition of triethylamine to an acetonitrile solution of the dimeric complex $[Cu^{II}_2(H_2L^{M1})_2(MeCN)_2](BF_4)_4$ (**18**) in a 1:1 molar ratio per ligand strand.

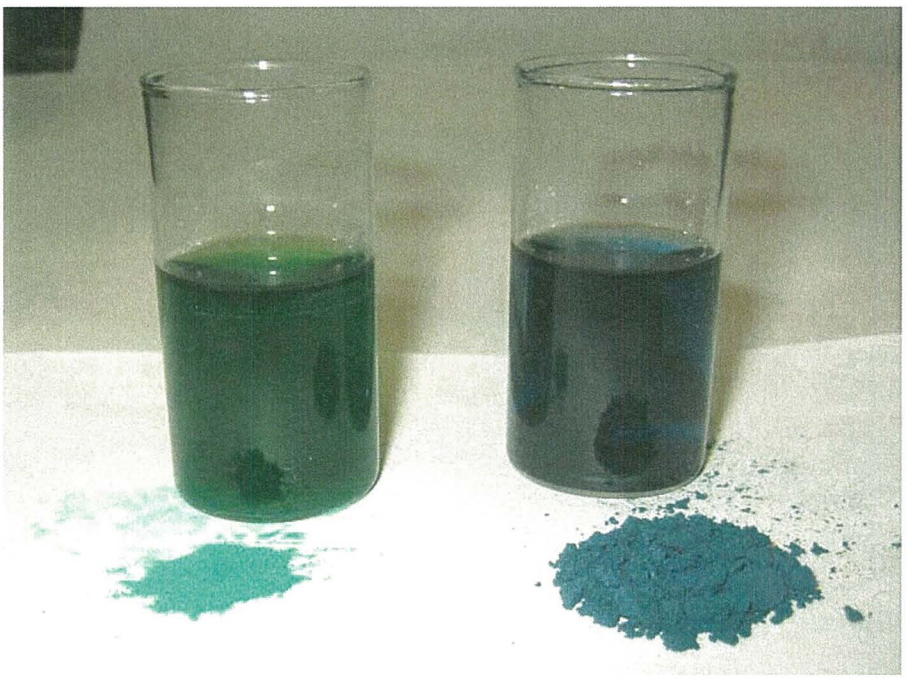

Figure 2.5.1. Colour change observed by the *in situ* deprotonation of a dark navy blue solution of H_2L^{M1} and copper(II) in a 1:1 molar ratio (right side) with 1 equivalent triethylamine, resulting in a grass green solution (left side).

By vapour diffusion of diethyl ether into the reaction mixture complex **23** was isolated as a grass green crystalline solid in around 70 % yield (Scheme 2.5.1). Complex **23** was also isolated, in around 60 % yield, by the treatment of a solution of the dimeric complex **18** in acetonitrile with triethylamine, resulting in an overall molar ratio of 1:1:1 of ligand to copper(II) to base (Scheme 2.5.1). The compound **23** was only slightly soluble in *N,N*-dimethylformamide and acetonitrile and was practically insoluble in other common polar solvents like alcohols, water or acetone. The use of a molar ratio of ligand H_2L^{M1} to triethylamine of 1:2 under otherwise identical reaction conditions resulted in the formation of an inhomogeneous unidentified amorphous green solid. Elemental analysis of **23** suggested that the compound could be formulated as $[Cu^{II}(HL^{M1})]_n(BF_4)_n$ which was in good agreement with the stoichiometry required for the desired [2 × 2] grid structure of the type b) in Scheme 2.4.1 (n = 4). It was therefore suggested that the diamide ligand was indeed

deprotonated, but only monodeprotonated. Conductivity measurements of **23** in acetonitrile solution [Λ_m(MeCN) = 110 mol^{-1} cm^2 Ω^{-1} per ligand] corroborated this result further.

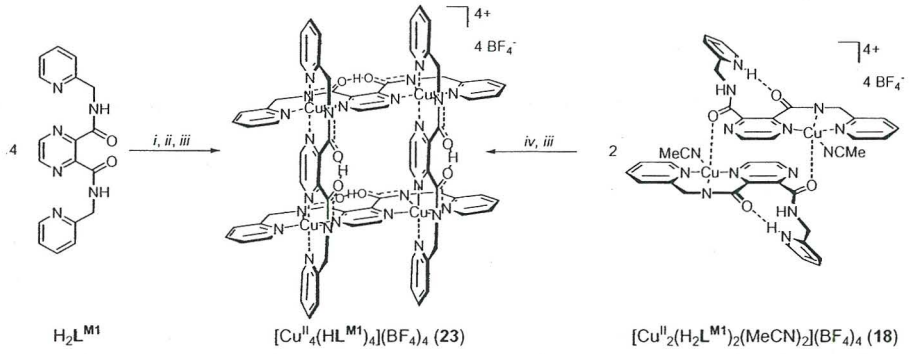

Scheme 2.5.1. Synthesis of **23**. Reagents and conditions: (*i*) 1 eq. $Cu(BF_4)_2 \cdot 4\ H_2O$, MeCN, RT; (*ii*) 1 eq. NEt_3; (*iii*) Et_2O (vapour diffusion); (*iv*) 2 eq. NEt_3.

The positive ion electrospray mass spectrum of **23** in acetonitrile (Figure 2.5.2) showed peaks at *m/z* = 908.0, 576.3 and 409.9 that were assigned to the tetranuclear species $\{[Cu^{II}_4(HL^{M1})_4](BF_4)_2\}^{2+}$, $\{[Cu^{II}_4(HL^{M1})_4](BF_4)\}^{3+}$ and $[Cu^{II}_4(HL^{M1})_4]^{4+}$, respectively, and revealed the stepwise loss of tetrafluoroborate counter ions, based on the tetranuclear parent complex $[Cu^{II}_4(HL^{M1})_4](BF_4)_4$ (**23**) and further supported the proposed [2 × 2] grid structure of the compound.

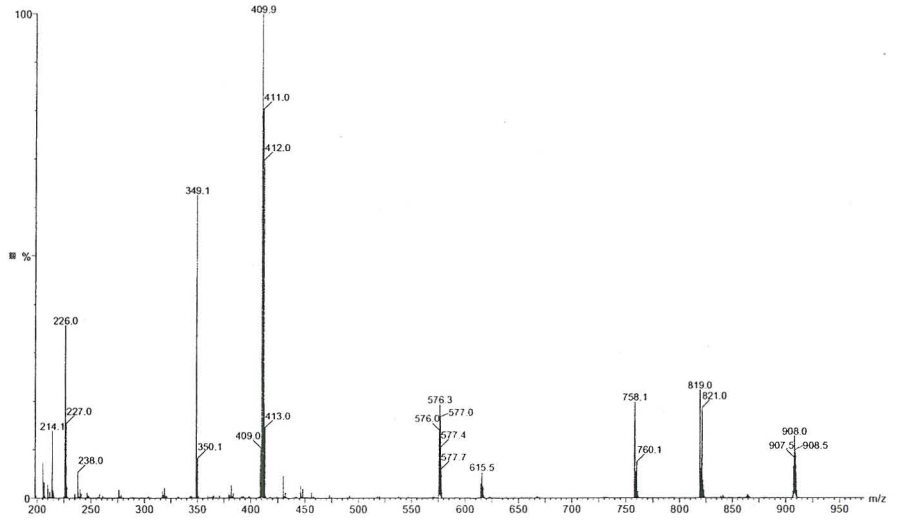

Figure 2.5.2. ESI-MS spectrum (MeCN) of $[Cu^{II}_4(HL^{M1})_4](BF_4)_4$ (**23**).

Furthermore a peak at *m/z* = 819.0 was assigned to the species $[Cu^{II}_4(HL^{M1})_2(L^{M1})_2]^{2+}$ revealing the loss of two of the four former N-H amide protons retained by the grid

complex. A smaller peak at m/z = 615.5 was assigned to the species $[Cu^{II}_6(HL^{M1})_4(L^{M1})_2]^{4+}$ indicating the formation of a hexanuclear species in the conditions of the experiment. The peak of the protonated ligand $(H_3L^{M1})^+$ was identified at m/z = 349.1.

IR spectroscopic studies on $[Cu^{II}_4(HL^{M1})_4](BF_4)_4$ (23)

The IR spectrum of **23** showed only one ν_{CO} absorption band at $\tilde{\upsilon}$ = 1651 cm^{-1}, supporting the assumption of the equivalence of the two amide functions of the ligands (Figure 2.5.3).

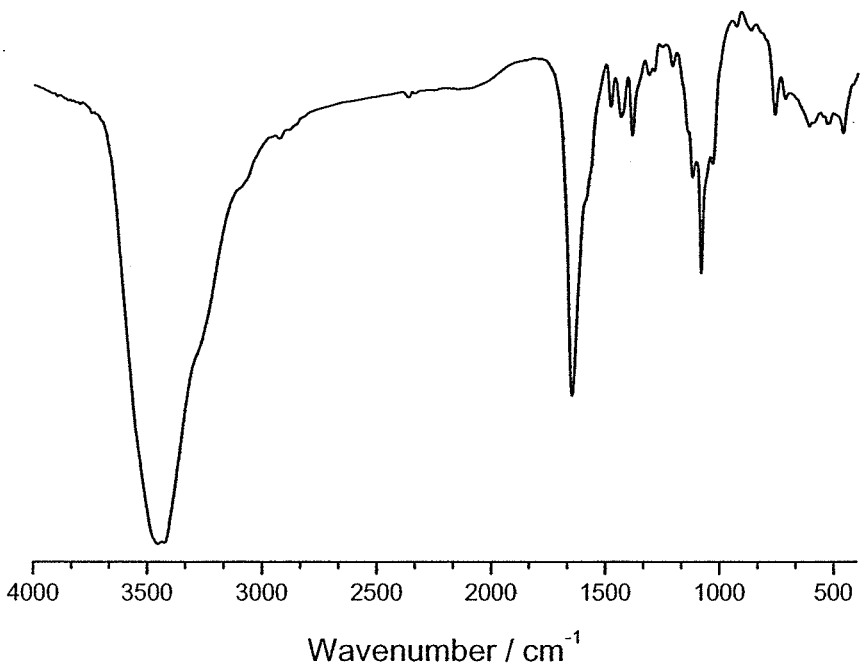

Figure 2.5.3. IR spectrum (KBr) of $[Cu^{II}_4(HL^{M1})_4](BF_4)_4$ (**23**).

Compared to the IR spectrum of the dinuclear complex $[Cu^{II}_2(HL^{M1})(MeCN)_2(H_2O)_2](BF_4)_3$ (**6**), the ν_{CO} vibration band was remarkably shifted to higher wavenumbers ($\Delta\nu_{CO(6,23)}$ = 42 cm^{-1}) (see Table 2.5.1). The expected presence of tetrafluoroborate ions was confirmed with a broad split band centred at $\tilde{\upsilon}$ = 1083 cm^{-1}.

Single crystal X-ray structural analysis of $[Cu^{II}_4(HL^{M1})_4](BF_4)_4 \cdot 3.5$ MeCN (23 · 3.5 MeCN)

Eventually, heavily twinned crystals of two different crystal types of $[Cu^{II}_4(HL^{M1})_4](BF_4)_4 \cdot 3.5$ MeCN (**23** · 3.5 MeCN) suitable for X-ray crystal structure determinations were obtained by vapour diffusion of diethyl ether into solutions of **23** in acetonitrile. As the two molecular structures obtained by the X-ray crystal structure determinations are very similar only the molecular structure of the monoclinic tetragonally twinned cation $[Cu^{II}_4(HL^{M1})_4]^{4+}$ of the complex **23** · 3.5 MeCN will be discussed (Figure 2.5.4).

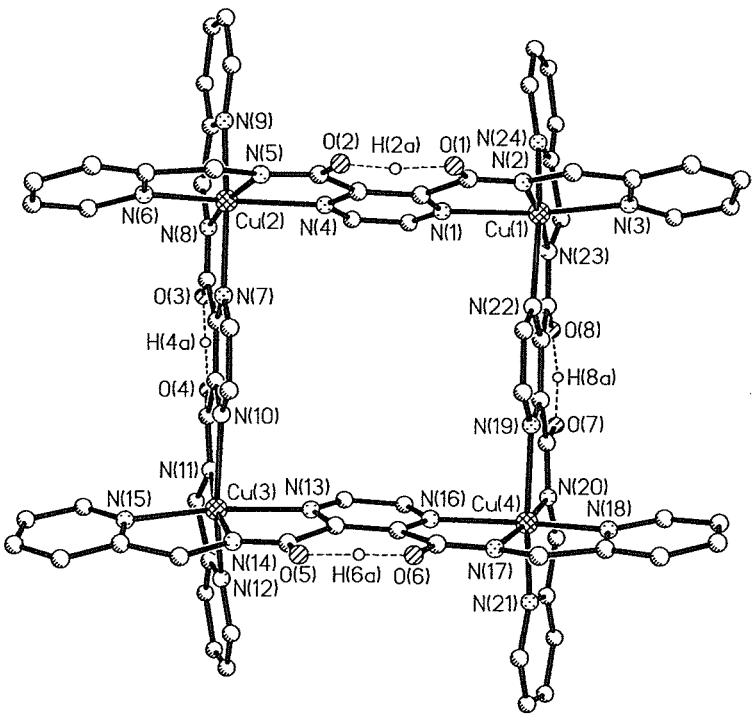

Figure 2.5.4. Molecular structure of $[Cu^{II}(HL^{M1})]_4^{4+}$, the cation of complex **23** · 3.5 MeCN. Hydrogen atoms, except H(2a), H(4a), H(6a) and H(8a), have been omitted for clarity. Selected distances (Å) and angles (°): Cu(1)-N(1) 2.232(8), Cu(1)-N(2) 1.90(1), Cu(1)-N(3) 2.170(9), Cu(1)-N(22) 2.22(1), Cu(1)-N(23) 2.00(1), Cu(1)-N(24) 2.193(9), Cu(1)···Cu(2) 7.150(3), Cu(2)···Cu(3) 7.108(3), Cu(3)···Cu(4) 7.101(3), Cu(4)···Cu(1) 7.132(3), Cu(1)···Cu(3) 10.051(3), Cu(2)···Cu(4) 10.035(3), O(1)···O(2) 2.44(1), O(3)···O(4) 2.30(1), O(5)···O(6) 2.45(1), O(7)···O(8) 2.35(1); N(1)-Cu(1)-N(2) 76.7(4), N(1)-Cu(1)-N(3) 155.7(3), N(1)-Cu(1)-N(22) 87.6(4), N(1)-Cu(1)-N(23) 98.9(3), N(1)-Cu(1)-N(24) 89.1(3), N(2)-Cu(1)-N(3) 79.1(4), N(2)-Cu(1)-N(22) 96.7(4), N(2)-Cu(1)-N(23) 172.6(4), N(2)-Cu(1)-N(24) 108.4(4), N(3)-Cu(1)-N(22) 93.2(3), N(3)-Cu(1)-N(23) 104.9(3), N(3)-Cu(1)-N(24) 100.5(3), N(22)-Cu(1)-N(23) 77.0(4), N(22)-Cu(1)-N(24) 153.2(4), N(23)-Cu(1)-N(24) 77.2(3), Cu(1)···Cu(2)···Cu(3) 89.64(4), Cu(2)···Cu(3)···Cu(4) 89.86(4), Cu(3)···Cu(4)···Cu(1) 89.85(4), Cu(4)···Cu(1)···Cu(2) 89.28(4).

The [2 × 2] grid-type molecular structure of **23** · 3.5 MeCN was unambiguously proven by the X-ray crystal structure determination and presents a rare example of a pyrazine-based grid compound,[101] and to the best of our knowledge was the first example of a grid-type structure being formed by a self-assembly following a precursor modification.[67] As expected, all four ligands in **23** · 3.5 MeCN act as bis-terdentate chelates, each terdentate binding pocket coordinating in a meridional fashion thus bridging the copper(II) ions via the pyrazine units and giving rise to a grid-like arrangement of the ligand strands. As was found for the tetrameric complex $[Cu^{II}_4(H_2L^{M2})_2(HL^{M2})_2](BF_4)_6 \cdot 3\ MeCN \cdot 0.5\ H_2O$ (**19** · 3 MeCN · 0.5 H_2O) of the higher ligand homologue, the $Cu^{II}\cdots Cu^{II}$ distances are similar but not equal and two shorter [Cu(2)···Cu(3) 7.108(3) Å and Cu(3)···Cu(4) 7.101(3) Å] and two slightly longer [Cu(1)···Cu(2) 7.150(3) Å and Cu(1)···Cu(4) 7.132(3) Å] distances are observed. The average $Cu^{II}\cdots Cu^{II}$ distance (7.123 Å) is slightly longer than the average $Cu^{II}\cdots Cu^{II}$ distance of the tetrameric complex **19** · 3 MeCN · 0.5 H_2O of the higher ligand homologue (7.024 Å) and is significantly longer than the $Cu^{II}\cdots Cu^{II}$ distance in the dinuclear complex **6b** · MeCN (6.745 Å). Exactly as in **19** · 3 MeCN · 0.5 H_2O, the copper(II) ions of **23** · 3.5 MeCN are shifted by ca. 0.28 Å in an up-down-up-down fashion relative to the Cu^{II}_4 mean plane, leading to a small tetrahedral distortion of the Cu^{II}_4 square. The average $Cu^{II}\cdots Cu^{II}\cdots Cu^{II}$ angle of the square is 89.7°. Unlike in **19** · 3 MeCN · 0.5 H_2O with its distorted N_4O square pyramidal copper(II) ions, the copper(II) ions of **19** · 3 MeCN · 0.5 H_2O are in a distorted N_6 octahedral coordination sphere, encapsulated by two N_3-terdentate binding sites of the perpendicular ligands. The mean planes defined by the donor atoms of the N_3-terdentate binding pockets are perpendicular to each other, forming an average angle of 89.6°. The bis-terdentate ligand strands are very flat and have a maximum deviation from the ligand plane of only 0.301 Å [$C(12)_{pyridine}$], 0.278 Å [$C(35)_{methylene}$], 0.254 Å [$C(52)_{pyridine}$] and 0.273 Å [$C(72)_{pyridine}$], respectively. The planes of the pyridine rings intersect with the plane of the pyrazine ring of the same ligand at angles in the range of 5.7–10.1°. As was found for the dimeric copper(II) complex $[Cu^{II}_2(H_2L^{M1})(MeCN)_2](BF_4)_4$ (**18**) of the same

ligand, the average Cu^{II}-N_{amide} bond length of **23** · 3.5 MeCN (1.94 Å) is significantly shorter than the average Cu^{II}-N_{pz} (2.22 Å) or Cu^{II}-N_{py} (2.14 Å) bond length. These values compare well to those of similar complexes of HL^{N1},[123] HL^{N2},[124] HL^{N11}[125] or HL^{N12} (Figure 2.2.4).[126] The tetragonality factor T is given by the mean in-plane Cu^{II}-L distance / mean out-of-plane Cu^{II}-L distance, where $T > 1$ for a compressed octahedron and $T < 1$ for a elongated octahedron.[130,182,189] For the tetranuclear complex **23** · 3.5 MeCN the mean planes around the copper(II) ions are defined by the $N_{heterocyle}$ atoms, which lie in the Cu^{II}_4 mean plane. The CuN_6 octahedra are compressed with the tetragonality factor[130] ranging from T = 1.103–1.132 and the average tetragonality factor T_{av} = 1.122. The compressed axes lie parallel to each other and perpendicular to the Cu^{II}_4 mean plane. As found for the dinuclear complex **6b** · MeCN, all N-H amide groups of the complex cation of **23** · 3.5 MeCN are deprotonated but each ligand still retains one former N-H amide proton in an O···H···O hydrogen bond between its two amide carbonyl oxygen atoms (see Section 3.4.8 and 3.4.9). The O···O separations in the resulting seven-membered rings range from 2.30–2.45 Å.

UV/VIS spectroscopic studies on $[Cu^{II}_4(HL^{M1})_4](BF_4)_4$ (23)

The UV/VIS spectrum of **23** in acetonitrile solution showed a very strong sharp absorption peak at λ_{max} = 266 nm (ε = 72500 M^{-1} cm^{-1}) (Figure 2.5.5).

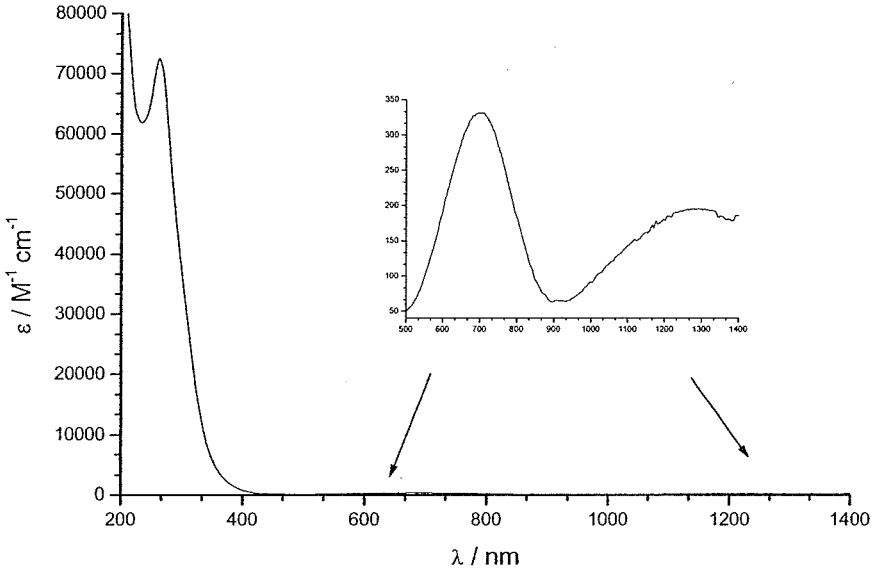

Figure 2.5.5. UV/VIS spectra [MeCN, 0.25 mM (inset) and 0.025 mM (main)] of $[Cu^{II}_4(HL^{M1})_4](BF_4)_4$ (**23**).

Furthermore a relatively weak broad absorption band was present at λ_{max} = 699 nm (ε = 331 M^{-1} cm^{-1}) that was assigned to the *d-d* transition $^2E_g \rightarrow {}^2T_{2g}$ of the copper(II) d^9 ion in an octahedral crystal field (Figure 2.5.6).[190] The width of the band was explained with the compressed octahedral environment of the copper(II) ions, which was expected to lead to a splitting of this transition band. The crystal field splitting energy was given by Δo = 14300 cm^{-1} ($[Cu^{II}(H_2O)_6]^{2+}$, Δo = 12600 cm^{-1}) (Figure 2.5.6).[190]

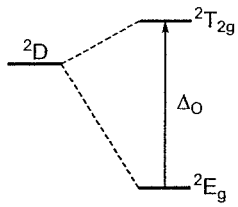

Figure 2.5.6. Point Charge splitting diagram for d^9 ions in an octahedral crystal field.

At very low energy an unexpected second very broad weak absorption band was observed at λ_{max} = 1290 nm (ε = 195 M^{-1} cm^{-1}, $\tilde{\upsilon}$ = 7750 cm^{-1}).

The deprotonation of the dark navy blue dimeric complex **18** and the formation of the grass green tetranuclear grid complex **23** could be monitored by UV/VIS titration using either triethylamine or 1,4-diazabicyclo[2,2,2]octane (DABCO) as base (Figure 2.5.7).

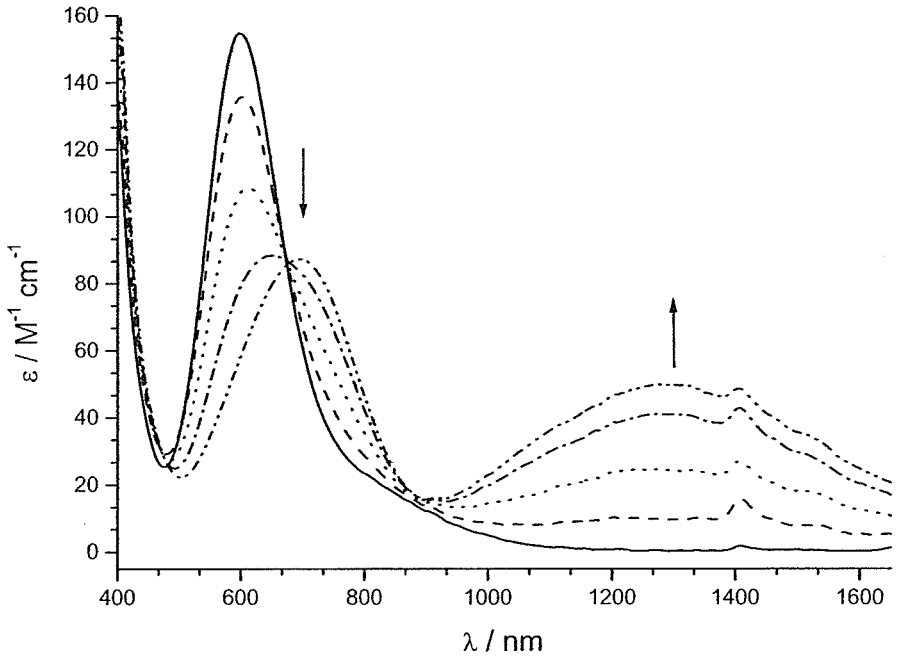

Figure 2.5.7. UV/VIS titration [MeCN, 1 mM per copper(II)] of $[Cu^{II}_2(H_2\mathbf{L}^{M1})_2(MeCN)_2](BF_4)_4$ (**18**) (solid line) with DABCO: [0.0 eq. DABCO = **18** (solid line), **18** + 0.25 eq. DABCO (dashed line), **18** + 0.5 eq. DABCO (dotted line), **18** + 0.75 eq. DABCO (dash-dotted line), **18** + 1.0 eq. DABCO (dash-dot-dotted line).

The reverse process of the protonation of the grass green grid compound **23** of the monodeprotonated ligand $(HL^{M1})^-$ with *p*-toluene sulfonic acid (*p*-TSA) and the formation of the dark navy blue complex **18** of the fully protonated zwitterionic form of the ligand H_2L^{M1} could also be monitored by UV/VIS titration (Figure 2.5.8). However, the back titration with *p*-toluene sulfonic acid was not complete and after a few minutes a bluish solid, probably a complex containing *p*-TSA as counter ion and/or coligand, started to precipitate.

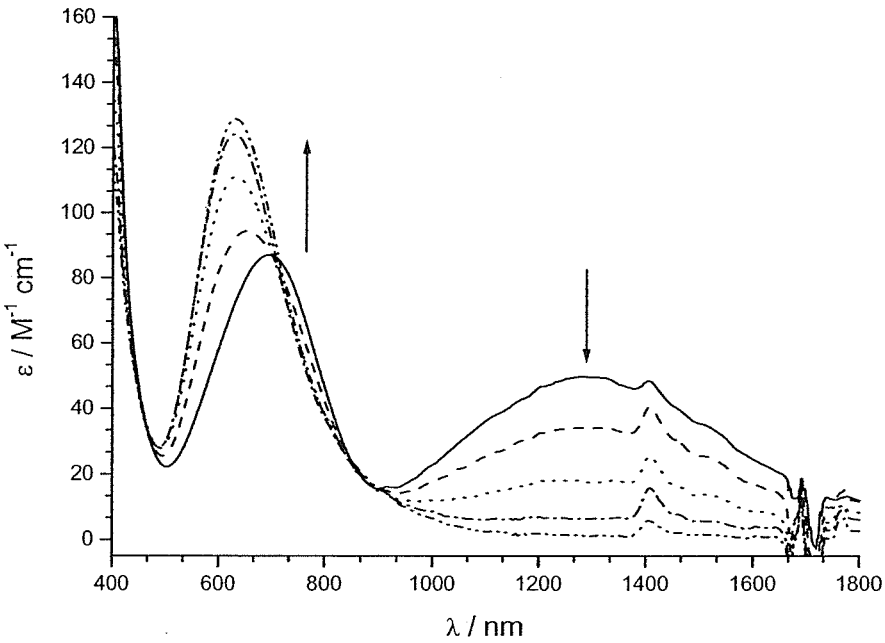

Figure 2.5.8. UV/VIS back titration [MeCN, 1 mM per copper(II)] of $[Cu^{II}_4(HL^{M1})_4](BF_4)_4$ (**23**) (**18** + 1 eq. DABCO) with *p*-TSA: [0.0 eq. *p*-TSA = **23** (solid line), **23** + 0.25 eq. *p*-TSA (dashed line), **23** + 0.5 eq. *p*-TSA (dotted line), **23** + 0.75 eq. *p*-TSA (dash-dotted line), **23** + 1.0 eq. *p*-TSA (dash-dot-dotted line)].

Cyclic voltammetric studies on $[Cu^{II}_4(HL^{M1})_4](BF_4)_4$ (23)

The cyclic voltammogram of the tetranuclear complex $[Cu^{II}_4(HL^{M1})_4](BF_4)_4$ (**23**) in acetonitrile solution showed one irreversible metal-centred two-electron reduction peak at E_{pc} = –0.89 V, relative to the Fc^+/Fc redox couple (Figure 2.5.9). Controlled potential coulometry at E = –0.90 V confirmed that the first process corresponded a two-electron reduction of the initial tetrameric copper(II) complex. The reduction was therefore assigned to $[Cu^{II}_4] \rightarrow [Cu^{II}_2Cu^{I}_2]$. At the slightly lower potential of E_{pc} = –0.99 V a second reduction wave was observed, associated with an oxidation process at E_{pa} = –0.61 V. Interestingly, the intensity of the oxidation process increased slightly on lowering the return voltage, but did not increase on decreasing the scan rate from 50 mV s^{-1} to 10 mV s^{-1}. Also the potential of the oxidation process was slightly shifted to less negative values on lowering the return voltage. Strikingly, in contrast to the cyclic voltammogram of the complex **6b** · MeCN, no intense stripping

peak was observed in the cyclic voltammogram of the grid compound **23**, even when scanning to E = –2.5 V. The shift and the increasing intensity observed for the oxidation process at around E_{pa} = –0.61 V could be due to a slow disproportionation process $[Cu^{I}_4] \rightarrow [Cu^{II}_2Cu^{0}_2]$ which, when the return voltage was lowered, had more time to proceed. Owing to the different redox behaviour it was unlikely that the oxidation process of **23** had occurred by a similar process to that observed in **6b** · MeCN.

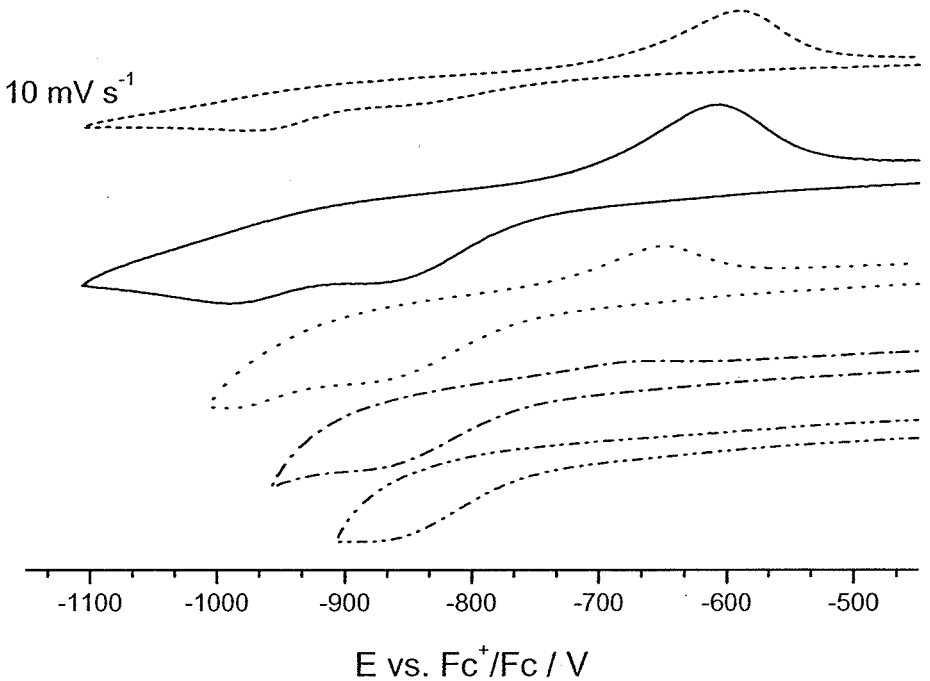

Figure 2.5.9. Cyclic voltammograms (0.5 mM, 0.1 M TBAP, MeCN, scan rate: 50 mV s^{-1}: solid line, dashed line, dash-dotted line and dash-dot-dotted line; 10 mV s^{-1}: short dashed line) of $[Cu^{II}_4(HL^{M1})_4](BF_4)_4$ (**23**).

Magnetic studies on $[Cu^{II}_4(HL^{M1})_4](BF_4)_4$ (23)

Figure 2.5.10 shows the temperature dependence of μ_{eff} per copper(II) ion and Figure 2.5.11 shows the temperature dependence of χ_m, per copper(II) ion of the [2 × 2] grid compound **23** respectively.

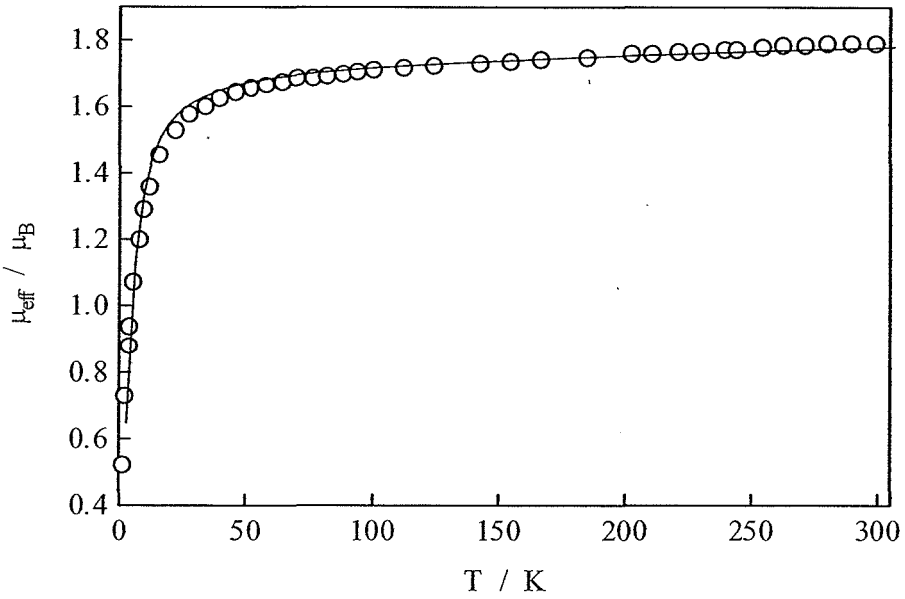

Figure 2.5.10. Thermal variation of the magnetic moment μ_{eff} (◦◦) of $[Cu^{II}_4(HL^{M1})_4](BF_4)_4$ (**23**). The solid line represents the best fit.

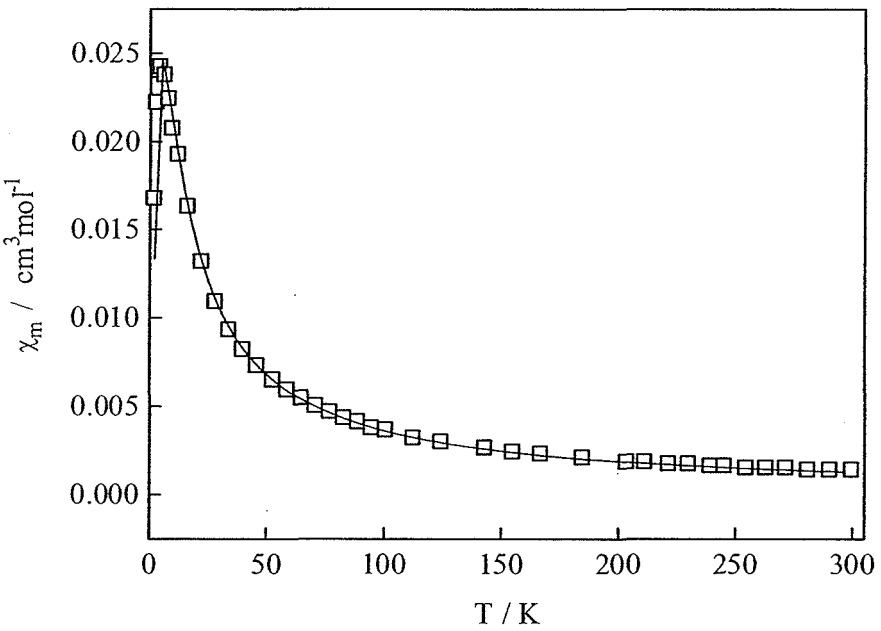

Figure 2.5.11. Thermal variation of the molar susceptibility χ_m (▫▫) of $[Cu^{II}_4(HL^{M1})_4](BF_4)_4$ (**23**). The solid line represents the best fit.

As similarly observed for the dinuclear complex **6b** · MeCN of the same ligand and the square-like tetranuclear complex **19** · 4 H_2O of the higher ligand homologue, the temperature dependence of the magnetic susceptibility showed a maximum at 6.3 K (0.024 cm^3 mol^{-1}) due to weak antiferromagnetic coupling. Consequently the value of μ_{eff} decreased continuously, when the temperature was lowered, from

μ_{eff} = 1.8 μ_B to μ_{eff} = 0.52 μ_B at 2 K. The best fit for the [2 × 2] grid-type complex $[Cu^{II}_4(HL^{M1})_4](BF_4)_4$ (**23**) was obtained using two slightly different coupling constants, compared to using one as anticipated for a perfect square. This might reflect the small differences in the copper(II)···copper(II) distances in the structure. The coupling constants were calculated as $J_{13} = J_{24} = -2.58$ cm^{-1} and $J_{14} = J_{23} = -3.36$ cm^{-1} (Figure 2.3.13), and were around half of the values, compared to $J_{(6b)}$ of the dinuclear complex **6b** · MeCN of the same ligand. The following parameters g = 2.00, and $TIP = 84 \times 10^{-6}$ cm^3 mol^{-1} and monomeric impurity = 4 % were calculated for **23**.

Metathesis of 23 with ammonium hexafluorophosphate

The first datasets obtained by X-ray crystal analyses of the (by eye) perfectly octahedrally shaped grass green crystals of the tetrafluoroborate complex **23** unfortunately did not yield a molecular structure. Initially, this was attributed to poor crystal quality but this was later found to be due to problems with the diffractometers. In the meantime a change of counter ion was expected to be a promising way to obtain single crystals of better quality

Metathesis of the tetrafluoroborate compound **23** into the corresponding hexafluorophosphate salt **23b** was carried out *in situ* in acetonitrile solution by the addition of a tenfold excess of ammonium hexafluorophosphate followed by precipitation of the resulting hexafluorophosphate compound with ethanol (Scheme 2.5.2). Addition of a second tenfold excess of ammonium hexafluorophosphate to an acetonitrile solution of the crude product and subsequent precipitation with ethanol gave analytically pure compound **23b** in 51 % yield. By vapour diffusion of diethyl ether into a solution of **23b** in acetonitrile a crystalline sample was isolated as a grass green solid.

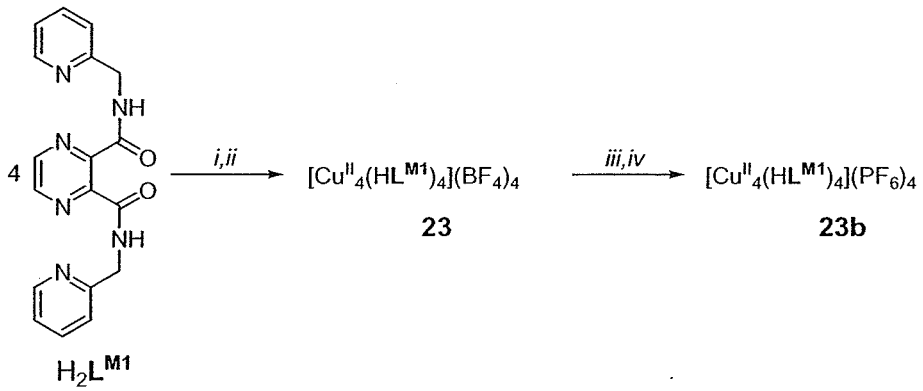

Scheme 2.5.2. Synthesis of **23b**. Reagents and conditions: (*i*) 1 eq. $Cu(BF_4)_2 \cdot 4\ H_2O$, MeCN, RT; (*ii*) 1 eq. NEt_3; (*iii*) 10 eq. H_4NPF_6, MeCN, RT, (*iv*) EtOH.

Results from elemental analysis and from conductivity measurements in acetonitrile solution [Λ_m = 110 mol^{-1} cm^2 Ω^{-1} per ligand] matched sufficiently well with the proposed formulation of $[Cu^{II}_4(HL^{M1})_4](PF_6)_4$ (**23b**). Unfortunately, the positive ion electrospray mass spectrum of **23b** in acetonitrile showed no evidence of polynuclear species but peaks at *m/z* = 410.0 and 266.0 were assigned to the mononuclear species $[Cu^{II}(HL^{M1})]^+$ and $[Cu^{II}(H_2L^{M1})(MeCN)]^{2+}$, respectively. Peaks of the protonated ligand species $[H_3L^{M1}]^+$ and $[H_4L^{M2}]^{2+}$ were identified at *m/z* = 349.1 and 175.0, respectively. Two smaller peaks at the higher values *m/z* = 456.0 and 537.9 could not be assigned. Crystals obtained by vapour diffusion of diethyl ether into a solution of **23b** in acetonitrile were very small and seemed, by eye, to be of no better quality than the crystals of the tetrafluoroborate complex **23**. Fortunately, recollection of data on freshly crystallised crystals of the tetrafluoroborate complex **23** eventually resulted in a molecular structure, which confirmed the proposed [2 × 2] grid-type structure of $[Cu^{II}_4(HL^{M1})_4](BF_4)_4$ (Figure 2.5.4).

IR spectroscopic studies on $[Cu^{II}_4(HL^{M1})_4](PF_6)_4$ (23b)

The IR spectrum of compound **23b** showed the presence of hexafluorophosphate with a band at $\tilde{\nu}$ = 843 cm^{-1}[141] and no evidence of remaining tetrafluoroborate anions (Figure 2.5.12, Table 2.5.1). It was noted that the band of the

νCO vibration in **23b** ($\tilde{\upsilon}$ = 1640 cm^{-1}) was shifted ($\Delta\tilde{\upsilon}_{(23,23b)}$ = 11 cm^{-1}) to lower wavenumbers, compared to the IR spectrum of **23**, and that a second band in this region was observed at $\tilde{\upsilon}$ = 1615 cm^{-1}.

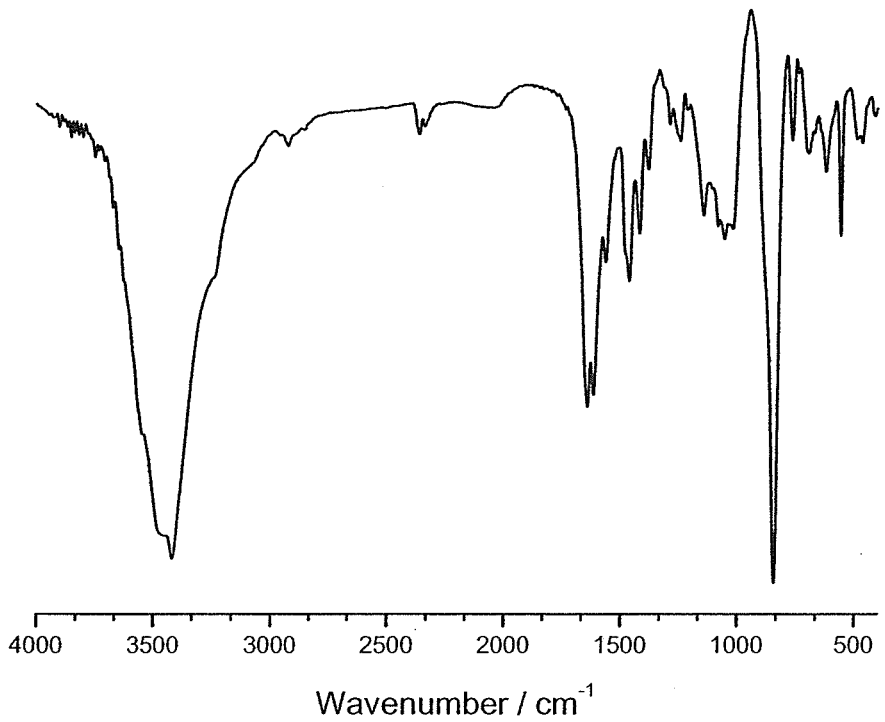

Figure 2.5.12. IR spectrum (KBr) of $[Cu^{II}_4(H\mathbf{L}^{M1})_4](PF_6)_4$ (**23b**).

Note: Just prior to submission of this thesis the X-ray crystal structure and the magnetic properties of $[Cu^{II}_4(HL^{M1})_4](ClO_4)_4 \cdot 5$ MeOH $\cdot$ 4 H_2O were reported by Cati, Stoeckli-Evans and co-workers.[143]

Complexation with H_2L^{M2} and copper(II) tetrafluoroborate tetrahydrate

As for the formation of the [2 × 2] grid complex **23** of the lower ligand homologue the analogous reaction of the higher ligand homologue H_2L^{M2} was carried out in acetonitrile solution. Thus the *in situ* deprotonation of a dark turquoise solution of a 1:1 molar ratio of H_2L^{M2} and copper(II) tetrafluoroborate tetrahydrate

with one molar equivalent of triethylamine resulted in a deep forest green solution (Figure 2.5.13).

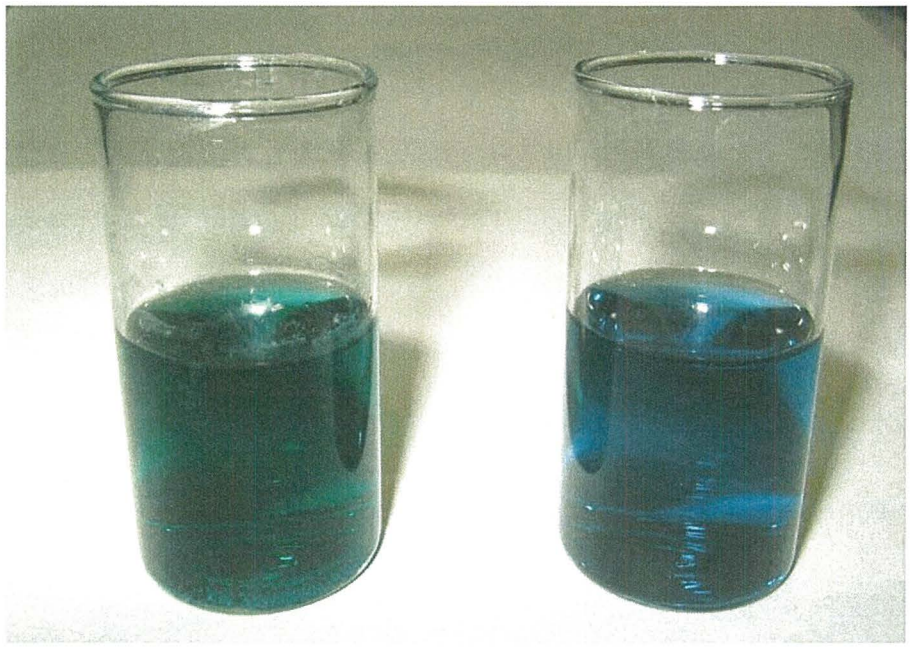

Figure 2.5.13. Colour change observed by the *in situ* deprotonation of a dark turquoise solution of $H_2\mathbf{L}^{\mathbf{M2}}$ and copper(II) in a 1:1 molar ratio (right side), with one equivalent of triethylamine, resulting in a deep bottle green solution (left side).

By precipitation with toluene, complex **24** could be isolated as a deep bottle green solid in 86 % yield (Scheme 2.5.3). Elemental analysis, in good agreement with the expected formulation of a [2 × 2] grid $[Cu^{II}_4(HL^{M2})_4](BF_4)_4$, suggested a 1:1 molar ratio of copper(II) complex to tetrafluoroborate counter ion.

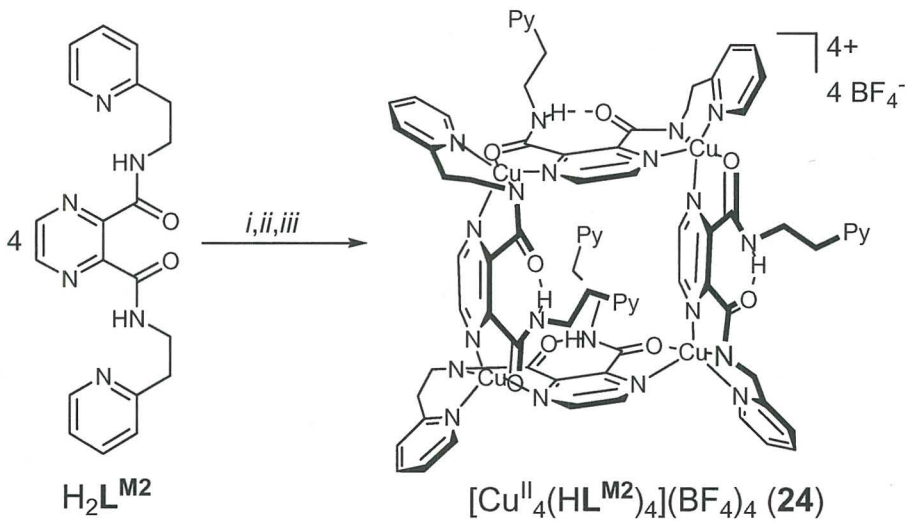

Scheme 2.5.3. Synthesis of **24**. Reagents and conditions: (*i*) 1 eq. $Cu(BF_4)_4 \cdot 4\ H_2O$, MeCN, RT; (*ii*) 1 eq. NEt_3; (*iii*) toluene (precipitation).

Conductivity measurements in acetonitrile solution [Λ_m = 133 mol^{-1} cm^2 Ω^{-1} per ligand] matched well with the proposed formulation of $[Cu^{II}_4(HL^{M2})_4](BF_4)_4$ (**24**). Unfortunately, the positive ion electrospray mass spectrum of **24** in acetonitrile gave no evidence of polynuclear species. The only peak ascribed to a copper containing species ($[Cu^{II}(HL^{M2})]^+$) was identified at *m/z* = 438.0. Peaks at *m/z* = 377.1 and 189.3 were assigned to the protonated ligand species $(H_3L^{M2})^+$ and $(H_4L^{M2})^{2+}$, respectively. A peak at the higher value of *m/z* = 483.9 could not be assigned.

IR spectroscopic studies on $[Cu^{II}_4(HL^{M2})_4](BF_4)_4$ (24)

The IR spectrum of **24** (Figure 2.5.14) compared reasonably well with the IR spectrum of the related [2 × 2] grid-type complex $[Cu^{II}_4(HL^{M1})_4](BF_4)_4$ **23** of the lower ligand homologue and with the IR spectrum of the precursor compound **19** · 4 H_2O. Only one ν_{CO} vibration absorption band at $\tilde{\upsilon}$ = 1636 cm^{-1} was present. Compared to the spectrum of complex **23** of the lower ligand homologue the band occurred with a shift of $\Delta\tilde{\upsilon}_{(23,24)}$ = 15 cm^{-1} to lower wavenumbers.

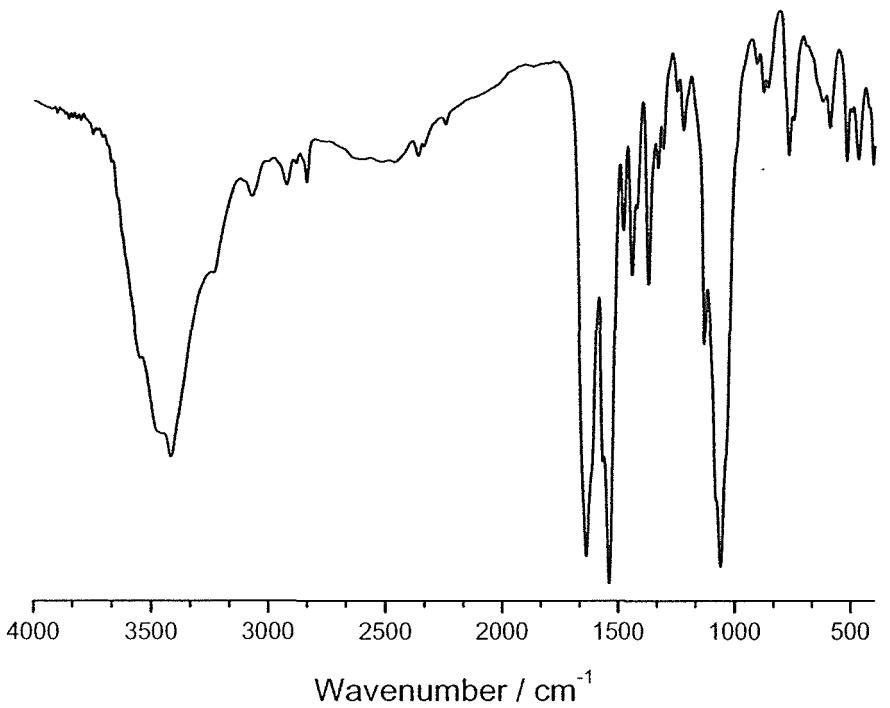

Figure 2.5.14. IR spectrum (KBr) of $[Cu^{II}_4(HL^{M2})_4](BF_4)_4$ (**24**).

As for the pair **6** *vs.* **23** of the lower ligand homologue, the ν_{CO} band of **24**, compared to the dinuclear complex **8** of the same ligand, occurred with a quite remarkable shift of $\Delta\nu_{(8,24)} = 31$ cm^{-1} to higher wavenumbers (see Table 2.5.1). As for the IR spectrum of the precursor complex **19** · 4 H_2O a second very strong absorption peak at $\tilde{\upsilon} = 1569$ cm^{-1} was observed in IR spectrum of **24**. Moreover the expected presence of tetrafluoroborate counter ions was confirmed with a broad split absorption band at $\tilde{\upsilon} = 1083$ cm^{-1}. Summarising these observations, it was suggested that both amide groups of the ligand were involved in metal coordination, possibly in a similar motif to that of **19** · 4 H_2O.

Single crystal X-ray structural analysis of $[Cu^{II}_4(HL^{M2})_4](BF_4)_4$ (24)

Single crystals of **24** were obtained by vapour diffusion of diethyl ether into an acetonitrile solution of the compound and the X-ray crystal structure determination confirmed its tetrameric structure (Figure 2.5.15). The centre of the tetranuclear square sits on a special position with $\bar{4}$ symmetry. Unlike the octahedrally coordinated copper(II) ions of the grid complex $[Cu^{II}_4(HL^{M1})_4](BF_4)_4$ (**23** · 3.5 MeCN) of the lower ligand homologue, but as seen for the square-like precursor complex $[Cu^{II}_4(H_2L^{M2})_2(HL^{M2})_2](BF_4)_6$ · 3 MeCN · 0.5 H_2O (**19** · 3 MeCN · 0.5 H_2O) of the same ligand, the copper(II) ions of the tetragonal complex **24** are in an N_4O coordination environment. The degree of trigonality of **24** ($\tau = 0.45$) is significantly higher than that of its precursor complex **19** · 3 MeCN · 0.5 H_2O ($\tau_{av} = 0.20$) and lies in-between the values for a perfect square pyramid and a perfect trigonal bipyramid.[127] In the following the coordination environment around the copper(II) ions in **24** will be described as distorted trigonal bipyramidal.

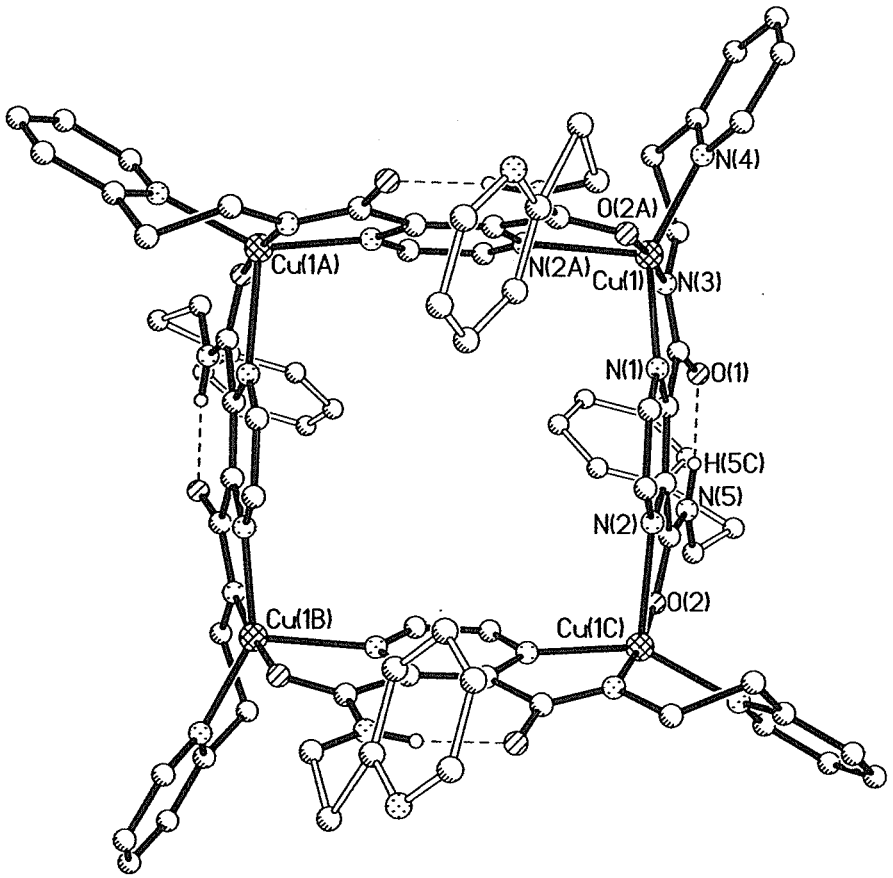

Figure 2.5.15. Molecular structure of $[Cu^{II}_4(HL^{M2})_4]^{4+}$, the complex cation of **24**. Hydrogen atoms not involved in hydrogen bonds have been omitted for clarity. The hollow bonds denote the strongly disordered free ligand arm, which was "SQUEEZEd away" in the refinement of the structure.[191] Selected distances (Å) and angles (°):Cu(1)-N(1) 2.024(6), Cu(1)-N(2A) 2.226(7), Cu(1)-N(3) 1.895(6), Cu(1)-N(4) 2.009(6), Cu(1)-O(2A) 1.966(5), Cu(1)···Cu(1A) 6.922(2), Cu(1)···Cu(1B) 9.777(3), O(1)···N(5) 2.551(9); N(1)-Cu(1)-N(2A) 99.6(2), N(1)-Cu(1)-N(3) 80.1(3), N(1)-Cu(1)-N(4) 147.3(2), N(1)-Cu(1)-O(2A) 94.3(2), N(2A)-Cu(1)-N(3) 102.1(3), N(2A)-Cu(1)-N(4) 113.1(2), N(2A)-Cu(1)-O(2A) 76.5(2), N(3)-Cu(1)-N(4) 93.9(3), N(3)-Cu(1)-O(2A) 174.0(3), N(4)-Cu(1)-O(2A) 92.0(2), Cu(1)···Cu(1A)···Cu(1B) 89.86(1). Symmetry operations used to generate equivalent atoms: A = 0.5–y, –0.5+x, 0.5–z; B = –x+1, –y, +z; C = 0.5–x, 0.5+y, 0.5–z.

The amide functions in **24** are not equivalent, but the ligand acts as a hybrid terdentate-bidentate N_3-NO chelate, as in the precursor complex **19** · 3 MeCN · 0.5 H_2O. The two apical positions of the distorted trigonal bipyramid are occupied by the amide nitrogen atom of the N_3-terdentate ligand half and the amide oxygen atom of the symmetry generated NO-bidentate ligand half. Two of the three equatorial coordination sites of the copper(II) ion are occupied by the pyridine nitrogen donor and the pyrazine nitrogen atom of the N_3-terdentate ligand half. The

distorted trigonal bipyramid is then completed by the pyrazine nitrogen atom of a symmetry generated N_3-terdentate ligand half. Thus, as seen in the tetranuclear complexes **19** · 3 MeCN · 0.5 H_2O and **23** · 3.5 MeCN, the pyrazine units of the square complex **24** act as $Cu^{II}\cdots Cu^{II}$ bridges. The resulting $Cu^{II}\cdots Cu^{II}$ distances (6.922(2) Å) of **24** are shorter even than the short $Cu^{II}\cdots Cu^{II}$ distances of **19** · 3 MeCN · 0.5 H_2O (7.00–7.05 Å) and **23** · 3.5 MeCN (7.10–7.15 Å). The $Cu^{II}\cdots Cu^{II}\cdots Cu^{II}$ angle (89.9°) of **24** is that of a regular square. However, as observed to a greater extent in the structures of **19** · 3 MeCN · 0.5 H_2O and **23** · 3.5 MeCN, the copper(II) ions of **24** are shifted by *ca.* 0.17 Å in an up-down-up-down fashion relative to the Cu^{II}_4 mean plane, leading to a small tetrahedral distortion of the Cu^{II}_4 square.

In **24** the O-coordinated amide group of the NO bidentate ligand half is still N-protonated, its proton being involved in a N-H···O hydrogen bond to the oxygen atom of the N-metalated amide function of the N_3-terdentate half of the same ligand. This results in the same sort of seven membered ring as found for complex **19** · 3 MeCN · 0.5 H_2O, with a similar N···O distance of 2.551(9) Å. Unlike the situation in **23** · 3.5 MeCN the ligand strands of **24** are not at all planer. Instead the ring mean plane of the coordinated pyridine forms an angle of 39.1° with the ring mean plane of the respective pyrazine. The pyridine ring of the bidentate ligand half points away from the square. It is very disordered (see Section 3.4.10), not coordinated to the copper(II) ion and not involved in any hydrogen bonds. So, the additional employment of base indeed resulted in the destruction of the intermolecular hydrogen bonds, which existed in the structure of **19** · 3 MeCN · 0.5 H_2O, and therefore freed the remaining uncoordinated pyridine arm of **24**. However, its donor atom is still not involved in copper(II) coordination, as was observed in the corresponding grid complex **23** · 3.5 MeCN of the lower ligand homologue.

UV/VIS spectroscopic studies on $[Cu^{II}_4(HL^{M2})_4](BF_4)_4$ (24)

The UV/VIS spectrum of **24** in acetonitrile solution showed one relatively intense absorption band at λ_{max} = 656 (ε = 603 M^{-1} cm^{-1}, $\tilde{\upsilon}$ = 15244 cm^{-1}) with a very pronounced shoulder at λ_{max} = 803 nm (ε = 356 M^{-1} cm^{-1}), which was assigned as overlapping bands of *d-d* transitions (Figure 2.5.16).

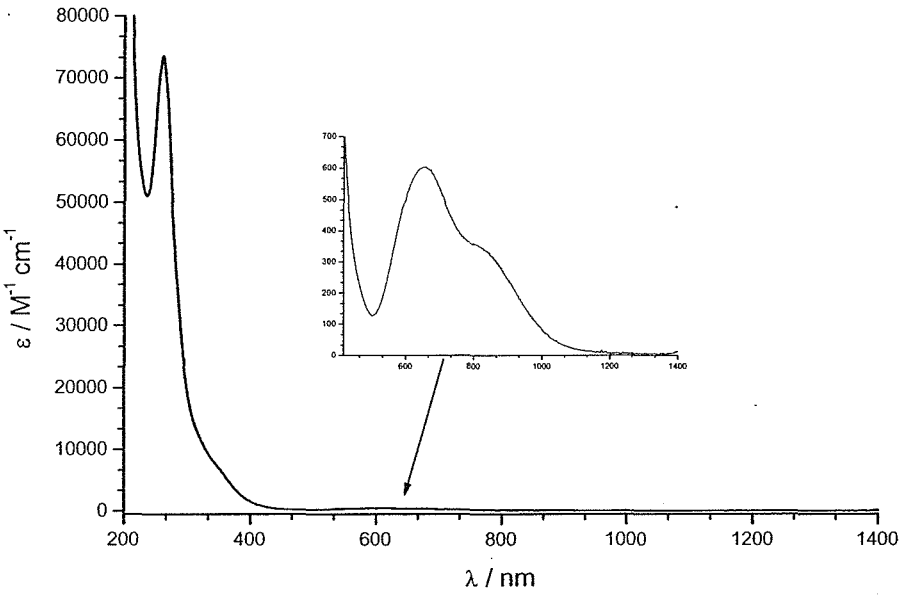

Figure 2.5.16. UV/VIS spectra [MeCN, 0.25 mM (inset) and 0.025 mM (main)] of $[Cu^{II}_4(HL^{M2})_4](BF_4)_4$ (**24**).

Compared to the corresponding band of the precursor complex **19** · 4 H_2O, the band of **24** appeared with a shift of $\Delta\tilde{\upsilon}_{(19,24)}$ = 833 cm^{-1} to lower energy. Remarkably, the molar extinction coefficient ε has increased by around 1.5 times (Figure 2.5.17).

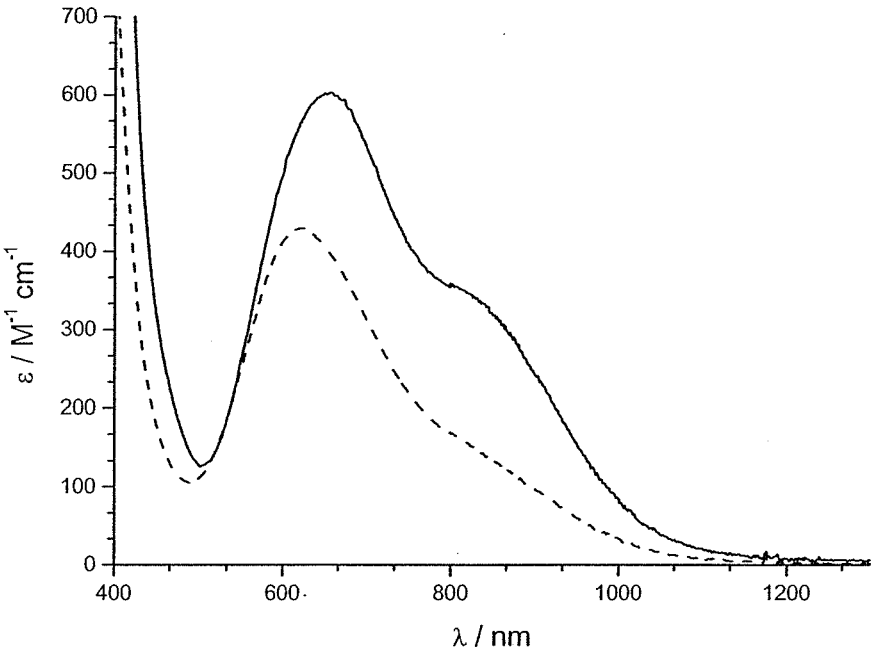

Figure 2.5.17. Comparison of the UV/VIS spectra of $[Cu^{II}_4(HL^{M2})_4](BF_4)_4$ (**24**) [MeCN 0.25 mM solid line] and $[Cu^{II}_4(H_2L^{M2})_2(HL^{M2})_2](BF_4)_6 \cdot 4\ H_2O$ (**19** · 4 H_2O) [MeCN, 0.5 mM dashed line].

Furthermore a relatively sharp intense band at λ_{max} = 263 nm (ε = 73200 M^{-1} cm^{-1}, $\tilde{\upsilon}$ = 38168 cm^{-1}) was observed.

Cyclic voltammetric studies on $[Cu^{II}_4(HL^{M2})_4](BF_4)_4$ (24)

The cyclic voltammogram of the tetranuclear square complex **24** only presented one irreversible reduction peak at E_{pc} = –0.55 V, relative to the Fc^+/Fc redox couple (Figure 2.5.18).

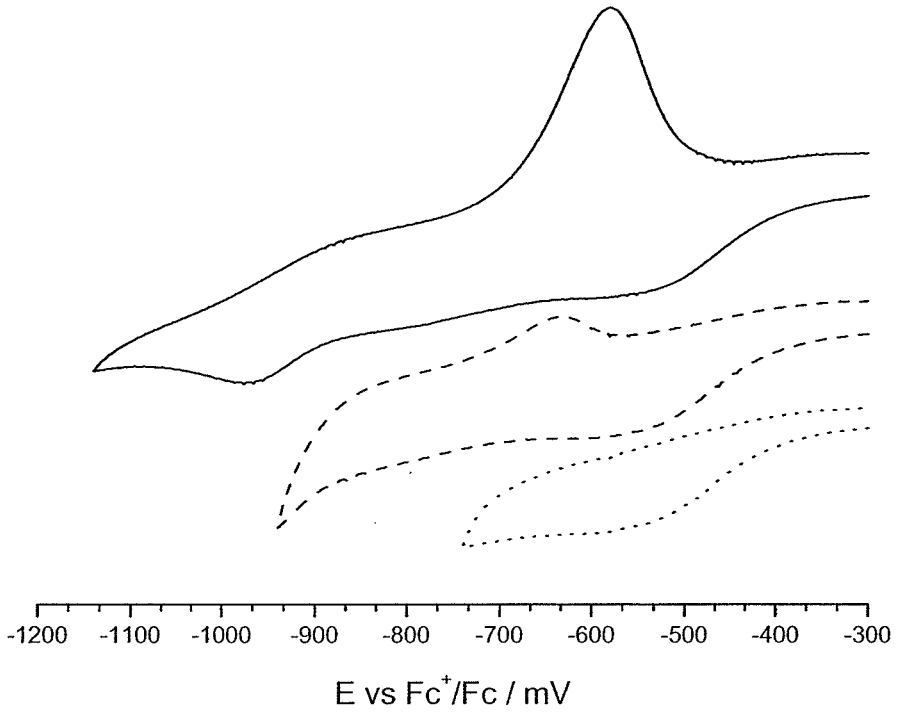

Figure 2.5.18. Cyclic voltammograms (0.5 mM, 0.1 M TBAP, MeCN, scan rate: 50 mV s^{-1}) of $[Cu^{II}_4(HL^{M2})_4](BF_4)_4$ (**24**).

This observation was quite unexpected, as in contrast the cyclic voltammograms of the dinuclear complex **8** and the precursor complex **19** · 4 H_2O of the same ligand, both showed two irreversible reduction waves in the region of 0.0 to –0.8 V, which for the latter was attributed to incomplete dissociation of the tetranuclear cation in acetonitrile solution (Figure 2.5.19). So although the tetranuclear complexes **19** · 4 H_2O and **24** exhibit very similar structures with similar coordination environments for the copper(II) ions, it appeared that the dissociation in acetonitrile solution of **24** was more complete than for **19** · 4 H_2O.

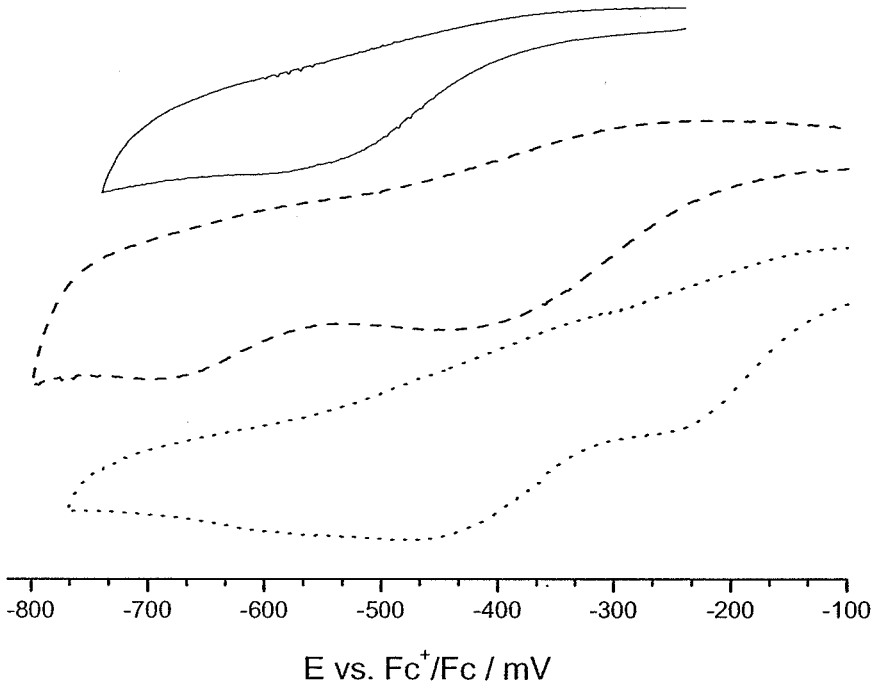

Figure 2.5.19. Comparison of the cyclic voltammograms (0.1 M TBAP, MeCN, scan rate: 50 mV s^{-1}) of the square complexes $[Cu^{II}_4(HL^{M2})_4](BF_4)_4$ (**24**) (0.5 mM, solid line) and $[Cu^{II}_4(H_2L^{M2})_2(HL^{M2})_2](BF_4)_6 \cdot 4\ H_2O$ (0.25 mM, **19** · 4 H_2O) (dashed line) and the dimeric complex $[Cu^{II}_2(HL^{M2})(H_2O)](ClO_4)_4$ (**8**) (1 mM, dotted line).

At lower potentials (E_{pc} = –0.97 V), a second reduction process was observed, associated with an oxidation wave (E_{pa} = –0.58 V). As for **23** the oxidation wave in the cyclic voltammogram of **24** increased in intensity when the turning voltage was lowered.

Magnetic studies on $[Cu^{II}_4(HL^{M2})_4](BF_4)_4$ (24)

The plots of μ_{eff} and χ_m versus the temperature (T) for the tetranuclear complex $[Cu^{II}_4(HL^{M2})_4](BF_4)_4$ (**24**) are shown in Figure 2.5.20 and Figure 2.5.21.

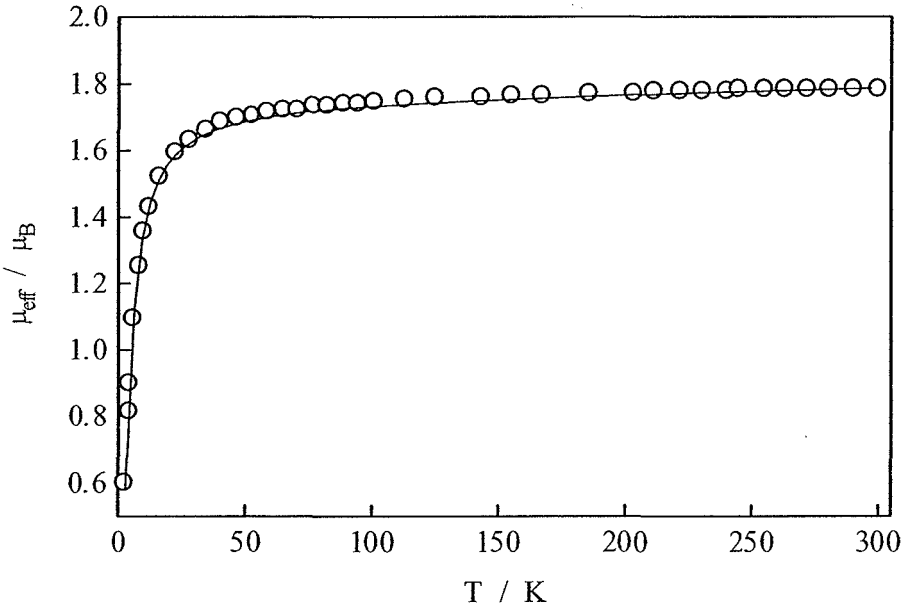

Figure 2.5.20. Thermal variation of the magnetic moment μ_{eff} (◦◦) for $[Cu^{II}_4(HL^{M2})_4](BF_4)_4$ (**24**). The solid line represents the best fit.

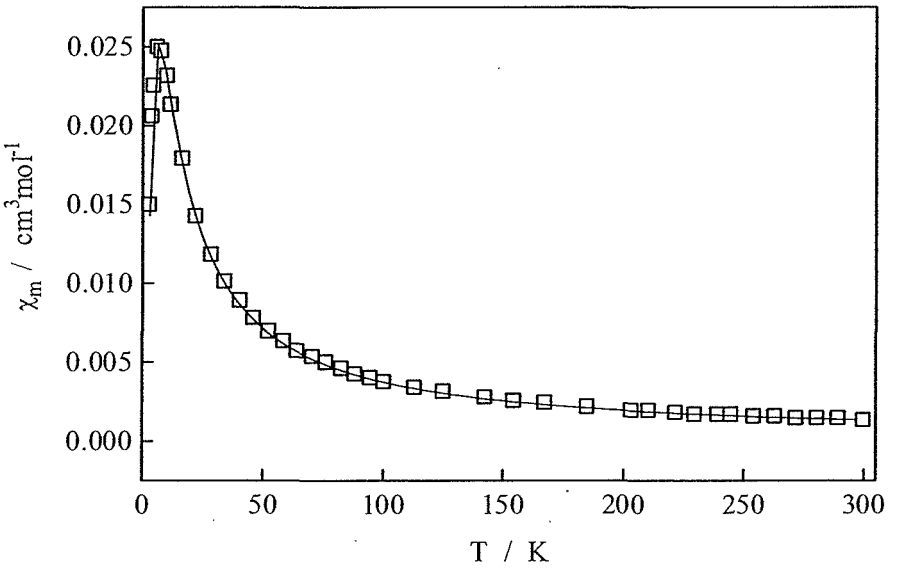

Figure 2.5.21. Thermal variation of the molar susceptibility χ_m (▫▫) for $[Cu^{II}_4(HL^{M2})_4](BF_4)_4$ (**24**). The solid line represents the best fit.

Once more, a maximum in χ_m at around 7 K was indicative of weak antiferromagnetic coupling. In contrast to the copper(II) grid complex **23** and the square complex **19** · 3 MeCN · 0.5 H_2O, only one coupling constant (J = –2.97 cm^{-1}) was needed for the square compound **24**. The following two parameters were calculated from the fit: g = 2.08 and $TIP = 65 \times 10^{-6}$ cm^3 mol^{-1}, monomeric impurity = 0.1 %.

2.5.2. *Nickel(II) salts*

Complexation with H_2L^{M2} and nickel(II) tetrafluoroborate hexahydrate

The complexation of H_2L^{M2} with nickel(II) tetrafluoroborate hexahydrate, employing a 1:1 molar ratio, was carried out in acetonitrile and resulted in a pale brown solution (see Section 2.4.2). On addition of one molar equivalent of triethylamine a colour change to dark red-brown was observed. By vapour diffusion of diethyl ether into the reaction solution compound **25** · 10 H_2O was obtained as a red-brown crystalline solid in around 60 % yield (Scheme 2.5.4). The compound proved to be readily soluble in *N,N*-dimethylformamide and acetonitrile but was insoluble in other polar solvents.

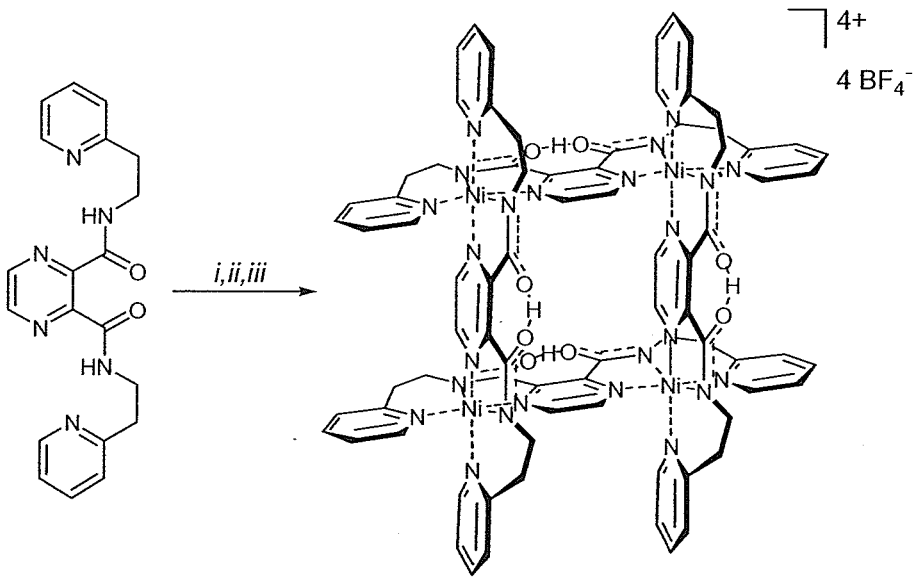

H_2L^{M2} $[Ni^{II}_4(HL^{M2})_4](BF_4)_4$ (**25**)

Scheme 2.5.4. Synthesis of **25**. Reagents and conditions: (*i*) 1 eq. $Ni(BF_4)_2 \cdot 6$ H_2O, MeCN, RT; (*ii*) 1 eq. NEt_3; (*iii*) Et_2O (vapour diffusion).

By means of elemental analysis, the compound was tentatively formulated as $[Ni^{II}(HL^{M2})]_n(BF_4)_n \cdot 2.5\ n\ H_2O$. This result was in agreement with the desired [2 × 2] grid-type structure (n = 4; **25** · 10 H_2O) and suggested that the diamide ligands were indeed deprotonated although, as observed before, only monodeprotonated. The use of two molar equivalents of base under otherwise identical conditions resulted in a

brown solid with the same empirical formula. The employment of a molar ratio of ligand to nickel(II) of 1:2 and the addition of base also resulted in the formation of a brown crystalline solid with the same empirical formula (see Section 2.2.5).

The positive ion electrospray mass spectrum of **25** · 10 H_2O in acetonitrile showed the most intense peaks at *m/z* = 953.1, 606.7, 433.0, 377.2 and 189.4. The first three peaks were assigned to the tetranuclear complex fragments $\{[Ni^{II}_4(HL^{M2})_4](BF_4)_2\}^{2+}$, $\{[Ni^{II}_4(HL^{M2})_4](BF_4)\}^{3+}$ and $[Ni^{II}_4(HL^{M2})_4]^{4+}$, respectively, and revealed the stepwise loss of counter ions, further supporting the proposed composition of **25** · 10 H_2O (Figure 2.5.22).

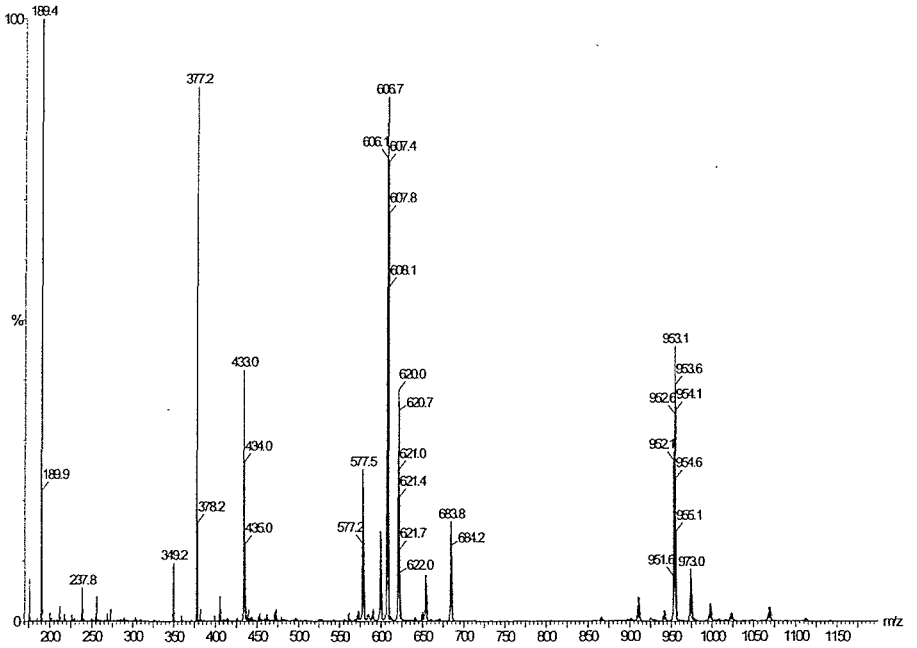

Figure 2.5.22. ESI-MS spectrum (MeCN) of $[Ni^{II}_4(HL^{M2})_4](BF_4)_4$ · 10 H_2O (**25** · 10 H_2O).

The peaks at *m/z* = 377.2 and 189.4 derived from the protonated ligand species $[H_3L^{M2}]^+$ and $[H_4L^{M2}]^{2+}$, respectively. The spectrum also showed various smaller peaks that supported the expected [2 × 2] structure of **25** · 10 H_2O. Thus the peaks at *m/z* = 997.0 and 683.8 were assigned to the species $\{[Ni^{II}_4(H_2L^{M2})(HL^{M2})_3](BF_4)_3\}^{2+}$ and $\{[Ni^{II}_4(H_2L^{M2})_2(HL^{M2})_2(H_2O)_3](BF_4)_3\}^{3+}$, respectively, containing mono- and fully protonated ligand and the peaks at *m/z* = 909.2 and 577.5 derived from the species $\{[Ni^{II}_4(HL^{M2})_3(L^{M2})](BF_4)_3\}^{2+}$ and $[Ni^{II}_4(HL^{M2})_3(L^{M2})]^{3+}$, respectively, containing mono-

and fully deprotonated ligand. Furthermore the peaks at m/z = 973.0 and 620.0 were assigned to the reduced nickel(I) species $\{[Ni^{I}_4(H_2L^{M2})_2(HL^{M2})_2(H_2O)_2](BF_4)_2\}^{2+}$ and $\{[Ni^{II}Ni^{I}_3(H_2L^{M2})_3(HL^{M2})(H_2O)_2](BF_4)\}^{3+}$. Unfortunately, no sensible fragments could be found for the relative intense peaks at m/z = 653.3 and 598.4.

IR spectroscopic studies on $[Ni^{II}_4(HL^{M2})_4](BF_4)_4 \cdot 10\ H_2O$ (25 · 10 H_2O)

Unexpectedly, the IR spectrum of **25** · 10 H_2O showed two strong bands at $\tilde{\upsilon}$ = 1652 and 1605 cm^{-1}, in the expected region of νCO vibration absorptions and a third strong absorption band $\tilde{\upsilon}$ = 1562 cm^{-1} (Figure 2.5.23).

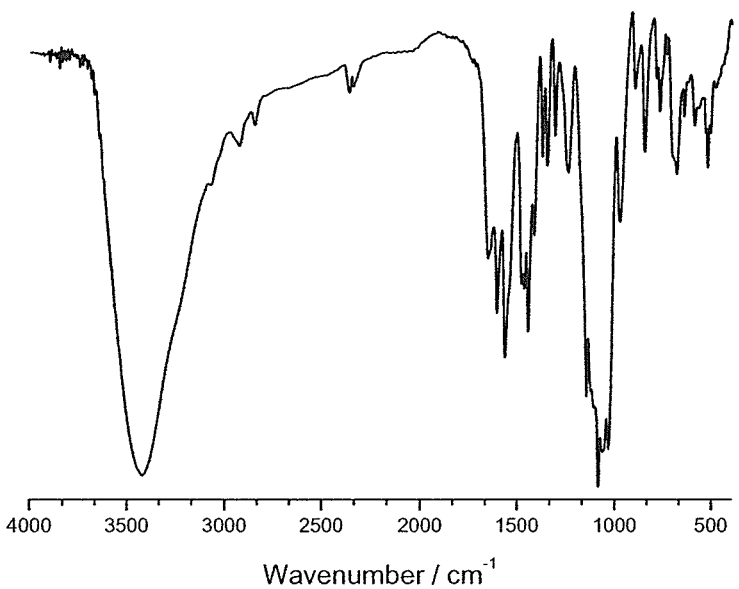

Figure 2.5.23. IR spectrum (KBr) of $[Ni^{II}_4(HL^{M2})_4](BF_4)_4$ · 10 H_2O (**25** · 10 H_2O).

The first band compared well to the νCO vibration of the related copper(II) [2 × 2] grid complex **23** of the lower ligand homologue, whereas the second band was more characteristic of the νCO vibration bands of the dinuclear complexes **6–12** (see Table 2.5.1). So whereas the IR spectrum of the related copper(II) square complex **24** of the same ligand, with asymmetrically coordinated amide functions, only showed one νCO vibration band at $\tilde{\upsilon}$ = 1636 cm^{-1}, the IR spectrum of the corresponding nickel(II)

compound **25** · 10 H_2O has two bands in the expected region of the ν_{CO} vibration. The strong band at $\tilde{\upsilon}$ = 1562 cm^{-1} was comparable to the bands observed in the IR spectra of **19** · 4 H_2O ($\tilde{\upsilon}$ = 1565 cm^{-1}), **22** · EtOH ($\tilde{\upsilon}$ = 1559 cm^{-1}) and **24** ($\tilde{\upsilon}$ = 1569 cm^{-1}). The expected presence of tetrafluoroborate counter ions was confirmed with a broad split band at $\tilde{\upsilon}$ = 1083 cm^{-1}.

Single crystal X-ray structural analysis of $[Ni^{II}_4(HL^{M2})_4](BF_4)_4$ · 10 MeCN (25 · 10 MeCN)

Single crystals of $[Ni^{II}_4(HL^{M2})_4](BF_4)_4$ · 10 MeCN (**25** · 10 MeCN) were obtained by vapour diffusion of diethyl ether into an acetonitrile solution of **25** · 10 H_2O and the subsequent X-ray crystal structure determination revealed the [2 × 2] grid-type nature of the compound (Figure 2.5.24). As the two independent tetrameric complex cations present in the asymmetric unit are very similar, only the cation incorporating Ni(1) to Ni(4) will be discussed in the following. In contrast to the N_4O distorted trigonal bipyramidal metal(II) coordination environments found in the related copper(II) square complex **24** of the same ligand, the nickel(II) ions of complex **25** · 10 MeCN adopt an N_6 distorted octahedral coordination sphere.

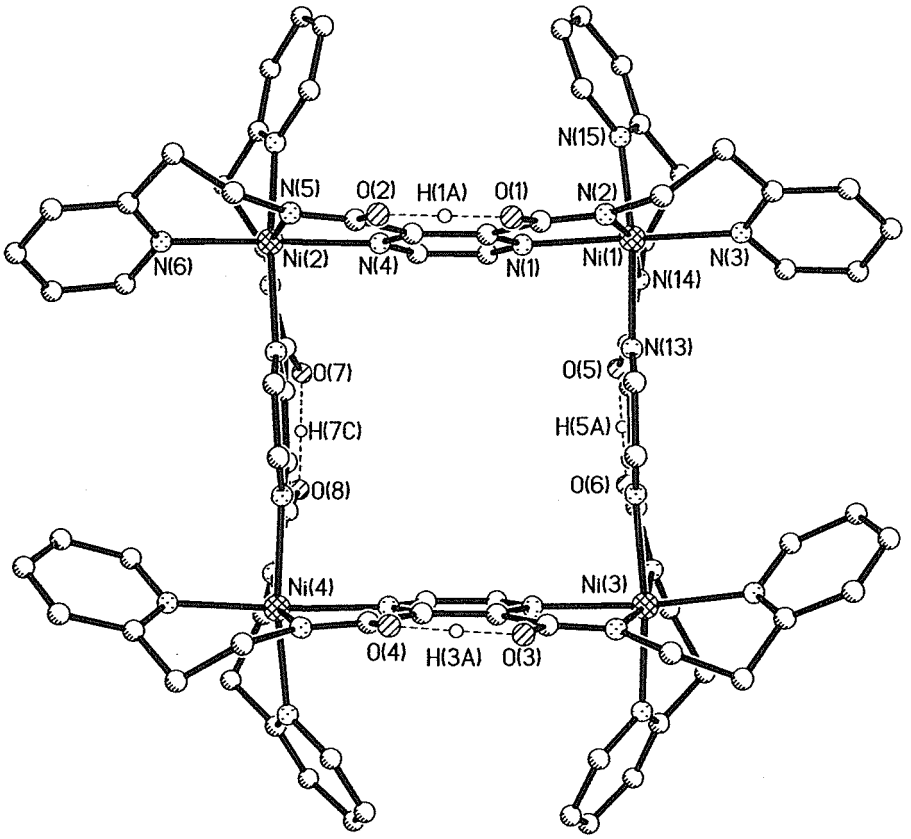

Figure 2.5.24. Molecular structure of $[Ni^{II}_4(HL^{M2})_4]^{4+}$, one of the two independent complex cations present in the asymmetric unit of complex **25** · 10 MeCN. Hydrogen atoms, except H(1A), H(3A), H(5A) and H(7C) have been omitted for clarity. Selected distances (Å) and angles (°): Ni(1)-N(1) 2.106(5), Ni(1)-N(2) 2.020(5), Ni(1)-N(3) 2.089(5), Ni(1)-N(13) 2.130(4), Ni(1)-N(14) 2.047(4), Ni(1)-N(15) 2.120(5), Ni(1)···Ni(2) 6.941(1), Ni(2)···Ni(4) 7.016(1), Ni(4)···Ni(3) 7.008(1), Ni(3)···Ni(1) 7.003(1), Ni(1)···Ni(4) 9.776(1), Ni(2)···Ni(3) 9.999(1), O(1)···O(2) 2.386(6), O(3)···O(4) 2.386(6), O(5)···O(6) 2.386(4), O(7)···O(8) 2.398(5); N(1)-Ni(1)-N(2) 77.4(2), N(1)-Ni(1)-N(3) 169.4(2), N(1)-Ni(1)-N(13) 87.0(2), N(1)-Ni(1)-N(14) 92.4(2), N(1)-Ni(1)-N(15) 86.4(2), N(2)-Ni(1)-N(3) 92.3(2), N(2)-Ni(1)-N(13) 92.3(2), N(2)-Ni(1)-N(14) 165.8(2), N(2)-Ni(1)-N(15) 96.9(2), N(3)-Ni(1)-N(13) 90.8(2), N(3)-Ni(1)-N(14) 97.2(2), N(3)-Ni(1)-N(15) 97.6(2), N(13)-Ni(1)-N(14) 77.1(2), N(13)-Ni(1)-N(15) 167.2(2), N(14)-Ni(1)-N(15) 92.3(2), Ni(2)···Ni(1)···Ni(3) 91.63(2), Ni(1)···Ni(2)···Ni(4) 88.92(2), Ni(1)···Ni(3)···Ni(4) 88.49(2), Ni(2)···Ni(4)···Ni(3) 90.96(2).

By analogy with the copper(II) [2 × 2] grid complex **23** · 3.5 MeCN of the lower ligand homologue, the ligands of **25** · 10 MeCN act as symmetrical bis-terdentate chelates. Each terdentate binding pocket coordinates in a meridional fashion, thus the nickel(II) ions are bridged *via* the pyrazine units, which gives rise to a grid-like arrangement of the ligand strands. The average angle between the mean planes defined by the donor atoms of the terdentate binding site is 89.8°. As expected, the average Ni^{II}-N_{amide} bond length (2.04 Å) is shorter than the average

Ni^{II}-N_{pz} (2.13 Å) or the average Ni^{II}-N_{py} bond distance (2.12 Å). The mean planes around the nickel(II) ions are defined by the $N_{heterocyle}$ atoms and therefore lie in the Ni^{II}_4 mean plane. The NiN_6 octahedra are compressed with the tetragonality factor ranging from $T = 1.051–1.038$,[189] giving the average tetragonality factor to $T_{av} = 1.045$. This is considerably closer to 1.0 than $T_{av(23)} = 1.122$ of the copper(II) grid **23** · 3.5 MeCN of the lower ligand homologue where, apart from the different donor atoms, the copper(II) d^9 ions are expected to experience a Jahn-Teller distortion. As found for the copper(II) grid **23** · 3.5 MeCN, all N-H amide functions are deprotonated but each ligand retains one former N-H amide proton in an O···H···O hydrogen bond between its two amide carbonyl oxygen atoms (see Section 3.4.11). The resulting O···O separations are all equal within experimental error (2.39 Å). The Ni^{II}···Ni^{II} distances of the grid compound **25** · 10 MeCN, with the exception of the shorter Ni(1)···Ni(2) distance of 6.941(1) Å, lie in the range of 7.003–7.016 Å, and are shorter than the Cu^{II}···Cu^{II} distances found for the grid complex **23** · 3.5 MeCN of the lower ligand homologue (7.101–7.150 Å), but are still slightly longer than the Cu^{II}···Cu^{II} distances of the square complex **24** of the same ligand (6.922(2) Å). The Ni^{II}···Ni^{II}···Ni^{II} angles show little deviation from 90° and range from 88.49–91.63°.

In contrast to the observed up-down-up-down shift of the copper(II) ions relative to the Cu^{II}_4 mean plane, observed in the structures of the [2 × 2] grid complex **23** · 3.5 MeCN (by 0.28 Å) and the square complexes **19** · 3 MeCN · 0.5 H_2O (by 0.28 Å) and **24** (by 0.17 Å), the up-down-up-down shift of the nickel(II) ions relative to the Ni^{II}_4 mean plane observed in **25** · 10 MeCN (by 0.01 Å) is negligible. Owing to the extra methylene link between the amide group and the pyridine, compared to **23** of the lower ligand homologue, the mean plane of each pyridine ring displays a relatively large angle with the plane of the pyrazine ring of the same ligand. The angles range from 32.7–39.8° and compare well to the respective angle of the square compound **24** of the same ligand (39.1°). It is noteworthy that the ligand strands of the corresponding grid compound **23** · 3.5 MeCN of the lower ligand

homologue were very flat indeed and the corresponding angles ranged only from 5.7–10.1°.

UV/VIS spectroscopic studies on $[Ni^{II}_4(HL^{M2})_4](BF_4)_4 \cdot 10\ H_2O$ (25 · 10 H_2O)

Nickel(II) ions in an octahedral environment are expected to show three characteristic *d-d*-transition bands, originating from the transitions $^3A_{2g} \rightarrow {}^3T_{2g}$, $^3A_{2g} \rightarrow {}^3T_{1g}(F)$ and $^3A_{2g} \rightarrow {}^3T_{1g}(P)$ (Figure 2.5.25).[190]

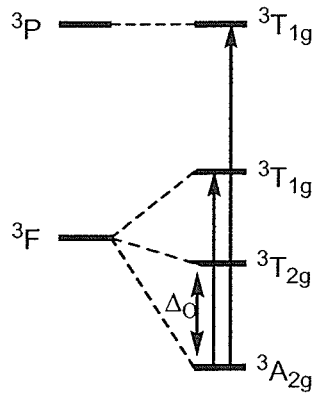

Figure 2.5.25. Term splitting diagram for d^8 ions in an octahedral crystal field.

The UV/VIS spectrum of **25** · 10 H_2O in acetonitrile solution showed only two absorption bands in the region of λ = 1400–200 nm (Figure 2.5.26). The band at λ_{max} = 260 nm (ε = 50000 M^{-1} cm^{-1}, $\tilde{\upsilon}$ = 38462 cm^{-1}) however, showed a distinct shoulder to lower energy. The second absorption band, observed at 853 nm (ε = 89 M^{-1} cm^{-1}, ε = 22 M^{-1} cm^{-1} per nickel(II) ion), was assigned to the lowest energy $^3A_{2g} \rightarrow {}^3T_{2g}$ transition giving the crystal field splitting energy of **25** · 10 H_2O as Δo = 11723 cm^{-1} ($[Ni^{II}(H_2O)_6]^{2+}$, Δo = 8500 cm^{-1}; $[Ni^{II}(bipy)_3]^{2+}$, Δo = 12650 cm^{-1}) (Figure 2.5.25).[190]

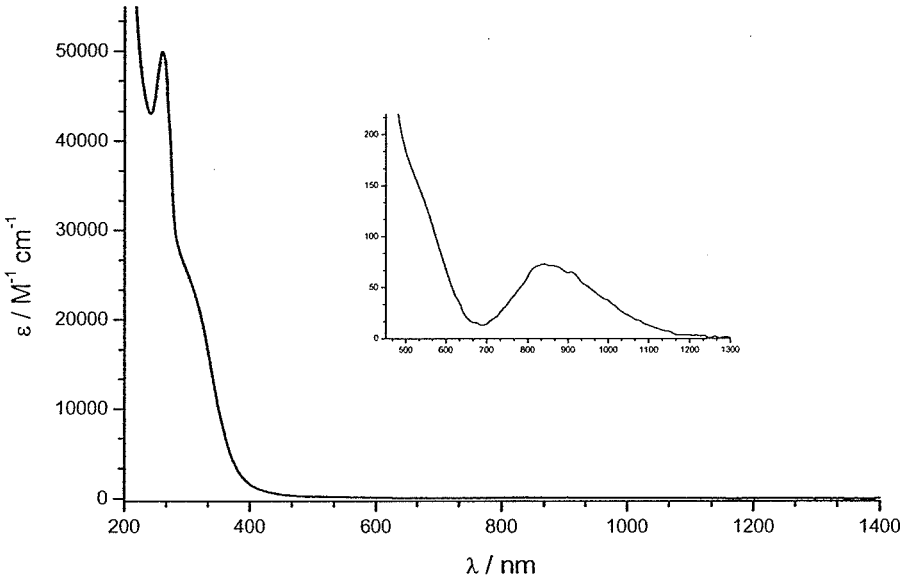

Figure 2.5.26. UV/VIS spectra [MeCN, 0.25 mM (inset) and 0.025 mM (main)] of $[Ni^{II}_4(HL^{M2})_4](BF_4)_4 \cdot 10\ H_2O$ (**25** · 10 H_2O).

Furthermore a weak shoulder at around λ = 550 nm was observed, presumably due to the transition $^3A_{2g} \rightarrow {}^3T_{1g}$ (F). An absorption band for the transition $^3A_{2g} \rightarrow {}^3T_{1g}$(P) could not be observed and was presumably masked by the strong band at higher energy.

Cyclic voltammetric studies on $[Ni^{II}_4(HL^{M2})_4](BF_4)_4 \cdot 10\ H_2O$ (25 · 10 H_2O)

The cyclic voltammogram of the [2 × 2] grid complex **25** · 10 H_2O in acetonitrile solution, showed two well separated reversible metal-centred reduction steps at $E_{1/2}$ = –1.18 V and $E_{1/2}$ = –1.57 V, relative to the Fc^+/Fc redox couple, respectively (Figure 2.5.27).

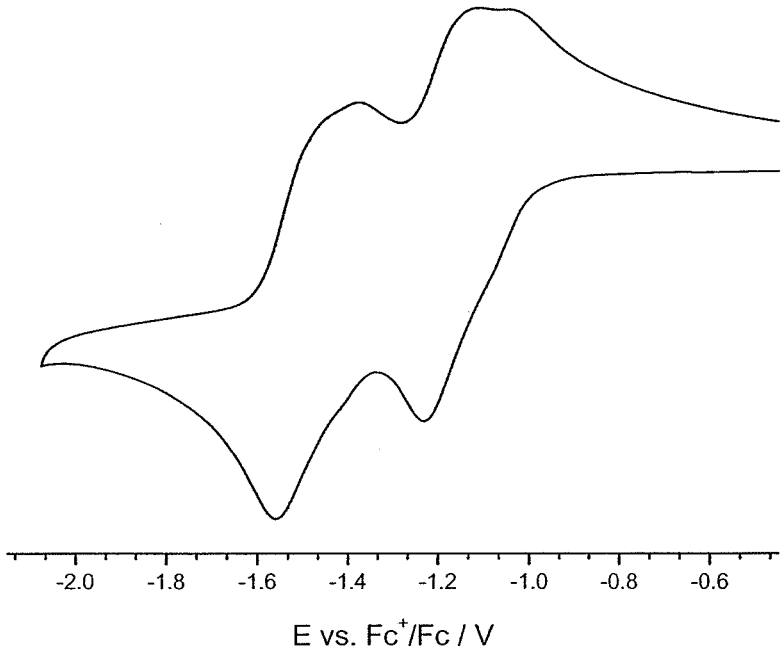

Figure 2.5.27. Cyclic voltammogram (0.5 mM, 0.1 M TBAP, MeCN, scan rate: 50 mV s^{-1}) of $[Ni^{II}_4(HL^{M2})_4](BF_4)_4 \cdot 10\ H_2O$ (**25** · 10 H_2O).

Controlled potential coulometry at E = –1.25 V confirmed that the first process corresponded a two-electron reduction of the initial tetrameric nickel(II) complex. The reductions were attributed to the processes $[Ni^{II}_4] \rightarrow [Ni^{II}_2Ni^{I}_2]$ and $[Ni^{II}_2Ni^{I}_2] \rightarrow [Ni^{I}_4]$, respectively, and demonstrated the low dissociation of the [2 × 2] grid cation in acetonitrile solution. Both oxidation processes clearly exhibited two bumps.

Magnetic studies on $[Ni^{II}_4(HL^{M2})_4](BF_4)_4 \cdot 10\ H_2O$ (25 · 10 H_2O)

The plots of the temperature dependence of μ_{eff} and of χ_m of **25** · 10 H_2O per nickel(II) ion are shown in Figure 2.5.28 and Figure 2.5.29.

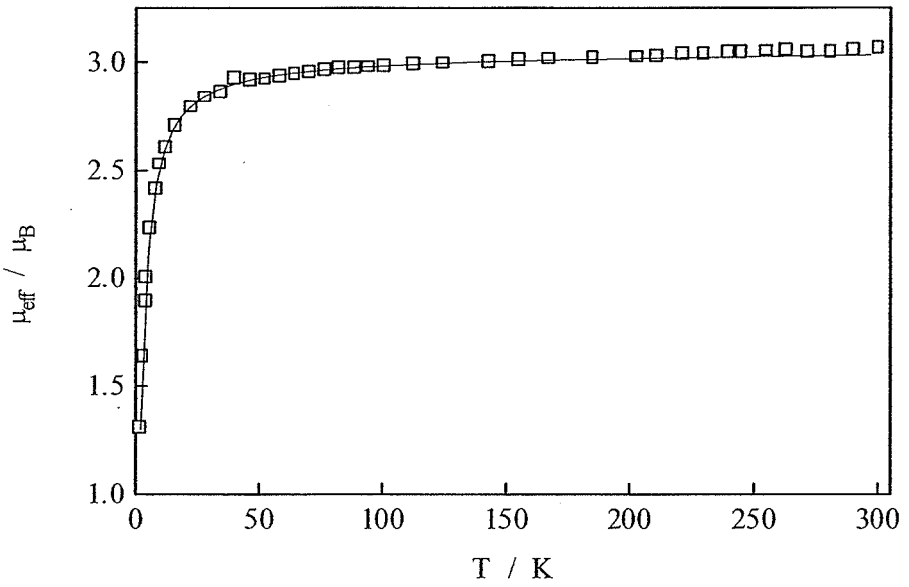

Figure 2.5.28. Thermal variation of the magnetic moment μ_{eff} (▫▫) of $[Ni^{II}_4(HL^{M2})_4](BF_4)_4 \cdot 10\ H_2O$ (**25** · 10 H_2O). The solid line represents the best fit.

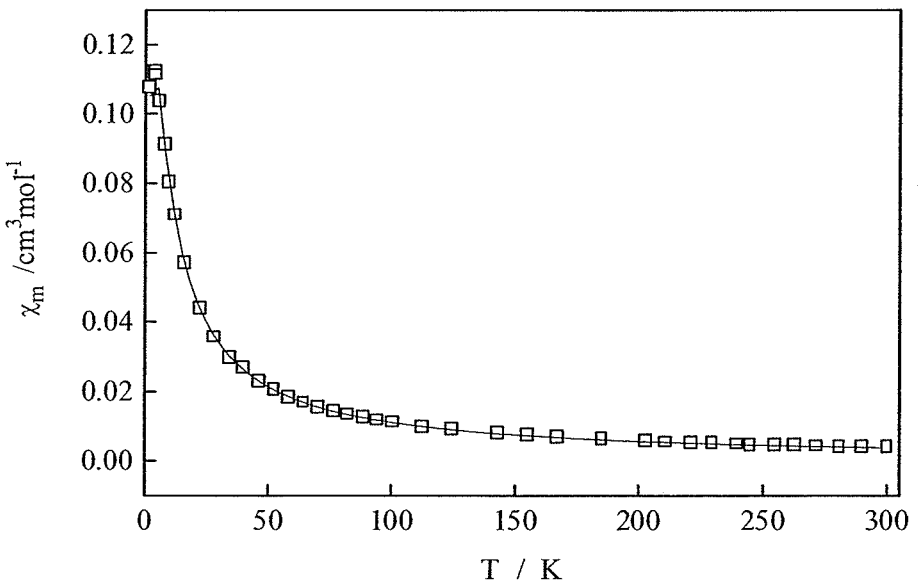

Figure 2.5.29. Thermal variation of the molar susceptibility χ_m (▫▫) of $[Ni^{II}_4(HL^{M2})_4](BF_4)_4 \cdot 10\ H_2O$ (**25** · 10 H_2O). The solid line represents the best fit.

As observed thus far for all pyrazine bridged metal(II) containing structures (**6b** · MeCN, **19** · 3 MeCN · 0.5 H_2O, **23** and **24**), the magnetic measurements of **25** · 10 H_2O obeyed the Curie-Weiss law above 50 K. Similarly to **6b** · MeCN, **19** · 3 MeCN · 0.5 H_2O, **23** and **24**, the value of χ_m increased below that temperature,

reaching a maximum value at 5.24 K (0.1076 $cm^3\ mol^{-1}$). Consequently the values of μ_{eff} decreased continuously, when the temperature was lowered, indicating the presence of antiferromagnetic interactions. In contrast to the copper(II) grid complex **23**, only one coupling constant ($J = -0.80\ cm^{-1}$, with $g = 2.14$, $TIP = 60 \times 10^{-6}\ cm^3\ mol^{-1}$) was needed for the nickel(II) [2 × 2] grid structure $[Ni^{II}_4(HL^{M2})_4](BF_4)_4 \cdot 10\ H_2O$ (**25** · 10 H_2O). A $S = 1$ cyclic square model was used. Compared to the pyrazine bridged copper(II) complexes described so far, the coupling constant of **25** · 10 H_2O appeared to be very low but the total spread of energy levels for $S = 1$ is bigger. The observed magnetic moment at room temperature was 3.03 μ_B, as was expected for weakly coupled nickel(II) d^8 ions.

Complexation with H_2L^{M1} and nickel(II) tetrafluoroborate hexahydrate

The analogous complexation of H_2L^{M1} with nickel(II) tetrafluoroborate hexahydrate and triethylamine, employing a 1:1:1 molar ratio, in acetonitrile led to the isolation of a pale beige inhomogeneous solid of unknown composition. Instead, the complexation of H_2L^{M1} with nickel(II) tetrafluoroborate hexahydrate was carried out with sodium hydroxide as base, employing a 1:1:1 molar ratio, in *N,N*-dimethylformamide solution (Scheme 2.5.5). Vapour diffusion of diethyl ether into the resulting dark red-brown reaction solution afforded the complex **26** · 4 H_2O as a dark brown crystalline solid in around 70 % yield. Elemental analysis led to the formulation of the compound as $[Ni^{II}(HL^{M1})]_n(BF_4)_n \cdot n\ H_2O$, suggesting the ligand was monodeprotonated. The results from conductivity measurements in *N,N*-dimethylformamide [$\Lambda_m = 57\ mol^{-1}\ cm^2\ \Omega^{-1}$, per ligand] were a little low but still acceptable for a 4:1 electrolyte. The compound was readily soluble only in *N,N*-dimethylformamide and practically insoluble in acetonitrile and other polar solvents. The use of a molar ratio of 2:1 of nickel(II) salt to ligand under otherwise identical

reaction conditions led to the formation of a brown crystalline material with the same empirical formula (see Section 2.2.5).

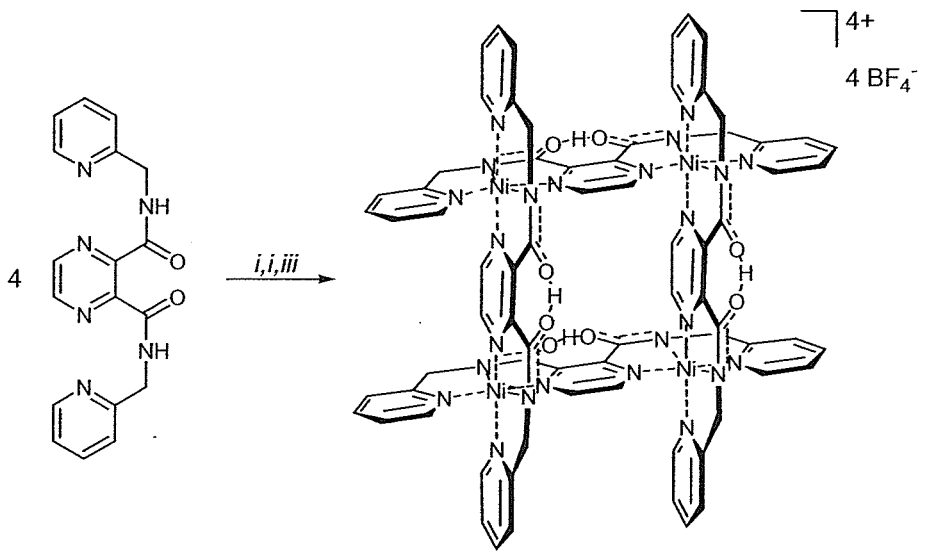

H_2L^{M1} $[Ni^{II}_4(HL^{M1})_4](BF_4)_4$ (**26**)

Scheme 2.5.5. Synthesis of **26**. Reagents and conditions: (*i*) 1 eq. $Ni(BF_4)_2 \cdot 6$ H_2O, DMF, RT; (*ii*) 1 eq. NaOH, DMF/H_2O (5:1); (*iii*) Et_2O (vapour diffusion).

The positive ion electrospray mass spectrum of **26** · 4 H_2O in acetonitrile gave some information about the polymeric nature of the compound, but unfortunately the spectrum obtained was very complex and only a few peaks could be assigned. As for the analogous copper(II) complex $[Cu^{II}_4(HL^{M1})_4](BF_4)_4$ (**23**), the peaks at *m/z* = 897.2, 569.5 and 406.1 were assigned to tetranuclear complex fragments $\{[Ni^{II}_4(HL^{M1})_4](BF_4)_2\}^{2+}$, $\{[Ni^{II}_4(HL^{M1})_4](BF_4)\}^{3+}$ and $[Ni^{II}_4(HL^{M1})_4]^{4+}$, respectively, revealing the sequential loss of tetrafluoroborate counter ions and thus confirming the complex formulation of $[Ni^{II}_4(HL^{M1})_4](BF_4)_4$ (*n* = 4). Furthermore three peaks at *m/z* = 809.3, 853.7 and 540.2 were assigned to the species $[Ni^{II}_4(HL^{M1})_2(L^{M1})_2]^{2+}$, $\{[Ni^{II}_4(HL^{M1})_3(L^{M1})](BF_4)\}^{2+}$ and $[Ni^{II}_4(HL^{M1})_3(L^{M1})]^{3+}$, respectively, demonstrating the loss of former N-H amide protons, further confirming the suggested structure of the compound. However, several peaks remained unassigned, so that a definite statement regarding the nuclearity of the compound could not be made. The peaks of the protonated ligand species $(H_3L^{M1})^+$ and $(H_4L^{M1})^{2+}$ were observed at *m/z* = 349.2 and 175.4, respectively.

IR spectroscopic studies on $[Ni^{II}_4(HL^{M1})_4](BF_4)_4 \cdot 4\ H_2O$ ($26 \cdot 4\ H_2O$)

The IR spectrum of **26** · 4 H_2O showed one sharp absorption band for the νCO vibration absorption at $\tilde{\upsilon}$ = 1606 cm^{-1} with a distinct shoulder to higher wavenumbers (Figure 2.5.30).

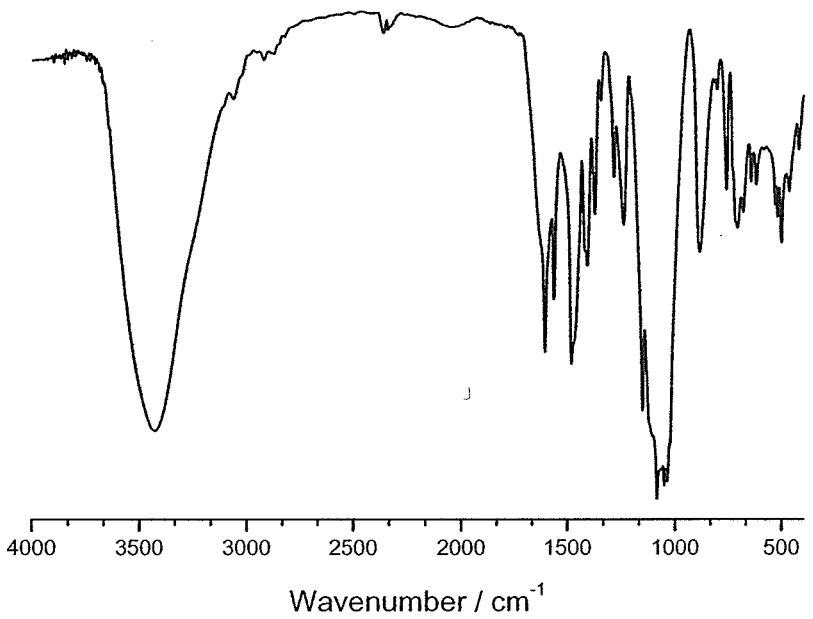

Figure 2.5.30. IR spectrum (KBr) of $[Ni^{II}_4(HL^{M1})_4](BF_4)_4 \cdot 4\ H_2O$ (**26** · 4 H_2O).

This band compared well with the split band ($\tilde{\upsilon}$ = 1652 and 1605 cm^{-1}) observed for the νCO absorption of the related nickel(II) grid compound **25** · 10 H_2O of the higher ligand homologue (see Table 2.5.1). As for the IR spectrum of **25** · 10 H_2O, an intense absorption band was observed in the spectrum of **26** · 4 H_2O at $\tilde{\upsilon}$ = 1565 cm^{-1}. Summarising these observations, it was suggested that the two compounds **25** · 10 H_2O and **26** · 4 H_2O exhibited similar molecular structures. The presence of tetrafluoroborate counter ions was confirmed in the IR spectrum of **26** · 4 H_2O with a broad split band at $\tilde{\upsilon}$ = 1083 cm^{-1}.

UV/VIS spectroscopic studies on $[Ni^{II}_4(HL^{M1})_4](BF_4)_4 \cdot 4\ H_2O$ (26 · 4 H_2O)

The UV/VIS spectrum of **26** · 4 H_2O in acetonitrile solution (Figure 2.5.31) compared well with the spectrum of the related grid compound **25** · 10 H_2O of the higher ligand homologue and featured two absorption bands in the region of λ = 1400–200 nm. As for the spectrum of the grid compound **25** · 10 H_2O, the band at higher energy (λ_{max} = 261 nm, ε = 43000 M^{-1} cm^{-1}, $\tilde{\upsilon}$ = 38314 cm^{-1}) showed a distinct shoulder to lower energy.

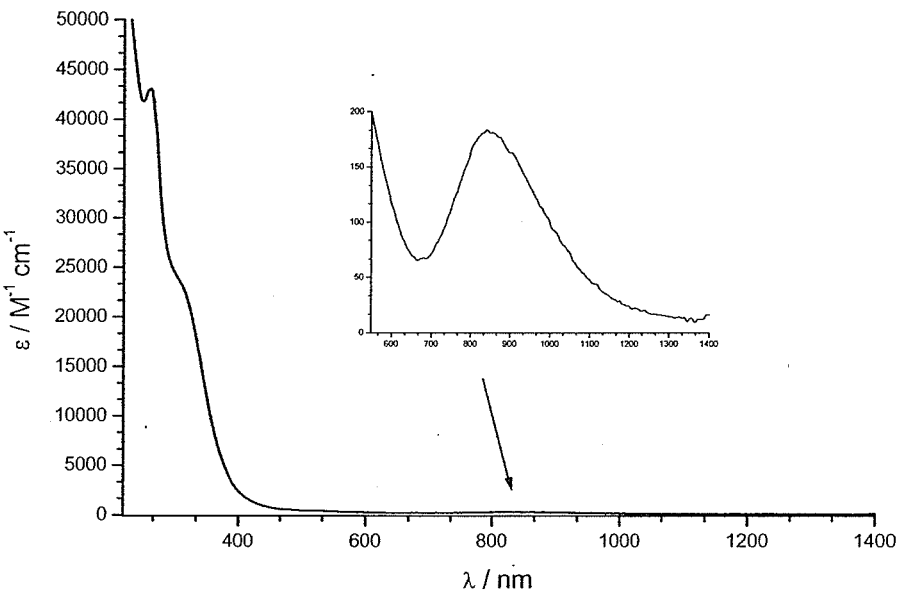

Figure 2.5.31. UV/VIS spectra [MeCN, 0.25 mM (inset) and 0.025 mM (main)] of $[Ni^{II}_4(H\mathbf{L}^{\mathbf{M1}})_4](BF_4)_4 \cdot 4\ H_2O$ (**26** · 4 H_2O).

By analogy with **25** · 10 H_2O, the band at λ_{max} = 853 nm (184 M^{-1} cm^{-1}, $\tilde{\upsilon}$ = 11723 cm^{-1}) was assigned to the $^3A_{2g} \rightarrow {}^3T_{2g}$ transition of octahedrally coordinated d^8 ions (Figure 2.5.25), confirming the expected octahedral coordination environment of the nickel(II) ions in **26** · 4 H_2O (ε = 46 M^{-1} cm^{-1} per nickel(II) ion). The crystal field splitting energy of **26** · 4 H_2O was therefore given to Δ_O = 11700 cm^{-1}, and was exactly the same as that for the related grid compound **25** · 10 H_2O of the higher ligand homologue. The expected absorption bands for the transitions $^3A_{2g} \rightarrow {}^3T_{1g}(F)$ and $^3A_{2g} \rightarrow {}^3T_{1g}(P)$ could not be observed and were probably masked by the strong band at higher energy. It is worthwhile noting that although the same energy of the

$^3A_{2g} \rightarrow {}^3T_{2g}$ transition was observed for the two homologous compounds **25** · 10 H_2O and **26** · 4 H_2O, the molar extinction coefficient was almost doubled for the latter compound **26** · 4 H_2O of the lower ligand homologue, relative to the former compound **25** · 10 H_2O of the higher ligand homologue (Figure 2.5.32). The same tendency has been observed before in the couples **6b** · MeCN *vs.* **8** and **18** *vs.* **19** · 4 H_2O, respectively (Figure 2.4.13).

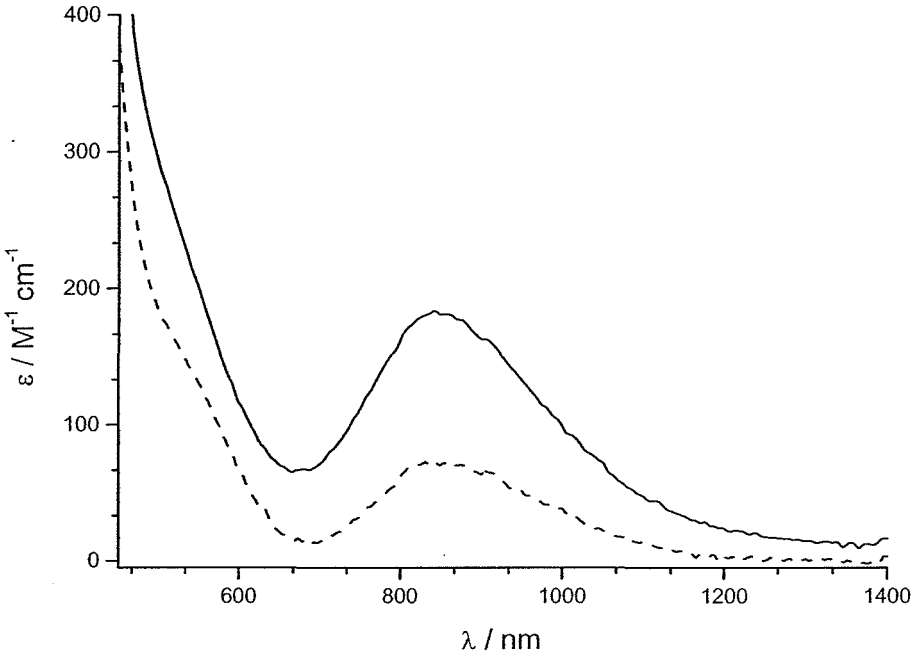

Figure 2.5.32. Comparison of the UV/VIS spectra [MeCN, 0.25 mM] (ε per nickel(II) ion) of $[Ni^{II}_4(HL^{M1})_4](BF_4)_4$ · 4 H_2O (**26** · 4 H_2O) (solid line) and $[Ni^{II}_4(HL^{M2})_4](BF_4)_4$ · 10 H_2O (**25** · 10 H_2O) (dashed line).

Cyclic voltammetric studies on $[Ni^{II}_4(HL^{M1})_4](BF_4)_4$ · 4 H_2O (26 · 4 H_2O)

As for compound **25** · 10 H_2O of the higher ligand homologue, the cyclic voltammogram of **26** · 4 H_2O in acetonitrile solution showed two metal-centred reduction waves, albeit very poorly resolved in the present case (Figure 2.5.33).

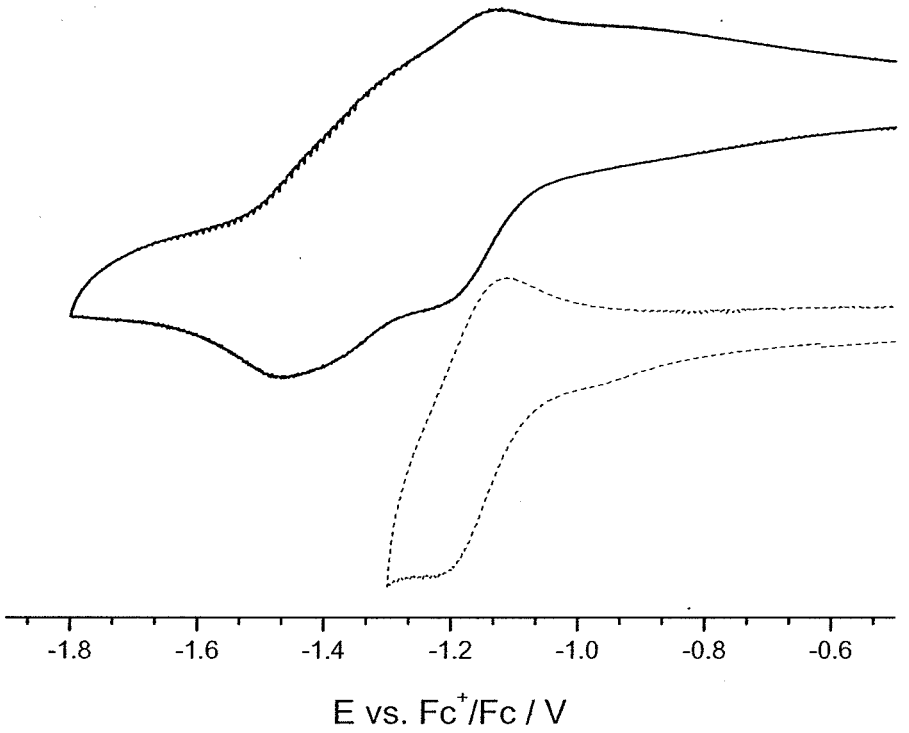

Figure 2.5.33. Cyclic voltammograms (0.25 mM, 0.1 M TBAP, MeCN, scan rate 200 mV s^{-1}) of $[Ni^{II}_4(HL^{M1})_4](BF_4)_4 \cdot 4\ H_2O$ (**26** · 4 H_2O).

At a scan rate of 200 mV s^{-1}, the reduction processes occurred at E_{pc} = –1.30 V and –1.54 V, relative to the Fc^+/Fc redox couple. The associated oxidation processes occurred as a series of overlapping waves with only one clear maximum, at E_{pa} = –1.19 V.

Magnetic studies on $[Ni^{II}_4(HL^{M1})_4](BF_4)_4 \cdot 4\ H_2O$ (26 · 4 H_2O)

As found for all complexes with pyrazine bridged metal centres described so far (**6b** · MeCN, **19** · 4 H_2O, **23**, **24** and **25** · 10 H_2O) the magnetic measurements of compound **26** · 4 H_2O obeyed the Curie-Weiss law above 50 K. In Figure 2.5.34 and Figure 2.5.35 are shown the temperature dependence of μ_{eff} and of χ_m per nickel(II) ion.

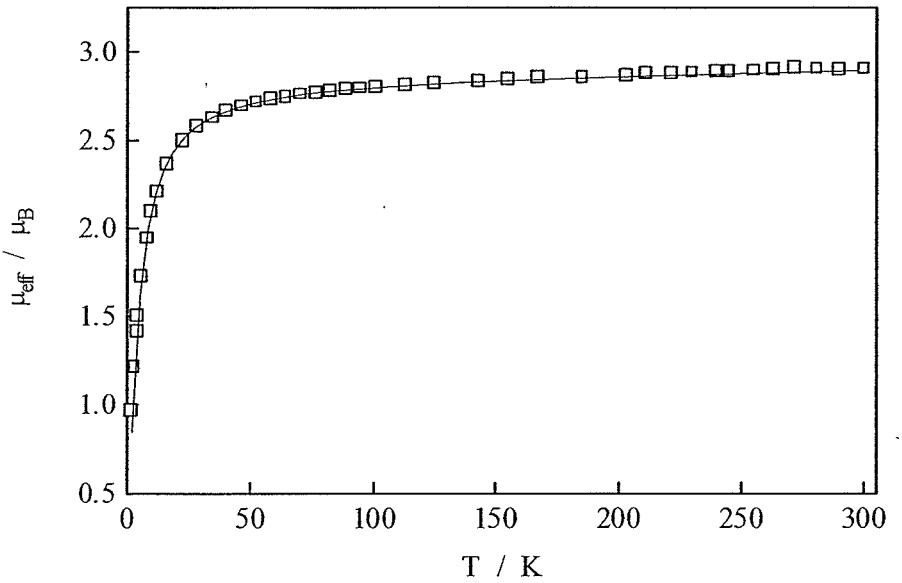

Figure 2.5.34. Thermal variation of the magnetic moment μ_{eff} (▫▫) of $[Ni^{II}_4(HL^{M1})_4](BF_4) \cdot 4\ H_2O$ (**26** · 4 H_2O). The solid line represents the best fit.

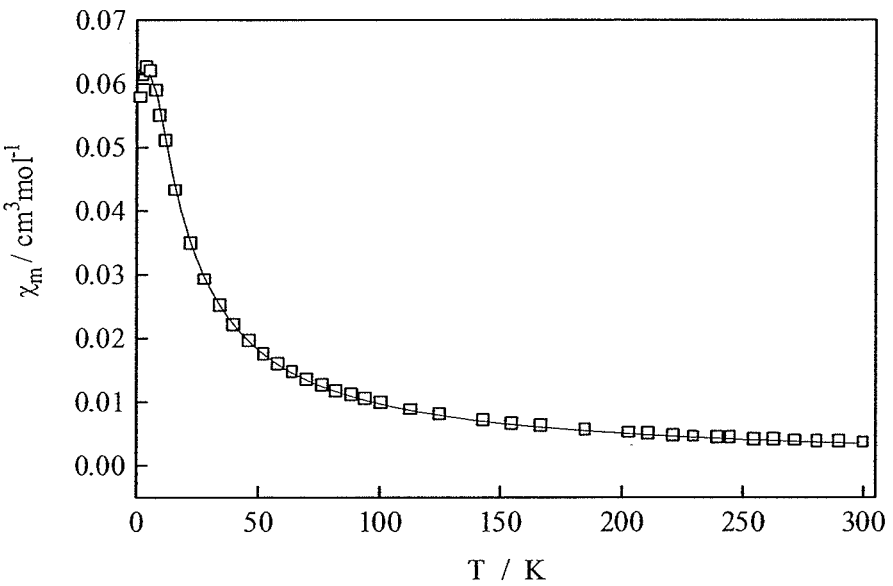

Figure 2.5.35. Thermal variation of the molar susceptibility χ_m (▫▫) of $[Ni^{II}_4(HL^{M1})_4](BF_4)_4 \cdot 4\ H_2O$ (**26** · 4 H_2O). The solid line represents the best fit.

Below 50 K, indicating the presence of antiferromagnetic interactions, the value of χ_m increased with decreasing temperature, reaching a maximum value at 5.24 K (0.0615 $cm^3\ mol^{-1}$) while the values of μ_{eff} decreased continuously. In contrast to the tetranuclear copper(II) complexes **19** · 4 H_2O and **24**, but by analogy with the nickel(II) grid compound **25** · 10 H_2O (J = –0.80 cm^{-1}), only one coupling constant

($J = -1.32$ cm^{-1}) was needed for compound **26** · 4 H_2O. It was noted that compared to the analogous grid complex **25** · 10 H_2O of the higher ligand homologue the coupling constant of **26** · 4 H_2O was almost doubled. The best fit for **26** · 4 H_2O was obtained from the parameters $g = 2.02$ and $TIP = 120 \times 10^{-6}$ cm^3 mol^{-1}. The calculated magnetic moment at room temperature was 2.89 μ_B.

Metathesis of 26 · 4 H_2O with ammonium hexafluorophosphate

Crystals of **26** · *n* solvent were obtained by various methods, such as vapour diffusion of diethyl ether into solutions of **26** · 4 H_2O in various solvents or solvent mixtures, layering with toluene or slow evaporation. The crystals were mostly seemingly beautiful but were all dreadfully twinned and no X-ray crystal structure determination could be carried out. In further attempts to obtain single crystals suitable for an X-ray crystal structure determination of the [2 × 2] grid-type complex cation of **26**, a change of counter ion was attempted. Unfortunately, complexations of $H_2\mathbf{L}^{M1}$ employing nickel(II) triflate hexahydrate or nickel(II) acetate tetrahydrate in *N,N*-dimethylformamide solution, employing sodium hydroxide as base, resulted in the isolation of dark brown solids of unknown compositions.

Metathesis of the tetrafluoroborate compound **26** · 4 H_2O into the corresponding hexafluorophosphate salt **26b** was carried out *in situ* in *N,N*-dimethylformamide by addition of a tenfold excess of ammonium hexafluorophosphate and subsequent precipitation with ethanol (Scheme 2.5.6). With this method compound **26b** was isolated in around 70 % yield.

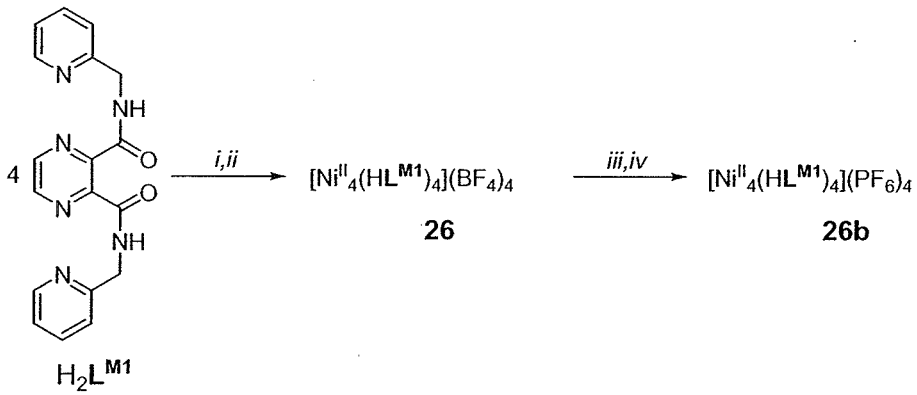

Scheme 2.5.6. Synthesis of **26b**. Reagents and conditions: (*i*) 1 eq. $Ni(BF_4)_2 \cdot 6\ H_2O$, DMF, RT; (*ii*) 1 eq. NaOH, DMF/H_2O (5:1); (*iii*) H_4NPF_6; (*iv*) EtOH.

Elemental analysis matched sufficiently well with the proposed formulation of $[Ni^{II}_4(HL^{M1})_4](PF_6)_4$ (**26b**) and the positive ion electrospray mass spectrum of **26b** in acetonitrile showed various peaks, which originated from tetranuclear species (Figure 5.2.4, Appendix). The peaks at *m/z* = 1911.8, 1765.6, 1619.0, 957.9, 883.9, 809.0, 589.0 and 404.9 were assigned to the tetranuclear complex fragments $[Ni^{II}_4(HL^{M1})(L^{M1})_3]^+$, $\{[Ni^{II}_4(HL^{M1})_2(L^{M1})_2](PF_6)\}^+$, $[Ni^{II}_4(HL^{M1})(L^{M1})_3]^+$, $\{[Ni^{II}_4(HL^{M1})_4](PF_6)_2\}^{2+}$, $\{[Ni^{II}_4(HL^{M1})_3(L^{M1})](PF_6)\}^{2+}$, $[Ni^{II}_4(HL^{M1})_2(L^{M1})_2]^{2+}$, $[Ni^{II}_4(HL^{M1})_4](PF_6)\}^{3+}$ and $[Ni^{II}_4(HL^{M1})_4]^{4+}$, respectively.

The IR spectrum of the compound compared reasonably well with the corresponding spectrum of **26** · 4 H_2O and showed no evidence of remaining tetrafluoroborate anions (Figure 5.3.10, Appendix; Table 2.5.1). The IR spectrum showed two strong bands at $\tilde{\upsilon}$ = 1636 and 1617 cm^{-1}, in the expected region of ν_{CO} vibration absorptions and a third strong absorption band $\tilde{\upsilon}$ = 1566 cm^{-1}.

Crystals obtained by vapour diffusion of diethyl ether into a solution of **26b** in *N,N*-dimethylformamide or acetonitrile although beautiful looking by eye were again dreadfully twinned and no X-ray crystal structure determination could be carried out.

Complexation of H_2L^{M1} and nickel(II) nitrate trihydrate

The complex **26c** · 4 H_2O was formed in around 80 % yield as a red-brown crystalline solid, by employing nickel(II) nitrate hexahydrate under otherwise identical reaction conditions to the formation to those used in the formation of **26**. Elemental analysis of **26c** · 4 H_2O matched well with the stoichiometry of the proposed [2 × 2] grid structure and the compound was accordingly formulated as $[Ni^{II}_4(HL^{M1})_4](NO_3)_4 \cdot 4\ H_2O$.

The IR spectrum of **26c** · 4 H_2O compared well to the IR spectrum of the parent compound **26** · 4 H_2O (Figure 5.3.11, Appendix; Table 2.5.1). In the expected region of the ν_{CO} vibration the IR spectrum of **26c** · 4 H_2O revealed a band at $\tilde{\upsilon}$ = 1606 cm^{-1} and a very small but distinct peak at $\tilde{\upsilon}$ = 1653 cm^{-1}. Furthermore a strong absorption band was observed at $\tilde{\upsilon}$ = 1564 cm^{-1}.

Table 2.5.1. Comparison of the absorption bands in the expected region of ν_{CO} absorptions in the IR spectra of the dinuclear complexes **6** and **8** and the tetranuclear complexes **23**, **23b**, **24**, **25** · 10 H_2O, **26** · 4 H_2O, **26b** and **26c** · 4 H_2O.

Complex	ν_{CO} absorptions (1) / cm^{-1}	ν_{CO} absorptions (2) / cm^{-1}
$[Cu^{II}_2(HL^{M1})(MeCN)_2(H_2O)_2](BF_4)_3$ (**6**)	1609	—
$[Cu^{II}_4(HL^{M1})_4](BF_4)_4$ (**23**)	—	1651
$[Cu^{II}_4(HL^{M1})_4](PF_4)_6$ (**23b**)	1615	1640
$[Ni^{II}_4(HL^{M1})_4](BF_4)_4$ · 4 H_2O (**26** · 4 H_2O)	1606	shoulder to higher energy
$[Ni^{II}_4(HL^{M1})_4](PF_4)_6$ (**26b**)	1617	1636
$[Ni^{II}_4(HL^{M1})_4](NO_3)_4$ · 4 H_2O (**26c** · 4 H_2O)	1606	1653
$[Cu^{II}_2(HL^{M2})(H_2O)](ClO_4)_3$ (**8**)	1605	—
$[Cu^{II}_4(HL^{M2})_4](BF_4)_4$ (**24**)	—	1636
$[Ni^{II}_4(HL^{M2})_4](BF_4)_4$ · 10 H_2O (**25** · 10 H_2O)	1605	1652

The positive ion electrospray mass spectrum of **26c** · 4 H_2O in acetonitrile showed, apart from the peaks of the protonated ligand species $[H_3L^{M1}]^+$ and $[H_4L^{M1}]^{2+}$ at *m/z* = 349.2 and 175.1, two major multiplets in the *m/z* = 560–570 and 840–860 regions (Figure 2.5.36). It was conspicuous that the increments between the major

peaks within each multiplet equalled *m/z* of oxygen. The main peak at *m/z* = 561.4 of the multiplet around *m/z* = 560–570 was assigned to the tetranuclear complex fragment $\{[Ni^{II}_4(HL^{M1})_4](NO_3)\}^{3+}$. The main peak at *m/z* = 856.6 of the second multiplet was attributed to the complex fragment $\{[Ni^{II}_4(HL^{M1})_4](NO_3)_2\}^{2+}$.

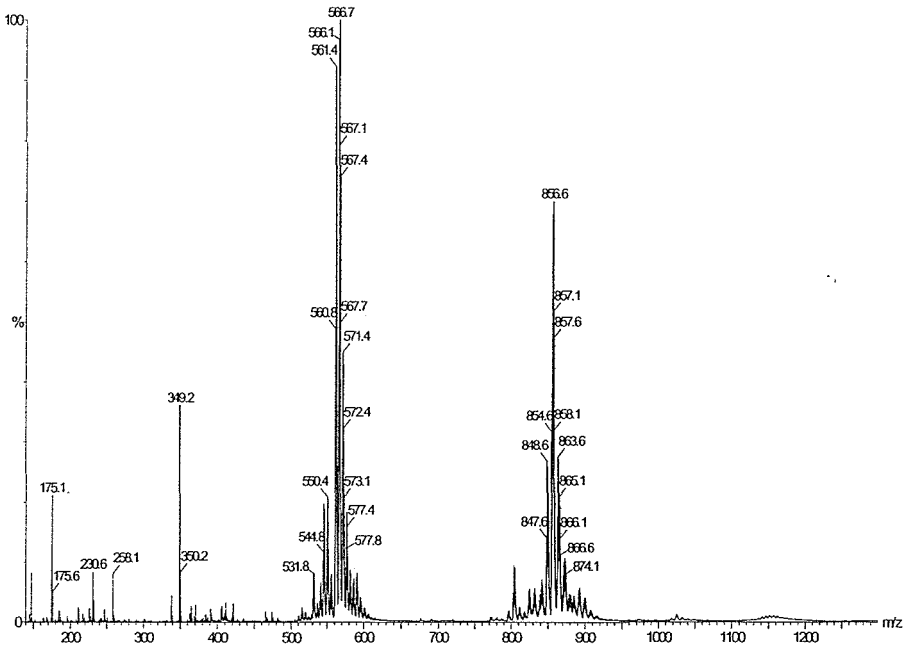

Figure 2.5.36. ESI-MS spectrum (MeCN) of $[Ni^{II}_4(HL^{M1})_4](NO_3)_4 \cdot 4\ H_2O$ (**26c** · 4 H_2O).

Conclusions

Unfortunately no single crystals of a quality suitable for X-ray crystal structure determination, of either of the complexes $[Ni^{II}_4(HL^{M1})_4](BF_4)_4 \cdot 4\ H_2O$ (**26** · 4 H_2O), $[Ni^{II}_4(HL^{M1})_4](PF_6)_4$ (**26b**) or $[Ni^{II}_4(HL^{M1})_4](NO_3)_4 \cdot 4\ H_2O$ (**26c** · 4 H_2O) were obtained. Nevertheless it was suggested that the complex cations of all three compounds probably exhibited the [2 × 2] grid-type structure as shown in Figure 2.5.37. In all three cases the assumption was supported by results from elemental analysis and positive ion electrospray mass spectroscopy. In the case of the tetrafluoroborate complex **26** · 4 H_2O this assumption was further supported by a UV/VIS

spectroscopic analysis that confirmed the octahedral coordination environment of the nickel(II) ions. The cyclic voltammogram of **26** · 4 H_2O in acetonitrile further corroborated the (at least dinuclearity but probably) higher nuclearity of the compound. The magnetic measurements were in good agreement with the proposed structure of **26**.

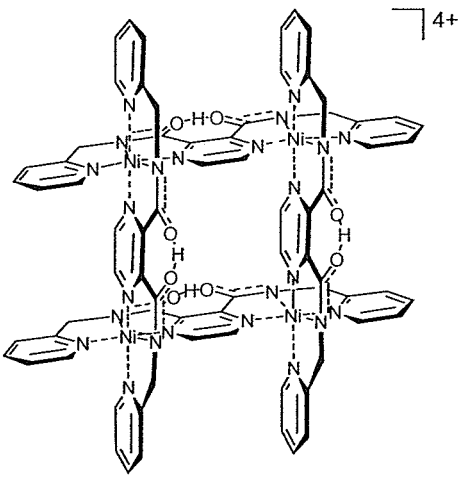

$[Ni^{II}_4(HL^{M1})_4]^{4+}$

Figure 2.5.37. The [2 × 2] grid complex cation $[Ni^{II}_4(H\mathbf{L}^{\mathbf{M1}})_4]^{4+}$ supposedly present in **26**, **26b** and **26c**.

Note: Just prior to submission of this thesis the X-ray crystal structure and the magnetic properties of $[Ni^{II}_4(HL^{M1})_4](Cl)_4$ · 5 MeCN · 13 H_2O were reported by Cati, Stoeckli-Evans and co-workers.[143]

2.5.3. *Metal(II) ions other than copper(II) or nickel(II)*

Complexations with manganese(II) and H_2L^{M1} or H_2L^{M2}

The reaction of H_2L^{M1} or H_2L^{M2} with manganese(II) perchlorate hexahydrate or manganese(II) chloride and triethylamine in a 1:1:1 molar ratio, respectively, resulted in the formation of inhomogeneous pale solids. Further attempts at isolating pure samples were unsuccessful.

Complexations with iron(II) and H_2L^{M1} or H_2L^{M2}

The reaction of H_2L^{M1} with iron(II) tetrafluoroborate hexahydrate and triethylamine employing a 1:1:1 molar ratio in acetonitrile solution and subsequent vapour diffusion of diethyl ether into the dark blue-black reaction mixture led to the formation of an inhomogeneous solid of brown and blue-black colouration. Attempts at purifying the compound were unsuccessful. A similar reaction outcome was observed in *N,N*-dimethylformamide solution with the employment of sodium hydroxide as base.

In acetonitrile solution the use of H_2L^{M2}, iron(II) tetrafluoroborate hexahydrate and triethylamine in a 1:1:1 molar ratio resulted in a dark purple-black solution from which, on addition of toluene, a blue-black solid was precipitated. On redissolving the solid in acetonitrile it was noted that in the blue-black solution a brown-black solid residue remained undisolved. On slow diffusion of toluene into the intensely coloured solution, very few, very tiny hexagonal crystals were obtained apart from the major bulk of an inhomogeneous blue-black solid. Elemental analysis of the crystals was consistent with a formulation of $[Fe^{II}Fe^{III}(HL^{M2})_2]_n(BF_4)_{3n}$, suggesting that the compound might be of a mixed-valent nature. Unfortunately, the crystals obtained were too small for X-ray crystal structure determination in New Zealand

and did not survive the journey to the Daresbury synchrotron intact. There was not enough of this compound isolated for cyclic voltammetry or other analytical methods, so that the true nature of the compound remains unknown. Under inert atmosphere and otherwise identical reaction conditions, the reaction outcome was basically identical. The sole difference was that the remaining brown-black solid residue, on redissolving the crude reaction product in acetonitrile, was a smaller mass percentage of the employed amount or crude product, relative to the reaction in air. This observation was consistent with the suggestion that air oxidation of the initially employed iron(II) ions led to the formation of a brown-black compound, which was poorly soluble in acetonitrile. Still, the main bulk on recrystallisation was an inhomogeneous blue-black solid, as described before and only a very small amount of crystalline material was obtained. A blue-black inhomogeneous solid was also obtained when reducing agents like hydroquinone or sodium dithionite were employed. A reaction carried out with a continuous stream of air through the reaction vessel, under otherwise identical conditions, led to the formation of a rust brown inhomogeneous solid of unknown composition, supporting the idea that the initially employed iron(II) ions were oxidised in air.

Complexations with cobalt(II) and H_2L^{M1} or H_2L^{M2}

The reaction of H_2L^{M1} with cobalt(II) tetrafluoroborate hexahydrate and triethylamine in a 1:1:1 molar ratio in acetonitrile solution resulted, after several hours of stirring at room temperature, in the precipitation of an orange-red amorphous solid. Under otherwise identical reaction conditions, the reaction in *N,N*-dimethylformamide with subsequent vapour diffusion of diethyl ether resulted in a dark brown amorphous solid. As observed by the employment of a molar ratio of 2:1 of ligand to cobalt(II) (see Section 2.2.5), the IR spectra of the two former compounds

revealed intense absorption peaks at $\tilde{\upsilon}$ = 1734 and 1727 cm^{-1}, respectively, suggesting the decomposition of the ligand.

The employment of a 1:1:1 molar ratio of H_2L^{M2}, cobalt(II) tetrafluoroborate hexahydrate and triethylamine in acetonitrile solution led to a dark brown reaction mixture, from which by vapour diffusion of diethyl ether a dark brown solid was precipitated. By recrystallisation from acetonitrile and vapour diffusion of diethyl ether, dark brown, very thin crystal plates could be isolated. Results from elemental analyses, of crystals obtained in various attempts, varied significantly with mass percentages for carbon and nitrogen between 42–52 and 14–19 %, respectively.

The IR spectra each revealed only one ν_{CO} vibration absorption at $\tilde{\upsilon}$ = 1636 cm^{-1} and the presence of tetrafluoroborate was confirmed.

A positive ion electrospray mass spectrum in acetonitrile showed the most intense peaks at m/z = 809.1, 433.0 and 405.1 that were assigned to the complex fragments $[Co^{III}(HL^{M2})_2]^+$, $[Co^{III}(L^{M2})]^+$ and $[Co^{III}(H_2L^{M2})(HL^{M2})]^{2+}$, respectively.

The cyclic voltammogram of the compound revealed one partially reversible reduction process at $E_{1/2}$ = –0.56 V, ΔE = 0.05 V (Figure 5.5.3, Appendix). It was therefore suggested that the original compound isolated probably contained cobalt(III) ions, which was consistent with the two related mononuclear compounds $[Co^{III}(H_2L^{M1})_2](BF_4)_3 \cdot 4\ H_2O$ (**21** · 4 H_2O) ($E_{pc(21)}$ = –0.60 V) and $[Co^{III}(H_2L^{M2})_2](BF_4)_3 \cdot$ EtOH (**22** · EtOH) ($E_{pc(22)}$ = –0.44 V). Two further irreversible reduction processes were observed in the cyclic voltammogram of the compound at E_{pa} = –1.52 and –1.97 V respectively.

Surprisingly no sensible NMR spectrum could be obtained but the ^1H NMR spectrum in d^3-MeCN exhibited very broad unresolved absorption peaks.

Unfortunately, recrystallisation attempts failed to give single crystals of a size suitable for X-ray crystal structure determination so that the structure of the compound remains unknown.

2.5.4. *Summary*

It has been shown that [2 × 2] grid-like arrangements can be formed with the monodeprotonated homologous ligands $(HL^{M1})^-$ and $(HL^{M2})^-$, respectively. To activate the second terdentate binding pocket towards metal ion coordination the deliberate deprotonation of the ligand was necessary in all cases. This observation was demonstrated effectively by the rearrangement of the dimeric complex **18** to the [2 × 2] grid complex **23**, which could be monitored by UV/VIS spectroscopic titration and by the molecular structures of both compounds. Nickel(II) and copper(II) grids were isolated by the use of the lower ligand homologue (H_2L^{M1}). Both grid complexes **23** and **26** · 4 H_2O revealed weak antiferromagnetic spin coupling between the metal(II) ions. The use of the higher ligand homologue (H_2L^{M2}) and copper(II) or nickel(II), led to the formation of tetranuclear complexes, respectively. The [2 × 2] nickel(II) grid **25** · 10 MeCN exhibited bis-terdentate ligands whereas the square-like tetranuclear copper(II) complex **24** employed hybrid terdentate-bidentate ligands, which led to a N_4O coordination for the copper(II) ions. Both compounds **24** and **25** · 10 H_2O displayed weak antiferromagnetic spin coupling between the metal(II) ions.

2.6. *The diamide ligands H_2L^{S1} and H_2L^{S2}*

The synthesis, properties and the complexation behaviour of the two homologous ligands H_2L^{M1} and H_2L^{M2} have been described in the Sections 2.1–2.5. With their terdentate binding pockets the ligands could coordinate to metal ions in a *mer* configuration, respectively, leading to a repeating linear array with parallel coordinate vectors (Figure 2.6.1). Even on occupation of both binding pockets, employing both amide nitrogen atoms, the resulting complex fragments $[M^{II}_2(HL^{M1})]^{3+}$ and $[M^{II}_2(HL^{M2})]^{3+}$ thus retained one of the former N-H amide protons in an O···H···O hydrogen bond, resulting in a seven-membered ring (Figure 2.2.22). This feature made the ligands geometrically flat and relatively rigid, despite the *ortho* position of the two bulky carbonyl groups. Thus the ligands could define one side of a square of a [2 × 2] grid-type arrangement. As the orientation of the coordinate vectors of the two terdentate units was parallel the resulting grid-type complexes were achiral (Figure 2.6.1).

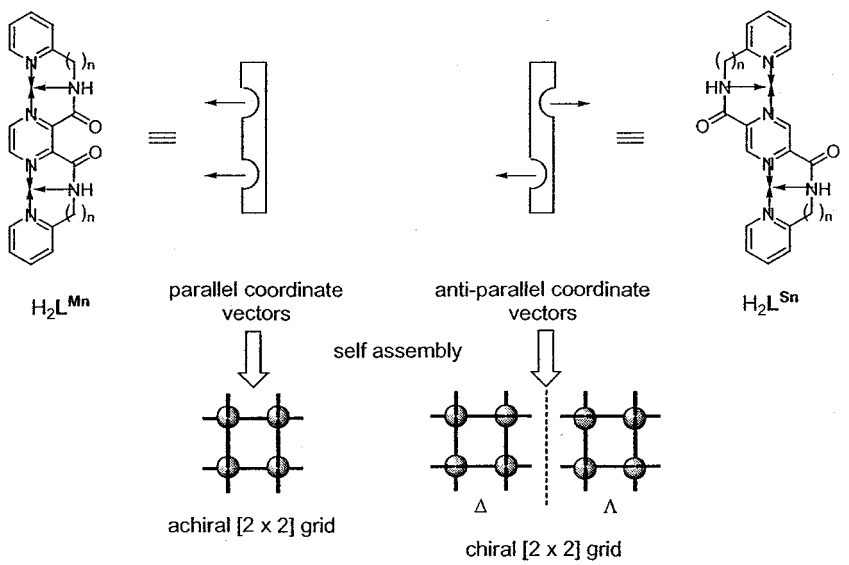

Figure 2.6.1. Definition of parallel and antiparallel coordinate vectors resulting in the formation of achiral and chiral [2 × 2] grid-type complexes, respectively.

The analogous S-type ligands *N,N'*-bis(2-pyridylmethyl)pyrazine-2,5-dicarboxamide (H_2L^{S1}) and *N,N'*-bis[2-(2-pyridyl)ethyl]pyrazine-2,5-dicarboxamide (H_2L^{S2}) also both feature two chelating terdentate binding sites in a repeating linear array (Figure 2.6.2). The main difference between the ligand pairs H_2L^{M1} *vs.* H_2L^{M2} and H_2L^{S1} *vs.* H_2L^{S2} is their physical construction. Whereas the M-type ligands H_2L^{M1} and H_2L^{M2} are 2,3-substituted pyrazine derivatives (Figure 2.1.1), which gives them an M-shaped appearance as drawn, the S-type ligands H_2L^{S1} and H_2L^{S2} are 2,5-substituted pyrazine derivatives, which gives them an S-shaped appearance as drawn.

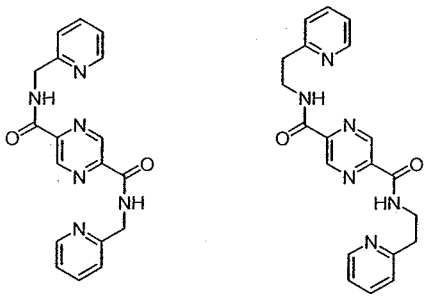

H_2L^{S1} H_2L^{S2}

Figure 2.6.2. The symmetrical diamide ligands H_2L^{S1} and H_2L^{S2}.

As indicated in Figure 2.6.1 the S-shape of the two homologous ligands H_2L^{S1} and H_2L^{S2} gives rise to antiparallel coordinate vectors, which on complexation is expected to lead to chiral grid molecules. As the two carbonyl groups of the S-type ligands are situated *para* to each other and are therefore further apart than in the M-type ligands, where they are situated in an *ortho* arrangement, they are not able to retain potential former N-H amide protons in a symmetrical intramolecular O···H···O hydrogen bond. Grid-type complexes of bivalent metals of the uncharged kind $[M^{II}_4(L^{S1})_4]^0$ and $[M^{II}_4(L^{S2})_4]^0$ are therefore expected (Scheme 2.4.1, b).

Synthesis of H_2L^{S1} and H_2L^{S2}

The common ligand precursor, dimethyl pyrazine-2,5-dicarboxylate (**29**), was synthesised from commercially available 2,5-dimethylpyrazine (**27**) in a one-pot two-step procedure giving diester **29** as a pure crystalline material. The first step consisted of the oxidation of the α-methyl groups with selenium dioxide in pyridine to obtain pyrazine-2,5-dicarboxylic acid (**28**).[192-194] By analogy with the synthesis of the 2,3-derivative **3**, the dicarboxylic acid **28** was not isolated but the subsequent esterification with methanol and thionyl chloride was carried out with the crude reaction mixture, after the removal of the precipitated elemental selenium by filtration (Scheme 2.6.1). Following this procedure, analytically pure diester **29** was obtained in good yields of around 50–60 %. It is noteworthy that the ^{1}H NMR spectrum of **29** consistently showed the curiosity of having a peak ratio for pz*H*:CO_2CH_3 of 1:3.7 to 1:4.5, even after purification by column chromatography.

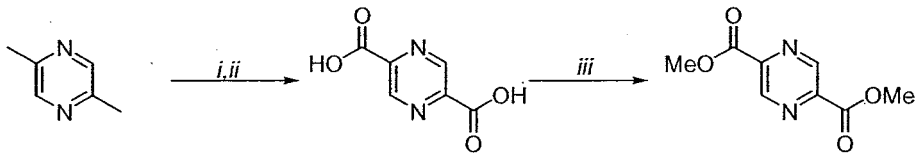

27 **28** **29**

Scheme 2.6.1. Synthesis of **29**. Reagents and conditions: (*i*) SeO_2, py/H_2O (10:1), reflux; (*ii*) H_2O, filtration; (*iii*) $SOCl_2$, MeOH, reflux.

The symmetrical S-type bis-terdentate diamide ligands *N,N'*-bis(2-pyridyl-methyl)pyrazine-2,5-dicarboxamide (H_2L^{S1}) and *N,N'*-bis[2-(2-pyridyl)ethyl]pyrazine-2,5-dicarboxamide (H_2L^{S2}) were obtained by reacting diester **29** with 2-(amino-methyl)pyridine (**4**) or 2-(2-aminoethyl)pyridine (**5**) in a molar ratio of 1:2.2, respectively (Scheme 2.6.2). The reactions were carried out in methanol solution in an open flask, respectively, thus allowing most of the solvent to evaporate. The ligands H_2L^{S1} and H_2L^{S2} were obtained by filtration in around 80 and 70 % yield as colourless solids, respectively.

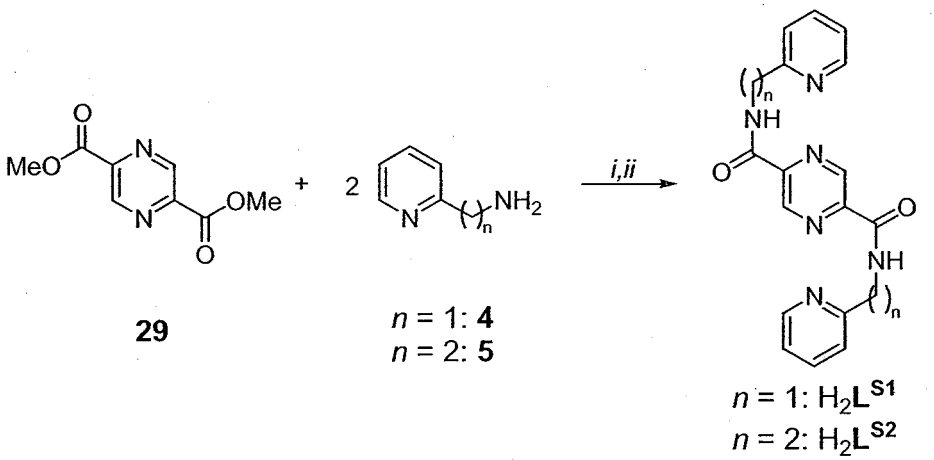

Scheme 2.6.2. Synthesis of $H_2\mathbf{L}^{S1}$ and $H_2\mathbf{L}^{S2}$. Reagents and conditions: (*i*) MeOH, 80–90°, open flask; (*ii*) filtration.

Both compounds proved to be virtually insoluble in all common solvents at room temperature. Little solubility was observed in chloroform and dichloromethane. Little solubility was also observed in refluxing methanol, acetonitrile and *N,N*-dimethylformamide.

IR spectroscopic studies on H_2L^{S1} and H_2L^{S2}

As discussed in Section 2.1 the IR spectra of the M-type ligands H_2L^{M1} and H_2L^{M2} exhibited two ν_{CO} and δ_{NH} absorption bands, respectively. This observation was explained by the *ortho* arrangement of their carbonyl groups, which was believed to give rise to the tautomeric equilibria shown in Figure 2.1.4, and to result in the splitting of the absorption bands in question. In contrast the symmetrical S-type ligands H_2L^{S1} and H_2L^{S2} exhibited a *para* arrangement of the carbonyl groups and lacked the possibility of expressing similar tautomeric equilibria. Therefore only one ν_{NH}, ν_{CO} and δ_{NH} absorption band was expected in the IR spectra of H_2L^{S1} and H_2L^{S2}, respectively. In fact as shown in Figure 2.6.3 and Figure 2.6.4 only one band occurred for the respective vibrations, which for each S-type ligand homologue occurred at a wavenumber in between the wavenumbers observed for the two bands of their analogous M-type ligand (see Table 2.6.1).

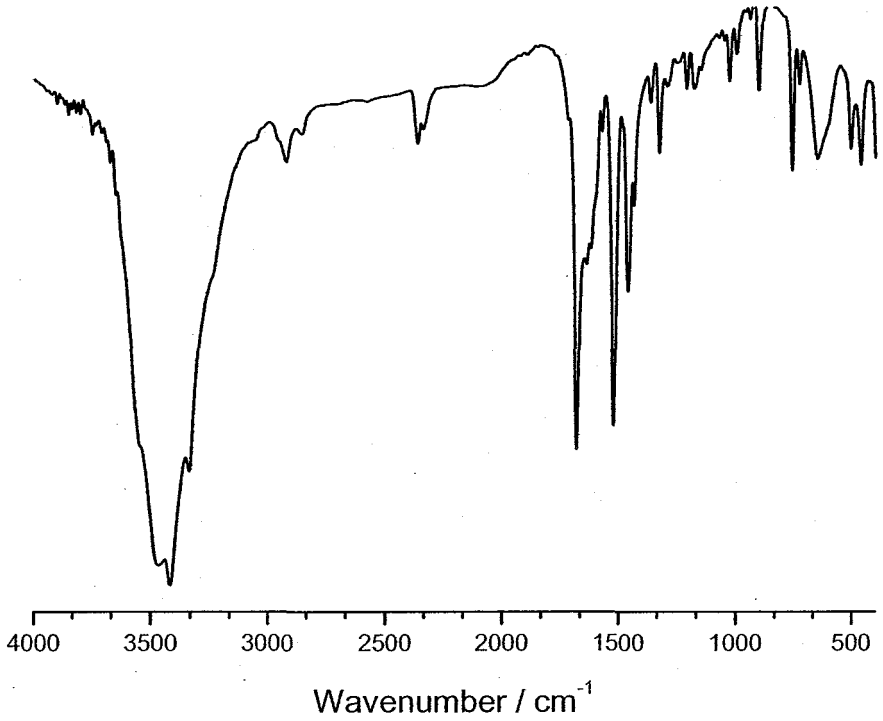

Figure 2.6.3. IR spectrum (KBr) of $H_2\mathbf{L}^{S1}$.

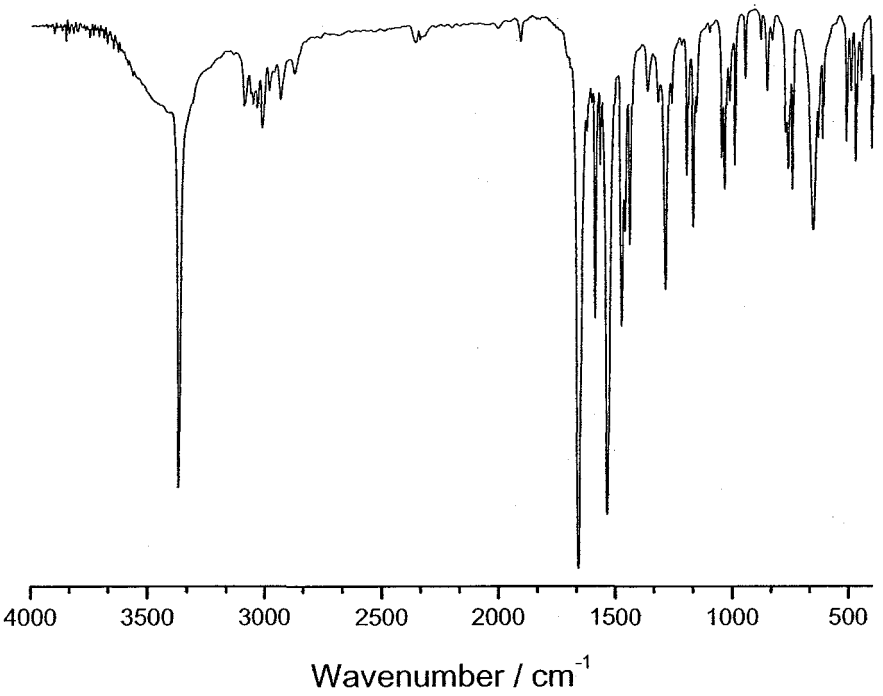

Figure 2.6.4. IR spectrum (KBr) of $H_2\mathbf{L}^{S2}$.

Table 2.6.1. Comparison of the ν_{CO} and δ_{NH} absorption bands in the IR spectra of $H_2\mathbf{L}^{M1}$, $H_2\mathbf{L}^{S1}$, $H_2\mathbf{L}^{M2}$ and $H_2\mathbf{L}^{S2}$.

Absorption	H_2L^{M1}	H_2L^{S1}	H_2L^{M2}	H_2L^{S2}
ν_{CO} / cm^{-1}	1690 1655	1681	1674 1651	1659
δ_{NH} / cm^{-1}	1533 1514	1522	1541 1509	1535

NMR spectroscopic studies on H_2L^{S1} and H_2L^{S2}

The aromatic region of the ^1H NMR spectra, measured in deutero chloroform, of H_2L^{S1} (Figures 2.6.5 and 5.1.5) and H_2L^{S2} (Figures 2.6.6 and 5.1.6) showed six signals and five signals including a multiplet of superposed signals, respectively. Compared to the spectra of their analogous M-type ligands the signals derived from the pyridine protons experienced only small shifts (see Table 2.6.2). The singlet belonging to the pyrazine proton experienced a relatively great shift of 0.81 ppm for H_2L^{S1} and 0.70 ppm for H_2L^{S2} to lower field, compared to their respective M-type analogues, and both occurred well above 9 ppm. Also a relatively large shift to lower field, of 0.65 ppm for H_2L^{S1} and 0.71 ppm for H_2L^{S2}, was observed for the signal derived from the amide protons, respectively.

In the series of the four M- and S-type ligands, the ^1H NMR spectrum of H_2L^{S1} was the only one that exhibited the signal of the amide protons at lower field than the signal derived from 6-py*H* (see Table 2.6.2).

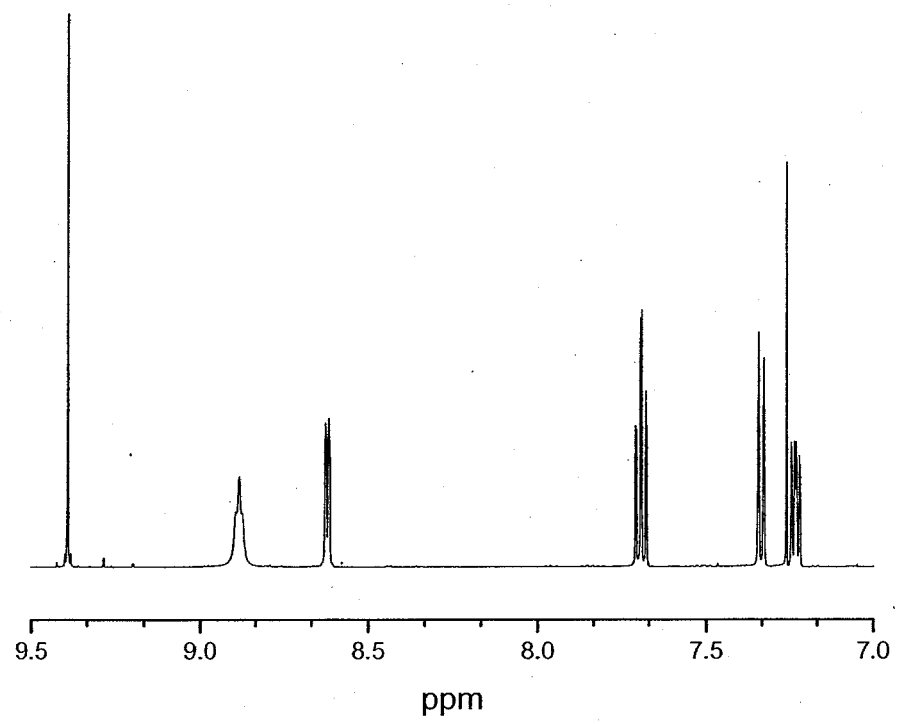

Figure 2.6.5. Aromatic region of the ^{1}H NMR spectrum ($CDCl_3$) of $H_2\mathbf{L}^{S1}$.

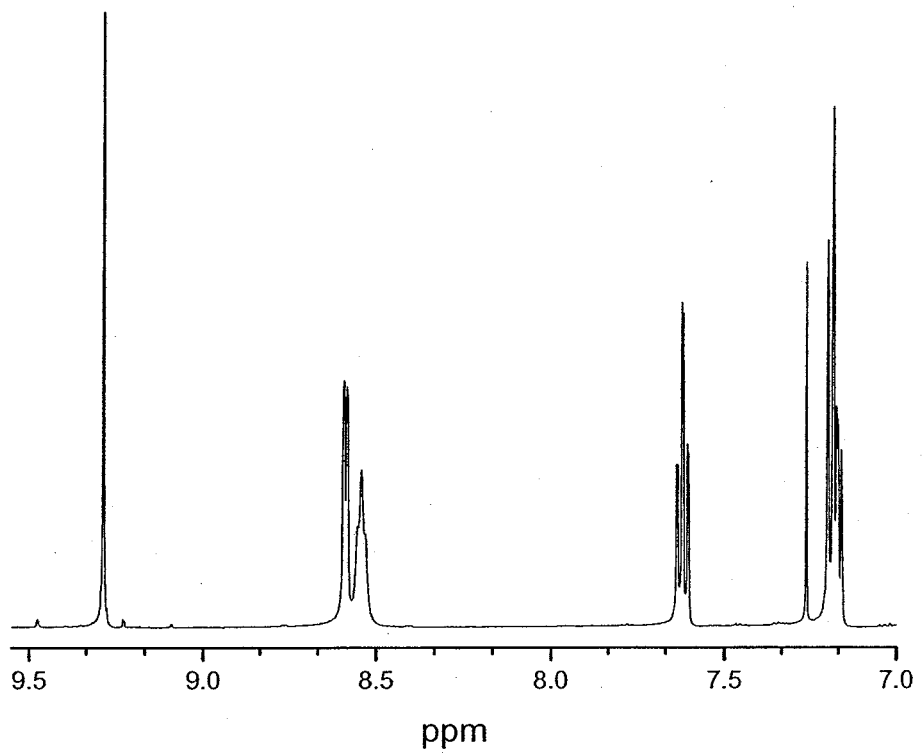

Figure 2.6.6. Aromatic region of the ^{1}H NMR spectrum ($CDCl_3$) of $H_2\mathbf{L}^{S2}$.

Table 2.6.2. Comparison of the ^{1}H NMR ($CDCl_3$) signals in the aromatic region of $H_2\mathbf{L}^{M1}$, $H_2\mathbf{L}^{S1}$, $H_2\mathbf{L}^{M2}$ and $H_2\mathbf{L}^{S2}$.

Signal / ppm	H_2L^{M1}	H_2L^{S1}	H_2L^{M2}	H_2L^{S2}
pz*H*	8.58 (s)	9.39 (s)	8.58 (s)	9.28 (s)
Amide-*H*	8.23 (t)	8.88 (t)	7.83 (s)†	8.54 (s)†
3-py*H*	7.35 (d)	7.34 (td)	7.20 (d)	7.20–7.16 (m)*
4-py*H*	7.60 (dt)	7.69 (dt)	7.61 (dt)	7.62 (dt)
5-py*H*	7.13 (ddd)	7.23 (ddd)	7.13 (ddd)	7.20–7.16 (m)*
6-py*H*	8.46 (ddd)	8.62 (ddd)	8.51 (ddd)	8.59 (d)

* overlapping multiplet signal, derived from 3-py*H* and 5-py*H*
† poorly resolved triplet

The ^{13}C NMR spectra of the compounds, measured in deutero chloroform, showed all of the expected signals (Figures 5.1.7 and 5.1.8, Appendix) and only very small shifts relative to the spectra of their analogous ligands, respectively. As had been observed for the M-type ligand couple, the signals of the *5*-py (122.6 ppm for H_2L^{S1} and 121.8 ppm for H_2L^{S2}) and *3*-py (122.1 ppm for H_2L^{S1} and 123.5 ppm for H_2L^{S2}) carbon atoms of the S-type ligand couple have switched their relative order with respect to each other.

2.7. *Coordination of the ligands H_2L^{S1} and H_2L^{S2}, employing a 1:1 molar ratio of ligand to copper(II) ions*

2.7.1. *Copper(II) salts without base*

Complexations

As the ligand H_2L^{S1} was insoluble in most solvents and practically insoluble in acetonitrile and *N,N*-dimethylformamide at room temperature, complexations were initially carried out in refluxing acetonitrile solution. It has been found however, that reactions with copper(II) ions did not require solutions of the ligand, as the suspended ligand readily dissolved on complexation. Complexations carried out with H_2L^{S1} and copper(II) tetrafluoroborate tetrahydrate in a molar ratio of 1:1 using a small volume of acetonitrile resulted in the immediate precipitation of a turquoise microcrystalline solid. Elemental analysis suggested a molar ratio of copper(II) to ligand to tetrafluoroborate of 2:1:2, proposing a possible formulation of $[Cu^{II}_2(L^{S1})](BF_4)_2 \cdot n$ solvent. Increasing the solvent volume, to avoid immediate precipitation, and slow evaporation of the solvent, did not alter the reaction outcome, but the compound was obtained as a turquoise-green crystalline material with the same empirical formulation (see Section 2.7.3, compound **33**). A change of reaction solvent to water instead of acetonitrile and slow evaporation resulted in a different, very unexpected but still dinuclear copper(II) complex (see Section 2.7.3, compound **34**).

The employment of the higher ligand homologue H_2L^{S2} and copper(II) in a molar ratio of 1:1 was carried out in acetonitrile by adding a solution of copper(II) tetrafluoroborate tetrahydrate to a suspension of the ligand. Compared to the lower

ligand homologue H_2L^{S1} the ligand H_2L^{S2} dissolved after the addition of the copper(II) salt only reluctantly and after several hours of stirring. By vapour diffusion of diethyl ether into the resulting grass green solution turquoise-green crystals of what turned out to be a dinuclear copper(II) complex could be isolated (see Section 2.7.4, compound **35**).

2.7.2. *Copper(II) salts and one equivalent of base*

In contrast to the reactions with the analogous M-type ligands H_2L^{M1} and H_2L^{M2}, no complexes of the S-type ligands H_2L^{S1} and H_2L^{S2}, exhibiting a 1:1 molar ratio of ligand to copper(II), were obtained without the employment of base.

Complexations with copper(II) tetrafluoroborate tetrahydrate

The addition of triethylamine to a turquoise-blue solution of a 1:1 molar ratio of copper(II) tetrafluoroborate tetrahydrate and the lower ligand homologue H_2L^{S1}, in a relatively large volume of acetonitrile, did not result in a drastic colour change, such as had been observed with the employment of the analogous M-type ligand H_2L^{M1} (Figure 2.5.1). In this case the initially turquoise-blue solution slowly became greener and eventually was dark grass green. With the addition of toluene to the reaction mixture a turquoise amorphous solid was precipitated and could be isolated in around 70 % yield (Scheme 2.7.1). The compound proved to be insoluble in ethanol, was only slightly soluble in acetonitrile but was readily soluble in water and *N*,*N*-dimethylformamide. Elemental analysis suggested that the compound could be formulated as $[Cu^{II}(HL^{S1})]_n(BF_4)_n \cdot n\ H_2O$ (**30**). As described in Section 2.5.1 a similar formulation had been found for the [2 × 2] grid compound $[Cu^{II}_4(HL^{M1})_4](BF_4)_4$ (**23**),

which originated from a reaction employing H_2L^{M1} under otherwise identical reaction conditions. However, for reasons discussed above, no grid-type structure was expected in the present case. The 1:1 compound **30** was rather believed to have a structure similar to $[Cu^{II}_2(H_2L^{M1})_2(MeCN)_2](BF_4)_4$ (**18**) of the M-type ligand analogue, which originated from the 1:1 molar reaction of copper(II) tetrafluoroborate tetrahydrate and ligand without the employment of base. The compound was therefore tentatively formulated as $[Cu^{II}(HL^{S1})(H_2O)]_n(BF_4)_n$ (**30**) and was expected to incorporate the copper(II) ion in one N_3-terdentate binding pocket of the ligand, as indicated in Scheme 2.7.1. The conductivity measurement carried out in water [$\Lambda_m(H_2O)$ = 119 mol^{-1} cm^2 Ω^{-1}] fitted well with the assumption of **30** being a 1:1 electrolyte. The positive ion electrospray mass spectrum of **30** in acetonitrile showed the most intense peak at m/z = 450.9 which was assigned to the mononuclear complex species $[Cu^{II}(HL^{S1})(MeCN)]^+$ further endorsing the expected formulation (Figure 5.2.5, Appendix). Peaks at m/z = 818.9 and 757.8 were assigned to the species $[Cu^{II}_2(HL^{S1})(L^{S1})]^+$ and $[Cu^{I}(H_2L^{S1})_2]^+$, respectively, containing two ligands and therefore suggesting a possible di- or polynuclear structure for **30**. Similarly to **18** of the M-type analogue, this could for example be achieved *via* coordination of the amide carbonyl group of one subunit to the copper(II) ion of a second subunit. Furthermore a relatively intense peak at m/z = 316.6 in the electrospray mass spectrum of **30** remained unassigned.

A change of the reaction solvent to *N,N*-dimethylformamide and subsequent vapour diffusion of diethyl ether into the reaction mixture, under otherwise identical reaction conditions to the formation of **30**, resulted in the formation of an amorphous solid of the same composition.

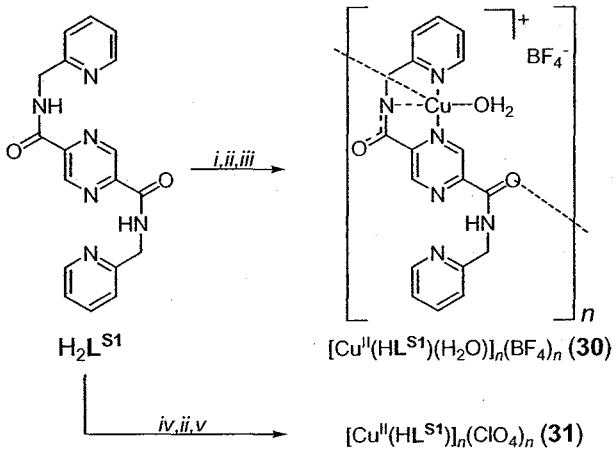

Scheme 2.7.1. Synthesis of **30** and **31**. Reagents and conditions: (*i*) 1 eq. $Cu(BF_4)_2 \cdot 4\ H_2O$, MeCN, RT; (*ii*) 1 eq. NEt_3; (*iii*) toluene (precipitation); (*iv*) 1 eq. $Cu(ClO_4) \cdot 6\ H_2O$, DMF, RT; (*v*) Et_2O (vapour diffusion).

Attempts at obtaining single crystals of **30** by vapour diffusion of diethyl ether into solutions of the compound in *N,N*-dimethylformamide or solvent mixtures with acetonitrile and ethanol, respectively, or by layering of the respective solutions with toluene, unfortunately failed to give single crystals of a size suitable for X-ray crystal structure determination. By slow evaporation of a solution of **30** in water a crystalline sample of what proved to be a dinuclear copper(II) complex was obtained (see Section 2.7.3, compound **33**).

Unlike what was observed for the lower ligand homologue H_2L^{S1}, the additional employment of one equivalent of triethylamine, to a 1:1 molar mixture of copper(II) tetrafluoroborate tetrahydrate and ligand, did not alter the reaction outcome, relative to the reaction without the addition of base.

Complexation with copper(II) perchlorate hexahydrate and H_2L^{S1}

The reaction of H_2L^{S1}, copper(II) perchlorate hexahydrate and triethylamine in a 1:1:1 molar ratio in *N,N*-dimethylformamide resulted in a deep bottle green solution

from which, after vapour diffusion of diethyl ether, a grey-blue crystalline material was isolated in around 70 % yield (Scheme 2.7.1). The compound proved to be insoluble in acetonitrile and ethanol and was only very poorly soluble in water and *N,N*-dimethylformamide. Elemental analysis suggested that the compound might have a similar formulation to **30**. Therefore the compound was tentatively formulated as $[Cu^{II}(HL^{S1})]_n(ClO_4)_n$ (**31**).

Attempts at obtaining single crystals of **31**, by similar methods as described for the related compound **30**, unfortunately failed to give single crystals of a size suitable for X-ray crystal structure determination.

IR spectroscopic studies on $[Cu^{II}(HL^{S1})(H_2O)]_n(BF_4)_n$ (30) and $[Cu^{II}(HL^{S1})]_n(ClO_4)_n$ (31)

As observed for the related dimeric complex $[Cu^{II}_2(H_2L^{M1})_2(MeCN)_2](BF_4)_4$ (**18**) of the analogous M-type ligand, the preparation of the KBr pellets for IR analyses of **30** and **31**, resulted in colour changes to green. In both cases the IR spectra showed one broad intense ν_{CO} absorption band, at $\tilde{\upsilon}$ = 1638 and 1656 cm^{-1}, respectively (Figure 2.7.1 and Figure 2.7.2). However, both bands exhibited a distinct shoulder (at $\tilde{\upsilon}$ = 1674 cm^{-1} for **30** and at $\tilde{\upsilon}$ = and 1679 cm^{-1} for **31**) to higher energy. Furthermore, in both IR spectra a second, less intense, absorption band was observed in the expected region of ν_{CO} vibrations, at $\tilde{\upsilon}$ = 1612 cm^{-1}, respectively. These values compared reasonably well with the three bands that were observed for the ν_{CO} vibrations in the IR spectrum of complex **18** of the M-type ligand analogue ($\tilde{\upsilon}(\nu_{CO(18)})$ = 1668, 1644 and 1618 cm^{-1}). However, unlike observed in the IR spectrum of **18**, in the IR spectra of **30** and **31**, no broad strong absorption bands were observed in the region $\tilde{\upsilon}$ = 3100–2700 cm^{-1}. The expected presence of tetrafluoroborate or perchlorate counter ions was affirmed in the IR spectra of **30** and **31**, with broad split bands at $\tilde{\upsilon}$ = 1083 and 1116 cm^{-1}, respectively.

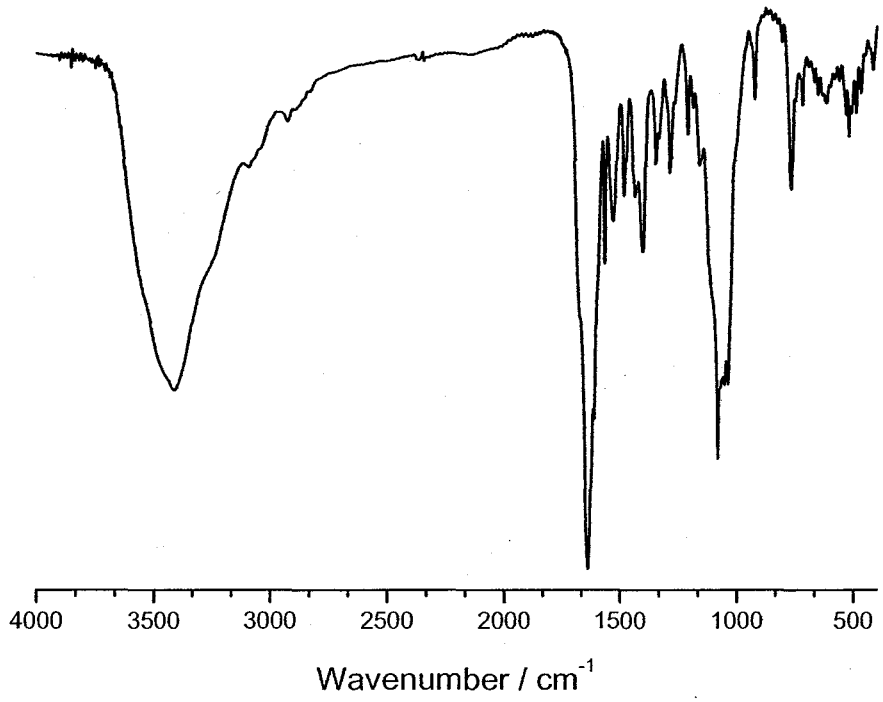

Figure 2.7.1. IR spectrum (KBr) of $[Cu^{II}(HL^{S1})(H_2O)]_n(BF_4)_n$ (**30**).

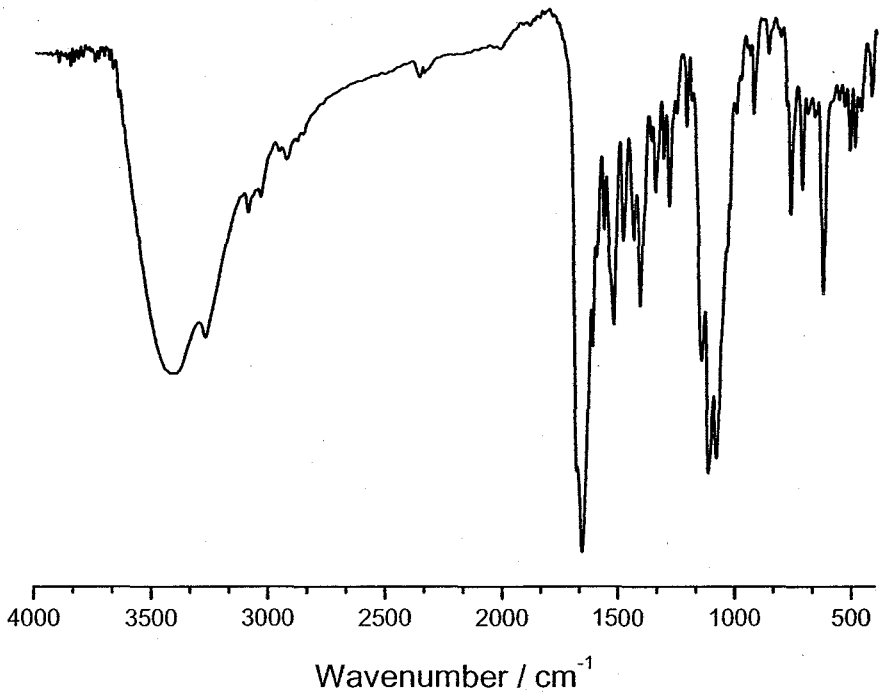

Figure 2.7.2. IR spectrum (KBr) of $[Cu^{II}(HL^{S1})]_n(ClO_4)_n$ (**31**).

UV/VIS spectroscopic studies on $[Cu^{II}(HL^{S1})(H_2O)]_n(BF_4)_n$ (30)

The UV/VIS spectrum of **30** in water showed three absorption peaks and one broad shoulder in the region of 1400–200 nm (Figure 5.4.3, Appendix). The intense absorption bands at λ_{max} = 217 nm (ε = 18350 M^{-1} cm^{-1}, $\tilde{\upsilon}$ = 46083 cm^{-1}) and 261 nm (ε = 15600 M^{-1} cm^{-1}, $\tilde{\upsilon}$ = 38314 cm^{-1}) were tentatively assigned as charge transfer absorption bands. Furthermore a relatively intense absorption shoulder, which was so far unique to the mononuclear complex **30** of the S-type ligand H_2L^{S1}, at λ_{max} = 330 nm (ε = 2963 M^{-1} cm^{-1}, $\tilde{\upsilon}$ = 30303 cm^{-1}) was observed. A broad weak absorption band at λ_{max} = 640 nm (ε = 88 M^{-1} cm^{-1}, $\tilde{\upsilon}$ = 15623 cm^{-1}) was assigned as a band derived from the overlapping *d-d* transitions.

2.7.3. Copper(II) salts and two equivalent of base

Summarising the results of the Section 2.7.1 and 2.7.2, the employment of at least two equivalents of base seemed necessary, in order to form [2 × 2] grid-type complexes of the neutral types $[M^{II}_4(L^{S1})_4]^0$ and $[M^{II}_4(L^{S2})_4]^0$ (Scheme 2.4.1, b) of fully deprotonated ligands $(L^{S1})^{2-}$ or $(L^{S2})^{2-}$.

Compleaxations with copper(II) tetrafluoroborate tetrahydrate and H_2L^{S1} or H_2L^{S2}

The addition of two equivalents of triethylamine to a turquoise-green solution of a 1:1 molar ratio of copper(II) tetrafluoroborate tetrahydrate and H_2L^{S1} even in a very large volume of acetonitrile led to the immediate quantitative precipitation of a grass green solid. Elemental analyses roughly suggested a 1:1 molar ratio of copper(II) to ligand. Under the same reaction conditions but using *N,N*-

imethylformamide as solvent a grass green solid with roughly the same empirical ormulation precipitated after a few minutes of stirring at room temperature in quantitative yield. The immediate precipitation of an amorphous solids could be prevented by using a very large volume of *N,N*-dimethylformamide under otherwise identical reaction conditions. In that case a colour change from dark grass green to bright grass green was observed on addition of the second equivalent of triethylamine and even after several hours of stirring the resulting solution at room temperature no precipitation was observed. By slow vapour diffusion of diethyl ether into the reaction mixture very, very tiny, perfectly octahedral grass green crystals were obtained in around 11 % yield, along with some grass green amorphous solid (Scheme 2.7.2). Again, elemental analyses roughly suggested a possible 1:1 molar ratio of copper(II) to ligand. Elemental analyses of the crystals fitted well with a suggested 1:1 molar ratio of copper(II) to fully deprotonated ligand, and the absence of tetrafluoroborate counter ions. Accordingly the compound was tentatively formulated as $[Cu^{II}_4(\mathbf{L}^{S1})_4] \cdot 6\ H_2O$ ($\mathbf{32} \cdot 6\ H_2O$) and was believed to be a [2 × 2] grid-type complex as indicated in Scheme 2.7.2. The compound proved to be insoluble in all common solvents so unfortunately no positive ion electrospray mass spectroscopic, UV/VIS spectroscopic or cyclic voltammetric studies could be carried out. Attempts at growing crystals of **32** of a size suitable for X-ray crystal structure determination, by lowering of the concentration of the reaction mixture even further or by slow diffusion of a solution containing base into a solution containing a 1:1 mixture of copper(II) salt and $H_2\mathbf{L}^{S1}$, unfortunately failed to succeed.

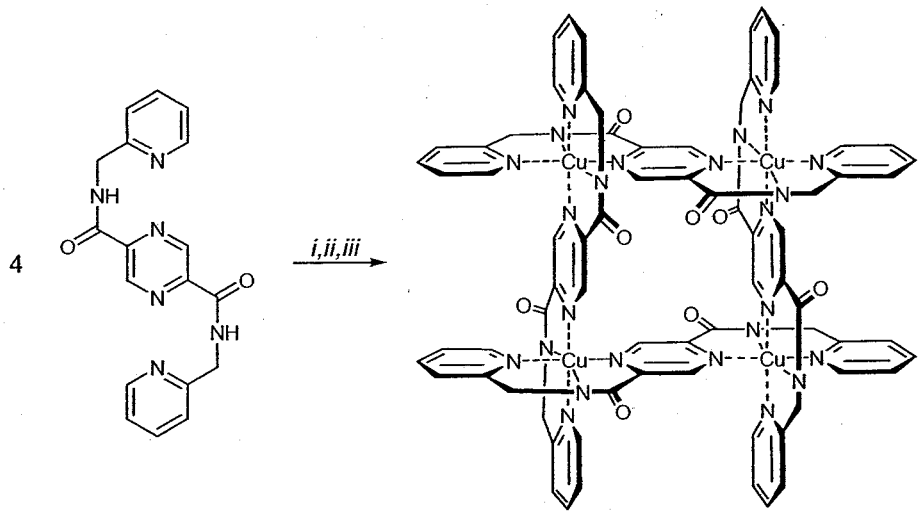

H_2L^{S1} $[Cu^{II}_4(L^{S1})_4]$ **(32)**

Scheme 2.7.2. Synthesis of **32**. Reagents and conditions: (*i*) 1 eq. $Cu(BF_4)_2 \cdot 4\ H_2O$, DMF, RT; (*ii*) 2 eq. NEt_3; (*iii*) Et_2O (vapour diffusion).

In acetonitrile solution, the employment of a 1:1:2 molar ratio of the higher ligand homologue H_2L^{S2}, copper(II) tetrafluoroborate tetrahydrate and triethylamine did not result in the spontaneous formation of a precipitate. By vapour diffusion of diethyl ether into the reaction mixture an inhomogeneous grass green solid of unknown composition was isolated. Similarly in *N,N*-dimethylformamide solution the employment of a 1:1:2 molar ratio of H_2L^{S2}, copper(II) tetrafluoroborate tetrahydrate and triethylamine did not result in the spontaneous formation of a precipitate. Again, the formation of an inhomogeneous amorphous solid of unknown composition was observed by the vapour diffusion of diethyl ether into the grass green reaction mixture.

IR spectroscopic studies on $[Cu^{II}_4(L^{S1})_4] \cdot 6\ H_2O$ (32 · 6 H_2O)

The IR spectrum of **32** · 6 H_2O showed one broad band for the ν_{CO} vibration at $\tilde{\nu}$ = 1606 cm^{-1}, with a distinct shoulder to higher wavenumbers (Figure 2.7.3). Compared to the IR spectrum of the analogous M-type [2 × 2] grid compound **23**, the

absorption band of the νCO vibration suffered a shift of $\Delta\tilde{\upsilon}_{(23,32)}$ = 45 cm^{-1} to lower energy. The respective shift compared to the related complex [Cu^{II}(HL^{S1})(H$_2$O)]$_n$(BF$_4$)$_n$ (**30**) of the same ligand is $\Delta\tilde{\upsilon}_{(30,32)}$ = 32 cm^{-1}. Furthermore an intense band at $\tilde{\upsilon}$ = 1566 cm^{-1} was observed in the IR spectrum of **32** · 6 H$_2$O. The expected absence of tetrafluoroborate counter ions was confirmed.

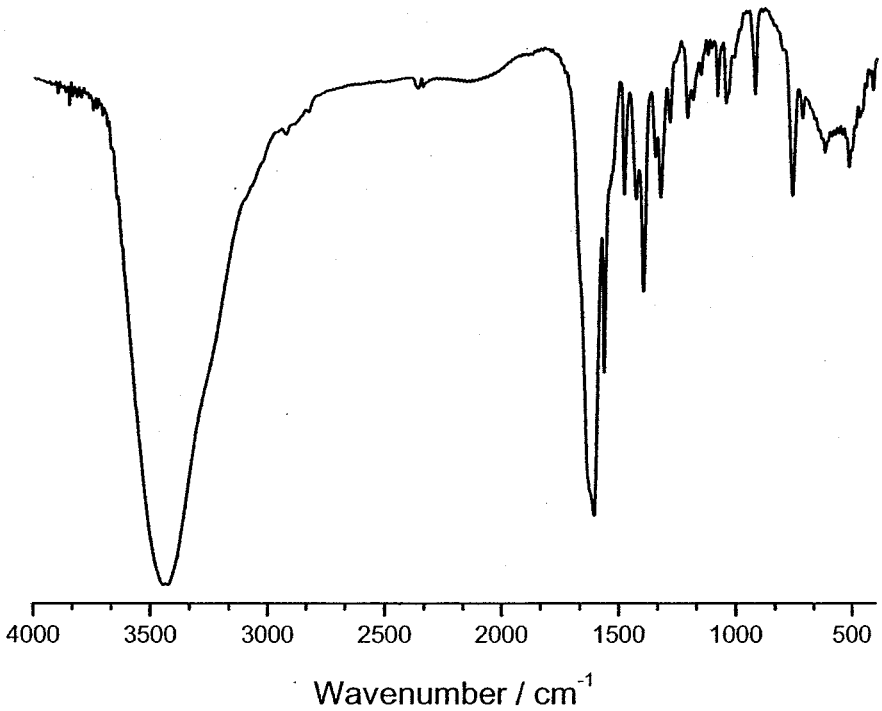

Figure 2.7.3. IR spectrum (KBr) of [Cu$^{II}_4$(**L^{S1}**)$_4$] · 6 H$_2$O (**32** · 6 H$_2$O).

2.8. *Coordination of the ligands H_2L^{S1} and H_2L^{S2}, employing a 1:2 molar ratio of ligand to copper(II) ions*

2.8.1. *Copper(II) tetrafluoroborate tetrahydrate and H_2L^{S1}*

Complexation in acetonitrile

As mentioned in Section 2.7.1 the reaction of $H_2\mathbf{L}^{S1}$ and copper(II) tetrafluoroborate tetrahydrate in a molar ratio of 1:1 in acetonitrile, resulted in the formation of a dinuclear copper(II) complex. Hence the complexation was repeated employing a 2:1 molar ratio of copper(II) salt to ligand. By vapour diffusion of diethyl ether into the dark green acetonitrile reaction mixture compound **33** was obtained as a dark turquoise microcrystalline solid in around 60 % yield (Scheme 2.8.1). The compound was insoluble in ethanol, was only marginally soluble in acetonitrile and *N,N*-dimethylformamide, but readily soluble in water. Elemental analysis confirmed the probable 2:1 molar ratio of copper(II) ions to ligand, and the compound was tentatively formulated as $[Cu^{II}_2(\mathbf{L}^{S1})(H_2O)_2](BF_4)_2$ (**33**). A conductivity measurement carried out in water [$\Lambda_m(H_2O)$ = 231 mol^{-1} cm^2 Ω^{-1}] was in good agreement with this formulation as a 2:1 electrolyte. The positive ion electrospray mass spectrum of **33** in acetonitrile showed the most intense peak at *m/z* = 276.9 which was assigned to the dinuclear species $[Cu^{II}_2(\mathbf{L}^{S1})(MeCN)_2]^{2+}$ further confirming the proposed structure of **33** (Figure 5.2.6, Appendix). Peaks at *m/z* = 450.7 and 225.9 were assigned to the mononuclear species $[Cu^{II}(HL^{S1})(MeCN)]^+$ and $[Cu^{II}(H_2\mathbf{L}^{S1})(MeCN)]^{2+}$, respectively and the remaining peaks at *m/z* = 571.5, 531.7 and 237.9 were assigned to the reduced dinuclear species $[Cu^{I}Cu^{II}(\mathbf{L}^{S1})(H_2O)(MeCN)_2]^+$, $[Cu^{I}Cu^{II}_2(\mathbf{L}^{S1})(H_2O)(MeCN)]^+$ and

$[Cu^{I}_2(H_2L^{S1})]^{2+}$. Single crystals of $[Cu^{II}_2(L^{S1})(H_2O)_2(MeCN)_2](BF_4)_2 \cdot H_2O$ (**33b** · H_2O) were obtained by slow evaporation of the dark green reaction mixture (Scheme 2.8.1).

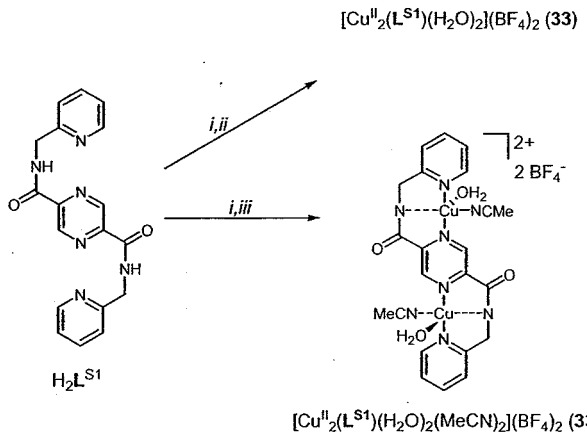

Scheme 2.8.1. Synthesis of **33** and **33b**. Reagents and conditions: (*i*) 2 eq. $Cu(BF_4)_2 \cdot 4\ H_2O$, MeCN, RT; (*ii*) Et_2O (vapour diffusion); (*iii*) slow evaporation.

IR spectroscopic studies on $[Cu^{II}_2(L^{S1})(H_2O)_2](BF_4)_2$ (33)

As observed earlier for the complexes $[Cu^{II}_2(HL^{M1})(MeCN)_2(H_2O)_2](BF_4)_3$ (**6**), $[Cu^{II}_2(HL^{M2})(H_2O)](ClO_4)_3$ (**8**) and $[Cu^{II}_2(H_2L^{M1})_2(MeCN)_2](BF_4)_4$ (**18**) of the M-type ligand analogue and the complexes $[Cu^{II}(HL^{S1})(H_2O)]_n(BF_4)_n$ (**30**) and $[Cu^{II}(HL^{S1})]_n(ClO_4)_n$ (**31**) of the same ligand, the preparation of a KBr pellet of $[Cu^{II}_2(L^{S1})(H_2O)_2](BF_4)_2$ (**33**) resulted in a colour change from dark turquoise to grass green, indicating coligand exchange with the bromide ions. The IR spectrum of **33** compared relatively well to the spectrum of the related dinuclear complex **6**. In the spectrum of **33** only one ν_{CO} vibration absorption band was observed, at $\tilde{\upsilon} = 1634\ cm^{-1}$ (Figure 2.8.1). The band experienced a shift to higher energy ($\Delta\nu_{CO(6,33)} = 25\ cm^{-1}$), compared to the related compound **6** (see Table 2.8.1). The expected presence of tetrafluoroborate counter ions was confirmed with a broad split band at $\tilde{\upsilon} = 1083\ cm^{-1}$.

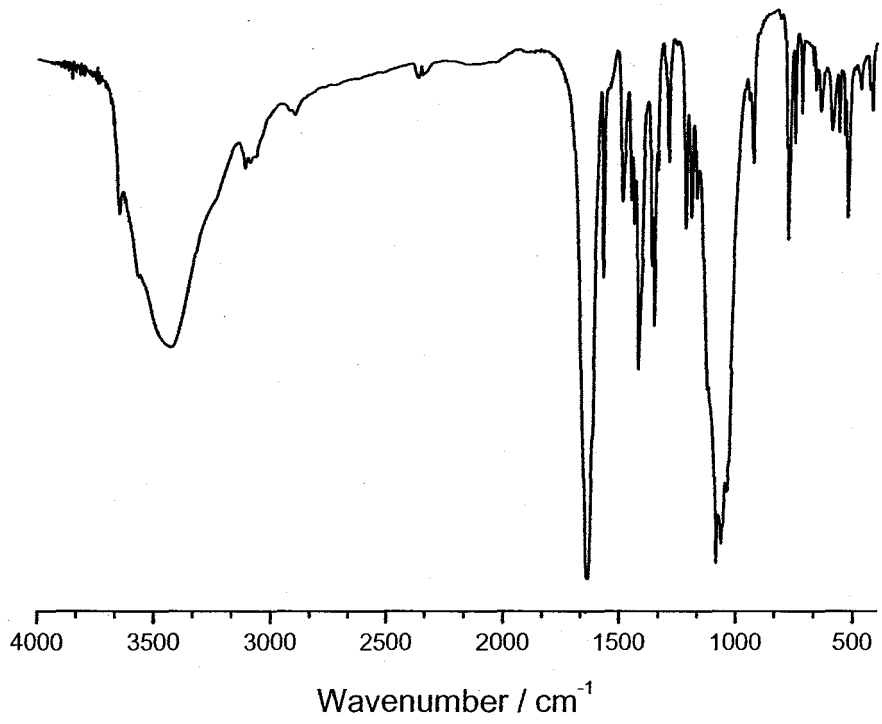

Figure 2.8.1. IR spectrum (KBr) of $[Cu^{II}_2(\mathbf{L^{S1}})(H_2O)_2](BF_4)_2$ (**33**).

Single crystal X-ray structural analysis of $[Cu^{II}_2(L^{S1})(H_2O)_2(MeCN)_2](BF_4)_2 \cdot H_2O$ (33b · H_2O)

By slow evaporation of the reaction mixture containing a 1:2 molar ratio of $H_2\mathbf{L^{S1}}$ and copper(II) tetrafluoroborate tetrahydrate in acetonitrile single crystals of $[Cu^{II}_2(\mathbf{L^{S1}})(H_2O)_2(MeCN)_2](BF_4)_2 \cdot H_2O$ (**33b** · H_2O) suitable for X-ray crystal structure determination were obtained (Figure 2.8.2).

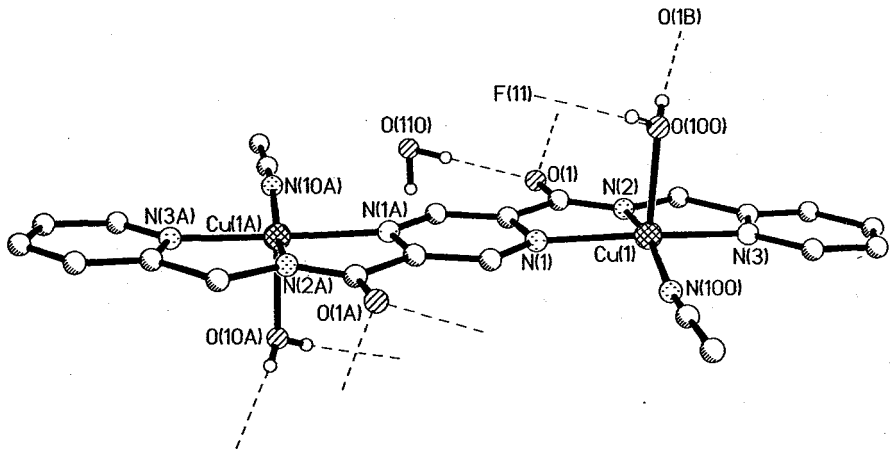

Figure 2.8.2. Molecular structure of $[Cu^{II}_2(\mathbf{L^{S1}})(H_2O)_2(MeCN)_2]^{2+}$, the complex cation of **33b** · H_2O. Hydrogen atoms not involved in hydrogen bonds have been omitted for clarity. Selected distances (Å) and angles (°): Cu(1)-N(1) 2.044(3), Cu(1)-N(2) 1.906(3), Cu(1)-N(3) 1.999(3), Cu(1)-N(100) 1.972(3), Cu(1)-O(100) 2.201(3), Cu(1)···Cu(1A) 6.811(3), O(1B)···O(100) 2.714(6), O(1)···O(110) 2.907(6), O(100)···F(11) 2.745(6); N(1)-Cu(1)-N(2) 81.1(1), N(1)-Cu(1)-N(3) 161.7(1), N(1)-Cu(1)-N(100) 95.9(1), N(1)-Cu(1)-O(100) 94.5(1), N(2)-Cu(1)-N(3) 81.9(1), N(2)-Cu(1)-N(100) 165.2(1), N(2)-Cu(1)-O(100) 103.5(1), N(3)-Cu(1)-N(100) 99.0(1), N(3)-Cu(1)-O(100) 95.8(1), N(100)-Cu(1)-O(100) 95.8(1). Symmetry operations used to generate equivalent atoms: A = 2-x, 1-y, 1-z; B = 1-x, 1-y, 1-z.

As expected the copper(II) ion of the centrosymmetrical complex cation of **33b** · H_2O is encapsulated by the N_3-terdentate binding pocket of one ligand half, which occupies three equatorial coordination sites. A fourth equatorial and an axial coordination site is occupied by the nitrogen donor of an acetonitrile coligand and the oxygen of a water molecule, respectively. The coordination geometry around the copper(II) ion is therefore best described as N_4O distorted square pyramidal. The distortion from the square pyramid of **33b** · H_2O is very small and given by the degree of trigonality[127] τ = 0.06, which compares well with the related compound $[Cu^{II}_2(HL^{M1})(MeCN)_4](BF_4)_3$ · MeCN (**6b** · MeCN) ($\tau_{(1)}$ = 0.04 and $\tau_{(2)}$ = 0.09) of the analogous M-type ligand. The copper(II) ion in **33b** · H_2O is pulled 0.200(2) Å out of the N_4 base in the direction of the axial coordinated water coligand. As in the related complex **6b** · MeCN both amide nitrogen atoms of the ligand in **33b** · H_2O are involved in copper(II) coordination and are therefore deprotonated. But unlike in **6b** · MeCN in the present case no former N-H amide proton is retained, as no intramolecular O···H···O hydrogen bond can be formed. As observed for copper(II)

complexes of the related ligands H_2L^{M1}, H_2L^{M2}, HL^{N1},[123] HL^{N2},[124] HL^{N11}[125] and HL^{N12}[126] (Figure 2.2.4) in **33b** · H_2O the Cu^{II}-N_{amide} bond length (1.906(3) Å) is shorter than the Cu^{II}-N_{py} (1.999(3) Å) or the Cu^{II}-N_{pz} (2.044(3) Å) distance. The two symmetry equivalent copper(II) ions of the dinuclear molecule are bridged by the pyrazine ring of the ligand and are separated by 6.811(3) Å, which is slightly further apart than was observed in **6b** · MeCN of the analogous M-type ligand (6.745(5) Å). The deprotonated ligand is very flat with the main deviation from the mean plane, defined by all non hydrogen atoms of the ligand, being only 0.104 Å for $C(10)_{pyridine}$. The acetonitrile coligand forms an angle of only 10.8° to this ligand mean plane. Both hydrogen atoms of the water coligand are involved in intermolecular hydrogen bonds (Figure 2.8.2 and Figure 2.8.3).

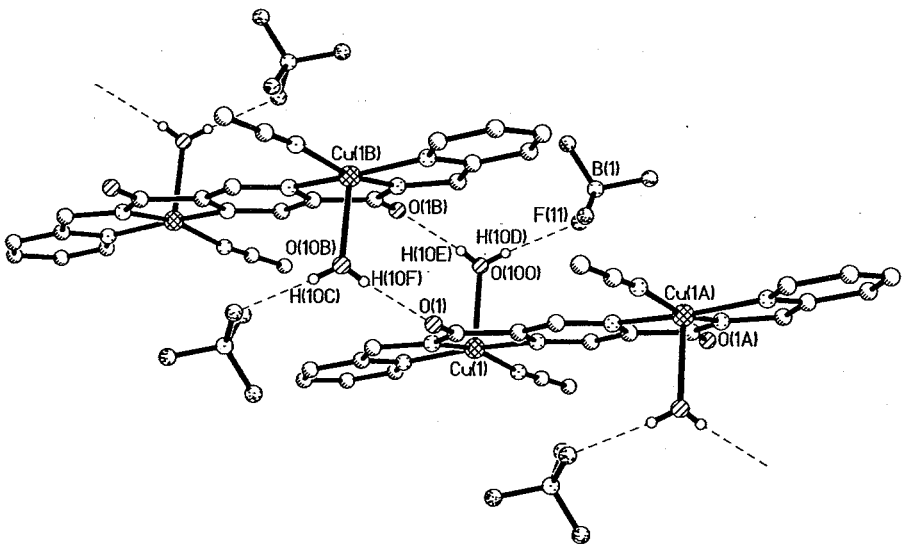

Figure 2.8.3. Section of the 3D structure of $[Cu^{II}_2(\mathbf{L^{S1}})(H_2O)_2(MeCN)_2](BF_4)_2 \cdot H_2O$ (**33b** · H_2O). Hydrogen atoms not involved in hydrogen bonds and solvent water molecules have been omitted for clarity. Symmetry operations used to generate equivalent atoms: A = 2–x, 1–y, 1–z; B = 1–x, 1–y, 1–z.

One proton is involved in an O-H···O hydrogen bond to the oxygen O(1) of the symmetry generated ligand carbonyl function, which itself is involved in a second hydrogen bond to the solvent water molecule (O(110), Figure 2.8.2). The water coligand of the latter molecule thus is intermolecularly hydrogen bonded to the carbonyl oxygen of the former molecule. Thus the centrosymmetrical molecules are

connected in a circular motif, which leads to a stair like chain structure as indicated in Figure 2.8.3. The other proton of the O(100) water coligand is O-H···F hydrogen bonded to a tetrafluoroborate counter ion (Figure 2.8.2, Figure 2.8.3).

UV/VIS spectroscopic studies on $[Cu^{II}_2(L^{S1})(H_2O)_2](BF_4)_2$ (33)

The UV/VIS spectrum of **33** in water was very similar to the UV/VIS spectrum of the related mononuclear complex **30** of the same ligand and showed four absorption peaks in the region of λ = 200–1400 nm (Figure 2.8.4). A broad relatively intense asymmetrical absorption band, which so far was unique to complexes of the S-type ligand $(L^{S1})^{2-}$, was observed at λ_{max} = 349 nm (ε = 4200 M^{-1} cm^{-1}, $\tilde{\upsilon}$ = 28653 cm^{-1}). A broad weak absorption band at λ_{max} = 641 nm (ε = 204 M^{-1} cm^{-1}, $\tilde{\upsilon}$ = 15600 cm^{-1}), by analogy with the related dinuclear complex $[Cu^{II}_2(HL^{M1})(MeCN)_4](BF_4)_3 \cdot MeCN$ (**6b** · MeCN) of the analogous M-type ligand $(HL^{M1})^-$, was assigned as a band of overlapping *d-d* transitions.[128-130] The molar extinction coefficient of this band per ligand strand of the dinuclear complex **33** was about doubled compared to the respective band of the analogous mononuclear complex **30**, but occurred at the same energy.

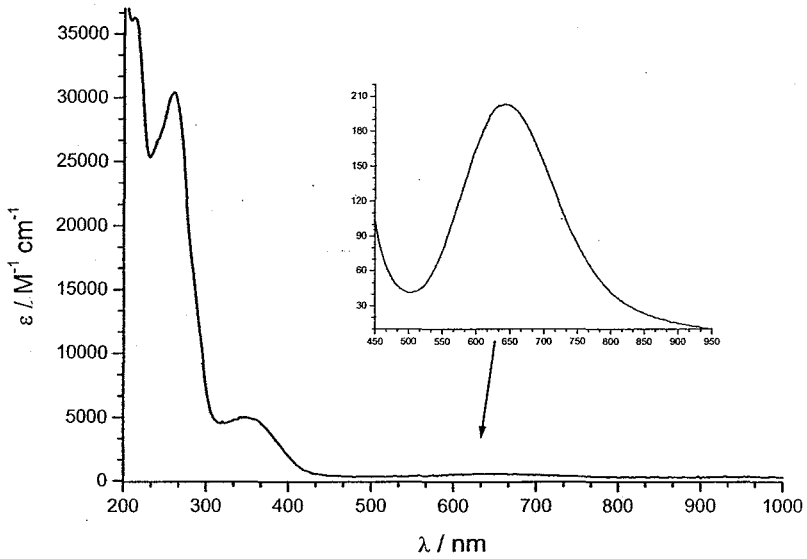

Figure 2.8.4. UV/VIS spectra [H_2O, 1 mM (inset) and 0.01 mM (main)] of $[Cu^{II}_2(\mathbf{L^{S1}})(H_2O)_2](BF_4)_2$ (**33**).

Compared to the *d-d* transition band of **6b** · MeCN a shift of $\Delta\tilde{\upsilon}_{(6b,33)}$ = 630 cm^{-1} to lower energy occurred for **33**. However, this shift was not surprising as the UV/VIS spectra of **6b** · MeCN and **33** were monitored in different solvent systems (acetonitrile and water, respectively). Accordingly the complex cation of **33** in water was suggested to be $[Cu^{II}_2(L^{S1})(H_2O)_4]^{2+}$, involving the weaker water coligand. Furthermore two very intense peaks at λ_{max} = 212 nm (ε = 34100 M^{-1} cm^{-1}, $\tilde{\upsilon}$ = 47170 cm^{-1}) and λ_{max} = 261 nm (ε = 20500 M^{-1} cm^{-1}, $\tilde{\upsilon}$ = 44248 cm^{-1}) were observed in the UV/VIS spectrum of **33**.

Magnetic studies on $[Cu^{II}_2(L^{S1})(H_2O)_2(MeCN)_2](BF_4)_2 \cdot H_2O$ (33b · H_2O)

The temperature dependence of μ_{eff} and of χ_m of **33b** · H_2O per copper(II) ion, respectively, are shown in Figure 2.8.5 and Figure 2.8.6. At higher temperatures the effective magnetic moment of **33b** · H_2O showed Curie-like behaviour and only below 20 K a decrease of μ_{eff} on lowering the temperature was observed. Consequently the molar magnetic susceptibility (χ_m) increased. However, in contrast to all other pyrazine bridged complexes described so far, no maximum in the plot of the molar magnetic susceptibility *vs.* temperature of **33b** · H_2O was observed.

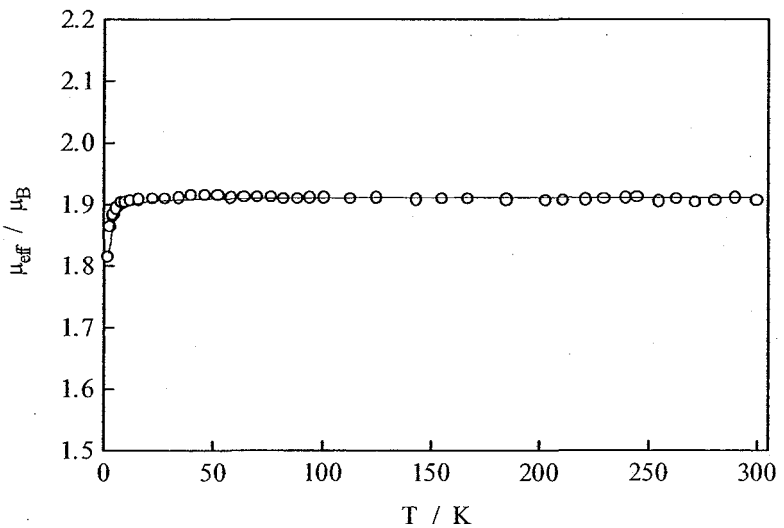

Figure 2.8.5. Thermal variation of the magnetic moment μ_{eff} (∘∘) of $[Cu^{II}_2(\mathbf{L^{S1}})(H_2O)_2(MeCN)_2](BF_4)_2 \cdot H_2O$ (**33b** · H_2O). The solid line represents the best fit.

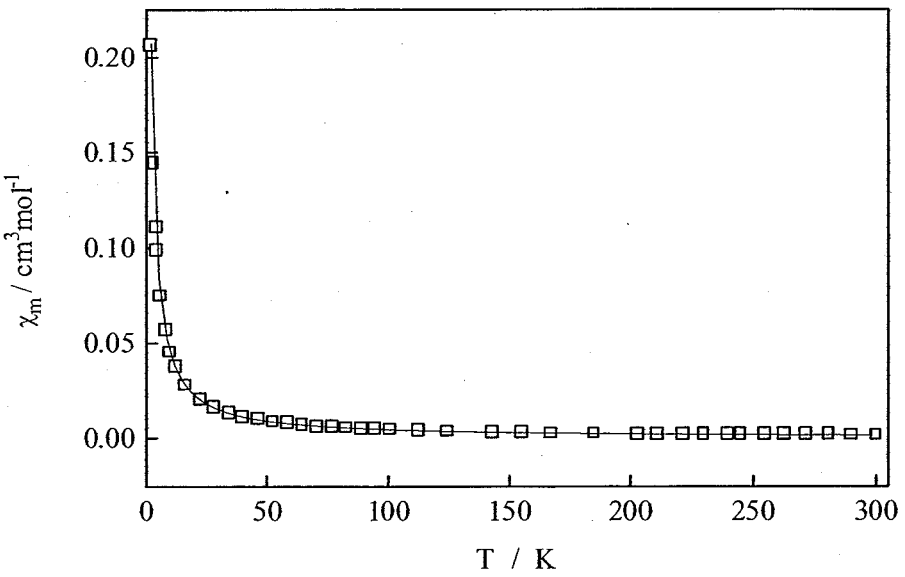

Figure 2.8.6. Thermal variation of the molar susceptibility χ_m (▫▫) of $[Cu^{II}_2(\mathbf{L^{S1}})(H_2O)_2(MeCN)_2](BF_4)_2 \cdot H_2O$ (**33b** · H_2O). The solid line represents the best fit.

The best fit for the dinuclear compound $[Cu^{II}_2(\mathbf{L^{S1}})(H_2O)_2(MeCN)_2](BF_4)_2 \cdot H_2O$ (**33b** · H_2O) was obtained from the parameters J = –0.24 cm^{-1}, g = 2.2 and $TIP = 60 \times 10^{-6}$ cm^3 mol^{-1}. Unexpectedly, the antiferromagnetic coupling interaction of **33b** · H_2O was around twenty times weaker than that of the analogous M-type complex $[Cu^{II}_2(H\mathbf{L^{M1}})(MeCN)_4](BF_4)_3 \cdot MeCN$ (**6b** · MeCN) (J = –5.1 cm^{-1}), despite the similar molecular structures of the two analogous S- and M-type complexes.

Complexation in water

As mentioned in Section 2.7.1 the reaction of a 1:1 molar ratio of copper(II) tetrafluoroborate tetrahydrate and $H_2\mathbf{L^{S1}}$ in water resulted, by slow evaporation of the dark green solution, in the formation of an unexpected dinuclear compound with a composition differing from **33**. The complexation in water was therefore repeated employing a molar ratio of ligand to copper(II) salt of 1:2. As observed on complexation of $H_2\mathbf{L^{S1}}$ with copper(II) in acetonitrile, the addition of copper(II) tetrafluoroborate tetrahydrate to a suspension of $H_2\mathbf{L^{S1}}$ in water quickly resulted in

the dissolution of the ligand. By slow evaporation (2–4 weeks) of the resulting dark green solution from a glass vessel, dark blue-green crystalline blocks could be isolated. X-ray crystal structure determination carried out on the crystal blocks, revealed two different closely related compounds (**34b** · 0.5 H_2O and **34c** · 4 H_2O). Both compounds had a rather unexpected octahedral counter ion in their molecular structures, which was first believed to be hexafluorophosphate even though the source could not be explained and the charge balance was confusing. Eventually the octahedral counter ion in the structures was shown to be hexafluorosilicate. The negative ion electrospray mass spectrum presented a peak at m/z = 123.0 that could unambiguously be assigned to the anion SiF_5^-. Furthermore the IR spectrum taken of the crystalline blocks presented the absorption bands expected for hexafluorosilicate. The compounds were accordingly formulated as $[Cu^{II}_2(\mathbf{L^{S1}})(H_2O)_4](SiF_6)$ · 0.5 H_2O (**34b** · 0.5 H_2O) and $\{[Cu^{II}_2(\mathbf{L^{S1}})(H_2O)_2(SiF_6)]$ · 4 $H_2O\}_\infty$ (**34c** · 4 H_2O).

The occurrence of hexafluorosilicate, rather than tetrafluoroborate as counter ion was unexpected as definitely copper(II) tetrafluoroborate tetrahydrate was employed in the reaction and hexafluorosilicate salts were altogether absent from the laboratories. A negative ion electrospray mass spectral analysis carried out on the copper(II) tetrafluoroborate tetrahydrate salt employed in the reaction showed no traces of hexafluorosilicate ions. However, it has been found before that hexafluorosilicate anions can arise in compounds originally containing tetrafluoroborate anions. Because partial hydrolysis of the tetrafluoroborate in the presence of moisture generates traces of HF which react with the glassware to form hexafluorosilicate.[91,195-198] In the present case the reaction was carried out in water and furthermore two protons were generated per ligand strand in the course of the copper(II) complexation, which facilitated the generation of HF.

The complexation of $H_2\mathbf{L^{S1}}$ with copper(II) tetrafluoroborate tetrahydrate in a molar ratio of 1:2 carried out in a glass vessel in distilled water (pH = 5.5–5.7), in Dunedin tap water (pH = 7.4–7.5) and in "milliQ" water (pH = 6.0–6.2), with subsequent slow evaporation of the solvent (over 2–4 weeks), resulted in all cases in

the formation of dark blue-green crystals in around 40–60 % yield, along with yellow crystals in around 20–40 % yield. Elemental analyses of the blue-green crystals were in agreement with a formulation of $[Cu^{II}_2(L^{S1})](SiF_6) \cdot n\ H_2O$ (n = 3–5.5) (**34**), respectively. The positive ion electrospray mass spectrum of **34** in acetonitrile showed two main peaks at m/z = 349.2 and 451.1 that were assigned to the species $(H_3L^{S1})^+$ and $[Cu^{II}(HL^{S1})(MeCN)]^+$, respectively. A third main peak at m/z = 238.0 could not be assigned and unfortunately no dinuclear complex fragment could be found. By means of elemental analysis and IR spectroscopy a formulation of $(H_4L^{S1})(BF_4)_2$ was suggested for the yellow crystals. The additional employment of 2 equivalents of triethylamine under otherwise identical reaction conditions resulted in the formation of the blue-green crystal type **34** only, in 83 % yield (Scheme 2.8.2). This observation was in good agreement with the assumption that the yellow crystals were $(H_4L^{S1})(BF_4)_2$ and formed on protonation of the free ligand with the former amide protons that were released on complexation. Thus the addition of base to the reaction mixture prevented the protonation of free ligand and at the same time nearly doubled the yield of the desired compound **34**.

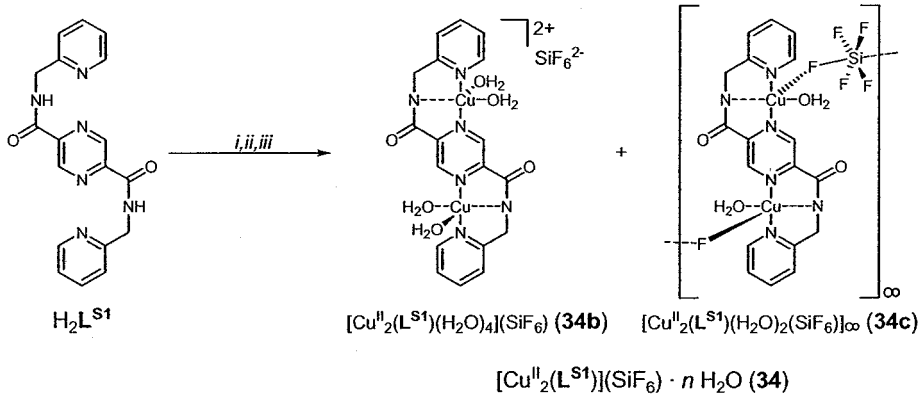

H_2L^{S1} $[Cu^{II}_2(L^{S1})(H_2O)_4](SiF_6)$ (**34b**) $[Cu^{II}_2(L^{S1})(H_2O)_2(SiF_6)]_\infty$ (**34c**)

$[Cu^{II}_2(L^{S1})](SiF_6) \cdot n\ H_2O$ (**34**)

Scheme 2.8.2. Synthesis of **34**. Reagents and conditions: (*i*) 2 eq. $Cu(BF_4)_2 \cdot 4\ H_2O$, H_2O, RT, glass vessel; (*ii*) 2 eq. NEt_3; (*iii*) slow evaporation (2–4 weeks).

IR spectroscopic studies on $[Cu^{II}_2(L^{S1})](SiF_6) \cdot n\ H_2O$ (34)

The IR spectrum of **34** compared reasonably well to the IR spectrum of the related compound $[Cu^{II}_2(L^{S1})(H_2O)_2](BF_4)_2$ (**33**) and showed one broad band at $\tilde{\upsilon}$ = 1628 cm^{-1}, with a shoulder to lower energy, in the expected region of the ν_{CO} vibration (Figure 2.8.7, Table 2.8.1). However, in contrast to the IR spectrum of **33**, the IR spectrum of **34** showed very broad strong absorption bands in the region of $\tilde{\upsilon}$ = 3100–2000 cm^{-1}.

For uncoordinated hexafluorosilicate two IR active vibrations are expected at $\tilde{\upsilon}$ = 740 cm^{-1} (ν_3) and at $\tilde{\upsilon}$ = 480 cm^{-1} (ν_4). On coordination, the symmetry of the hexafluorosilicate is lowered, which results in the splitting of the two bands.[141] The IR spectrum of **34** showed an intense broad split band at $\tilde{\upsilon}$ = 780 and 750 cm^{-1} that was assigned as vibration of the hexafluorosilicate counter ion.

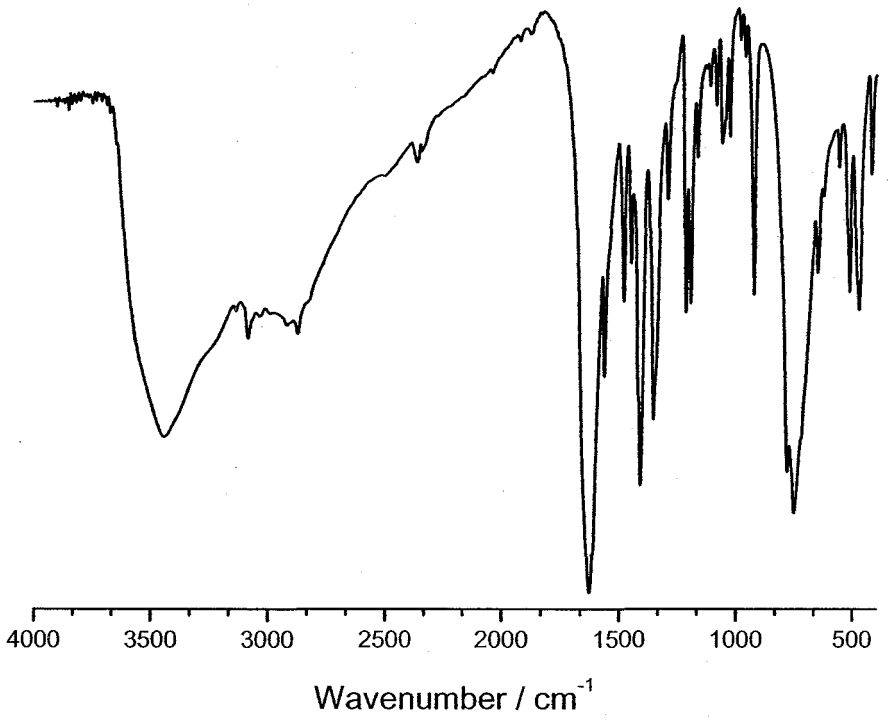

Figure 2.8.7. IR spectrum (KBr) of $[Cu^{II}_2(\mathbf{L^{S1}})](SiF_6) \cdot n\ H_2O$ (**34**).

Single crystal X-ray structural analysis of $[Cu^{II}_2(L^{S1})(H_2O)_4](SiF_6) \cdot 0.5\ H_2O$ ($\mathbf{34b} \cdot 0.5\ H_2O$)

Single crystals of $[Cu^{II}_2(\mathbf{L}^{S1})(H_2O)_4](SiF_6) \cdot 0.5\ H_2O$ (**34b** · 0.5 H_2O), along with single crystals of **34c** · 4 H_2O, suitable for X-ray crystal structure determination, were obtained by slow evaporation of a reaction solution containing $H_2\mathbf{L}^{S1}$ and copper(II) tetrafluoroborate tetrahydrate in a 1:2 molar ratio in water in a glass vessel. The molecular structure of **34b** · 0.5 H_2O (Figure 2.8.8) is similar to the structure of the analogous tetrafluoroborate containing complex $[Cu^{II}_2(\mathbf{L}^{S1})(H_2O)_2(MeCN)_2](BF_4)_2 \cdot H_2O$ (**33b** ·H_2O).

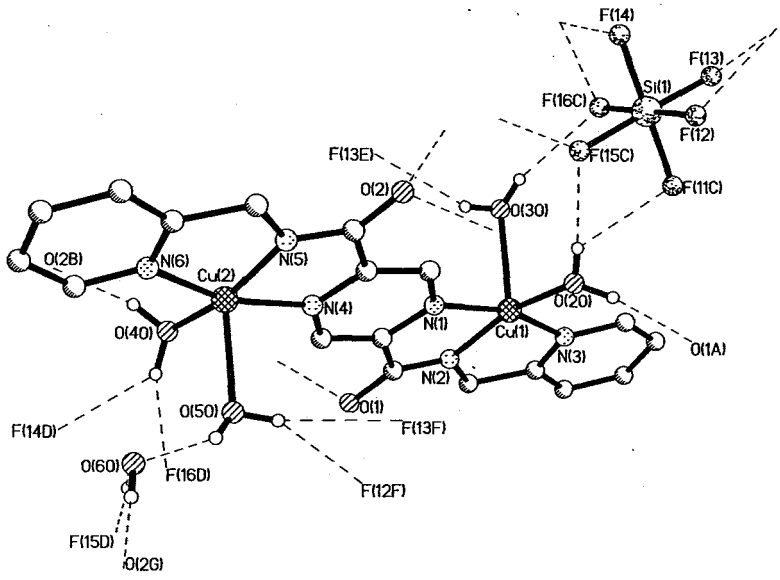

Figure 2.8.8. Molecular structure of $[Cu^{II}_2(\mathbf{L}^{S1})(H_2O)_4](SiF_6) \cdot 0.5\ H_2O$ (**34b** · 0.5 H_2O). Hydrogen atoms not involved in hydrogen bonds have been omitted for clarity. Selected distances (Å) and angles (°): Cu(1)-N(1) 2.031(4), Cu(1)-N(2) 1.904(4), Cu(1)-N(3) 2.011(4), Cu(1)-O(20) 1.945(4), Cu(1)-O(30) 2.289(4), Cu(2)-N(4) 2.031(4), Cu(2)-N(5) 1.908(4), Cu(2)-N(6) 2.000(4), Cu(2)-O(40) 1.951(4), Cu(2)-O(50) 2.240(4), Cu(1)···Cu(2) 6.772(1), O(20)···O(1A), 2.588(7), O(40)···O(2B) 2.627(7), O(20)···F(15C) 2.750(7), O(20)···F(11C) 2.799(7), O(40)···F(16D) 2.755(7), O(40)···F(14D) 2.794(7), O(30)···F(13E) 3.083(7), O(30)···F(16C) 3.060(7), O(50)···F(12F) 2.920(7), O(50)···F(13F) 3.213(7), O(50)···O(60) 2.305(7), O(60)···F(15D) 2.670(7), O(60)···O(2G) 2.714(7); N(1)-Cu(1)-N(2) 81.5(2), N(1)-Cu(1)-N(3) 162.7(2), N(1)-Cu(1)-O(20) 91.7(2), N(1)-Cu(1)-O(30) 96.6(2), N(2)-Cu(1)-N(3) 82.1(2), N(2)-Cu(1)-O(20) 160.8(2), N(2)-Cu(1)-O(30) 106.2(2), N(3)-Cu(1)-O(20) 102.0(2), N(3)-Cu(1)-O(30) 93.4(2), O(20)-Cu(1)-O(30) 92.3(2), N(4)-Cu(2)-N(5) 81.8(2), N(4)-Cu(2)-N(6) 163.1(2), N(4)-Cu(2)-O(40) 92.4(2), N(4)-Cu(2)-O(50) 95.3(2), N(5)-Cu(2)-N(6) 82.3(2), N(5)-Cu(2)-O(40) 161.5(2), N(5)-Cu(2)-O(50) 106.2(2), N(6)-Cu(2)-O(40) 101.1(2), N(6)-Cu(2)-O(50) 94.5(2), O(40)-Cu(2)-O(50) 91.8(2). Symmetry operations to generate equivalent atoms: A = x, y+1, z; B = x, y−1, z; C = −x+1, y+0.5, −z+1.5; D = −x+1, −y, −z+2; E = −x+1, y−0.5, −z+1.5; F = −x+1, −y+1, −z+2; G = x, −y+0.5, z+0.5.

Just as in **33b** · H_2O, the copper(II) ions of **34b** · 0.5 H_2O are encapsulated by the antiparallel terdentate binding pockets of the S-type ligand. The copper(II)-N_{ligand} distances thus are very similar to the distances in **33b** · H_2O, and as expected the average Cu^{II}-N_{amide} bond length in **34b** · 0.5 H_2O is shorter (1.906 Å) than the average Cu^{II}-N_{py} (2.006 Å) or Cu^{II}-N_{pz} (2.031 Å) bond length. Interestingly, the average N_{ligand}-Cu^{II}-N_{ligand} angles observed in **34b** · 0.5 H_2O are slightly greater than for **33b** · H_2O. A major difference between the structures **33b** · H_2O and **34b** · 0.5 H_2O, is that each coordination environment of the copper(II) ions in the latter complex is completed by two water coligands, rather than one water and one acetonitrile coligand as was found in the former complex. Thus the coordination environment around the copper(II) in **34b** · 0.5 H_2O is best described as N_3O_2 distorted square pyramidal. The average degree of trigonality[127] of **34b** · 0.5 H_2O is very small (τ = 0.03) and about half of that, compared to **33b** · H_2O. As observed in the analogous complexes **33b** · H_2O and $[Cu^{II}_2(HL^{M1})(MeCN)_4](BF_4)_3$ · MeCN (**6b** · MeCN), the copper(II) ions of **34b** · 0.5 H_2O are pulled 0.227(2) Å and 0.221(2) Å out of the basal plane in direction of the axial coligand, respectively. The pyrazine bridged copper(II) ions of **34b** · 0.5 H_2O are separated by 6.772(1) Å, which compares well with the similar complexes **33b** · H_2O (6.811(3) Å) of the same ligand and **6b** · MeCN (6.745(5) Å) of the analogous M-type ligand. As expected the ligand $(L^{S1})^{2-}$ is very flat with the main deviation from the mean plane, defined by all non hydrogen atoms of the ligand, being only 0.142 Å for $C(7)_{methylene}$. The equatorially coordinated water coligands are intermolecularly O-H···O hydrogen bonded to the carbonyl oxygen atom of the same ligand half of the neighbouring symmetry generated complex molecule, leading to a chain like polynuclear strand of dinuclear subunits [O(20)···O(1A): 2.588(7) Å, O(40)···O(2B): 2.627(7) Å] (Figure 2.8.8). All four water coligands are involved in intermolecular O-H···F hydrogen bonds to hexafluorosilicate counter ions. The two equatorial water coligands thus form  hydrogen bonds linking two chain like strands [O(20)···F(15C): 2.750(7) Å, O(20)···F(11C): 2.799(7) Å, O(40)···F(16D): 2.755(7) Å, O(40)···F(14D): 2.794(7) Å]

(Figures 2.8.8–2.8.10). Other interstrand connections are formed by the axial coordinated water coligands: four relatively weak O-H···F hydrogen bonds are formed by O(30) [O(30)···F(13E): 3.083(7) Å, O(30)···F(16C): 3.060(7) Å] and O(50) [O(50)···F(12F): 2.920(7) Å, [O(50)···F(13F): 3.213(7) Å] and an 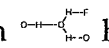 hydrogen bond, involving the solvate water, a carbonyl oxygen and the hexafluorosilicate counter ion [O(50)···O(60): 2.305(7) Å, O(60)···F(15D): 2.670(7) Å, O(60)···O(2G): 2.714(7) Å]. Figure 2.8.10 shows a section of the 3D structure of **34b** · 0.5 H_2O.

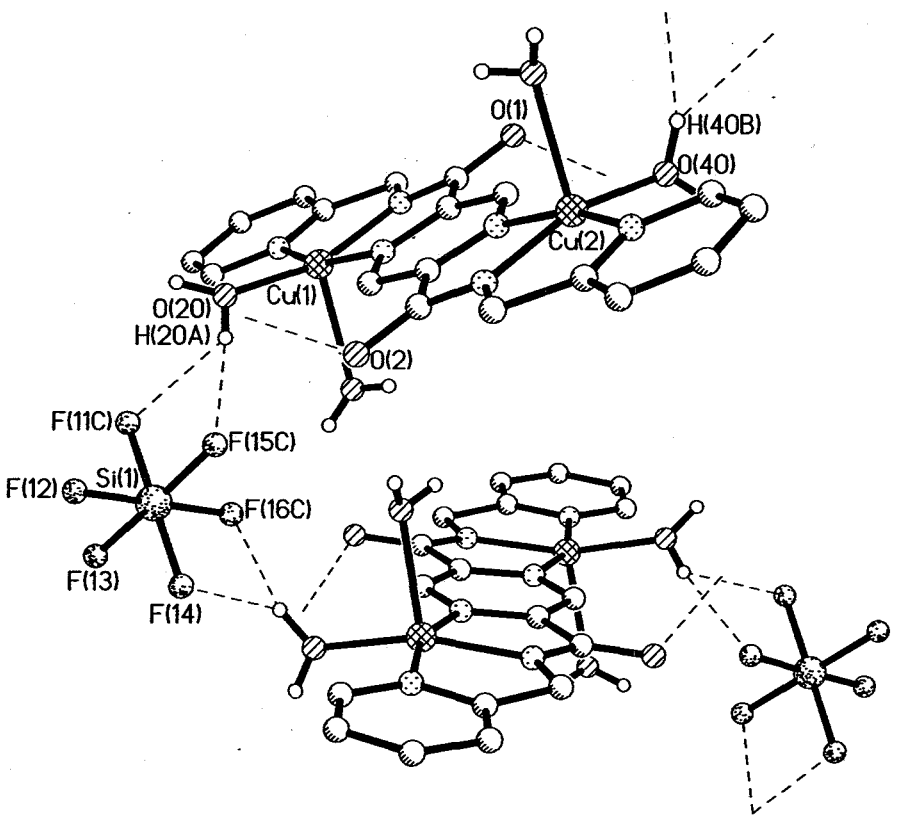

Figure 2.8.9. Section of the 3D structure of $[Cu^{II}_2(\mathbf{L^{S1}})(H_2O)_4](SiF_6)$ · 0.5 H_2O (**34b** · 0.5 H_2O), with emphasis on the hydrogen bonds involving the hexafluorosilicate counter ion. Hydrogen atoms not involved in hydrogen bonds and solvent molecules have been omitted for clarity.

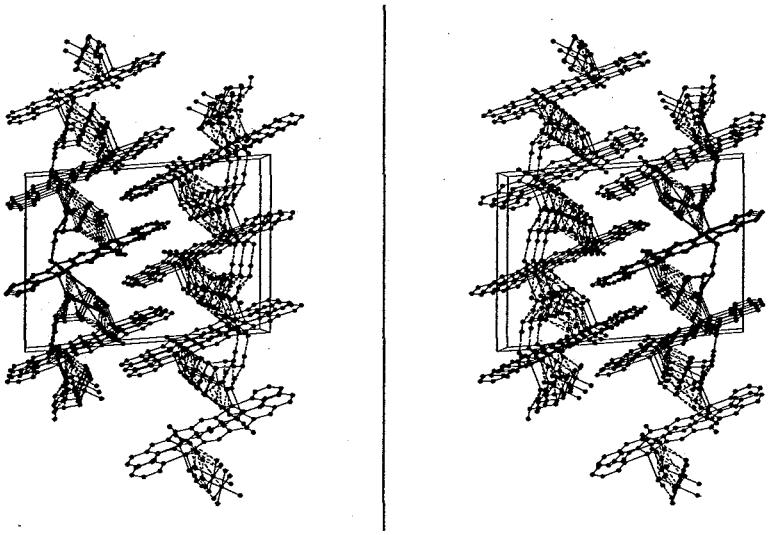

Figure 2.8.10. Stereo picture of a section of the 3D structure of $[Cu^{II}_2(\mathbf{L^{S1}})(H_2O)_4](SiF_6) \cdot 0.5\ H_2O$ (**34b** · 0.5 H_2O). Hydrogen atoms not involved in hydrogen bonds have been omitted for clarity.

Single crystal X-ray structural analysis of $\{[Cu^{II}_2(L^{S1})(H_2O)_2(SiF_6)] \cdot 4\ H_2O\}_\infty$ (34c · 4 H_2O)

Single crystals of $\{[Cu^{II}_2(\mathbf{L^{S1}})(H_2O)_2(SiF_6)] \cdot 4\ H_2O\}_\infty$ **34c** · 4 H_2O suitable for X-ray crystal structure determination were collected along with crystals of **34b** · 0.5 H_2O. Not surprisingly the molecular structure of the centrosymmetrical complex building block (Figure 2.8.11) is very similar to the structures of $[Cu^{II}_2(\mathbf{L^{S1}})(H_2O)_2(MeCN)_2](BF_4)_2 \cdot H_2O$ (**33b** · H_2O) and $[Cu^{II}_2(\mathbf{L^{S1}})(H_2O)_4](SiF_6) \cdot 0.5\ H_2O$ (**34b** · 0.5 H_2O). The copper(II) ions of **34c** · 4 H_2O are coordinated in a equatorial fashion by the antiparallel oriented terdentate binding pockets of the ligand $(\mathbf{L^{S1}})^{2-}$. As observed in the M-type analogous compound $[Cu^{II}_2(HL^{M1})(MeCN)_4](BF_4)_3 \cdot MeCN$ (**6b** · MeCN) and the similar complexes **33b** · H_2O and **34b** · 0.5 H_2O of the same ligand, the ligand in **34c** · 4 H_2O is very flat, with a main deviation from the mean plane defined by all non-hydrogen atoms of the ligand being only 0.057 Å for $C(1)_{pz}$. The main difference between the compounds **33b** · H_2O, **34b** · 0.5 H_2O and **34c** · 4 H_2O is given by the different coligands involved in the copper(II) coordination.

Whereas in **33b** · H_2O the coordination environment is N_4O distorted square pyramidal and the coligands are water (axial) and acetonitrile (equatorial), the coordination sphere in **34b** · H_2O is N_3O_2 distorted square pyramidal involving two water coligands, and in **34c** · 4 H_2O water coligands are bound equatorially and hexafluorosilicato coligands are coordinated axially (Figure 2.8.11). The coordination environment around the copper(II) ion in **34c** · 4 H_2O is therefore best described as N_3OF distorted square pyramidal with an extremely small degree of trigonality of only $\tau = 0.001$.[127] The Cu^{II}-N_{ligand} bond lengths and angles of **34c** · 4 H_2O all compare well with the values in **34b** · 0.5 H_2O. In **34c** · 4 H_2O the symmetry equivalent pyrazine bridged copper(II) ions are separated by 6.827(1) Å which is slightly longer than that observed in **34b** · 0.5 H_2O (6.772(1) Å).

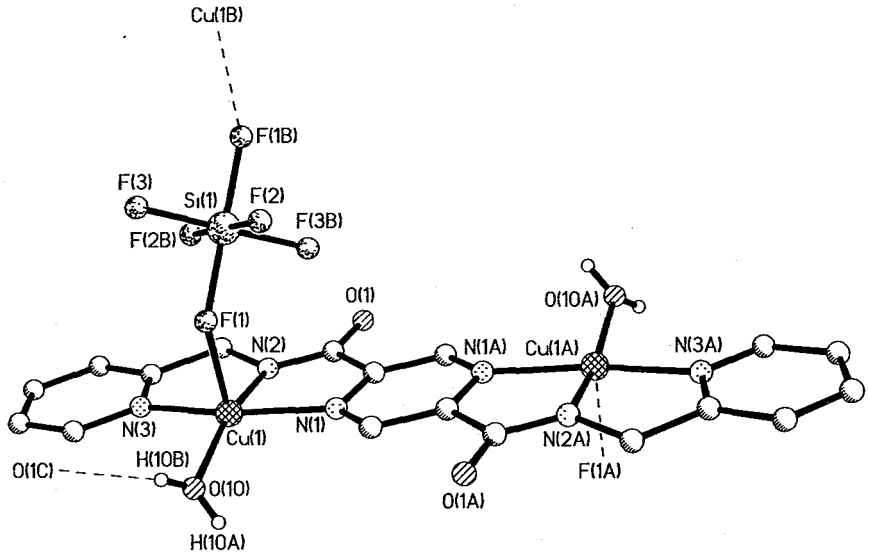

Figure 2.8.11. Molecular subunit $[Cu^{II}_2(\mathbf{L^{S1}})(H_2O)_2(SiF_6)]$ of the polymeric chain structure of the complex cation of **34c** · 4 H_2O emphasising the coordination environment about Cu(1). Hydrogen atoms not involved in hydrogen bonds have been omitted for clarity. Selected distances (Å) and angles (°): Cu(1)-N(1) 2.052(2), Cu(1)-N(2) 1.912(2), Cu(1)-N(3) 2.012(2), Cu(1)-O(10) 1.951(2), Cu(1)-F(1) 2.235(1), Cu(1)···Cu(1A) 6.827(1), Cu(1)···Cu(1B) 7.166(1), O(10)···O(1C) 2.662(3); N(1)-Cu(1)-N(2) 81.27(7), N(1)-Cu(1)-N(3) 163.58(7), N(1)-Cu(1)-O(10) 97.53(7), N(1)-Cu(1)-F(1) 87.19(6), N(2)-Cu(1)-N(3) 82.40(7), N(2)-Cu(1)-O(10) 163.68(8), N(2)-Cu(1)-F(1) 105.31(6), N(3)-Cu(1)-O(10) 97.68(7), N(3)-Cu(1)-F(1) 98.75(6), O(10)-Cu(1)-F(1) 90.84(6). Symmetry operations used to generate equivalent atoms: A = –x, –y–1, –z; B = –x, –y, –z; C = x+1, y, z.

In **34c** · 4 H_2O the distorted square pyramidal copper(II) ions of neighbouring dinuclear subunits are bridged *via* the apical positions by hexafluorosilicato coligands, thus forming a stair like polymeric chain structure (Figure 2.8.11 and Figure 2.8.13). The first crystal structure of a chain compound containing hexafluorosilicato bridging ligands was $[Co^{II}(viz)_4(SiF_6)]_\infty$ (viz = *N*-vinylimidazole) and was only reported in 1982 by Reedijk and co-workers.[199] Even up to now polynuclear compounds with bridging hexafluorosilicato ligands are not very common, and all reported compounds incorporate six coordinate metal ions and mononuclear subunits.[196,200-202] To the best of our knowledge **34c** · 4 H_2O is the first polymeric chain compound incorporating square pyramidal metal ions, and at the same time it is the first polymeric compound with hexafluorosilicato bridged discrete dinuclear subunits. The Cu^{II}-F bond length in **34c** · 4 H_2O (2.235(1) Å) is around 0.3 Å shorter than in $[\{Cu^{II}(HL)(H_2O)\}_2(SiF_6)]$ · 2 H_2O (2.522 Å)[203] or in $[\{Cu^{II}(HL')(H_2O)\}_2(SiF_6)]$ · 2 H_2O (2.528 Å),[197] the only crystal structures reported to date (1995 and 1993, respectively) containing square pyramidal copper(II) ions, bridged *via* the apical positions by hexafluorosilicate ions (Figure 2.8.12).

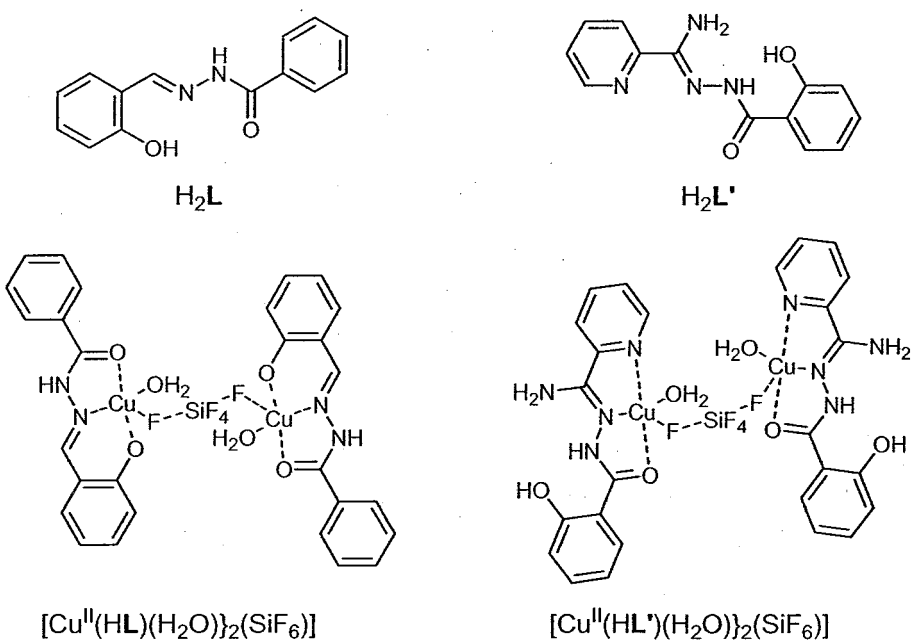

Figure 2.8.12. The ligands H_2**L**, H_2**L'** and their hexafluorosilicato bridged dinuclear complexes.[197,203]

The intermolecular $Cu^{II}\cdots Cu^{II}$ distance in **34c** · 4 H_2O is 7.166(1) Å and thus lies in-between the distances reported for [{Cu^{II}(HL)(H_2O)}$_2$(SiF_6)] · 2 H_2O (6.04 Å)[203] and [{Cu^{II}(HL')(H_2O)}$_2$(SiF_6)] · 2 H_2O (7.951 Å).[197] The Cu^{II}-F-Si angle in **34c** · 4 H_2O is only 130.45(7)° and thus smaller than in [{Cu^{II}(HL)(H_2O)}$_2$(SiF_6)] · 2 H_2O (144.0°)[203] or in [{Cu^{II}(HL')(H_2O)}$_2$(SiF_6)] · 2 H_2O (140.1°)[197] and considerably smaller than in the six coordinated polymeric chain structures, where the M-F-Si angle ranges from 180° to 152°.[196,199,204]

As observed in **34b** · 0.5 H_2O the equatorial water coligands in **34c** · 4 H_2O are involved in intermolecular hydrogen bonds to a symmetry generated carbonyl oxygen [O(10)···O(1C): 2.662 Å], in the present case interconnecting parallel stair like polymeric strands. Furthermore two solvent water molecules per asymmetric unit are involved in a network of hydrogen bonds involving all uncoordinated fluoride atoms of the hexafluorosilicate and the equatorial water coligand (Figure 2.8.13).

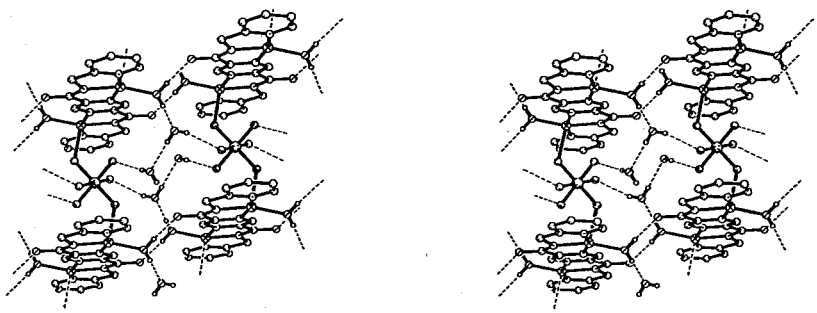

Figure 2.8.13. Stereo picture of a section of the 3D structure of {[Cu^{II}_2($\mathbf{L^{S1}}$)(H_2O)$_2$(SiF_6)] · 4 H_2O}$_\infty$ (**34c** · 4 H_2O). Hydrogen atoms not involved in hydrogen bonds have been omitted for clarity.

2.8.2. *Copper(II) tetrafluoroborate tetrahydrate and H_2L^{S2}*

Complexation in acetonitrile

As mentioned in Section 2.7.2 the reaction of $H_2\mathbf{L}^{S2}$ and copper(II) tetrafluoroborate tetrahydrate in a molar ratio of 1:1 in acetonitrile resulted, after vapour diffusion of diethyl ether into the reaction mixture, in the formation of a few bottle green crystals of a dinuclear copper(II) complex along with some bottle green amorphous precipitate. By means of elemental analysis the crystalline solid was tentatively formulated as $[Cu^{II}_2(\mathbf{L}^{S2})](BF_4)_2 \cdot$ solvent (**35**) (solvent = H_2O), the amorphous solid was also believed to be dinuclear in nature. Hence the complexation was repeated with a 2:1 molar ratio of copper(II) salt to ligand. Owing to the moderate solubility of the ligand the complexation was carried out in hot acetonitrile (60 °C) and the resulting bottle green reaction mixture was kept at that temperature until a homogeneous solution had formed. After stirring the resulting solution at room temperature for a further ten hours a bottle green microcrystalline precipitate was filtered off. With this method $[Cu^{II}_2(\mathbf{L}^{S2})](BF_4)_2 \cdot$ solvent (**35**) (solvent = 0.5 MeCN + H_2O) could be isolated in around 50 % yield (Scheme 2.8.3). The compound proved to be insoluble in ethanol and was only slightly soluble in acetonitrile but readily soluble in water. Conductivity measurements carried out in water [$\Lambda_m(H_2O)$ = 186 mol^{-1} cm^2 Ω^{-1}] gave relatively low but still acceptable values for a 2:1 electrolyte. The positive ion electrospray mass spectrum of **35** in acetonitrile was very noisy but showed the most intense peak at m/z = 1058.7, which was assigned to the dinuclear species $[Cu^{II}_2(HL^{S2})(MeCN)(H_2O)_3]^+$.

Single crystals of $[Cu^{II}_2(\mathbf{L}^{S2})(H_2O)_2(MeCN)_2](BF_4)_2$ (**35b**) suitable for X-crystal structure determination were obtained by diethyl ether vapour diffusion into a reaction mixture containing a 1:1 molar ratio of copper(II) to ligand, as described above. Slow evaporation of the dark bottle green solution of **35** in a 1:1 mixture of

acetonitrile and ethanol afforded single crystals of $[Cu^{II}_2(L^{S2})(H_2O)_4(BF_4)_2] \cdot 2\ H_2O$ (**35c** · 2 H_2O) suitable for X-ray crystal structure determination (Scheme 2.8.3).

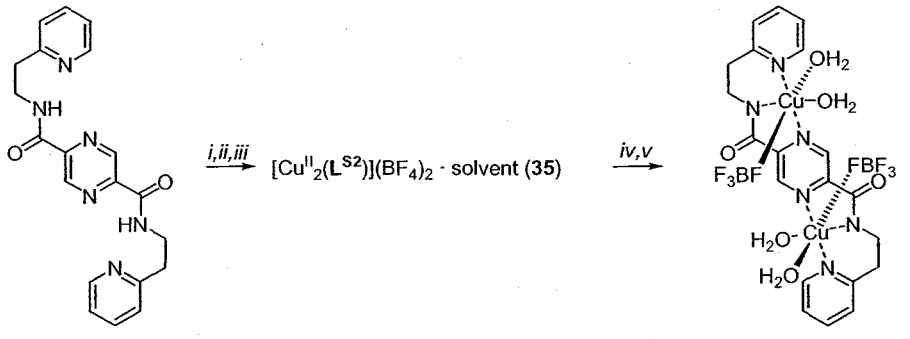

Scheme 2.8.3. Synthesis of **35**. Reagents and conditions: (*i*) 2 eq. $Cu(BF_4)_2 \cdot 4\ H_2O$, MeCN, 60 °C; (*ii*) RT, 10 h; (*iii*) filtration; (*iv*) MeCN/EtOH (1:1); (*v*) slow evaporation.

Complexation in water

By analogy with the synthesis of the hexafluorosilicate containing compounds $[Cu^{II}_2(L^{S1})(H_2O)_4](SiF_6) \cdot 0.5\ H_2O$ (**34b** · 0.5 H_2O) and $\{[Cu^{II}_2(L^{S1})(H_2O)_2(SiF_6)] \cdot 4\ H_2O\}_\infty$ (**34c** · 4 H_2O) of the lower ligand homologue, the reaction of H_2L^{S2} with copper(II) tetrafluoroborate tetrahydrate in a molar ratio of 1:2 was repeated in water in a glass vessel. Slow evaporation of the resulting solution led to the formation of bottle green crystals of **35**. IR analysis of the crystals showed no evidence for the presence of hexafluorosilicate anions, rather the counter ion was found to be tetrafluoroborate.

IR spectroscopic studies on $[Cu^{II}_2(L^{S2})](BF_4)_2 \cdot$ solvent (35)

The IR spectrum of **35** (Figure 2.8.14) showed one ν_{CO} vibration band at 1607 cm^{-1}, which compared well to the respective band of the M-type analogous perchlorate complex **8** (see Table 2.8.1), but expressed a distinct shoulder to higher

energy ($\tilde{\upsilon}$ = 1663 cm^{-1}). Compared to the IR spectrum of **33** of the lower ligand homologue the band of **35** experienced a shift of $\Delta\tilde{\upsilon}_{(35,33)}$ = 27 cm^{-1} to lower energy. The presence of tetrafluoroborate anions in **35** was confirmed with a broad split band at $\tilde{\upsilon}$ = 1083 cm^{-1}.

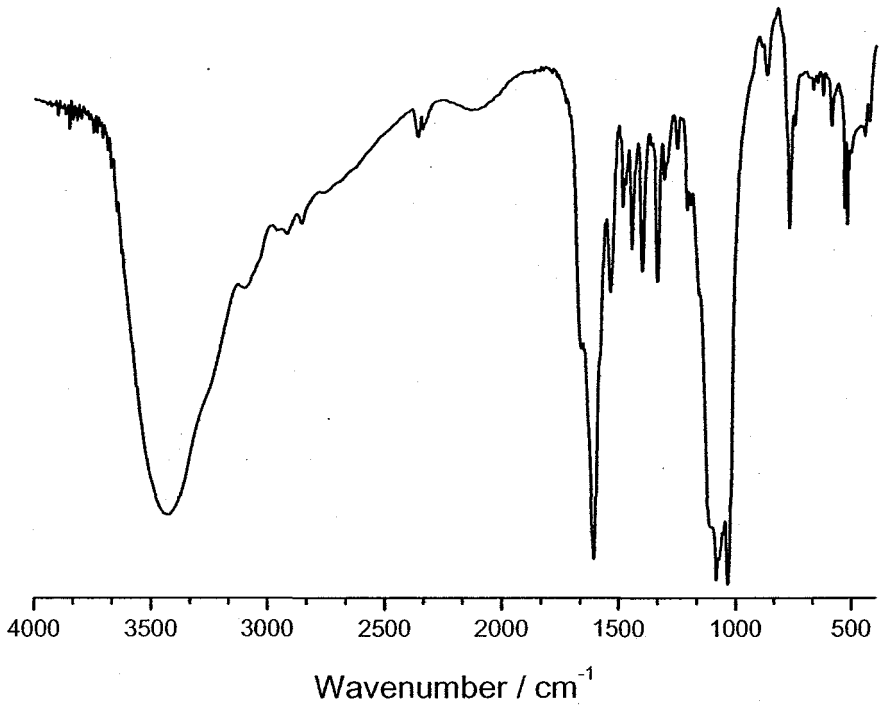

Figure 2.8.14. IR spectrum (KBr) of $[Cu^{II}_2(\mathbf{L^{S2}})](BF_4)_2$ · solvent (**35**).

Table 2.8.1. Comparison of the absorption bands in the expected region of ν_{CO} absorptions in the IR spectra of the dinuclear complexes **6** and **8** of the M-type ligands and **33**, **34** and **35** of the S-type ligands.

Complex	ν_{CO} vibration / cm^{-1}
$[Cu^{II}_2(HL^{M1})(MeCN)_2(H_2O)_2](BF_4)_3$ (**6**)	1609
$[Cu^{II}_2(HL^{M2})(H_2O)](ClO_4)_3$ (**8**)	1605
$[Cu^{II}_2(\mathbf{L^{S1}})(H_2O)_2](BF_4)_3$ (**33**)	1634
$[Cu^{II}_2(\mathbf{L^{S1}})](SiF_6) \cdot n\ H_2O$ (**34**)	1628, shoulder to lower energy
$[Cu^{II}_2(\mathbf{L^{S2}})](BF_4)_2$ · solvent (**35**)	1663, 1607

Single crystal X-ray structural analysis of $[Cu^{II}_2(L^{S2})(H_2O)_2(MeCN)_2](BF_4)_2$ (35b)

Single crystals of $[Cu^{II}_2(L^{S2})(H_2O)_2(MeCN)_2](BF_4)_2$ (**35b**) suitable for X-ray crystal structure determination were obtained by vapour diffusion of diethyl ether into the reaction mixture of a 1:1 molar ratio of ligand to copper(II) tetrafluoroborate tetrahydrate, as described before (Figure 2.8.15). The crystallographic solution showed two independent but chemically similar centrosymmetric molecules in the asymmetric unit.

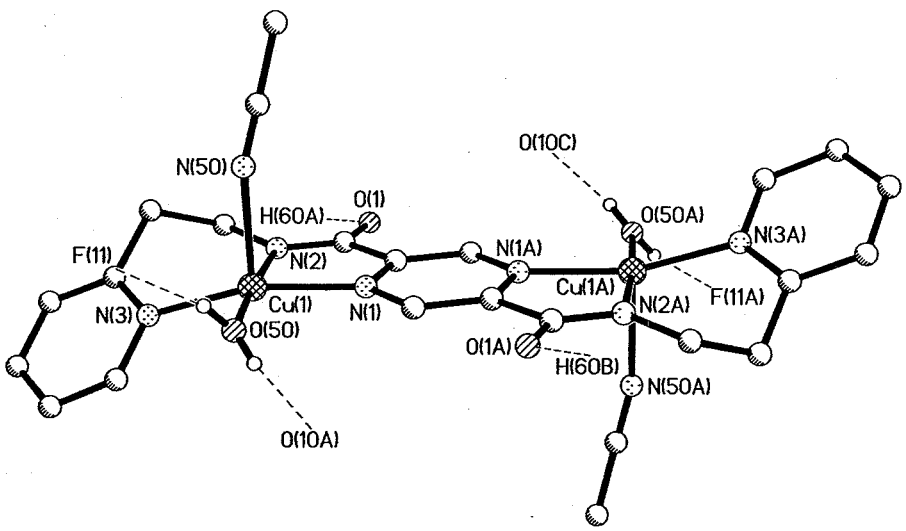

Figure 2.8.15. Molecular structure of $[Cu^{II}_2(\mathbf{L^{S2}})(H_2O)_2(MeCN)_2]^{2+}$, one of the two independent cations of **35b**. Hydrogen atoms except those of the water coligands have been omitted for clarity. Selected distances (Å) and angles (°): Cu(1)-N(1) 2.027(2), Cu(1)-N(2) 1.936(2), Cu(1)-N(3) 2.011(3), Cu(1)-O(50) 1.972(2), Cu(1)-N(50) 2.321(3), Cu(2)-N(11) 2.021(2), Cu(2)-N(12) 1.929(2), Cu(2)-N(13) 1.992(3), Cu(2)-O(60) 1.996(2), Cu(2)-N(60) 2.299(3), Cu(1)···Cu(1A) 6.784(2), Cu(2)···Cu(2B) 6.756(2), O(50)···O(10C) 2.598(4), O(50)···F(11) 2.738(4), O(60)···O(1) 2.595(4), O(60)···F(12D) 2.801(4); N(1)-Cu(1)-N(2) 82.1(1), N(1)-Cu(1)-N(3) 161.2(1), N(1)-Cu(1)-O(50) 93.5(1), N(50)-Cu(1)-N(1) 91.4(1), N(2)-Cu(1)-N(3) 92.3(1), N(2)-Cu(1)-O(50) 175.6(1), N(2)-Cu(1)-N(50) 92.8(1), N(3)-Cu(1)-O(50) 91.9(1), N(3)-Cu(1)-N(50) 106.9(1), N(50)-Cu(1)-O(50) 87.1(1), N(11)-Cu(2)-N(12) 82.3(1), N(11)-Cu(2)-N(13) 175.7(1), N(11)-Cu(2)-O(60) 93.7(1), N(60)-Cu(2)-N(11) 84.9(1), N(12)-Cu(2)-N(13) 94.3(1), N(12)-Cu(2)-O(60) 151.4(1), N(12)-Cu(2)-N(60) 102.8(1), N(13)-Cu(2)-O(60) 90.5(1), N(13)-Cu(2)-N(60) 93.3(1), O(60)-Cu(2)-N(60) 105.0(1). Symmetry operations used to generate equivalent atoms: A = 1–x, 2–y, 1–z; B = –x, 2–y, –z; C = x+1, y, z+1; D = x, y, z–1.

Not surprisingly, the molecular structure of **35b** is very similar to the structure of the related compound $[Cu^{II}_2(L^{S1})(H_2O)_2(MeCN)_2](BF_4)_2 \cdot H_2O$ (**33b** · H_2O) of the

lower ligand homologue. As in **33b** · H_2O the copper(II) ions of the two independent centrosymmetric molecules of **35b** are in an N_4O distorted square pyramidal coordination environment. As expected the nitrogen atoms of the N_3-terdentate binding pockets are functioning as equatorial donors. The Cu^{II}-N_{ligand} bond lengths, with shorter Cu^{II}-N_{amide} distances [Cu(1)-N(2): 1.936(2) Å and Cu(2)-N(12): 1.929(2) Å] than Cu^{II}-N_{py} [Cu(1)-N(3): 2.011(3) Å and Cu(2)-N(13): 1.992(3) Å] or Cu^{II}-N_{pz} [Cu(1)-N(1): 2.027(2) Å and Cu(2)-N(11): 2.021(2) Å] bond lengths, are comparable to the corresponding distances in **33b** · H_2O. The two remaining coordination sites of the copper(II) ions are occupied by a water and an acetonitrile coligand. In contrast to the molecular structure of **33b** · H_2O, where the remaining equatorial coordination site is occupied by the acetonitrile coligand leaving the water to coordinate to the axial position, in **35b** the two coligands are positioned the opposite way: the water coligand is coordinated equatorially leaving the axial coordination position to the acetonitrile coligand. The trigonal distortion of the square pyramids of the two independent copper(II) centers in **35b** is relatively large. The degree of trigonality of Cu(1) ($\tau_{(1)} = 0.24$) is around four times greater than that of **33b** · H_2O ($\tau = 0.06$) of the lower ligand homologue but still only about half the value observed for Cu(2) ($\tau_{(2)} = 0.40$) of the copper(II) center in the other independent molecule of **35b**. The copper(II) ions are pulled out of the N_3O plane in the direction of the axially coordinated acetonitrile coligand [Cu(1): 0.162(1) Å and Cu(2): 0.224(1) Å]. The ligand strands, with their extra methylene linkers compared to the lower ligand homologue, are not flat. The pyridine ring planes form an angle of 39.5(1)° [pyridine ring incorporating N(3)] and 33.4(1)° [pyridine ring incorporating N(13)] with the pyrazine ring plane of the respective ligand. The two pyrazine bridged symmetry equivalent copper(II) ions of **35b** are separated by 6.784(2) Å [Cu(1)···Cu(1A)] and 6.756(2) Å [Cu(2)···Cu(2B)], respectively, which is slightly closer together than in **33b** · H_2O (6.811(3) Å) of the lower ligand homologue.

As observed in the homologous complex **33b** · H_2O both hydrogen atoms of the water coligand in **35b** are involved in intermolecular hydrogen bonds. One proton is

involved in an O-H···O hydrogen bond to the carbonyl oxygen [O(1) and O(10), respectively] of the other independent molecule. This feature leads to a linear strand of dinuclear subunits (Figure 2.8.16). Each water coligand is further intermolecularly hydrogen bonded to a tetrafluoroborate counter ion, which itself is hydrogen bonded to a second water coligand. In this way, the polymeric linear strands are 3D connected *via* O-H···F-BF_2-F···H-O hydrogen bonds, as indicated in Figure 2.8.16.

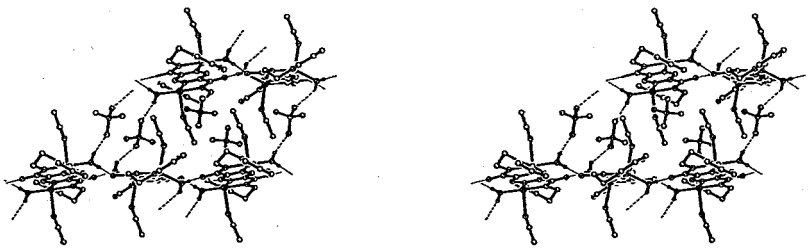

Figure 2.8.16. Stereo picture of a section of the 3D structure of $[Cu^{II}_2(\mathbf{L}^{S2})(H_2O)_2(MeCN)_2](BF_4)_2$ **35b**. Hydrogen atoms, except from water molecules have been omitted for clarity.

Single crystal X-ray structural analysis of $[Cu^{II}_2(L^{S2})(H_2O)_4(BF_4)_2] \cdot 2\ H_2O$ (35c · 2 H_2O)

By redissolving the initially obtained microcrystalline material **35** in a solvent mixture containing one part of acetonitrile and one part of ethanol and by slow evaporation of the resulting solution single crystals of $[Cu^{II}_2(L^{S2})(H_2O)_4(BF_4)_2] \cdot 2\ H_2O$ (**35c** · 2 H_2O) suitable for X-ray crystal structure determination were obtained (Figure 2.8.17).

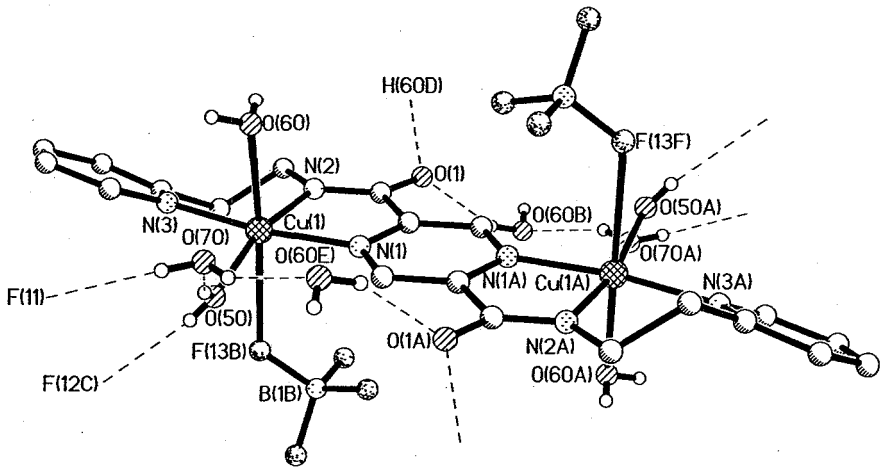

Figure 2.8.17. Molecular structure of $[Cu^{II}_2(\mathbf{L}^{S2})(H_2O)_4(BF_4)_2]$ the complex molecule of **35c** · 2 H_2O. Hydrogen atoms except of water molecules have been omitted for clarity. Selected distances (Å) and angles (°): Cu(1)-N(1) 2.021(4), Cu(1)-N(2) 1.946(4), Cu(1)-N(3) 1.981(4), Cu(1)-O(50) 1.961(4), Cu(1)-O(60) 2.516(5), Cu(1)-F(13B) 2.598(3), Cu(1)···Cu(1A) 6.764(1), O(50)···O(70) 2.620(4), O(50)···F(12C) 2.771(4), O(60B)···O(1) 2.828(4), O(60D)···O(1) 2.747(4), O(70)···(F11) 2.756(4), O(70)···O(60E) 2.794(4); N(1)-Cu(1)-N(2) 81.1(2), N(1)-Cu(1)-N(3) 173.5(1), N(1)-Cu(1)-O(50) 91.4(2), N(1)-Cu(1)-O(60) 85.5(2), N(1)-Cu(1)-F(13) 91.6(1), N(2)-Cu(1)-N(3) 95.0(2), N(2)-Cu(1)-O(50) 165.7(1), N(2)-Cu(1)-O(60) 102.0(2), N(2)-Cu(1)-F(13) 91.4(1), N(3)-Cu(1)-O(50) 93.5(2), N(3)-Cu(1)-O(60) 90.3(2), N(3)-Cu(1)-F(13) 93.7(1), O(50)-Cu(1)-O(60) 89.5(2), O(50)-Cu(1)-F(13) 76.5(1), O(60)-Cu(1)-F(13) 165.7(1). A = 1-x, 1-y, 1-z; B = x-1, y, z; C = -x+2, -y+1, -z+2; D = -x, -y+1, -z; E = -x+2, -y+1, -z+1.

The molecular structure of the centrosymmetric complex molecule of **35c** · 2 H_2O is very similar to the molecular structure of $[Cu^{II}_2(\mathbf{L}^{S2})(H_2O)_2(MeCN)_2](BF_4)_2$ (**35b**) and the copper(II) ions are coordinated in an equatorial fashion by the bis-terdentate ligand $(\mathbf{L}^{S2})^{2-}$. As observed in all structures described so far the Cu^{II}-N_{amide} bond length in **35c** · 2 H_2O (1.946(4) Å) is shorter than the Cu^{II}-N_{py} (1.981(4) Å) or the Cu^{II}-N_{pz} (2.021(4) Å) distance. Again, the ligand strand is not flat but the pyridine ring forms an angle of 28.19(3)° with the pyrazine ring. The two pyrazine bridged symmetry equivalent copper(II) ions are separated by 6.764(1) Å, which compares well with the structures described so far. The main difference between the compounds **35b** and **35c** · 2 H_2O is the different coordination environment around the copper(II) ions. Whereas in **35b** the coordination environment is N_4O distorted square pyramidal and the coligands are water (equatorial) and acetonitrile (axial), the coordination sphere in **35c** · 2 H_2O is best

described as a distorted N_3O_2F octahedral with two water coligands in the remaining equatorial and an axial position, leaving the second axial position for the tetrafluoroborate anion. Tetrafluoroborate is commonly regarded as a "non-coordinating anion" but nevertheless a number of structures with coordinated tetrafluoroborate ions are known.[140] In copper(II) complexes with coordinated tetrafluoroborate ions Cu^{II}-F distances between 2.07 Å[205] and 2.85 Å[206] have been observed, but mostly the distances lie in the range of 2.40–2.71 Å. The Cu^{II}-F distance in **35c** · 2 H_2O is 2.598(3) Å and thus notably longer than the Cu^{II}-$O_{(ax)}$ distance of 2.516(5) Å. The tetragonality factor[189] for **35c** · 2 H_2O is given by T = 0.773. The elongated axis of the distorted copper(II) octahedron is very close to perpendicular (89.4°) to the N_3-chelate plane. This is in contrast to the compressed octahedra of the [2 × 2] copper(II) grid **23** of the M-type lower ligand analogue, where the out of plane axis is defined by the Cu^{II}-N_{amide} bonds and thus is parallel to the N_3-chelate planes.

All of the water coligands of **35c** · 2 H_2O are involved in intermolecular hydrogen bonds. A common feature for these structures with water coligands is an O-H···O hydrogen bond to the carbonyl oxygen atom of a second molecule. In the present case this involves the axially coordinated water coligand, which bridges two molecules that are additionally bridged by a water coligand of a third molecule, leading to a  circular arrangement as shown in Figure 2.8.18.

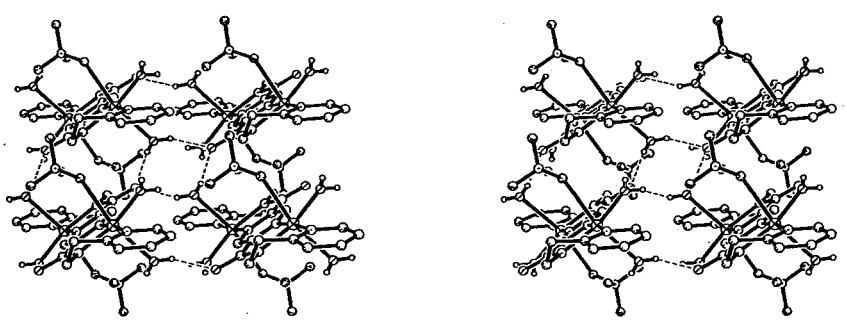

Figure 2.8.18. Stereo picture of a section of the 3D structure of $[Cu^{II}_2(\mathbf{L^{S2}})(H_2O)_4(BF_4)_2]$ · 2 H_2O (**35c** · 2 H_2O), with emphasis on the cyclic motif that involves water coligands. Solvent molecules and hydrogen atoms except of water molecules and have been omitted for clarity.

Another circular motif is formed by the equatorial water coligand, which is hydrogen bound to the coordinated tetrafluoroborato ligand of a second molecule, which *vice versa* is hydrogen bonded *via* its equatorial water coligand to the tetrafluoroborato ligand of the former molecule (Figure 2.8.19). The equatorial water coligand is involved in a further hydrogen bond to a water solvate molecule, which is additionally involved in hydrogen bonds to the tetrafluoroborato and the axial water coligand of a second complex molecule.

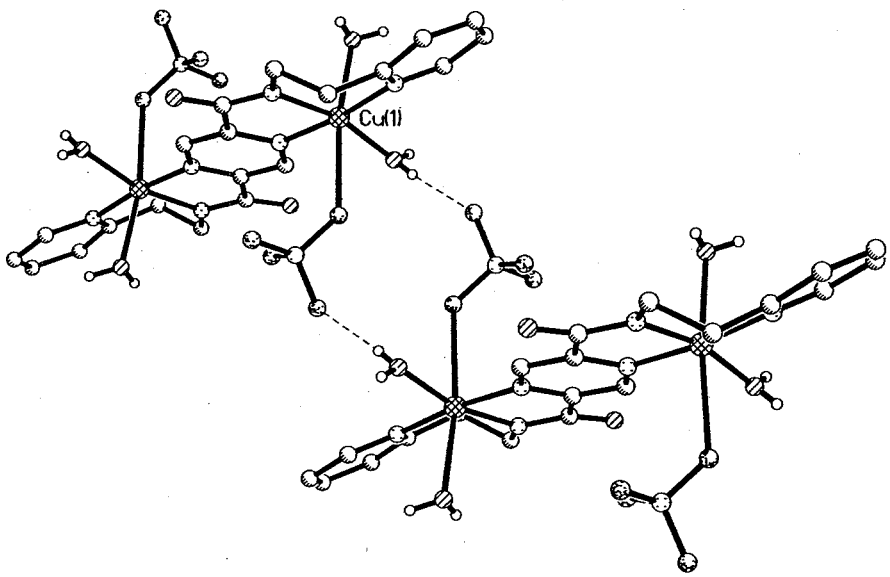

Figure 2.8.19. Section of the 3D structure of $[Cu^{II}_2(\mathbf{L}^{S2})(H_2O)_4(BF_4)_2] \cdot 2\ H_2O$ (**35c** · 2 H_2O), with emphasis on the tetrafluoroborato involving cyclic motif. Solvent molecules and hydrogen atoms except of water molecules have been omitted for clarity.

UV/VIS spectroscopic studies on $[Cu^{II}_2(L^{S2})](BF_4)$ · solvent (35)

The UV/VIS spectrum of **35** in water was very similar to the spectrum of $[Cu^{II}_2(\mathbf{L}^{S1})(H_2O)_2](BF_4)_2$ (**33**) of the lower ligand homologue but showed only three distinct absorptions in the region of $\lambda = 200–1400$ nm.

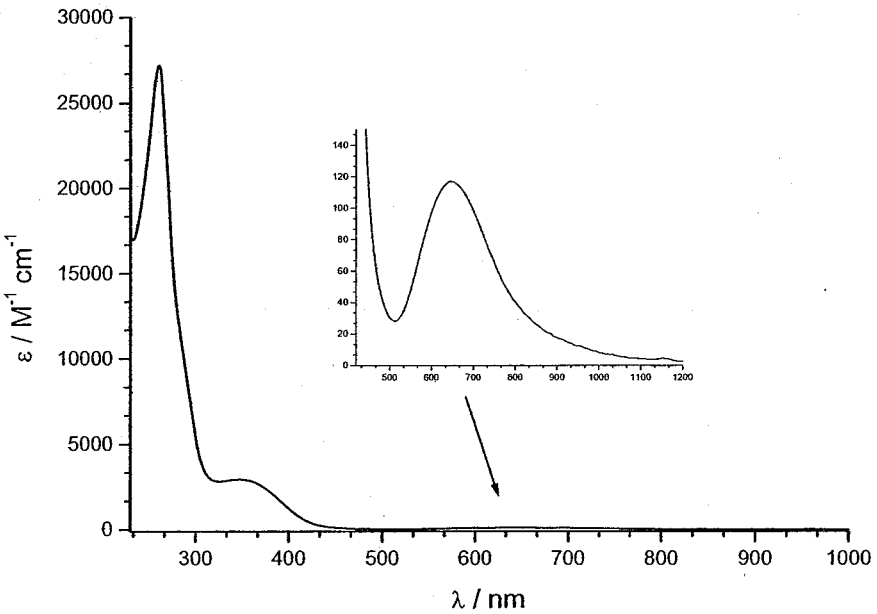

Figure 2.8.20. UV/VIS spectra [H_2O, 1 mM (inset) and 0.1 mM (main)] of $[Cu^{II}_2(\mathbf{L}^{S2})](BF_4)_2 \cdot$ solvent (**35**).

As observed in the UV/VIS spectrum of **33** of the lower ligand homologue, the spectrum of **35** showed a relatively intense asymmetrical absorption band, unique to complexes of the S-type ligands, at λ_{max} = 346 nm (ε = 2930 M^{-1} cm^{-1}, $\tilde{\upsilon}$ = 28902 cm^{-1}). Furthermore a weak broad absorption peak at λ_{max} = 647 nm (ε = 113 M^{-1} cm^{-1}, $\tilde{\upsilon}$ = 15456 cm^{-1}) was assigned as the absorption band of the overlapping copper(II) *d-d* transitions. An expected shift of $\Delta\tilde{\upsilon}_{(8,35)}$ = 595 cm^{-1} to lower energy occurred, comparing the UV/VIS spectra of **8** (in MeCN) and **35** (in H_2O). Again, as for the complex pair $[Cu^{II}_2(HL^{M1})(MeCN)_4](BF_4)_3 \cdot$ MeCN (**6b** · MeCN) (in MeCN) *vs.* **33** (in H_2O) of the analogous lower ligand homologues H_2L^{M1} and H_2L^{S1}, this shift was attributed to the different solvent systems: acetonitrile for the former and water for the latter. The complex cation of **35** in water was hence formulated as $[Cu^{II}_2(\mathbf{L}^{S2})(H_2O)_4]^{2+}$, accounting for the involvement of the weaker water coligand. Compared to **33** of the lower ligand homologue the molar extinction coefficient of the copper(II) *d-d* transition of **35** was approximately halved (Figure 2.8.21). Interestingly the same observation has been made for all pairs of similar complexes involving the two homologous M-type ligands H_2L^{M1} and H_2L^{M2}, respectively, *i.e.* **6b** · MeCN *vs.* **8**, **18** *vs.* **19** · 4 H_2O and **26** · 4 H_2O *vs.* **25** · 10 H_2O (Figure 2.4.13 and Figure 2.5.32).

Furthermore a very intense peak was observed at λ_{max} = 261 nm (ε = 26400 M^{-1} cm^{-1}, $\tilde{\upsilon}$ = 38314 cm^{-1}) in the UV/VIS spectrum of **35** (Figure 2.8.20).

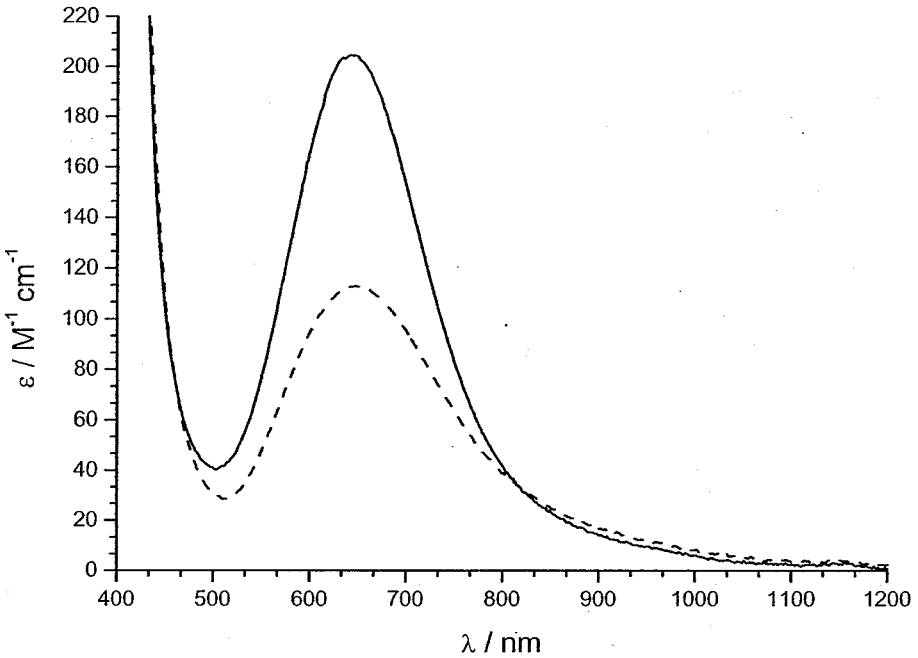

Figure 2.8.21. Comparison of the UV/VIS spectra [H_2O, 1 mM] of $[Cu^{II}_2(\mathbf{L^{S1}})(H_2O)_2](BF_4)_2$ (**33**) (solid line) and $[Cu^{II}_2(\mathbf{L^{S2}})](BF_4)_2$ · solvent (**35**) (dashed line).

2.8.3. *Summary*

By means of the molecular structure of $[Cu^{II}_2(\mathbf{L^{S1}})(H_2O)_2(MeCN)_2](BF_4)_2 \cdot H_2O$ (**33b** · H_2O) it has been shown that dinuclear complexes of the fully deprotonated S-type ligand $(\mathbf{L^{S1}})^{2-}$ could be formed. The overall molecular structure of the dinuclear copper(II) complex **33b** · H_2O thus proved to be very similar to the structure of the related complex $[Cu^{II}_2(HL^{M1})(MeCN)_4](BF_4)_3 \cdot MeCN$ (**6b** · MeCN) of the M-type ligand analogue $(HL^{M1})^-$. As the bis-terdentate S-type ligand was not able to retain former N-H amide protons the resulting complex fragment $[Cu^{II}(\mathbf{L^{S1}})]^{2+}$ held

a 2+ charge, rather than the 3+ charge observed for the analogous M-type complex fragment.

Serendipitously the molecular structures of the hexafluorosilicate containing complexes $[Cu^{II}_2(\mathbf{L}^{S1})(H_2O)_4](SiF_6) \cdot 0.5\ H_2O$ (**34b** · 0.5 H_2O) and $\{[Cu^{II}_2(\mathbf{L}^{S1})(H_2O)_2(SiF_6)] \cdot 4\ H_2O\}_\infty$ (**34c** · 4 H_2O) were obtained. Thus it has been shown that on carrying out the complexation of $H_2\mathbf{L}^{S1}$ with copper(II) tetrafluoroborate tetrahydrate in water, a compound containing solely hexafluorosilicate as a counter ion crystallised quantitatively. In contrast the recrystallisation of the dinuclear copper(II) complex **33b** · H_2O in water did not result in any hexafluorosilicate containing species.

Also, under identical reaction conditions but employing $H_2\mathbf{L}^{S2}$ instead of $H_2\mathbf{L}^{S1}$ the complexation with copper(II) tetrafluoroborate tetrahydrate did not result in any hexafluorosilicate containing species.

From the examples of $[Cu^{II}_2(\mathbf{L}^{S2})(H_2O)_2(MeCN)_2](BF_4)_2$ (**35b**) and $[Cu^{II}_2(\mathbf{L}^{S2})(H_2O)_4(BF_4)_2] \cdot 2\ H_2O$ (**35c** · 2 H_2O) it has been shown that dinuclear copper(II) complexes of the fully deprotonated higher S-type ligand homologue $(\mathbf{L}^{S2})^{2-}$ could form. The molecular structures were found to be very similar to the structure of **33b** · H_2O.

It was believed that a [2 × 2] grid complex $[Cu^{II}_4(\mathbf{L}^{S1})_4]$ (**32**) has formed following the reaction of 1:1:2 molar ratio of $H_2\mathbf{L}^{S1}$, copper(II) tetrafluoroborate tetrahydrate and triethylamine. Owing to the extreme insolubility of the neutral grid compound further analyses unfortunately could not be carried out.

2.9. *Coordination of the ligands H_2L^{S1} and H_2L^{S2}, employing metal ions other than copper(II)*

2.9.1. *Iron(II) salts*

Complexations with H_2L^{S1} and H_2L^{S2}

On treating a suspension of the lower ligand homologue H_2L^{S1} in acetonitrile with a solution of iron(II) tetrafluoroborate hexahydrate in acetonitrile, in either a 1:1 or 1:2 molar ratio, the ligand quickly dissolved and a dark green-black solution formed. With addition of triethylamine a darkening of the solution to deep black was achieved. Unfortunately in no case could a homogeneous solid be isolated.

The employment of the higher ligand homologue H_2L^{S2} under otherwise identical conditions merely resulted in the recovery of pure ligand H_2L^{S2}.

2.9.2. *Iron(III) salts*

As described in Section 2.6 the formation of [2 × 2] grid-type complexes employing either of the S-type ligands H_2L^{S1} or H_2L^{S2} and metal(II) ions was expected to lead to neutral species like $[M^{II}_4(L^{S1})_4]^0$ or $[M^{II}_4(L^{S2})_4]^0$. As has been observed for **32** · 6 H_2O, which was believed to be a [2 × 2] grid of the fully deprotonated ligand $(L^{S1})^{2-}$, these types of neutral complexes were expected to have marginal solubility in any solvent systems, which hampers recrystallisation attempts and indeed full characterisation. By the employment of metal(III) ions rather than metal(II) ions, the

formation of quadruply charged grid-type species like $[M^{III}_4(L^{S1})_4]^{4+}$ or $[M^{III}_4(L^{S2})_4]^{4+}$, hopefully with more favourable solubility properties, was expected.

Complexations with H_2L^{S1} and H_2L^{S2}

The reaction of iron(III) perchlorate hexahydrate with the higher ligand homologue H_2L^{S2} in acetonitrile solution, employing a molar ratio of 1:1, initially led to an orange-brown solution. A golden flaky solid precipitated after the addition of two equivalents of triethylamine. Elemental analysis of the compound revealed an unexpected high mass percentage of carbon (around 56 %), hydrogen (around 5 %) and nitrogen (around 20 %), so that the compound was believed to have a molar ratio of iron(III) to ligand of 1:3.

The reaction of the lower ligand homologue H_2L^{S1} under otherwise identical reaction conditions initially led to the formation of a dark red-brown solution, which turned to deep purple after the addition of triethylamine. By vapour diffusion of diethyl ether into the reaction mixture a dark purple inhomogeneous solid of unknown composition was isolated.

Very different observations were made in methanol solution on reacting the lower ligand homologue H_2L^{S1}, iron(III) salts and lithium hydroxide or sodium hydroxide as base. The addition of iron(III) perchlorate hexahydrate to a suspension of the ligand H_2L^{S1} in methanol did not result in the immediate dissolution of the ligand, but resulted instead in a yellow suspension, even after the addition of the base. In order to dissolve the ligand the suspension was subsequently heated to reflux and, on doing so, the mixture slowly became darker in colour and became deep blue-black on refluxing. The resulting solution, left to cool to room temperature overnight, adopted a yellow colouration in the morning and on reheating it darkened

again to blue-black before once again becoming yellow on cooling overnight. This cycle could be maintained for several days. Unfortunately all attempts to isolate discrete solids, either blue-black or yellow failed. For example, by layering the blue-black solution with toluene or by vapour diffusion of diethyl ether into the black solution, no solid separated but the mixture merely slowly turned yellow. By the addition of excess counter ion, no solid could be isolated and on slow evaporation of the yellow solution only an inhomogeneous sticky yellowish solid was obtained.

Basically the same observations were made employing iron(III) nitrate nonahydrate instead of the corresponding perchlorate salt. The initially formed yellow suspension turned to a black solution on refluxing, but on cooling to room temperature overnight a small amount of something close to colloidal but not isolable black solid formed. The reaction was subsequently carried out in ethanol under otherwise identical reaction conditions and resulted in the formation of a more coarse isolable black solid. Elemental analysis of the compound thus revealed unexpectedly low mass percentages of carbon (around 28 %) and nitrogen (around 12 %) so that no statement about the likely formulation of this compound could be made. Unfortunately, further attempts to recrystallise the isolated compound failed.

2.9.3. *Cobalt(II) salts*

Complexation with H_2L^{S1}

In acetonitrile solution the reaction of H_2L^{S1} with cobalt(II) tetrafluoroborate hexahydrate in a 1:1 or 1:2 molar ratio employing additional base resulted, after vapour diffusion of diethyl ether into the reaction mixtures, respectively, in the formation of a dark brown solid. As had been observed for reactions employing the analogous M-type ligand H_2L^{M1} under otherwise identical reaction conditions the

reaction products in the present cases showed intense absorption bands in the region of $\tilde{\upsilon}$ = 1720–1730 cm^{-1} in their IR spectra, which possibly indicated the disintegration of the ligand (Section 2.5.3).

Complexation with H_2L^{S2}

The treatment of a suspension of H_2L^{S2} with a solution of one molar equivalent cobalt(II) tetrafluoroborate hexahydrate in acetonitrile, resulted in the immediate formation of a cherry red solution. After vapour diffusion of diethyl ether into the reaction mixture, red-brown-to-red crystals were isolated in around 30 % yield, along with some unidentified red-brown solid. Elemental analysis of the crystals suggested a 1:1:1 molar ratio of cobalt ions to ligand to tetrafluoroborate. The addition of triethylamine leading to a 1:1:2 molar ratio of cobalt(II) ions to ligand to base, under otherwise identical reaction conditions, led to the clean isolation of red-brown-to-red crystals in 85 % yield (Scheme 2.9.1). The compound was readily soluble in most polar solvents like acetonitrile, ethanol, water or *N*,*N*-dimethylformamide. By means of elemental analysis the compound was tentatively formulated as $[Co^{III}(L^{S2})]_n(BF_4)_n \cdot 2.5n\ H_2O$ (**36** · 2.5*n* H_2O), assuming that the initially employed cobalt(II) ions had been oxidised to cobalt(III) on complexation. A similar oxidation had occurred in the synthesis of the cobalt(III) complexes $[Co^{III}(H_2L^{M1})_2](BF_4)_3 \cdot 4\ H_2O$ (**21** · 4 H_2O) and $[Co^{III}(H_2L^{M2})_2](BF_4)_3 \cdot EtOH$ (**22** · EtOH) (Section 2.4.2). The formulation of $[Co^{III}(L^{S2})]_n(BF_4)_n \cdot 2.5n\ H_2O$ (**36** · 2.5*n* H_2O) fitted well with the expected [2 × 2] grid-type molecular structure of the compound (n = 4), as indicated in Scheme 2.9.1. The conductivity measurement carried out in acetonitrile solution [Λ_m(MeCN) = 133 mol^{-1} cm^2 Ω^{-1} per ligand] also fitted well with that proposal. The tetranuclear [2 × 2] grid structure of **36** · 2.5*n* H_2O was further corroborated by the positive ion electrospray mass spectrum in acetonitrile. Three distinct peaks at m/z = 433.4, 443.4 and 453.7 were assigned to the [2 × 2] complex fragments

$[Co^{III}_4(L^{S2})_4]^{4+}$, $\{[Co^{III}_4(L^{S2})_4] \cdot MeCN\}^{4+}$ and $\{[Co^{III}_4(L^{S2})_4] \cdot 2\ MeCN\}^{4+}$, respectively. Similarly, the four peaks at *m/z* = 577.9, 591.5, 605.2 and 619.8 were assigned to the tetranuclear complex fragments $[Co^{III}_3Co^{II}(L^{S2})_4]^{3+}$, $\{[Co^{III}_3Co^{II}(L^{S2})_4] \cdot MeCN\}^{3+}$, $\{[Co^{III}_3Co^{II}(L^{S2})_4] \cdot 2\ MeCN\}^{3+}$ and $\{[Co^{III}_3Co^{II}(L^{S2})_4] \cdot 3\ MeCN\}^{3+}$ and by analogy the two peaks at m/z = 866.8 and 887.3 were assigned to the [2 × 2] complex fragments $[Co^{III}_2Co^{II}_2(L^{S2})_4]^{2+}$ and $\{[Co^{III}_2Co^{II}_2(L^{S2})_4] \cdot MeCN\}^{2+}$, respectively. The compound was accordingly formulated as $[Co^{III}_4(L^{S2})_4](BF_4)_4 \cdot 10\ H_2O$ (**36** · 10 H_2O), as shown in Scheme 2.9.1.

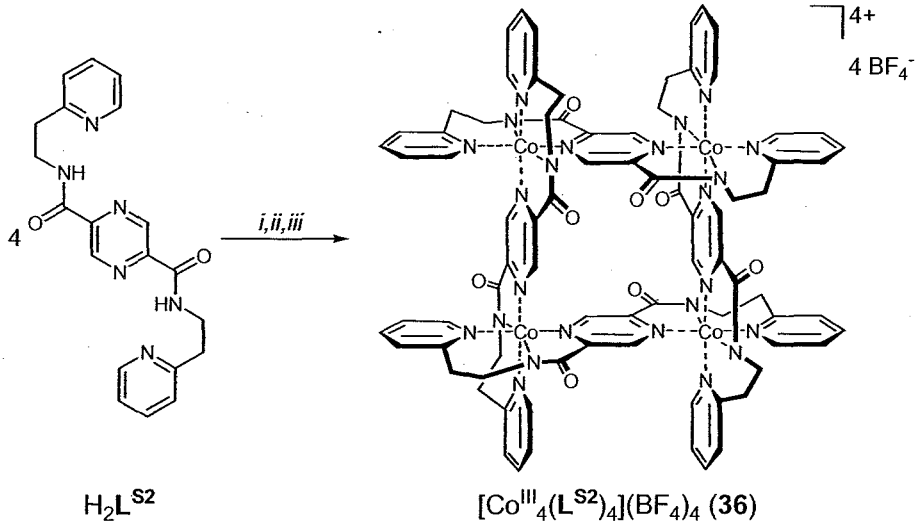

H_2L^{S2} $[Co^{III}_4(L^{S2})_4](BF_4)_4$ (**36**)

Scheme 2.9.1. Synthesis of **36**. Reagents and conditions: (*i*) 1 eq. $Co(BF_4)_2 \cdot 6\ H_2O$, MeCN, RT; (*ii*) 2 eq. NEt_3; (*iii*) Et_2O (vapour diffusion).

IR spectroscopic studies on $[Co^{III}_4(L^{S2})_4](BF_4)_4 \cdot 10\ H_2O$ (36 · 10 H_2O)

As expected for a symmetrical [2 × 2] grid-type structure the IR spectrum of **36** · 10 H_2O showed only one absorption for the νCO vibration at $\tilde{\nu}$ = 1623 cm^{-1}. In contrast to the IR spectrum of the analogous [2 × 2] nickel(II) complex **25** · 10 H_2O, no splitting was observed for that band. A shift of $\Delta\tilde{\nu}_{(25,36)}$ = 18 cm^{-1} occurred for the νCO vibration band of **36** with respect to the main νCO band of **25** ($\tilde{\nu}$ = 1605 cm^{-1}). The

expected presence of tetrafluoroborate counter ions was confirmed with a broad split peak at $\tilde{\upsilon}$ = 1083 cm^{-1} (Figure 2.9.1).

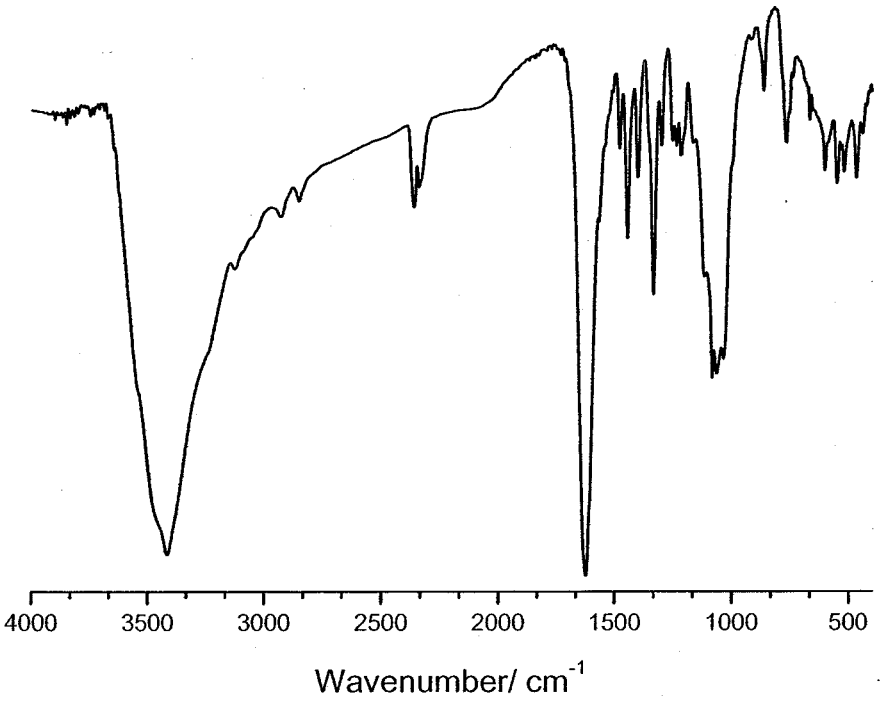

Figure 2.9.1. IR spectrum (KBr) of $[Co^{III}_4(\mathbf{L^{S2}})_4](BF_4)_4 \cdot 10\ H_2O$ (**36** · 10 H_2O).

Single crystal X-ray structural analysis of 36 · 12.75 MeCN

Single crystals of **36** · 12.75 MeCN suitable for X-ray crystal structure determination were obtained by vapour diffusion of diethyl ether into a solution of **36** · 10 H_2O in acetonitrile. The structural analysis subsequently carried out affirmed the [2 × 2] type structure of the racemic compound $[Co^{III}_4(L^{S2})_4](BF_4)_4 \cdot 12.75$ MeCN (Figure 2.9.2).

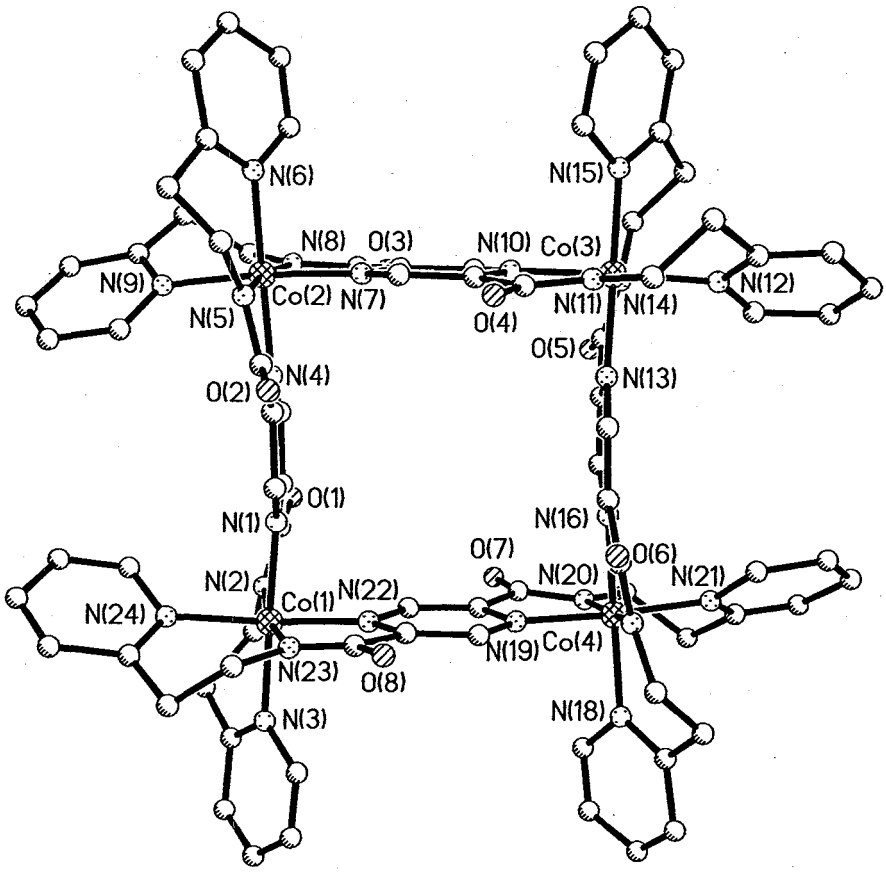

Figure 2.9.2. Molecular structure of $[Co^{III}_4(\mathbf{L^{S2}})_4]^{4+}$, the complex cation of the racemic compound **36** · 12.75 MeCN. Hydrogen atoms have been omitted for clarity. Only one of the enantiomers is shown (*Δ*). Selected distances (Å) and angles (°): Co(1)-N(1) 1.941(3), Co(1)-N(2) 1.931(4), Co(1)-N(3) 2.003(3), Co(1)-N(22) 1.933(3), Co(1)-N(23) 1.929(3), Co(1)-N(24) 1.988(4), Co(1)···Co(2) 6.605(3), Co(2)···Co(3) 6.636(3), Co(3)···Co(4) 6.592(3), Co(4)···Co(1) 6.641(3), Co(1)···Co(3) 9.283(3), Co(2)···Co(4) 9.400(3); N(1)-Co(1)-N(2) 82.0(2), N(1)-Co(1)-N(3) 174.8(1), N(1)-Co(1)-N(22) 87.4(1), N(1)-Co(1)-N(23) 91.2(1), N(1)-Co(1)-N(24) 88.2(1), N(2)-Co(1)-N(3) 92.9(2), N(2)-Co(1)-N(22) 90.6(1), N(2)-Co(1)-N(23) 170.4(2), N(2)-Co(1)-N(24) 94.4(2), N(3)-Co(1)-N(22) 91.3(1), N(3)-Co(1)-N(23) 93.7(1), N(3)-Co(1)-N(24) 93.5(1), N(22)-Co(1)-N(23) 82.2(1), N(22)-Co(1)-N(24) 172.9(1), N(23)-Co(1)-N(24) 92.2(1), Co(1)···Co(2)···Co(3) 89.0(2), Co(2)···Co(3)···Co(4) 90.5(2), Co(3)···Co(4)···Co(1) 89.1(2), Co(4)···Co(1)···Co(2) 90.4(2).

As shown in Figure 2.9.2 all four ligands of **36** · 12.75 MeCN act as bis-terdentate chelates with antiparallel coordinate vectors. Consequently two enantiomers (*Δ* and *Λ*, see Figure 2.6.1) are present in the unit cell. Each terdentate binding pocket of **36** · 12.75 MeCN coordinates in a meridional fashion to the cobalt(III) ions and both amide N-H functions of the ligand are deprotonated. The cobalt(III) ions adopt a distorted N_6 octahedral coordination sphere, encapsulated by two N_3-terdentate binding pockets of a pair of perpendicularly arranged ligands. In

the tetranuclear complex, the cobalt(III) ions are bridged *via* the ligand pyrazine rings which gives rise to a grid-like arrangement of interwoven ligand strands (Figure 2.9.2). As observed for the [2 × 2] copper(II) grid **23** · 3.5 MeCN of the lower M-type ligand analogue, two shorter [Co(1)···Co(2): 6.605(3) Å, Co(3)···Co(4): 6.592(3) Å] and two slightly longer [Co(2)···Co(3): 6.636(3) Å, Co(4)···Co(1): 6.641 Å] Co^{III}···Co^{III} distances are observed. Compared to the M···M distances found in **23** · 3.5 MeCN (7.101–7.150 Å), and in the nickel(II) [2 × 2] grid-type complex **25** · 10 MeCN of the higher M-type ligand analogue (7.003–7.150 Å) the Co^{III}···Co^{III} distances observed in **36** · 12.75 MeCN are relatively short. Like in **25** · 10 H_2O, the ligand strands in **36** · 12.75 MeCN are not flat but the average angle formed by the pyridine rings with the pyrazine ring of the same ligand is relatively huge (36.4°). The individual angles range from 31.5–42.5°. As observed in all structures of either the M-type or the S-type ligands so far, the average M-N_{ligand} distances are not similar but the average Co^{III}-N_{amide} bond length (1.92 Å) is shorter than the average Co^{III}-N_{pz} (1.94 Å) or Co^{III}-N_{py} (1.98 Å) bond length. These values compare well to those of the similar mononuclear complex **22** · EtOH of the M-type ligand analogue $H_2\mathbf{L}^{M2}$. The tetragonality factors for the distorted N_6 octahedra of tetranuclear complex **36** · 12.75 MeCN range from T = 1.003–1.027 giving the average tetragonality factor to T_{av} = 1.018. This is considerably closer to 1.0 than $T_{av(23)}$ = 1.122 or $T_{av(25)}$ = 1.045 of the [2 × 2] grid-type complexes **23** · 3.5 MeCN and **25** · 10 MeCN, respectively. As in the analogous [2 × 2] grid structures **23** · 3.5 MeCN of the lower M-type ligand analogue $(H\mathbf{L}^{M1})^-$ and **25** · 10 MeCN of the higher M-type ligand analogue $(H\mathbf{L}^{M2})^-$, in **36** · 12.75 MeCN the mean planes around the cobalt(III) ions are defined by the $N_{heterocyle}$ atoms and therefore lie in the Co^{III}_4 mean plane. The compressed axes lie parallel to each other and perpendicular to the Co^{III}_4 mean plane.

NMR spectroscopic studies on $[Co^{III}_4(L^{S2})_4](BF_4)_4 \cdot 10\ H_2O$ (36 · 10 H_2O)

As the cobalt(III) ions of the complex $[Co^{III}_4(L^{S2})_4](BF_4)_4 \cdot 10\ H_2O$ (**36** · 10 H_2O) exist in a diamagnetic ground state, the compound is readily analysable by NMR spectroscopy. The ^1H and ^{13}C NMR spectra of **36** · 10 H_2O were measured in d^3-MeCN and unequivocally proved the highly symmetrical environment of all four ligands of the grid and underlined the very low dissociation of the [2 × 2] grid cation in acetonitrile solution. The aromatic region of the ^1H NMR spectrum of **36** · 10 H_2O as expected showed five well-resolved peaks (Figure 2.9.3).

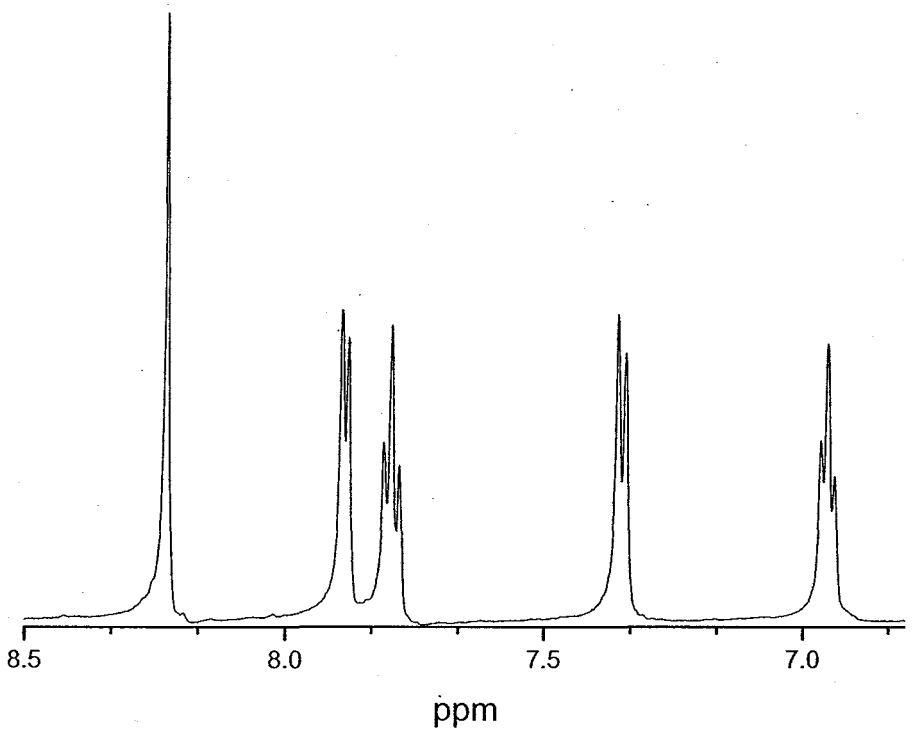

Figure 2.9.3. Aromatic region of the ^1H NMR spectrum (d^3-MeCN) of $[Co^{III}_4(\mathbf{L^{S2}})_4](BF_4)_4 \cdot 10\ H_2O$ (**36** · 10 H_2O).

The singlet at 8.23 ppm derived from the pyrazine protons and, compared to the ^1H NMR spectrum of the free ligand H_2L^{S2}, it experienced a relatively large shift of 1.05 ppm to higher field. The signals derived from the pyridine hydrogen atoms positioned on the ligand side facing the pyrazine ring (5-py*H* and 6-py*H*) also both experienced a minor shift to higher field, compared to the spectrum of the free ligand. The signals of the pyridine hydrogen atoms positioned on the opposite ligand

side (3-py*H* and 4-py*H*) both experienced a minor shift to lower field. Consistent with the molecular structure, no signal of amide hydrogen atoms was identified. In the ^{1}H NMR spectrum of **36** · 10 H_2O the hydrogen atoms of the methylene groups experienced a splitting and showed a doublet and a triplet, respectively. Furthermore a very broad peak derived from water protons was observed (Figure 5.1.9, Appendix). The ^{13}C NMR spectrum of **36** · 10 H_2O showed all expected peaks (Figure 5.1.10, Appendix).

Cyclic voltammetric studies on $[Co^{III}_4(L^{S2})_4](BF_4)_4$ · 10 H_2O (36 · 10 H_2O)

At a scan rate of 200 mV s^{-1} the cyclic voltammogram of the cobalt(III) [2 × 2] grid complex **36** · 10 H_2O in acetonitrile solution showed two poorly separated reduction steps at around E_{pa} = –0.50 V (Figure 2.9.4). The associated oxidation processes occurred at E_{pc} = –0.42 V and E_{pc} = –0.25 V and appeared somewhat better resolved. At lower potentials a second partially reversible reduction process was observed at E_{pa} = –1.74 V (E_{pc} = –1.65 V).

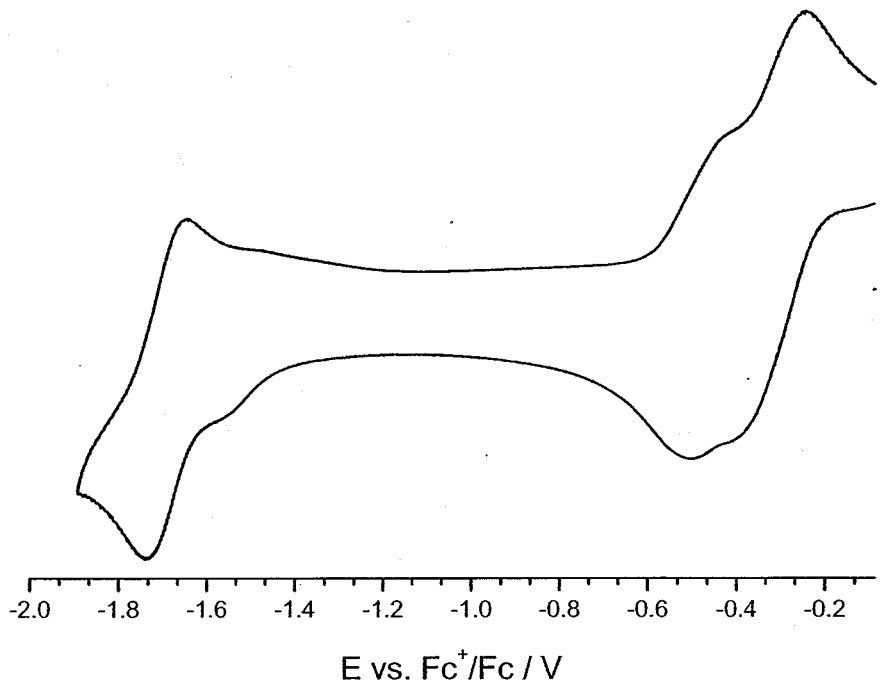

Figure 2.9.4. Cyclic voltammogram (0.5 mM, 0.1 M TBAP, MeCN, scan rate: 200 mV s^{-1}) of $[Co^{III}_4(\mathbf{L^{S2}})_4](BF_4)_4$ · 10 H_2O (**36** · 10 H_2O).

2.9.4. *Nickel(II) salts*

Complexations with H_2L^{S1} and H_2L^{S2}

The treatment of a hot (60 °C) acetonitrile solution of the lower ligand homologue H_2L^{S1} with nickel(II) tetrafluoroborate hexahydrate in a 1:1 molar ratio led to the formation of a very pale canary yellow solution. The addition of one or more equivalents of triethylamine resulted in the formation of an inhomogeneous dark brown precipitate of unknown composition, respectively.

The employment of a 2:1 molar ratio of nickel(II) tetrafluoroborate hexahydrate to H_2L^{S1} in hot (60 °C) acetonitrile or in *N,N*-dimethylformamide under otherwise identical reaction conditions did not alter the reaction outcome.

The treatment of a refluxing solution of H_2L^{S2} in acetonitrile with nickel(II) tetrafluoroborate hexahydrate, in a 1:1 or 1:2 molar ratio of ligand to nickel(II) salt, resulted in a yellow-green solution. On cooling to room temperature pure H_2L^{S2} precipitated out of the reaction mixture. The addition of base did not alter the reaction outcome.

2.9.5. *Summary*

A soluble [2 × 2] grid compound $[Co^{III}_4(L^{S2})_4](BF_4)_4 \cdot 10\ H_2O$ (**36** · 10 H_2O) of the higher ligand homologue was synthesised and structurally characterised. Thus it has been shown that racemic grid-type complexes of the S-type ligands could be formed. The employment of metal(III) rather than metal(II) ions in the [2 × 2] complex fragment was beneficial as the resulting complex fragment was not neutral and thus the compound had better solubility properties.

No discrete metal complexes containing metal ions other than copper(II) or cobalt(III) have been isolated to date.

2.10. *Dinuclear complexes as building blocks*

In Section 2.3 it has been shown that the dinuclear complex cations $[Cu^{II}_2(HL^{M1})(MeCN)_4]^{3+}$ and $[Cu^{II}_2(HL^{M2})(MeCN)_4]^{3+}$ could be used as building blocks in self-assembly processes incorporating appropriate bridging ligands. The azide ion thus proved to be an effective bridging ligand. By analogy with the reactions described in Section 2.3, similar reactions were carried out employing the analogous S-type complex cores as building blocks.

2.10.1. *Azido ligand*

Reactions with $[Cu^{II}_2(L^{S1})(H_2O)_4]^{2+}$ and $[Cu^{II}_2(L^{S2})(H_2O)_4]^{2+}$

On treating a dark green solution of the *in situ* prepared parent complex cation $[Cu^{II}_2(\mathbf{L^{S1}})(H_2O)_4]^{2+}$ with a solution of sodium azide in water, no obvious changes were observed. The resulting dark green solution was left for slow evaporation of the solvent, and by this method huge blue-green crystal blocks could be isolated. Surprisingly, the IR spectra of the compound did not show any of the characteristic absorption bands expected for the azide ion, but instead evidence of hexafluorosilicate ions was present. Elemental analysis suggested that the compound could be formulated as $[Cu^{II}_2(\mathbf{L^{S1}})](SiF_6) \cdot n\ H_2O$ ($n = 4$) (**34**).

Under otherwise identical reaction conditions the reaction of the *in situ* prepared parent complex cation $[Cu^{II}_2(L^{S2})(H_2O)_4]^{2+}$ and sodium azide resulted in a dark green solution. Dark green crystal plates were isolated after slow evaporation of some solvent. Again the IR spectrum of the compound did not show any evidence of

the presence of azide ions. Elemental analysis suggested that the compound could be formulated as $[Cu^{II}_2(\mathbf{L}^{S2})](BF_4)_2 \cdot$ solvent (**35**) (solvent = 3–4 H_2O).

In summary none of the complex cations $[Cu^{II}_2(\mathbf{L}^{S1})(H_2O)_4]^{2+}$ or $[Cu^{II}_2(\mathbf{L}^{S2})(H_2O)_4]^{2+}$ easily acted as parent cores in a self-assembly process involving azido bridging ligands. Remarkably the azide ions did not appear to influence the reaction outcome at all. Especially in regard to the similar reactions employing the analogous M-type ligands, respectively, where the complex parent cores reacted even with solid sodium azide in an inhomogeneous reaction mixture, this observation was quite unexpected.

2.11. Conclusions

The pyrazine-based homologous M-type ligands $H_2\mathbf{L}^{M1}$ and $H_2\mathbf{L}^{M2}$ have been synthesised and characterised. The structural analysis of $H_2\mathbf{L}^{M2}$ has been carried out. The coordination chemistry with first row transition metal ions of the two ligands has been investigated. A summary of syntheses leading to some of the fundamental complexes of this work is presented in Scheme 2.11.1.

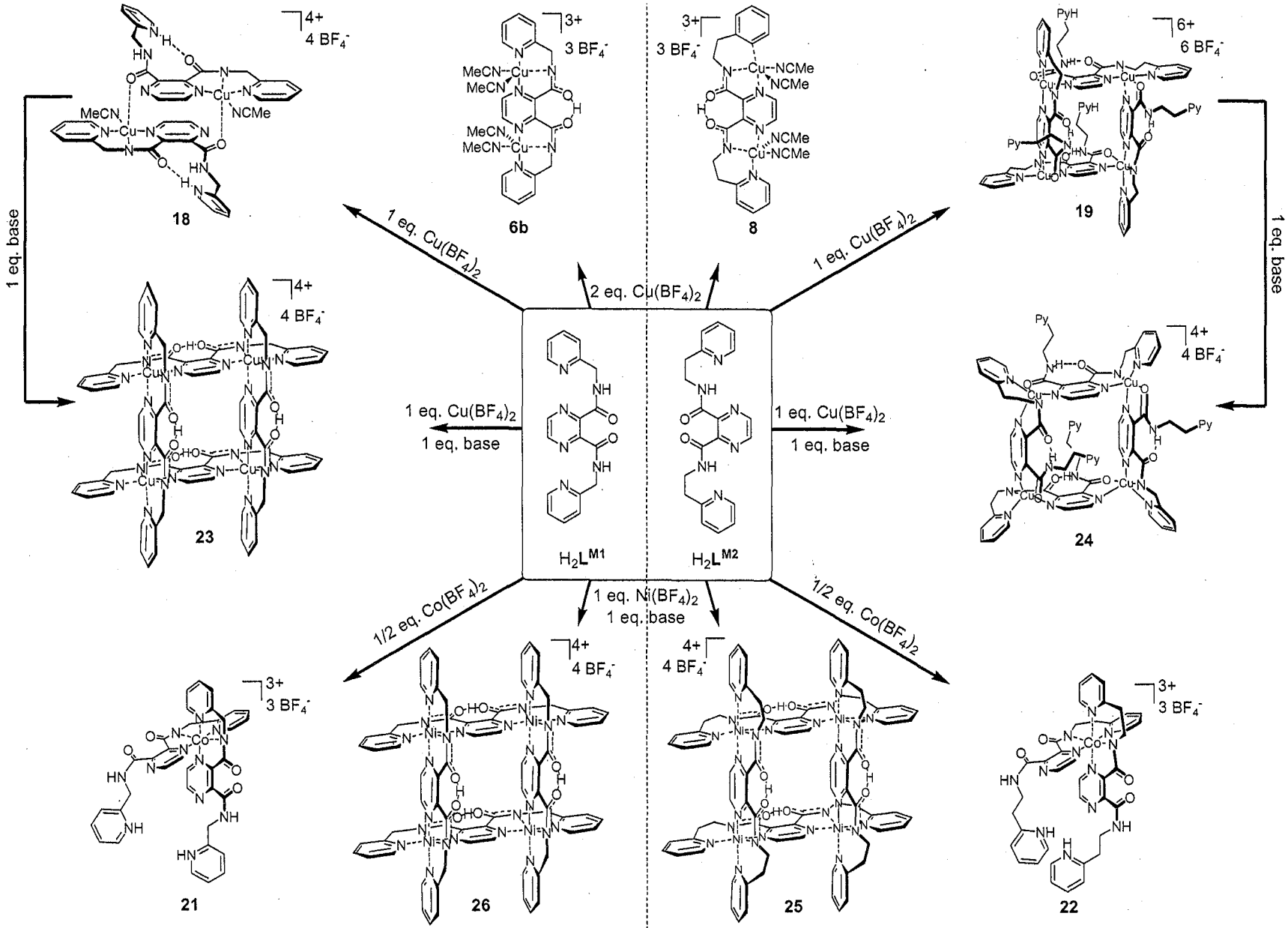

Scheme 2.11.1. Summary of complexations of $H_2\mathbf{L}^{M1}$ and $H_2\mathbf{L}^{M2}$.

Dinuclear copper(II) complexes of monodeprotonated $(HL^{M1})^-$ and $(HL^{M2})^-$ have been obtained employing a molar ratio of ligand to copper(II) salt of 1:2, respectively (*e.g.* **6b**, **8**, Scheme 2.11.1). It has been shown that the *ortho* arranged amide carbonyl functions of the M-type ligands were capable of retaining one former N-H amide proton in an O···H···O hydrogen bond. The X-ray crystal structure analysis of the dinuclear complex $[Cu^{II}_2(HL^{M1})(MeCN)_4](BF_4)_3 \cdot MeCN$ (**6b** · MeCN) of the lower ligand homologue has been carried out. Cyclic voltammetric studies on **6b** · MeCN have suggested an electronic interaction between the two copper(II) ions, showing two separate reduction processes for the reduction of $[Cu^{II}Cu^{II}] \rightarrow [Cu^{II}Cu^{I}]$ and $[Cu^{II}Cu^{I}] \rightarrow [Cu^{I}Cu^{I}]$. Similar observations have been made for the related complex $[Cu^{II}_2(HL^{M2})(H_2O)](ClO_4)_3$ (**8**) of the higher ligand homologue. Magnetic studies on the pyrazine bridged dinuclear copper(II) complex **6b** · MeCN of the lower ligand homologue have revealed a weak antiferromagnetic coupling of the copper(II) centres. Thus **6b** · MeCN was believed to be an example of a complex with pyrazine bridged metal centres showing spin coupling through a σ-type exchange pathway, as due to geometric reasons, a π-type pathway had to be ruled out.[11,33,34,133,135,207]

With a 1:1 molar ratio of H_2L^{M1} and copper(II) tetrafluoroborate tetrahydrate the dimeric complex $[Cu^{II}_2(H_2L^{M1})_2(MeCN)_2](BF_4)_4$ (**18**) of a zwitterionic form of H_2L^{M1} has been obtained (Scheme 2.11.1). An X-ray crystal structure determination has been carried out. The two copper(II) ions of **18** were not bridged by the pyrazine rings of the ligands. Only one reduction wave for copper(II) → copper(I) has been observed in the cyclic voltammogram of the compound, and no spin coupling has been observed in the magnetic measurements carried out. Under identical reaction conditions, but with the use of the higher ligand homologue H_2L^{M2}, the square-like tetranuclear complex $[Cu^{II}_4(H_2L^{M2})_2(HL^{M2})_2](BF_4)_6 \cdot 4\ H_2O$ (**19** · 4 H_2O) has been obtained (Scheme 2.11.1). An X-ray crystal structure determination has been carried out on **19** · 3 MeCN · 0.5 H_2O. The tetranuclear square-like complex **19** incorporated two neutral ligands H_2L^{M2} in a zwitterionic form and two monodeprotonated ligands

$(HL^{M2})^-$. Neighbouring copper(II) ions of the square were bridged by the pyrazine rings of the ligands. Infinite strands of tetranuclear subunits were formed at a further level of organisation, through N-H···N hydrogen bonds between the zwitterionic ligands (H_2L^{M2}) and the monodeprotonated ligands $(HL^{M2})^-$ of neighbouring subunits, respectively. The cyclic voltammogram of **19** · 4 H_2O has shown two independent reduction processes in the region E = 0.0 to –0.8 V. Weak antiferromagnetic spin coupling has been observed for **19** · 4 H_2O, with two coupling constants accounting for the two longer and the two shorter Cu^{II}··· Cu^{II} distances observed in the structure, respectively.

The tetranuclear complexes $[Cu^{II}_4(HL^{M1})_4](BF_4)_4$ (**23**) of the lower ligand homologue and $[Cu^{II}_4(HL^{M2})_4](BF_4)_4$ (**24**) of the higher ligand homologue have been obtained under identical reaction conditions to those used in the preparation of **18** and **19**, respectively, but with the addition of base. Both compounds have been characterised by X-ray crystal structure determinations. Complex **23** of the lower ligand homologue displayed the expected [2 × 2] grid-type structure and thus to the best of our knowledge was the first example of a grid structure being formed by a self-assembly following a precursor modification[67] and represented a rare example of a structurally characterised discrete grid structure with pyrazine bridged metal centres.[101] The titration of the dimeric precursor complex **18** of the lower ligand homologue with DABCO, to form the [2 × 2] grid compound **23** has been monitored by UV/VIS spectroscopy, and a partial reformation of **18** has been achieved by the back titration with *p*-TSA. The cyclic voltammogram of the pyrazine bridged [2 × 2] complex **23** has shown two separate reduction waves in the region E = 0 to –0.9 V, and weak antiferromagnetic spin coupling has been observed between the metal centres, with two coupling constants accounting for the two longer and the two shorter sets of Cu^{II}··· Cu^{II} distances observed in the structure.

Complex **24** of the higher ligand homologue was revealed to be a square-like tetranuclear complex. Even though the same donor atoms were involved for both the

square-like precursor complex **19** and the square-like complex **24**, a notably different coordination geometry was found for the copper(II) ions of **24** compared to **19**.

The [2 × 2] grid-type complexes $[Ni^{II}_4(HL^{M1})_4](BF_4)_4$ (**26**) of the lower ligand homologue and $[Ni^{II}_4(HL^{M2})_4](BF_4)_4$ (**25**) of the higher ligand homologue have been obtained by the addition of base to the reaction mixture containing ligand and nickel(II) tetrafluoroborate hexahydrate in a 1:1 molar ratio, respectively. An X-ray crystal structure determination has been carried out on **25** · 10 MeCN of the higher ligand homologue. The cyclic voltammogram of **25** has shown two clearly resolved reduction processes that have been attributed to the reduction $[Ni^{II}_4] \rightarrow [Ni^{II}_2Ni^{I}_2]$ and $[Ni^{II}_2Ni^{I}_2] \rightarrow [Ni^{I}_4]$, suggesting an electronic interaction between the nickel(II) centres. The reduction processes of the grid complex **26** of the lower ligand homologue were shown to be similar, though poorly resolved. Both pyrazine bridged [2 × 2] nickel(II) complexes **25** and **26** have shown very weak antiferromagnetic spin coupling.

The two precursor "corner complexes" $[Co^{III}(H_2L^{M1})_2](BF_4)_3$ (**21**) of the lower ligand homologue and $[Co^{III}(H_2L^{M2})_2](BF_4)_3$ (**22**) of the higher ligand homologue have been obtained by the 2:1 molar reaction of ligand to cobalt(II) tetrafluoroborate hexahydrate, respectively. An X-ray crystal structure determination has been carried out on **22** · 2 EtOH of the higher ligand homologue. Owing to the relative inertness of the cobalt(III) centres reactions of these "corner complexes" with further metal ions and additional base are expected to lead to heteronuclear grid-type structures as indicated in Scheme 2.11.2.

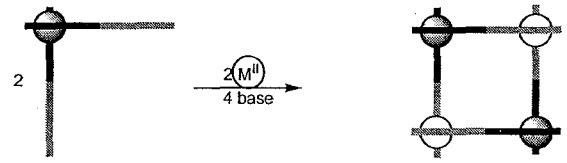

$[Co^{III}(H_2L^{M1})_2]^{3+}$ (**21**) or
$[Co^{III}(H_2L^{M2})_2]^{3+}$ (**22**)

$[Co^{III}_2M^{II}_2(HL^{M1})_4]^{6+}$ or
$[Co^{III}_2M^{II}_2(HL^{M2})_4]^{6+}$

Figure 2.11.2. Formation of a heteronuclear grid complex from the "precursor corner type" complexes **21** or **22**.

By means of the reactions with azide ions the dinuclear complex cores $[Cu^{II}_2(HL^{M1})]^{3+}$ of the lower ligand homologue and $[Cu^{II}_2(HL^{M2})]^{3+}$ of the higher ligand homologue have been shown to be suitable acceptor type building blocks for subsequent self-assembly processes involving complementary donor building blocks. An X-ray crystal structure analysis has been carried out on the dimeric tetranuclear azido compound $[Cu^{II}_4(HL^{M1})_2(\mu_{(1,1)}\text{-}N_3)_2(N_3)_2(MeCN)_2](BF_4)_2 \cdot MeCN$ (**14b** · MeCN) of the lower ligand homologue. The compound incorporated two different types of azido ligands: with a $\mu_{(1,1)}$-bridging and an end-on coordinating mode. An X-ray crystal structure analysis of $\{[Cu^{II}_2(HL^{M2})(\mu_{(1,3)}\text{-}N_3)_2](BF_4) \cdot MeCN\}_\infty$ (**16b** · MeCN) of the higher ligand homologue has revealed the infinite chain structure of the compound, built up exclusively of $\mu_{(1,3)}$-bridging azido coligands.

By analogy with the M-type ligands, the pyrazine-based homologous S-type ligands H_2L^{S1} and H_2L^{S2} have been synthesised and characterised. A summary of syntheses leading to some of the structurally characterised S-type complexes presented in this work is outlined in Scheme 2.11.3.

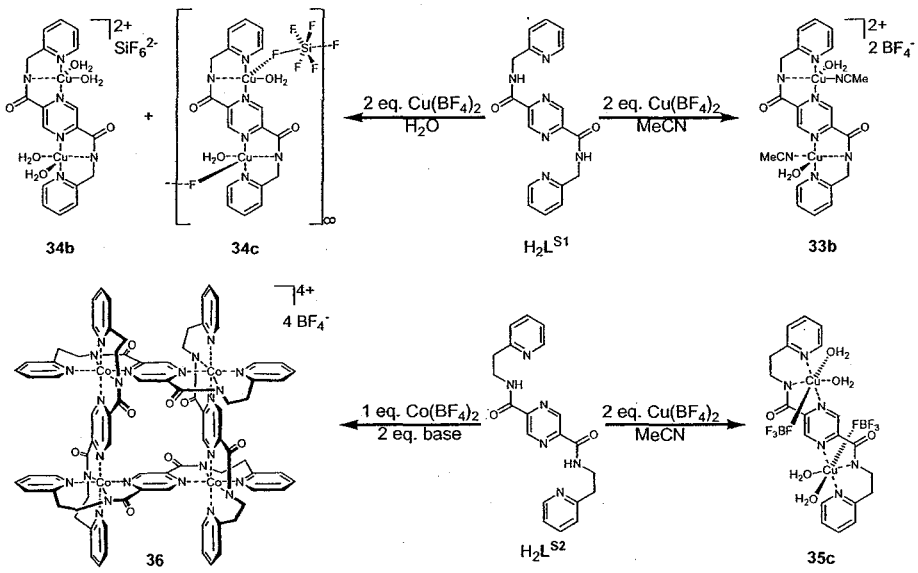

Scheme 2.11.3. Summary of syntheses of some S-type complexes.

Copper(II) complexes of both homologous S-type ligands H_2L^{S1} and H_2L^{S2} have been obtained from reactions carried out in acetonitrile or water. Dinuclear

complexes of both ligands have been obtained without the addition of base (Scheme 2.11.3). X-ray crystal structure determinations of $[Cu^{II}_2(\mathbf{L}^{S1})(H_2O)_2(MeCN)_2](BF_4)_2 \cdot H_2O$ (**33b** · H_2O), $[Cu^{II}_2(\mathbf{L}^{S1})(H_2O)_4](SiF_6) \cdot 0.5\ H_2O$ (**34b** · 0.5 H_2O) and $\{[Cu^{II}_2(\mathbf{L}^{S1})(H_2O)_2(SiF_6)] \cdot 4\ H_2O\}_\infty$ (**34c** · 4 H_2O) of the lower ligand homologue and of $[Cu^{II}_2(\mathbf{L}^{S2})(H_2O)_2(MeCN)_2](BF_4)_2$ (**35b**) and $[Cu^{II}_2(\mathbf{L}^{S2})(H_2O)_4(BF_4)_2] \cdot 2\ H_2O$ (**35c** · 2 H_2O) of the higher ligand homologue have been carried out.

Magnetic studies have been carried out for $[Cu^{II}_2(\mathbf{L}^{S1})(H_2O)_2(MeCN)_2](BF_4)_2 \cdot H_2O$ (**33b** · H_2O) of the lower ligand homologue and have revealed an antiferromagnetic spin coupling around 20 times weaker than that observed for the analogous M-type complex $[Cu^{II}_2(HL^{M1})(MeCN)_4](BF_4)_3$ (**6b**).

Two types of single crystals were obtained from the reaction of the lower ligand homologue $H_2\mathbf{L}^{S1}$ with copper(II) tetrafluoroborate tetrahydrate in water (Scheme 2.11.3). Both structures incorporated hexafluorosilicate ions that had arisen through partial hydrolysis of the tetrafluoroborate anions and the formation of hydrofluoric acid, which reacted with the glassware. In $[Cu^{II}_2(\mathbf{L}^{S1})(H_2O)_4](SiF_6) \cdot 0.5\ H_2O$ (**34b** · 0.5 H_2O) the hexafluorosilicate ions were not metal coordinated but were involved in hydrogen bonds to the water coligands of the complex. In $\{[Cu^{II}_2(\mathbf{L}^{S1})(H_2O)_2(SiF_6)] \cdot 4\ H_2O\}_\infty$ (**34c** · 4 H_2O) a bridging coordination of the hexafluorosilicato ions has been found, which led to an infinite polymeric chain structure of the compound. To the best of our knowledge **34c** · 4 H_2O displayed the first polynuclear chain compound where hexafluorosilicato ligands bridge the apical positions of five coordinated copper(II) ions, and at the same time was the first polymeric compound with hexafluorosilicato bridged discrete dinuclear subunits.

The dinuclear complex $[Cu^{II}_2(\mathbf{L}^{S2})(H_2O)_4(BF_4)_2] \cdot 2\ H_2O$ (**35c** · 2 H_2O) of the higher ligand homologue has been the first structurally characterised dinuclear complex of either M- or S-type ligand, with distorted octahedral copper(II) environment. It exhibited tetrafluoroborate coordination.

In all of the structurally characterised dinuclear compounds of either homologue S-type ligand, **33b** · H_2O, **34b** · 0.5 H_2O, **34c** · 4 H_2O, **35b** and **35c** · 2 H_2O,

the water coligands and the amide carbonyl oxygen atoms were involved in a 3D network based on hydrogen bonds.

The racemic [2 × 2] grid-type complex $[Co^{III}_4(L^{S2})_4](BF_4)_4$ (**36**) of the higher S-type ligand homologue has been obtained by the reaction of H_2L^{S2} with cobalt(II) tetrafluoroborate hexahydrate and base in a 1:1:2 molar ratio (Scheme 2.11.3). In the course of the reaction the initially employed cobalt(II) ions have been oxidised so that the resulting grid compound **36** incorporated cobalt(III) ions.

2.12. Outlook

2.12.1. Multi-grid networks

The formation of the tetranuclear copper(II) compounds **19** and **24** of the higher ligand homologue and the copper(II) [2 × 2] grid compound **23** of the lower ligand homologue, as well as the two nickel(II) [2 × 2] grid compounds **25** and **26** may be construed as the first dimension of a self-assembly process. In a second and/or third dimension of self-assembly the initially assembled coordination architectures could organise into higher-assembled arrangements of multi-grid networks. The possibility of a second and/or third dimension of self-assembly is potentially given if the ligands[91] or the coordinated metal ions exhibit further binding or coordination sites, respectively. In the case of the five coordinate copper(II) square **24** of the higher ligand homologue for example, the employment of linear bridging ligands, which can coordinate to the sixth coordination sites, respectively, could potentially lead to

multi-grid networks as shown in Figure 2.11.1. It is therefore of interest to isolate grid complexes with five- rather then six coordinate metal(II) ions.

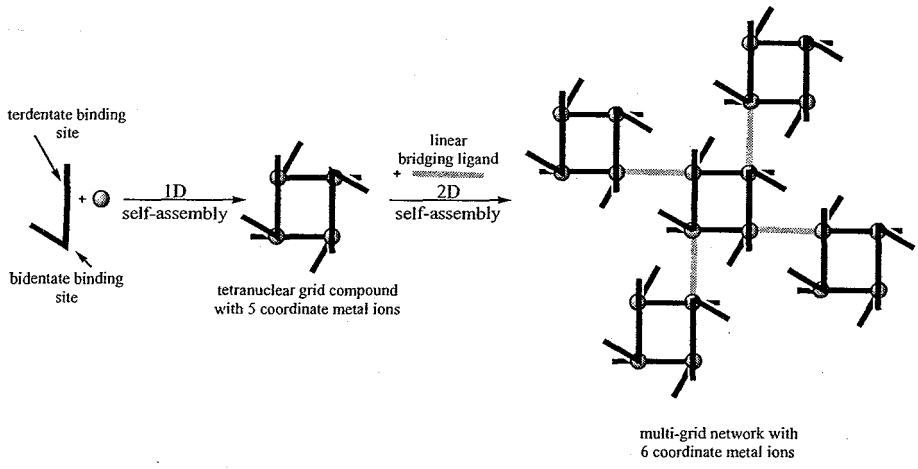

Figure 2.11.1. Formation of a multi-grid network in a 2D self-assembly process *via* bridging of initially formed discrete tetranuclear grid complexes that have free coordination sites on the metal ions.

For the controlled synthesis of grid-type complexes with potentially free coordination sites theoretically two different synthetic approaches are accessible: the employment of asymmetrical hybrid bidentate-terdentate ligands or the combination of bis-terdentate with bis-bidentate ligands. In Scheme 2.11.4 a survey of potential hybrid bidentate-terdentate and bis-bidentate ligands based on 2,3-substituted pyrazine derivatives is shown, including a proposed synthetic route starting from quinoxaline (**1**), respectively.

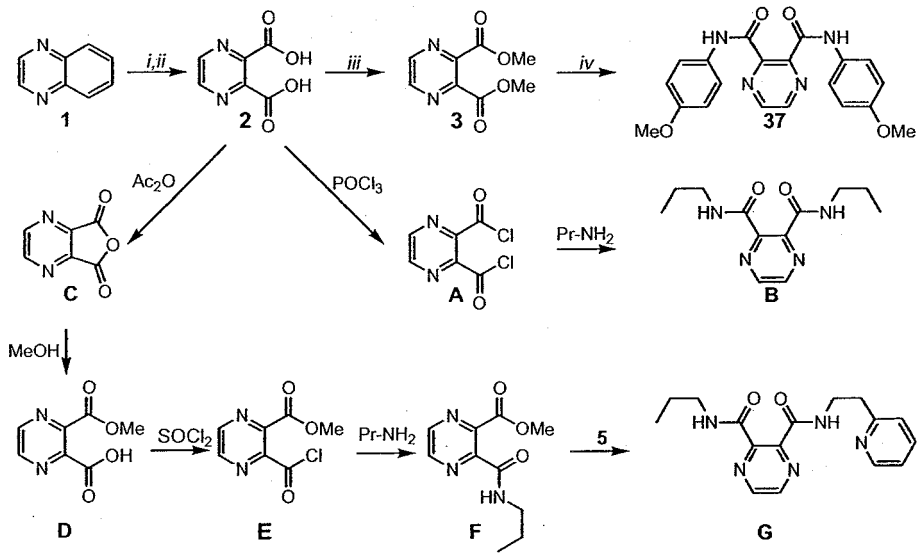

Scheme 2.11.4. Survey of ligand syntheses potentially leading to bis-bidentate ligands (**37** and **B**) or to a hybrid bidentate–terdentate ligand (**G**). Literature known intermediates: **A**,[109] **C**,[208-210] **D**,[209] **E**.[209] Synthesis of **37**. Reagents and conditions: (*i*) $KMnO_4$, H_2O, 80–90 °C; (*ii*) conc. HCl, H_2O, RT; (*iii*) $SOCl_2$, MeOH, reflux; (*iv*) 4-methoxyaniline, MeOH, reflux, 2 d.

Synthesis of *N,N'*-(4-methoxyphenyl)pyrazine-2,3-dicarboxamide (37)

In a first introductory step the symmetrical bis-bidentate diamide ligand *N,N'*-(4-methoxyphenyl)pyrazine-2,3-dicarboxamide (**37**) was synthesised and characterised. As for H_2L^{M1} and H_2L^{M2}, the reaction of **37** started with the common ligand precursor **3**. The bis-bidentate ligand thus was formed by reacting the diester **3** with 4-methoxyaniline in a 1:2 molar ratio in a small volume of methanol. Analytically pure slightly purple crystalline **37** was obtained by recrystallisation of the initially obtained brown solid from dichloromethane/methanol in around 35 % yield (Scheme 2.11.4).

Bis-bidentate ligand B

In theory the common ligand precursor **3** can be reacted with any amine, leading to the corresponding amide compound. With the synthesis of the amide ligands H_2L^{M1} and H_2L^{M2} it has been found however, that the syntheses were most successful if the compounds were reacted in an open flask, allowing the methanol formed in the reaction to evaporate. Following this procedure, syntheses are limited to amines with a suitably high vapour pressure, commonly amines with an aromatic moiety, to prevent the evaporation in the course of the reaction. For the synthesis of bis-bidentate ligands like **B**, employing aliphatic amines, a more reactive precursor molecule may be necessary, so that subsequent reactions can be carried out effectively under normal reflux conditions. Such a more reactive ligand precursor is believed to be the acid chloride derivative **A** (Scheme 2.11.4).[109] It is believed that **A** is accessible reacting the free acid **2** with thionyl chloride,[109,211] phosphorus pentachloride[193] or phosphorus oxychloride[210] in the absence of methanol. Bis-bidentate ligands like **B** will then be formed on reacting the acid chloride **A** with the respective amine like for example propylamine in excess (Scheme 2.11.4).

Hybrid bidentate-terdentate ligand G

For the synthesis of asymmetric diamide ligands like **G** an asymmetric precursor molecule, ideally with a more reactive and a more selective carbonyl function, is necessary. For example the acid chloride-monomethyl ester derivative **E**[209] is believed to be an effective precursor for asymmetrical diamide ligands like **G**. The reaction of **E** with aliphatic amines like propylamine is believed to lead under mild conditions in a first step to the formation of the amide-monomethyl ester derivative **F**. The more selective carbonyl function of **F** will then react with appropriate amines like **5** probably only under more harsh conditions, to finally result in an asymmetrical hybrid bidentate-terdentate diamide ligand (**G**).

For the preparation of the asymmetrical acid chloride-monomethyl ester derivative **E**, the anhydride derivative **C**[208-210] is believed to be an effective precursor. It has been reported that the acid anhydride **C** can easily be synthesised by refluxing **2** in acetic anhydride.[208,209] The subsequent reaction of **C** with methanol, as reported in the literature, would conveniently result in the formation of the monomethyl ester **D**.[209] And on reacting **D** with thionyl chloride hopefully the desired acid chloride-monomethyl ester **E** would be formed, according to the literature.[209]

2.12.2. *Ligand formation and metal complexation in one pot*

A new strategy for the formation of grid-type complexes is the ligand formation and metal complexation in one-pot. In this strategy ligand precursor molecules (*e.g.* **Precursor 1** and **Precursor 2** in Figure 2.11.2) will, in diverse equilibria, react with each other and with the metal ions present in the reaction mixture (**M** in Figure 2.11.2), which ideally will lead to a thermodynamically stable product that can be isolated (Figure 2.11.2).

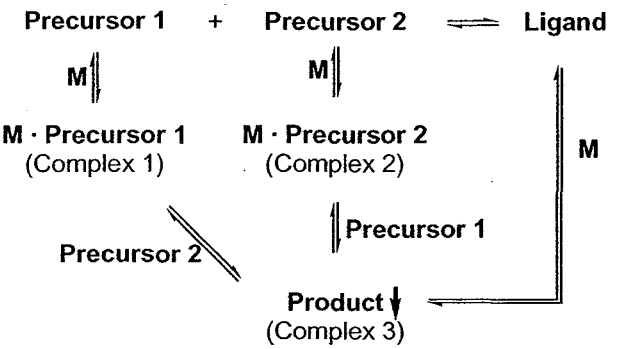

Figure 2.11.2. One-pot formation of a thermodynamically stable product, from two ligand precursor molecules and metal ions.

Suitable ligand precursor molecules for such reversible reactions may for example be carbaldehydes and amines, respectively. In a reversible reaction

carbaldehydes react with amines to form Schiff-base ligands and water, as it is shown on two examples in Figure 2.11.3.

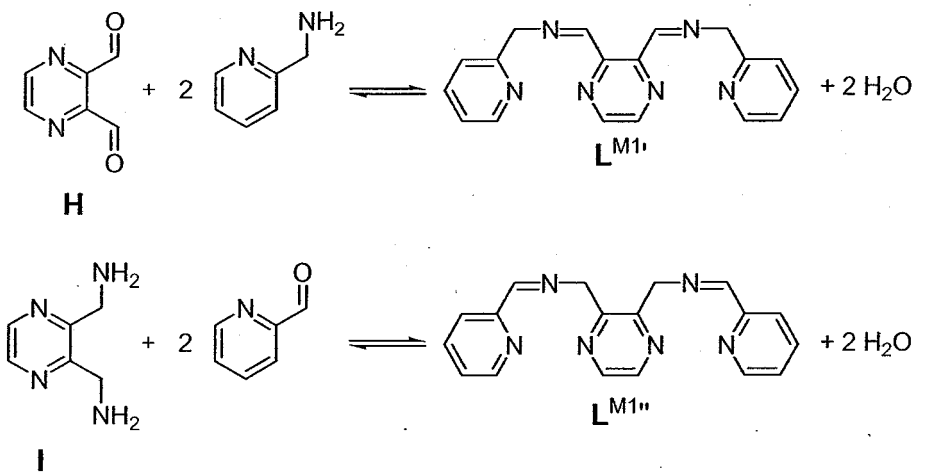

Figure 2.11.3. Formation of the two Schiff-base ligands $\mathbf{L^{M1\prime}}$ and $\mathbf{L^{M1\prime\prime}}$.

By analogy with the symmetrical bis-terdentate diamide ligands H_2L^{M1}, H_2L^{M2}, H_2L^{S1} and H_2L^{S2} which have been shown to form [2 × 2] grid-type complexes, similar Schiff-base ligands like $L^{M1\prime}$ or $L^{M1\prime\prime}$, as shown in Figure 2.11.3 are desirable target molecules. Equally desirable are their higher ligand homologues, as well as their S-type ligand analogues. As common ligand precursor molecules pyrazine-2,3-dicarbaldehyde, the respective 2,5-substituted derivative, or the respective amine derivatives are eligible.

2,3-disubstituted pyrazine derivatives

In Scheme 2.11.5 is shown a survey of synthetic routes potentially leading to pyrazine-2,3-dicarbaldehyde (**H**) or 2,3-bis(aminomethyl)pyrazine (**J**).

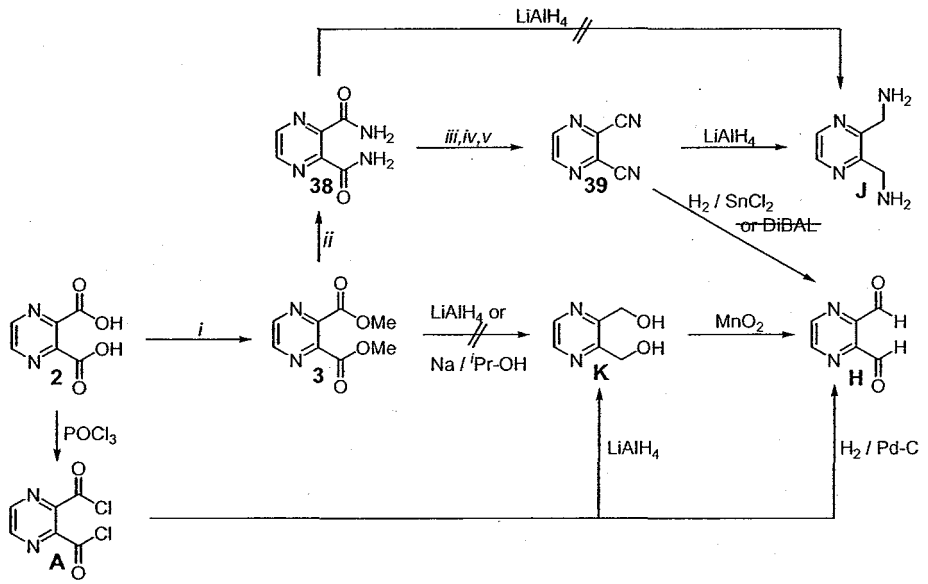

Scheme 2.11.5. Survey of syntheses potentially leading to pyrazine-2,3-dicarbaldehyde (**H**) or 2,3-bis(aminomethyl)pyrazine (**J**). Literature known compounds, being mentioned for the first time in this thesis: **38**,[113,208,210] **39**.[210] Synthesis of **39**. Reagents and conditions: (*i*) $SOCl_2$, MeOH, reflux; (*ii*) NH_3 (aq); (*iii*) $POCl_3$, reflux; (*iv*) Na_2CO_3 (aq), 0 °C; (*v*) Et_2O (extraction).

An easy synthetic route for the preparation of pyrazine-2,3-dicarbaldehyde (**H**) was believed to be the reduction of the diester **3** with lithium aluminium hydride to form the dialcohol **K**, followed by mild oxidation of **K** with manganese dioxide, as this is a commonly used approach to obtain dialdehydes.[212] Surprisingly first attempts at reducing **3** with lithium aluminium hydride resulted merely in the recovery of starting material. Also no dialcohol was obtained with the Bouvleault-Blanc reduction[213] of **3** with elemental sodium.

As an alternative route the reduction of the acid chloride derivative **A** with lithium aluminium hydride is suggested.[214] Also for example the Rosenmund reduction,[215,216] *i.e.* the hydrogenation of the acid chloride **A** is a potential route for directly obtaining the dicarbaldehyde **H**.

Synthesis of pyrazine-2,3-dicarboxamide (38)

Following the route outlined in Scheme 2.11.5, and a modification of a literature procedure,[113,192] in a first step the reaction of **3** with aqueous ammonia was carried out. By digesting **3** for 15 minutes in aqueous ammonia and subsequent filtration of the resulting milky mixture pyrazine-2,3-dicarboxamide (**38**) was isolated in excellent yields of 85–90 % in the form of a colourless amorphous solid. Unfortunately the solid proved to be very insoluble in solvents suitable for reductions with lithium aluminium hydride, so that first attempts at reducing **38** to **J** were not successful.

Synthesis of pyrazine-2,3-dicarbonitrile (39)

As an alternative route for the preparation of the diamine **J** the reduction of the dinitrile **39** was attempted. In a first attempt the dehydration of the diamide **38** to the dinitrile **39** was carried out with phosphorus oxychloride, following a modified literature procedure.[210] Crude dinitrile **39** was obtained in around 60 % yield as a pale brown solid. Reduction of **39** with lithium aluminium hydride has not yet been tried, but is believed to lead to the desired diamine **J**.[214]

First attempts to reduce the dinitrile **39** to the desired dicarbaldehyde **H** with diisobutyl aluminium hydride (DIBAL) unfortunately did not result in any isolable product.[217] An alternative route to reduce nitriles to carbaldehydes is believed to be the Stevens reduction with hydrogen chloride and tin(II) chloride.[216]

2,5-disubstituted pyrazine derivatives

The reactions pointed out in Scheme 2.11.5 are also applicable for the analogous 2,5-disubstituted pyrazine derivatives. Some initial reactions carried out are

summarised in Scheme 2.11.6, including a new strategy for the synthesis of bis(hydroxymethyl)pyrazines.

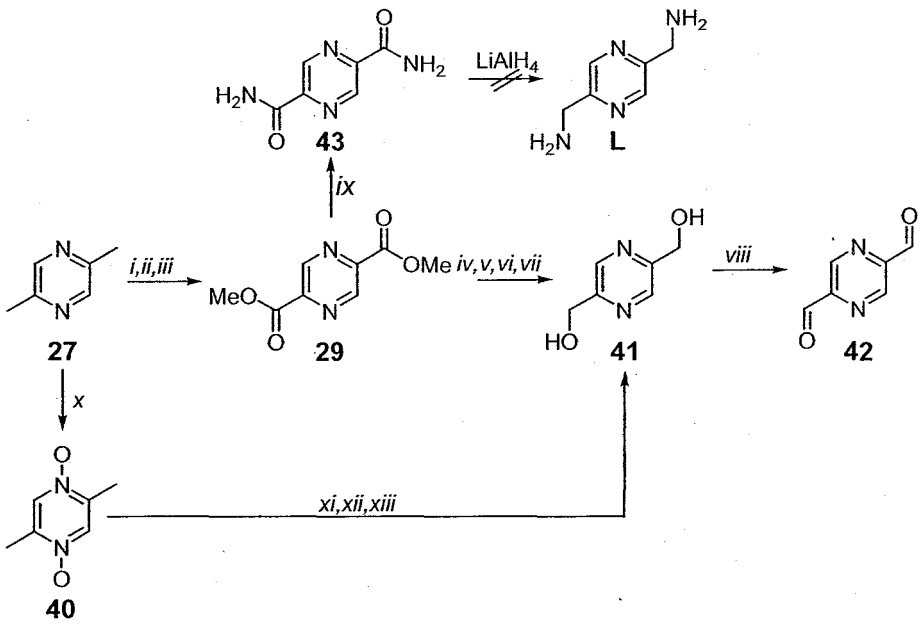

Scheme 2.11.6. Survey of syntheses potentially leading to pyrazine-2,5-dicarbaldehyde (**42**) or 2,5-bis(aminomethyl)pyrazine (**L**). Literature known compounds, being mentioned for the first time in this thesis: **40**,[218-220] **41**,[221,222] **42**,[223] **43**.[192,193] Synthesis of **40**–**43**. Reagents and conditions: (*i*) SeO_2, py/H_2O (10:1), reflux; (*ii*) H_2O, filtration; (*iii*) $SOCl_2$, MeOH, reflux; (*iv*) $NaBH_4$, EtOH, RT, 2 d; (*v*) HCl (conc); (*vi*) NH_3 (aq), filtration; (*vii*) column chromatography (CH_2Cl_2/10 % MeOH); (*viii*) MnO_2, $CHCl_3$, reflux; (*ix*) NH_3 (aq); (*x*) AcOH, H_2O_2 (30 % aq), 95 °C, 3 d; (*xi*) $CHCl_3$, $(F_3CCO)_2O$, 4-(dimethylamino)pyridine; (*xii*) Na_2CO_3 (aq); (*xiii*) continuous extraction (CH_2Cl_2), 28 d.

Synthesis of 2,5-dimethylpyrazine-1,4-dioxide (40), 2,5-bis(hydroxymethyl)pyrazine (41) and pyrazine-2,5-dicarbaldehyde (42)

As a promising and simple way of obtaining the desired 2,5-bis(hydroxymethyl)pyrazine (**41**) a slight modification[224] of the Boekelheide reaction[220,225,226] was followed. The Boekelheide reaction is a procedure for the introduction of oxygen on an alkyl group α to a ring nitrogen atom. The key step of the Boekelheide reaction is the conversion of heterocyclic α-alkyl N-oxides to the corresponding α-hydroxyalkyl

heterocyclic amine *via* a radical mechanism with acylating agents followed by basic workup (Scheme 2.11.7).

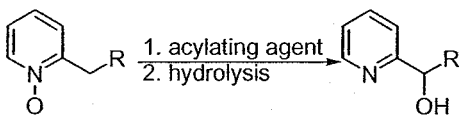

Scheme 2.11.7. Rearrangement of the Boekelheide reaction.

Following this strategy, and a modified literature procedure,[218,219] the synthesis of **41** started with the oxidation of commercially available 2,5-dimethylpyrazine (**27**) with aqueous hydrogen peroxide in acetic acid (Scheme 2.11.6). Following this procedure 2,5-dimethylpyrazine-1,4-dioxide (**40**) could be isolated after 3 days in 90 % yield in the form of a colourless solid (Scheme 2.11.6). The conversion of the dioxide **40** to the desired 2,5-bis(hydroxymethyl)pyrazine (**41**) was carried out with trifluoroacetic anhydride as acylating agent and 4-(dimethylamino)pyridine as catalyst, followed by aqueous basic workup (Scheme 2.11.6).[224] Unfortunately the isolation of the dialcohol **41** from the resulting aqueous solution was tedious and extremely time consuming. The pure dialcohol **41** was obtained in around 25 % yield by continuous extraction with dichloromethane over two weeks.

As an alternative route to obtain the desired dialcohol **41** the reduction of the dimethyl ester **29** with sodium borohydride in ethanol was carried out modifying a procedure of Staab and Appel,[221] with a notedly different workup (Scheme 2.11.6). The dialcohol **41** was conveniently obtained in around 25 % yield as an analytically pure slightly yellow solid after only two days.

In a first attempt the oxidation of a small amount of dialcohol **41** to the desired dialdehyde **42** was carried out with manganese dioxide in chloroform and gave crude dialdehyde **42** in around 60 % yield (Scheme 2.11.6). These results were promising, however, the reaction procedure has not been optimised yet.

Synthesis of pyrazine-2,5-dicarboxamide (43)

By analogy with the similar reaction of the 2,3-disubstituted carboxamide **38**, dimethyl 2,5-pyrazinedicarboxylate (**29**) was digested for 15 minutes in aqueous ammonia, following a modified literature procedure.[192,193] By filtration of the resulting colourless solid pyrazine-2,5-dicarboxamide (**43**) was obtained in around 90 % yield.

Unfortunately, similarly to the attempted reduction of **38**, first attempts of reducing **43** to **L** with lithium aluminium hydride were not successful, probably due to the very poor solubility of **43** in solvents suitable for the reduction.

3. Experimental

3.1. *General*

All commercially available chemicals were purchased from Aldrich, Fluka, Merck, Ajax, Scharlau or BDH and used as received. Unless stated otherwise all solvents used were LR grade. Dry solvents required for some reactions were obtained by treatment of the respective HPLC grade solvents as follows: tetrahydrofuran was distilled from sodium; diethyl ether was distilled from sodium, chloroform was washed with water, dried over phosphorus pentoxide and distilled over potassium carbonate; *N*,*N*-dimethylformamide was distilled from calcium hydride; acetonitrile was distilled from calcium hydride.

Elemental analyses (C, H, N, Br, S) were performed by the Campbell Microanalytical Laboratory at the University of Otago.

Melting points were determined on a Gallenkamp melting point apparatus in open glass capillaries and are uncorrected.

Column chromatography was carried out under gravity on Merck silica gel 60, 200–400 mesh, 40-63 μm. For TLC analysis Macherey-Nagel Alugram SIL G/UV_{254} aluminium sheets were used. Visualisation was achieved with UV light (254 nm).

^{1}H and ^{13}C NMR spectra were recorded by the author on a Varian INOVA-300 or by Dr. Mervyn Thomas, Mr. Wayne A. Redmond or Mr. Ian Stewart on a Varian INOVA-500 spectrometer at 25 °C. For measurements in deuterated organic solvents chemical shifts are given relative to tetramethylsilane (TMS) using the residual

solvent signals as secondary reference (chloroform: δ_H = 7.26 ppm, δ_C = 77.16 ppm; acetonitrile: δ_H = 1.94 ppm, δ_C = 118.26 ppm; *N*,*N*-dimethylformamide: δ_H = 8.02 ppm, δ_C = 163.15 ppm).[227] Peak assignments were made on the basis of chemical shifts, integration patterns and coupling constants. Where necessary, two-dimensional correlation experiments where carried out.

IR spectra were recorded on a Perkin-Elmer Spectrum BX FT-IR spectrophotometer in the range of 4000–400 cm^{-1}. All solid samples were measured as potassium bromide pellets, if not stated otherwise.

UV/VIS/NIR spectra were recorded on a Varian CARY 500 Scan UV/VIS/NIR spectrophotometer in the range of 200–1400 nm. HPLC grade solvents were used for the measurements.

Molar conductivities were measured with a Suntex SC-170 conductivity meter with 1 mM solutions of the compounds. HPLC grade solvents were used for the measurements.

Cyclic voltammetric studies were carried out in 0.1 M of Bu_4NPF_6 and 0.1 mM of compound in acetonitrile, if not stated otherwise. A classical three-electrode cell was used, connected to a computerised electrochemical device EG & G Princeton Applied Research, Potentiostat / Galvanostat Model 273 A. The reference electrode was an Ag/AgCl electrode. The cyclic voltammograms were recorded at a scan rate of 50 mV s^{-1}, if not stated otherwise. Ferrocene was used as an internal standard. HPLC grade solvents were used for the measurements.

ESI mass spectra were recorded by Mr. Bruce M. Clark at the University of Canterbury on a MicroMass LCT spectrometer, or by Dr. N. Davies at the University of Tasmania. For all compounds acetonitrile was used as the solvent.

X-Ray data were collected by Assoc. Prof. Peter D. W. Boyd, Prof. George R. Clark or Assoc. Prof. Clifford E. F. Rickard at the University of Auckland, by Prof. Ward T. Robinson or Dr. Jan Wikaira at the University of Canterbury or by Dr. Christopher E. Anson at the University of Karlsruhe. The Bruker SMART diffractometers at Auckland and Canterbury as well as the STOE IPDS diffractometer

at Karlsruhe were equipped with CCD area detectors. The structures, except for **22** · 2 EtOH, were solved by direct methods using SHELXS-97,[228,229] and refined against F^2 using full-matrix least-squares techniques with SHELXL-97.[230] Structure **22** · 2 EtOH was solved using the Patterson option in SHELXS-97. Refinements of the structures of **23** · 3.5 MeCN, **24** and **25** · 10 MeCN were carried out by Prof. Geoffrey B. Jameson at the Institute of Fundamental Sciences, Massey University in Palmerston North, New Zealand. Refinement of all other structures was carried out by the author, assistance was provided by Assoc. Prof. Sally Brooker.

Magnetic measurements and data analyses were carried out by Prof. Keith S. Murray and Dr. Boujemaa Moubaraki at Monash University, Australia. Magnetic data were recorded in the range of 320–4.2 K using a Quantum Design MPMS5 SQUID magnetometer with an applied field of 1 T.

3.2. Organic syntheses

3.2.1. Pyrazine-2,3-dicarboxylic acid (2)[112,113]

To a suspension of quinoxaline (**1**) (12.0 g, 92.2 mmol) in hot (70–80 °C) water (600 ml) was slowly added, over approximately 3 hours, solid potassium permanganate (79.0 g, 0.50 mol). The resulting mixture was maintained at 80 °C for 1 hour then ethanol (20 ml) was added to destroy the excess potassium permanganate. The resulting dark brown suspension was filtered and the remaining manganese dioxide cake was stirred vigorously with water (4 × 100 ml) and was then filtered off. The combined aqueous solutions were reduced in volume (to 300 ml)

under reduced pressure and then concentrated hydrochloric acid (45 ml) was slowly added. The resulting suspension was evaporated to dryness under reduced pressure and the colourless solid residue obtained was mixed with water/acetone (170 ml, 1:9), refluxed for 15 minutes and the mixture filtered whilst hot. The remaining solid was refluxed for a further 15 minutes with more water/acetone (2 × 80 ml, 1:9) and was filtered off. The combined filtrates were evaporated to dryness under reduced pressure. The resulting brown solid was dissolved in acetone (200 ml), treated with decolourising charcoal (800 mg) and the mixture was refluxed for 15 minutes. Filtration of the hot mixture and removal of the solvent under reduced pressure gave 12.1 g (72.0 mmol, 78 %) of crude pyrazine-2,3-dicarboxylic acid (**2**) in the form of a brown solid. An analytically pure sample was obtained by recrystallisation from water.

Mp.: 167–170 °C — elemental analysis (%) found: C 42.56, H 2.41, N 16.96; calcd. for $C_6H_4N_2O_4$ (168.11 g mol^{-1}): C 42.87, H 2.40, N 16.66 — ^1H NMR (300 MHz, d^6-DMSO): δ (ppm) = 8.84 (s, 2 H, pz*H*), 2.07 (s, 2 H, CO_2H) — $^{13}C\{^1H\}$ NMR (75 MHz, d^6-DMSO): δ (ppm) = 166.0 (CO_2H), 145.5, 145.4 — IR (KBr, disk): $\tilde{\upsilon}$ (cm^{-1}) = 3263, 2849, 2612, 2511, 1753, 1716, 1687, 1576, 1540, 1444, 1397, 1357, 1264, 1225, 1209, 1182, 1098, 996, 936, 868, 834, 792, 766, 737, 724, 693, 678, 642, 584, 532, 428.

3.2.2. *Dimethyl pyrazine-2,3-dicarboxylate (3)*[112,113,218]

To a solution of quinoxaline (**1**) (24.0 g, 184 mmol) in hot (70–80 °C) water (2 l) was slowly added, over approximately 3 hours, solid potassium permanganate (174 g, 1.10 mol). The resulting mixture was maintained at that temperature for 1 hour, was then allowed to cool to room temperature and was stirred for another 8 hours. Then ethanol (40 ml) was added to destroy excess potassium permanganate

and the resulting mixture was filtered. The remaining manganese dioxide cake was stirred vigorously with water (5 × 400 ml) and was filtered off again. The combined aqueous solutions were reduced in volume (to 300 ml) under reduced pressure, then concentrated hydrochloric acid (90 ml) was added and the resulting pale yellow suspension was stirred at room temperature for 1 hour. Removal of the solvent under reduced pressure gave a pale yellow solid, which was taken up in methanol (250 ml) and treated with thionyl chloride (10 ml). The resulting suspension was refluxed for 5 hours, was allowed to cool to room temperature and was then filtered. The remaining colourless solid was washed with methanol (3 × 50 ml) and the combined filtrates were evaporated to dryness under reduced pressure. The resulting orange solid was taken up in diethyl ether (100 ml) and the suspension was filtered. The remaining solid was stirred vigorously with diethyl ether (5 × 100 ml) and was then filtered off. The filtrates were combined. Removal of the solvent under reduced pressure gave 32.8 g (167 mmol, 91 %) of dimethyl pyrazine-2,3-dicarboxylate (**3**) in the form of an analytically pure colourless crystalline material.

Mp.: 52–55 °C — elemental analysis (%) found: C 48.73, H 3.99, N 14.28; calcd. for $C_8H_8N_2O_4$ (196.16 g mol^{-1}): C 48.98, H 4.11, N 14.28 — TLC (SiO_2, DCM/10 % MeOH): R_f = 0.80 — ^1H NMR (300 MHz, $CDCl_3$): δ (ppm) = 8.54 (s, 2 H, pz*H*), 3.70 (s, 6 H, C*H*$_3$) — $^{13}C\{^1H\}$ NMR (75 MHz, $CDCl_3$): δ (ppm) = 164.0 (CO_2), 145.3 (*pz*CO_2), 144.0 (*pz*H), 52.8 (CH_3) — IR (KBr, disk): $\tilde{\upsilon}$ (cm^{-1}) = 3550, 3465, 3414, 3004, 2957, 1742, 1730, 1637, 1617, 1564, 1531, 1451, 1433, 1405, 1315, 1301, 1216, 1149, 1087, 951, 886, 820, 763, 730, 637, 580, 435.

3.2.3. *N,N′-Bis(2-pyridylmethyl)pyrazine-2,3-dicarboxamide (H_2L^{M1})*

A solution of dimethyl pyrazine-2,3-dicarboxylate (**3**) (784 mg, 4.00 mmol) and 2-(aminomethyl)pyridine (**4**) (865 mg, 8.00 mmol) in methanol (10 ml) was maintained at 80–90 °C for 5 hours in an open flask, allowing the methanol formed in the reaction to distil off and was then allowed to cool to room temperature. The resulting golden caramel like solid was dissolved in dichloromethane (20 ml) and the remaining brown solid was filtered off. Removal of the solvent under reduced pressure gave 1.34 g (3.84 mmol, 96 %) of the crude product H_2L^{M1} in the form of a slightly yellow foamy solid. An analytically pure sample of H_2L^{M1} was obtained by redissolving the crude product in benzene/dichloromethane (5:1) and by slow evaporation of the solvent on air.

Mp.: 106–109 °C — elemental analysis (%) found: C 62.33, H 4.73, N 24.43; calcd. for $C_{18}H_{16}N_6O_2$ (348.36 g mol^{-1}): C 62.06, H 4.63, N 24.12 — TLC (SiO_2, DCM/10 % MeOH): R_f = 0.40 — ^{1}H NMR (500 MHz, $CDCl_3$): δ (ppm) = 8.58 (s, 2 H, 2 × pz*H*), 8.46 (ddd, $^3J_{6,5}$ = 4.8 Hz, $^4J_{6,4}$ = 1.8 Hz, $^5J_{6,3}$ = 0.9 Hz, 2 H, 2 × 6-py*H*), 8.23 (t, J = 5.0 Hz, 2 H, 2 × N*H*), 7.60 (dt, $^3J_{4,5}$ = $^3J_{4,3}$ = 7.7 Hz, $^4J_{4,6}$ = 1.8 Hz, 2 H, 2 × 4-py*H*), 7.35 (d, J = 7.9 Hz, 2 H, 2 × 3-py*H*), 7.13 (ddd, $^3J_{5,4}$ = 7.7 Hz, $^3J_{5,6}$ = 4.8 Hz, $^4J_{5,3}$ = 0.7 Hz, 2 H, 2 × 5-py*H*), 4.76 (d, J = 5.4 Hz, 4 H, 2 × pyCH_2) — $^{13}C\{^1H\}$ NMR (125 MHz, $CDCl_3$): δ (ppm) = 164.5 (CO), 156.1 (2-*py*), 148.9 (6-*py*), 146.7 (*pz*CO), 144.2 (*pz*H), 136.8 (4-*py*), 122.3 (5-*py*), 122.0 (3-*py*), 44.6 (CH_2) — IR (KBr, disk): $\tilde{\nu}$ (cm^{-1}) = 3338, 3293, 3048, 2938, 1690, 1655, 1589, 1568, 1533, 1514, 1479, 1434, 1311, 1291, 1250, 1234, 1208, 1185, 1171, 1133, 1098, 1071, 1048, 995, 914, 874, 829, 752, 727, 658, 640, 607, 571, 538, 491, 444.

3.2.4. *N,N'-Bis[2-(2-pyridyl)ethyl]pyrazine-2,3-dicarboxamide (H_2L^{M2})*[108,109,122]

A solution of dimethyl pyrazine-2,3-dicarboxylate (**3**) (2.00 g, 10.2 mmol) and 2-(2-aminoethyl)pyridine (**5**) (2.49 g, 20.4 mmol) in methanol (20 ml) was maintained at 80–90 °C for 5 hours in an open flask, allowing the methanol formed in the reaction to distil off and was then allowed to cool to room temperature. Removal of the remaining methanol under reduced pressure gave the crude product as a pale brown foamy solid in quantitative yield. Redissolving the crude product in dichloromethane/acetone (2:1, 50 ml), reduction of the solvent under reduced pressure (to 10 ml) and filtration of the resulting colourless solid gave 3.22 g (8.55 mmol, 83 %) of analytically pure H_2L^{M2} in the form of a colourless crystalline material. Single crystals of H_2L^{M2} suitable for X-ray crystal structure determination were obtained through recrystallisation from acetone.

Mp.: 130–133 °C — elemental analysis (%) found: C 63.78, H 5.37, N 22.35; calcd. for $C_{20}H_{20}N_6O_2$ (376.42 g mol^{-1}): C 63.82, H 5.36, N 22.33 — TLC (SiO_2, DCM/10 % MeOH): R_f = 0.38 — ^{1}H NMR (300 MHz, $CDCl_3$): δ (ppm) = 8.58 (s, 2 H, 2 × pz*H*), 8.51 (ddd, $^3J_{6,5}$ = 4.9 Hz, $^4J_{6,4}$ = 1.7 Hz, $^5J_{6,3}$ = 0.9 Hz, 2 H, 2 × 6-py*H*), 7.83 (s, 2 H, 2 × N*H*), 7.61 (dt, $^3J_{4,5} = {}^3J_{4,3}$ = 7.6 Hz, $^4J_{4,6}$ = 1.7 Hz, 2 H, 2 × 4-py*H*), 7.20 (d, J = 7.8 Hz, 2 H, 2 × 3-py*H*), 7.13 (ddd, $^3J_{5,4}$ = 7.6 Hz, $^3J_{5,6}$ = 4.9 Hz, $^4J_{5,3}$ = 1.1 Hz, 2 H, 2 × 5-py*H*), 3.91 (q, J = 6.2 Hz, 4 H, 2 × NHCH_2), 3.14 (t, J = 6.5 Hz, 4 H, 2 × pyCH_2) — ^{13}C{^{1}H} NMR (75 MHz, $CDCl_3$): δ (ppm) = 164.5 (*C*O), 159.5 (2-*py*), 149.3 (6-*py*), 147.1 (*pz*CO), 144.0 (*pz*H), 136.6 (4-*py*), 123.6 (3-*py*), 121.6 (5-*py*), 39.1 (NHCH$_2$), 36.9 (pyCH$_2$) — IR (KBr, disk): $\tilde{\nu}$ (cm^{-1}) = 3410, 3300, 3076, 3010, 2939, 2981, 1674, 1651, 1590, 1560, 1541, 1509, 1474, 1450, 1433, 1366, 1314, 1297, 1275, 1216, 1192, 1160, 1153, 1119, 1074, 1052, 1023, 1006, 991, 886, 774, 761, 749, 650, 612, 567, 511, 445.

3.2.5. *Dimethyl pyrazine-2,5-dicarboxylate (29)*[192-194]

A solution of 2,5-dimethylpyrazine (**27**) (8.11 g, 75.0 mmol) in pyridine (150 ml) was treated with solid selenium dioxide (37.5 g, 338 mmol). Water (15 ml) was added and the resulting suspension was refluxed for 18 hours. The resulting dark red-brown mixture was evaporated to dryness under reduced pressure. Water (250 ml) was added and the solid elemental selenium was filtered off, the red solution was evaporated to dryness. The resulting dark red-brown solid was taken up in methanol (150 ml), treated with thionyl chloride (3.5 ml) and refluxed for 8 hours. The resulting suspension was then filtered hot and the remaining solid was washed with dichloromethane (5 × 20 ml). The combined organic layers were reduced in volume under reduced pressure (to 100 ml) to give the product in the form of pale yellow orange feathery crystals. The solid was filtered off and washed with ice-cold methanol (20 ml) to give 8.98 g (45.8 mmol, 61 %) of analytically pure dimethyl pyrazine-2,5-dicarboxylate (**29**).

Mp.: 167–168 °C — elemental analysis (%) found: C 49.24, H 3.87, N 14.25; calcd. for $C_8H_8N_2O_4$ (196.16 g mol^{-1}): C 48.98, H 4.11, N 14.28 — TLC (SiO_2, DCM/10 % MeOH): R_f = 0.83 — ^1H NMR (300 MHz, $CDCl_3$): δ (ppm) = 9.39 (s, 2 H, pz*H*), 4.07 (s, 6 H, C*H*$_3$) — $^{13}C\{^1H\}$ NMR (75 MHz, $CDCl_3$): δ (ppm) = 163.6 (pzCO), 145.6 (*pz*H), 145.3 (*pz*CO), 53.6 (OCH_3) — IR (KBr, disk): $\tilde{\upsilon}$ (cm^{-1}) = 3549, 3472, 3417, 3077, 3015, 2960, 2853, 1720, 1637, 1618, 1472, 1431, 1359, 1279, 1202, 1181, 1144, 1020, 959, 824, 759, 616 495, 466, 425.

3.2.6. *N,N'-Bis(2-pyridylmethyl)pyrazine-2,5-dicarboxamide (H_2L^{S1})*

A suspension of dimethyl pyrazine-2,5-dicarboxylate (**29**) (1.96 g, 10.0 mmol) in methanol (70 ml) was treated with a solution of 2-(aminomethyl)pyridine (**4**) (2.38 g, 22.0 mmol) in methanol (30 ml) and the resulting solution was kept in an open flask at 80–90 °C for 4 hours, allowing most of the solvent to evaporate. Filtration of the resulting suspension gave 2.92 g (8.38 mmol, 84 %) of H_2L^{S1} in the form of an analytically pure colourless powder.

Mp.: 205–206 °C — elemental analysis (%) found: C 61.94, H 4.66, N 24.30; calcd. for $C_{18}H_{16}N_6O_2$ (348.36 g mol^{-1}): C 62.06, H 4.63, N 24.12 — TLC (SiO_2, DCM/10 % MeOH): R_f = 0.60 — ^{1}H NMR (500 MHz, $CDCl_3$): δ (ppm) = 9.39 (s, 2 H, 2 × pz*H*), 8.88 (t, J = 5.0 Hz, 2 H, 2 × N*H*), 8.62 (ddd, $^3J_{6,5}$ = 5.0 Hz, $^4J_{6,4}$ = 2.0 Hz, $^5J_{6,3}$ = 1.0 Hz, 2 H, 2 × 6-py*H*), 7.69 (dt, $^3J_{4,5} = {}^3J_{4,3}$ = 7.5 Hz, $^4J_{4,6}$ = 2.0 Hz, 2 H, 2 × 4-py*H*), 7.34 (td, $^3J_{3,4}$ = 7.5 Hz, $^4J_{3,5} = {}^5J_{3,6}$ = 1.0 Hz, 2 H, 2 × 3-py*H*), 7.23 (ddd, $^3J_{5,4}$ = 7.5 Hz, $^3J_{5,6}$ = 5.0 Hz, $^4J_{5,3}$ = 1.0 Hz, 2 H, 2 × 5-py*H*), 4.82 (d, J = 5.0 Hz, 4 H, 2 × pyCH_2) — ^{13}C{^{1}H} NMR (75 MHz, $CDCl_3$): δ (ppm) = 162.6 (pzCO), 156.0 (2-*py*), 149.5 (6-*py*), 146.4 (*pz*CO), 142.4 (*pz*H), 136.9 (4-*py*), 122.6 (5-*py*), 122.1 (3-*py*), 44.7 (CH_2) — IR (KBr, disk): $\tilde{\upsilon}$ (cm^{-1}) = 3458, 3417, 3338, 2922, 1681, 1572, 1522, 1461, 1434, 1363, 1325, 1208, 1177, 1027, 997, 902, 758, 726, 648, 504, 460.

3.2.7. *N,N'-Bis[2-(2-pyridyl)ethyl]pyrazine-2,5-dicarboxamide (H_2L^{S2})*

A solution of dimethyl pyrazine-2,5-dicarboxylate (**29**) (1.96 g, 10.0 mmol) in hot (60 °C) methanol (80 ml) was treated with a solution of 2-(2-aminoethyl)pyridine (**5**)

(2.69 g, 22.0 mmol) in methanol (20 ml) and the resulting solution was kept in an open flask at 80–90 °C for 4 hours, allowing most of the solvent to evaporate. The resulting suspension was allowed to cool to room temperature. Filtration gave 2.68 g (7.12 mmol, 71 %) of H_2L^{S2} in the form of an analytically pure colourless powder.

Mp.: 225–227 °C — elemental analysis (%) found: C 63.51, H 5.42, N 22.69; calcd. for $C_{20}H_{20}N_6O_2$ (376.42 g mol^{-1}): C 63.82, H 5.36, N 22.33 — TLC (SiO_2, DCM/10 % MeOH): R_f = 0.70 — ^{1}H NMR (500 MHz, $CDCl_3$): δ (ppm) = 9.28 (s, 2 H, 2 × pz*H*), 8.59 (d, J = 5.0 Hz, 2 H, 6-py*H*), 8.54 (s, 2 H, 2 × N*H*), 7.62 (dt, $^3J_{4,5} = {}^3J_{4,3}$ = 7.8 Hz, $^4J_{4,6}$ = 2.0 Hz, 2 H, 2 × 4-py*H*), 7.20–7.16 (m, 4 H, 2 × 3-py*H* and 2 × 5-py*H*), 3.92 (q, J = 6.5 Hz, 4 H, 2 × NHCH_2), 3.13 (t, J = 6.5 Hz, 4 H, 2 × pyCH_2) — ^{13}C{^{1}H} NMR (75 MHz, $CDCl_3$): δ (ppm) = 162.5 (pzCO), 159.1 (2-*py*), 149.5 (6-*py*), 146.4 (*pz*CO), 142.2 (*pz*H), 136.7 (4-*py*), 123.5 (3-*py*), 121.8 (5-*py*), 38.8 (HNCH_2), 37.0 (pyCH_2) — IR (KBr, disk): $\tilde{\nu}$ (cm^{-1}) = 3369, 3092, 3036, 3013, 1985, 2973, 1659, 1590, 1569, 1535, 1475, 1461, 1441, 1367, 1321, 1286, 1263, 1196, 1169, 1049, 1036, 1017, 993, 951, 884, 857, 763, 745, 654, 633, 614, 512, 494, 472, 449.

3.2.8. N,N'-Bis(4-methoxyphenyl)-2,3-dicarboxamide (37)

A solution of dimethyl pyrazine-2,3-dicarboxylate (**29**) (0.98 g, 5.00 mmol) in hot (60 °C) methanol (80 ml) was treated with solid 4-methoxyaniline (1.23 g, 10.0 mmol) and the resulting solution was kept in an open flask at 80–90 °C for 4 hours, allowing most of the solvent to evaporate. While a small volume (10 ml) of solvent was still present in the flask the heating was continued under reflux for 2 days. The resulting mixture was evaporated to dryness to give a dark brown solid in quantitative yield. By digesting the crude product in dichloromethane/methanol (1:1), filtration of the remaining solid and evaporating the filtrate under reduced pressure 729 mg

(1.93 mmol, 38 %) of **37** were obtained in the form of an analytically pure slightly purple powder.

Mp.: 178–180 °C — elemental analysis (%) found: C 63.19, H 5.11, N 14.56; calcd. for $C_{20}H_{18}N_4O_4$ (378.39 g mol^{-1}): C 63.49, H 4.79, N 14.81 — TLC (SiO_2, DCM/10 % MeOH): R_f = 0.64 — ^1H NMR (500 MHz, $CDCl_3$): δ (ppm) = 8.93 (s, 2 H, 2 × N*H*), 8.66 (s, 2 H, 2 × pz*H*), 7.63 (d, ^3J = 9.0 Hz, 4 H, 2 × 2,6-ph*H*), 6.89 (d, ^3J = 9.0 Hz, 4 H, 2 × 3,5-ph*H*), 3.80 (s, 6 H, 2 × OCH_3) — $^{13}C\{^1H\}$ NMR ($CDCl_3$, 125 MHz): δ (ppm) = 161.7 (*C*O), 156.9 (4-*ph*), 146.8 (*pz*C), 144.1 (*pz*H), 130.6 (1-*ph*), 122.0 (3,5-*ph*), 114.3 (2,6-*ph*), 55.5 (OCH_3) — IR (KBr, disk): $\tilde{\nu}$ (cm^{-1}) = 3549, 3417, 3349, 3058, 3010, 2960, 2929, 2905, 2833, 1666, 1594, 1526, 1511, 1462, 1440, 1420, 1400, 1315, 1303, 1260, 1228, 1178, 1126, 1108, 1048, 1032, 1021, 896, 870, 824, 773, 717, 661, 546, 519, 450, 409.

3.2.9. Pyrazine-2,3-dicarboxamide (38)[113]

Solid dimethyl pyrazine-2,3-dicarboxylate (**3**) (5.88 g, 30.0 mmol) was suspended in concentrated aqueous ammonia (38 %, 20 ml) and the mixture was stirred for 15 minutes at room temperature. The resulting colourless suspension was filtered and the solid was washed with tetrahydrofuran (2 × 5 ml) to give 4.50 g (27.1 mmol, 90 %) of pyrazine-2,3-dicarboxamide (**38**) in the form of an analytically pure colourless solid.

Mp.: 211–217 °C (dec.) — elemental analysis (%) found: C 43.29, H 3.51, N 33.47; calcd. for $C_6H_6N_4O_2$ (166.14 g mol^{-1}): C 43.38, H 3.64, N 33.72 — TLC (SiO_2, DCM/10 % MeOH): R_f = 0.24 — ^1H NMR (500 MHz, $CDCl_3$): δ (ppm) = 8.73 (s, 2 H, pz*H*), 7.98 (s, 2 H, ½ NH_2), 7.63 (s, 2 H, ½ NH_2) — $^{13}C\{^1H\}$ NMR (125 MHz, $CDCl_3$): δ (ppm) = 166.6, ($CONH_2$), 147.1 (*pz*$CONH_2$), 144.1 (*pz*H) — IR (KBr, disk): $\tilde{\nu}$ (cm^{-1}) = 3431, 3312,

3204, 1697, 1677, 1613, 1561, 1444, 1395, 1347, 1190, 1171, 1103, 1077, 1059, 879, 856, 759, 742, 702, 649, 621, 559, 431.

3.2.10. Pyrazine-2,3-dicarbonitrile (39)[210]

Pyrazine-2,3-dicarboxamide (**38**) (1.66 g, 10.0 mmol) was suspended in phosphorus oxychloride (15 ml), the resulting mixture was refluxed for 90 minutes, resulting in a dark black mixture, which was evaporated to dryness under reduced pressure. With ice-cooling, saturated aqueous sodium carbonate solution (40 ml) was slowly added and the resulting mixture was extracted with diethyl ether (5 × 50 ml). The combined organic layers were washed with brine (15 ml) and dried over anhydrous sodium sulphate. Filtration of the remaining solid and evaporation of the solvent gave 794 mg (6.10 mmol, 61 %) of pyrazine-2,3-dicarbonitrile (**39**) in the form of an analytically pure pale brown solid.

Mp.: 125–126 °C (dec.) — elemental analysis (%) found: C 55.24, H 1.36, N 42.85; calcd. for $C_6H_2N_4$ (130.11 g mol^{-1}): C 55.37, H 1.55, N 43.07 — TLC (SiO_2, DCM/10 % MeOH): R_f = 0.77 — ^{1}H NMR (300 MHz, $CDCl_3$): δ (ppm) = 8.94 (s, 2 H, pz*H*) — $^{13}C\{^1H\}$ NMR (75 MHz, $CDCl_3$): δ (ppm) = 161.7, 147.3 (*pz*H), 110.2 — IR (KBr, disk): $\tilde{\upsilon}$ (cm^{-1}) = 3414, 3102, 3071, 2925, 2359, 2244, 1974, 1860, 1732, 1687, 1549, 1524, 1454, 1389, 1309, 1213, 1176, 1118, 1051, 874, 722, 692, 611, 151, 536, 467, 443.

3.2.11. *2,5-Dimethylpyrazine-1,4-dioxide (40)*[218,219,222]

A solution of 2,5-dimethylpyrazine (**27**) (15.5 g, 143 mmol) in glacial acetic acid (70 ml) was treated with aqueous hydrogen peroxide (30 %, 30 ml, 286 mmol) and maintained at 95 °C. After 24 hours, another portion of aqueous hydrogen peroxide (30 %, 30 ml, 286 mmol) was added and the reaction mixture was maintained at 95 °C for further 48 hours. After testing for the absence of hydrogen peroxide with starch iodide paper the mixture was reduced in volume (to 50 ml) under reduced pressure and diethyl ether (50 ml) was added. The resulting precipitate was filtered off and washed with diethyl ether (10 ml) to obtain 18.0 g (129 mmol, 90 %) of analytically pure 2,5-dimethylpyrazine-1,4-dioxide (**40**) in the form of a colourless solid.

Mp.: >230 °C — elemental analysis (%) found: C 51.42, H 5.58, N 20.22; calcd. for $C_6H_8N_2O_2$ (140.14 g mol^{-1}): C 51.42, H 5.75, N 19.99 — TLC (SiO_2, DCM/10 % MeOH): R_f = 0.41 — ^1H NMR (300 MHz, D_2O): δ (ppm) = 8.50 (s, 2 H, pz*H*), 2.44 (s, 6 H, C*H*$_3$) — $^{13}C\{^1H\}$ NMR (75 MHz, D_2O): δ (ppm) = 146.3 (*pz*CH_3), 136.5 (*pz*H), 14.1 (CH_3) — IR (KBr, disk): $\tilde{\upsilon}$ (cm^{-1}) = 3538, 3430, 3385, 3051, 1664, 1641, 1616, 1525, 1451, 1422, 1399, 1383, 1359, 1274, 1207, 1163, 1141, 1010, 901, 873, 715.

3.2.12. *2,5-Bis(hydroxymethyl)pyrazine (41)*

a:[218,224] A suspension of 2,5-dimethylpyrazine-1,4-dioxide (**40**) (2.10 g, 15.0 mmol) in dry chloroform (90 ml) was treated with trifluoroacetic anhydride (10.5 ml, 75 mmol) and 4-(dimethylamino)pyridine (0.75 mmol, 91.5 mmol) and the resulting mixture was refluxed for two days. The mixture was then evaporated to dryness under reduced pressure and the resulting solid was dissolved in

dichloromethane (30 ml). The solution was treated with aqueous sodium carbonate (2 M, 45 ml) and the mixture was stirred vigorously for 4 hours at room temperature. The resulting mixture was extracted continuously for three days with dichloromethane. The first crop of dichloromethane layer, containing only impurities, was discarded and the extraction was continued with fresh dichloromethane for two weeks. Separation of the dichloromethane layer and removal of the solvent under reduced pressure gave 533 mg (3.80 mmol, 25 %) of 2,5-bis(hydroxymethyl)pyrazine (**41**) in the form of a pure pale tan solid.

b:[221] A suspension of sodium borohydride (3.8 g, 0.1 mol) in ethanol (300 ml) was slowly treated with solid dimethyl pyrazine-2,5-dicarboxylate (**29**) (2.10 g, 10.7 mmol) so that the temperature was not raised above 40 °C. The resulting slightly yellow solution was stirred at room temperature for 2 days, then hydrochloric acid (conc.) (7.5 ml) was added slowly over 1 hour and the resulting mixture was stirred at room temperature for another hour. After the addition of aqueous ammonia (conc.) (7.5 ml) and stirring for another hour at room temperature, the resulting voluminous inorganic precipitate was filtered off and washed with ethanol (4 × 50 ml). The slightly yellow combined organic layers were reduced to dryness under reduced pressure and the resulting solid was separated from remaining inorganic solids by column chromatography (SiO_2, h = 24 cm, $\varnothing$ = 3.5 cm, DCM/10 % MeOH) to obtain 390 mg (2.78 mmol, 26 %) of 2,5-bis-(hydroxymethyl)pyrazine (**41**) in the form of a slightly yellow analytically pure solid.

Mp.: 82–83 °C — elemental analysis (%) found: C 51.45, H 5.72, N 19.91; calcd. for $C_6H_8N_2O_2$ (140.14 g mol^{-1}): C 51.42, H 5.75, N 19.99 — TLC (SiO_2, DCM/10 % MeOH): R_f = 0.26 — ^1H NMR (300 MHz, $CDCl_3$): δ (ppm) = 8.59 (s, 2 H, pz*H*), 4.86 (d, J = 4.5 Hz, 4 H, C*H*$_2$OH), 2.95 (t, J = 4.5 Hz, CH$_2$O*H*) — $^{13}C\{^1H\}$ NMR (75 MHz, $CDCl_3$): δ (ppm) = 153.6 (*pz*H), 141.6 (*pz*H), 62.9 (*C*H$_2$) — IR (KBr, disk): $\tilde{\upsilon}$ (cm^{-1}) =

3319, 2929, 2871, 1639, 1495, 1451, 1352, 1316, 1280, 1214, 1155, 1067, 1027, 971, 911, 880, 864, 789, 742, 731, 670, 606, 531, 482, 445, 413.

3.2.13. *Pyrazine-2,5-dicarbaldehyde (42)*[223]

A hot solution (50–60 °C) of 2,5-bis(dihydroxymethyl)pyrazine (**41**) (400 mg, 2.85 mmol) in dry chloroform (210 ml) was treated with manganese dioxide (3.0 g, 35 mol). The resulting suspension was stirred for two days at room temperature. Filtration of the manganese dioxide and removal of the solvent under reduced pressure gave 233 mg (1.71 mmol, 60 %) of crude pyrazine-2,5-dicarbaldehyde (**42**) in the form of a slightly yellow solid.

TLC (SiO_2, DCM/10 % MeOH): R_f = 0.46 — ^{1}H NMR (300 MHz, $CDCl_3$): δ (ppm) = 10.24 (s, 2 H, C*H*O), 9.31 (s, 2 H, pz*H*).

3.2.14. *Pyrazine-2,5-dicarboxamide (43)*[113,193,208,211]

Solid dimethyl pyrazine-2,5-dicarboxylate (**29**) (1.00 g, 5.10 mmol) was suspended in concentrated aqueous ammonia (38 %, 15 ml) and the mixture was stirred for 15 minutes at room temperature. The resulting colourless suspension was filtered and the solid was washed with water (3 × 5 ml) and dried under reduced pressure to give 777 mg (4.68 mmol, 92 %) of pyrazine-2,5-dicarboxamide (**43**) in the form of an analytically pure colourless solid.

Mp.: >300 °C (dec.) — elemental analysis (%) found: C 43.40, H 3.56, N 33.32; calcd. for $C_6H_6N_4O_2$ (166.14 g mol^{-1}): C 43.38, H 3.64, N 33.72 — TLC (SiO_2, DCM/10 % MeOH): R_f = 0.00 — ^1H NMR (300 MHz, d^6-DMSO): δ (ppm) = 8.32 (s, 2 H, pz*H*), 7.53 (s, 2 H, ½ N*H*$_2$), 7.10 (s, 2 H, ½ N*H*$_2$) — IR (KBr, disk): $\tilde{\upsilon}$ (cm^{-1}) = 3418, 3279, 3169, 1671, 1601, 1490, 1414, 1344, 1306, 1184, 1091, 1037, 941, 800, 726, 575, 503, 462, 449.

3.3. *Complexations*

3.3.1. *$[Cu^{II}_2(HL^{M1})(MeCN)_2(H_2O)_2](BF_4)_3$ (6) and $[Cu^{II}_2(HL^{M1})(MeCN)_4](BF_4)_3 \cdot MeCN$ (6b · MeCN)*

To a solution of *N,N'*-bis(2-pyridylmethyl)pyrazine-2,3-dicarboxamide (H_2L^{M1}) (200 mg, 574 µmol) in acetonitrile (15 ml) was added a solution of copper(II) tetrafluoroborate tetrahydrate (355 mg, 1.15 mmol) in acetonitrile (15 ml) and the resulting dark navy blue solution was stirred at room temperature for 4 hours. Toluene (60 ml) was added and a dark navy blue solid precipitated. Filtration gave 389 mg (456 µmol, 79 %) of $[Cu^{II}_2(HL^{M1})(MeCN)_2(H_2O)_2](BF_4)_3$ (**6**) in the form of a dark navy blue amorphous solid. Single crystals of $[Cu^{II}_2(HL^{M1})(MeCN)_4](BF_4)_3 \cdot MeCN$ (**6b** · MeCN) suitable for X-ray crystal structure determination were obtained by vapour diffusion of diethyl ether into a solution of **6** in acetonitrile.

Elemental analysis (%) found: C 31.25, H 2.95, N 13.14; calcd. for $[Cu^{II}_2(HL^{M1})(MeCN)_2(H_2O)_2](BF_4)_3$, $C_{22}H_{25}B_3N_8O_4F_{12}Cu_2$ (852.99 g mol^{-1}): C 30.98, H 2.95, N 13.14 — IR (KBr, disk): $\tilde{\upsilon}$ (cm^{-1}) = 3454, 1609, 1564, 1476, 1398, 1281, 1242, 1159,

1083, 1034, 872, 777, 730, 702, 650, 628, 533, 521, 501 — ESI-MS (MeCN): *m/z* (fragment) = 410.0 ($[Cu^{II}(HL^{M1})]^+$), 277.0 ($[Cu^{II}_2(L^{M1})(MeCN)_2]^{2+}$), 256.5 ($[Cu^{II}_2(L^{M1})(MeCN)]^{2+}$), 226.0 ($[Cu^{II}(H_2L^{M1})(MeCN)]^{2+}$), 205.5 ($[Cu^{II}(H_2L^{M1})]^{2+}$) — UV/VIS (MeCN): λ_{max} (ε) = 254 (26100), 616 nm (322 M^{-1} cm^{-1}) — Λ_m(MeCN) = 378 mol^{-1} cm^2 Ω^{-1}.

3.3.2. $[Cu^{II}_2(HL^{M1})(MeCN)_2](ClO_4)_3$ (7)

Caution! Perchlorate salts of metal complexes with organic ligands are potentially explosive. Although no problems have been experienced during this work only small amounts of material should be prepared and these should be handled with the appropriate care.

To a solution of *N,N'*-bis(2-pyridylmethyl)pyrazine-2,3-dicarboxamide (H_2L^{M1}) (200 mg, 574 µmol) in acetonitrile (15 ml) was added a solution of copper(II) perchlorate hexahydrate (425 mg, 1.15 mmol) in acetonitrile (15 ml) and the resulting dark navy blue solution was stirred at room temperature for 4 hours. By vapour diffusion of diethyl ether into the reaction mixture 320 mg (374 µmol, 65 %) of $[Cu^{II}_2(HL^{M1})(MeCN)_2](ClO_4)_3$ (7) were obtained in the form of dark navy blue feathery crystals.

Elemental analysis (%) found: C 30.87, H 2.44, N 13.37; calcd. for $[Cu^{II}_2(HL^{M1})(MeCN)_2](ClO_4)_3$, $C_{22}H_{21}N_8O_{14}Cl_3Cu_2$ (854.90 g mol^{-1}): C 30.91, H 2.48, N 13.11 — IR (KBr, disk): $\tilde{\nu}$ (cm^{-1}) = 3446, 3048, 1608, 1564, 1474, 1447, 1398, 1348, 1283, 1243, 1145, 1116, 1088, 1023, 940, 871, 776, 730, 701, 651, 626, 502, 469.

3.3.3. $[Cu^{II}_2(HL^{M2})(H_2O)](ClO_4)_3$ (8)

Caution! Perchlorate salts of metal complexes with organic ligands are potentially explosive. Although no problems have been experienced during this work only small amounts of material should be prepared and these should be handled with the appropriate care.

To a solution of *N,N'*-bis[2-(2-pyridyl)ethyl]pyrazine-2,3-dicarboxamide (H_2L^{M2}) (75.3 mg, 200 μmol) in acetonitrile (5 ml) was added a solution of copper(II) perchlorate hexahydrate (148 mg, 400 μmol) in acetonitrile (5 ml) and the resulting dark turquoise solution was stirred at room temperature for 4 hours. By vapour diffusion of diethyl ether into the reaction mixture, 118 mg (144 μmol, 72 %) of $[Cu^{II}_2(HL^{M2})(H_2O)](ClO_4)_3$ (**8**) were obtained in the form of dark sky blue feathery crystals.

Elemental analysis (%) found: C 30.50, H 2.70, N 10.84; calcd. for $[Cu^{II}_2(HL^{M2})(H_2O)](ClO_4)_3$, $C_{20}H_{21}N_6O_{15}Cl_3Cu_2$ (818.87 g mol^{-1}): C 30.76, H 2.71, N 10.76 — IR (KBr, disk): $\tilde{\nu}$ (cm^{-1}) = 3447, 3072, 2954, 2863, 1605, 1561, 1481, 1460, 1446, 1406, 1373, 1351, 1311, 1237, 1148, 1118, 1085, 1028, 975, 899, 841, 792, 770, 731, 681, 636, 626, 592, 525, 485 — ESI-MS (MeCN): *m/z* (fragment) = 599.0 ($\{[Cu^{II}_2(\mathbf{L}^{M2})](ClO_4)_3\}^+$), 538.0 ($[Cu^{I}_2(HL^{M2})(H_2O)_2]^+$), 499.1 ($[Cu^{I}(H_2L^{M2})(H_2O)(MeCN)]^+$), 477.1 ($[Cu^{II}(HL^{M2})(MeCN)]^+$), 474.0 ($[Cu^{II}(HL^{M2})(H_2O)_2]^+$), 439.0 ($[Cu^{I}(H_2L^{M2})]^+$), 377.1 ($[H_3L^{M2}]^+$), 189.1 ($[H_4L^{M2}]^{2+}$), 147.1 ($[Cu^{I}(H_4L^{M2})]^{3+}$) — UV/VIS (MeCN): λ_{max} (ε) = 259 (32400), 623 nm (190 M^{-1} cm^{-1}) — Λ_m(MeCN) = 328 mol^{-1} cm^2 Ω^{-1}.

3.3.4. $[Cu^{II}_2(HL^{M1})(NO_3)_3]_n$ (9)

To a solution of *N,N'*-bis(2-pyridylmethyl)pyrazine-2,3-dicarboxamide (H_2L^{M1}) (100 mg, 287 μmol) in acetonitrile (10 ml) was added a solution of copper(II) nitrate trihydrate (139 mg, 574 μmol) in acetonitrile (10 ml) and the resulting dark turquoise mixture was stirred at room temperature for 8 hours. Filtration of the turquoise precipitate gave 106 mg (160 μmol, 56 %) of $[Cu^{II}_2(HL^{M1})(NO_3)_3]_n$ (**9**) in the form of a microcrystalline solid.

Elemental analysis (%) found: C 32.61, H 2.43, N 18.70; calcd. for $[Cu^{II}_2(HL^{M1})(NO_3)_3]_n$, $C_{18}H_{15}N_9O_{11}Cu_2$ (660.46 g mol^{-1}): C 32.73, H 2.29, N 19.09 — IR (KBr, disk): $\tilde{\upsilon}$ (cm^{-1}) = 3446, 3068, 1609, 1580, 1565, 1474, 1384, 1320, 1291, 1159, 1053, 1016, 874, 776, 731, 688, 651, 625, 585, 524, 502, 470, 419 — UV/VIS (MeCN): λ_{max} (ε) = 247 (shoulder) (23100), 649 nm (252 M^{-1} cm^{-1}).

3.3.5. $[Cu^{II}_2(HL^{M2})(NO_3)_3]_n$ (10)

To a solution of *N,N'*-bis[2-(2-pyridyl)ethyl]pyrazine-2,3-dicarboxamide (H_2L^{M2}) (100 mg, 366 μmol) in acetonitrile (10 ml) was added a solution of copper(II) nitrate trihydrate (128 mg, 531 μmol) in acetonitrile (10 ml). The resulting dark turquoise suspension was stirred at room temperature for 8 hours. Filtration of the mixture gave 166 mg (241 μmol, 66 %) of $[Cu^{II}_2(HL^{M2})(NO_3)_3]_n$ (**10**) in the form of a microcrystalline dark turquoise solid.

Elemental analysis (%) found: C 34.88, H 3.05, N 18.21; calcd. for $[Cu^{II}_2(HL^{M2})(NO_3)_3]_n$, $C_{20}H_{19}N_9O_{11}Cu_2$ (688.52 g mol^{-1}): C 34.89, H 2.78, N 18.31 — IR

(KBr, disk): $\tilde{\upsilon}$ (cm^{-1}) = 3447, 3073, 2924, 2861, 1606, 1567, 1481, 1474, 1445, 1384, 1282, 1237, 1150, 1113, 1053, 1030, 975, 901, 842, 797, 773, 732, 684, 648, 577, 521, 505, 429 — ESI-MS (MeCN): *m/z* (fragment) = 439.1 ($[Cu^{I}(H_2L^{M2})]^+$), 377.1 ($[H_3L^{M2}]^+$), 189.1 ($[H_4L^{M2}]^{2+}$), 147.1 ($[Cu^{I}(H_4L^{M2})]^{3+}$) — UV/VIS (MeCN): λ_{max} (ε) = 257 (28400), 645 nm (176 M^{-1} cm^{-1}).

3.3.6. $\{[Cu^{II}_2(HL^{M1})(Br)_3] \cdot H_2O\}_\infty$ (11 · H_2O)

To a solution of *N,N'*-bis(2-pyridylmethyl)pyrazine-2,3-dicarboxamide (H_2L^{M1}) (69.7 mg, 200 µmol) in water (10 ml) was added a solution of copper(II) bromide (89.3 mg, 400 µmol) in water (10 ml) and the resulting dark bottle green solution was stirred at room temperature for 18 hours. Filtration of the resulting grass green precipitate gave 58 mg (79 µmol, 40 %) of $\{[Cu^{II}_2(HL^{M1})(Br)_3] \cdot H_2O\}_\infty$ (**11** · H_2O) in the form of an amorphous solid.

Elemental analysis (%) found: C 29.36, H 2.24, N 10.94, Br 32.93; calcd. for $\{[Cu^{II}_2(HL^{M1})(Br)_3] \cdot H_2O\}_\infty$, $C_{18}H_{17}N_6O_3Br_3Cu_2$ (732.18 g mol^{-1}): C 29.53, H 2.34, N 11.48, Br 32.74 — IR (KBr, disk): $\tilde{\upsilon}$ (cm^{-1}) = 3418, 3067, 1608, 1564, 1463, 1394, 1382, 1348, 1288, 1257, 1145, 1055, 1026, 1011, 878, 808, 785, 733, 710, 685, 650, 624, 585, 541, 503, 467.

3.3.7. $[Cu^{II}_2(HL^{M2})(Br)_3]_\infty$ (12)

To a solution of *N,N'*-bis[2-(2-pyridyl)ethyl]pyrazine-2,3-dicarboxamide (H_2L^{M2}) (50.0 mg, 133 μmol) in acetonitrile (10 ml) was added a solution of copper(II) bromide (59.4 mg, 266 μmol) in acetonitrile (20 ml). The resulting dark green suspension was stirred at room temperature for 8 hours. Filtration of the mixture gave 71 mg (96 μmol, 72 %) of $[Cu^{II}_2(HL^{M2})(Br)_3]_\infty$ (**12**) in the form of a dark green amorphous solid.

Elemental analysis (%) found: C 32.68, H 2.41, N 11.37, Br 32.49; calcd. for $[Cu^{II}_2(HL^{M2})(Br)_3]_\infty$, $C_{20}H_{19}N_6O_2Br_3Cu_2$ (742.21 g mol^{-1}): C 32.37, H 2.58, N 11.32, Br 32.30 — IR (KBr, disk): $\tilde{\upsilon}$ (cm^{-1}) = 3445, 3070, 2953, 2862, 1604, 1561, 1480, 1445, 1405, 1371, 1351, 1310, 1234, 1149, 1110, 1127, 975, 899, 840, 793, 770, 731, 680, 646, 592, 524, 505, 431 — ESI-MS (MeCN): *m/z* (fragment) = 1203.5 ($[Cu^{II}_4(HL^{M2})(L^{M2})(MeCN)(Br)_2]^+$), 1060.7 ($[Cu^{II}_4(HL^{M2})(L^{M2})(MeCN)(H_2O)]^+$), 660.6 ($[Cu^{II}_2(HL^{M2})(Br)_2]^+$), 581.7 ($[Cu^{II}_2(L^{M2})(Br)]^+$), 519.9 ($[Cu^{II}(HL^{M2})(MeCN)_2]^+$), 452.1 ($[Cu^{I}_2(HL^{M2})(MeCN)]^+$), 439.0 ($[Cu^{I}(H_2L^{M2})]^+$), 377.1 ($[H_3L^{M2}]^+$).

3.3.8. $[Cu^{II}_2(HL^{M1})(SCN)_2(H_2O)_2]_n(BF_4)_n$ (13)

To a navy blue solution of $[Cu^{II}_2(HL^{M1})(MeCN)_2(H_2O)_2](BF_4)_3$ (**6**) (74 mg, 87 μmol) in acetonitrile (20 ml) was added a solution of potassium thiocyanate (16.9 mg, 174 μmol) in acetonitrile (10 ml). The resulting green suspension was reduced in volume under reduced pressure (to 10 ml). Filtration of the mixture gave 34 mg of a green amorphous solid of unknown composition. Vapour diffusion

of diethyl ether into the filtrate gave 50 mg (70 μmol, 80 %) of $[Cu^{II}_2(HL^{M1})(SCN)_2(H_2O)_2]_n(BF_4)_n$ (**13**) in the form of a turquoise crystalline solid.

Elemental analysis (%) found: C 33.57, H 2.92, N 15.44, S 8.54; calcd. for $[Cu^{II}_2(HL^{M1})(SCN)_2(H_2O)_2]_n(BF_4)_n$, $C_{20}H_{19}BN_8O_4F_4S_2Cu_2$ (713.44 g mol^{-1}): C 33.67, H 2.68, N 15.71, S 8.99 — IR (KBr, disk): $\tilde{\upsilon}$ (cm^{-1}) = 3449, 3084, 2922, 2094, 1610, 1566, 1472, 1411, 1389, 1287, 1244, 1162, 1082, 1064, 1028, 875, 769, 689, 650, 624, 599, 582, 560, 537, 520, 500, 475, 457, 436, 416 — ESI-MS (MeCN): *m/z* (fragment) = 469.1 ($[Cu^{II}(H_2L^{M1})(SCN)]^+$), 410.1 ($[(Cu^{II}(HL^{M1})]^+$), 349.2 ($[H_3L^{M1}]^+$), 226.0 ($[Cu^{II}(H_2L^{M1})(MeCN)]^{2+}$).

3.3.9. $[Cu^{II}_4(HL^{M1})_2(N_3)_4](BF_4)_2$ (14) and $[Cu^{II}_4(HL^{M1})_2(\mu_{(1,1)}\text{-}N_3)_2(N_3)_2(MeCN)_2](BF_4)_2 \cdot MeCN$ (14b · MeCN)

Caution! Azide derivatives are potentially explosive. Although no problems have been experienced during this work only small amounts of material should be prepared and these should be handled with the appropriate care.

To a navy blue solution of $[Cu^{II}_2(HL^{M1})(MeCN)_2(H_2O)_2](BF_4)_3$ (**6**) (188 mg, 220 μmol) in acetonitrile (50 ml) was added solid sodium azide (28.6 mg, 440 μmol). The resulting mixture was stirred for 24 hours at room temperature and was then filtered. Slow evaporation of the solvent gave 40 mg (31 μmol, 28 %) of $[Cu^{II}_2(HL^{M1})(N_3)_2]_n(BF_4)_n$ (**14**) in the form of a dark bottle green crystalline solid. Single crystals of $[Cu^{II}_4(HL^{M1})_2(\mu_{(1,1)}\text{-}N_3)_2(N_3)_2(MeCN)_2](BF_4)_2 \cdot MeCN$ (**14b** · MeCN) suitable for X-ray crystal structure determination were obtained by vapour diffusion of diethyl ether into the filtrate of the reaction mixture.

Elemental analysis (%) found: C 33.89, H 2.06, N 25.90; calcd. for $[Cu^{II}_2(HL^{M1})(N_3)_2]_n(BF_4)_n$, $C_{18}H_{15}BN_{12}O_2F_4Cu_2$ (645.29 g mol^{-1}): C 33.50, H 2.34, N 26.05 — IR (KBr, disk): $\tilde{\upsilon}$ (cm^{-1}) = 3417, 3075, 2072, 2063, 1610, 1577, 1566, 1478, 1462, 1404, 1385, 1346, 1289, 1234, 1158, 1124, 1083, 1067, 1026, 867, 774, 732, 689, 668, 651, 623, 587, 521, 499 — ESI-MS (MeCN): *m/z* (fragment) = 562.7, 517.8, 456.0, 410.0 ($[Cu^{II}(HL^{M1})]^+$), 277.2 ($[Cu^{II}_2(L^{M1})(MeCN)_2]^{2+}$), 256.7 ($[Cu^{II}_2(L^{M1})(MeCN)]^{2+}$), 226.3 ($[Cu^{II}(H_2L^{M1})(MeCN)]^{2+}$), 214.3 ($[Cu^{II}(H_2L^{M1})(H_2O)]^{2+}$), 205.8 ($[Cu^{II}(H_2L^{M1})]^{2+}$) — UV/VIS (MeCN, **14b**): λ_{max} (ε) = 384 (11500) 640 nm (1130 M^{-1} cm^{-1}) — Λ_m(DMF, **14b**) = 136 mol^{-1} cm^2 Ω^{-1}.

3.3.10. $[Cu^{II}_2(L^{M1})(N_3)_2]_n$ (15)

Caution! Azide derivatives are potentially explosive. Although no problems have been experienced during this work only small amounts of material should be prepared and these should be handled with the appropriate care.

To a dark navy blue solution of $[Cu^{II}_2(HL^{M1})(MeCN)_2(H_2O)_2](BF_4)_3$ (**6**) (28 mg, 33 µmol) in acetonitrile (15 ml) was added solid sodium azide (8.71 mg, 134 µmol). The resulting mixture was stirred for 2 days at room temperature. Filtration of the resulting suspension gave 18 mg (33 µmol, 100 %) of $[Cu^{II}_2(L^{M1})(N_3)_2]_n$ (**15**) in the form of a grass green amorphous solid.

Elemental analysis (%) found: C 38.90, H 2.33, N 29.69; calcd. for $[Cu^{II}_2(L^{M1})(N_3)_2]_n$, $C_{18}H_{14}N_{12}O_2Cu_2$ (557.48 g mol^{-1}): C 38.78, H 2.53, N 30.15 — IR (KBr, disk): $\tilde{\upsilon}$ (cm^{-1}) = 3448, 2054, 1633, 1609, 1592, 1586, 1566, 1485, 1429, 1381, 1343, 1285, 1152, 1026, 984, 933, 767, 716, 501, 495.

3.3.11. $[Cu^{II}_4(HL^{M2})_2(\mu_{(1,1)}\text{-}N_3)_2(N_3)_2(H_2O)_2](BF_4)_2 \cdot 2\,H_2O$ (16 · 2 H_2O) and $\{[Cu^{II}_2(HL^{M2})(\mu_{(1,3)}\text{-}N_3)_2](BF_4) \cdot MeCN\}_\infty$ (16b · MeCN)

Caution! Azide derivatives are potentially explosive. Although no problems have been experienced during this work only small amounts of material should be prepared and these should be handled with the appropriate care.

A dark navy blue solution of *N,N'*-bis[2-(2-pyridyl)ethyl]pyrazine-2,3-dicarboxamide (H_2L^{M2}) (188 mg, 500 µmol) and copper(II) tetrafluoroborate tetrahydrate (309 mg, 1.00 mmol) in acetonitrile (20 ml) was treated with solid sodium azide (65 mg, 1.0 mmol) and the resulting mixture was stirred for 24 hours at room temperature. Filtration of the resulting suspension gave 41 mg (58 µmol, 12 %) of $[Cu^{II}_2(HL^{M2})(N_3)_2]_n(BF_4)_n \cdot 2n\ H_2O$ (**16** · 2 H_2O) as a grass green microcrystalline solid. Addition of ethanol (10 ml) to the filtrate and slow evaporation of the solvent in air gave 123 mg (183 µmol, 37 %) of $\{[Cu^{II}_2(HL^{M2})(\mu_{(1,3)}\text{-}N_3)_2](BF_4)\}_\infty$ (**16b**) in the form of a dark bottle green crystalline solid. Single crystals of $\{[Cu^{II}_2(HL^{M2})(\mu_{(1,3)}\text{-}N_3)_2](BF_4) \cdot MeCN\}_\infty$ (**16b** · MeCN) suitable for X-ray crystal structure determination were obtained by this method.

16 · 2 H_2O: Elemental analysis (%) found: C 34.01, H 2.95, N 23.36; calcd. for $[Cu^{II}_2(HL^{M2})(N_3)_2]_n(BF_4)_n \cdot 2n\ H_2O$, $C_{20}H_{23}BN_{12}O_4F_4Cu_2$ (709.38 g mol^{-1}): C 33.86, H 3.27, N 23.69 — IR (KBr, disk): $\tilde{\nu}$ (cm^{-1}) = 3419, 3079, 2919, 2075, 2059, 1606, 1569, 1459, 1415, 1375, 1338, 1309, 1285, 1234, 1153, 1083, 1055, 1029, 971, 903, 845, 788, 771, 732, 686, 649, 595, 520 — Λ_m(DMF) = 306 $mol^{-1}\ cm^2\ \Omega^{-1}$.

16b: Elemental analysis (%) found: C 35.41, H 2.85, N 24.71; calcd. for $\{[Cu^{II}_2(HL^{M2})(N_3)_2](BF_4)\}_\infty$, $C_{20}H_{19}BN_{12}O_2F_4Cu_2$ (673.35 g mol^{-1}): C 35.68, H 2.84, N 24.96 — IR (KBr, disk): $\tilde{\nu}$ (cm^{-1}) = 3413, 3079, 2957, 2072, 2042, 1607, 1568, 1484, 1463, 1446, 1413, 1377, 1348, 1312, 1252, 1237, 1155, 1083, 1058, 1029, 966, 901, 893, 844, 789, 773, 754, 735, 682, 649, 581, 520 — ESI-MS (MeCN): *m/z* (fragment) = 377.1 ($[H_3L^{M2}]^+$), 189.1

($[H_4L^{M2}]^+$), 147.1 ($[Cu^I(H_4L^{M2})]^{3+}$) — UV/VIS (MeCN): λ_{max} (ε) = 257 (26000), 396 (6260), 625 nm (588 M^{-1} cm^{-1}) — Λ_m(DMF) = 129 mol^{-1} cm^2 Ω^{-1} (per ligand).

3.3.12. $[Cu^{II}_2(HL^{M1})(O_4C_8H_4)(H_2O)_2]_n(BF_4)_n \cdot 2n\ H_2O$ (17 · 2 H_2O)

To a dark navy blue solution of $[Cu^{II}_2(HL^{M1})(MeCN)_2(H_2O)_2](BF_4)_3$ (**6**) (30 mg, 35 µmol) in acetonitrile (10 ml) was added solid disodium terephthalate (6.5 mg, 35 µmol) and the mixture was treated with water (1 ml). The resulting suspension was stirred for 24 hours at room temperature. Filtration of the suspension gave 24 mg (15 µmol, 90 %) of $[Cu^{II}_2(HL^{M1})(O_4C_8H_4)(H_2O)_2]_n(BF_4)_n \cdot 2n\ H_2O$ (**17** · 2 H_2O) in the form of a dark sky blue microcrystalline solid.

Elemental analysis (%) found: C 39.18, H 3.21, N 10.25; calcd. for $[Cu^{II}_2(HL^{M1})(C_8H_4O_4)(H_2O)_2]_n(BF_4)_n \cdot 2n\ H_2O$, $C_{26}H_{27}BN_6O_{10}F_4Cu_2$ (797.43 g mol^{-1}): C 39.16, H 3.41, N 10.54 — IR (KBr, disk): $\tilde{\upsilon}$ (cm^{-1}) = 3446, 1683, 1636, 1565, 1506, 1484, 1443, 1409, 1386, 1287, 1214, 1153, 1124, 1083, 1026, 944, 891, 880, 864, 827, 784, 760, 737, 714, 496.

3.3.13. $[Cu^{II}_2(H_2L^{M1})_2(MeCN)_2](BF_4)_4$ (18)

To a solution of *N*,*N*'-bis(2-pyridylmethyl)pyrazine-2,3-dicarboxamide (H_2L^{M1}) (80.1 mg, 230 µmol) in acetonitrile (15 ml) was added a solution of copper(II) tetrafluoroborate tetrahydrate (71.1 mg, 230 µmol) in acetonitrile (10 ml) and the resulting dark navy blue solution was stirred at room temperature for 4 hours. By

vapour diffusion of diethyl ether into the reaction mixture, 97 mg (77 μmol, 67 %) of $[Cu^{II}_2(H_2L^{M1})_2(MeCN)_2](BF_4)_4$ (**18**) were obtained in the form of a navy blue crystalline solid. Single crystals of $[Cu^{II}_2(H_2L^{M1})_2(MeCN)_2](BF_4)_4$ (**18**) suitable for X-ray crystal structure determination were obtained by vapour diffusion of diethyl ether into a solution of **18** in acetonitrile.

Elemental analysis (%) found: C 38.33, H 2.99, N 15.37; calcd. for $[Cu^{II}_2(H_2L^{M1})_2(MeCN)_2](BF_4)_4$, $C_{40}H_{44}B_4N_{14}O_4F_{16}Cu_2$ (1253.14 g mol^{-1}): C 38.34, H 3.06, N 15.65 — IR (KBr, disk): $\tilde{\upsilon}$ (cm^{-1}) = 3416, 3066, 2937, 2803, 2733, 1668, 1644, 1618, 1577, 1564, 1539, 1471, 1447, 1423, 1388, 1349, 1319, 1287, 1213, 1145, 1083, 1035, 930, 882, 824, 775, 722, 667, 629, 549, 533, 521, 502, 463 — ESI-MS (MeCN): *m/z* (fragment) = 538.1 ($\{[Cu^{II}(HL^{M1})(MeCN)](BF_4)\}^+$), 410.1 ($[Cu^{II}(HL^{M1})]^+$), 349.2 ($[H_3L^{M1}]^+$), 226.1 ($[Cu^{II}(H_2L^{M1})(MeCN)]^{2+}$), 175.2 ($[H_4L^{M1}]^{2+}$) — UV/VIS (MeCN): λ_{max} (ε) = 262 (49500), 600 nm (299 M^{-1} cm^{-1}) — Λ_m(MeCN) = 576 mol^{-1} cm^2 Ω^{-1}.

3.3.14. $[Cu^{II}_4(H_2L^{M2})_2(HL^{M2})_2](BF_4)_6 \cdot 4\ H_2O$ (19 · 4 H_2O) and $[Cu^{II}_4(H_2L^{M2})_2(HL^{M2})_2](BF_4)_6 \cdot 3\ MeCN \cdot 0.5\ H_2O$ (19 · 3 MeCN · 0.5 H_2O)

To a solution of *N,N'*-bis[2-(2-pyridyl)ethyl]pyrazine-2,3-dicarboxamide (H_2L^{M2}) (75.3 mg, 200 μmol) in acetonitrile (10 ml) was added a solution of copper(II) tetrafluoroborate tetrahydrate (61.8 mg, 200 μmol) in acetonitrile (5 ml) and the resulting dark turquoise solution was stirred at room temperature for 2 hours. By vapour diffusion of diethyl ether into the reaction mixture, 108 mg (175 μmol, 88 %) of $[Cu^{II}_4(H_2L^{M2})_2(HL^{M2})_2](BF_4)_6 \cdot 4\ H_2O$ (**19** · 4 H_2O) were obtained in the form of turquoise-green feathery crystals. Single crystals of $[Cu^{II}_4(H_2L^{M2})_2(HL^{M2})_2](BF_4)_6 \cdot 3\ MeCN \cdot 0.5\ H_2O$ (**19** · 3 MeCN · 0.5 H_2O) suitable for

X-ray crystal structure determination were obtained by vapour diffusion of diethyl ether into a dilute (1 mg ml^{-1}) solution of **19** · 4 H_2O in acetonitrile.

Elemental analysis (%) found: C 40.82, H 3.71, N 14.58; calcd. for $[Cu^{II}_4(H_2L^{M2})_2(HL^{M2})_2](BF_4)_6 \cdot 4\ H_2O$, $[C_{80}H_{86}B_6N_{24}O_{12}F_{24}Cu_4]$ (2350.72 g mol^{-1}): C 40.88, H 3.69, N 14.30 — IR (KBr, disk): $\tilde{\nu}$ (cm^{-1}) = 3422, 3076, 2924, 2854, 1636, 1607, 1569, 1542, 1484, 1446, 1423, 1376, 1338, 1310, 1253, 1226, 1132, 1083, 1062, 1037, 904, 870, 770, 745, 681, 650, 626, 591, 576, 521 — ESI-MS (MeCN): *m/z* (fragment) = 438.0 ($[Cu^{II}(HL^{M2})]^+$), 377.1 ($[H_3L^{M2}]^+$), 189.3 ($[H_4L^{M2}]^{2+}$) — UV/VIS (MeCN): λ_{max} (ε) = 262 (87300), 622 nm (434 M^{-1} cm^{-1}) — Λ_m(MeCN) = 768 mol^{-1} cm^2 Ω^{-1}.

3.3.15. $[Fe^{II}(H_2L^{M1})(MeCN)]_n(BF_4)_{2n}$ (20)

To a solution of *N,N'*-bis(2-pyridylmethyl)pyrazine-2,3-dicarboxamide (H_2L^{M1}) (52.2 mg, 150 µmol) in acetonitrile (5 ml) was added a solution of iron(II) tetrafluoroborate hexahydrate (50.6 mg, 150 µmol) in acetonitrile (10 ml) and the resulting dark deep purple solution was stirred at room temperature for 4 hours. By vapour diffusion of diethyl ether into the reaction mixture, 57 mg (92 µmol, 61 %) of $[Fe^{II}(H_2L^{M1})(MeCN)]_n(BF_4)_{2n}$ (**20**) were obtained in the form of a dark blue solid.

Elemental analysis (%) found: C 38.82, H 3.54, N 15.39; calcd. for $[Fe^{II}(H_2L^{M1})(MeCN)]_n(BF_4)_{2n}$, $C_{20}H_{19}BN_7O_2F_4Fe$ (618.87 g mol^{-1}): C 38.82, H 3.09, N 15.84 — IR (KBr, disk): $\tilde{\nu}$ (cm^{-1}) = 3414, 1636, 1616, 1580, 1558, 1475, 1426, 1384, 1368, 1283, 1215, 1083, 1053, 891, 764, 690, 668, 627, 595, 533, 521, 472 — ESI-MS (MeCN): *m/z* (fragment) = 750.0 ($[Fe^{III}(HL^{M1})_2]^+$), 349.1 ($[H_3L^{M1}]^+$) — UV/VIS (MeCN): λ_{max} (ε) = 252 (20600), 358 (3060), 533 (shoulder) (5320), 658 nm (8140 M^{-1} cm^{-1}) — Λ_m(MeCN) = 281 mol^{-1} cm^2 Ω^{-1}.

3.3.16. $[Co^{III}(H_2L^{M1})_2](BF_4)_3 \cdot 4\,H_2O$ (21 · 4 H_2O)

To a solution of *N,N'*-bis(2-pyridylmethyl)pyrazine-2,3-dicarboxamide (H_2L^{M1}) (80.1 mg, 230 μmol) in acetonitrile (2 ml) was added a solution of cobalt(II) tetrafluoroborate hexahydrate (39.2 mg, 115 μmol) in acetonitrile (5 ml) and the resulting dark red-brown mixture was stirred at room temperature for 18 hours. By filtration of the resulting dark red-brown suspension, 64 mg (59 μmol, 51 %) of $[Co^{III}(H_2L^{M1})_2](BF_4)_3 \cdot 4\,H_2O$ (**21** · 4 H_2O) were isolated in the form of a dark red-brown solid.

Elemental analysis (%) found: C 39.49, H 3.24, N 15.28; calcd. for $[Co^{III}(H_2L^{M1})_2](BF_4)_3 \cdot 4\,H_2O$, $C_{36}H_{40}B_3N_{12}O_8F_{12}Co$ (1088.13 g mol^{-1}): C 39.74, H 3.71, N 15.45 — IR (KBr, disk): $\tilde{\nu}$ (cm^{-1}) = 3424, 3054, 2830, 1734, 1678, 1644, 1614, 1579, 1565, 1534, 1467, 1432, 1388, 1321, 1299, 1281, 1208, 1123, 1070, 1036, 928, 858, 764, 716, 628, 622, 533, 521, 488, 463 — ESI-MS (MeCN): *m/z* (fragment) = 928.7 ($\{[Co^{III}(H_2L^{M1})_2](BF_4)_2\}^+$), 840.7 ($\{[Co^{III}(H_2L^{M1})(HL^{M1})](BF_4)\}^+$), 753.1 ($[Co^{III}(HL^{M1})_2]^+$), 377.1 — UV/VIS (MeCN): λ_{max} (ε) = 250 (37700), 504 (shoulder) nm (984 M^{-1} cm^{-1}) — Λ_m(MeCN) = 391 mol^{-1} cm^2 Ω^{-1}.

3.3.17. $[Co^{III}(H_2L^{M2})_2](BF_4)_3 \cdot EtOH$ (22 · *EtOH*) *and* $[Co^{III}(H_2L^{M2})_2](BF_4)_3 \cdot 2\,EtOH$ (22 · 2 *EtOH*)

To a solution of *N,N'*-bis[2-(2-pyridyl)ethyl]pyrazine-2,3-dicarboxamide (H_2L^{M2}) (113 mg, 300 μmol) in acetonitrile (10 ml) was added a solution of cobalt(II) tetrafluoroborate hexahydrate (51.1 mg, 150 μmol) in acetonitrile (5 ml) and the resulting dark brick red mixture was stirred at room temperature for 4 hours. Ethanol (45 ml) was added and by slow evaporation of the solvent in air, 106 mg

(94.8 μmol, 63 %) of $[Co^{III}(H_2L^{M2})_2](BF_4)_3 \cdot EtOH$ (**22** · EtOH) were obtained in the form of a dark brick red crystalline solid. Single crystals of $[Co^{III}(H_2L^{M2})_2](BF_4)_3 \cdot 2\ EtOH$ (**22** · 2 EtOH) were obtained by slow evaporation of a solution of **22** · EtOH containing one part of acetonitrile and four parts of ethanol.

Elemental analysis (%) found: C 45.06, H 4.35, N 15.11; calcd. for $[Co^{III}(H_2L^{M2})_2](BF_4)_3 \cdot EtOH$, $C_{42}H_{46}B_3N_{12}O_5F_{12}Co$ (1118.25 g mol^{-1}): C 45.11, H 4.15, N 15.03 — ^1H NMR (500 MHz, d^3-MeCN): δ (ppm) = 8.68 (s, 2 H, 2 × pz*H*), 8.56 (s, 2 H, 2 × pz*H*), 8.20–8.10 (m, 4 H, 4 × 6-py*H*), 7.87 (t, J = 7.5 Hz, 2 H, 2 × N*H*), 7.70 (s, 2 H, 2 × 4-py*H*), 7.62 (s, 2 H, 2 × 4-py*H*), 7.41 (d, J = 7.5 Hz, 2 H, 2 × 3-py*H*), 7.32 (t, J = 6.3 Hz, 2 H, 2 × 3-py*H*), 7.16 (broad s, 4 H, 4 × 5-py*H*), 4.68 (d, J = 13.5 Hz, 2 H, 2 × pyN*H*), 3.77 (broad s, 8 H, 4 × NHCH_2), 3.30–3.24 (m, 8 H, 4 × pyCH_2) — IR (KBr, disk): $\tilde{\nu}$ (cm^{-1}) = 3415, 2944, 2852, 2758, 1652, 1559, 1478, 1446, 1418, 1373, 1300, 1255, 1220, 1142, 1083, 1062, 909, 869, 771, 750, 627, 596, 578, 533, 521, 491 — ESI-MS (MeCN): *m/z* (fragment) = 809.1 ($[Co^{III}(HL^{M2})_2]^+$) — UV/VIS (MeCN): λ_{max} (ε) = 623 (29800), 510 (shoulder) nm (257 $M^{-1}\ cm^{-1}$) — Λ_m(MeCN) = 356 $mol^{-1}\ cm^2\ \Omega^{-1}$.

3.3.18. $[Cu^{II}_4(HL^{M1})_4](BF_4)_4$ (23) and $[Cu^{II}_4(HL^{M1})_4](BF_4)_4 \cdot 3.5\ MeCN$ (23 · 3.5 MeCN)

a: To a solution of *N,N'*-bis(2-pyridylmethyl)pyrazine-2,3-dicarboxamide (H_2L^{M1}) (120 mg, 345 μmol) in acetonitrile (30 ml) was added a solution of copper(II) tetrafluoroborate tetrahydrate (107 mg, 345 μmol) in acetonitrile (20 ml). The dark navy blue solution was treated with triethylamine (34.9 mg, 345 μmol), and the resulting grass green solution was stirred at room temperature for 4 hours. By vapour diffusion of diethyl ether into the reaction mixture, 120 mg (60.3 μmol, 70 %) of $[Cu^{II}_4(HL^{M1})_4](BF_4)_4$ (**23**) were obtained in the form of shiny grass green octahedral

crystals. Strongly twinned crystals of the two different crystal types of $[Cu^{II}_4(HL^{M1})_4](BF_4)_4 \cdot 3.5$ MeCN (**23** · 3.5 MeCN) suitable for X-ray crystal structure determination were obtained by vapour diffusion of diethyl ether into a solution of **23** in acetonitrile.

b: A dark navy blue solution of $[Cu^{II}_2(H_2L^{M1})_2(MeCN)_2](BF_4)_4$ (**18**) (125 mg, 100 μmol) in acetonitrile (30 ml) was treated with a solution of triethylamine (20.2 mg, 200 μmol) in acetonitrile (10 ml) and the resulting grass green solution was stirred for 4 hours at room temperature. By vapour diffusion of diethyl ether into the reaction mixture, 60 mg (30 μmol, 60 %) of $[Cu^{II}_4(HL^{M1})_4](BF_4)_4$ (**23**) were obtained in the form of shiny grass green octahedral crystals.

Elemental analysis (%) found: C 43.71, H 3.31, N 17.39; calcd. for $[Cu^{II}_4(HL^{M1})_4](BF_4)_4$, $C_{72}H_{60}B_4N_{24}O_8F_{16}Cu_4$ (1990.82 g mol^{-1}): C 43.44, H 3.04, N 16.89 — IR (KBr, disk): $\tilde{\nu}$ (cm^{-1}) = 3456, 1651, 1482, 1438, 1386, 1315, 1287, 1211, 1124, 1083, 1035, 762, 612, 533, 521 — ESI-MS (MeCN): *m/z* (fragment) = 908.0 ($\{[Cu^{II}_4(HL^{M1})_4](BF_4)_2\}^{2+}$), 819.0 ($[Cu^{II}_4(L^{M1})_2(HL^{M1})_2]^{2+}$), 615.5 ($[Cu^{II}_6(L^{M1})_2(HL^{M1})_4]^{4+}$), 576.3 ($\{[Cu^{II}_4(HL^{M1})_4](BF_4)\}^{3+}$), 409.9 ($[Cu^{II}_4(HL^{M1})_4]^{4+}$), 349.1 ($[H_3L^{M1}]^+$) — UV/VIS (MeCN): λ_{max} (ε) = 262 (72500), 699 (331), 1290 (195 M^{-1} cm^{-1}) — Λ_m(MeCN) = 440 mol^{-1} cm^2 Ω^{-1}.

3.3.19. $[Cu^{II}_4(HL^{M1})_4](PF_6)_4$ (23b)

To a solution of *N,N'*-bis(2-pyridylmethyl)pyrazine-2,3-dicarboxamide (H_2L^{M1}) (400 mg, 1.15 mmol) in acetonitrile (50 ml) was added a solution of copper(II) tetrafluoroborate tetrahydrate (355 mg, 1.15 mmol) in acetonitrile (30 ml). The dark navy blue solution was treated with triethylamine (116 mg, 1.15 μmol), and the

resulting grass green solution was stirred at room temperature for 4 hours. Solid ammonium hexafluorophosphate (1.90 g, 11.7 mmol) was added and the resulting solution was filtered and then reduced in volume (to 30 ml). Ethanol (20 ml) was added and the resulting suspension was further reduced in volume (to 15 ml). Filtration of the suspension gave 400 mg of a grass green solid which was redissolved in acetonitrile (45 ml). The mixture was filtered and solid ammonium hexafluorophosphate (1.90 g, 11.7 mmol) was added. The solution was reduced in volume (to 20 ml) and ethanol (15 ml) was added. Filtration of the resulting grass green precipitate gave 332 mg (0.15 mmol, 51 %) of $[Cu^{II}_4(HL^{M1})_4](PF_6)_4$ (**23b**) in the form of a shiny grass green amorphous solid. An analytically pure crystalline sample of compound **23b** was obtained by vapour diffusion of diethyl ether into a solution of **23b** in acetonitrile.

Elemental analysis (%) found: C 39.05, H 2.66, N 15.51; calcd. for $[Cu^{II}_4(HL^{M1})_4](PF_6)_4$, $C_{72}H_{60}N_{24}O_8F_{24}P_4Cu_4$ (2223.47 g mol^{-1}): C 38.89, H 2.72, N 15.10 — IR (KBr, disk): $\tilde{\nu}$ (cm^{-1}) = 3417, 1640, 1615, 1564, 1463, 1418, 1381, 1289, 1211, 1124, 1054, 843, 766, 696, 622, 558 — ESI-MS (MeCN): *m/z* (fragment) = 456.0, 537.9, 410.0 ($[Cu^{II}(HL^{M1})]^+$), 349.1 ($[H_3L^{M1}]^+$), 266.0 ($[Cu^{II}(H_2L^{M1})(MeCN)]^{2+}$), 175 ($[H_4L^{M1}]^{2+}$) — Λ_m(MeCN) = 440 mol^{-1} cm^2 Ω^{-1}.

3.3.20. $[Cu^{II}_4(HL^{M2})_4](BF_4)_4$ (24)

To a solution of *N,N'*-bis[2-(2-pyridyl)ethyl]pyrazine-2,3-dicarboxamide (H_2L^{M2}) (400 mg, 1.06 mmol) in acetonitrile (60 ml) was added a solution of copper(II) tetrafluoroborate tetrahydrate (329 mg, 1.06 mmol) in acetonitrile (15 ml). The dark turquoise solution was treated with triethylamine (107 mg, 1.06 mmol) and the resulting dark bottle green solution was stirred at room temperature for 4 hours.

Toluene (220 ml) was added and a dark bottle green solid precipitated. Filtration of the solid gave 480 mg (0.23 mmol, 86 %) of $[Cu^{II}_4(HL^{M2})_4](BF_4)_4$ (**24**) in the form of a bottle green amorphous solid. Single crystals of **24** suitable for X-ray crystal structure determination were obtained by vapour diffusion of diethyl ether into a solution of **24** in acetonitrile.

Elemental analysis (%) found: C 45.36, H 3.63, N 15.77; calcd. for $[Cu^{II}_4(HL^{M2})_4](BF_4)_4$, $C_{80}H_{76}B_4N_{24}O_8F_{16}Cu_4$ (2103.04 g mol^{-1}): C 45.69, H 3.64, N 15.98 — IR (KBr, disk): $\tilde{\upsilon}$ (cm^{-1}) =.3417, 3074, 2924, 2838, 1636, 1569, 1539, 1484, 1446, 1422, 1373, 1332, 1310, 1250, 1225, 1133, 1083, 1060, 881, 771, 595, 520 — ESI-MS (MeCN): *m/z* (fragment) = 483.9, 438.0 ($[Cu^{II}(HL^{M2})]^+$), 377.1 ($[H_3L^{M2}]^+$), 189.3 ($[H_4L^{M2}]^{2+}$) — UV/VIS (MeCN): λ_{max} (ε) = 263 (73200), 656 (603), 803 nm (shoulder) (356 M^{-1} cm^{-1}) — Λ_m(MeCN) = 531 mol^{-1} cm^2 Ω^{-1}.

3.3.21. $[Ni^{II}_4(HL^{M2})_4](BF_4)_4 \cdot 10\ H_2O$ (25 · 10 H_2O) and $[Ni^{II}_4(HL^{M2})_4](BF_4)_4 \cdot 10$ MeCN (25 · 10 MeCN)

To a solution of *N,N'*-bis[2-(2-pyridyl)ethyl]pyrazine-2,3-dicarboxamide (H_2L^{M2}) (80.2 mg, 213 µmol) in acetonitrile (7 ml) was added a solution of nickel(II) tetrafluoroborate hexahydrate (72.5 mg, 213 µmol) in acetonitrile (5 ml). The pale brown solution was treated with a solution of triethylamine (21.6 mg, 213 µmol) in acetonitrile (4 ml) and the resulting dark red-brown solution was stirred at room temperature for 4 hours. By vapour diffusion of diethyl ether into the reaction mixture, 72 mg (32 µmol, 60 %) of $[Ni^{II}_4(HL^{M2})_4](BF_4)_4 \cdot 10\ H_2O$ (**25** · 10 H_2O) were obtained in the form of dark red-brown crystals. Single crystals of **25** · 10 MeCN suitable for X-ray crystal structure determination were obtained by vapour diffusion of diethyl ether into a solution of **25** · 10 H_2O in acetonitrile.

Elemental analysis (%) found: C 42.53, H 3.91, N 14.70; calcd. for $[Ni^{II}_4(HL^{M2})_4](BF_4)_4 \cdot 10\ H_2O$, $C_{80}H_{96}B_4N_{24}O_{18}F_{16}Ni_4$ (2263.77 g mol^{-1}): C 42.45, H 4.27, N 14.85 — IR (KBr, disk): $\tilde{\upsilon}$ (cm^{-1}) = 3419, 1652, 1605, 1562, 1464, 1443, 1413, 1371, 1346, 1307, 1238, 1145, 1083, 1063, 1031, 976, 898, 847, 769, 735, 680, 643, 588, 521 — ESI-MS (MeCN): *m/z* (fragment) = 997.0 ($\{[Ni^{II}_4(H_2L^{M2})(HL^{M2})_3](BF_4)_3\}^{2+}$), 973.0 ($\{[Ni^{II}_4(H_2L^{M2})_2(HL^{M2})_2(H_2O)_2](BF_4)_2\}^{2+}$), 953.1 ($\{[Ni^{II}_4(HL^{M2})_4](BF_4)_2\}^{2+}$), 909.2 ($\{[Ni^{II}_4(HL^{M2})_3(L^{M2})](BF_4)_3\}^{2+}$), 683.8 ($\{[Ni^{II}_4(H_2L^{M2})_2(HL^{M2})_2(H_2O)_3](BF_4)_3\}^{3+}$), 653.3, 620.0 ($\{[Ni^{II}Ni^{II}_3(H_2L^{M2})_3(HL^{M2})(H_2O)_2](BF_4)\}^{3+}$), 606.7 ($\{[Ni^{II}_4(HL^{M2})_4](BF_4)\}^{3+}$), 598.4, 577.5 ($[Ni^{II}_4(HL^{M2})_3(L^{M2})]^{3+}$), 433.0 ($[Ni^{II}_4(HL^{M2})_4]^{4+}$), 377.2 ($[H_3L^{M2}]^+$), 189.4 ($[H_4L^{M2}]^{2+}$) — UV/VIS (MeCN): λ_{max} (ε) = 260 (50000), 853 nm (89 M^{-1} cm^{-1}) — Λ_m(MeCN) = 454 mol^{-1} cm^2 Ω^{-1}.

3.3.22. $[Ni^{II}_4(HL^{M1})_4](BF_4)_4 \cdot 4\ H_2O$ (26 · 4 H_2O)

To a solution of *N,N'*-bis(2-pyridylmethyl)pyrazine-2,3-dicarboxamide (H_2L^{M1}) (80.1 mg, 230 µmol) in *N,N*-dimethylformamide (5 ml) was added a solution of nickel(II) tetrafluoroborate hexahydrate (78.3 mg, 230 µmol) in *N,N*-dimethyl-formamide (3 ml). The resulting brown solution was treated with a solution of sodium hydroxide (9.5 mg, 230 µmol) in *N,N*-dimethylformamide/water (5:1, 6 ml) and the resulting dark red-brown solution was stirred for 8 hours at room temperature. By vapour diffusion of diethyl ether into the reaction mixture, 80 mg (40 µmol, 70 %) of $[Ni^{II}_4(HL^{M1})_4](BF_4)_4 \cdot 4\ H_2O$ (**26** · 4 H_2O) were obtained in the form of dark red-brown octahedral crystals.

Elemental analysis (%) found: C 42.33, H 3.73, N 16.70; calcd. for $[Ni^{II}_4(HL^{M1})_4](BF_4)_4 \cdot 4\ H_2O$, $C_{72}H_{68}B_4N_{24}O_{12}F_{16}Ni_4$ (2043.46 g mol^{-1}): C 42.32, H 3.35, N 16.45 — IR (KBr, disk): $\tilde{\upsilon}$ (cm^{-1}) = 3424, 1606, 1565, 1483, 1408, 1374, 1347, 1286, 1240,

1151, 1083, 1050, 1036, 886, 804, 760, 709, 682, 645, 621, 533, 521, 502, 467, 423 — ESI-MS (MeCN): *m/z* (fragment) = 897.2 ($\{[Ni^{II}_4(HL^{M1})_4](BF_4)_2\}^{2+}$), 853.7 ($\{[Ni^{II}_4(HL^{M1})_3(L^{M1})](BF_4)\}^{2+}$), 809.3 ($[Ni^{II}_4(HL^{M1})_2(L^{M1})_2]^{2+}$), 569.5 ($\{[Ni^{II}_4(HL^{M1})_4](BF_4)\}^{3+}$), 540.2 ($[Ni^{II}_4(HL^{M1})_3(L^{M1})]^{3+}$), 406.1 ($[Ni^{II}_4(HL^{M1})_4]^{4+}$), 349 ($[H_3L^{M1}]^+$), 175.4 ($[H_4L^{M1}]^{2+}$) — UV/VIS (MeCN): λ_{max} (ε) = 261 (43000), 307 (shoulder) (23600), 853 nm (184 M^{-1} cm^{-1}) — Λ_m(DMF) = 285 mol^{-1} cm^2 Ω^{-1}.

3.3.23. $[Ni^{II}_4(HL^{M1})_4](PF_6)_4$ (26b)

To a solution of *N,N'*-bis(2-pyridylmethyl)pyrazine-2,3-dicarboxamide (H_2L^{M1}) (240 mg, 696 μmol) in *N,N*-dimethylformamide (5 ml) was added a solution of nickel(II) tetrafluoroborate hexahydrate (237 mg, 696 μmol) in *N,N*-dimethylformamide (10 ml). The resulting brown solution was treated with a solution of sodium hydroxide (28.5 mg, 696 μmol) in *N,N*-dimethylformamide/water (5:1, 10 ml) and the resulting dark red-brown solution was stirred for 8 hours at room temperature. The dark brown solution was then evaporated to dryness under reduced pressure. The resulting dark red-brown solid was redissolved in *N,N*-dimethylformamide (50 ml) and the solution was treated with solid ammonium hexafluorophosphate (1.13 g, 6.96 mmol) and was then reduced in volume under reduced pressure (to 10 ml). With ethanol (20 ml), 261 mg (118 μmol, 68 %) of $[Ni^{II}_4(HL^{M1})_4](PF_6)_4$ (**26b**) were precipitated. Crystalline samples of **26b** were obtained by vapour diffusion of diethyl ether into solutions of **26b** in *N,N*-dimethylformamide or acetonitrile.

Elemental analysis (%) found: C 39.05, H 3.09, N 15.13; calc. for $[Ni^{II}_4(HL^{M1})_4](PF_6)_4$, $C_{72}H_{60}N_{24}O_8F_{24}P_4Ni_4$ (2204.04 g mol^{-1}): C 39.24, H 2.74, N 15.25 — IR (KBr, disk): $\tilde{\nu}$ (cm^{-1}) = 3417, 1636, 1617, 1566, 1483, 1409, 1389, 1287, 1237, 1150,

1121, 1083, 1049, 1021, 845, 761, 678, 618, 559, 467 — ESI-MS (MeCN): *m/z* (fragment) = 1911.8 ($[Ni^{II}_4(HL^{M1})(L^{M1})_3]^+$), 1765.6 ($\{[Ni^{II}_4(HL^{M1})_2(L^{M1})_2](PF_6)\}^+$), 1619.0 ($[Ni^{II}_4(HL^{M1})(L^{M1})_3]^+$), 957.9 ($\{[Ni^{II}_4(HL^{M1})_4](PF_6)_2\}^{2+}$), 883.9 ($\{[Ni^{II}_4(HL^{M1})_3(L^{M1})](PF_6)\}^{2+}$), 809.0 ($[Ni^{II}_4(HL^{M1})_2(L^{M1})_2]^{2+}$), 589.0 ($[Ni^{II}_4(HL^{M1})_4](PF_6)\}^{3+}$), 404.9 ($[Ni^{II}_4(HL^{M1})_4]^{4+}$).

3.3.24. $[Ni^{II}_4(HL^{M1})_4](NO_3)_4 \cdot 4\,H_2O$ (26c · 4 H₂O)

To a solution of *N,N'*-bis(2-pyridylmethyl)pyrazine-2,3-dicarboxamide (H_2L^{M1}) (100 mg, 287 μmol) in *N,N*-dimethylformamide (5 ml) was added a solution of nickel(II) nitrate hexahydrate (83 mg, 287 μmol) in *N,N*-dimethylformamide (5 ml). The resulting brown solution was treated with a solution of sodium hydroxide (11.5 mg, 287 μmol) in *N,N*-dimethylformamide/water (5:1, 6 ml) and the resulting dark red-brown solution was stirred for 8 hours at room temperature. By vapour diffusion of diethyl ether into the reaction mixture, 114 mg (58.6 μmol, 82 %) of $[Ni^{II}_4(HL^{M1})_4](NO_3)_4 \cdot 4\,H_2O$ (**26c** · 4 H_2O) were obtained in the form of dark red-brown crystals.

Elemental analysis (%) found: C 44.39, H 3.84, N 19.83; calcd. for $[Ni^{II}_4(HL^{M1})_4](NO_3)_4 \cdot 4\,H_2O$, $C_{72}H_{68}N_{28}O_{24}Ni_4$ (1944.27 g mol^{-1}): C 44.48, H 3.53, N 20.17 — IR (KBr, disk): $\tilde{\upsilon}$ (cm^{-1}) = 3421, 1653, 1606, 1564, 1481, 1383, 1286, 1240, 1152, 1049, 1021, 884, 761, 706, 645, 620, 503 — ESI-MS (MeCN): *m/z* (fragment) = 864.6, 856.6 ($\{[Ni^{II}_4(HL^{M1})_4](NO_3)_2\}^{2+}$), 849.6, 571.4, 566.1, 561.4 ($\{[Ni^{II}_4(HL^{M1})_4](NO_3)\}^{3+}$), 349.2 ($[H_3L^{M1}]^+$), 175.1 ($[H_4L^{M1}]^{2+}$).

3.3.25. $[Cu^{II}(HL^{S1})(H_2O)]_n(BF_4)_n$ (30)

To a suspension of *N,N'*-bis(2-pyridylmethyl)pyrazine-2,5-dicarboxamide (H_2L^{S1}) (100 mg, 287 μmol) in acetonitrile (25 ml) was added a solution of copper(II) tetrafluoroborate tetrahydrate (88.7 mg, 287 μmol) in acetonitrile (25 ml) and the resulting turquoise solution was stirred at room temperature for 30 minutes. The mixture was treated with a solution of triethylamine (29.0 mg, 287 μmol) in acetonitrile (20 ml). Reduction of the solvent volume under reduced pressure (to 20 ml) and addition of toluene (60 ml) afforded 102 mg (198 μmol, 69 %) of $[Cu^{II}(HL^{S1})(H_2O)]_n(BF_4)_n$ (**30**) in the form of a turquoise amorphous solid.

Elemental analysis (%) found: C 41.92, H 4.01, N 16.85; calcd. for $[Cu^{II}(HL^{S1})(H_2O)]_n(BF_4)_n$, $C_{18}H_{17}BN_6O_3F_4Cu$ (515.72 g mol^{-1}): C 41.92, H 3.32, N 16.30 — IR (KBr, disk): $\tilde{\upsilon}$ (cm^{-1}) = 3412, 1674, 1638, 1612, 1566, 1529, 1483, 1436, 1402, 1348, 1287, 1212, 1160, 1083, 1038, 923, 805, 766, 718, 668, 651, 616, 533, 521, 489, 468 — ESI-MS (MeCN): *m/z* (fragment) = 818.9 ($[Cu^{II}_2(HL^{S1})(L^{S1})]^+$), 757.8 ($[Cu^{I}(H_2L^{S1})_2]^+$), 450.9 $[(Cu^{II}(HL^{S1})(MeCN)]^+$), 316.6 — UV/VIS ($H_2O$): λ_{max} (ε) = 217 (18350), 261 (15600), 330 (shoulder) (2960), 640 nm (88 M^{-1} cm^{-1}) — $\Lambda_m(H_2O)$ = 119 mol^{-1} cm^2 Ω^{-1}.

3.3.26. $[Cu^{II}(HL^{S1})]_n(ClO_4)_n$ (31)

Caution! Perchlorate salts of metal complexes with organic ligands are potentially explosive. Although no problems have been experienced during this work only small amounts of material should be prepared and these should be handled with the appropriate care.

To a suspension of *N,N'*-bis(2-pyridylmethyl)pyrazine-2,5-dicarboxamide (H_2L^{S1}) (69.7 mg, 200 μmol) in *N,N*-dimethylformamide (5 ml) was added a solution of copper(II) perchlorate hexahydrate (74.1 mg, 200 μmol) in *N,N*-dimethylformamide (5 ml) and the resulting deep bottle green solution was stirred at room temperature for 30 minutes. The mixture was then treated with a solution of triethylamine (20.2 mg, 200 μmol) in *N,N*-dimethylformamide (5 ml). By vapour diffusion of diethyl ether into the reaction mixture, 87.8 mg (172 μmol, 86 %) of $[Cu^{II}(HL^{S1})]_n(ClO_4)_n$ (**31**) were isolated in the form of a grey-blue crystalline solid.

Elemental analysis (%) found: C 42.35, H 3.33, N 16.36; calcd. for $[Cu^{II}(HL^{S1})]_n(ClO_4)_n$, $C_{18}H_{15}N_6O_6ClCu$ (510.35 g mol^{-1}): C 42.36, H 2.96, N 16.47 — IR (KBr, disk): $\tilde{\upsilon}$ (cm^{-1}) = 3420, 1679, 1656, 1612, 1566, 1522, 1483, 1438, 1408, 1346, 1311, 1287, 1255, 1213, 1146, 1116, 1081, 998, 924, 862, 764, 716, 692, 662, 624, 558, 533, 511, 489.

3.3.27. $[Cu^{II}_4(L^{S1})_4] \cdot 6\,H_2O$ ($32 \cdot 6\,H_2O$)

To a solution of *N,N'*-bis(2-pyridylmethyl)pyrazine-2,5-dicarboxamide (H_2L^{S1}) (50.2 mg, 144 μmol) in *N,N*-dimethylformamide (20 ml) was added a solution of copper(II) tetrafluoroborate tetrahydrate (44.5 mg, 144 μmol) in *N,N*-dimethylformamide (20 ml) and the resulting dark grass green solution was stirred at room temperature for 1 hour. Then the mixture was treated with a solution of triethylamine (29.1 mg, 288 μmol) in *N,N*-dimethylformamide (20 ml) and was left for 18 hour to stir at room temperature. By vapour diffusion of diethyl ether into the bright grass green solution, 7.0 mg (4.0 μmol, 11 %) of $[Cu^{II}_4(\mathbf{L}^{S1})_4] \cdot 6\,H_2O$ (**32** · 6 H_2O) were obtained in the form of very tiny grass green octahedrally shaped crystals.

Elemental analysis (%) found: C 49.56, H 4.04, N 18.85; calcd. for $[Cu^{II}_4(L^{S1})_4] \cdot 6\ H_2O$, $C_{72}H_{68}N_{24}O_{14}Cu_4$ (1747.67 g mol^{-1}): C 49.48, H 3.92, N 19.23 — IR (KBr, disk): $\tilde{\nu}$ (cm^{-1}) = 3443, 1606, 1566, 1481, 1430, 1397, 1348, 1325, 1286, 1211, 1154, 1083, 1047, 923, 763, 720, 623, 518.

3.3.28 *$[Cu^{II}_2(L^{S1})(H_2O)_2](BF_4)_2$ (33) and $[Cu^{II}_2(L^{S1})(H_2O)_2(MeCN)_2](BF_4)_2 \cdot H_2O$ (33b · H₂O)*

To a hot (60 °C) solution of *N,N'*-bis(2-pyridylmethyl)pyrazine-2,5-dicarboxamide (H_2L^{S1}) (84.0 mg, 241 µmol) in acetonitrile (10 ml) was added a solution of copper(II) tetrafluoroborate tetrahydrate (149 mg, 482 µmol) in acetonitrile (10 ml) and the resulting dark bottle green solution was left at that temperature for 10 minutes and was then allowed to cool to room temperature. By vapour diffusion of diethyl ether into the reaction mixture, 106 mg (155 µmol, 64 %) of $[Cu^{II}_2(\mathbf{L}^{S1})(H_2O)_2](BF_4)_2$ (**33**) were obtained in the form of a dark turquoise solid. Single crystals of $[Cu^{II}_2(\mathbf{L}^{S1})(H_2O)_2(MeCN)_2](BF_4)_2 \cdot H_2O$ (**33b** · H_2O) suitable for X-ray crystal structure determination were obtained by slow evaporation of the reaction mixture.

Elemental analysis (%) found: C 31.86, H 2.23, N 12.30; calcd. for $[Cu^{II}_2(L^{S1})(H_2O)_2](BF_4)_2$, $C_{18}H_{18}B_2N_6O_4F_8Cu_2$ (683.08 g mol^{-1}): C 31.65, H 2.66, N 12.30 — IR (KBr, disk): $\tilde{\nu}$ (cm^{-1}) = 3424, 3110, 2897, 1634, 1567, 1485, 1449, 1436, 1416, 1361, 1350, 1335, 1288, 1214, 1190, 1167, 1083, 1062, 923, 772, 743, 715, 656, 635, 585, 556, 533, 521, 465, 415 — ESI-MS (MeCN): *m/z* (fragment) = 571.5 ($[Cu^{I}Cu^{II}(L^{S1})(H_2O)(MeCN)_2]^+$), 531.7 ($[Cu^{I}Cu^{II}(L^{S1})(H_2O)(MeCN)]^+$), 450.7 ($[Cu^{II}(HL^{S1})(MeCN)]^+$), 276.9 ($[Cu^{II}_2(L^{S1})(MeCN)_2]^{2+}$), 237.9 ($Cu^{I}_2(H_2L^{S1})]^{2+}$), 225.9

($[Cu^{II}(H_2L^{S1})(MeCN)]^{2+}$) — UV/VIS (MeCN): λ_{max} (ε) = 212 (34100), 261 (20500), 349 (4200), 641 nm (204 M^{-1} cm^{-1}) — Λ_m(MeCN) = 231 mol^{-1} cm^2 Ω^{-1}.

3.3.29. *$[Cu^{II}_2(L^{S1})](SiF_6) \cdot n\ H_2O$ (34): $[Cu^{II}_2(L^{S1})(H_2O)_4](SiF_6) \cdot 0.5\ H_2O$ (34b · 0.5 H_2O) and $\{[Cu^{II}_2(L^{S1})(H_2O)_2(SiF_6)] \cdot 4\ H_2O\}_\infty$ (34c · 4 H_2O)*

Solid *N,N'*-bis(2-pyridylmethyl)pyrazine-2,5-dicarboxamide (H_2L^{S1}) (40.1 mg, 115 μmol) was treated with a solution of copper(II) tetrafluoroborate tetrahydrate (71.1 mg, 230 μmol) in water (5 ml) and the resulting dark bottle green solution was further treated with a solution of triethylamine (23.3 mg, 230 μmol) in water (3 ml). The resulting blue-green solution was transferred into a sample vial (SAMCO specimen tubes – Soda glass, 75 × 25/26 mm, ISO 9002) and was left to slowly evaporate. After 4 weeks 66 mg (96 μmol, 83 %) of $[Cu^{II}_2(\mathbf{L}^{S1})](SiF_6) \cdot n\ H_2O$ (*n* = 4) (**34**) were isolated by filtration, in the form of huge blue-green crystal blocks. Single crystals suitable for X-ray crystal structure determination of $[Cu^{II}_2(\mathbf{L}^{S1})(H_2O)_4](SiF_6) \cdot 0.5\ H_2O$ (**34b** · 0.5 H_2O) and $\{[Cu^{II}_2(\mathbf{L}^{S1})(H_2O)_2(SiF_6)] \cdot 4\ H_2O\}_\infty$ (**34c** · 4 H_2O) could be isolated from the crystal blocks **34**.

Elemental analysis (%) found: C 31.45, H 3.23, N 12.08; calcd. for $[Cu^{II}_2(\mathbf{L}^{S1})](SiF_6) \cdot 4\ H_2O$, $C_{18}H_{22}N_6O_6F_6SiCu_2$ (687.58 g mol^{-1}): C 31.44, H 3.23, N 12.22 — IR (KBr, disk): $\tilde{\upsilon}$ (cm^{-1}) = 3442, 3084, 2872, 1628, 1563, 1481, 1449, 1407, 1352, 1289, 1214, 1193, 1163, 1111, 1083, 1060, 1026, 981, 961, 923, 780, 750, 651, 556, 512, 472, 417 — ESI-MS (MeCN): *m/z* (fragment) = 451.1 ($[Cu^{II}(\mathbf{L}^{S1})(MeCN)_2]^+$), 349.2 ($[H_3\mathbf{L}^{S1}]^+$) — ESI-MS (negative) (MeCN): *m/z* (fragment) = 123.0 ($[SiF_5]^-$).

3.3.30. *$[Cu^{II}_2(L^{S2})](BF_4)_2 \cdot$ solvent (35): $[Cu^{II}_2(L^{S2})(H_2O)_2(MeCN)_2](BF_4)_2$ (35b) and $[Cu^{II}_2(L^{S2})(H_2O)_4(BF_4)_2] \cdot 2\ H_2O$ (35c · 2 H_2O)*

To a hot (60 °C) solution of *N,N'*-bis[2-(2-pyridyl)ethyl]pyrazine-2,3-dicarboxamide (H_2L^{S2}) (75.3 mg, 200 μmol) in acetonitrile (20 ml) was added a solution of copper(II) tetrafluoroborate tetrahydrate (124 mg, 400 μmol) in acetonitrile (10 ml). The resulting bottle green suspension was stirred at that temperature for 2 hours until the ligand had dissolved, and the solution was stirred for a further 10 hours at room temperature. Filtration of the bottle green precipitate gave 74.2 mg (104 μmol, 52 %) of $[Cu^{II}_2(\mathbf{L}^{S2})](BF_4)_2 \cdot 0.5$ MeCN · H_2O (**35**) in the form of a microcrystalline solid. Single crystals of $[Cu^{II}_2(\mathbf{L}^{S2})(H_2O)_4(BF_4)_2] \cdot 2\ H_2O$ (**35c** · 2 H_2O) suitable for X-ray crystal structure determination were obtained by slow evaporation of a solution of **35** in acetonitrile/ethanol (1:1). Single crystals of $[Cu^{II}_2(\mathbf{L}^{S1})(H_2O)_2(MeCN)_2](BF_4)_2$ (**35b**) suitable for X-ray crystal structure determination were obtained by vapour diffusion of diethyl ether into the reaction filtrate of an analogous 1:1 molar reaction of ligand to copper(II) tetrafluoroborate tetrahydrate.

Elemental analysis (%) found (2:1 reaction): C 34.94, H 3.26, N 13.30; calcd. for $[Cu^{II}_2(\mathbf{L}^{S2})](BF_4)_2 \cdot 0.5$ MeCN · H_2O, $C_{21}H_{21.5}B_2N_{6.5}O_3F_8Cu_2$ (713.65 g mol^{-1}): C 35.34, H 3.04, N 12.76; found (1:1 reaction): C 34.59, H 3.31, 12.71; calcd. for $[Cu^{II}_2(\mathbf{L}^{S2})](BF_4)_2 \cdot H_2O$, $C_{20}H_{20}B_2N_6O_3F_8Cu_2$ — IR (KBr, disk): $\tilde{\nu}$ (cm^{-1}) = 3423, 1607, 1539, 1484, 1445, 1400, 1336, 1307, 1254, 1210, 1083, 1034, 869, 770, 688, 626, 590, 533, 521 — ESI-MS (MeCN): *m/z* (fragment) = 1058.7 ($[(Cu^{II}_2(HL^{S2})(MeCN)(H_2O)_3]^+$) — UV/VIS (MeCN): λ_{max} (ε) = 261 (26400), 346 (2930), 647 nm (113 M^{-1} cm^{-1}) — Λ_m(MeCN) = 186 mol^{-1} cm^2 Ω^{-1}.

3.3.31. *$[Co^{III}_4(L^{S2})_4](BF_4)_4 \cdot 10\ H_2O$ (36 · 10 H_2O) and $[Co^{III}_4(L^{S2})_4](BF_4)_4 \cdot 12.75$ MeCN (36 · 12.75 MeCN)*

A suspension of *N,N'*-bis[2-(2-pyridyl)ethyl]pyrazine-2,3-dicarboxamide (H_2L^{S2}) (226 mg, 600 μmol) in acetonitrile (30 ml) was treated with a solution of cobalt(II) tetrafluoroborate hexahydrate (204 mg, 600 μmol) in acetonitrile (15 ml). The resulting cherry red solution was stirred at room temperature for 1 hour and was then treated with a solution of triethylamine (121 mg, 1.20 mmol) in acetonitrile (15 ml). By vapour diffusion of diethyl ether into the resulting red-brown reaction mixture, 288 mg (127 μmol, 85 %) of $[Co^{III}_4(L^{S2})_4](BF_4)_4 \cdot 10\ H_2O$ (**36** · 10 H_2O) were obtained in the form of red-brown crystal plates. Single crystals of $[Co^{III}_4(L^{S2})_4](BF_4)_4 \cdot 12.75$ MeCN (**36** · 12.75 MeCN) suitable for X-ray crystal structure determination were obtained by vapour diffusion of diethyl ether into a solution of **36** · 10 H_2O in acetonitrile.

Elemental analysis (%) found: C 42.25, H 4.04, N 14.59; calcd. for $[Co^{III}_4(L^{S2})_4](BF_4)_4 \cdot 10\ H_2O$, $C_{80}H_{92}B_4N_{24}O_{18}F_{16}Co_4$ (2260.71 g mol^{-1}): C 42.50, H 4.10, N 14.87 — ^{1}H NMR (500 MHz, d^3-MeCN): δ (ppm) = 8.23 (s, 8 H, 8 × pz*H*), 7.88 (d, J = 7.0 Hz, 8 H, 8 × 6-py*H*), 7.79 (t, $^3J_{4,5} = {}^3J_{4,3}$ = 7.0 Hz, 8 H, 8 × 4-py*H*), 7.35 (d, J = 7.0 Hz, 8 H, 8 × 3-py*H*), 6.95 (t, $^3J_{5,6} = {}^3J_{5,4}$ = 7.0 Hz, 8 H, 8 × 5-py*H*), 4.58 (d, J = 14 Hz, 8 H, 8 × ½ NCH_2), 3.52 (t, J = 17 Hz, 8 H, 8 × ½ NCH_2), 3.21 (d, J = 17 Hz, 8 H, 8 × ½ pyCH_2), 2.23 (t, J = 14 Hz, 8 H, 8 × ½ pyCH_2) — ^{13}C{^{1}H} NMR (75 MHz, d^3-MeCN): δ (ppm) = 168.5 (pzCO), 165.3 (2-*py*), 154.3 (6-*py*), 153.2 (*pz*CO), 148.4 (*pz*H), 142.4 (4-*py*), 129.7 (3-*py*), 125.6 (5-*py*), 42.0 (NCH_2), 37.6 ($pyCH_2$) — IR (KBr, disk): $\tilde{\nu}$ (cm^{-1}) = 3414, 1623, 1479, 1445, 1400, 1334, 1299, 1253, 1236, 1216, 1083, 1063, 1036, 864, 768, 667, 602, 550, 520, 467 — ESI-MS (MeCN): *m/z* (fragment) = 887.3 ({$[Co^{III}_2Co^{II}_2(L^{S2})_4] \cdot MeCN\}^{2+}$), 866.8 ($[Co^{III}_2Co^{II}_2(L^{S2})_4]^{2+}$), 619.8 ({$[Co^{III}_3Co^{II}(L^{S2})_4] \cdot 3\ MeCN\}^{3+}$), 605.2 ({$[Co^{III}_3Co^{II}(L^{S2})_4] \cdot 2\ MeCN\}^{3+}$), 591.5 ({$[Co^{III}_3Co^{II}(L^{S2})_4] \cdot MeCN\}^{3+}$), 577.9 ($[Co^{III}_3Co^{II}(L^{S2})_4]^{3+}$), 453.7 ({$[Co^{III}_4(L^{S2})_4] \cdot 2\ MeCN\}^{4+}$), 443.4 ({$[Co^{III}_4(L^{S2})_4] \cdot MeCN\}^{4+}$), 433.4 ($[Co^{III}_4(L^{S2})_4]^{4+}$) —

UV/VIS (MeCN): λ_{max} (ε) = 225 (156900), 437 nm (5580 M^{-1} cm^{-1}) — Λ_m(MeCN) = 531 mol^{-1} cm^2 Ω^{-1}.

3.4. *Crystal Data*

3.4.1. H_2L^{M2}

The asymmetric unit of $H_2\mathbf{L}^{M2}$ consisted of one neutral ligand molecule $H_2\mathbf{L}^{M2}$. All non-hydrogen atoms were refined anisotropically. All hydrogen atoms were placed at calculated positions using a riding model except for the amide protons H(2B) and H(5A), which were located from the difference map and were allowed to refine freely. All other hydrogen atoms had thermal parameters 1.2 times the equivalent isotropic thermal parameter of the atom to which they were bonded.

Table 3.4.1. Crystal data and structure refinement of $H_2\mathbf{L}^{M2}$.

Empirical formula	$C_{20}H_{20}N_6O_2$	
Formula weight M_r	376.42 g mol^{-1}	
Temperature T	83(2) K	
Wavelength	0.71073 Å	
Crystal system	Monoclinic	
Space group	$P2(1)/n$	
Unit cell dimensions	a = 5.0400(2) Å	α = 90°
	b = 20.6432(6) Å	β = 93.204(2)°
	c = 17.8496(2) Å	γ = 90°
Volume V	1854.20(9) $Å^3$	
Z	4	
Density $\rho_{cacld.}$	1.348 g cm^{-3}	
Absorption coefficient μ	0.092 mm^{-1}	

$F(000)$	792
Crystal colour and shape	Colourless needles
Crystal size	0.26 × 0.06 × 0.05 mm^3
θ range for data collection	$1.51° \leq \theta \leq 25.69°$
Index ranges	$-5 \leq h \leq 6$, $-25 \leq k \leq 24$, $-20 \leq l \leq 21$
Reflections collected	10187
Independent reflections	3494 [$R_{int} = 0.0765$]
Completeness to $\theta = 25.69°$	99.2 %
Absorption correction	Semi-empirical (SADABS)
Max. / min. transmission	0.9954 / 0.9766
Refinement method	Full-matrix least-squares on F^2
Data / restraints / parameters	3494 / 0 / 261
Goodness-of-fit on F^2	1.063
Final R indices [$I>2\sigma(I)$]	$R1 = 0.0604$, $wR2 = 0.1066$
R indices (all data)	$R1 = 0.1226$, $wR2 = 0.1315$
Largest diff. peak / hole	0.256 / –0.279 e Å^{-3}

Table 3.4.2. Atomic coordinates (× 10^4) and equivalent isotropic displacement parameters U_{eq} (× 10^3) [Å^2] for $H_2\mathbf{L^{M2}}$.

Atom	x	y	z	U_{eq}
O(1)	–4473(4)	4698(1)	–2908(1)	24(1)
O(2)	–3928(4)	3744(1)	–1753(1)	23(1)
N(1)	–3392(5)	3375(1)	–4107(1)	22(1)
N(2)	–6993(4)	4358(1)	–3922(1)	19(1)
N(3)	–10876(4)	6261(1)	–4537(1)	23(1)
N(4)	209(5)	3015(1)	–2925(1)	23(1)
N(5)	532(5)	3933(1)	–1706(1)	22(1)
N(6)	4(5)	3560(1)	846(1)	32(1)
C(1)	–1689(6)	2883(1)	–4169(2)	23(1)
C(2)	148(6)	2721(1)	–3599(2)	24(1)
C(3)	–1592(5)	3489(1)	–2842(2)	18(1)
C(4)	–3313(5)	3689(1)	–3445(2)	17(1)
C(5)	–4984(5)	4289(1)	–3400(2)	19(1)
C(6)	–8623(5)	4944(1)	–3923(2)	21(1)
C(7)	–7171(6)	5531(1)	–4219(2)	22(1)
C(8)	–8681(5)	6150(1)	–4086(2)	19(1)
C(9)	–7857(6)	6573(1)	–3511(2)	24(1)
C(10)	–9280(6)	7132(1)	–3398(2)	25(1)
C(11)	–11538(6)	7251(1)	–3852(2)	26(1)
C(12)	–12255(6)	6804(1)	–4405(2)	26(1)
C(13)	–1760(6)	3747(1)	–2051(2)	19(1)
C(14)	698(6)	4138(1)	–918(1)	23(1)

C(15)	1814(6)	3607(1)	–391(2)	26(1)
C(16)	1853(6)	3818(1)	419(2)	22(1)
C(17)	3713(6)	4266(2)	705(2)	30(1)
C(18)	3656(6)	4466(2)	1443(2)	33(1)
C(19)	1773(6)	4204(2)	1884(2)	28(1)
C(20)	20(7)	3758(2)	1563(2)	36(1)

3.4.2. $[Cu^{II}_2(HL^{M1})(MeCN)_4](BF_4)_3 \cdot MeCN$ (6b · MeCN)

The asymmetric unit of $[Cu^{II}_2(HL^{M1})(MeCN)_4](BF_4)_3 \cdot MeCN$ (**6b** · MeCN) consisted of one complex cation $[Cu^{II}_2(HL^{M1})(MeCN)_4]^{3+}$, three tetrafluoroborate counter ions and one acetonitrile solvent molecule. Three fluorine atoms of one tetrafluoroborate were disordered over two sites (twirling about the B(2)-F(21) bond), with a site occupancy factor of 0.54 for F(22), F(23) and F(24) and 0.46 for F(25), F(26) and F(27). Pairs of "opposite" fluorine atoms were given equal anisotropic displacement parameters. The acetonitrile solvent molecule was disordered over two sites (restrained to be similar by the "SAME" instruction) with a site occupancy factor of 0.55 for N(140)-C(140)-C(141) and 0.45 for N(150)-C(150)-C(151). All non-hydrogen atoms were refined anisotropically, except the partial occupancy acetonitrile molecules. All hydrogen atoms were placed at calculated positions using a riding model. All hydrogen atoms had thermal parameters 1.2 times the equivalent isotropic thermal parameter of the atom to which they were bonded. High peaks were found close to the copper(II) atoms and are possibly Fourier ripples.

Table 3.4.3. Crystal data and structure refinement of $[Cu^{II}_2(HL^{M1})(MeCN)_4](BF_4)_3 \cdot MeCN$ (**6b** · MeCN).

Empirical formula	$C_{28}H_{30}B_3Cu_2F_{12}N_{11}O_2$
Formula weight M_r	940.14 g mol^{-1}
Temperature T	168(2) K

Wavelength	0.71073 Å	
Crystal system	Triclinic	
Space group	*P*–1	
Unit cell dimensions	$a = 10.719(7)$ Å	$\alpha = 87.444(8)°$
	$b = 13.724(8)$ Å	$\beta = 76.744(8)°$
	$c = 14.709(9)$ Å	$\gamma = 83.671(9)°$
Volume *V*	2093(2) Å^3	
Z	2	
Density $\rho_{calcd.}$	1.492 g cm^{-3}	
Absorption coefficient μ	1.110 mm^{-1}	
F(000)	944	
Crystal colour and shape	Blue block	
Crystal size	0.40 × 0.20 × 0.08 mm^3	
θ range for data collection	$1.96° \leq \theta \leq 26.36°$	
Index ranges	$-13 \leq h \leq 13$, $-13 \leq k \leq 16$, $-18 \leq l \leq 18$	
Reflections collected	26178	
Independent reflections	8233 [$R_{int} = 0.0912$]	
Completeness to $\theta = 26.36°$	96.3 %	
Absorption correction	Semi-empirical (SADABS)	
Max. / min. transmission	1 / 0.69	
Refinement method	Full-matrix least-squares on F^2	
Data / restraints / parameters	8233 / 3 / 537	
Goodness-of-fit on F^2	1.074	
Final *R* indices [$I>2\sigma(I)$]	$R1 = 0.1564$, $wR2 = 0.3933$	
R indices (all data)	$R1 = 0.1931$, $wR2 = 0.4141$	
Largest diff. peak / hole	2.565 / –2.183 e Å^{-3}	

Table 3.4.4. Atomic coordinates (× 10^4) and equivalent isotropic displacement parameters U_{eq} (× 10^3) [Å^2] for $[Cu^{II}_2(HL^{M1})(MeCN)_4](BF_4)_3 \cdot MeCN$ (**6b** · MeCN).

Atom	x	y	z	U_{eq}
Cu(1)	1128(2)	4788(1)	1848(1)	26(1)
Cu(2)	2832(2)	–89(1)	1946(1)	31(1)
N(1)	1650(11)	3342(8)	2017(8)	27(2)
C(2)	2075(12)	2843(9)	1191(8)	22(3)
C(3)	2438(12)	1860(9)	1212(9)	23(3)
N(4)	2370(12)	1388(8)	2049(7)	29(2)
C(4)	1973(14)	1867(10)	2853(10)	33(3)
C(5)	1609(14)	2872(10)	2824(9)	31(3)
C(6)	2080(11)	3542(9)	341(8)	20(2)
O(1)	2506(10)	3220(7)	–493(6)	33(2)

N(2)	1617(10)	4407(8)	554(8)	25(2)
C(7)	1622(13)	5182(9)	–156(9)	27(3)
C(10)	1118(12)	6120(10)	342(9)	25(3)
C(11)	925(15)	7029(11)	–160(11)	38(3)
C(12)	477(15)	7856(10)	345(11)	39(4)
C(13)	215(15)	7795(10)	1334(11)	37(3)
C(14)	383(15)	6959(11)	1759(12)	41(4)
N(3)	849(11)	6089(8)	1299(8)	30(3)
C(16)	2874(13)	1145(10)	389(9)	29(3)
O(2)	3000(11)	1472(7)	–471(7)	38(2)
N(5)	3081(11)	266(8)	628(8)	30(3)
C(17)	3412(16)	–528(10)	–48(10)	39(4)
C(20)	3566(14)	–1464(11)	505(12)	40(4)
C(21)	4025(14)	–2365(10)	41(11)	38(4)
C(22)	4158(15)	–3202(11)	538(15)	51(5)
C(23)	3843(15)	–3155(11)	1539(13)	44(4)
C(24)	3409(15)	–2237(11)	1947(13)	42(4)
N(6)	3303(11)	–1424(8)	1424(9)	32(3)
N(100)	–970(12)	4400(11)	2449(9)	44(3)
C(100)	–1704(16)	3892(12)	2793(11)	41(4)
C(101)	–2681(17)	3251(14)	3314(14)	57(5)
N(110)	1271(12)	5182(9)	3098(8)	35(3)
C(110)	1614(15)	5299(12)	3756(12)	42(4)
C(111)	2040(20)	5449(17)	4616(15)	74(7)
N(120)	2177(13)	–419(9)	3274(9)	41(3)
C(120)	1892(16)	–590(12)	4081(12)	42(4)
C(121)	1610(20)	–799(17)	5052(14)	71(6)
N(130)	4865(14)	–60(12)	2305(10)	50(4)
C(130)	5704(15)	–457(12)	2545(11)	41(4)
C(131)	6841(19)	–969(15)	2807(15)	63(5)
B(1)	790(20)	2525(16)	5542(14)	53(5)
F(11)	1561(14)	2644(13)	6147(10)	100(5)
F(12)	–444(12)	2447(10)	6056(9)	76(4)
F(13)	1258(14)	1696(9)	5001(8)	83(4)
F(14)	819(17)	3318(10)	4971(9)	101(5)
B(2)	–911(19)	10820(20)	2040(14)	54(6)
F(21)	–413(11)	11834(8)	1972(8)	63(3)
F(22)	–1970(30)	10980(20)	1730(30)	106(10)
F(23)	170(30)	10340(20)	1500(20)	105(8)
F(24)	–1020(40)	10590(30)	2924(18)	96(8)
F(25)	–1250(40)	10540(30)	1530(30)	96(8)
F(26)	0(40)	10270(30)	2470(30)	106(10)
F(27)	–1990(40)	10930(20)	2840(30)	105(8)
B(3)	4745(12)	–5913(11)	2010(10)	23(3)
F(31)	4504(10)	–6976(7)	2129(9)	63(3)
F(32)	3970(11)	–5536(8)	1433(8)	65(3)
F(33)	5991(10)	–5906(9)	1683(8)	69(3)

F(34)	4307(12)	–5549(10)	2901(9)	78(4)
N(140)	4240(30)	7210(30)	4070(30)	84(10)
C(140)	5130(40)	6700(30)	3670(30)	80(12)
C(141)	6370(30)	6150(20)	3020(20)	48(7)
N(150)	4170(40)	–2190(30)	4360(30)	64(10)
C(150)	4810(40)	–2120(30)	4910(30)	58(11)
C(151)	5510(40)	–2000(30)	5730(30)	57(10)

3.4.3. *$[Cu^{II}_4(HL^{M1})_2(\mu_{(1,1)}\text{-}N_3)_2(N_3)_2(MeCN)_2](BF_4)_2 \cdot MeCN$ (14b· MeCN)*

The asymmetric unit of $[Cu^{II}_4(HL^{M1})_2(\mu_{(1,1)}\text{-}N_3)_2(N_3)_2(MeCN)_2](BF_4)_2 \cdot MeCN$ (**14b**· MeCN) consisted of one dinuclear complex core $[Cu^{II}_2(HL^{M1})(\mu_{(1,1)}\text{-}N_3)(N_3)(MeCN)]^+$ one tetrafluoroborate counter ion and half an acetonitrile solvent molecule. All non-hydrogen atoms were refined anisotropically. All hydrogen atoms were placed at calculated positions using a riding model. except for the former N-H amide proton H(12), which was located from the difference map and its coordinates were allowed to refine freely. All hydrogen atoms had thermal parameters 1.2 times the equivalent isotropic thermal parameter of the atom to which they were bonded. The tetrafluoroborate counter ion was disordered over two sites with a site occupancy factor of 0.55 for B(1), F(1), F(2), F(3) and F(4) and 0.45 for B(2), F(5), F(6), F(7) and F(8). The B-F and F···F distances were restrained by the use of two "SADI" instructions.

Table 3.4.5. Crystal data and structure refinement of $[Cu^{II}_4(HL^{M1})_2(\mu_{(1,1)}\text{-}N_3)_2(N_3)_2(MeCN)_2](BF_4)_2 \cdot MeCN$ (**14b**· MeCN).

Empirical formula	$C_{21}H_{19.5}BCu_2F_4N_{13.5}O_2$
Formula weight M_r	706.89 g mol^{-1}
Temperature T	200(2) K
Wavelength	0.71073 Å

Crystal system	Triclinic	
Space group	*P*–1	
Unit cell dimensions	$a = 8.7773(2)$ Å	$\alpha = 74.551(1)°$
	$b = 12.9357(3)$ Å	$\beta = 88.697(1)°$
	$c = 13.5036(3)$ Å	$\gamma = 87.016(1)°$
Volume *V*	1475.74(6) Å^3	
Z	2	
Density $\rho_{calcd.}$	1.591 g cm^{-3}	
Absorption coefficient μ	1.512 mm^{-1}	
F(000)	710	
Crystal colour and shape	Green needles	
Crystal size	0.40 × 0.08 × 0.05 mm^3	
θ range for data collection	$1.56° \leq \theta \leq 25.75°$	
Index ranges	$-10 \leq h \leq 10$, $-14 \leq k \leq 15$, $0 \leq l \leq 16$	
Reflections collected	5566	
Independent reflections	5566 [$R_{int} = 0.0000$]	
Completeness to $\theta = 25.75°$	98.4 %	
Absorption correction	Semi-empirical (SADABS)	
Data / restraints / parameters	5566 / 94 / 456	
Goodness-of-fit on F^2	1.060	
Final *R* indices [$I>2\sigma(I)$]	$R1 = 0.0475$, $wR2 = 0.1344$	
R indices (all data)	$R1 = 0.0684$, $wR2 = 0.1487$	
Largest diff. peak / hole	0.944 / –0.471 e Å^{-3}	

Table 3.4.6. Atomic coordinates (× 10^4) and equivalent isotropic displacement parameters U_{eq} (× 10^3) [Å^2] for $[Cu^{II}_4(HL^{M1})_2(\mu_{(1,1)}\text{-}N_3)_2(N_3)_2(MeCN)_2](BF_4)_2 \cdot MeCN$ (**14b** · MeCN).

Atom	x	y	z	U_{eq}
Cu(1)	7284(1)	10748(1)	7078(1)	29(1)
Cu(2)	12811(1)	7604(1)	5512(1)	29(1)
O(1)	11450(3)	10072(3)	8403(2)	36(1)
O(2)	13366(3)	8906(3)	7881(2)	34(1)
N(1)	8789(4)	9741(3)	6549(3)	26(1)
N(2)	9038(4)	10724(3)	7925(3)	29(1)
N(3)	6201(4)	11241(3)	8200(3)	33(1)
N(4)	11005(4)	8487(3)	5914(2)	26(1)
N(5)	13659(4)	8004(3)	6654(3)	31(1)
N(6)	14901(4)	6946(3)	5455(3)	32(1)
C(1)	8515(5)	9259(3)	5822(3)	28(1)
C(2)	9627(5)	8636(3)	5493(3)	28(1)
C(3)	11297(4)	8938(3)	6687(3)	25(1)
C(4)	10185(4)	9580(3)	7007(3)	25(1)

C(5)	10261(5)	10165(3)	7844(3)	28(1)
C(6)	8833(5)	11258(4)	8745(3)	34(1)
C(7)	7137(5)	11428(3)	8910(3)	31(1)
C(8)	6570(5)	11744(4)	9747(3)	37(1)
C(9)	5004(6)	11830(4)	9901(4)	46(1)
C(10)	4057(6)	11621(5)	9191(4)	50(1)
C(11)	4683(5)	11343(4)	8346(4)	43(1)
C(13)	12882(5)	8612(3)	7118(3)	28(1)
C(15)	15198(5)	7591(4)	6975(3)	36(1)
C(17)	17333(5)	6584(4)	6266(4)	41(1)
C(16)	15843(5)	7019(3)	6210(3)	33(1)
C(18)	17848(6)	6056(4)	5540(4)	49(1)
C(19)	16885(6)	5999(4)	4774(4)	50(1)
C(20)	15426(6)	6448(4)	4742(4)	42(1)
N(20)	5708(4)	10535(3)	6175(3)	38(1)
N(21)	4385(4)	10826(3)	6127(3)	31(1)
N(22)	3106(4)	11085(3)	6050(3)	38(1)
N(30)	12101(4)	7679(3)	4127(3)	33(1)
N(31)	11347(5)	7048(3)	3878(3)	38(1)
N(32)	10615(7)	6475(4)	3587(4)	74(2)
N(40)	11670(5)	6041(3)	6467(3)	45(1)
C(40)	11511(7)	5438(5)	7203(5)	61(2)
C(41)	11328(14)	4629(8)	8178(7)	143(4)
B(1)	8893(17)	7326(11)	8968(11)	86(9)
F(1)	9415(16)	7196(8)	8076(7)	103(3)
F(2)	7867(12)	6652(8)	9359(9)	114(4)
F(3)	8340(20)	8313(6)	8801(13)	171(8)
F(4)	10040(20)	7200(20)	9588(13)	316(16)
B(2)	9276(16)	7259(10)	8985(8)	35(4)
F(5)	9270(20)	7893(18)	9571(17)	236(16)
F(6)	10677(14)	7282(9)	8588(12)	119(4)
F(7)	8310(20)	7652(17)	8225(14)	218(14)
F(8)	8980(20)	6304(11)	9491(13)	189(9)
N(50)	15282(16)	4273(9)	7631(11)	87(4)
C(50)	16002(18)	4400(10)	8173(13)	74(4)
C(51)	16830(30)	4491(12)	8874(19)	174(12)

3.4.4. *{[Cu^{II}_2(HL^{M2})($\mu_{(1,3)}$-N_3)$_2$](BF$_4$) · MeCN}$_\infty$ (16b · MeCN)*

The asymmetric unit of {[Cu^{II}_2(HL^{M2})($\mu_{(1,3)}$-N_3)$_2$](BF$_4$) · MeCN}$_\infty$ (**16b** · MeCN) consisted of half of a complex core [Cu^{II}_2(HL^{M2})($\mu_{(1,3)}$-N_3)$_2$]$^+$, half a BF_4^- and half an acetonitrile solvent molecule. Three fluorine atoms of the half tetrafluoroborate were disordered over two sites (twirling about the B(1)-F(11) bond) with a site occupancy factor of 0.30 for F(12), F(13) and F(14) and 0.20 for F(15), F(16) and F(17). The B-F and F···F distances were restrained by the use of two "SADI" instructions. The half acetonitrile solvent molecule [N(50A)-C(50)-C(51)] was located over a centre of inversion; N(50) and C(50) were therefore given equal coordinates and anisotropic displacement parameters. All non-hydrogen atoms were refined anisotropically. All hydrogen atoms were placed at calculated positions using a riding model except for the half occupancy former N-H amide proton H(1A), which was located from the difference map on a two fold axis and its coordinates were allowed to refine freely. All hydrogen atoms had thermal parameters 1.2 times the equivalent isotropic thermal parameter of the atom to which they were bonded.

Table 3.4.7. Crystal data and structure refinement of {[Cu^{II}_2(HL^{M2})($\mu_{(1,3)}$-N_3)$_2$](BF$_4$) · MeCN}$_\infty$ (**16b** · MeCN).

Empirical formula	$C_{22}H_{22}B_1Cu_2F_4N_{13}O_2$	
Formula weight M_r	714.40	
Temperature T	200(2) K	
Wavelength	0.71073 Å	
Crystal system	Monoclinic	
Space group	C2/c	
Unit cell dimensions	a = 20.8447(5) Å	α = 90°
	b = 15.2208(4) Å	β = 106.4340(10)°
	c = 9.0272(2) Å	γ = 90°
Volume V	2747.08(12) Å^3	
Z	4	
Density $\rho_{calcd.}$	1.727 g cm^{-3}	
Absorption coefficient	1.625 mm^{-1}	
F(000)	1440	
Crystal colour and shape	Green needle	

Crystal size	0.36 × 0.12 × 0.10 mm^3
Theta range for data collection	$1.68° \leq \theta \leq 26.39°$
Index ranges	$-18 \leq h \leq 26$, $-19 \leq k \leq 16$, $-11 \leq l \leq 11$
Reflections collected	8160
Independent reflections	2796 [$R_{int} = 0.0288$]
Completeness to $\theta = 26.39°$	99.0 %
Absorption correction	Semi-empirical (SADABS)
Max. / min. transmission	0.8878 / 0.7151
Refinement method	Full-matrix least-squares on F^2
Data / restraints / parameters	2796 / 51 / 251
Goodness-of-fit on F^2	1.100
Final R indices [$I>2\sigma(I)$]	$R1 = 0.0295$, $wR2 = 0.0780$
R indices (all data)	$R1 = 0.0329$, $wR2 = 0.0803$
Largest diff. peak / hole	0.335 / –0.550 e Å^{-3}

Table 3.4.8. Atomic coordinates (× 10^4) and equivalent isotropic displacement parameters U_{eq} (× 10^3) [Å^2] for $\{[Cu^{II}_2(HL^{M2})(\mu_{(1,3)}\text{-}N_3)_2](BF_4) \cdot MeCN\}_\infty$ (**16b** · MeCN).

Atom	x	y	z	U_{eq}
Cu(1)	1406(1)	–1161(1)	500(1)	26(1)
N(1)	540(1)	–1053(1)	–1226(2)	23(1)
C(1)	273(1)	–304(2)	–1836(3)	26(1)
C(2)	283(1)	–1831(2)	–1864(2)	23(1)
C(3)	683(1)	–2606(2)	–1051(3)	25(1)
N(2)	1230(1)	–2400(1)	–25(2)	27(1)
O(1)	482(1)	–3395(1)	–1402(2)	35(1)
C(4)	1649(1)	–3114(2)	835(3)	35(1)
C(5)	1947(1)	–2846(2)	2518(3)	40(1)
C(6)	2475(1)	–2152(2)	2736(3)	35(1)
C(7)	3124(1)	–2288(2)	3677(3)	47(1)
C(8)	3594(1)	–1628(3)	3857(3)	53(1)
C(9)	3423(1)	–855(3)	3068(3)	49(1)
C(10)	2776(1)	–754(2)	2133(3)	39(1)
N(3)	2308(1)	–1383(2)	1976(2)	32(1)
N(20)	1313(1)	51(2)	1186(2)	38(1)
N(21)	1622(1)	381(1)	2363(2)	28(1)
N(22)	1914(1)	735(2)	3491(2)	37(1)
B(1)	0	2069(3)	7500	64(2)
F(11)	–519(5)	1521(6)	7750(12)	98(4)
F(12)	589(6)	1619(9)	7807(19)	81(6)
F(13)	41(9)	2736(8)	8507(13)	118(7)
F(14)	–177(7)	2326(12)	6031(12)	154(13)
F(15)	503(10)	1920(12)	8620(30)	220(30)

F(16)	–294(6)	2888(6)	7570(20)	80(4)
F(17)	–17(10)	1915(12)	6111(19)	115(8)
N(50)	–123(3)	4727(3)	9378(8)	118(2)
C(50)	–123(3)	4727(3)	9378(8)	118(2)
C(51)	–442(4)	4330(5)	7851(9)	56(2)

3.4.5. $[Cu^{II}_2(H_2L^{M1})_2(MeCN)_2](BF_4)_4$ (18)

The asymmetric unit of $[Cu^{II}_2(H_2L^{M1})_2(MeCN)_2](BF_4)_4$ (**18**) consisted of one mononuclear complex core $[Cu^{II}(H_2L^{M1})(MeCN)]^{2+}$ and two tetrafluoroborate counter ions. All non-hydrogen atoms were refined anisotropically. All hydrogen atoms were placed at calculated positions using a riding model except for the N-H amide proton H(5) and the former N-H amide proton H(6), which were located from the difference map and were allowed to refine freely. All hydrogen atoms, except H(5) and H(6) had thermal parameters 1.2 times the equivalent isotropic thermal parameter of the atom to which they were bonded.

Table 3.4.9. Crystal data and structure refinement of $[Cu^{II}_2(H_2\mathbf{L^{M1}})_2(MeCN)_2](BF_4)_4$ (**18**).

Empirical formula	$C_{20}H_{19}B_2CuF_8N_7O_2$	
Formula weight	626.58 g mol^{-1}	
Temperature	150(2) K	
Wavelength	0.71073 Å	
Crystal system	Triclinic	
Space group	*P*–1	
Unit cell dimensions	a = 10.5129(3) Å	α = 87.8400(10)°
	b = 10.7093(3) Å	β = 74.2720(10)°
	c = 11.9977(3) Å	γ = 72.5870(10)°
Volume V	1239.22(6) Å^3	
Z	2	
Density $\rho_{calcd.}$	1.679 g cm^{-3}	
Absorption coefficient	0.976 mm^{-1}	

$F(000)$	630
Crystal size	0.40 × 0.35 × 0.02 mm^3
θ range for data collection	$1.77° \leq \theta \leq 25.40°$.
Index ranges	$-12 \leq h \leq 12$, $-12 \leq k \leq 12$, $-14 \leq l \leq 14$
Reflections collected	11056
Independent reflections	4480 [R_{int} = 0.0201]
Completeness to θ = 25.40°	98.4 %
Absorption correction	Semi-empirical (SADABS)
Max. / min. transmission	0.9807 / 0.6961
Refinement method	Full-matrix least-squares on F^2
Data / restraints / parameters	4480 / 0 / 370
Goodness-of-fit on F^2	1.027
Final R indices [$I>2\sigma(I)$]	$R1$ = 0.0272, $wR2$ = 0.0707
R indices (all data)	$R1$ = 0.0319, $wR2$ = 0.0731
Largest diff. peak / hole	0.626 / –0.354 e Å^{-3}

Table 3.4.10. Atomic coordinates (× 10^4) and equivalent isotropic displacement parameters U_{eq} (× 10^3) [Å^2] [$Cu^{II}_2(H_2\mathbf{L^{M1}})_2(MeCN)_2](BF_4)_4$ (**18**).

Atom	x	y	z	U_{eq}
Cu(1)	7066(1)	9335(1)	6011(1)	21(1)
C(1)	8267(2)	10768(2)	7435(2)	24(1)
C(2)	9058(2)	11594(2)	7517(2)	25(1)
C(3)	9254(2)	12086(2)	5618(2)	20(1)
C(4)	8493(2)	11257(2)	5508(2)	19(1)
N(1)	7997(2)	10601(2)	6437(1)	21(1)
N(4)	9556(2)	12248(2)	6621(1)	24(1)
C(5)	8198(2)	10956(2)	4397(2)	20(1)
C(6)	7131(2)	9655(2)	3578(2)	23(1)
C(7)	6380(2)	8651(2)	4015(2)	23(1)
C(8)	5877(2)	8038(2)	3296(2)	31(1)
C(9)	5229(2)	7104(2)	3743(2)	37(1)
C(10)	5096(2)	6800(2)	4900(2)	35(1)
C(11)	5608(2)	7438(2)	5570(2)	29(1)
N(2)	7482(2)	10114(2)	4548(1)	22(1)
O(1)	8657(2)	11448(1)	3467(1)	29(1)
N(3)	6236(2)	8358(2)	5141(1)	24(1)
C(15)	9850(2)	12836(2)	4614(2)	22(1)
C(16)	9407(2)	14814(2)	3505(2)	30(1)
C(17)	8922(2)	14684(2)	2450(2)	27(1)
C(18)	8729(2)	15670(2)	1676(2)	35(1)
C(19)	8302(2)	15477(2)	712(2)	40(1)
C(20)	8070(2)	14307(2)	519(2)	40(1)

C(21)	8289(2)	13337(2)	1298(2)	35(1)
N(5)	8985(2)	13985(2)	4440(2)	24(1)
N(6)	8690(2)	13555(2)	2229(2)	28(1)
O(2)	11064(1)	12423(1)	4025(1)	29(1)
N(50)	6203(2)	8879(2)	7591(2)	26(1)
C(50)	5735(2)	8504(2)	8465(2)	24(1)
C(51)	5130(2)	8021(2)	9573(2)	31(1)
B(1)	6313(2)	14869(2)	7705(2)	29(1)
F(11)	6775(1)	14559(1)	6493(1)	39(1)
F(12)	5042(1)	15833(1)	7929(1)	41(1)
F(13)	6186(2)	13750(1)	8276(1)	49(1)
F(14)	7274(1)	15326(2)	8029(1)	49(1)
B(2)	11819(2)	10885(2)	–244(2)	29(1)
F(21)	10942(1)	11592(1)	–882(1)	40(1)
F(22)	11710(2)	9631(1)	–66(1)	44(1)
F(23)	13185(2)	10779(2)	–869(1)	55(1)
F(24)	11547(2)	11564(2)	800(1)	53(1)

3.4.6. $[Cu^{II}_4(H_2L^{M2})_2(HL^{M2})_2](BF_4)_6 \cdot 3\ MeCN \cdot 0.5\ H_2O$ (19 · 3 MeCN · 0.5 H_2O)

The asymmetric unit of $[Cu^{II}_4(H_2L^{M2})_2(HL^{M2})_2](BF_4)_6 \cdot 3$ MeCN · 0.5 H_2O (**19** · 3 MeCN · 0.5 H_2O) consisted of one tetranuclear square complex $[Cu^{II}_4(H_2L^{M2})_2(HL^{M2})_2]^{6+}$, six tetrafluoroborate counter ions, three acetonitrile solvent molecules and half a water solvent molecule. All non-hydrogen atoms were refined anisotropically. All hydrogen atoms were placed at calculated positions using a riding model except for the four N-H amide protons H(5C), H(11C), H(17C) and H(23C), the two former N-H amide protons H(18C) and H(24C) and the half occupancy water hydrogen atoms H(70C) and H(70D), all of which were located from the difference map and fixed at that position. All hydrogen atoms had thermal parameters 1.2 times the equivalent isotropic thermal parameter of the atom to which they were bonded. Four of the six tetrafluoroborate counter ions were disordered.

One was disordered over two sites with a site occupancy factor of 0.73 for B(3), F(31), F(32), F(33) and F(34) and 0.27 for B(3'), F(35), F(36), F(37) and F(38). In each of the other three disordered tetrafluoroborate ions, three fluorine atoms were disordered (twirling about the B(X)-F(X1) bond) with an occupancy factor of 0.61 [0.39] for F(42), F(43) and F(44) [F(45), F(46) and F(47)], 0.53 [0.47] for F(52), F(53) and F(54) [F(55), F(56) and F(57)] and 0.56 [0.44] for F(62), F(63) and F(64) [F(65), F(66) and F(67)], respectively. Pairs of "opposite" fluorine atoms in these three molecules were given equal anisotropic displacement parameters. The "SAME" instruction was applied to the B(2), B(3'), B(4), B(5) and B(6) tetrafluoroborate ions, restraining them to have similar geometry to that of the well behaved B(1) tetrafluoroborate ion.

Table 3.4.11. Crystal data and structure refinement of $[Cu^{II}_4(H_2\mathbf{L}^{\mathbf{M2}})_2(H\mathbf{L}^{\mathbf{M2}})_2](BF_4)_6 \cdot 3\ MeCN \cdot 0.5\ H_2O$ (**19** · 3 MeCN · 0.5 H_2O).

Empirical formula	$C_{86}H_{88}B_6Cu_4F_{24}N_{27}O_{8.5}$	
Formula weight M_r	2411.83 g mol^{-1}	
Temperature T	150(2) K	
Wavelength	0.71073 Å	
Crystal system	Triclinic	
Space group	$P\bar{1}$	
Unit cell dimensions	a = 13.9483(2) Å	α = 82.3380(10)°
	b = 14.1741(2) Å	β = 86.1350(10)°
	c = 26.0046(2) Å	γ = 87.7230(10)°
Volume V	5081.28(11) Å^3	
Z	2	
Density $\rho_{calcd.}$	1.576 g cm^{-3}	
Absorption coefficient μ	0.939 mm^{-1}	
$F(000)$	2446	
Crystal colour and shape	Green blocks	
Crystal size	0.40 × 0.22 × 0.20 mm^3	
θ range for data collection	$0.79° \leq \theta \leq 25.11°$	
Index ranges	$-16 \leq h \leq 16$, $-16 \leq k \leq 16$, $0 \leq l \leq 30$	
Reflections collected	43733	
Independent reflections	17828 [R_{int} = 0.0331]	
Completeness to θ = 25.11°	98.5 %	
Absorption correction	Semi-empirical (SADABS)	
Max. / min. transmission	0.86 / 0.63	
Refinement method	Full-matrix least-squares on F^2	
Data / restraints / parameters	17828 / 339 / 1480	

Goodness-of-fit on F^2	1.049
Final R indices [$I>2\sigma(I)$]	$R1 = 0.0673$, $wR2 = 0.1976$
R indices (all data)	$R1 = 0.0840$, $wR2 = 0.2126$
Largest diff. peak / hole	2.101 / –0.968 e Å^{-3}

Table 3.4.12. Atomic coordinates (× 10^4) and equivalent isotropic displacement parameters U_{eq} (× 10^3) [Å^2] for $[Cu^{II}_4(H_2\mathbf{L}^{\mathbf{M2}})_2(H\mathbf{L}^{\mathbf{M2}})_2](BF_4)_6 \cdot 3\ MeCN \cdot 0.5\ H_2O$ (**19** · 3 MeCN · 0.5 H_2O).

Atom	x	y	z	U_{eq}
Cu(1)	6688(1)	7913(1)	2908(1)	26(1)
Cu(2)	9333(1)	3717(1)	2478(1)	29(1)
Cu(3)	5053(1)	1340(1)	2405(1)	25(1)
Cu(4)	2492(1)	5697(1)	2395(1)	25(1)
N(1)	5445(3)	7441(3)	2682(2)	27(1)
N(2)	5969(3)	7757(4)	3565(2)	30(1)
N(3)	7627(4)	8788(4)	3131(2)	30(1)
N(4)	3837(3)	6555(3)	2480(2)	28(1)
N(5)	3093(4)	6384(4)	3832(2)	34(1)
N(6)	3209(5)	6462(4)	5431(2)	50(2)
O(1)	4533(3)	7359(3)	4000(2)	39(1)
O(2)	2537(3)	5814(3)	3149(2)	28(1)
C(1)	5307(4)	7292(4)	2200(2)	31(1)
C(2)	4487(4)	6846(5)	2102(2)	32(1)
C(3)	3972(4)	6711(4)	2975(2)	26(1)
C(4)	4793(4)	7175(4)	3080(2)	25(1)
C(5)	5090(4)	7439(4)	3600(2)	27(1)
C(6)	6346(5)	8028(5)	4038(2)	32(1)
C(7)	7433(5)	7920(4)	4014(2)	34(1)
C(8)	7941(4)	8638(4)	3617(2)	32(1)
C(9)	8706(5)	9147(5)	3746(3)	42(2)
C(10)	9126(5)	9824(5)	3386(3)	46(2)
C(11)	8776(5)	10011(5)	2897(3)	42(2)
C(12)	8026(5)	9473(4)	2783(3)	35(1)
C(13)	3158(4)	6280(4)	3336(2)	27(1)
C(14)	2288(5)	5982(5)	4173(2)	39(2)
C(15)	2255(5)	6323(5)	4705(2)	39(2)
C(16)	3016(5)	5906(5)	5067(2)	37(1)
C(17)	3442(5)	5018(5)	5072(3)	45(2)
C(18)	4074(6)	4685(5)	5450(3)	51(2)
C(19)	4261(6)	5246(6)	5828(3)	55(2)
C(20)	3830(7)	6125(6)	5801(3)	59(2)
N(7)	8669(3)	4915(3)	2718(2)	26(1)
N(8)	9566(3)	4593(3)	1858(2)	30(1)

N(9)	10341(4)	2738(4)	2277(2)	37(1)
N(10)	7640(3)	6538(3)	2900(2)	27(1)
N(11)	8558(4)	7627(3)	1665(2)	32(1)
N(12)	8443(4)	6795(4)	463(2)	39(1)
O(3)	9666(3)	6175(3)	1555(2)	39(1)
O(4)	7320(3)	7996(3)	2208(2)	29(1)
C(21)	8162(4)	4958(4)	3165(2)	31(1)
C(22)	7653(5)	5788(4)	3256(2)	32(1)
C(23)	8161(4)	6512(4)	2445(2)	23(1)
C(24)	8709(4)	5688(4)	2351(2)	24(1)
C(25)	9360(4)	5506(4)	1878(2)	30(1)
C(26)	10180(5)	4355(5)	1413(3)	39(2)
C(27)	10124(5)	3302(5)	1357(3)	42(2)
C(28)	10597(5)	2640(5)	1777(3)	40(2)
C(29)	11259(6)	1934(5)	1650(4)	56(2)
C(30)	11669(7)	1323(6)	2042(5)	78(3)
C(31)	11428(6)	1450(6)	2543(4)	69(3)
C(32)	10760(5)	2151(5)	2656(4)	52(2)
C(33)	7993(4)	7435(4)	2083(2)	25(1)
C(34)	8452(5)	8518(4)	1311(2)	37(1)
C(35)	8147(5)	8309(5)	790(3)	39(2)
C(36)	8825(5)	7596(5)	559(2)	35(1)
C(37)	9803(5)	7758(5)	465(2)	42(2)
C(38)	10398(5)	7077(6)	264(3)	46(2)
C(39)	10000(6)	6265(6)	155(3)	55(2)
C(40)	9019(5)	6144(6)	260(3)	49(2)
N(13)	6341(3)	1991(3)	2344(2)	23(1)
N(14)	5463(4)	962(3)	3100(2)	27(1)
N(15)	4111(3)	292(3)	2456(2)	29(1)
N(16)	8015(3)	2925(3)	2366(2)	26(1)
N(17)	8156(4)	1900(4)	3686(2)	40(1)
N(18)	6966(6)	1622(4)	4787(2)	50(2)
O(5)	6698(3)	899(3)	3632(2)	37(1)
O(6)	9011(3)	2975(3)	3161(2)	32(1)
C(41)	6675(4)	2555(4)	1933(2)	28(1)
C(42)	7523(4)	3026(4)	1940(2)	28(1)
C(43)	7684(4)	2355(4)	2792(2)	24(1)
C(44)	6827(4)	1858(4)	2786(2)	24(1)
C(45)	6318(4)	1190(4)	3211(2)	26(1)
C(46)	4911(5)	358(5)	3499(2)	32(1)
C(47)	3856(5)	380(4)	3389(2)	33(1)
C(48)	3676(4)	–66(4)	2915(2)	31(1)
C(49)	3080(5)	–835(5)	2949(3)	43(2)
C(50)	2912(5)	–1216(5)	2499(3)	47(2)
C(51)	3359(5)	–850(5)	2034(3)	41(2)
C(52)	3952(5)	–107(4)	2026(3)	35(1)
C(53)	8333(4)	2409(4)	3235(2)	28(1)

C(54)	8752(6)	1987(6)	4129(3)	58(2)
C(55)	8644(7)	1151(6)	4542(3)	64(2)
C(56)	7656(7)	941(6)	4757(2)	54(2)
C(57)	7367(10)	–8(7)	4957(3)	81(3)
C(58)	6484(10)	–147(7)	5186(3)	83(4)
C(59)	5842(10)	595(7)	5210(4)	84(3)
C(60)	6091(8)	1465(6)	5005(3)	64(2)
N(19)	3150(3)	4390(3)	2470(2)	24(1)
N(20)	2557(3)	5465(3)	1681(2)	25(1)
N(21)	1518(3)	6779(3)	2285(2)	28(1)
N(22)	4129(3)	2680(3)	2479(2)	25(1)
N(23)	3784(3)	2767(3)	1134(2)	27(1)
N(24)	3451(4)	3659(4)	–538(2)	33(1)
O(7)	2833(3)	4348(3)	1126(2)	32(1)
O(8)	4694(3)	1836(3)	1687(1)	27(1)
C(61)	3474(4)	3946(4)	2907(2)	29(1)
C(62)	3969(4)	3079(4)	2916(2)	30(1)
C(63)	3812(4)	3123(4)	2031(2)	21(1)
C(64)	3298(4)	4000(4)	2019(2)	23(1)
C(65)	2870(4)	4633(4)	1564(2)	23(1)
C(66)	2149(4)	6139(4)	1261(2)	28(1)
C(67)	2192(4)	7161(4)	1384(2)	31(1)
C(68)	1523(4)	7384(4)	1834(2)	30(1)
C(69)	943(5)	8206(5)	1793(3)	37(1)
C(70)	338(5)	8409(5)	2211(3)	44(2)
C(71)	295(5)	7754(5)	2664(3)	42(2)
C(72)	897(4)	6959(5)	2688(2)	34(1)
C(73)	4129(4)	2539(4)	1591(2)	22(1)
C(74)	3977(5)	2140(4)	725(2)	34(1)
C(75)	3461(5)	2532(5)	241(2)	35(1)
C(76)	3955(4)	3299(4)	–127(2)	31(1)
C(77)	4880(5)	3608(5)	–103(3)	42(2)
C(78)	5267(5)	4260(6)	–500(3)	49(2)
C(79)	4740(6)	4594(5)	–920(3)	50(2)
C(80)	3816(6)	4291(5)	–927(3)	46(2)
B(1)	5952(4)	4737(4)	2531(2)	35(2)
F(11)	5425(4)	5243(3)	2867(2)	65(1)
F(12)	5337(3)	4437(3)	2179(2)	58(1)
F(13)	6654(3)	5220(4)	2260(2)	66(1)
F(14)	6313(3)	3916(3)	2829(2)	58(1)
B(2)	5052(6)	1384(5)	–760(3)	47(2)
F(21)	5335(9)	525(7)	–923(5)	200(5)
F(22)	5093(10)	1207(7)	–224(3)	191(5)
F(23)	4310(7)	1757(7)	–977(3)	166(4)
F(24)	5755(8)	2051(8)	–944(4)	193(5)
B(3)	1914(9)	203(11)	578(4)	53(3)
F(31)	1612(5)	1161(4)	501(2)	54(2)

F(32)	1145(8)	–356(6)	652(5)	133(5)
F(33)	2491(10)	27(10)	166(3)	181(7)
F(34)	2391(7)	35(7)	1017(3)	97(3)
B(3')	–663(9)	5529(9)	4344(5)	44(7)
F(35)	–516(9)	6065(8)	3878(4)	38(3)
F(36)	–1110(8)	4666(8)	4266(4)	37(3)
F(37)	78(9)	5344(9)	4611(5)	47(4)
F(38)	–1377(11)	6009(10)	4633(7)	78(6)
B(4)	3552(6)	2824(5)	4345(3)	73(3)
F(41)	3515(4)	3703(3)	4081(2)	71(2)
F(42)	4204(8)	2238(6)	4087(3)	78(3)
F(43)	2794(7)	2491(10)	4586(6)	145(6)
F(44)	4196(8)	2956(7)	4765(3)	99(3)
F(45)	2968(11)	2323(9)	4003(5)	99(3)
F(46)	3160(12)	2612(9)	4789(3)	78(3)
F(47)	4417(10)	2326(14)	4241(8)	145(6)
B(5)	1248(6)	–1238(7)	3996(3)	81(4)
F(51)	2154(4)	–1347(5)	4146(2)	85(2)
F(52)	792(12)	–436(10)	4213(7)	141(6)
F(53)	1072(9)	–1287(18)	3529(4)	132(6)
F(54)	719(9)	–1993(11)	4306(8)	158(6)
F(55)	1302(11)	–354(13)	3635(8)	158(6)
F(56)	959(13)	–1926(12)	3786(9)	141(6)
F(57)	556(8)	–954(17)	4367(5)	132(6)
B(6)	7293(5)	3565(6)	506(3)	68(3)
F(61)	6461(3)	3442(4)	795(2)	61(1)
F(62)	7888(7)	2748(7)	700(4)	83(3)
F(63)	7374(8)	3832(12)	32(3)	131(6)
F(64)	7820(7)	4248(7)	757(4)	87(2)
F(65)	7285(9)	2818(8)	158(5)	87(2)
F(66)	7253(10)	4353(7)	185(5)	83(3)
F(67)	8139(7)	3385(16)	737(4)	131(6)
N(600)	8685(7)	965(6)	1699(3)	83(3)
C(600)	8940(7)	992(6)	1280(4)	60(2)
C(601)	9239(8)	1040(8)	740(4)	84(3)
N(610)	6234(7)	–4(9)	1915(6)	104(4)
C(610)	6363(9)	264(10)	1493(8)	92(5)
C(611)	6516(9)	629(9)	963(8)	118(6)
N(620)	952(6)	4510(6)	2899(4)	76(2)
C(620)	933(7)	4210(6)	3319(6)	73(3)
C(621)	916(10)	3837(9)	3859(6)	119(5)
O(70)	1165(13)	1444(10)	3924(8)	111(6)

3.4.7. $[Co^{III}(H_2L^{M2})_2](BF_4)_3 \cdot 2\ EtOH$ (**22** · 2 EtOH)

The asymmetric unit of $[Co^{III}(H_2\mathbf{L}^{M2})_2](BF_4)_3 \cdot 2$ EtOH (**22** · 2 EtOH) consisted of one mononuclear complex cation $[Co^{III}(H_2\mathbf{L}^{M2})_2]^{3+}$, three tetrafluoroborate counter ions and two ethanol solvent molecules. All non-hydrogen atoms were refined anisotropically. All hydrogen atoms were placed at calculated positions using a riding model except for the N-H amide protons H(5N) and H(11N) and the former N-H amides proton H(6N) and H(12N), which were located from the difference map and their coordinates were allowed to refine freely. All hydrogen atoms had thermal parameters 1.2 times the equivalent isotropic thermal parameter of the atom to which they were bonded. One of the tetrafluoroborate counter ions was disordered with a site occupancy factor of 0.55 for F(31), F(32), F(33) and F(34) and 0.45 for F(35), F(36), F(37) and F(38). The hydroxyl group of one of the ethanol solvent molecules was disordered over two sites with a site occupancy factor of 0.45 for O(60)-H(60) and 0.55 for O(61)-H(61). The O-C distances of the disordered ethanol molecule were restrained using two "SADI" instructions.

Table 3.4.13. Crystal data and structure refinement of $[Co^{III}(H_2\mathbf{L}^{M2})_2](BF_4)_3 \cdot 2$ EtOH (**22** · 2 EtOH).

Empirical formula	$C_{44}H_{52}B_3CoF_{12}N_{12}O_6$	
Formula weight M_r	1164.34 g mol^{-1}	
Temperature T	163(2) K	
Wavelength	0.71073 Å	
Crystal system	Monoclinic	
Space group	$P2(1)/c$	
Unit cell dimensions	$a = 11.6949(8)$ Å	$\alpha = 90°$
	$b = 19.2367(14)$ Å	$\beta = 100.4370(10)°$
	$c = 22.1692(16)$ Å	$\gamma = 90°$
Volume V	4904.9(6) Å^3	
Z	4	
Density $\rho_{calcd.}$	1.577 g cm^{-3}	
Absorption coefficient μ	0.458 mm^{-1}	
$F(000)$	2392	
Crystal colour and shape	Red block	
Crystal size	0.60 × 0.45 × 0.40 mm^3	

θ range for data collection	$1.87° \leq \theta \leq 26.45°$
Index ranges	$-14 \leq h \leq 10, -24 \leq k \leq 24, -27 \leq l \leq 27$
Reflections collected	60533
Independent reflections	10050 [$R_{int} = 0.0336$]
Completeness to $\theta = 26.45°$	99.4 %
Absorption correction	Semi-empirical (SADABS)
Max. / min. transmission	1.00 / 0.83
Refinement method	Full-matrix least-squares on F^2
Data / restraints / parameters	10050 / 2 / 762
Goodness-of-fit on F^2	1.040
Final R indices [$I>2\sigma(I)$]	$R1 = 0.0475$, $wR2 = 0.1158$
R indices (all data)	$R1 = 0.0621$, $wR2 = 0.1243$
Largest diff. peak / hole	0.887 / –0.644 e Å^{-3}

Table 3.4.14. Atomic coordinates (× 10^4) and equivalent isotropic displacement parameters U_{eq} (× 10^3) [Å^2] for $[Co^{III}(H_2\mathbf{L^{M2}})_2](BF_4)_3 \cdot 2$ EtOH (**22** · 2 EtOH).

Atom	x	y	z	U_{eq}
Co(1)	6717(1)	7398(1)	8045(1)	17(1)
N(1)	7681(2)	8118(1)	7767(1)	20(1)
N(2)	7814(2)	7510(1)	8798(1)	21(1)
N(3)	5832(2)	6725(1)	8459(1)	23(1)
N(4)	9077(2)	9227(1)	7556(1)	28(1)
N(5)	10943(2)	9258(1)	8763(1)	29(1)
N(6)	11485(2)	8029(1)	9735(1)	31(1)
O(1)	9228(2)	8251(1)	9294(1)	29(1)
O(2)	9340(2)	9855(1)	8896(1)	43(1)
C(1)	7660(2)	8353(1)	7202(1)	23(1)
C(2)	8380(2)	8905(1)	7101(1)	27(1)
C(3)	9085(2)	8987(1)	8124(1)	25(1)
C(4)	8414(2)	8423(1)	8235(1)	21(1)
C(5)	8506(2)	8058(1)	8837(1)	22(1)
C(6)	7993(2)	7031(1)	9317(1)	29(1)
C(7)	7633(2)	6296(1)	9111(1)	29(1)
C(8)	6349(2)	6260(1)	8880(1)	26(1)
C(9)	5682(2)	5781(2)	9138(1)	36(1)
C(10)	4490(3)	5797(2)	8994(2)	41(1)
C(11)	3963(2)	6297(2)	8592(1)	33(1)
C(12)	4653(2)	6740(1)	8327(1)	25(1)
C(13)	9807(2)	9398(1)	8642(1)	29(1)
C(14)	11714(3)	9610(2)	9261(1)	36(1)
C(15)	11674(3)	9282(2)	9892(1)	40(1)
C(16)	12180(2)	8570(2)	9944(1)	34(1)

C(17)	13337(3)	8420(2)	10178(2)	48(1)
C(18)	13729(3)	7746(2)	10185(2)	56(1)
C(19)	12986(3)	7210(2)	9960(2)	47(1)
C(20)	11849(3)	7367(2)	9734(1)	36(1)
N(7)	5721(2)	8167(1)	8230(1)	20(1)
N(8)	5602(2)	7394(1)	7287(1)	20(1)
N(9)	7660(2)	6677(1)	7727(1)	21(1)
N(10)	4294(2)	9312(1)	8300(1)	30(1)
N(11)	2345(2)	9141(1)	7143(1)	26(1)
N(12)	1783(2)	7796(1)	6285(1)	36(1)
O(3)	4090(2)	8017(1)	6722(1)	26(1)
O(4)	3920(2)	9663(1)	6884(1)	34(1)
C(21)	5779(2)	8517(1)	8755(1)	26(1)
C(22)	5053(2)	9083(1)	8785(1)	30(1)
C(23)	4252(2)	8958(1)	7777(1)	24(1)
C(24)	4938(2)	8376(1)	7736(1)	21(1)
C(25)	4850(2)	7913(1)	7190(1)	20(1)
C(26)	5495(2)	6852(1)	6818(1)	25(1)
C(27)	5906(2)	6157(1)	7103(1)	25(1)
C(28)	7188(2)	6159(1)	7345(1)	21(1)
C(29)	7890(2)	5655(1)	7154(1)	27(1)
C(30)	9077(2)	5669(2)	7345(1)	33(1)
C(31)	9558(2)	6204(1)	7719(1)	30(1)
C(32)	8836(2)	6695(1)	7898(1)	25(1)
C(33)	3480(2)	9276(1)	7217(1)	25(1)
C(34)	1525(2)	9432(2)	6628(1)	32(1)
C(35)	1523(3)	9029(2)	6029(1)	38(1)
C(36)	1052(2)	8309(2)	6050(1)	35(1)
C(37)	–104(3)	8136(2)	5846(1)	44(1)
C(38)	–470(3)	7459(2)	5883(2)	51(1)
C(39)	318(3)	6948(2)	6121(2)	49(1)
C(40)	1453(3)	7131(2)	6324(1)	43(1)
B(1)	6735(3)	6185(2)	5399(2)	37(1)
F(11)	6323(2)	6833(1)	5164(1)	64(1)
F(12)	7077(2)	5810(1)	4934(1)	57(1)
F(13)	7641(2)	6282(1)	5878(1)	60(1)
F(14)	5857(2)	5838(1)	5609(1)	68(1)
B(2)	11666(3)	7704(2)	8005(2)	41(1)
F(21)	12449(2)	8186(1)	8315(1)	83(1)
F(22)	12245(2)	7273(1)	7686(1)	77(1)
F(23)	11163(2)	7357(1)	8420(1)	80(1)
F(24)	10828(2)	8060(1)	7598(1)	79(1)
B(3)	1465(4)	5328(2)	9315(2)	48(1)
F(31)	2366(11)	5588(8)	9698(6)	107(4)
F(32)	1719(11)	5296(6)	8741(5)	91(4)
F(33)	1193(11)	4704(6)	9508(6)	120(5)
F(34)	497(14)	5746(7)	9338(8)	110(5)

F(35)	1794(8)	5439(7)	8746(5)	76(4)
F(36)	2476(14)	5348(8)	9783(6)	61(3)
F(37)	734(16)	5825(6)	9403(8)	75(4)
F(38)	1014(10)	4656(7)	9294(6)	68(3)
O(50)	7284(4)	10649(2)	8543(2)	100(1)
C(50)	7318(6)	10623(3)	7933(4)	122(3)
C(51)	6490(4)	9970(2)	7524(4)	142(3)
O(60)	6835(6)	8035(4)	5827(3)	78(2)
O(61)	5829(4)	9172(2)	6388(2)	53(1)
C(60)	5341(4)	8941(2)	5790(2)	68(1)
C(61)	6274(5)	8507(2)	5546(2)	78(1)

3.4.8. a: $[Cu^{II}_4(HL^{M1})_4](BF_4)_4 \cdot 3.5\ MeCN$ (23 · 3.5 MeCN)

The asymmetric unit of $[Cu^{II}_4(HL^{M1})_4](BF_4)_4 \cdot 3.5$ MeCN (**23** · 3.5 MeCN) consisted of one [2 × 2] grid-type complex cation $[Cu^{II}_4(HL^{M1})_4]^{4+}$, four tetrafluoroborate counter ions and 3.5 acetonitrile solvent molecules without assigned hydrogen atoms. All non-hydrogen atoms were refined anisotropically. All hydrogen atoms were placed at calculated positions using a riding model, except the former N-H amide protons H(2A), H(4A), H(6A) and H(8A) (see below). All hydrogen atoms had thermal parameters 1.2 times the equivalent isotropic thermal parameter of the atom to which they were bonded. Three of the acetonitrile solvent molecules were disordered over two sites with site occupancies of 0.5.

Because of the near tetragonality of the unit cell, a variety of monoclinic twin laws were tested both with and without inversion twinning (in matrix form, row by row): (0 0 1, 0 –1 0, 1 0 0); (0 1 0, 1 0 0, 0 0 –1), all led to *R*1 ($F>4\sigma(F)$) greater than 0.15. The adopted twin law (0 1 0, –1 0 0 , 0 0 –1), which led to satisfactory elaboration of the initial structure and to stable least-squares refinements, led to four non-inversion-related twin domains with fractional sizes of the three independent components: 0.184(2), 0.112(2), 0.311(2). Reflections of the class *h h* 0, $h = 2n+1$ are systematically

very weak. Intensity statistics (E^2–1 = 0.708) are consistent with acentric twinned data (and with the consequences that incorrectly assigned features of Fourier maps tended to refine quite well, and missing atoms of disordered BF_4^- groups were not strongly differentiated from noise). Moreover, as the molecular species has *4mm* symmetry and refinement in space group *Cc* revealed no signs of disorder, centrosymmetric monoclinic space groups, which would impose inversion symmetry, can be eliminated. Merging of data into orthorhombic or tetragonal crystal classes led to $R_{int} > 0.15$, whereas monoclinic merging led to $R_{int} = 0.074$. Thus, orthorhombic and tetragonal crystal classes can be eliminated also. Merging of data in triclinic symmetry was no better (or worse) than for monoclinic. Because of the near-tetragonal data symmetry and near-*4mm* symmetry of the complex, considerable correlation exists among formally chemically equivalent bond distances and angles, leading to patterns of unnaturally long and short interatomic distances. Therefore, bond distances that are formally chemically equivalent were refined by means of free variables. In addition tight planarity restraints were applied to appropriate rings and tight restraints to nearly spherical ellipsoids were applied to the atomic displacement parameters of B, C, N, O and F atoms. Although the fluorine atoms of the BF_4^- groups exhibited large anisotropic displacement parameters, and were flagged by SHELXL for contemplation of disorder, various disordered models applied to the BF_4^- groups led to unstable refinements, despite very tight restraints on geometry and especially on atomic displacement parameters. The former N-H amide hydrogen atoms shared between pairs of oxygen atoms O(2) and O(1), O(3) and O(4), O(5) and O(6), and O(7) and O(8) were not observed in this structure. As the electron density is shared between two strongly electronegative atoms, and as the hydrogen atom is formally a proton, the amount of electron density to be expected on the hydrogen atom is very small, and will only be observable in extremely well behaved structures. Therefore, these hydrogen atoms have been inserted symmetrically between pairs of oxygen atoms to make chemical sense.

Table 3.4.15. Crystal data and structure refinement of $[Cu^{II}_4(HL^{M1})_4](BF_4)_4 \cdot 3.5$ MeCN (**23** · 3.5 MeCN).

Empirical formula	$C_{79}H_{60}B_4Cu_4F_{16}N_{27.5}O_8$
Formula weight M_r	2123.95
Temperature T	200(2) K
Wavelength	0.71073 Å
Crystal system	Monoclinic
Space group	Cc
Unit cell dimensions	$a = 21.4502(5)$ Å $\quad \alpha = 90°$
	$b = 21.4616(5)$ Å $\quad \beta = 90.156(2)°$
	$c = 19.9220(5)$ Å $\quad \gamma = 90°$
Volume V	9171.2(4) Å^3
Z	4
Density $\rho_{calcd.}$	1.538 g cm^{-3}
Absorption coefficient μ	1.017 mm^{-1}
$F(000)$	4282
Crystal colour and shape	Green block
Crystal size	0.42 × 0.36 × 0.20 mm^3
θ range for data collection	$2.04° \leq \theta \leq 26.48°$
Index ranges	$-26 \leq h \leq 25, -17 \leq k \leq 26, -22 \leq l \leq 24$
Reflections collected	21082
Independent reflections	15580 [$R_{int} = 0.0741$]
Completeness to $\theta = 26.48°$	98.4 %
Absorption correction	Semi-empirical (SADABS)
Max. / min. transmission	0.8225 / 0.6747
Refinement method	Full-matrix least-squares on F^2
Data / restraints / parameters	15580 / 1451 / 1314
Goodness-of-fit on F^2	0.909
Final R indices [$I>2\sigma(I)$]	$R1 = 0.0603$, $wR2 = 0.1166$
R indices (all data)	$R1 = 0.1137$, $wR2 = 0.1366$
Largest diff. peak / hole	0.487 / –0.401 e Å^{-3}

Table 3.4.16. Atomic coordinates (× 10^4) and equivalent isotropic displacement parameters U_{eq} (× 10^3) [Å^2] for $[Cu^{II}_4(HL^{M1})_4](BF_4)_4 \cdot 3.5$ MeCN (**23** · 3.5 MeCN).

Atom	x	y	z	U_{eq}
Cu(1)	1547(1)	4802(1)	6746(1)	48(1)
Cu(2)	–352(1)	2079(1)	7054(1)	59(1)
Cu(3)	2364(1)	192(1)	6857(1)	48(1)
Cu(4)	4253(1)	2899(1)	7101(1)	52(1)
N(3)	1982(2)	5607(4)	7210(5)	57(3)

N(2)	1195(5)	4767(5)	7621(6)	49(3)
N(1)	959(3)	3943(4)	6714(4)	42(3)
N(4)	229(3)	2922(4)	6835(5)	51(3)
N(5)	–315(5)	2547(5)	7900(5)	43(3)
N(6)	–814(2)	1424(4)	7681(6)	69(3)
O(1)	708(5)	4217(5)	8438(5)	65(3)
O(2)	85(6)	3275(5)	8572(5)	69(3)
N(9)	–1129(3)	2505(3)	6618(6)	53(3)
N(8)	–292(5)	1719(6)	6159(6)	52(3)
N(7)	486(4)	1512(3)	7092(5)	51(3)
N(10)	1533(4)	808(4)	7030(5)	55(3)
N(11)	1983(5)	275(6)	5972(6)	54(3)
N(12)	3057(4)	–250(3)	6211(5)	57(3)
O(3)	274(5)	1206(5)	5370(5)	68(3)
O(4)	1199(5)	665(6)	5281(5)	64(3)
N(15)	1928(2)	–618(4)	7337(5)	62(3)
N(14)	2712(6)	261(5)	7765(6)	48(3)
N(13)	2918(3)	1037(4)	6812(5)	45(3)
N(16)	3686(3)	2060(5)	6899(5)	49(3)
N(17)	4212(5)	2488(5)	7948(5)	42(3)
N(18)	4707(2)	3570(4)	7678(6)	56(3)
O(5)	3143(5)	836(5)	8574(5)	62(3)
O(6)	3756(6)	1798(5)	8670(5)	61(3)
N(21)	5035(3)	2467(3)	6681(5)	39(3)
N(20)	4234(5)	3244(6)	6223(6)	52(3)
N(19)	3401(4)	3492(3)	7115(5)	56(3)
N(22)	2357(6)	4190(5)	6956(5)	51(3)
N(23)	1955(4)	4725(4)	5847(5)	41(3)
N(24)	878(3)	5261(3)	6075(5)	46(3)
O(7)	3669(6)	3763(6)	5374(5)	71(3)
O(8)	2738(6)	4323(6)	5212(5)	63(3)
C(12)	2368(4)	5973(5)	6860(7)	61(4)
C(11)	2581(5)	6496(6)	7139(6)	60(3)
C(10)	2390(4)	6639(6)	7771(6)	59(3)
C(9)	1980(4)	6243(5)	8133(7)	59(4)
C(8)	1779(4)	5705(5)	7811(6)	55(3)
C(7)	1399(7)	5196(6)	8143(7)	63(4)
C(5)	867(7)	4298(6)	7843(6)	50(3)
C(4)	720(3)	3828(4)	7306(6)	49(3)
C(1)	854(3)	3589(4)	6191(6)	50(3)
C(2)	490(4)	3086(5)	6268(6)	51(3)
C(3)	337(4)	3291(5)	7382(6)	49(3)
C(13)	15(7)	3042(6)	7998(6)	55(3)
C(15)	–555(6)	2199(5)	8484(6)	45(3)
C(16)	–916(3)	1596(5)	8311(6)	57(3)
C(20)	–1027(4)	841(6)	7512(8)	70(4)
C(19)	–1328(5)	423(7)	7918(7)	73(4)

C(18)	–1419(5)	622(6)	8533(8)	91(5)
C(17)	–1210(4)	1217(6)	8750(7)	71(4)
C(32)	–1567(6)	2897(5)	6831(8)	65(4)
C(31)	–2076(7)	3113(7)	6496(7)	70(4)
C(30)	–2177(6)	2936(5)	5844(7)	69(4)
C(29)	–1722(5)	2527(5)	5614(8)	77(4)
C(28)	–1235(5)	2335(5)	5998(6)	60(4)
C(27)	–777(6)	1894(7)	5678(7)	60(4)
C(25)	177(6)	1379(7)	5964(6)	53(3)
C(24)	645(4)	1260(3)	6504(6)	42(3)
C(21)	831(5)	1418(4)	7627(7)	63(4)
C(22)	1375(6)	1060(5)	7628(7)	67(4)
C(23)	1188(5)	894(4)	6461(6)	45(3)
C(33)	1457(6)	556(7)	5867(6)	44(3)
C(35)	2198(6)	–122(7)	5403(7)	63(4)
C(36)	2848(5)	–333(4)	5596(6)	54(3)
C(40)	3606(6)	–456(5)	6430(8)	79(4)
C(39)	3938(8)	–771(6)	5929(8)	89(5)
C(38)	3748(7)	–874(6)	5302(8)	92(5)
C(37)	3157(7)	–639(5)	5098(8)	81(4)
C(52)	1572(4)	–978(6)	6955(8)	64(4)
C(51)	1360(5)	–1510(7)	7251(7)	62(4)
C(50)	1522(5)	–1632(7)	7896(8)	82(4)
C(49)	1900(5)	–1234(5)	8284(8)	69(4)
C(48)	2103(4)	–696(5)	7950(5)	46(3)
C(47)	2531(7)	–213(6)	8261(7)	51(4)
C(45)	3019(7)	749(6)	7971(6)	44(3)
C(44)	3167(3)	1208(4)	7412(6)	43(3)
C(41)	3047(4)	1358(5)	6283(7)	55(4)
C(42)	3443(4)	1883(5)	6332(6)	41(3)
C(43)	3559(4)	1734(5)	7450(6)	41(3)
C(53)	3838(7)	2022(6)	8084(6)	43(3)
C(55)	4441(7)	2826(6)	8563(6)	48(3)
C(56)	4773(3)	3420(5)	8334(6)	57(4)
C(60)	4948(4)	4125(6)	7500(9)	73(4)
C(59)	5247(5)	4558(7)	7863(8)	80(4)
C(58)	5303(6)	4391(6)	8506(8)	87(4)
C(57)	5070(5)	3823(6)	8769(8)	76(4)
C(72)	5446(6)	2060(5)	6957(8)	70(4)
C(71)	5967(7)	1843(7)	6609(8)	83(5)
C(70)	6086(7)	2043(5)	5974(8)	72(4)
C(69)	5659(5)	2459(5)	5702(8)	65(4)
C(68)	5163(5)	2643(4)	6074(6)	45(3)
C(67)	4721(6)	3081(7)	5744(7)	53(4)
C(65)	3738(6)	3557(7)	5988(6)	48(3)
C(64)	3268(4)	3736(3)	6497(6)	42(3)
C(61)	3032(4)	3593(4)	7636(7)	56(4)

C(62)	2498(6)	3952(5)	7547(7)	62(4)
C(63)	2719(4)	4101(3)	6414(6)	48(3)
C(73)	2468(6)	4395(7)	5777(6)	43(3)
C(75)	1726(6)	5088(7)	5278(7)	52(4)
C(76)	1095(4)	5329(4)	5467(5)	39(3)
C(80)	305(6)	5502(5)	6242(8)	66(4)
C(79)	–34(6)	5814(5)	5775(6)	56(3)
C(78)	188(6)	5898(5)	5134(7)	65(4)
C(77)	768(6)	5638(4)	4986(7)	63(4)
B(1)	599(6)	3367(6)	4300(6)	60(4)
F(11)	418(5)	3513(6)	3698(5)	128(4)
F(12)	1049(5)	3741(5)	4542(5)	106(4)
F(13)	147(4)	3271(6)	4733(5)	111(4)
F(14)	865(5)	2788(4)	4186(8)	176(5)
B(2)	5968(8)	3904(7)	4480(7)	97(5)
F(21)	5565(8)	4307(6)	4173(8)	255(7)
F(22)	6497(6)	4049(7)	4205(7)	212(6)
F(23)	5749(6)	3330(4)	4303(6)	107(4)
F(24)	5967(7)	3968(6)	5130(5)	140(5)
B(3)	2942(7)	3922(7)	9437(7)	93(5)
F(31)	2893(7)	3951(6)	10094(5)	144(5)
F(32)	3396(7)	4285(6)	9197(9)	235(7)
F(33)	2431(6)	4086(7)	9125(6)	174(5)
F(34)	3113(6)	3325(4)	9247(6)	103(4)
B(4)	3370(7)	8493(7)	9347(8)	88(5)
F(41)	3765(5)	8208(5)	9767(5)	103(4)
F(42)	3179(6)	8108(7)	8881(7)	225(6)
F(43)	3661(7)	8957(7)	9046(9)	248(7)
F(44)	2871(4)	8726(5)	9672(6)	97(4)
N(600)	9690(30)	10090(20)	4956(11)	190(20)
C(600)	9740(30)	9960(20)	5526(11)	138(19)
C(601)	9794(16)	10058(15)	6246(11)	78(5)
N(60A)	9100(12)	10007(12)	6205(9)	78(5)
C(60A)	9331(11)	9993(12)	5698(8)	40(6)
C(60B)	9410(20)	9920(20)	4963(10)	92(15)
N(610)	2236(10)	2714(10)	4879(9)	65(7)
C(610)	2065(13)	2560(14)	5425(12)	73(9)
C(611)	1659(12)	2127(12)	5799(13)	66(8)
N(620)	4379(13)	–115(14)	8901(8)	69(9)
C(620)	4490(30)	–120(30)	8334(10)	190(30)
C(621)	4438(19)	–36(18)	7612(9)	69(5)
N(62A)	4458(13)	529(12)	7641(8)	69(5)
C(62A)	4501(9)	339(9)	8170(7)	22(5)
C(62B)	4591(10)	293(10)	8907(7)	27(4)
N(630)	1660(12)	2775(11)	8501(10)	80(6)
C(630)	1724(14)	2667(15)	7926(11)	74(10)
C(631)	2010(30)	2450(30)	7305(14)	161(16)

N(63A)	2084(14)	2410(13)	8030(9)	79(9)
C(63A)	2093(15)	2437(16)	8637(11)	80(6)
C(63B)	1766(14)	2766(14)	9203(12)	74(10)

3.4.9. b: $[Cu^{II}_4(HL^{M1})_4](BF_4)_4 \cdot 3.5\ MeCN$ (23 · 3.5 MeCN)

As the molecular structure of **23** · 3.5 MeCN in the monoclinic space group *P*2(1) was not discussed in Chapter 2, Results and Discussion, some selected distances and angles of the complex cation are given in Tables 3.4.19 and 3.4.20.

The asymmetric unit of $[Cu^{II}_4(HL^{M1})_4](BF_4)_4 \cdot 3.5$ MeCN (**23** · 3.5 MeCN) consisted of one [2 × 2] grid-type complex cation $[Cu^{II}_4(HL^{M1})_4]^{4+}$, four tetrafluoroborate counter ions and 3.5 acetonitrile solvent molecules. All non-hydrogen atoms were refined anisotropically. All hydrogen atoms were placed at calculated positions using a riding model, except the former N-H amide protons H(12), H(34), H(56) and H(78) (see below). All hydrogen atoms had thermal parameters 1.2 times the equivalent isotropic thermal parameter of the atom to which they were bonded. Three of the tetrafluoroborate counter ions are disordered with a site occupancy factor of 0.75 [0.25] for B(1A), F(11A), F(12A), F(13A) and F(14A) [B(1B), F(11B), F(12B), F(13B) and F(14B)], 0.75 [0.25] for B(2A), F(21A), F(22A), F(23A) and F(24A) [B(2B), F(21B), F(22B), F(23B) and F(24B)] and 0.5 for B(4A), B(4B), F(41A), F(42A), F(43A), F(44A), F(41B), F(42B), F(43B) and F(44B) (see below).

Because of the near tetragonality of the unit cell, a variety of monoclinic twin laws were tested both with and without inversion twinning (in matrix form, row by row): (0 0 1, 0 –1 0, 1 0 0); (0 1 0, 1 0 0, 0 0 –1). All led to *R*1 ($F>4\sigma(F)$) greater than 0.15. The adopted twin law (0 1 0, –1 0 0 , 0 0 –1), which led to satisfactory elaboration of the initial structure and to stable least-squares refinements, leads to four non-inversion-related twin domains with fractional sizes: 0.229(2), 0.066(2), 0.216(2) and

0.489. Reflections of the class 0 0 *l*, $l = 2n + 1$ are systematically very weak, indicating the possibility of a second screw axis (and at least intrinsic orthorhombic symmetry) or a glide plane (noting that twinning would overlap reflections *h* 0 *l* and 0 *k l*). Refinements in the monoclinic space group *P*a were less successful than in *P*2(1). Space group *P*2(1)/a would impose a centre of symmetry on the cation, leading to a disordered cation, which was not observed (see below). Intensity statistics (E^2–1 = 0.648) are consistent with acentric twinned data (and with the consequences that incorrectly assigned features of Fourier maps tended to refine quite well, and missing atoms of disordered BF_4^- groups were not strongly differentiated from noise). Moreover, as the molecular species has *4mm* symmetry and refinement in space group *P*2(1) revealed no signs of disorder, centrosymmetric monoclinic space groups, which would impose inversion symmetry, can be eliminated. Merging of data into orthorhombic or tetragonal crystal classes led to $R_{int} > 0.15$, whereas monoclinic merging led to $R_{int} = 0.058$. Thus, orthorhombic crystal classes can be eliminated also. Merging of data in triclinic symmetry was no better (or worse) than for monoclinic. That more than 300 reflections are flagged as inconsistent equivalents and that R_{int} is significantly greater than R_σ is indicative of the difficulties of processing variably and partially overlapped data, consequent upon a monoclinic β angle of 90.409°. Accordingly, in final cycles of refinement 22 reflections with very poor agreement between F_{obs} and F_{calcd} were eliminated. Although the extinction parameter is significantly different from zero [0.047(2)], this is attributed to incomplete recording of reflection data, rather than to extinction itself. Data in shells with resolution better than 0.85 Å were not included, as their mean $I/\sigma(I)$ were less than two. Because of the near-tetragonal data symmetry and near *4mm* symmetry of the complex, considerable correlation exists among formally chemically equivalent bond distances and angles, leading to patterns of unnaturally long and short interatomic distances. Therefore, bond distances that are formally chemically equivalent were refined by means of free variables. In addition tight planarity restraints were applied to appropriate rings and tight restraints to nearly spherical ellipsoids were applied to

the atomic displacement parameters of B, C, N, O and F atoms. Three of the BF_4^- groups are substantially disordered. Residual electron density was concentrated in the vicinity of the copper atoms. The former N-H amide hydrogen atoms shared between pairs of oxygen atoms O(1) and O(2), O(3) and O(4), O(5) and O(6), and O(7) and O(8) were not observed in this structure. As the electron density is shared between two strongly electronegative atoms, and the hydrogen atom is formally a proton, the amount of electron density to be expected on the hydrogen atom is very small, and will only be observable in extremely well behaved structures. Therefore, these hydrogen atoms have been inserted symmetrically between pairs of oxygen atoms to make chemical sense.

Table 3.4.17. Crystal data and structure refinement of $[Cu^{II}_4(H\mathbf{L}^{\mathbf{M1}})_4](BF_4)_4 \cdot 3.5$ MeCN (**23** · 3.5 MeCN).

Empirical formula	$C_{79}H_{70.5}B_4Cu_4F_{16}N_{27.5}O_8$	
Formula weight M_r	2134.53 g mol^{-1}	
Temperature T	200(2) K	
Wavelength	0.71073 Å	
Crystal system	Monoclinic	
Space group	$P2(1)$	
Unit cell dimensions	$a = 15.189(3)$ Å	$\alpha = 90°$
	$b = 15.191(3)$ Å	$\beta = 90.41(3)°$
	$c = 20.048(4)$ Å	$\gamma = 90°$
Volume V	4625.8(16) Å^3	
Z	2	
Density $\rho_{calcd.}$	1.518 g cm^{-3}	
Absorption coefficient	1.007 mm^{-1}	
$F(000)$	2140	
Crystal colour and shape	Green block	
Crystal size	0.38 × 0.35 × 0.22 mm^3	
θ range for data collection	$4.24° \leq \theta \leq 24.71°$	
Index ranges	$-17 \leq h \leq 16$, $-17 \leq k \leq 17$, $-23 \leq l \leq 23$	
Reflections collected	24008	
Independent reflections	15222 [$R_{int} = 0.0575$]	
Completeness to $\theta = 24.71°$	98.9 %	
Absorption correction	Semi-empirical from equivalents	
Max. / min. transmission	0.9076 / 0.8183	
Refinement method	Full-matrix least-squares on F^2	
Data / restraints / parameters	15222 / 1487 / 1290	

Goodness-of-fit on F^2	1.025
Final R indices [$I>2\sigma(I)$]	$R1 = 0.0800$, $wR2 = 0.1952$
R indices (all data)	$R1 = 0.1025$, $wR2 = 0.2204$
Largest diff. peak / hole	0.801 / –0.868 e Å^{-3}

Table 3.4.18. Atomic coordinates (× 10^4) and equivalent isotropic displacement parameters U_{eq} (× 10^3) [Å^2] for $[Cu^{II}_4(H\mathbf{L}^{\mathbf{M1}})_4](BF_4)_4 \cdot 3.5$ MeCN (**23** · 3.5 MeCN).

Atom	x	y	z	U_{eq}
Cu(1)	4796(2)	2813(1)	2267(1)	53(1)
Cu(2)	5613(2)	7431(2)	2684(1)	63(1)
Cu(3)	10251(2)	6579(1)	2470(1)	57(1)
Cu(4)	9386(2)	2003(1)	2595(1)	63(1)
O(1)	4477(9)	4203(7)	4007(5)	70(3)
O(2)	4857(10)	5747(7)	4156(5)	67(3)
O(3)	7086(8)	7714(8)	1017(5)	60(3)
O(4)	8607(8)	7347(9)	930(5)	65(3)
O(5)	10373(10)	5071(8)	4156(5)	74(4)
O(6)	10034(10)	3546(7)	4206(5)	65(3)
O(7)	7953(9)	1883(9)	861(5)	70(3)
O(8)	6450(8)	2220(9)	726(4)	63(3)
N(1)	5046(4)	4252(6)	2275(5)	60(3)
N(2)	4490(9)	3208(6)	3142(5)	50(3)
N(3)	4448(3)	1569(6)	2694(5)	55(3)
N(4)	5413(4)	6009(6)	2440(4)	49(3)
N(5)	5266(9)	6911(7)	3530(5)	53(3)
N(6)	5822(3)	8516(6)	3331(5)	70(4)
N(7)	7037(7)	7179(4)	2740(5)	57(3)
N(8)	6018(8)	7753(8)	1807(5)	55(3)
N(9)	4401(7)	7758(4)	2223(5)	61(3)
N(10)	8813(7)	6826(4)	2655(5)	56(3)
N(11)	9787(8)	6961(9)	1608(5)	63(3)
N(12)	11348(6)	6363(4)	1830(6)	76(4)
N(13)	9962(4)	5184(7)	2409(5)	55(3)
N(14)	10530(9)	6173(7)	3353(5)	55(3)
N(15)	10611(3)	7812(7)	2916(5)	62(3)
N(16)	9636(4)	3434(6)	2450(5)	61(4)
N(17)	9712(10)	2445(7)	3474(5)	61(4)
N(18)	9137(3)	835(6)	3165(6)	61(3)
N(19)	7960(7)	2305(3)	2597(5)	52(3)
N(20)	9026(9)	1753(10)	1692(6)	72(4)
N(21)	10596(7)	1654(3)	2185(5)	62(3)
N(22)	6201(8)	2560(7)	2469(5)	57(3)

N(23)	5267(7)	2468(4)	1390(4)	50(3)
N(24)	3685(7)	3028(4)	1660(5)	64(3)
C(1)	5326(3)	4744(8)	1773(7)	63(4)
C(2)	5516(5)	5642(8)	1848(6)	58(4)
C(3)	5133(5)	5548(7)	2966(5)	51(4)
C(4)	4948(5)	4645(7)	2872(6)	52(3)
C(5)	4649(11)	3993(7)	3397(6)	51(3)
C(7)	4204(14)	2562(7)	3648(7)	65(4)
C(8)	4160(4)	1678(6)	3315(6)	54(4)
C(9)	3824(6)	939(6)	3650(7)	57(4)
C(10)	3797(7)	109(7)	3328(7)	58(3)
C(11)	4103(8)	17(9)	2684(8)	70(4)
C(12)	4422(7)	792(7)	2398(7)	55(3)
C(13)	5054(13)	6079(8)	3590(5)	61(4)
C(15)	5254(14)	7469(8)	4126(5)	60(4)
C(16)	5526(5)	8377(7)	3948(6)	57(4)
C(17)	5558(7)	9028(8)	4449(7)	80(5)
C(18)	5911(8)	9860(10)	4301(9)	86(5)
C(19)	6224(9)	10014(10)	3659(8)	82(5)
C(20)	6170(7)	9325(7)	3178(9)	75(5)
C(21)	7492(9)	6885(4)	3269(6)	60(4)
C(22)	8382(10)	6704(5)	3237(6)	67(4)
C(23)	8365(8)	7118(5)	2127(5)	56(3)
C(24)	7457(8)	7301(5)	2161(5)	48(3)
C(25)	6844(9)	7660(8)	1628(6)	49(3)
C(27)	5378(9)	8052(12)	1318(8)	67(4)
C(28)	4443(9)	8100(5)	1599(6)	58(3)
C(29)	3737(10)	8418(6)	1242(9)	77(4)
C(30)	2900(13)	8396(11)	1535(9)	95(5)
C(31)	2923(13)	8093(11)	2186(9)	81(4)
C(32)	3644(11)	7725(9)	2507(9)	85(5)
C(33)	8954(9)	7147(11)	1520(6)	62(3)
C(35)	10307(10)	6989(10)	1005(7)	63(3)
C(36)	11219(9)	6684(5)	1204(6)	68(4)
C(37)	11838(10)	6661(7)	698(8)	83(4)
C(38)	12658(13)	6263(8)	878(9)	94(5)
C(39)	12813(13)	5928(9)	1513(8)	90(5)
C(40)	12139(10)	5984(7)	1994(9)	79(4)
C(41)	9749(3)	4767(8)	1856(6)	66(4)
C(42)	9581(4)	3854(8)	1882(7)	60(4)
C(43)	9854(5)	3864(7)	3017(6)	54(4)
C(44)	10023(5)	4760(6)	3005(5)	41(3)
C(45)	10298(13)	5392(8)	3547(6)	57(4)
C(47)	10862(12)	6799(7)	3862(7)	57(4)
C(48)	10838(4)	7692(7)	3562(6)	53(3)
C(49)	11136(6)	8414(8)	3925(9)	72(4)
C(50)	11201(8)	9254(10)	3628(8)	83(5)

C(51)	10965(8)	9347(11)	2973(8)	86(5)
C(52)	10663(7)	8592(8)	2619(8)	61(4)
C(53)	9888(12)	3260(7)	3612(6)	51(3)
C(55)	9718(13)	1799(7)	4031(6)	58(4)
C(56)	9367(4)	922(6)	3814(6)	50(3)
C(57)	9268(7)	217(8)	4243(8)	78(5)
C(58)	8929(8)	–599(9)	4020(8)	82(5)
C(59)	8706(9)	–665(9)	3373(8)	83(5)
C(60)	8821(7)	72(7)	2962(9)	68(4)
C(61)	7531(9)	2511(3)	3145(7)	70(4)
C(62)	6604(10)	2648(5)	3064(6)	68(4)
C(63)	6669(8)	2360(3)	1921(5)	48(3)
C(64)	7578(8)	2222(5)	1988(6)	53(3)
C(65)	8224(10)	1920(11)	1473(6)	64(3)
C(67)	9696(10)	1450(13)	1203(8)	70(4)
C(68)	10567(9)	1380(4)	1548(6)	61(3)
C(69)	11255(11)	1064(6)	1153(9)	83(5)
C(70)	12060(13)	1044(9)	1485(9)	104(6)
C(71)	12043(13)	1337(8)	2149(9)	89(5)
C(72)	11333(11)	1657(8)	2536(9)	82(4)
C(73)	6107(8)	2360(11)	1298(5)	51(3)
C(75)	4656(8)	2471(11)	806(6)	51(3)
C(76)	3771(8)	2791(4)	1024(6)	57(3)
C(77)	3083(9)	2831(6)	568(8)	69(4)
C(78)	2220(11)	3127(8)	742(9)	89(5)
C(79)	2106(13)	3388(8)	1406(9)	85(4)
C(80)	2867(10)	3311(7)	1816(9)	78(4)
B(1A)	1997(10)	1823(10)	4838(7)	62(5)
F(11A)	1655(11)	990(8)	4799(10)	127(6)
F(14A)	2849(7)	1787(11)	5098(8)	93(4)
F(13A)	1487(9)	2350(9)	5242(6)	92(4)
F(12A)	2015(11)	2202(12)	4206(5)	101(4)
B(1B)	2145(15)	2029(15)	5013(11)	62(5)
F(11B)	2160(20)	2849(14)	5323(17)	127(6)
F(14B)	2981(14)	1660(20)	5060(20)	93(4)
F(13B)	1550(18)	1497(18)	5338(14)	92(4)
F(12B)	1910(30)	2120(30)	4348(11)	101(4)
B(2A)	2912(9)	7184(9)	5007(8)	51(4)
F(21A)	2695(12)	6306(7)	5037(10)	141(6)
F(24A)	2220(7)	7688(8)	5251(6)	65(3)
F(23A)	3676(6)	7369(10)	5366(6)	83(4)
F(22A)	3025(11)	7442(11)	4351(5)	93(4)
B(2B)	3018(14)	7415(14)	5082(11)	51(4)
F(21B)	3280(20)	8292(13)	5130(20)	141(6)
F(24B)	2192(13)	7330(20)	5357(15)	65(3)
F(23B)	3628(16)	6874(19)	5399(16)	83(4)
F(22B)	2970(30)	7180(30)	4413(11)	93(4)

B(3)	9833(12)	4266(11)	–114(8)	121(8)
F(31)	9168(11)	4042(10)	–561(9)	202(7)
F(32)	10579(12)	4367(10)	–512(10)	208(8)
F(33)	9989(12)	3617(9)	334(6)	139(6)
F(34)	9601(10)	5041(8)	191(7)	120(5)
N(400)	7500(20)	5228(18)	1358(12)	97(10)
C(400)	7530(50)	4670(30)	960(15)	138(17)
C(401)	7682(7)	4279(5)	290(3)	200(30)
B(4A)	5151(7)	5135(5)	–25(3)	83(5)
F(41A)	4256(7)	4965(5)	91(3)	185(9)
F(42A)	5270(7)	5255(5)	–710(3)	111(6)
F(43A)	5633(7)	4398(5)	177(3)	95(5)
F(44A)	5444(7)	5860(5)	331(3)	91(5)
B(4B)	5273(7)	5201(5)	–120(3)	83(5)
F(41B)	6137(7)	5475(5)	–200(3)	185(9)
F(42B)	4811(7)	5250(5)	–722(3)	111(6)
F(43B)	5254(7)	4321(5)	93(3)	95(5)
F(44B)	4846(7)	5711(5)	354(3)	91(5)
N(100)	6934(7)	4626(5)	4857(3)	149(9)
C(100)	6998(7)	4722(5)	4267(3)	125(9)
C(101)	7562(7)	4839(5)	3664(3)	400(30)
N(200)	12339(15)	4313(14)	4473(7)	103(6)
C(200)	12327(16)	4417(15)	3869(8)	101(7)
C(201)	12091(17)	4286(16)	3179(8)	113(7)
N(300)	6990(20)	10190(20)	1777(11)	195(13)
C(300)	7260(20)	9970(20)	1259(10)	129(9)
C(301)	7410(30)	9770(20)	542(10)	148(11)

Table 3.4.19. Selected distances [Å] of **23** · 3.5 MeCN.

Atom(1)-Atom(2)	Distance	Atom(1)-Atom(2)	Distance
Cu(1)-N(1)	2.218(10)	Cu(3)-N(10)	2.250(11)
Cu(1)-N(2)	1.913(10)	Cu(3)-N(11)	1.951(11)
Cu(1)-N(3)	2.142(10)	Cu(3)-N(12)	2.136(10)
Cu(1)-N(22)	2.203(12)	Cu(3)-N(13)	2.167(10)
Cu(1)-N(23)	1.975(9)	Cu(3)-N(14)	1.919(10)
Cu(1)-N(24)	2.098(10)	Cu(3)-N(15)	2.144(10)
Cu(2)-N(4)	2.234(10)	Cu(4)-N(16)	2.226(9)
Cu(2)-N(5)	1.948(10)	Cu(4)-N(17)	1.946(10)
Cu(2)-N(6)	2.121(10)	Cu(4)-N(18)	2.147(10)
Cu(2)-N(7)	2.198(11)	Cu(4)-N(19)	2.215(10)
Cu(2)-N(8)	1.929(11)	Cu(4)-N(20)	1.925(11)
Cu(2)-N(9)	2.114(10)	Cu(4)-N(21)	2.086(11)

Table 3.4.20. Selected angles [°] of **23** · 3.5 MeCN.

A(1)-A(2)-A(3)	Angle	A(1)-A(2)-A(3)	Angle
N(1)-Cu(1)-N(2)	74.2(4)	N(10)-Cu(3)-N(11)	75.6(5)
N(1)-Cu(1)-N(3)	155.4(4)	N(10)-Cu(3)-N(12)	152.5(4)
N(1)-Cu(1)-N(22)	90.3(3)	N(10)-Cu(3)-N(13)	88.6(2)
N(1)-Cu(1)-N(23)	101.8(3)	N(10)-Cu(3)-N(14)	96.3(5)
N(1)-Cu(1)-N(24)	89.3(3)	N(10)-Cu(3)-N(15)	91.8(2)
N(2)-Cu(1)-N(3)	81.3(4)	N(11)-Cu(3)-N(12)	78.0(5)
N(2)-Cu(1)-N(22)	97.3(5)	N(11)-Cu(3)-N(13)	99.7(5)
N(2)-Cu(1)-N(23)	172.4(5)	N(11)-Cu(3)-N(14)	171.5(6)
N(2)-Cu(1)-N(24)	106.5(5)	N(11)-Cu(3)-N(15)	101.5(5)
N(3)-Cu(1)-N(22)	90.8(3)	N(12)-Cu(3)-N(13)	88.5(3)
N(3)-Cu(1)-N(23)	102.3(3)	N(12)-Cu(3)-N(14)	109.7(5)
N(3)-Cu(1)-N(24)	99.8(3)	N(12)-Cu(3)-N(15)	100.8(3)
N(22)-Cu(1)-N(23)	76.1(4)	N(13)-Cu(3)-N(14)	77.4(4)
N(22)-Cu(1)-N(24)	155.1(4)	N(13)-Cu(3)-N(15)	158.2(4)
N(23)-Cu(1)-N(24)	79.6(4)	N(14)-Cu(3)-N(15)	81.0(4)
N(4)-Cu(2)-N(5)	76.2(4)	N(16)-Cu(4)-N(17)	74.9(4)
N(4)-Cu(2)-N(6)	154.8(4)	N(16)-Cu(4)-N(18)	155.2(4)
N(4)-Cu(2)-N(7)	88.6(2)	N(16)-Cu(4)-N(19)	88.0(2)
N(4)-Cu(2)-N(8)	95.2(4)	N(16)-Cu(4)-N(20)	96.8(5)
N(4)-Cu(2)-N(9)	90.9(2)	N(16)-Cu(4)-N(21)	92.6(2)
N(5)-Cu(2)-N(6)	79.8(4)	N(17)-Cu(4)-N(18)	81.2(4)
N(5)-Cu(2)-N(7)	99.1(5)	N(17)-Cu(4)-N(19)	99.7(5)
N(5)-Cu(2)-N(8)	170.6(5)	N(17)-Cu(4)-N(20)	171.2(6)
N(5)-Cu(2)-N(9)	103.6(5)	N(21)-Cu(4)-N(17)	103.0(5)
N(6)-Cu(2)-N(7)	87.8(3)	N(18)-Cu(4)-N(19)	89.6(2)
N(6)-Cu(2)-N(8)	108.2(4)	N(18)-Cu(4)-N(20)	106.7(6)
N(6)-Cu(2)-N(9)	102.1(3)	N(18)-Cu(4)-N(21)	99.1(3)
N(7)-Cu(2)-N(8)	76.8(4)	N(19)-Cu(4)-N(20)	76.8(5)
N(7)-Cu(2)-N(9)	156.5(4)	N(19)-Cu(4)-N(21)	156.6(4)
N(8)-Cu(2)-N(9)	79.9(4)	N(20)-Cu(4)-N(21)	79.9(5)

3.4.10. $[Cu^{II}_4(HL^{M2})_4](BF_4)_4$ (24)

The asymmetric unit of $[Cu^{II}_4(HL^{M2})_4](BF_4)_4$ (**24**) consisted of a quarter tetranuclear square complex $[Cu^{II}_4(HL^{M2})_4]^{4+}$, with the uncoordinated free pyridyl moiety and the methylene linker removed (see below). Tetrafluoroborate counter ions were also removed (see below). All non-hydrogen atoms were refined anisotropically. All hydrogen atoms were placed at calculated positions using a riding model and had thermal parameters 1.2 times the equivalent isotropic thermal parameter of the atom to which they were bonded.

The calculated molar mass, density and absorption coefficient pertain only to the ordered part of the cation. The disordered pyridyl group, anion and solvate species were removed and final refinements were made with data that had been subjected to the SQUEEZE procedure from the PLATON suite.[191]

The overall apparent thermal motion is quite high, leading to a rapid drop-off in intensity at moderate resolution. Refinement died with $R1 = 0.096$, with badly disordered non-coordinated pyridyl, solvent and BF_4^- moieties. The non-coordinated pyridyl group occupied two different sites with approximately equal occupancy, with substantial librational motions in each site about the methylene linker groups. In addition these sites were alternately occupied by a BF_4^- counter ion. In view of the serious disorder, which could not be properly modelled, the structure was subjected to SQUEEZE from the PLATON suite,[191] which calculated a void volume of 2497 $Å^3$ and 768 electrons per unit cell (I-centring led to SQUEEZE apparently mis-reporting the electron density by a factor of two *i.e.* 384 electrons; this error was clearly seen by comparison of calc. electron count with calc. void volume). Methylene carbon C(26) was eliminated for the accurate calculation of the void volume of the attached pyridyl side chain and electron density in the void volume, but this carbon was readily apparent in the subsequent difference Fourier map and was accordingly re-included in the model. Metrical parameters of the copper complex had improved

internal consistency as a result of proper treatment of the disordered components of the structure. Inversion twinning was apparent (minor component 0.195(32)).

Table 3.4.21. Crystal data and structure refinement of $[Cu^{II}_4(HL^{M2})_4](BF_4)_4$ (**24**).

Empirical formula	$C_{54}H_{44}Cu_4N_{20}O_8$	
Formula weight M_r	1355.25 g mol^{-1}	
Temperature T	168(2) K	
Wavelength	0.71073 Å	
Crystal system	Tetragonal	
Space group	$I\bar{4}$	
Unit cell dimensions	a = 16.152(3) Å	α = 90°
	b = 16.152(3) Å	β = 90°
	c = 17.855(8) Å	γ = 90°
Volume V	4658(2) Å^3	
Z	2	
Density $\rho_{calcd.}$	0.966 g cm^{-3}	
Absorption coefficient μ	0.945 mm^{-1}	
F(000)	1760	
Crystal colour and shape	Bottle green plate	
Crystal size	0.37 × 0.31 × 0.11 mm^3	
θ range for data collection	5.11° ≤ 24.69°	
Index ranges	$-17 \le h \le 8$, $-18 \le k \le 18$, $-20 \le l \le 20$	
Reflections collected	9277	
Independent reflections	3910 [R_{int} = 0.0883]	
Completeness to θ = 24.69°	98.9 %	
Absorption correction	Semi-empirical (SADABS)	
Max. / min. transmission	1.00 / 0.64	
Refinement method	Full-matrix least-squares on F^2	
Data / restraints / parameters	3910 / 12 / 195	
Goodness-of-fit on F^2	0.859	
Final R indices [$I>2\sigma(I)$]	$R1$ = 0.0613, $wR2$ = 0.1286	
R indices (all data)	$R1$ = 0.1252, $wR2$ = 0.1479	
Largest diff. peak / hole	0.281 / –0.373 e Å^{-3}	

Table 3.4.22. Atomic coordinates (× 10^4) and equivalent isotropic displacement parameters U_{eq} (× 10^3) [Å^2] for $[Cu^{II}_4(HL^{M2})_4](BF_4)_4$ (**24**).

Atom	X	y	z	U_{eq}
Cu(1)	4599(1)	3000(1)	2403(1)	46(1)
N(1)	5648(3)	2342(3)	2579(3)	40(1)
C(2)	6121(6)	2198(5)	1966(5)	50(2)
C(3)	6795(6)	1678(5)	1994(4)	46(2)
N(2)	6966(4)	1309(4)	2664(4)	49(2)
C(4)	6542(5)	1464(5)	3250(4)	46(2)
C(5)	5889(6)	1993(6)	3225(4)	54(3)
C(6)	5767(6)	2684(5)	1289(4)	50(2)
O(1)	6176(4)	2745(4)	685(3)	74(2)
N(3)	5048(4)	3013(4)	1423(3)	42(2)
C(7)	4705(6)	3499(6)	795(5)	72(3)
C(8)	3812(5)	3764(6)	987(4)	56(2)
C(9)	3751(5)	4365(5)	1625(5)	53(2)
C(10)	3401(5)	5144(7)	1558(5)	66(3)
C(11)	3351(5)	5649(6)	2166(6)	68(3)
C(12)	3673(5)	5394(6)	2832(5)	60(3)
C(13)	4007(5)	4618(6)	2859(5)	53(2)
N(4)	4073(3)	4121(4)	2302(4)	42(2)
O(2)	7883(3)	794(3)	1560(3)	46(1)
N(5)	7371(5)	1715(5)	754(4)	79(3)
C(26)	7396(5)	1374(6)	1399(4)	47(2)
C(27)	7890(20)	1487(18)	268(16)	134(10)

3.4.11. $[Ni^{II}_4(HL^{M2})_4](BF_4)_4 \cdot 10\,MeCN$ (25 · 10 MeCN)

The asymmetric unit of $[Ni^{II}_4(HL^{M2})_4](BF_4)_4 \cdot 10$ MeCN (**25** · 10 MeCN) consisted of two independent tetranuclear grid complexes $[Ni^{II}_4(HL^{M2})_4]^{4+}$ and four full occupancy tetrafluoroborate counter ions. Four disordered tetrafluoroborate counter ions and all solvent molecules were removed (see below). All non–hydrogen atoms were refined anisotropically. All hydrogen atoms were placed at calculated positions using a riding model and had thermal parameters 1.2 times the equivalent isotropic thermal parameters of the atom to which they were bonded.

As one of the two independent complex cations has not been discussed in Chapter 2, Results and Discussion, selected bond distances and angles of this complex cation [involving Ni(5) to Ni(8)] are given in Tables 3.4.25 and 2.3.26.

Calculations of molar mass, density, $F(000)$ and absorption coefficient are based upon the well defined cations and four ordered BF_4^- anions. Acetonitrile solvent molecules and four tetrafluoroborate anions were marginally visible in electron density maps, and were badly disordered. Because of disorder and the large amounts of missing electron density, the structure was subjected to the SQUEEZE procedure from the PLATON suite.[191]

Refinements with four ordered BF_4^- and four disordered BF_4^- ions distributed over 6 sites and 10 disordered acetonitrile moieties converged at $R1$ ($I>2\sigma(I)$) ~0.13. There was much residual uninterpretable electron density away from the grid complexes. Therefore, the two crystallographically independent Ni_4 grid complexes and the four ordered $(BF_4)^-$ groups were retained and the structure subjected to SQUEEZE from the PLATON suite.[191] A total solvent-accessible void volume of 4264 $Å^3$ containing 1349 electrons per unit cell was calculated ($2 \times \{10 \times MeCN + 4 \times BF_4^-\}$ = 1168). Final refinement converged at $R1 = 0.0631$ (0.072 with inclusion of contribution from contents of the void volume). Somewhat to our surprise 4 of the 8 former N-H amide protons turned up. None were exactly symmetrical with the shorter O-H separations in the range of 1.12–1.16 Å and the longer separations in the range 1.29–1.21 Å. On reflection this is not so surprising as the crystal environment is full of charges and dipoles. These hydrogen atoms curiously are all on opposite sides of the square and all four observed O···H···O pointed "North-South".

Four of the pyridyl rings on one of the two crystallographically independent molecules have anomalously high apparent thermal motion due to apparent libration about CH_2-CH_2 bonds. A disorder model was imposed, including bond distance and planarity restraints: atoms were restricted to isotropic displacement factors with tight similarity restraints imposed on sites closer than 1 Å apart, but this did not lead to an improved model. Significant residual electron density remained in the vicinity of

these putatively disordered pyridyl rings. Although the ellipsoids are rather eccentric, their sizes and relative orientations seem more consistent with free librational motion than with two discrete non-resolved conformations. No significant residual electron density was present in these regions, and $R1$ and $wR2$ were slightly lower.

Table 3.4.23. Crystal data and structure refinement of $[Ni^{II}_4(HL^{M2})_4](BF_4)_4 \cdot 10$ MeCN (**25** · 10 MeCN).

Empirical formula	$C_{80}H_{78}B_2F_8N_{24}Ni_4O_8$	
Formula weight M_r	1912.12 g mol^{-1}	
Temperature T	150(2) K	
Wavelength	0.71073 Å	
Crystal system	Triclinic	
Space group	$P\bar{1}$	
Unit cell dimensions	a = 21.7134(3) Å	α = 108.8230(10)°
	b = 21.8434(3) Å	β = 103.0400(10)°
	c = 26.24680(10) Å	γ = 90.7210(10)°
Volume V	11429.8(2) Å^3	
Z	4	
Density $\rho_{calcd.}$	1.111 g cm^{-3}	
Absorption coefficient μ	0.714 mm^{-1}	
$F(000)$	3936	
Crystal colour and shape	Red-brown block	
Crystal size	0.40 × 0.20 × 0.12 mm^3	
θ range for data collection	2.72° ≤ 24.71°	
Index ranges	$-25 \le h \le 24$, $-25 \le k \le 24$, $0 \le l \le 30$	
Reflections collected	93504	
Independent reflections	38305 [R_{int} = 0.0996]	
Completeness to θ = 24.71°	98.3 %	
Absorption correction	Semi-empirical (SADABS)	
Max. / min. transmission	0.94 / 0.71	
Refinement method	Full-matrix least-squares on F^2	
Data / restraints / parameters	38305 / 0 / 2270	
Goodness-of-fit on F^2	0.750	
Final R indices [$I>2\sigma(I)$]	$R1$ = 0.0631, $wR2$ = 0.1402	
R indices (all data)	$R1$ = 0.1487, $wR2$ = 0.1639	
Largest diff. peak / hole	0.481 / –0.321 e Å^{-3}	

Table 3.4.24. Atomic coordinates (× 10^4) and equivalent isotropic displacement parameters U_{eq} (× 10^3) [$Å^2$] for $[Ni^{II}_4(HL^{M2})_4](BF_4)_4 \cdot 10$ MeCN (**25** · 10 MeCN).

Atom	x	y	z	U_{eq}
Ni(1)	6386(1)	1478(1)	1791(1)	63(1)
Ni(2)	9587(1)	1427(1)	1813(1)	56(1)
Ni(3)	6145(1)	4164(1)	878(1)	50(1)
Ni(4)	9381(1)	4132(1)	915(1)	47(1)
O(1)	7828(2)	2488(2)	3168(2)	84(1)
O(2)	8927(2)	2435(2)	3180(1)	71(1)
O(3)	7581(2)	5306(3)	2184(2)	139(2)
O(4)	8686(2)	5234(2)	2230(2)	96(2)
O(5)	6028(2)	1341(2)	143(1)	52(1)
O(6)	5904(2)	2258(2)	–165(1)	51(1)
O(7)	9024(2)	1318(2)	173(1)	53(1)
O(8)	8995(2)	2240(2)	–136(1)	49(1)
N(1)	7340(2)	1464(2)	1739(2)	55(1)
N(2)	6862(3)	1958(3)	2582(2)	73(2)
N(3)	5507(3)	1624(2)	1986(2)	76(2)
N(4)	8604(2)	1419(2)	1754(2)	56(1)
N(5)	9548(3)	1884(2)	2610(2)	64(1)
N(6)	10588(2)	1594(2)	2035(2)	67(1)
N(7)	7114(2)	4113(2)	830(2)	48(1)
N(8)	6634(2)	4864(2)	1585(2)	63(1)
N(9)	5288(2)	4261(2)	1139(2)	49(1)
N(10)	8385(2)	4093(2)	848(2)	42(1)
N(11)	9301(2)	4812(2)	1635(2)	50(1)
N(12)	10381(2)	4230(2)	1159(2)	54(1)
N(13)	6371(2)	2341(2)	1578(2)	53(1)
N(14)	6056(2)	1135(2)	946(2)	57(1)
N(15)	6455(3)	527(3)	1831(2)	72(2)
N(16)	6289(2)	3398(2)	1217(2)	47(1)
N(17)	5830(2)	3349(2)	202(1)	39(1)
N(18)	6045(2)	4757(2)	350(2)	57(1)
N(19)	9504(2)	2298(2)	1603(2)	52(1)
N(20)	9451(2)	1107(2)	971(2)	50(1)
N(21)	9548(2)	461(2)	1819(2)	61(1)
N(22)	9394(2)	3354(2)	1248(2)	42(1)
N(23)	9306(2)	3323(2)	242(2)	42(1)
N(24)	9204(2)	4743(2)	403(2)	58(1)
C(1)	7532(3)	1144(3)	1289(2)	59(2)
C(2)	8166(3)	1122(3)	1295(2)	53(2)
C(3)	8425(3)	1760(3)	2227(2)	54(2)
C(4)	7776(3)	1775(3)	2210(2)	56(2)
C(5)	7451(4)	2107(3)	2698(2)	61(2)
C(6)	6551(3)	2216(4)	3044(2)	93(2)

C(7)	5992(4)	1741(4)	2968(3)	99(2)
C(8)	5423(4)	1721(4)	2511(3)	94(2)
C(9)	4828(5)	1816(4)	2615(3)	98(2)
C(10)	4318(4)	1833(4)	2208(4)	113(3)
C(11)	4390(4)	1752(3)	1671(3)	92(2)
C(12)	4994(4)	1654(3)	1606(3)	81(2)
C(15)	9018(4)	2052(3)	2714(2)	63(2)
C(16)	10100(3)	2115(3)	3086(2)	72(2)
C(17)	10608(3)	1650(3)	2990(2)	85(2)
C(18)	10939(4)	1687(3)	2548(3)	73(2)
C(19)	11600(4)	1846(3)	2677(4)	100(3)
C(20)	11880(4)	1867(4)	2259(4)	117(3)
C(21)	11521(4)	1782(3)	1745(3)	98(2)
C(22)	10870(4)	1648(3)	1648(3)	77(2)
C(31)	7313(3)	3743(2)	393(2)	47(1)
C(32)	7951(3)	3735(2)	404(2)	42(1)
C(33)	8201(3)	4477(3)	1299(2)	50(1)
C(34)	7556(3)	4498(2)	1291(2)	49(1)
C(35)	7252(3)	4912(3)	1728(3)	80(2)
C(36)	6334(3)	5350(3)	1977(3)	100(3)
C(37)	5654(3)	5394(3)	1701(3)	87(2)
C(38)	5206(3)	4789(3)	1561(2)	63(2)
C(39)	4750(3)	4781(3)	1855(2)	68(2)
C(40)	4348(3)	4226(3)	1707(2)	75(2)
C(41)	4408(3)	3672(3)	1266(2)	72(2)
C(42)	4882(3)	3722(3)	998(2)	58(2)
C(45)	8756(3)	4868(3)	1755(3)	62(2)
C(46)	9854(3)	5233(3)	2049(2)	74(2)
C(47)	10369(3)	5335(3)	1758(2)	72(2)
C(48)	10719(3)	4755(3)	1563(2)	53(2)
C(49)	11370(3)	4763(3)	1807(2)	62(2)
C(50)	11672(3)	4200(3)	1606(2)	71(2)
C(51)	11335(3)	3661(3)	1201(2)	64(2)
C(52)	10697(3)	3694(3)	987(2)	59(2)
C(61)	6484(3)	2937(3)	1931(2)	66(2)
C(62)	6455(3)	3472(3)	1758(2)	63(2)
C(63)	6179(2)	2783(3)	839(2)	40(1)
C(64)	6219(2)	2235(3)	1018(2)	47(1)
C(65)	6099(2)	1544(3)	674(2)	53(2)
C(66)	5872(3)	459(3)	606(2)	67(2)
C(67)	5631(3)	102(3)	959(2)	78(2)
C(68)	6134(3)	15(4)	1422(3)	72(2)
C(69)	6257(3)	–619(3)	1394(3)	84(2)
C(70)	6741(4)	–716(4)	1814(3)	92(2)
C(71)	7058(4)	–162(4)	2243(3)	90(2)
C(72)	6899(3)	423(3)	2235(3)	81(2)
C(75)	5958(2)	2787(3)	251(2)	43(1)

C(76)	5504(2)	3324(3)	–362(2)	50(1)
C(77)	5224(3)	3961(3)	–338(2)	56(2)
C(78)	5721(3)	4521(3)	–185(3)	59(2)
C(79)	5847(3)	4764(3)	–585(3)	81(2)
C(80)	6312(4)	5255(4)	–451(4)	101(3)
C(81)	6631(3)	5511(3)	90(4)	92(2)
C(82)	6487(3)	5267(3)	493(3)	75(2)
C(91)	9585(3)	2901(3)	1973(2)	56(2)
C(92)	9518(2)	3423(3)	1785(2)	51(2)
C(93)	9289(2)	2753(3)	873(2)	40(1)
C(94)	9339(2)	2208(2)	1046(2)	41(1)
C(95)	9268(2)	1504(3)	706(2)	47(1)
C(96)	9443(3)	422(2)	624(2)	55(2)
C(97)	9880(3)	65(3)	950(2)	64(2)
C(98)	9633(3)	–54(3)	1404(2)	59(2)
C(99)	9523(3)	–696(3)	1398(3)	73(2)
C(100)	9304(3)	–800(3)	1818(3)	80(2)
C(101)	9190(3)	–276(4)	2234(3)	83(2)
C(102)	9315(3)	354(3)	2232(2)	69(2)
C(105)	9176(2)	2765(3)	284(2)	40(1)
C(106)	9305(3)	3313(2)	–323(2)	56(2)
C(107)	9603(3)	3944(3)	–309(2)	53(2)
C(108)	9220(3)	4498(3)	–135(3)	62(2)
C(109)	8855(3)	4733(3)	–536(3)	77(2)
C(110)	8476(3)	5240(4)	–363(4)	103(3)
C(111)	8488(3)	5497(3)	186(4)	88(2)
C(112)	8855(3)	5242(3)	554(3)	64(2)
Ni(5)	2111(1)	6857(1)	4447(1)	70(1)
Ni(6)	5373(1)	6951(1)	4579(1)	70(1)
Ni(7)	1673(1)	8850(1)	2797(1)	52(1)
Ni(8)	4910(1)	8887(1)	2869(1)	52(1)
O(9)	3472(2)	8162(2)	5714(2)	89(1)
O(10)	4576(2)	8123(2)	5796(2)	83(1)
O(11)	3021(2)	10278(2)	3928(1)	65(1)
O(12)	4143(2)	10258(2)	3984(1)	66(1)
O(13)	1757(2)	6166(2)	2737(2)	62(1)
O(14)	1530(2)	6840(2)	2169(1)	56(1)
O(15)	4971(2)	6222(2)	2873(2)	76(1)
O(16)	4788(2)	6872(2)	2281(1)	65(1)
N(25)	3098(2)	6799(2)	4462(2)	62(1)
N(26)	2553(3)	7530(3)	5177(2)	74(2)
N(28)	4385(2)	6817(2)	4509(2)	56(1)
N(29)	5260(3)	7602(2)	5295(2)	71(2)
N(31)	2647(2)	8814(2)	2764(2)	48(1)
N(32)	2099(3)	9708(2)	3372(2)	58(1)
N(33)	811(2)	9018(3)	3032(2)	61(1)
N(34)	3921(2)	8809(2)	2808(2)	51(1)

N(35)	4784(3)	9727(2)	3437(2)	59(1)
N(36)	5912(2)	9123(2)	3100(2)	57(1)
N(37)	2092(2)	7522(2)	3995(2)	53(1)
N(38)	1819(2)	6271(2)	3641(2)	62(1)
N(40)	1900(2)	8286(2)	3350(2)	51(1)
N(41)	1420(2)	7909(2)	2291(2)	52(1)
N(42)	1484(2)	9190(2)	2110(2)	52(1)
N(43)	5161(2)	7582(2)	4101(2)	57(1)
N(44)	5315(2)	6360(2)	3795(2)	68(2)
N(46)	4994(2)	8347(2)	3435(2)	51(1)
N(47)	4909(2)	7944(2)	2380(2)	50(1)
N(48)	4715(2)	9206(2)	2172(2)	50(1)
C(121)	3315(4)	6361(3)	4060(2)	69(2)
C(122)	3954(4)	6384(3)	4094(2)	61(2)
C(123)	4165(4)	7252(3)	4916(2)	58(2)
C(124)	3519(4)	7245(3)	4893(2)	63(2)
C(125)	3151(4)	7663(3)	5285(2)	68(2)
C(126)	2222(3)	7927(3)	5570(2)	82(2)
C(127)	1640(4)	7538(4)	5581(3)	101(3)
N(27)	1207(3)	7121(3)	4567(3)	90(2)
C(128)	1084(5)	7421(4)	5070(4)	111(3)
C(129)	491(6)	7620(6)	5125(5)	178(5)
C(130)	14(5)	7538(6)	4657(5)	197(6)
C(131)	120(5)	7236(5)	4140(5)	161(4)
C(132)	715(5)	7044(4)	4124(3)	103(2)
C(135)	4699(4)	7691(3)	5366(2)	63(2)
C(136)	5781(4)	8012(3)	5736(2)	96(2)
C(137)	6408(5)	7694(5)	5745(4)	171(5)
N(30)	6341(4)	7306(4)	4767(4)	118(3)
C(138)	6671(6)	7659(6)	5279(5)	134(4)
C(139)	7270(8)	8004(8)	5360(8)	256(10)
C(140)	7536(8)	8011(11)	4911(9)	304(12)
C(141)	7162(8)	7666(8)	4381(6)	244(8)
C(142)	6593(6)	7331(6)	4340(6)	161(4)
C(151)	2870(3)	8343(2)	2408(2)	51(2)
C(152)	3510(3)	8339(3)	2427(2)	55(2)
C(153)	3711(3)	9293(3)	3180(2)	50(2)
C(154)	3063(3)	9294(2)	3160(2)	48(2)
C(155)	2712(3)	9795(3)	3518(2)	52(2)
C(156)	1753(3)	10234(3)	3666(2)	67(2)
C(157)	1086(3)	10203(3)	3332(2)	74(2)
C(158)	674(3)	9628(4)	3291(2)	74(2)
C(159)	130(4)	9709(5)	3510(3)	103(3)
C(160)	–251(5)	9184(6)	3472(3)	123(4)
C(161)	–106(4)	8568(4)	3218(3)	93(2)
C(162)	424(4)	8515(4)	3006(2)	78(2)
C(165)	4241(3)	9796(2)	3564(2)	55(2)

C(166)	5288(3)	10252(3)	3749(2)	72(2)
C(167)	5757(3)	10280(3)	3405(2)	72(2)
C(168)	6172(3)	9742(3)	3345(2)	63(2)
C(169)	6838(4)	9859(4)	3534(2)	84(2)
C(170)	7235(4)	9364(5)	3483(3)	96(2)
C(171)	6947(3)	8734(4)	3228(3)	79(2)
C(172)	6294(3)	8638(3)	3049(2)	66(2)
C(181)	2190(3)	8152(3)	4225(2)	56(2)
C(182)	2080(3)	8553(3)	3893(2)	58(2)
C(183)	1821(2)	7637(2)	3098(2)	43(1)
C(184)	1910(2)	7237(3)	3432(2)	50(1)
C(185)	1835(3)	6508(3)	3247(3)	55(2)
C(186)	1643(3)	5572(3)	3480(2)	85(2)
C(187)	1305(4)	5430(3)	3902(3)	103(3)
N(39)	2100(3)	6058(3)	4739(3)	96(2)
C(188)	1730(5)	5512(4)	4444(3)	116(3)
C(189)	1735(6)	4982(4)	4654(4)	190(6)
C(190)	2130(6)	5082(5)	5176(5)	185(5)
C(191)	2533(6)	5641(5)	5478(4)	159(4)
C(192)	2477(4)	6105(4)	5228(3)	122(3)
C(195)	1584(2)	7451(3)	2483(2)	44(1)
C(196)	1107(2)	7712(3)	1693(2)	52(2)
C(197)	708(3)	8248(3)	1583(2)	56(2)
C(198)	1076(3)	8847(3)	1619(2)	51(1)
C(199)	1034(3)	9034(3)	1153(2)	51(2)
C(200)	1395(3)	9580(3)	1190(2)	63(2)
C(201)	1797(3)	9939(3)	1691(2)	62(2)
C(202)	1828(3)	9724(3)	2133(2)	65(2)
C(211)	5150(3)	8222(3)	4314(2)	60(2)
C(212)	5071(3)	8610(3)	3970(2)	56(2)
C(213)	4974(3)	7700(3)	3207(2)	52(2)
C(214)	5068(3)	7294(3)	3545(2)	53(2)
C(215)	5117(3)	6574(3)	3392(3)	60(2)
C(216)	5455(3)	5678(3)	3643(2)	80(2)
C(217)	6023(4)	5622(3)	4110(3)	120(3)
N(45)	5557(3)	6175(3)	4894(2)	100(2)
C(218)	5806(5)	5649(4)	4648(3)	142(4)
C(219)	5976(6)	5165(4)	4866(4)	181(5)
C(220)	5916(6)	5229(4)	5366(4)	199(6)
C(221)	5626(6)	5759(5)	5635(3)	213(7)
C(222)	5489(5)	6221(3)	5384(3)	150(4)
C(225)	4881(3)	7484(3)	2576(2)	55(2)
C(226)	4884(3)	7748(2)	1779(2)	56(2)
C(227)	5213(3)	8284(3)	1650(2)	55(2)
C(228)	4834(3)	8865(3)	1684(2)	51(2)
C(229)	4600(3)	9050(3)	1227(2)	57(2)
C(230)	4277(3)	9563(3)	1255(2)	70(2)

C(231)	4154(3)	9902(3)	1741(2)	64(2)
C(232)	4386(3)	9714(3)	2187(2)	62(2)
B(1)	777(5)	1812(5)	235(4)	89(3)
F(11)	490(2)	2172(2)	616(2)	110(1)
F(12)	728(2)	1169(2)	231(2)	141(2)
F(13)	506(3)	1860(3)	–266(2)	161(2)
F(14)	1419(2)	2037(2)	401(2)	154(2)
B(2)	2807(5)	6870(4)	1097(3)	75(2)
F(21)	2281(2)	7145(3)	929(2)	155(2)
F(22)	2749(2)	6237(2)	802(2)	137(2)
F(23)	2942(3)	6983(2)	1641(2)	163(2)
F(24)	3278(2)	7189(3)	984(2)	166(2)
B(3)	4302(6)	1835(6)	203(5)	113(4)
F(31)	4820(2)	2184(2)	570(2)	115(1)
F(32)	4352(3)	1190(3)	181(2)	163(2)
F(33)	3788(3)	2025(3)	371(3)	195(3)
F(34)	4318(3)	1866(3)	–309(2)	174(2)
B(4)	8583(6)	709(5)	3464(5)	100(3)
F(41)	8534(2)	39(2)	3263(2)	116(1)
F(42)	9184(3)	963(3)	3604(2)	166(2)
F(43)	8387(4)	860(3)	3944(3)	277(5)
F(44)	8248(3)	980(3)	3133(3)	225(4)

Table 3.4.25. Selected distances [Å] of the complex cation involving Ni(5)–Ni(8) of **25** · 10 MeCN.

Atom(1)-Atom(2)	Distance	Atom(1)-Atom(2)	Distance
Ni(5)-N(25)	2.141(5)	Ni(7)-N(31)	2.137(4)
Ni(5)-N(26)	2.017(5)	Ni(7)-N(32)	2.036(5)
Ni(5)-N(27)	2.116(6)	Ni(7)-N(33)	2.102(5)
Ni(5)-N(37)	2.148(4)	Ni(7)-N(40)	2.174(4)
Ni(5)-N(38)	2.035(4)	Ni(7)-N(41)	2.043(4)
Ni(5)-N(39)	2.122(5)	Ni(7)-N(42)	2.122(4)
Ni(6)-N(28)	2.119(5)	Ni(8)-N(34)	2.117(5)
Ni(6)-N(29)	2.028(5)	Ni(8)-N(35)	2.024(4)
Ni(6)-N(30)	2.124(8)	Ni(8)-N(36)	2.130(5)
Ni(6)-N(43)	2.135(4)	Ni(8)-N(46)	2.154(4)
Ni(6)-N(44)	2.019(4)	Ni(8)-N(47)	2.044(4)
Ni(6)-N(45)	2.117(5)	Ni(8)-N(48)	2.120(4)

Table 3.4.26. Selected angles [°] of the complex cation involving Ni(5)–Ni(8) of **25** · 10 MeCN.

A(1)-A(2)-A(3)	Angle	A(1)-A(2)-A(3)	Angle
N(25)-Ni(5)-N(26)	76.2(2)	N(31)-Ni(7)-N(32)	76.50(19)
N(25)-Ni(5)-N(27)	167.2(2)	N(31)-Ni(7)-N(33)	166.05(17)
N(25)-Ni(5)-N(37)	88.12(16)	N(31)-Ni(7)-N(40)	85.49(15)
N(25)-Ni(5)-N(38)	93.77(19)	N(31)-Ni(7)-N(41)	93.95(17)
N(25)-Ni(5)-N(39)	90.9(2)	N(31)-Ni(7)-N(42)	89.56(16)
N(26)-Ni(5)-N(27)	91.7(3)	N(32)-Ni(7)-N(33)	91.5(2)
N(26)-Ni(5)-N(37)	93.33(19)	N(32)-Ni(7)-N(40)	95.28(17)
N(26)-Ni(5)-N(38)	166.3(2)	N(32)-Ni(7)-N(41)	167.43(18)
N(26)-Ni(5)-N(39)	97.2(2)	N(32)-Ni(7)-N(42)	96.17(18)
N(27)-Ni(5)-N(37)	88.36(19)	N(33)-Ni(7)-N(40)	88.57(17)
N(27)-Ni(5)-N(38)	97.4(2)	N(33)-Ni(7)-N(41)	96.8(2)
N(27)-Ni(5)-N(39)	94.9(2)	N(33)-Ni(7)-N(42)	98.95(17)
N(37)-Ni(5)-N(38)	76.81(18)	N(40)-Ni(7)-N(41)	75.59(17)
N(37)-Ni(5)-N(39)	168.8(2)	N(40)-Ni(7)-N(42)	166.11(16)
N(38)-Ni(5)-N(39)	92.2(2)	N(41)-Ni(7)-N(42)	91.84(17)
N(28)-Ni(6)-N(29)	77.0(2)	N(34)-Ni(8)-N(35)	76.84(19)
N(28)-Ni(6)-N(30)	166.7(2)	N(34)-Ni(8)-N(36)	167.53(16)
N(28)-Ni(6)-N(43)	87.66(16)	N(34)-Ni(8)-N(46)	86.45(16)
N(28)-Ni(6)-N(44)	93.79(19)	N(34)-Ni(8)-N(47)	93.91(16)
N(28)-Ni(6)-N(45)	92.1(2)	N(34)-Ni(8)-N(48)	88.19(16)
N(29)-Ni(6)-N(30)	91.1(3)	N(35)-Ni(8)-N(36)	91.3(2)
N(29)-Ni(6)-N(43)	95.38(18)	N(35)-Ni(8)-N(46)	93.78(16)
N(29)-Ni(6)-N(44)	168.2(2)	N(35)-Ni(8)-N(47)	166.65(18)
N(29)-Ni(6)-N(45)	95.9(2)	N(35)-Ni(8)-N(48)	97.29(17)
N(30)-Ni(6)-N(43)	87.6(3)	N(36)-Ni(8)-N(46)	90.64(17)
N(30)-Ni(6)-N(44)	97.2(3)	N(36)-Ni(8)-N(47)	97.13(18)
N(30)-Ni(6)-N(45)	95.1(3)	N(36)-Ni(8)-N(48)	97.19(17)
N(43)-Ni(6)-N(44)	76.61(18)	N(46)-Ni(8)-N(47)	75.83(16)
N(43)-Ni(6)-N(45)	168.3(2)	N(46)-Ni(8)-N(48)	166.27(16)
N(44)-Ni(6)-N(45)	91.8(2)	N(47)-Ni(8)-N(48)	91.95(17)

3.4.12. $[Cu^{II}_2(L^{S1})(H_2O)_2(MeCN)_2](BF_4)_2 \cdot H_2O$ (33b · H_2O)

The asymmetric unit of $[Cu^{II}_2(L^{S1})(H_2O)_2(MeCN)_2](BF_4)_2 \cdot H_2O$ (**33b** · H_2O) consisted of half of a dinuclear complex cation $[Cu^{II}_2(L^{S1})(H_2O)_2(MeCN)_2]^{2+}$ one tetrafluoroborate counter ion and half a water solvent molecule. All non-hydrogen atoms were refined anisotropically. All hydrogen atoms were placed at calculated positions using a riding model except for the hydrogen atoms of the water coligand H(10D) and H(10E), which were located from the difference map and were allowed to refine freely and the hydrogen atoms of the half occupancy solvent water molecule H(11A) and H(11B), which were located from the difference map and fixed at that position. All hydrogen atoms, except H(10D) and H(10E), were given thermal parameters 1.2 times the equivalent isotropic thermal parameters of the atom to which they were bonded.

Table 3.4.27. Crystal data and structure refinement of $[Cu^{II}_2(\mathbf{L^{S1}})(H_2O)_2(MeCN)_2](BF_4)_2 \cdot H_2O$ (**33b** · H_2O).

Empirical formula	$C_{22}H_{26}B_2Cu_2F_8N_8O_5$	
Formula weight M_r	783.21 g mol^{-1}	
Temperature T	150(2) K	
Wavelength	0.71073 Å	
Crystal system	Triclinic	
Space group	P–1	
Unit cell dimensions	a = 8.29650(10) Å	α = 74.5940(10)°
	b = 10.0428(2) Å	β = 69.3420(10)°
	c = 10.1034(2) Å	γ = 84.32°
Volume V	759.37(2) Å^3	
Z	1	
Density $\rho_{calcd.}$	1.713 g cm^{-3}	
Absorption coefficient μ	1.498 mm^{-1}	
F(000)	394	
Crystal colour and shape	Green block	
Crystal size	0.38 × 0.26 × 0.08 mm^3	
θ range for data collection	2.10° ≤ 25.48°	
Index ranges	$-9 \le h \le 10$, $-11 \le k \le 12$, $0 \le l \le 12$	
Reflections collected	6914	
Independent reflections	2803 [R_{int} = 0.0235]	

Completeness to $\theta = 25.48°$	99.5 %
Absorption correction	Semi-empirical (SADABS)
Max. / min. transmission	0.92 / 0.70
Refinement method	Full-matrix least-squares on F^2
Data / restraints / parameters	2803 / 0 / 226
Goodness-of-fit on F^2	1.046
Final R indices [$I>2\sigma(I)$]	$R1 = 0.0464$, $wR2 = 0.1210$
R indices (all data)	$R1 = 0.0507$, $wR2 = 0.1244$
Largest diff. peak / hole	1.294 / –1.364 e Å^{-3}

Table 3.4.28. Atomic coordinates (× 10^4) and equivalent isotropic displacement parameters U_{eq} (× 10^3) [Å^2] for $[Cu^{II}_2(\mathbf{L^{S1}})(H_2O)_2(MeCN)_2](BF_4)_2 \cdot H_2O$ (**33b** · H_2O).

Atom	x	y	z	U_{eq}
Cu(1)	6541(1)	6969(1)	6374(1)	23(1)
N(1)	8703(4)	5834(3)	5637(3)	22(1)
C(2)	8717(4)	5423(3)	4477(4)	22(1)
C(5)	9979(4)	5414(4)	6167(4)	23(1)
C(6)	7266(4)	5943(3)	3907(4)	21(1)
O(1)	7197(3)	5598(3)	2838(3)	29(1)
N(3)	6218(4)	6737(3)	4673(3)	24(1)
C(7)	4744(5)	7386(4)	4315(4)	25(1)
C(10)	3843(4)	8249(4)	5373(4)	24(1)
C(11)	2432(5)	9069(4)	5262(4)	32(1)
C(12)	1657(5)	9835(4)	6269(5)	35(1)
C(13)	2299(5)	9759(4)	7378(4)	33(1)
C(14)	3705(5)	8937(4)	7428(4)	31(1)
N(4)	4483(4)	8200(3)	6432(3)	24(1)
N(100)	7291(4)	7579(3)	7766(4)	30(1)
C(100)	7566(5)	7807(4)	8695(4)	29(1)
C(101)	7870(7)	8121(5)	9907(5)	47(1)
O(100)	5129(4)	5224(3)	8110(3)	32(1)
B(1)	7771(7)	2035(6)	8417(5)	45(1)
F(11)	7294(9)	3197(6)	8954(5)	152(3)
F(12)	8939(4)	1340(3)	9012(3)	51(1)
F(13)	8443(4)	2472(3)	6935(3)	49(1)
F(14)	6406(6)	1263(7)	8797(6)	169(3)
O(110)	9096(8)	3766(8)	1012(8)	53(2)

3.4.13. $[Cu^{II}_2(L^{S1})(H_2O)_4](SiF_6) \cdot 0.5\ H_2O$ (**34b** · 0.5 H_2O)

The asymmetric unit of $[Cu^{II}_2(\mathbf{L}^{S1})(H_2O)_4](SiF_6) \cdot 0.5\ H_2O$ (**34b** · 0.5 H_2O) consisted of one dinuclear complex cation $[Cu^{II}_2(\mathbf{L}^{S1})(H_2O)_4]^{2+}$, one hexafluorosilicate counter ion and half a water solvent molecule. All non-hydrogen atoms were refined anisotropically. All hydrogen atoms were placed at calculated positions using a riding model except for the hydrogen atoms of three of the water coligands H(20A), H(20B), H(30A), H(30B), H(40A) and H(40B), which were located from the difference map and their coordinates allowed to refine freely, and the hydrogen atoms of the remaining water coligand, H(50A) and H(50B), and the hydrogen atoms of the half occupancy water solvent molecule, H(60A) and H(60B), which were located from the difference map and fixed at that position. All hydrogen atoms had thermal parameter 1.2 times the equivalent isotropic thermal parameters of the atom to which they were bonded.

Table 3.4.29. Crystal data and structure refinement of $[Cu^{II}_2(\mathbf{L}^{S1})(H_2O)_4](SiF_6) \cdot 0.5\ H_2O$ (**34b** · 0.5 H_2O).

Empirical formula	$C_{18}H_{23}Cu_2F_6N_6O_{6.5}Si$	
Formula weight M_r	696.59 g mol^{-1}	
Temperature T	200(2) K	
Wavelength	0.71073 Å	
Crystal system	Monoclinic	
Space group	$P2(1)/c$	
Unit cell dimensions	$a = 21.1697(3)$ Å	$\alpha = 90°$
	$b = 7.55260(10)$ Å	$\beta = 94.4300(10)°$
	$c = 15.1687(2)$ Å	$\gamma = 90°$
Volume V	2418.02(6) $Å^3$	
Z	4	
Density $\rho_{calcd.}$	1.914 g cm^{-3}	
Absorption coefficient μ	1.907 mm^{-1}	
$F(000)$	1404	
Crystal colour and shape	Blue-green plates	
Crystal size	0.20 × 0.15 × 0.08 mm^3	
θ range for data collection	$0.96° \leq 27.16°$	
Index ranges	$-27 \leq h \leq 27, 0 \leq k \leq 9, 0 \leq l \leq 19$	
Reflections collected	14503	

Independent reflections	5239 [R_{int} = 0.0380]
Completeness to θ = 27.16°	97.6 %
Absorption correction	Semi-empirical (SADABS)
Max. / min. transmission	0.94 / 0.72
Refinement method	Full-matrix least-squares on F^2
Data / restraints / parameters	5239 / 0 / 379
Goodness-of-fit on F^2	1.061
Final R indices [$I>2\sigma(I)$]	$R1$ = 0.0582, $wR2$ = 0.1247
R indices (all data)	$R1$ = 0.0889, $wR2$ = 0.1403
Largest diff. peak / hole	0.784 / –0.886 e Å^{-3}

Table 3.4.30. Atomic coordinates (× 10^4) and equivalent isotropic displacement parameters U_{eq} (× 10^3) [Å^2] for $[Cu^{II}_2(\mathbf{L^{S1}})(H_2O)_4](SiF_6) \cdot 0.5\ H_2O$ (**34b** · 0.5 H_2O).

Atom	x	y	z	U_{eq}
Cu(1)	3717(1)	4844(1)	9141(1)	30(1)
Cu(2)	1377(1)	175(1)	10870(1)	34(1)
O(1)	3992(2)	–160(5)	9975(2)	39(1)
O(2)	1091(2)	5185(5)	10040(2)	38(1)
O(20)	3349(2)	7161(5)	9329(3)	41(1)
O(30)	3302(2)	4745(8)	7703(3)	63(1)
O(40)	1758(2)	–2150(5)	10727(3)	44(1)
O(50)	1789(2)	372(8)	12272(3)	89(2)
N(1)	2985(2)	3604(5)	9673(2)	28(1)
N(2)	4110(2)	2608(5)	9375(3)	33(1)
N(3)	4589(2)	5479(6)	8806(2)	36(1)
N(4)	2108(2)	1425(5)	10340(2)	29(1)
N(5)	969(2)	2385(6)	10606(3)	35(1)
N(6)	512(2)	–501(6)	11197(3)	43(1)
C(1)	2400(2)	4205(6)	9778(3)	30(1)
C(2)	1953(2)	3089(6)	10118(3)	29(1)
C(3)	2688(2)	846(6)	10243(3)	31(1)
C(4)	3134(2)	1933(6)	9901(3)	29(1)
C(5)	3799(2)	1362(6)	9746(3)	32(1)
C(7)	4756(2)	2372(7)	9148(3)	39(1)
C(8)	5002(2)	4130(7)	8859(3)	36(1)
C(9)	5620(2)	4338(9)	8637(3)	50(2)
C(10)	5812(3)	5979(9)	8356(4)	54(2)
C(11)	5386(3)	7371(9)	8296(3)	52(2)
C(12)	4774(2)	7083(8)	8527(3)	43(1)
C(13)	1288(2)	3664(6)	10251(3)	32(1)
C(15)	316(2)	2599(7)	10810(3)	41(1)
C(16)	83(2)	821(8)	11100(3)	45(1)

C(17)	–537(3)	553(10)	11314(4)	60(2)
C(18)	–713(3)	–1110(12)	11609(4)	74(2)
C(19)	–268(3)	–2449(11)	11699(4)	64(2)
C(20)	332(3)	–2086(8)	11494(3)	53(2)
Si(1)	7517(1)	4832(2)	7418(1)	51(1)
F(11)	6799(1)	4925(5)	6899(2)	60(1)
F(12)	7772(2)	6444(6)	6776(2)	65(1)
F(13)	7302(2)	6369(6)	8136(2)	76(1)
F(14)	8235(2)	4727(6)	7950(3)	85(1)
F(15)	7712(2)	3255(7)	6686(3)	98(2)
F(16)	7270(2)	3184(6)	8071(3)	91(2)
O(60)	1291(4)	–1102(11)	13353(5)	57(2)

3.4.14. {[$Cu^{II}_2(L^{S1})(H_2O)_2(SiF_6)$] · 4 H_2O}$_\infty$ (34c · 4 H_2O)

The asymmetric unit of {[Cu^{II}_2(**L^{S1}**)(H_2O)$_2$(SiF_6)] · 4 H_2O}$_\infty$ (**34c** · 4 H_2O) consisted of half of a dinuclear complex molecule [Cu^{II}_2(**L^{S1}**)(H_2O)$_2$(SiF_6)] and two full occupancy water solvent molecules. The coordinated SiF_6^{2-} ion was located such that the silicon atom was on a centre of inversion and half of the ion generated the other half *via* this symmetry operation. All non-hydrogen atoms were refined anisotropically. All hydrogen atoms were placed at calculated positions using a riding model except for the hydrogen atoms of the water coligand, H(10A) and H(10B), and of the water solvent molecules, H(50A), H(50B), H(60A) and H(60B), which were located from the difference map and their coordinates allowed to refine freely. All hydrogen atoms had thermal parameters 1.2 times the equivalent isotropic thermal parameter of the atom to which they were bonded.

Table 3.4.31. Crystal data and structure refinement of {[Cu^{II}_2(**L^{S1}**)(H_2O)$_2$(SiF_6)] · 4 H_2O}$_\infty$ (**34c** · 4 H_2O).

Empirical formula	$C_{18}H_{26}Cu_2F_6N_6O_8Si$
Formula weight M_r	723.62 g mol^{-1}

Temperature T	200(2) K	
Wavelength	0.71073 Å	
Crystal system	Triclinic	
Space group	$P\bar{1}$	
Unit cell dimensions	a = 8.00020(10) Å	α = 71.3330(10)°
	b = 8.96160(10) Å	β = 77.7600(10)°
	c = 10.2285(2) Å	γ = 69.0230(10)°
Volume V	644.760(17) Å^3	
Z	1	
Density $\rho_{calcd.}$	1.864 g cm^{-3}	
Absorption coefficient μ	1.796 mm^{-1}	
F(000)	366	
Crystal colour and shape	Blue-green prism	
Crystal size	0.40 × 0.20 × 0.08 mm^3	
θ range for data collection	2.11° ≤ 26.42°	
Index ranges	$-9 \le h \le 9$, $-10 \le k \le 11$, $0 \le l \le 12$	
Reflections collected	6211	
Independent reflections	2598 [R_{int} = 0.0359]	
Completeness to θ = 26.42°	98.5 %	
Absorption correction	Semi-empirical (SADABS)	
Max. / min. transmission	0.95 / 0.73	
Refinement method	Full-matrix least-squares on F^2	
Data / restraints / parameters	2598 / 0 / 205	
Goodness-of-fit on F^2	1.129	
Final R indices [$I>2\sigma(I)$]	$R1$ = 0.0277, $wR2$ = 0.0766	
R indices (all data)	$R1$ = 0.0294, $wR2$ = 0.0775	
Largest diff. peak / hole	0.694 / –0.524 e Å^{-3}	

Table 3.4.32. Atomic coordinates (× 10^4) and equivalent isotropic displacement parameters U_{eq} (× 10^3) [Å^2] for {[Cu^{II}_2(**L^{S1}**)(H_2O)$_2$(SiF_6)] · 4 H_2O}$_\infty$ (**34c** · 4 H_2O).

Atom	x	y	z	U_{eq}
Cu(1)	1181(1)	–3945(1)	2519(1)	15(1)
C(1)	1782(3)	–5303(2)	–24(2)	15(1)
C(2)	–1102(3)	–4443(2)	1050(2)	14(1)
N(1)	676(2)	–4750(2)	1021(2)	14(1)
C(3)	–2296(3)	–3720(2)	2193(2)	14(1)
N(2)	–1367(2)	–3477(2)	2966(2)	16(1)
O(1)	–3981(2)	–3390(2)	2290(2)	20(1)
C(5)	–2244(3)	–2644(3)	4057(2)	19(1)
C(6)	–791(3)	–2540(2)	4729(2)	18(1)

C(7)	–1208(3)	–1884(3)	5863(2)	22(1)
C(8)	164(4)	–1783(3)	6427(2)	26(1)
C(9)	1931(3)	–2338(3)	5836(2)	25(1)
C(10)	2258(3)	–2975(3)	4710(2)	21(1)
N(3)	925(2)	–3079(2)	4163(2)	18(1)
O(10)	3779(2)	–5038(2)	2414(2)	25(1)
Si(1)	0	0	0	16(1)
F(1)	1550(2)	–1740(2)	828(1)	28(1)
F(2)	1185(2)	–181(2)	–1536(1)	34(1)
F(3)	1185(2)	1153(2)	137(2)	32(1)
O(50)	5343(3)	–7752(3)	1690(3)	58(1)
O(60)	3818(3)	–10016(2)	1837(2)	37(1)

3.4.15. $[Cu^{II}_2(L^{S2})(H_2O)_2(MeCN)_2](BF_4)_2$ (35b)

The asymmetric unit of $[Cu^{II}_2(\mathbf{L}^{S2})(H_2O)_2(MeCN)_2](BF_4)_2$ (**35b**) consisted of two independent half dinuclear complex cations $[Cu^{II}_2(\mathbf{L}^{S2})(H_2O)_2(MeCN)_2]^{2+}$ and two full occupancy tetrafluoroborate counter ions. All non-hydrogen atoms were refined anisotropically. All hydrogen atoms were placed at calculated positions using a riding model except for the hydrogen atoms of the water coligands, H(50A), H(50B), H(60A) and H(60B), which were located from the difference map and were allowed to refine freely. All other hydrogen atoms had thermal parameters 1.2 times the equivalent isotropic thermal parameter of the atom to which they were bonded.

Table 3.4.33. Crystal data and structure refinement of $[Cu^{II}_2(\mathbf{L}^{S2})(H_2O)_2(MeCN)_2](BF_4)_2$ (**35b**).

Empirical formula	$C_{24}H_{28}B_2Cu_2F_8N_8O_4$	
Formula weight M_r	793.24 g mol^{-1}	
Temperature T	168(2) K	
Wavelength	0.71073 Å	
Crystal system	Triclinic	
Space group	P–1	
Unit cell dimensions	a = 9.312(3) Å	α = 106.649(4)°

	$b = 13.156(4)$ Å	$\beta = 101.489(4)°$
	$c = 13.802(4)$ Å	$\gamma = 99.121(4)°$
Volume V	1545.0(8) Å^3	
Z	2	
Density $\rho_{calcd.}$	1.705 g cm^{-3}	
Absorption coefficient μ	1.471 mm^{-1}	
$F(000)$	800	
Crystal colour and shape	Green block	
Crystal size	0.50 × 0.40 × 0.35 mm^3	
θ range for data collection	1.59° ≤ 26.37°	
Index ranges	$-11 \le h \le 11$, $-16 \le k \le 16$, $-17 \le l \le 14$	
Reflections collected	19871	
Independent reflections	6216 [$R_{int} = 0.0432$]	
Completeness to $\theta = 26.37°$	98.3 %	
Absorption correction	Semi-empirical (SADABS)	
Max. / min. transmission	1.00 / 0.53	
Refinement method	Full-matrix least-squares on F^2	
Data / restraints / parameters	6216 / 0 / 451	
Goodness-of-fit on F^2	1.027	
Final R indices [$I>2\sigma(I)$]	$R1 = 0.0426$, $wR2 = 0.1127$	
R indices (all data)	$R1 = 0.0538$, $wR2 = 0.1194$	
Largest diff. peak / hole	1.212 / –0.758 e Å^{-3}	

Table 3.4.34. Atomic coordinates (× 10^4) and equivalent isotropic displacement parameters U_{eq} (× 10^3) [Å^2] for $[Cu^{II}_2(\mathbf{L^{S2}})(H_2O)_2(MeCN)_2](BF_4)_2$ (**35b**).

Atom	x	y	z	U_{eq}
Cu(1)	3100(1)	7621(1)	5093(1)	18(1)
N(1)	4344(3)	9049(2)	5127(2)	17(1)
C(1)	5493(3)	9769(2)	5878(2)	17(1)
C(2)	3862(3)	9269(2)	4255(2)	17(1)
C(3)	2592(3)	8427(2)	3423(2)	17(1)
O(1)	2151(2)	8585(2)	2572(2)	23(1)
N(2)	2068(3)	7620(2)	3728(2)	18(1)
C(4)	727(3)	6805(2)	3035(2)	22(1)
C(5)	–28(3)	6188(3)	3652(3)	24(1)
C(6)	905(3)	5500(2)	4049(2)	22(1)
C(7)	428(4)	4371(3)	3723(3)	30(1)
C(8)	1342(5)	3757(3)	4087(3)	37(1)
C(9)	2716(4)	4289(3)	4791(3)	36(1)
C(10)	3135(4)	5410(3)	5092(3)	28(1)
N(3)	2260(3)	6015(2)	4732(2)	21(1)

Cu(2)	–1359(1)	7438(1)	–63(1)	21(1)
N(11)	–404(3)	8966(2)	34(2)	19(1)
C(11)	729(3)	9711(2)	784(2)	20(1)
C(12)	–1124(3)	9243(2)	–742(2)	19(1)
C(13)	–2367(3)	8359(2)	–1578(2)	20(1)
O(10)	–3009(2)	8572(2)	–2352(2)	28(1)
N(12)	–2583(3)	7449(2)	–1361(2)	21(1)
C(14)	–3647(4)	6476(2)	–2124(2)	24(1)
C(15)	–3071(4)	5460(3)	–2104(3)	28(1)
C(16)	–3087(3)	5162(3)	–1136(3)	25(1)
C(17)	–3743(4)	4121(3)	–1178(3)	34(1)
C(18)	–3743(4)	3885(3)	–268(3)	38(1)
C(19)	–3120(4)	4704(3)	675(3)	36(1)
C(20)	–2489(4)	5722(3)	681(3)	30(1)
N(13)	–2448(3)	5951(2)	–201(2)	25(1)
O(50)	4247(3)	7734(2)	6499(2)	26(1)
N(50)	1487(3)	8516(2)	5910(2)	30(1)
C(50)	778(4)	9119(3)	6139(3)	33(1)
C(51)	–148(5)	9894(4)	6442(4)	65(2)
O(60)	517(3)	7233(2)	777(2)	24(1)
N(60)	–2529(4)	8287(3)	1152(2)	37(1)
C(60)	–3332(4)	8820(3)	1393(3)	34(1)
C(61)	–4381(5)	9505(3)	1696(3)	43(1)
B(1)	2124(6)	7870(4)	8692(4)	41(1)
F(11)	2875(3)	7353(2)	7982(2)	56(1)
F(12)	1103(4)	7070(2)	8831(2)	70(1)
F(13)	3056(5)	8399(4)	9644(3)	115(2)
F(14)	1413(4)	8540(3)	8313(3)	92(1)
B(2)	–3360(5)	7643(4)	3756(4)	41(1)
F(21)	–4606(3)	7114(2)	4022(3)	75(1)
F(22)	–2251(4)	8019(3)	4639(3)	95(1)
F(23)	–3006(4)	6853(3)	3027(2)	95(1)
F(24)	–3871(5)	8375(4)	3366(3)	117(2)

3.4.16. $[Cu^{II}_2(L^{S2})(H_2O)_4(BF_4)_2] \cdot 2\,H_2O$ (35c · 2 H_2O)

The asymmetric unit of $[Cu^{II}_2(\mathbf{L}^{S2})(H_2O)_4(BF_4)_2] \cdot 2\,H_2O$ (**35c** · 2 H_2O) consisted of half of a dinuclear complex molecules $[Cu^{II}_2(\mathbf{L}^{S2})(H_2O)_4(BF_4)_2]$ and one water solvent

molecule. All non-hydrogen atoms were refined anisotropically. All hydrogen atoms were placed at calculated positions using a riding model except for the hydrogen atoms of the water coligands, H(50A), H(50B), H(60A) and H(60B), and the hydrogen atoms of the water solvent molecule, H(70A) and H(70B), which were located from the difference map and were allowed to refine freely. All other hydrogen atoms had thermal parameters 1.2 times the equivalent isotropic thermal parameter of the atom to which they were bonded.

Table 3.4.35. Crystal data and structure refinement of $[Cu^{II}_2(\mathbf{L^{S2}})(H_2O)_4(BF_4)_2] \cdot 2\ H_2O$ (**35c** · 2 H_2O).

Empirical formula	$C_{20}H_{30}B_2Cu_2F_8N_6O_8$	
Formula weight M_r	783.20 g mol^{-1}	
Temperature T	168(2) K	
Wavelength	0.71073 Å	
Crystal system	Triclinic	
Space group	$P\bar{1}$	
Unit cell dimensions	a = 7.898(16) Å	α = 84.98(6)°
	b = 8.101(20) Å	β = 80.11(6)°
	c = 11.19(3) Å	γ = 85.62(8)°
Volume V	701(3) Å^3	
Z	1	
Density $\rho_{calcd.}$	1.855 g cm^{-3}	
Absorption coefficient μ	1.628 mm^{-1}	
F(000)	396	
Crystal colour and shape	Green block	
Crystal size	0.70 × 0.20 × 0.10 mm^3	
θ range for data collection	2.53° ≤ 26.38°	
Index ranges	$-6 \le h \le 9, -10 \le k \le 7, -13 \le l \le 13$	
Reflections collected	3172	
Independent reflections	2497 [R_{int} = 0.1674]	
Completeness to θ = 26.38°	87.4 %	
Absorption correction	Semi-empirical (SADABS)	
Max. / min. transmission	1.00 / 0.47	
Refinement method	Full-matrix least-squares on F^2	
Data / restraints / parameters	2497 / 0 / 232	
Goodness-of-fit on F^2	1.108	
Final R indices [$I>2\sigma(I)$]	$R1$ = 0.0470, $wR2$ = 0.1250	
R indices (all data)	$R1$ = 0.0542, $wR2$ = 0.1302	
Largest diff. peak / hole	0.750 / –0.728 e Å^{-3}	

Table 3.4.36. Atomic coordinates (× 10^4) and equivalent isotropic displacement parameters U_{eq} (× 10^3) [$Å^2$] for $[Cu^{II}_2(\mathbf{L^{S2}})(H_2O)_4(BF_4)_2] \cdot 2\ H_2O$ (**35c** · 2 H_2O).

Atom	x	y	z	U_{eq}
Cu(1)	6309(1)	7401(1)	6951(1)	17(1)
N(1)	5628(4)	5848(4)	5821(3)	16(1)
C(1)	6331(5)	4360(5)	5521(3)	17(1)
C(2)	4307(4)	6475(4)	5301(3)	16(1)
C(3)	3547(4)	8152(4)	5686(3)	15(1)
O(1)	2223(3)	8737(3)	5299(3)	21(1)
N(2)	4426(4)	8778(4)	6393(3)	16(1)
C(4)	3756(5)	10331(4)	6909(3)	17(1)
C(5)	4047(5)	10302(5)	8224(3)	18(1)
C(6)	5894(5)	10382(5)	8326(3)	19(1)
C(7)	6474(5)	11672(5)	8835(4)	23(1)
C(8)	8176(5)	11665(5)	8965(4)	25(1)
C(9)	9273(5)	10355(5)	8557(4)	26(1)
C(10)	8646(5)	9125(5)	8024(4)	23(1)
N(3)	6997(4)	9116(4)	7899(3)	17(1)
O(50)	7755(4)	5627(4)	7653(3)	23(1)
O(60)	8786(4)	8010(4)	5269(3)	22(1)
O(70)	10628(4)	4428(5)	6400(3)	35(1)
B(1)	12803(6)	5248(6)	8764(4)	25(1)
F(11)	13168(3)	4178(3)	7827(2)	31(1)
F(12)	12384(4)	4335(4)	9857(3)	46(1)
F(13)	14231(3)	6108(3)	8789(3)	34(1)
F(14)	11469(4)	6337(4)	8528(3)	50(1)

3.4.17. $[Co^{III}_4(L^{S2})_4](BF_4)_4 \cdot 12.75\ MeCN$ (36 · 12.75 MeCN)

The asymmetric unit of $[Co^{III}_4(\mathbf{L^{S2}})_4](BF_4)_4 \cdot 12.75$ MeCN (**36** · 12.75 MeCN) consisted of one [2 × 2] grid-type complex molecule $[Co^{III}_4(\mathbf{L^{S2}})_4](BF_4)_4$. All non-hydrogen atoms were refined anisotropically. All hydrogen atoms were placed at calculated positions using a riding model. All hydrogen atoms had thermal

parameters 1.2 times the equivalent isotropic thermal parameter of the atom to which they were bonded.

In view of the disordered anions (four tetrafluoroborate per tetranuclear grid) and solvent (many MeCN) sites, and the fact that the best attempt to model this situation gave an $R1$ on observed data of 0.129, *cf.* R_{int} = 0.072, the structure was subjected to the SQUEEZE procedure of the PLATON suite.[191] A total potential solvent / anion accessible volume of 7451 Å^3 per cell containing 1798 electrons was calculated. The electron count is very close to that calculated (1794 electrons) for 16 BF_4^- and 51 MeCN per cell. The final value for $R1$ on observed data on reincorporation of electron density in the void volume was 0.077. The chemical formulae, electron count, absorption coefficient and other derived parameters reported below are for the cation only.

Table 3.4.37. Crystal data and structure refinement of $[Co^{III}_4(\mathbf{L^{S2}})_4](BF_4)_4 \cdot 12.75$ MeCN (**36** · 12.75 MeCN).

Empirical formula	$C_{80}H_{72}Co_4N_{24}O_8$	
Formula weight M_r	1733.34 g mol^{-1}	
Temperature T	164(2) K	
Wavelength	0.71073 Å	
Crystal system	Monoclinic	
Space group	$P2(1)/c$	
Unit cell dimensions	a = 19.3906(19) Å	α = 90°
	b = 19.6881(19) Å	β = 91.916(2)°
	c = 35.419(3) Å	γ = 90°
Volume V	13514(2) Å^3	
Z	4	
Density $\rho_{calcd.}$	0.852 g cm^{-3}	
Absorption coefficient μ	0.525 mm^{-1}	
$F(000)$	3568	
Crystal colour and shape	Red-brown block	
Crystal size	0.70 × 0.60 × 0.20 mm^3	
θ range for data collection	1.53 ° ≤ 26.41°	
Index ranges	$-22 \le h \le 24$, $-24 \le k \le 24$, $-18 \le l \le 44$	
Reflections collected	93070	
Independent reflections	27173 [R_{int} = 0.0736]	
Completeness to θ = 26.38°	97.9 %	
Absorption correction	Semi-empirical (SADABS)	

Max. / min. transmission	1.00 / 0.79
Refinement method	Full-matrix least-squares on F^2
Data / restraints / parameters	27173 / 0 / 1045
Goodness-of-fit on F^2	0.983
Final R indices [$I>2\sigma(I)$]	$R1 = 0.0772$, $wR2 = 0.1982$
R indices (all data)	$R1 = 0.1180$, $wR2 = 0.2116$
Largest diff. peak / hole	0.980 / –1.220 e Å^{-3}

Table 3.4.38. Atomic coordinates (× 10^4) and equivalent isotropic displacement parameters U_{eq} (× 10^3) [Å^2] for $[Co^{III}_4(\mathbf{L^{S2}})_4](BF_4)_4 \cdot 12.75$ MeCN (**36** · 12.75 MeCN).

Atom	x	y	z	U_{eq}
Co(1)	3596(1)	6714(1)	8420(1)	25(1)
Co(2)	1477(1)	4090(1)	8458(1)	24(1)
Co(3)	1217(1)	4189(1)	6586(1)	24(1)
Co(4)	3652(1)	6525(1)	6551(1)	24(1)
N(1)	2924(2)	5984(2)	8382(1)	24(1)
N(2)	4226(2)	5962(2)	8490(1)	30(1)
N(3)	4357(2)	7402(2)	8453(1)	23(1)
N(4)	2147(2)	4821(2)	8407(1)	21(1)
N(5)	847(2)	4829(2)	8510(1)	27(1)
N(6)	740(2)	3409(2)	8500(1)	27(1)
O(1)	4326(2)	4820(2)	8367(1)	37(1)
O(2)	725(2)	5971(1)	8343(1)	36(1)
C(1)	3219(2)	5355(2)	8379(1)	25(1)
C(2)	2831(2)	4771(2)	8390(1)	24(1)
C(3)	1842(2)	5445(2)	8381(1)	26(1)
C(4)	2249(2)	6024(2)	8366(1)	27(1)
C(5)	4012(2)	5363(2)	8411(1)	25(1)
C(6)	4968(2)	6057(2)	8578(1)	36(1)
C(7)	5093(2)	6649(2)	8843(1)	40(1)
C(8)	4932(2)	7317(2)	8666(1)	37(1)
C(9)	5421(3)	7851(3)	8708(2)	46(1)
C(10)	5287(3)	8445(2)	8524(2)	45(1)
C(11)	4720(2)	8505(3)	8296(1)	42(1)
C(12)	4277(2)	8000(2)	8257(1)	32(1)
C(13)	1080(2)	5442(2)	8407(1)	26(1)
C(14)	130(2)	4754(2)	8599(1)	38(1)
C(15)	34(2)	4204(2)	8879(1)	37(1)
C(16)	178(2)	3502(2)	8712(1)	36(1)
C(17)	–308(3)	2975(3)	8775(1)	47(1)
C(18)	–175(3)	2343(3)	8615(2)	45(1)
C(19)	359(2)	2276(2)	8373(2)	44(1)

C(20)	786(2)	2806(2)	8323(1)	33(1)
N(7)	1344(2)	4142(2)	7913(1)	24(1)
N(8)	2162(2)	3418(2)	8330(1)	26(1)
N(9)	1731(2)	4052(2)	9005(1)	28(1)
N(10)	1333(2)	4095(2)	7135(1)	21(1)
N(11)	491(2)	4810(2)	6712(1)	26(1)
N(12)	1075(2)	4360(2)	6035(1)	28(1)
O(3)	2753(2)	3001(2)	7821(1)	36(1)
O(4)	33(2)	5358(2)	7226(1)	38(1)
C(21)	1794(2)	3734(2)	7724(1)	21(1)
C(22)	1780(2)	3730(2)	7334(1)	22(1)
C(23)	894(2)	4511(2)	7320(1)	23(1)
C(24)	884(2)	4516(2)	7712(1)	23(1)
C(25)	2287(2)	3352(2)	7968(1)	26(1)
C(26)	2559(2)	2997(2)	8604(1)	34(1)
C(27)	2112(2)	2868(2)	8952(1)	35(1)
C(28)	1998(2)	3476(2)	9174(1)	31(1)
C(29)	2192(3)	3500(3)	9564(1)	45(1)
C(30)	2100(3)	4074(3)	9770(1)	44(1)
C(31)	1839(3)	4660(3)	9592(1)	48(1)
C(32)	1675(2)	4628(2)	9214(1)	37(1)
C(33)	428(2)	4946(2)	7077(1)	27(1)
C(34)	15(2)	5135(2)	6434(1)	32(1)
C(35)	–168(2)	4630(3)	6117(1)	42(1)
C(36)	448(2)	4519(2)	5870(1)	33(1)
C(37)	364(3)	4535(2)	5481(1)	41(1)
C(38)	930(3)	4507(3)	5250(1)	62(2)
C(39)	1560(3)	4387(3)	5422(1)	57(2)
C(40)	1619(3)	4316(2)	5813(1)	36(1)
N(13)	1893(2)	4918(2)	6612(1)	24(1)
N(14)	2025(2)	3652(2)	6522(1)	30(1)
N(15)	593(2)	3396(2)	6563(1)	31(1)
N(16)	2995(2)	5791(2)	6595(1)	23(1)
N(17)	2850(2)	7068(2)	6481(1)	24(1)
N(18)	4271(2)	7324(2)	6507(1)	26(1)
O(5)	3198(2)	3659(2)	6660(1)	36(1)
O(6)	1667(2)	7049(2)	6600(1)	38(1)
C(41)	2553(2)	4688(2)	6624(1)	21(1)
C(42)	3105(2)	5128(2)	6624(1)	23(1)
C(43)	2328(2)	6033(2)	6607(1)	24(1)
C(44)	1777(2)	5581(2)	6620(1)	21(1)
C(45)	2641(2)	3926(2)	6607(1)	30(1)
C(46)	2000(3)	2917(2)	6438(1)	38(1)
C(47)	1399(3)	2758(2)	6166(1)	40(1)
C(48)	716(2)	2835(2)	6334(1)	38(1)
C(49)	210(3)	2343(3)	6270(2)	51(1)
C(50)	–419(3)	2399(3)	6454(2)	56(2)

C(51)	–500(3)	2912(3)	6704(2)	46(1)
C(52)	–3(2)	3393(2)	6756(1)	32(1)
C(53)	2233(2)	6789(2)	6563(1)	24(1)
C(54)	2830(2)	7796(2)	6372(1)	37(1)
C(55)	3413(2)	7930(2)	6101(1)	40(1)
C(56)	4104(3)	7854(2)	6275(1)	38(1)
C(57)	4603(3)	8382(2)	6227(2)	45(1)
C(58)	5224(3)	8342(3)	6406(2)	48(1)
C(59)	5347(3)	7839(3)	6663(1)	42(1)
C(60)	4887(2)	7351(2)	6699(1)	36(1)
N(19)	3611(2)	6651(2)	7094(1)	22(1)
N(20)	4399(2)	5924(2)	6690(1)	25(1)
N(21)	3712(2)	6307(2)	6008(1)	30(1)
N(22)	3670(2)	6650(2)	7878(1)	25(1)
N(23)	2901(2)	7376(2)	8281(1)	26(1)
N(24)	3395(2)	6789(2)	8965(1)	31(1)
O(7)	4899(2)	5383(2)	7205(1)	39(1)
O(8)	2259(2)	7788(2)	7767(1)	35(1)
C(61)	4055(2)	6237(2)	7291(1)	24(1)
C(62)	4097(2)	6242(2)	7680(1)	21(1)
C(63)	3217(2)	7027(2)	7676(1)	25(1)
C(64)	3199(2)	7039(2)	7290(1)	23(1)
C(65)	4508(2)	5789(2)	7061(1)	28(1)
C(66)	4848(2)	5575(2)	6431(1)	29(1)
C(67)	4959(2)	6025(2)	6081(1)	35(1)
C(68)	4307(2)	6119(2)	5842(1)	30(1)
C(69)	4325(3)	5976(3)	5466(1)	51(1)
C(70)	3728(3)	6036(3)	5228(1)	52(1)
C(71)	3097(3)	6192(3)	5406(2)	51(1)
C(72)	3104(2)	6327(2)	5786(1)	35(1)
C(73)	2734(2)	7438(2)	7922(1)	28(1)
C(74)	2529(2)	7804(2)	8543(1)	34(1)
C(75)	3004(2)	7966(2)	8883(1)	34(1)
C(76)	3146(3)	7367(2)	9126(1)	39(1)
C(77)	3001(3)	7369(3)	9517(1)	53(1)
C(78)	3079(3)	6819(3)	9728(1)	64(2)
C(79)	3322(3)	6213(3)	9562(2)	62(2)
C(80)	3454(3)	6218(2)	9190(1)	44(1)

4. References

[1] A. E. A. Porter, in *Comprehensive Heterocyclic Chemistry - The Structure, Reactions, Synthesis and Uses of Heterocyclic Compounds, Vol. 3*, Pergamon Press, Oxford, **1984**, pp. 157-199.

[2] T. L. Gilchrist, *Heterocyclic Chemistry*, 2 ed., Longman Scientific & Technical, Liverpool, **1987**.

[3] *Heterocyclic Compounds, Vol. 6*, John Wiley & Sons, Inc., New York, **1957**.

[4] J. A. Joule, G. F. Smith, *Heterocylclic Chemistry*, 2 ed., Van Nostrand Reinhold, Padstow, **1978**.

[5] J. A. Joule, K. Mills, G. F. Smith, *Heterocyclic Chemistry*, 3 ed., Chapman & Hall, Padstow, **1995**.

[6] N. Sato, *Comprehensive Heterocyclic Chemistry II - A Review of the Literature 1982-1995, Vol. 6*, 1 ed., Pergamon, Glasgow, **1996**.

[7] G. Aylward, T. Findlay, *SI Chemical Data*, 4 ed., John Wiley & Sons, Singapore, **1998**.

[8] A. B. Blake, W. E. Hatfield, *J. Chem. Soc., Dalton Trans.* **1978**, 868-871.

[9] E. Coronado, M. Drillon, D. Beltrán, *Inorg. Chim. Acta* **1984**, *82*, 13-17.

[10] H. Grove, J. Sletten, M. Julve, F. Lloret, *J. Chem. Soc., Dalton Trans.* **2001**, 2487-2493.

[11] M. S. Haddad, D. N. Hendrickson, J. P. Cannady, R. S. Drago, *J. Am. Chem. Soc.* **1979**, *101*, 898-906.

[12] H. Oshio, K. Toriumi, Y. Hayashi, *J. Chem. Soc., Dalton Trans.* **1990**, 293-298.

[13] B. Serli, E. Zangrando, E. Iengo, E. Alessio, *Inorg. Chim. Acta* **2002**, *339*, 265-272.

[14] G. R. Newkome, D. K. Kohli, F. R. Fronczek, *J. Am. Chem. Soc.* **1982**, *104*, 994-998.

[15] E. Iengo, G. Mestroni, S. Geremia, M. Calligaris, E. Alessio, *J. Chem. Soc., Dalton Trans.* **1999**, 3361-3371.

[16] A. Bino, P. A. Lay, H. Taube, J. F. Wishart, *Inorg. Chem.* **1985**, *24*, 3969-3671.

[17] D.-M. Hong, H.-H. Wei, K.-H. Chang, G.-H. Lee, Y. Wang, *Polyhedron* **1998**, *17*, 3565-3573.

[18] M. K. Ellison, W. R. Scheidt, *J. Am. Chem. Soc.* **1999**, *121*, 5210-5219.

[19] Q. Wang, X. Wu, P. Lin, W. Zhang, T. Sheng, H. Yu, L. Chen, J. Li, *Polyhedron* **1999**, *18*, 1411-1417.

[20] S. A. Warda, *Acta Crystallogr. C* **1998**, *54*, 1756-1758.

[21] X.-Y. Yu, M. Maekawa, M. Kondo, S. Kitagawa, G.-X. Jin, *Chem. Lett.* **2001**, 168-169.
[22] T. Fetzer, R. Jooss, A. Lentz, T. Debaerdemaeker, *Z. Anorg. Allg. Chem.* **1994**, *620*, 1750-1754.
[23] B. J. Coe, T. J. Meyer, P. S. White, *Inorg. Chem.* **1995**, *34*, 593-602.
[24] C. Creutz, H. Taube, *J. Am. Chem. Soc.* **1969**, *91*, 3988-3989.
[25] C. Creutz, H. Taube, *J. Am. Chem. Soc.* **1973**, *95*, 1086-1094.
[26] D. Xu, C. Chen, Y. Xu, C. Cheng, J. Chen, W. Tang, *Acta Crystallogr. C* **1991**, *47*, 72-75.
[27] R. Kuhlman, G. L. Schimek, J. W. Kolis, *Polyhedron* **1999**, *18*, 1379-1387.
[28] C. Nather, J. Greve, I. Jess, *Z. Naturforsch., B: Chem. Sci.* **2003**, *58*, 52-58.
[29] B.-Q. Ma, S. Gao, T. Yi, G.-X. Xu, *Polyhedron* **2001**, *20*, 1255-1261.
[30] E. Kwiatkowski, G. Romanowski, W. Nowicki, K. Suwinska, *Polyhedron* **2001**, *20*, 1097-1100.
[31] O.-S. Jung, C. G. Pierpont, *J. Am. Chem. Soc.* **1994**, *116*, 2229-2230.
[32] L. Carlucci, G. Ciani, D. M. Proserpio, A. Sironi, *J. Am. Chem. Soc.* **1995**, *117*, 4562-2569.
[33] H. W. Richardson, J. R. Wasson, W. E. Hatfield, *Inorg. Chem.* **1977**, *16*, 484-486.
[34] W. H. Richard, W. E. Hatfield, *J. Am. Chem. Soc.* **1976**, *98*, 835-839.
[35] L. R. MacGillivray, S. Subramanian, M. J. Zaworotko, *Chem. Commun.* **1994**, 1325-1326.
[36] P. W. Carreck, M. Goldstein, E. M. McPartlin, W. D. Unsworth, *J. Chem. Soc. D* **1971**, 1634-1635.
[37] M. James, *Aust. J. Chem.* **2002**, *55*, 219-223.
[38] J. S. Haynes, S. J. Rettig, J. R. Sams, R. C. Thompson, J. Trotter, *Can. J. Chem.* **1987**, *65*, 420-426.
[39] S. A. Bourne, M. Kilkenny, L. R. Nassimbeni, *J. Chem. Soc., Dalton Trans.* **2001**, 1176-1179.
[40] F. Lloret, G. D. Munno, M. Julve, J. Cano, R. Ruiz, A. Caneschi, *Angew. Chem. Int. Ed.* **1998**, *37*, 135-138.
[41] J. Lu, T. Paliwala, S. C. Lim, C. Yu, T. Niu, A. J. Jacobson, *Inorg. Chem.* **1997**, *36*, 923-929.
[42] J. A. Real, G. D. Munno, M. C. Munoz, M. Julve, *Inorg. Chem.* **1991**, *30*, 2701-2704.
[43] L. Carlucci, G. Ciani, F. Porta, D. M. Prosperio, L. Santagostini, *Angew. Chem. Int. Ed.* **2002**, *41*, 1907-1911.
[44] M. Schweiger, S. R. Seidel, A. M. Arif, P. J. Stang, *Angew. Chem. Int. Ed.* **2001**, *40*, 3467-3469.
[45] T. Rajendran, B. Manimaran, F.-Y. Lee, P.-J. Chen, S.-C. Lin, G.-H. Lee, S.-M. Peng, Y.-J. Chen, K.-L. Lu, *J. Chem. Soc., Dalton Trans.* **2001**, 3346-3351.
[46] V. C. Lau, L. A. Berben, J. R. Long, *J. Am. Chem. Soc.* **2002**, *124*, 9042-9043.
[47] L. Carlucci, G. Ciani, D. M. Proserpio, A. Sironi, *Angew. Chem. Int. Ed.* **1995**, *34*, 1895-1898.

[48] L. Carlucci, G. Ciani, D. M. Proserpio, A. Sironi, *J. Am. Chem. Soc.* **1995**, *117*, 4562-4569.
[49] A. Klein, V. Kasack, R. Reinhardt, T. Sixt, T. Scheiring, S. Zalis, J. Fiedler, W. Kaim, *J. Chem. Soc., Dalton Trans.* **1999**, 575-582.
[50] M. Graf, H. Stoeckli-Evans, A. Escuer, R. Vicente, *Inorg. Chim. Acta* **1997**, *257*, 89-97.
[51] H. Oshio, *J. Chem. Soc., Dalton Trans.* **1990**, 2985-2989.
[52] J. Suárez-Varela, E. Colacio, A. Romerosa, J. C. Avila-Rosón, M. A. Hidalgo, J. Romero, *Inorg. Chim. Acta* **1994**, *217*, 39-44.
[53] H. Oshio, U. Nagashima, *Inorg. Chem.* **1990**, *29*, 3321-3325.
[54] J.-M. Lehn, *Science* **1985**, *227*, 849-856.
[55] J.-M. Lehn, *Angew. Chem. Int. Ed.* **1988**, *27*, 89-112.
[56] J.-M. Lehn, *Angew. Chem. Int. Ed.* **1990**, *29*, 1304-1319.
[57] J. S. Lindsey, *New J. Chem.* **1991**, *15*, 153-180.
[58] J.-M. Lehn, *Science* **1993**, *260*, 1762-1763.
[59] D. S. Lawrence, T. Jiang, M. Levett, *Chem. Rev.* **1995**, *95*, 2229-2260.
[60] P. J. Stang, B. Olenyuk, *Acc. Chem. Res.* **1997**, *30*, 502-518.
[61] C. Piguet, G. Bernardinelli, G. Hopfgartner, *Chem. Rev.* **1997**, *97*, 2005-2062.
[62] B. Olenyuk, A. Fechtenkötter, P. J. Stang, *J. Chem. Soc., Dalton Trans.* **1998**, 1707-1728.
[63] D. L. Caulder, K. N. Raymond, *Acc. Chem. Res.* **1999**, *32*, 975-982.
[64] L. R. MacGillivray, J. L. Atwood, *Angew. Chem. Int. Ed.* **1999**, *38*, 1018-1033.
[65] D. L. Caulder, K. N. Raymond, *Acc. Chem. Res.* **1999**, *32*, 975-982.
[66] D. L. Caulder, K. N. Raymond, *J. Chem. Soc., Dalton Trans.* **1999**, 1185-1200.
[67] G. F. Swiegers, T. J. Malefetse, *Chem. Rev.* **2000**, *100*, 3483-3537.
[68] S. Leininger, B. Olenyuk, P. J. Stang, *Chem. Rev.* **2000**, *100*, 853-908.
[69] S. Leininger, J. Fan, M. Schmitz, P. J. Stang, *Proc. Nat. Acad. Soc. USA* **2000**, *97*, 1380-1384.
[70] J.-M. Lehn, *Chem. Eur. J.* **2000**, *6*, 2097-2102.
[71] V. G. Machado, P. N. W. Baxter, J.-M. Lehn, *J. Braz. Chem. Soc.* **2001**, *12*, 431-462.
[72] B. J. Holliday, C. A. Mirkin, *Angew. Chem. Int. Ed.* **2001**, *40*, 2022-2043.
[73] G. F. Swiegers, T. J. Malefetse, *Coord. Chem. Rev.* **2002**, *225*, 91-121.
[74] L. K. Thompson, *Coord. Chem. Rev.* **2002**, *233-234*, 193-206.
[75] The Royal Swedish Academy of Sciences, *Press Release: The 1987 Nobel Prize in Chemistry*, **1987**.
[76] D. Voet, J. G. Voet, C. W. Pratt, *Lehrbuch der Biochemie*, Wiley-VCH, **2002**.
[77] H. Fraenkel-Conrat, R. C. Williams, *Proc. Nat. Acad. Soc. USA* **1955**, *41*, 690-698.
[78] B. Hasenknopf, J.-M. Lehn, N. Boumediene, A. Dupont-Gervais, A. V. Dorsselaer, B. Kneisel, D. Fenske, *J. Am. Chem. Soc.* **1997**, *119*, 10956-10962.
[79] M. C. T. Fyfe, J. F. Stoddart, *Acc. Chem. Res.* **1997**, *30*, 393-401.
[80] M.-T. Youinou, N. Rahmouni, J. Fischer, J. A. Osborn, *Angew. Chem. Int. Ed.* **1992**, *31*, 733-735.

[81] P. N. W. Baxter, J.-M. Lehn, J. Fischer, M.-T. Youinou, *Angew. Chem. Int. Ed.* **1994**, *33*, 2284-2287.
[82] P. N. W. Baxter, J.-M. Lehn, G. Baum, D. Fenske, *Chem. Eur. J.* **2000**, *6*, 4510-4517.
[83] Y. Lan, D. K. Kennepohl, B. Moubaraki, K. S. Murray, J. D. Cashion, G. B. Jameson, S. Brooker, *Chem. Eur. J.* **2003**, *9*, 3772-3784.
[84] P. N. W. Baxter, J.-M. Lehn, B. O. Kneisel, D. Fenske, *Chem. Commun.* **1997**, 2231-2232.
[85] S. Toyota, C. R. Woods, M. Benaglia, R. Haldimann, K. Wärnmark, K. Hardcastle, J. S. Siegel, *Angew. Chem. Int. Ed.* **2001**, *40*, 751-754.
[86] M. Ferrer, M. Mounir, O. Rossell, E. Ruiz, M. A. Maestro, *Inorg. Chem.* **2003**, *42*, 5890-5899.
[87] J. Rojo, F. J. Romero-Salguero, J.-M. Lehn, G. Baum, D. Fenske, *Eur. J. Inorg. Chem.* **1999**, 1421-1428.
[88] A. N. Garcia, F. J. Romero-Salguero, D. M. Bassani, J.-M. Lehn, G. Baum, D. Fenske, *Chem. Eur. J.* **1999**, *5*, 1803-1808.
[89] M. Ruben, E. Breuning, J.-P. Gisselbrecht, J.-M. Lehn, *Angew. Chem. Int. Ed.* **2000**, *39*, 4139-4142.
[90] E. Breuning, M. Ruben, J.-M. Lehn, F. Renz, Y. Garcia, V. Ksenofontov, P. Gütlich, E. Wegelius, K. Rissanen, *Angew. Chem. Int. Ed.* **2000**, *39*, 2504-2507.
[91] E. Breuning, U. Ziener, J.-M. Lehn, E. Wegelius, K. Rissanen, *Eur. J. Inorg. Chem.* **2001**, 1515-1521.
[92] E. Breuning, G. S. Hanan, F. J. Romero-Salguero, A. N. Garcia, P. N. W. Baxter, J.-M. Lehn, E. Wegelius, K. Rissanen, H. Nierengarten, A. V. Dorsselaer, *Chem. Eur. J.* **2002**, *8*, 3458-3466.
[93] M. Ruben, E. Breuning, M. Barboiu, J.-P. Gisselbrecht, J.-M. Lehn, *Chem. Eur. J.* **2003**, *9*, 291-299.
[94] M. Barboiu, G. Vaughan, R. Graff, J.-M. Lehn, *J. Am. Chem. Soc.* **2003**, *125*, 10257-10265.
[95] M. Ruben, E. Breuning, J.-M. Lehn, V. Ksenofontov, F. Renz, P. Gütlich, G. B. M. Vaughan, *Chem. Eur. J.* **2003**, *9*, 4422-4429.
[96] V. Patroniak, P. N. W. Baxter, J.-M. Lehn, M. Kubicki, M. Nissinen, K. Rissanen, *Eur. J. Inorg. Chem.* **2003**, 4001-4009.
[97] O. Waldmann, J. Hassmann, P. Müller, D. Volkmer, U. S. Schubert, J.-M. Lehn, *Phys. Rev. B* **1998**, *58*, 3277-3285.
[98] R. Krämer, L. Kovbasynk, H. Pritzkow, *New J. Chem.* **2002**, *26*, 516-518.
[99] W. Bietsch, A. Mirea, T. Kamleiter, M. Weiss, U. S. Schubert, C. H. Weidl, C. Eschbaumer, I. Ovchinnikov, N. Domracheva, *Mol. Phys.* **2002**, *100*, 1957-1968.
[100] S. T. Onions, A. M. Frankin, P. N. Horton, M. B. Hursthouse, C. J. Matthews, *Chem. Commun.* **2003**, 2864-2865.
[101] T. Bark, M. Düggeli, H. Stoeckli-Evans, A. von Zelewsky, *Angew. Chem. Int. Ed.* **2001**, *40*, 2848-2851.
[102] L. Zhao, C. J. Matthews, L. K. Thompson, S. L. Heath, *Chem. Commun.* **2000**, 265-266.

[103] L. Zhao, Z. Xu, L. K. Thompson, S. L. Heath, D. O. Miller, M. Ohba, *Angew. Chem. Int. Ed.* **2000**, *39*, 3114-3117.
[104] L. K. Thompson, L. Zhao, Z. Xu, D. O. Miller, W. M. Reiff, *Inorg. Chem.* **2003**, *42*, 128-139.
[105] A. Gelasco, A. Askenas, V. L. Pecoraro, *Inorg. Chem.* **1996**, *35*, 1419-1420.
[106] J. Rojo, J.-M. Lehn, G. Baum, D. Fenske, O. Waldmann, P. Müller, *Eur. J. Inorg. Chem.* **1999**, 517-522.
[107] H. Gang, G. Dong, D. Chun-Ying, M. Hong, M. Qing-jin, *New J. Chem.* **2002**, *26*, 1371-1377.
[108] E. B. Fleischer, M. B. Lawson, *Inorg. Chem.* **1972**, *11*, 2772-2775.
[109] I. Mallik, S. Mallik, *Synlett* **1996**, 734-736.
[110] D. S. Marlin, M. M. Olmstead, P. K. Mascharak, *Inorg. Chim. Acta* **2001**, *323*, 1-4.
[111] M. Nonoyama, K. Yamasaki, *Inorg. Chim. Acta* **1971**, *5*, 124-128.
[112] R. G. Jones, K. C. McLaughlin, *Org. Synth.* **1950**, *30*, 87-90.
[113] S. Gabriel, A. Sonn, *Ber. Dtsch. Chem. Ges.* **1907**, *40*, 4850-4860.
[114] I. A. Solomons, P. E. Spoerri, *J. Am. Chem. Soc.* **1953**, *75*, 679-680.
[115] K. Nonoyama, W. Mori, M. Nonoyama, *Polyhedron* **1994**, *13*, 891-897.
[116] A. Braibanti, F. Dallavalle, G. Mori, B. Veroni, *Talanta* **1982**, *29*, 725-731.
[117] B. C. Challis, J. A. Challis, in *Comprehensive Organic Chemistry, Vol. 2*, Pergamon Press, Liverpool, **1979**, pp. 957-1067.
[118] M. H. Klingele, *PhD Thesis*, **2004**, *University of Otago*.
[119] D. S. Cati, H. Stoeckli-Evans, *Acta Crystallogr. E* **2004**, *60*, o210-o212.
[120] O. Clement, B. M. Rapko, B. P. Hay, *Coord. Chem. Rev.* **1998**, *170*, 203-243.
[121] H. Sigel, R. B. Martin, *Chem. Rev.* **1982**, *82*, 385-426.
[122] E. B. Fleischer, D. Jeter, R. Florian, *Inorg. Chem.* **1974**, *13*, 1042-1047.
[123] C.-Y. Wu, C.-C. Su, *Polyhedron* **1997**, *16*, 383-392.
[124] C.-Y. Wu, C.-C. Su, *Polyhedron* **1997**, *16*, 2465-2474.
[125] J. M. Rowland, M. M. Olmstead, P. K. Mascharak, *Inorg. Chem.* **2000**, *39*, 5326-5332.
[126] J. M. Rowland, M. M. Olmstead, P. K. Mascharak, *Inorg. Chem.* **2002**, *41*, 1545-1549.
[127] A. W. Addison, T. N. Rao, J. Reedijk, J. van Rijn, G. C. Verschoor, *J. Chem. Soc., Dalton Trans.* **1984**, 1349-1356.
[128] M. Duggan, N. Ray, B. J. Hathaway, *J. Chem. Soc., Dalton Trans.* **1980**, 1342-1348.
[129] B. J. Hathaway, *J. Chem. Soc., Dalton Trans.* **1972**, 1196-1199.
[130] A. B. P. Lever, *Inorganic Electronic Spectroscopy*, 2nd ed., Elsevier, Amsterdam, **1984**.
[131] J. A. McCleverty, M. D. Ward, *Acc. Chem. Res.* **1998**, *31*, 842-851.
[132] D. B. Losee, R. H. Wayne, W. E. Hatfield, *J. Chem. Phys.* **1993**, *59*, 3600-3603.
[133] M. Julve, M. Verdaguer, J. Faus, F. Tinti, J. Moratal, A. Monge, E. Gutierrez-Puebla, *Inorg. Chem.* **1987**, *26*, 3520-3527.
[134] J. P. Hay, J. C. Thibeault, R. Hoffmann, *J. Am. Chem. Soc.* **1975**, *97*, 4884-4899.

[135] R. C. E. Belford, D. E. Fenton, M. E. Truter, *J. Chem. Soc., Dalton Trans.* **1974**, 17-24.
[136] M. D. Ward, *Chem. Soc. Rev.* **1995**, *24*, 121-134.
[137] B. J. Hathaway, *Coord. Chem. Rev.* **1982**, *41*, 423-487.
[138] M. Inoue, M. Kubo, *Coord. Chem. Rev.* **1976**, *21*, 1-27.
[139] D. L. Lewis, E. D. Estes, D. J. Hodgson, *J. Cryst. Mol. Struct.* **1975**, *5*, 67-74.
[140] M. R. Rosenthal, *J. Chem. Ed.* **1973**, *50*, 331-335.
[141] K. Nakamoto, *Infrared and Raman Spectra of Inorganic Coordination Compounds*, 5 ed., Wiley-Interscience, New York, **1997**.
[142] N. M. N. Gowda, S. B. Naikar, G. K. N. Reddy, *Adv. Inorg. Chem. Radiochem.* **1984**, *28*, 255-299.
[143] D. S. Cati, J. Ribas, J. Ribas-Ariño, H. Stoeckli-Evans, *Inorg. Chem.* **2004**, *43*, 1021-1030.
[144] R. J. H. Clark, C. S. Williams, *Spectrochim. Acta* **1966**, *22*, 1081-1090.
[145] C. V. Depree, U. Beckmann, K. Heslop, S. Brooker, *J. Chem. Soc., Dalton Trans.* **2003**, 3071-3081.
[146] S. M. Nelson, F. S. Esho, M. G. B. Drew, *Chem. Commun.* **1981**, *8*, 388-389.
[147] G. A. van Albada, M. T. Lakin, N. Veldman, A. L. Spek, J. Reedijk, *Inorg. Chem.* **1995**, *34*, 4910-4917.
[148] R. Cortés, J. I. R. de Larramendi, L. Lezama, T. Rojo, K. Urtiaga, M. I. Arriortua, *J. Chem. Soc., Dalton Trans.* **1992**, 2723-2728.
[149] R. Cortés, J. L. Pizzaro, L. Lezama, M. I. Arriortua, T. Rojo, *Inorg. Chem.* **1994**, *33*, 2697-2700.
[150] Z. Dori, R. F. Ziolo, *Chem. Rev.* **1973**, *73*, 247-254.
[151] A. E. Goeta, L. K. Thompson, C. L. Sheppard, S. S. Tandon, C. W. Lehmann, J. Cosier, C. Webster, J. A. K. Howard, *Acta Crystallogr. C* **1999**, *55*, 1243-1246.
[152] J. Lorösch, H. Paulus, W. Haase, *Inorg. Chim. Acta* **1985**, *106*, 101-108.
[153] T. C. W. Mak, M. A. S. Goher, *Inorg. Chim. Acta* **1986**, *115*, 17-23.
[154] G. D. Munno, J. A. Real, M. Julve, M. C. Muños, *Inorg. Chim. Acta* **1993**, *211*, 227-233.
[155] S. S. Tandon, L. K. Thompson, M. E. Manuel, J. N. Bridson, *Inorg. Chem.* **1994**, *33*, 5555-5570.
[156] S. S. Tandon, L. K. Thompson, D. O. Miller, *Chem. Commun.* **1995**, 1907-1908.
[157] S. Koner, S. Saha, K.-I. Okamoto, J.-P. Tuchagues, *Inorg. Chem.* **2003**, *42*, 4668-4672.
[158] M. A. S. Goher, T. C. W. Mak, *Inorg. Chim. Acta* **1984**, *85*, 117-122.
[159] J. E. Pate, P. K. Ross, T. J. Thamann, C. A. Reed, K. D. Karlin, T. N. Sorrell, E. I. Solomon, *J. Am. Chem. Soc.* **1989**, *111*, 5198-5209.
[160] F. A. Mautner, M. A. S. Goher, *Polyhedron* **1996**, *15*, 1133-1139.
[161] J. Comarmond, P. Plumeré, J.-M. Lehn, Y. Agnus, R. Louis, R. Weiss, O. Kahn, I. Morgenstern-Badarau, *J. Am. Chem. Soc.* **1982**, *104*, 6330-6340.
[162] G. D. Munno, M. G. Lombardi, M. Julve, F. Lloret, J. Faus, *Inorg. Chim. Acta* **1998**, *282*, 82-89.

[163] C. L. Sheppard, S. S. Tandon, L. K. Thompson, J. N. Bridson, D. O. Miller, M. Handa, F. Lloret, *Inorg. Chim. Acta* **1996**, *250*, 227-239.
[164] L. Zhang, L.-F. Tang, Z.-H. Wang, M. Du, M. Julve, F. Lloret, J.-T. Wang, *Inorg. Chem.* **2001**, *40*, 3619-3622.
[165] A. Escuer, R. Vicente, J. Ribas, X. Solans, *Inorg. Chem.* **1995**, *34*, 1793-1798.
[166] Q.-L. Wang, L.-H. Yu, D.-Z. Liao, S.-P. Yan, Z.-H. Jiang, P. Cheng, *Helv. Chim. Acta* **2003**, *86*, 2441-2451.
[167] V. Amendola, L. Fabbrizzi, C. Mangano, P. Pallavicini, M. Zema, *Inorg. Chim. Acta* **2002**, *70*, 70-74.
[168] M. G. B. Drew, J. Hunter, D. J. Marrs, J. Nelson, C. Harding, *J. Chem. Soc., Dalton Trans.* **1992**, 3235-3242.
[169] C. J. Harding, F. E. Mabbs, E. J. L. MacInnes, V. McKee, J. Nelson, *J. Chem. Soc., Dalton Trans.* **1996**, 3227-3230.
[170] A. Escuer, M. Font-Bardía, E. Peñalba, X. Solans, R. Vicente, *Polyhedron* **1999**, *18*, 211-215.
[171] M. A. S. Goher, F. A. Mautner, *J. Chem. Soc., Dalton Trans.* **1999**, 1535-1536.
[172] T. K. Maji, P. S. Mukherjee, S. Koner, G. Mostafa, J.-P. Tuchagues, N. R. Chaudhuri, *Inorg. Chim. Acta* **2001**, *314*, 111-116.
[173] G. S. Papaefstathiou, A. Escuer, R. Vicente, M. Font-Bardia, X. Solans, S. P. Perlepes, *Chem. Commun.* **2001**, 2414-2415.
[174] G. S. Papaefstathiou, S. P. Perlepes, A. Escuer, R. Vicente, M. Font-Bardia, X. Solans, *Angew. Chem. Int. Ed.* **2001**, *40*, 884-886.
[175] M. L. Boillot, Y. Journaux, A. Bencini, D. Gatteschi, O. Kahn, *Inorg. Chem.* **1985**, *24*, 263-267.
[176] M. S. Ray, A. Ghosh, R. Bhattacharya, G. Mukhopadhyay, M. G. B. Drew, J. Ribas, *J. Chem. Soc., Dalton Trans.* **2004**, 252-259.
[177] Y. Agnus, R. Remy, J.-P. Gisselbrecht, R. Weiss, *J. Am. Chem. Soc.* **1984**, *106*, 93-102.
[178] I. Bkouche-Waksman, M.-L. Boillot, O. Kahn, S. Sikorav, *Inorg. Chem.* **1984**, *23*, 4454-4459.
[179] F. Fabrizzi de Biani, E. Ruiz, J. J. Novoa, S. Alvarez, *Inorg. Chem.* **2000**, *39*, 3221-3229.
[180] F. Holleman, N. Wiberg, *Lehrbuch der Anorganischen Chemie*, de Gruyter, **2001**.
[181] K. S. Murray, *Adv. Inorg. Chem.* **1995**, *43*, 261-358.
[182] B. J. Hathaway, D. E. Billing, *Coord. Chem. Rev.* **1970**, *5*, 143-207.
[183] T. Yano, R. Tanaka, T. Nishioka, I. Kinoshita, K. Isobe, L. J. Wright, T. J. Collins, *Chem. Commun.* **2002**, 1396-1397.
[184] D. S. Cati, H. Stoeckli-Evans, *Acta Crystallogr. E* **2004**, *60*, m177-179.
[185] K. J. Brewer, W. R. J. Murphy, J. D. Petersen, *Inorg. Chem.* **1987**, *26*, 3376-3379.
[186] D. S. Cati, H. Stoeckli-Evans, *Acta Crystallogr. E* **2004**, *60*, m174-m176.
[187] L. H. Uppadine, J.-M. Lehn, *Angew. Chem.* **2004**, *116*, 242-245.
[188] J. M. Rowland, M. M. Olmstead, P. K. Mascharak, *Inorg. Chem.* **2002**, *41*, 2754-2760.

[189] B. J. Hathaway, A. A. G. Tomlinson, *Coord. Chem. Rev.* **1970**, *5*, 1-43.
[190] C. Janiak, T. Klapötke, H.-J. Meyer, E. Riedel, *Moderne Anorganische Chemie*, de Gruyter, **1998**.
[191] P. Van der Sluis, A. L. Spek, *Acta Crystallogr. A* **1990**, *46*, 194-201.
[192] W. J. Schut, H. I. X. Mager, W. Berends, *Recueil* **1961**, *80*, 391-398.
[193] P. E. Spoerri, A. Erickson, *J. Am. Chem. Soc.* **1938**, *60*, 400-402.
[194] T. Sakasai, T. Sakamoto, H. Yamanaka, *Heterocycles* **1979**, *13*, 235-238.
[195] R. R. Gagné, M. W. McCool, R. E. Marsh, *Acta Crystallogr. B* **1980**, *36*, 2420-2422.
[196] F. S. Keij, R. A. G. de Graaff, J. G. Haasnoot, J. Reedijk, *Inorg. Chim. Acta* **1989**, *156*, 65-70.
[197] P. J. van Konigsbruggen, J. G. Haasnoot, R. A. G. de Graaff, J. Reedijk, *J. Chem. Soc., Dalton Trans.* **1993**, *1993*, 483-484.
[198] J. S. Fleming, K. L. V. Mann, S. M. Couchman, J. C. Jeffery, J. A. McCleverty, M. D. Ward, *J. Chem. Soc., Dalton Trans.* **1998**, 2047-2052.
[199] R. A. J. Driessen, F. B. Hulsbergen, W. J. Vermin, J. Reedijk, *Inorg. Chem.* **1982**, *21*, 3594-3597.
[200] S.-i. Noro, R. Kitaura, M. Kondo, S. Kitagawa, T. Ishii, H. Matsuzaka, M. Yamashita, *J. Am. Chem. Soc.* **2002**, *124*, 2568-2583.
[201] S.-i. Noro, S. Kitagawa, M. Kondo, K. Seki, *Angew. Chem. Int. Ed.* **2000**, *39*, 2081-2084.
[202] S. Subramanian, M. J. Zaworotko, *Angew. Chem. Int. Ed.* **1995**, *34*, 2127-2129.
[203] E. W. Ainscough, A. M. Brodie, J. D. Ranford, J. M. Waters, *Inorg. Chim. Acta* **1995**, *236*, 83-88.
[204] M. J. R. Clark, J. E. Fleming, H. Lynton, *Can. J. Chem.* **1969**, *47*, 3859-3861.
[205] J. A. Campo, M. Cano, J. V. Heras, M. C. Lagunas, J. Perles, E. Pinilla, M. R. Torres, *Helv. Chim. Acta* **2002**, *85*, 1079-1095.
[206] C.-C. Su, C.-B. Li, *Polyhedron* **1994**, *13*, 825-834.
[207] D. B. Losee, R. H. Wayne, W. E. Hatfield, *J. Chem. Phys.* **1973**, *59*, 3600-3603.
[208] P. R. Buckland, *J. Heterocycl. Chem.* **1980**, *17*, 397-398.
[209] J. J. Chen, J. M. Hinkley, D. S. Wise, L. B. Townsend, *Synth. Commun.* **1996**, *26*, 617-622.
[210] N. R. Patel, R. N. Castle, *J. Heterocycl. Chem.* **1966**, *3*, 512-517.
[211] K. Kanakarajan, A. W. Czarnik, *J. Heterocycl. Chem.* **1988**, *25*, 1869-1871.
[212] E. P. Papadopoulos, A. Jarrar, C. H. Issidorides, *J. Org. Chem.* **1966**, 615-615.
[213] E. Chablay, *Compt. Rend.* **1913**, *156*, 1020-1022.
[214] W. G. Brown, *Org. React.* **1951**, *6*, 469-510.
[215] E. Mosettig, R. Mozingo, *Org. React.* **1948**, *4*, 362-377.
[216] E. Mosettig, *Org. React.* **1954**, *8*, 218-257.
[217] J. Raap, S. Nieuwenhuis, A. Creemers, S. Hexspoor, U. Kragl, J. Lugtenburg, *Eur. J. Org. Chem.* **1999**, 2609-2621.
[218] G. T. Newbold, F. S. Spring, *J. Chem. Soc.* **1947**, 1183-1185.
[219] B. Klein, J. Berkowitz, *J. Am. Chem. Soc.* **1959**, *81*, 5160-5166.
[220] B. Klein, J. Berkowitz, N. E. Hetman, *J. Org. Chem.* **1961**, *26*, 126-131.

[221] H. A. Staab, W. K. Appel, *Liebigs Ann. Chem.* **1981**, 1065-1072.
[222] C. F. Koelsch, W. H. Gumprecht, *J. Org. Chem.* **1958**, *23*, 1603-1606.
[223] V. V. Kastron, I. G. Iovel, I. P. Skrastyn'sh, Y. S. Gol'dberg, M. V. Shimanskaya, G. Y. Dubur, *Chem. Coord. Comp.* **1986**, 915-917.
[224] C. Fontenas, E. Bejan, H. A. Haddou, G. G. A. Balavoine, *Synth. Commun.* **1995**, *25*, 629-633.
[225] H. Hopf, *Angew. Chem.* **2003**, *115*, 5698-5698.
[226] V. Boekelheide, W. J. Linn, *J. Am. Chem. Soc.* **1954**, *76*, 1286-1291.
[227] H. E. Gottlieb, V. Kotlyar, A. Nudelman, *J. Org. Chem.* **1997**, *62*, 7512-7515.
[228] G. M. Sheldrick, *Methods Enzymol.* **1997**, *276*, 628-641.
[229] G. M. Sheldrick, *Acta Crystallogr. A* **1990**, *46*, 467-473.
[230] G. M. Sheldrick, T. R. Schneider, *Methods Enzymol.* **1997**, *277*, 319-343.

5. Appendix

5.1. *Selected ^{1}H- and ^{13}C NMR spectra*

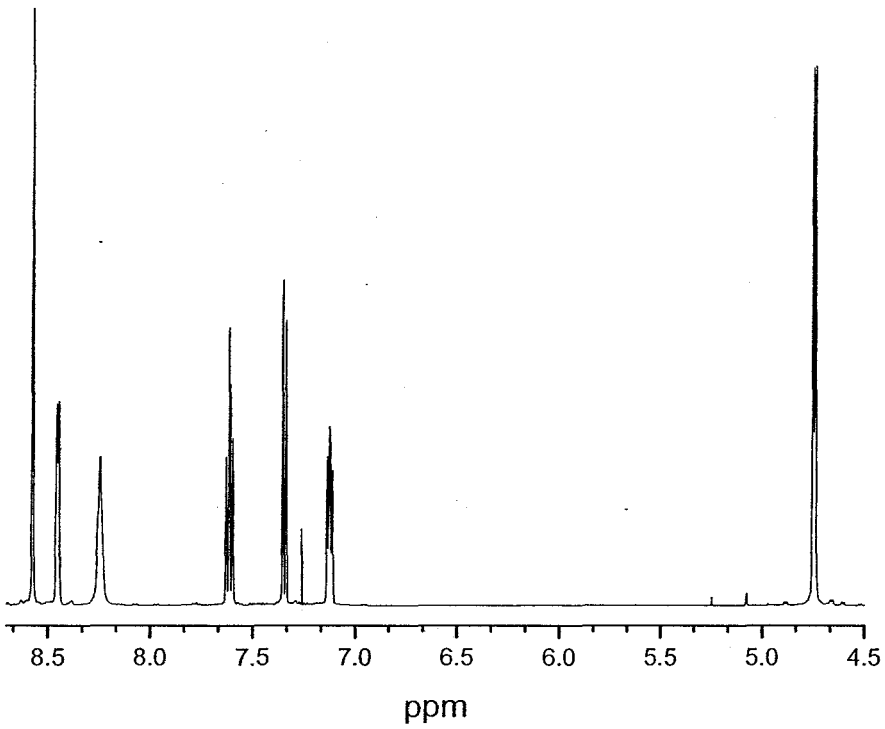

Figure 5.1.1. ^{1}H NMR spectrum ($CDCl_3$) of $H_2\mathbf{L}^{\mathbf{M1}}$.

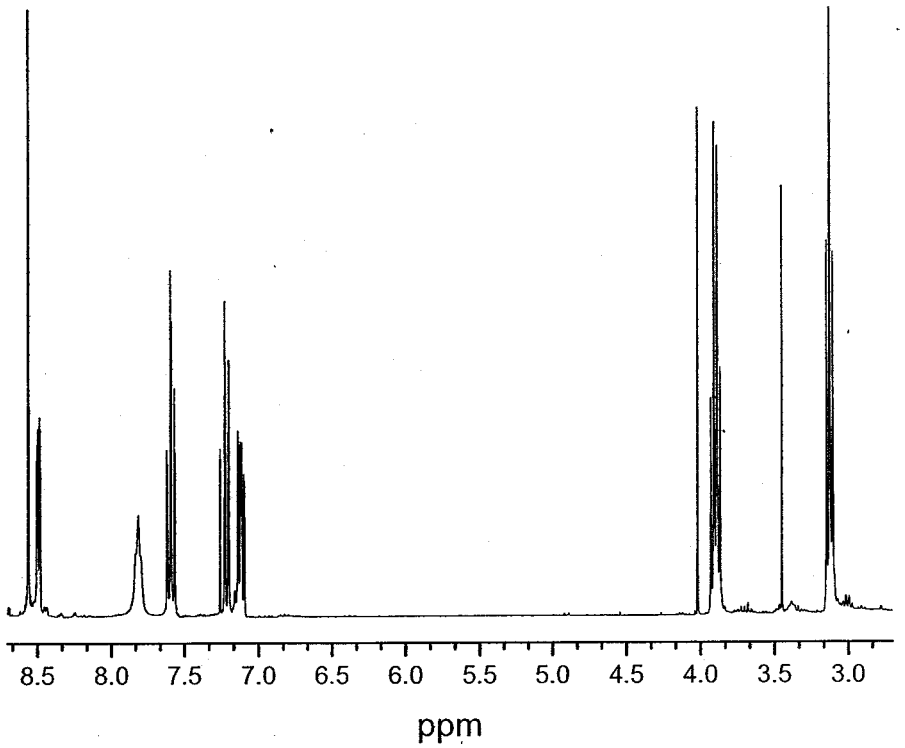

Figure 5.1.2. ^{1}H NMR spectrum ($CDCl_3$) of $H_2\mathbf{L}^{M2}$.

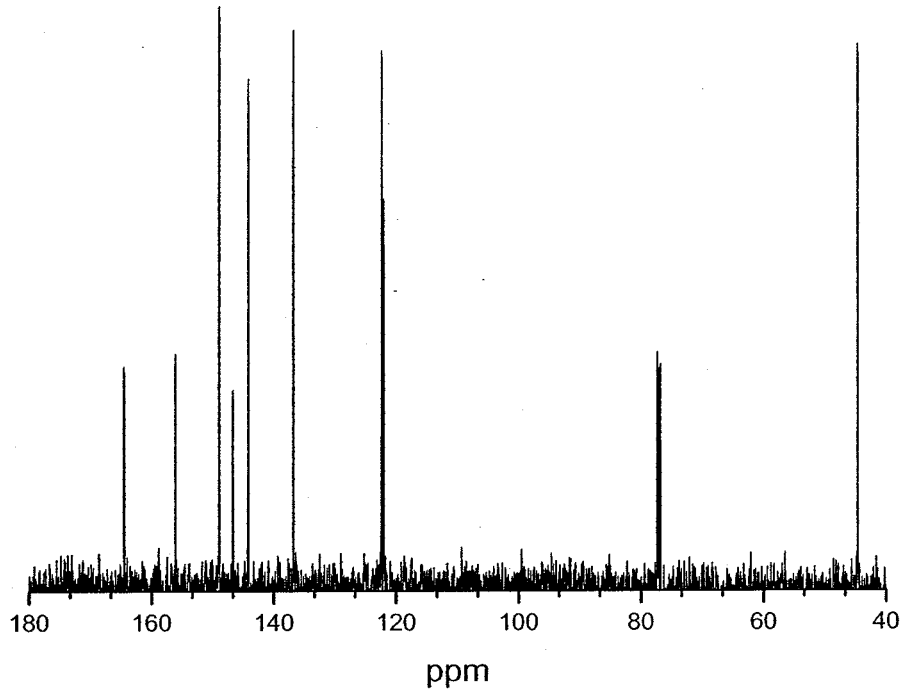

Figure 5.1.3. ^{13}C NMR spectrum ($CDCl_3$) of $H_2\mathbf{L}^{M1}$.

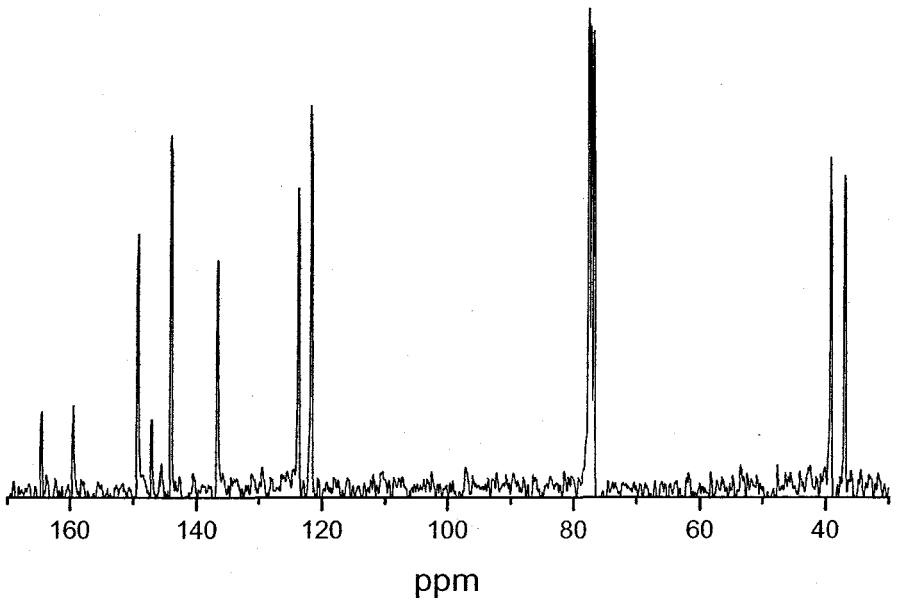

Figure 5.1.4. ^{13}C NMR spectrum ($CDCl_3$) of $H_2\mathbf{L}^{M2}$.

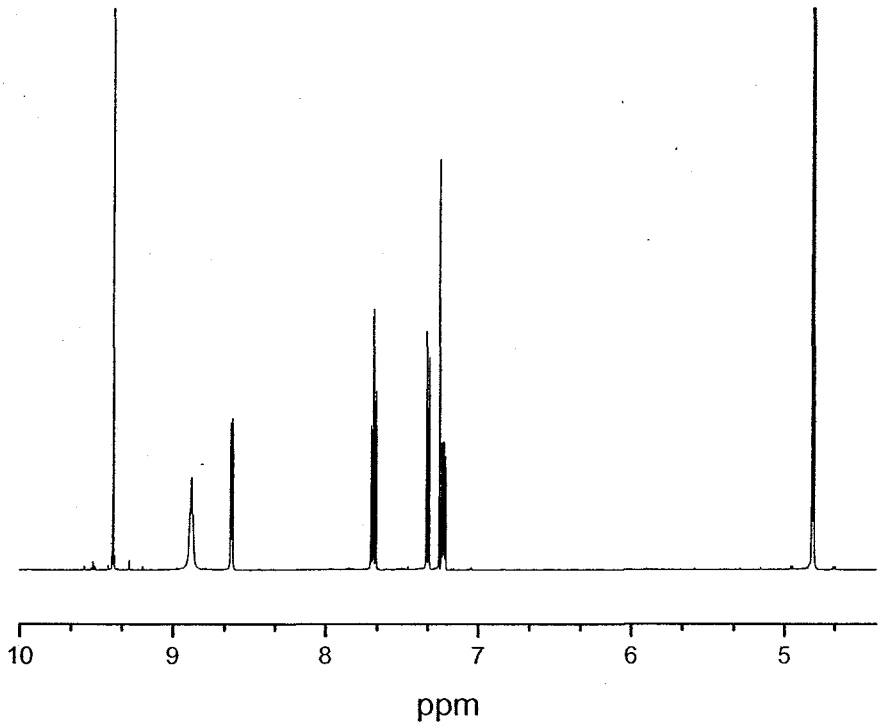

Figure 5.1.5. ^{1}H NMR spectrum ($CDCl_3$) of $H_2\mathbf{L}^{S1}$.

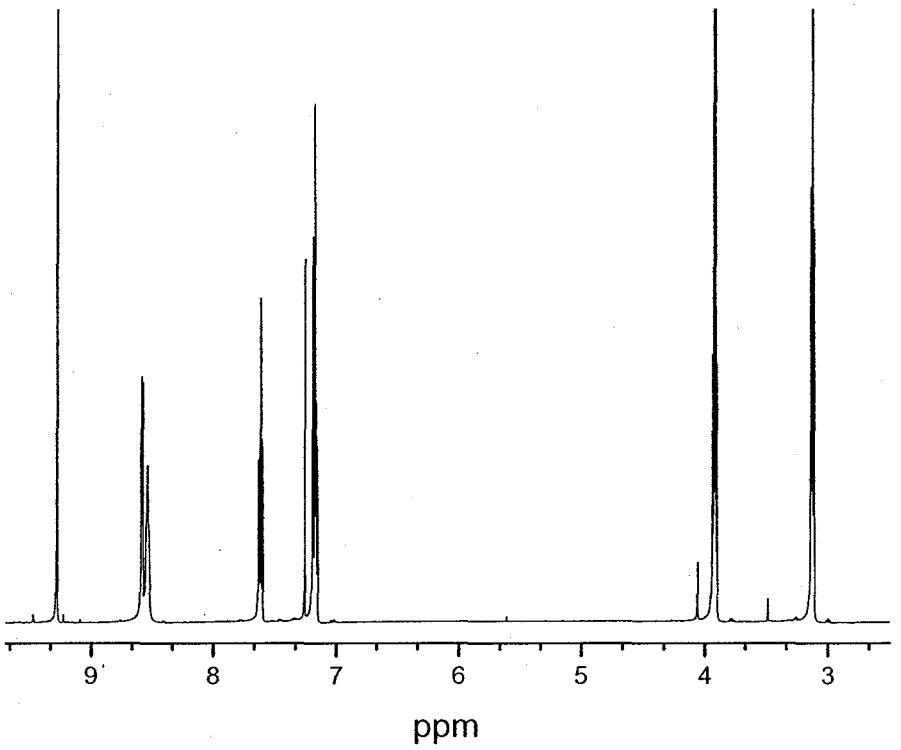

Figure 5.1.6. ^{1}H NMR spectrum ($CDCl_3$) of $H_2\mathbf{L}^{S2}$.

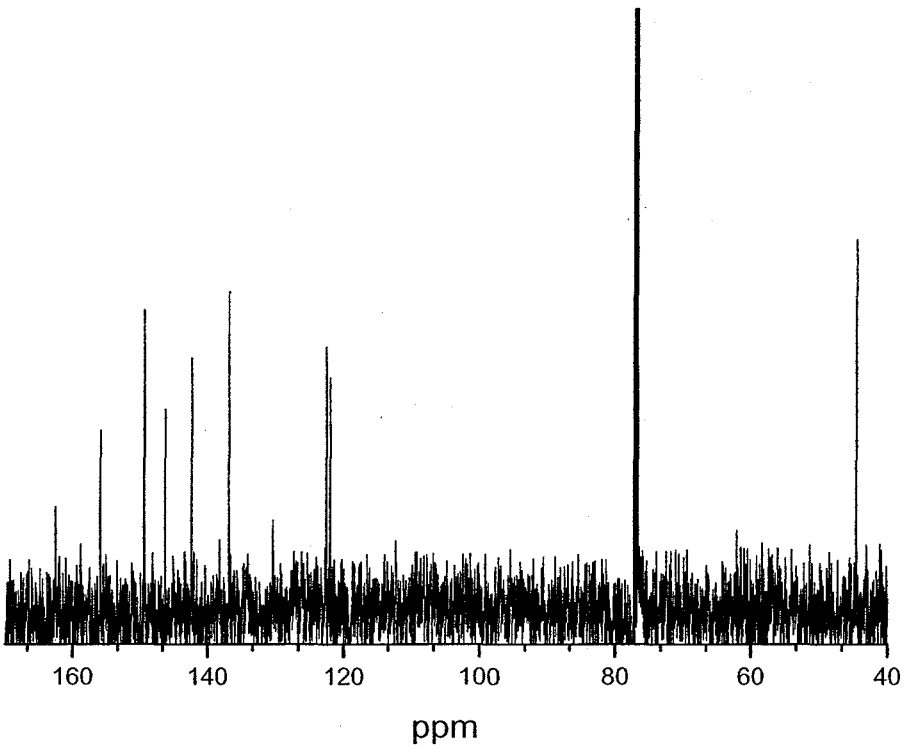

Figure 5.1.7. ^{13}C NMR spectrum ($CDCl_3$) of $H_2\mathbf{L}^{S1}$.

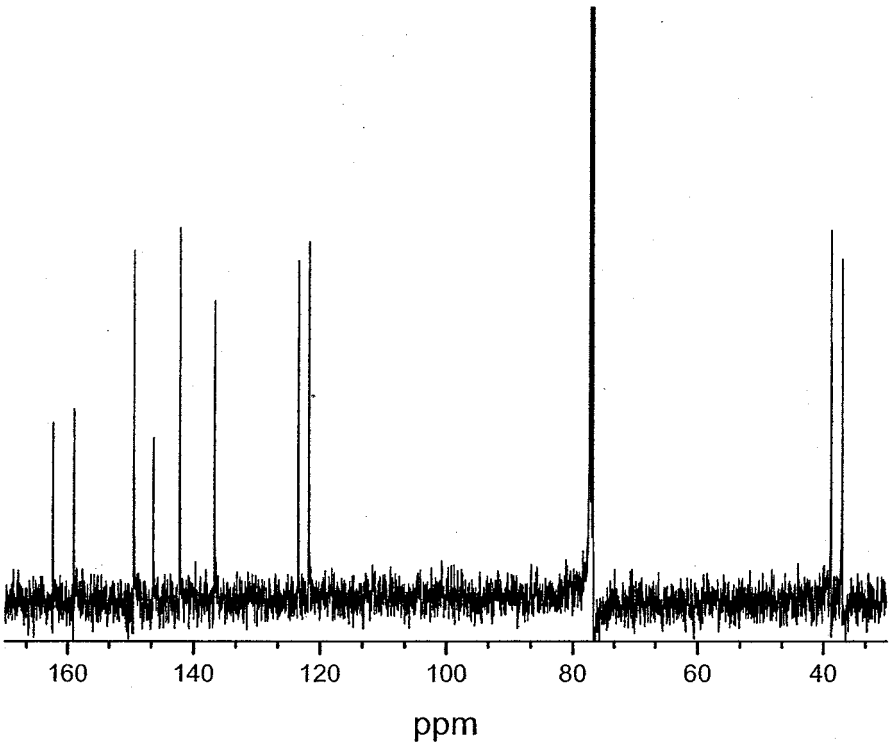

Figure 5.1.8. ^{13}C NMR spectrum ($CDCl_3$) of $H_2\mathbf{L}^{S2}$.

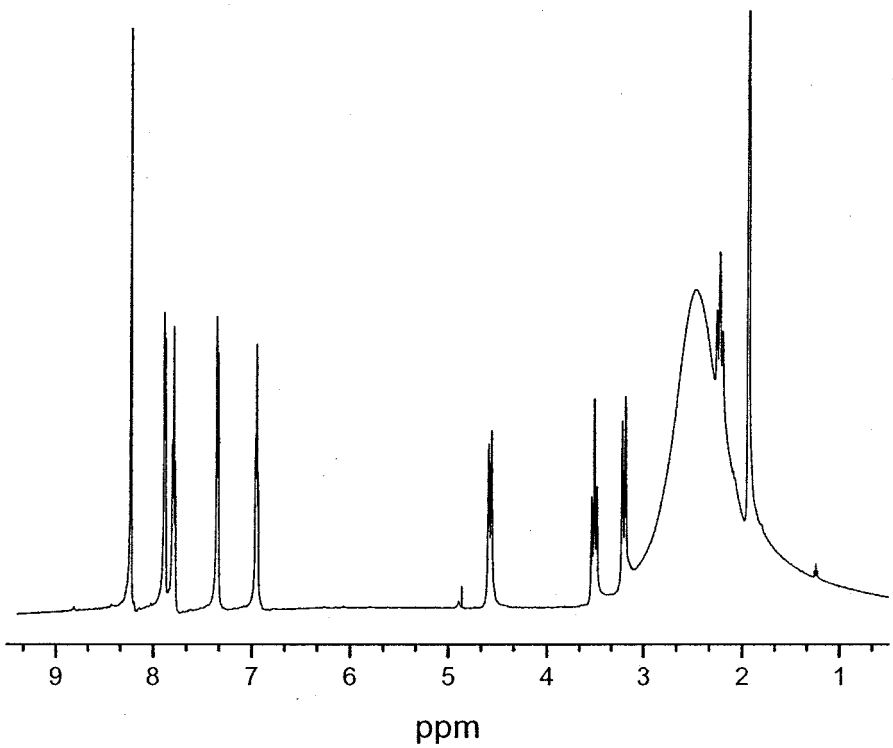

Figure 5.1.9. ^1H NMR spectrum (d^3-MeCN) of $[Co^{III}_4(\mathbf{L}^{S2})_4](BF_4)_4 \cdot 10\ H_2O$ (**36** · 10 H_2O).

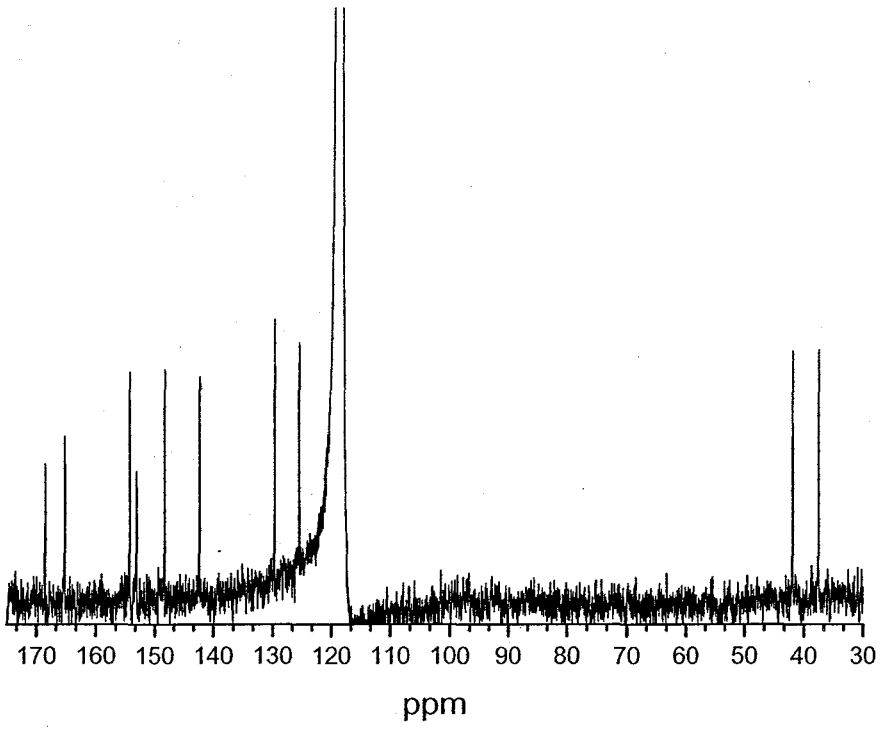

Figure 5.1.10. ^{13}C NMR spectrum (d^3-MeCN) of $[Co^{III}_4(\mathbf{L^{S2}})_4](BF_4)_4 \cdot 10\ H_2O$ (**36** · 10 H_2O).

5.2. *Selected positive ion electrospray mass spectra*

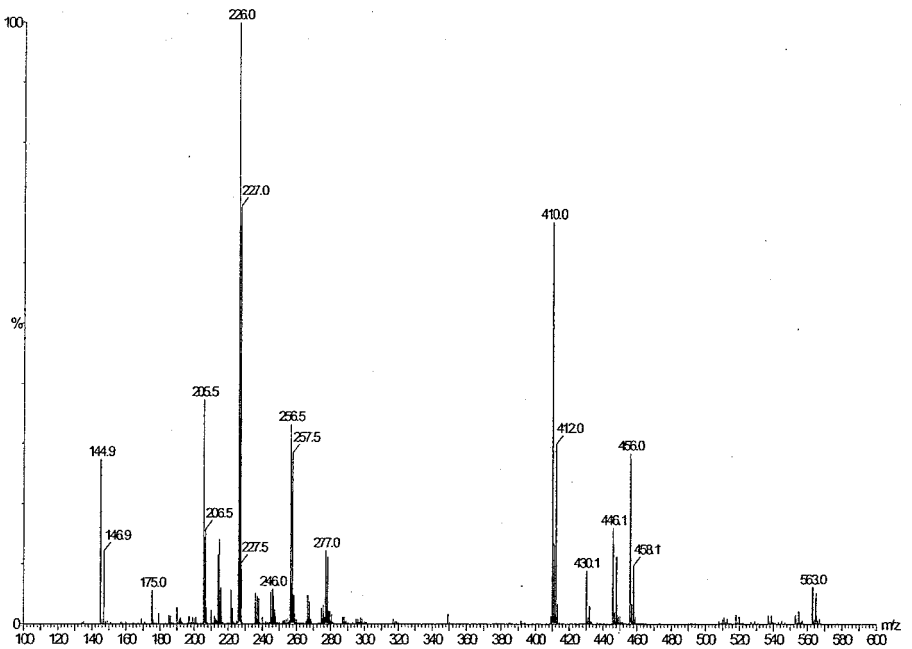

Figure 5.2.1. ESI-MS spectrum (MeCN) of $[Cu^{II}_2(HL^{M1})(MeCN)_2(H_2O)_2](BF_4)_3$ (**6**).

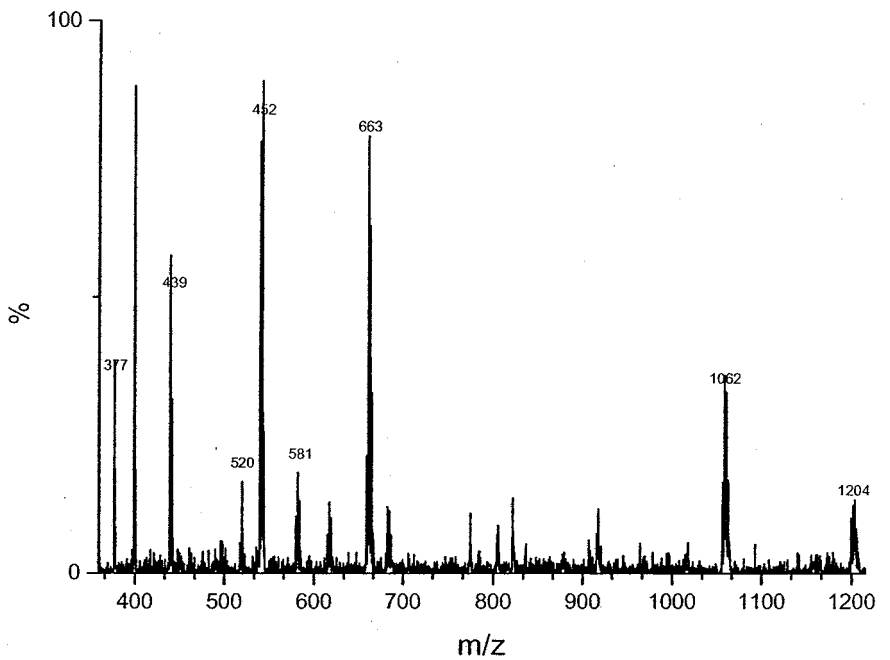

Figure 5.2.2. ESI-MS spectrum (MeCN) of $[Cu^{II}_2(HL^{M2})(Br)_3]_\infty$ (**12**).

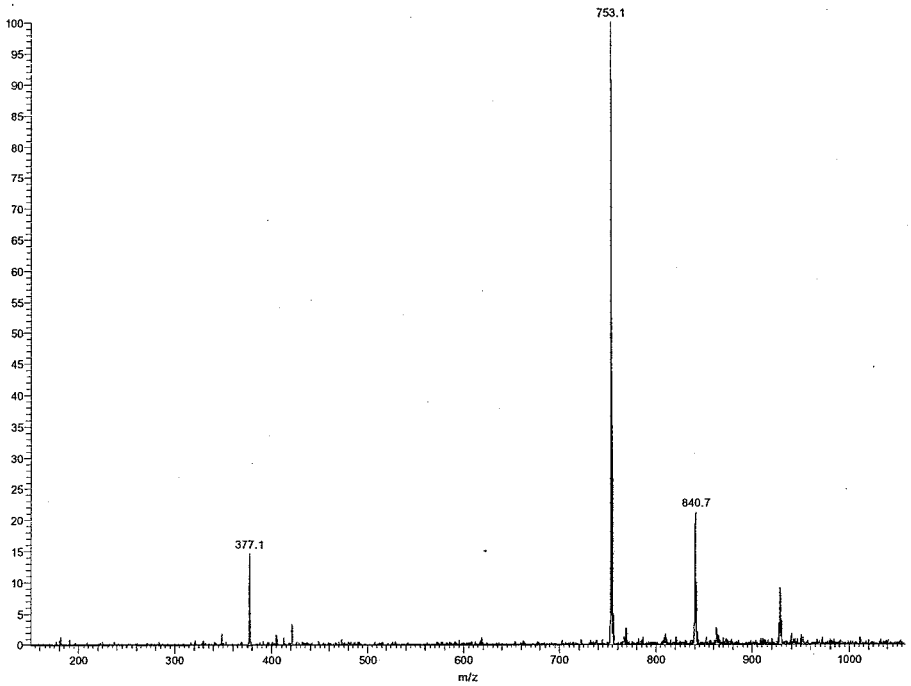

Figure 5.2.3. ESI-MS spectrum (MeCN) of $[Co^{III}(H_2\mathbf{L^{M1}})_2](BF_4)_3 \cdot 4\ H_2O$ (**21** · 4 H_2O).

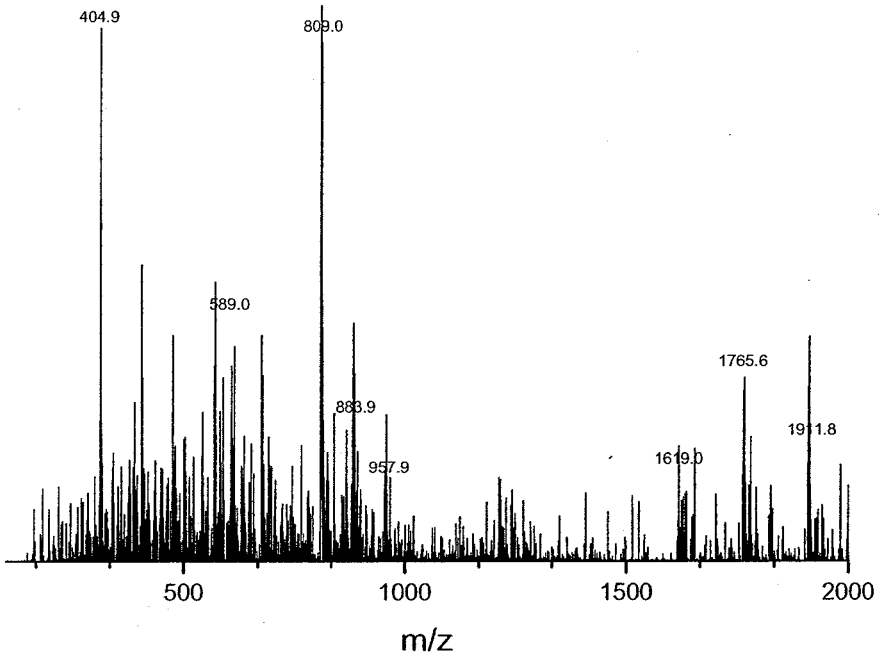

Figure 5.2.4. ESI-MS spectrum (MeCN) of $[Ni^{II}_4(H\mathbf{L^{M1}})_4](PF_6)_4$ (**26b**).

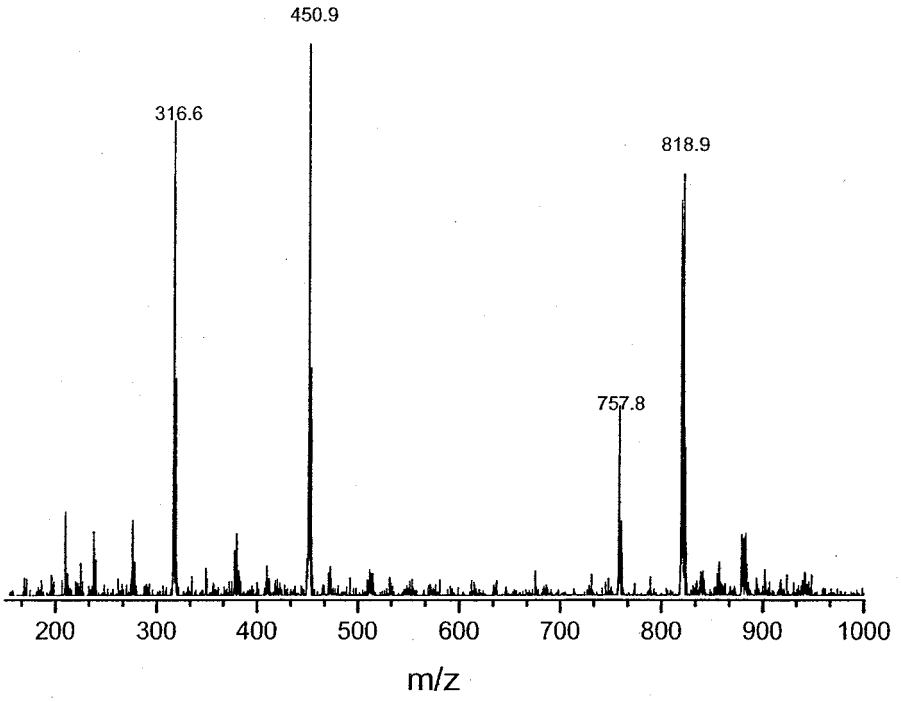

Figure 5.2.5. ESI-MS spectrum (MeCN) of $[Cu^{II}(H\mathbf{L^{S1}})(H_2O)]_n(BF_4)_n$ (**30**).

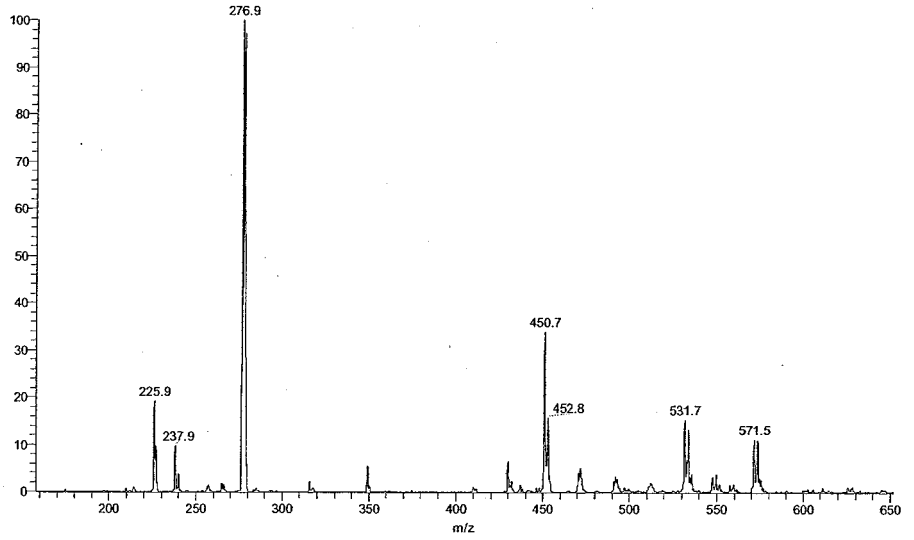

Figure 5.2.6. ESI-MS spectrum (MeCN) of $[Cu^{II}_2(\mathbf{L^{S1}})(H_2O)_2](BF_4)_2$ (**33**).

5.3. *Selected IR spectra*

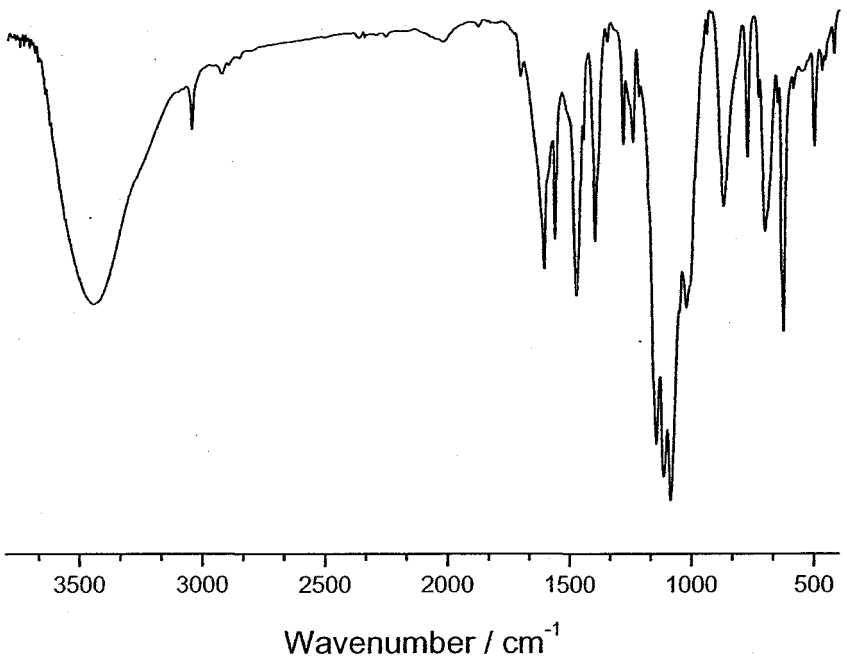

Figure 5.3.1. IR spectrum (KBr) of $[Cu^{II}_2(HL^{M1})(MeCN)_2](ClO_4)_3$ (**7**).

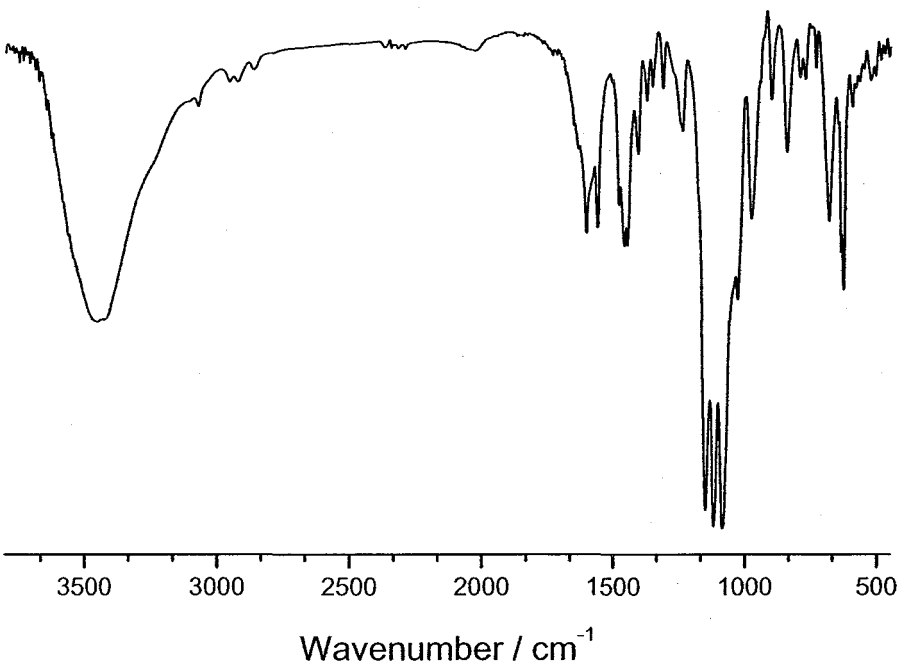

Figure 5.3.2. IR spectrum (KBr) of $[Cu^{II}_2(HL^{M2})(H_2O)](ClO_4)_3$ (**8**).

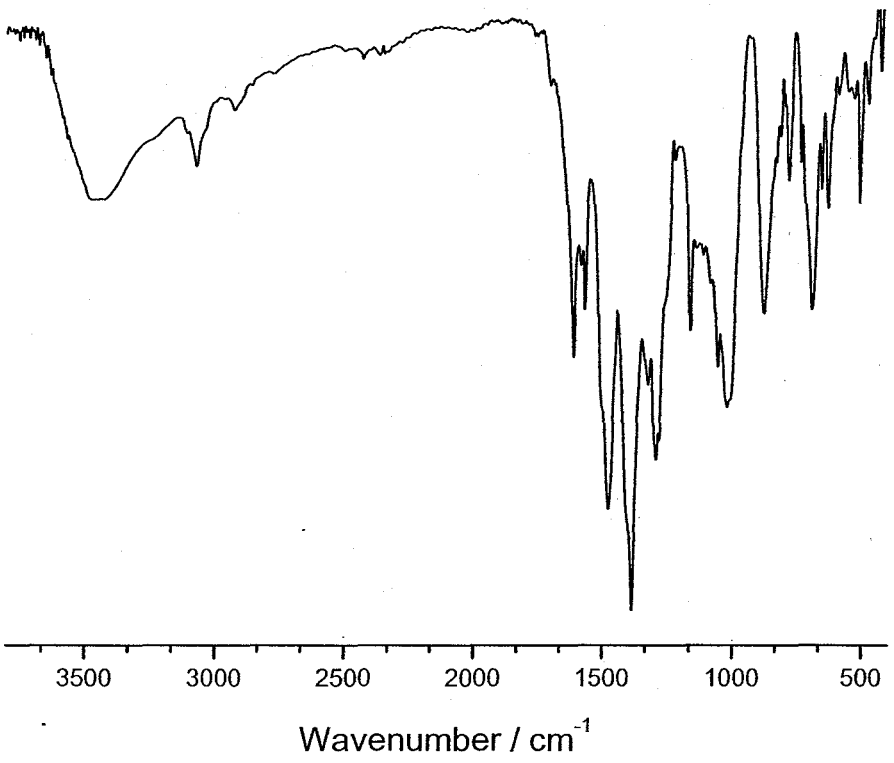

Figure 5.3.3. IR spectrum (KBr) of $[Cu^{II}_2(H\mathbf{L}^{M1})(NO_3)_3]_n$ (**9**).

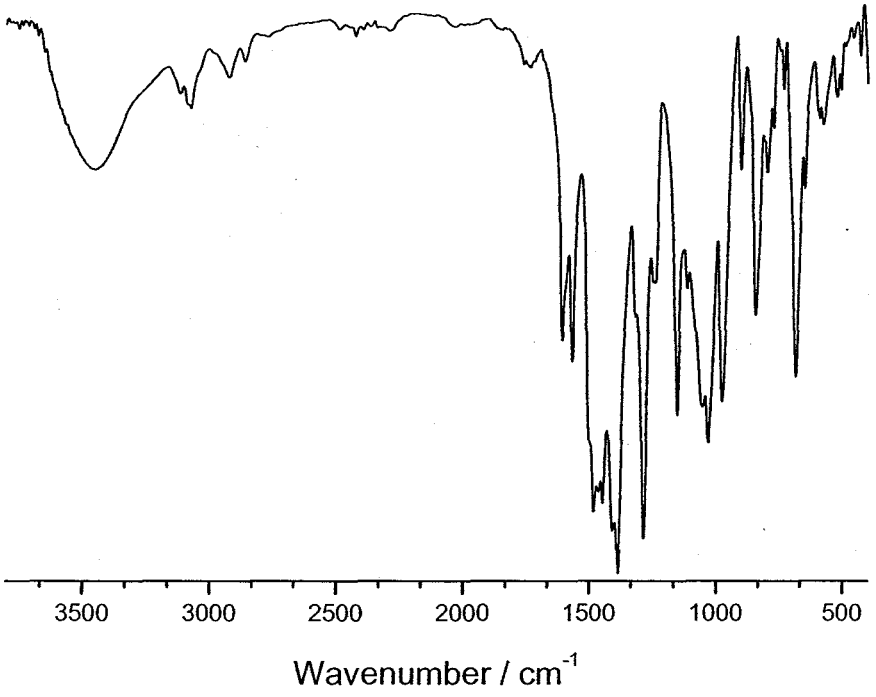

Figure 5.3.4. IR spectrum (KBr) of $[Cu^{II}_2(H\mathbf{L}^{M2})(NO_3)_3]_n$ (**10**).

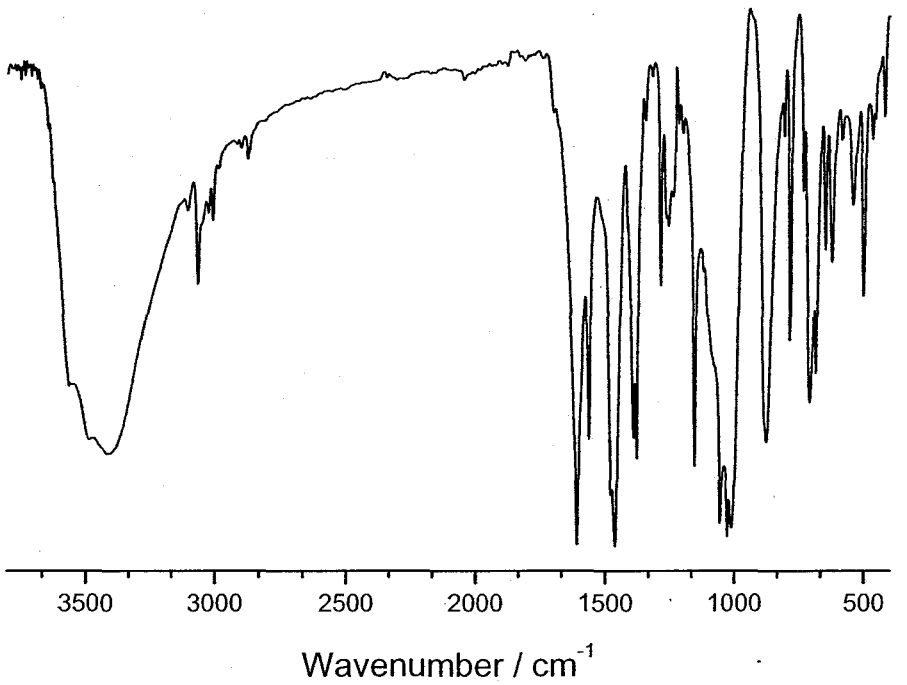

Figure 5.3.5. IR spectrum (KBr) of $\{[Cu^{II}_2(HL^{M1})(Br)_3] \cdot H_2O\}_\infty$ (**11** · H_2O).

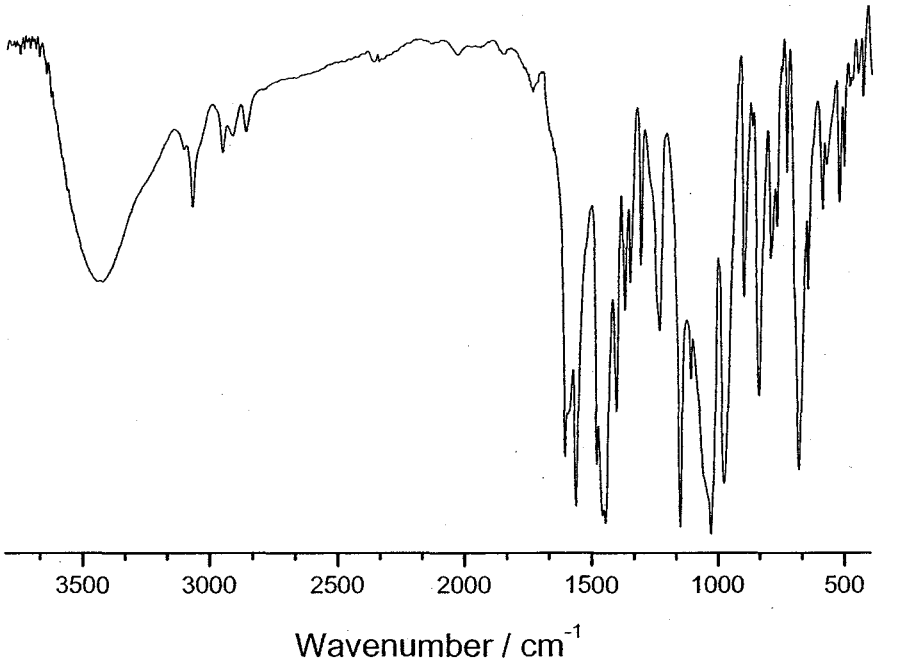

Figure 5.3.6. IR spectrum (KBr) of $[Cu^{II}_2(HL^{M2})(Br)_3]_\infty$ (**12**).

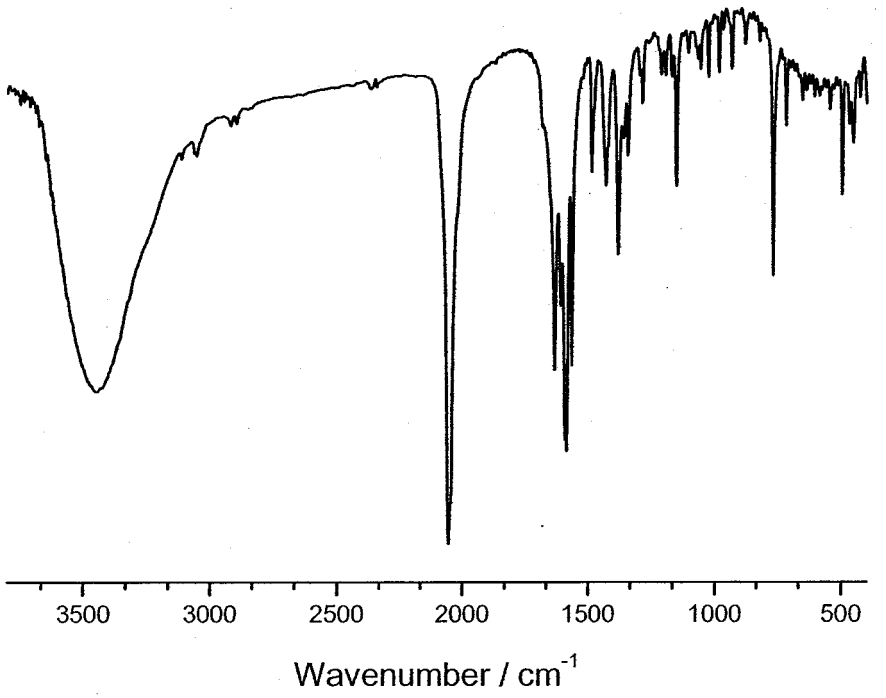

Figure 5.3.7. IR spectrum (KBr) of $[Cu^{II}_2(\mathbf{L^{M1}})(N_3)_2]_n$ (**15**).

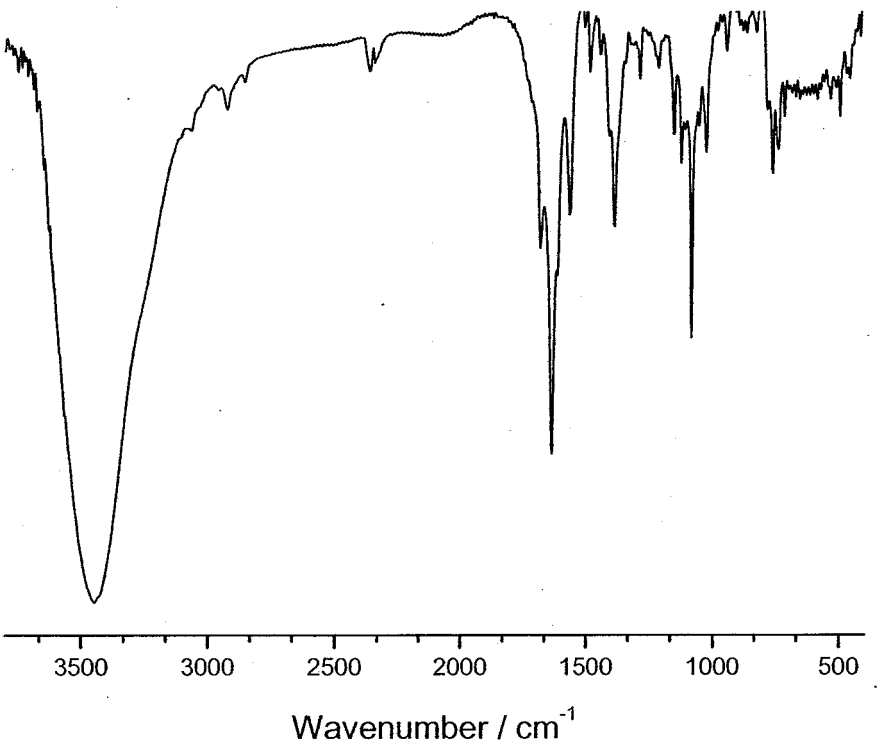

Figure 5.3.8. IR spectrum (KBr) of $[Cu^{II}_2(H\mathbf{L^{M1}})(O_4C_8H_4)(H_2O)_2]_n(BF_4)_n \cdot 2n\ H_2O$ (**17** · 2 H_2O).

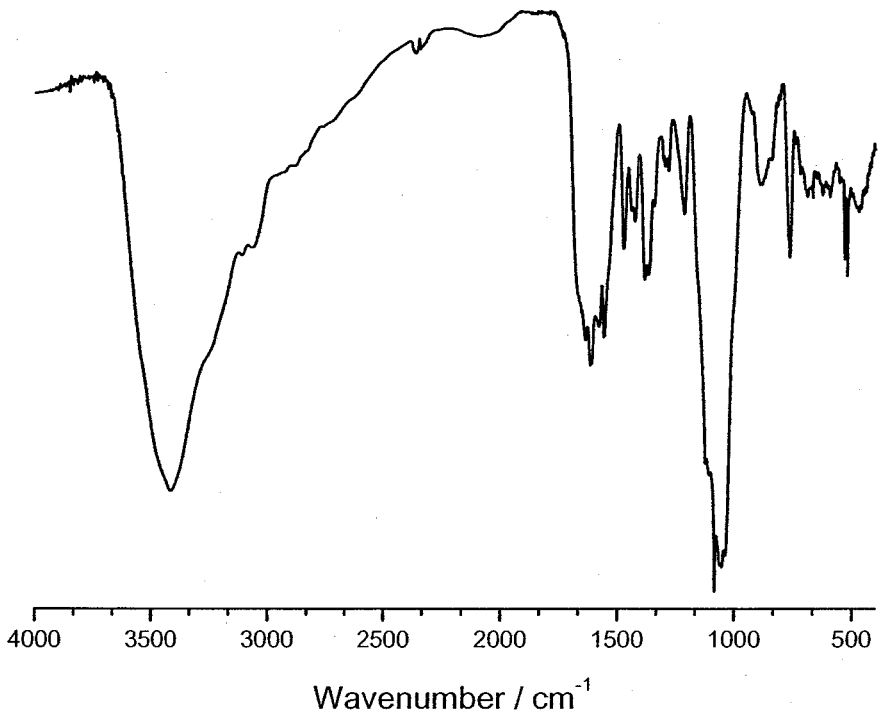

Figure 5.3.9. IR spectrum (KBr) of $[Fe^{II}(H_2\mathbf{L}^{M1})(MeCN)]_n(BF_4)_{2n}$ (**20**).

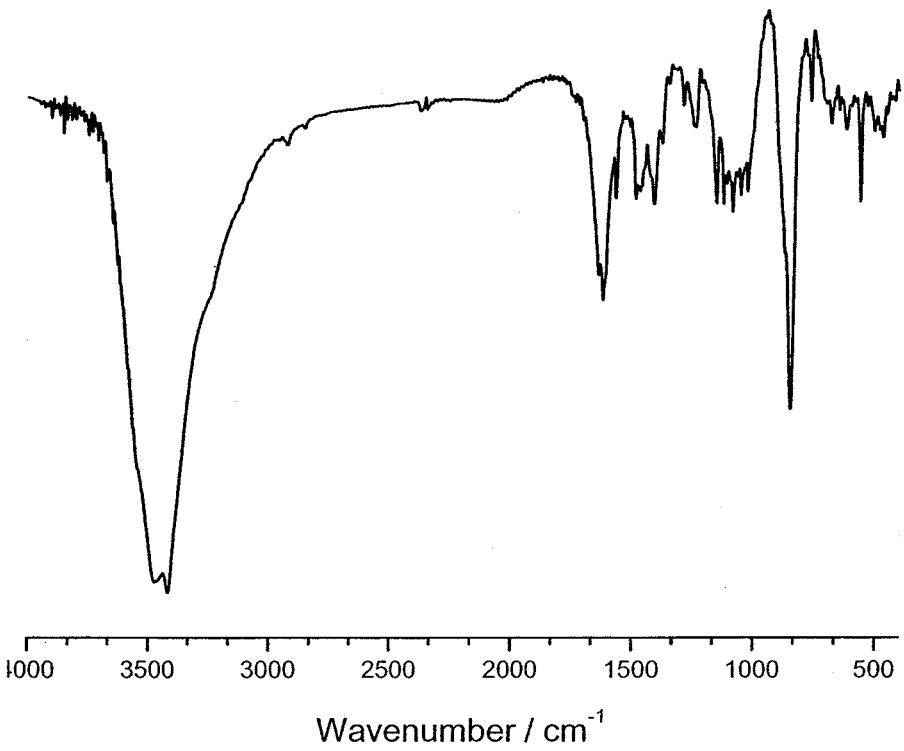

Figure 5.3.10. IR spectrum (KBr) of $[Ni^{II}_4(H\mathbf{L}^{M1})_4](PF_6)_4$ (**26b**).

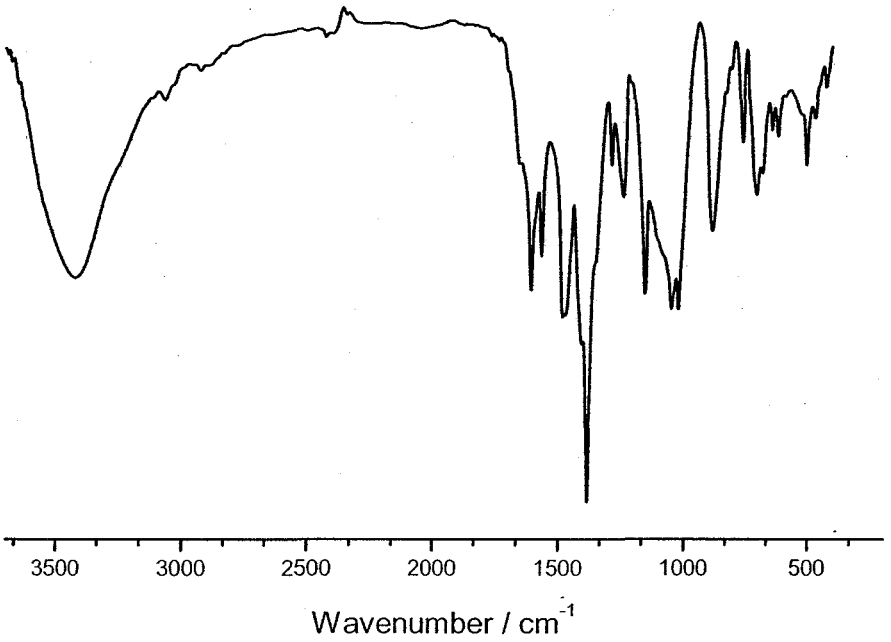

Figure 5.3.11. IR spectrum (KBr) of $[Ni^{II}_4(H\mathbf{L}^{M1})_4](NO_3)_4 \cdot 4\ H_2O$ (**26c** · 4 H_2O).

5.4. *Selected UV/VIS spectra*

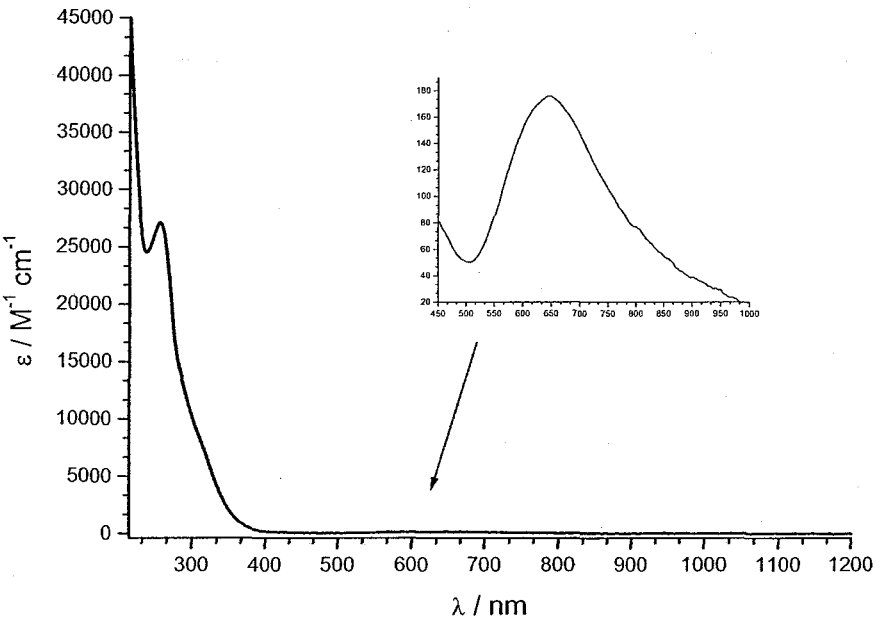

Figure 5.4.1. UV/VIS spectra [MeCN, 0.25 (inset) and 0.025 (main) mM] of $[Cu^{II}_2(H\mathbf{L}^{M2})(NO_3)_3]_n$ (**12**).

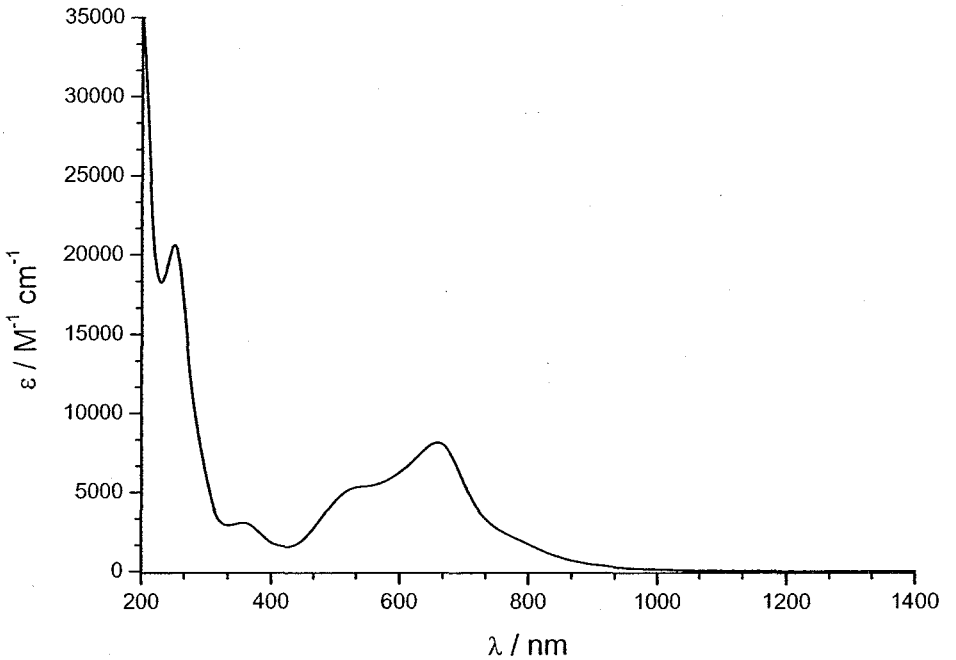

Figure 5.4.2. UV/VIS spectrum [MeCN, 0.1 mM] of $[Fe^{II}(H_2\mathbf{L}^{M1})(MeCN)]_n(BF_4)_{2n}$ (**20**).

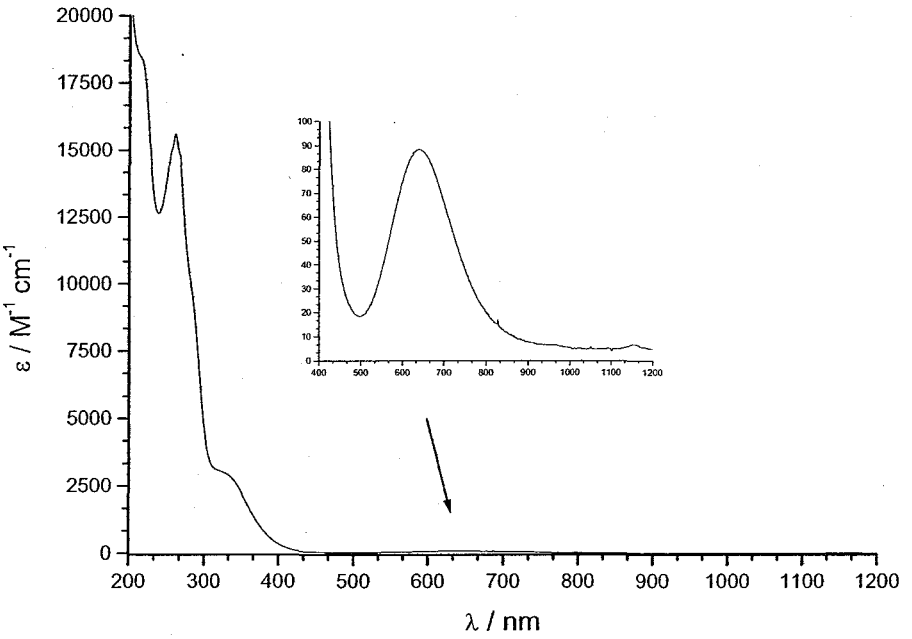

Figure 5.4.3. UV/VIS spectra [MeCN, 0.25 (inset) and 0.025 (main) mM] of $[Cu^{II}(H\mathbf{L}^{\mathbf{S1}})(H_2O)]_n(BF_4)_n$ (**30**).

5.5. *Selected cyclic voltammograms*

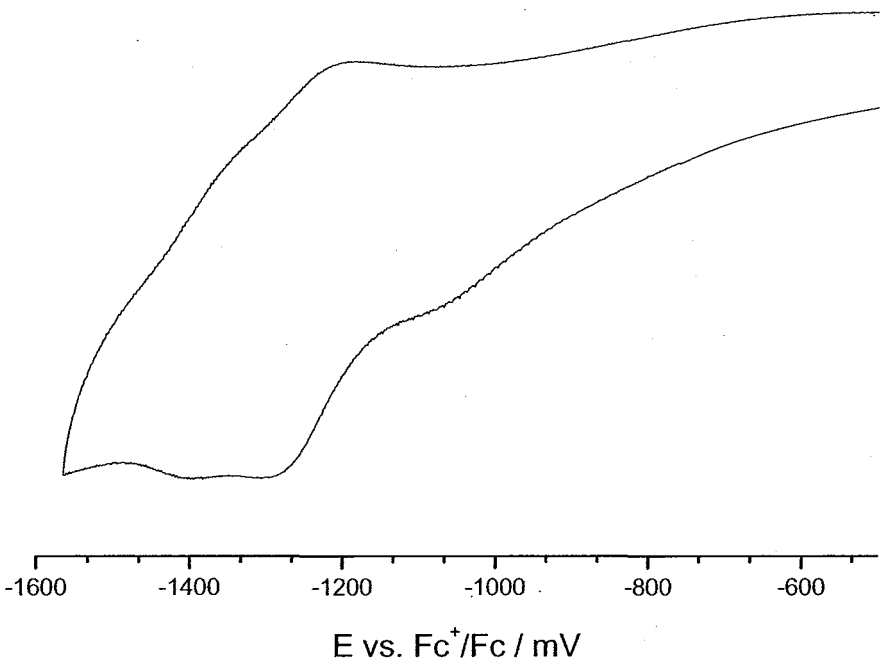

Figure 5.5.1. Cylic voltammogram (0.1 mM, 0.1 M TBAP, MeCN, scan rate: 200 mV s^{-1}) of $[Fe^{II}(H_2\mathbf{L^{M1}})(MeCN)]_n(BF_4)_{2n}$ (**20**).

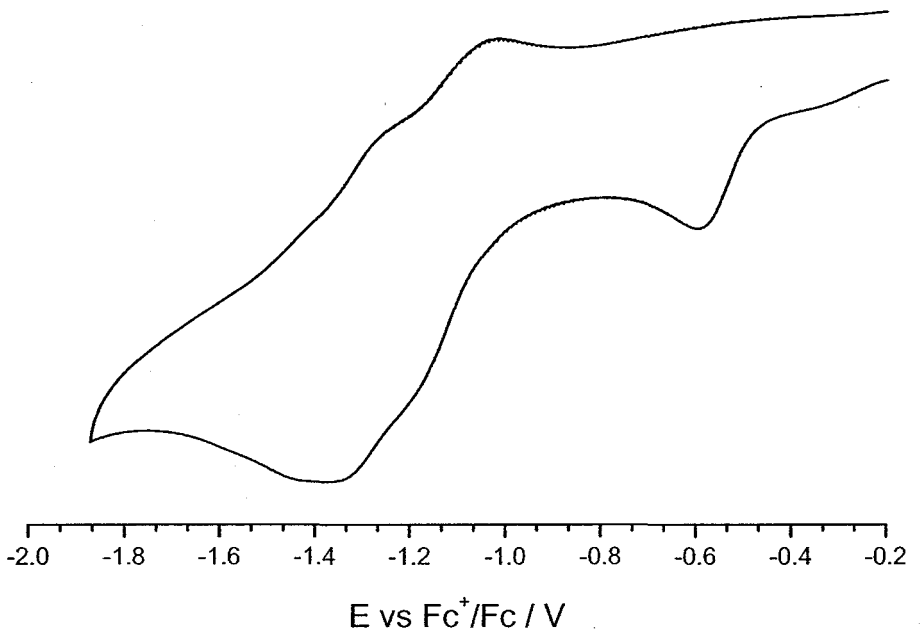

Figure 5.5.2. Cyclic voltammogram (0.1 mM, 0.1 M TBAP, MeCN, scan rate: 50 mV s^{-1}) of $[Co^{III}(H_2\mathbf{L^{M1}})_2](BF_4)_3 \cdot 4\ H_2O$ (**21** · 4 H_2O).

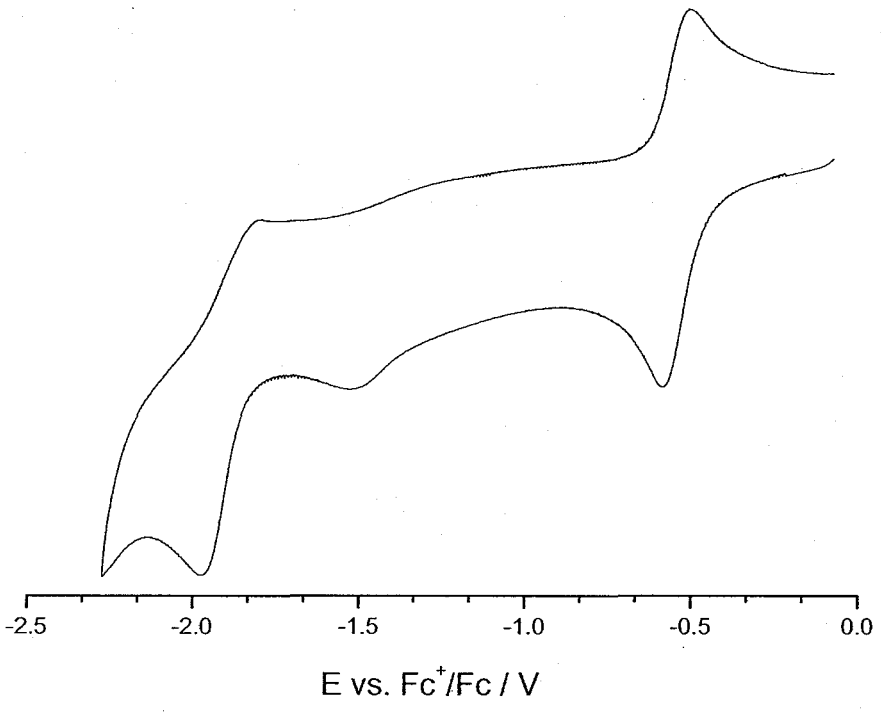

Figure 5.5.3. Cyclic voltammogram (MeCN, scan rate: 50 mV s^{-1}) of the reaction product obtained by the 1:1:1 molar reaction of $H_2\mathbf{L}^{\mathbf{M2}}$ to $Co(BF_4)_2 \cdot 6$ H_2O to NEt_3 in MeCN and subsequent vapour diffusion of Et_2O into the reaction mixture (see Section 2.5.3).

5.6. *Determination of the acid dissociation constants of the ligands H_2L^{M1} and H_2L^{M2}*

Theory

The acid dissociation constants of the two ligands H_2L^{M1} and H_2L^{M2} were measured by potentiometric titration with standard alkali solution using established methods.[137] This method involves titrating a known amount of the ligand with standard alkali, with measurement of pH using a glass electrode-calomel reference electrode combination. A small amount of standard HCl is added to the sample before titration. This serves both to set the initial pH to a low value and for *in situ* calibration of the glass electrode, as described below. The potentiometric titration produces a set of data points comprising the measured potential E of the glass electrode as a function of the volume V of added standard alkali. The acid dissociation constants of the ligand are then calculated from these results using a non-linear least squares method in which the required parameters (*e.g.* dissociation constants) are adjusted until a best fit is obtained to the measured E values.

The theory of this approach will be illustrated by reference to the example of a simple monoprotic weak acid HA having a single proton dissociation constant K_1 (Equation 5.6.1).

Equation 5.6.1. $$HA \rightleftharpoons H^+ + A^- \qquad K_1 = \frac{[H^+]\,[A^-]}{[HA]}$$

The electroneutrality condition for a solution containing both HA and HCl being titrated with NaOH is given in Equation 5.6.2.

Equation 5.6.2. $$[Na^+] + [H^+] = [A^-] + [Cl^-] + [OH^-]$$

Let c_X denote the stoichiometric concentration of species X at any given titration point after allowing for dilution of the analyte (initial volume V_0) by added titrant solution (volume V). Thus, the stoichiometric ligand concentration for any point V is given in Equation 5.6.3, where $[HA]_0$ is the initial concentration of HA in the analyte.

Equation 5.6.3. $$c_{HA} = \frac{V_0}{V_0 + V} [HA]_0$$

A similar equation applies to the stoichiometric concentration of HCl, denoted c_A at any point (Equation 5.6.4).

Equation 5.6.4. $$c_A = \frac{V_0}{V_0 + V} [HCl]_0$$

The stoichiometric concentration of added NaOH, denoted c_B is similarly given in Equation 5.6.5.

Equation 5.6.5. $$c_B = \frac{V}{V_0 + V} [NaOH]_0$$

Since the species Na^+ and Cl^- undergo no acid base reactions, their concentrations can be equated to c_B and c_A respectively as stated in Equation 5.6.6.

Equation 5.6.6. $$c_B + [H^+] = [A^-] + c_A + [OH^-]$$

Finally, the terms for A^- and OH^- in Equation 5.6.6 may be replaced with expressions derived from the acid dissociation Equilibrium 5.6.1 and the self dissociation equilibrium for water (equilibrium constant K_w) which, after rearrangement, produces an equation valid for any point in the titration which depends only on $[H^+]$ as a variable (Equation 5.6.7).

Equation 5.6.7. $$c_A - c_B = [H^+] - \frac{K_W}{[H^+]} - c_{HA}\frac{K_1}{[H^+] + K_1}$$

Note that this equation implicitly assumes that the equilibrium constants K_1 and K_w are conditional constants expressed in terms of the stoichiometric concentrations (not activities) of all the species involved.

Since Equation 5.6.7 is a monotonic increasing function in $[H^+]$, for any given titre volume V, and known or assumed values for the various constants, it can be solved numerically (*e.g.* by a simple bisection method) to compute $[H^+]$ for that point. This value can then be used to calculate the theoretical glass electrode potential E_{calc} using the Nernst equation where k is the Nernst slope (59.16 mV at 298 K) and E_0 is a constant that must be determined experimentally, either by separate calibration or by using the titration data points (Equation 5.6.8).

Equation 5.6.8. $$E = E_0 + k \log [H^+]$$

In the latter case, this is facilitated by the addition of standard HCl to the analyte, which is titrated first providing data for the calculation of E_0.

The procedure used to determine the dissociation constant K_1 is thus as follows: for each titre volume V, the known constant values (k, V, V_0, K_w, c_A, c_B and c_{HA}) are combined with an initial guessed value of K_1 to compute E_{calc}. Then, the squared differences between E_{calc} and the corresponding measured value of E are summed over all titre points to form a sum of squares SSQ (Equation 5.6.9).

Equation 5.6.9. $$SSQ = \sum_{\text{all } V} (E - E_{calc})^2$$

Finally, using a computer-based minimization routine, the value of the variable parameters (*e.g.* K_1 and E_0) is varied to obtain the minimum value of SSQ, which corresponds to the statistical best fit to the titration data.

This scheme is easily generalized to encompass more than one dissociation equilibrium. For the two diamide ligands H_2L^{M1} and H_2L^{M2} studied here, a triprotic model having constants K_1, K_2 and K_3 was chosen as this best fitted the expected equilibria. It should be noted that this approach can only find the best fit to the chosen model (monoprotic, diprotic etc.) and cannot independently assess the validity of the model. This is because in any non-linear minimization routine, the more parameters that are chosen, the better is the fit that is obtained. The general principle is to choose the minimum number of parameters consistent with what is known about the analyte.

Experimental methods

The titrations were conducted in aqueous solution in a 300 ml water-jacketed Pyrex glass cell connected to a thermostatted water bath. The cell top contained apertures for the introduction of the NaOH titrant, glass and reference electrodes and a N_2 gas bubbling tube. Electrode potentials were measured using a high-precision Metrohm pH meter in mV mode with a resolution of 0.1 mV. Titrant was introduced manually for each point using a Metrohm digital burette. Standard 0.1 M HCl was prepared using a Volucon ampoule, while CO_2-free 0.1 M NaOH was prepared and standardized against the HCl in a separate potentiometric titration using the same apparatus.

Titrations were carried out in the presence of 0.1 M $NaClO_4$ as an inert electrolyte designed to control changes in activity coefficients during the titration, thus ensuring the both equilibrium constants and the Nernst equation were expressed in terms of stoichiometric concentrations.

For each titration, approximately 200 g of 0.1 M $NaClO_4$ electrolyte solution were weighed into the cell and a known quantity (typically 0.2–0.3 mmol) of ligand dissolved in it. Next, 1.000 ml of standard HCl were added and the sample spurged

with N_2 gas to remove dissolved CO_2. The gas bubbling tube was then raised above the solution to provide a blanketing jacket of CO_2-free gas and the titration commenced. For each point, the potential reading E was taken when variations over 1–2 min were no greater than the 0.1 mV resolution of the pH meter. About 50 titration points were taken for each case, and both ligands were titrated in duplicate.

The results of the titration were then processed using a custom computer application to calculate the required pK_a values.

Results

The results for the duplicate titrations of both ligands are given in Table 2.1.2.

The complete titration data are presented graphically in the Figures 5.6.1 to 5.6.4. Each shows the original titration curve and a residuals curve corresponding to the difference δE between the calculated and measured E value for each point.

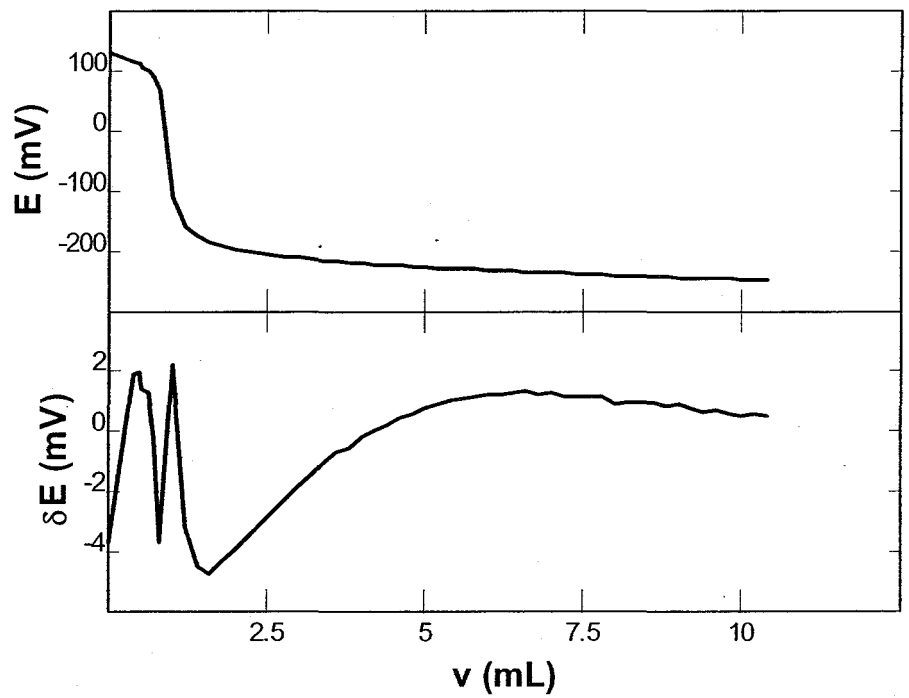

Figure 5.6.1. E and δE for $H_2\mathbf{L}^{M1}$ (first titration).

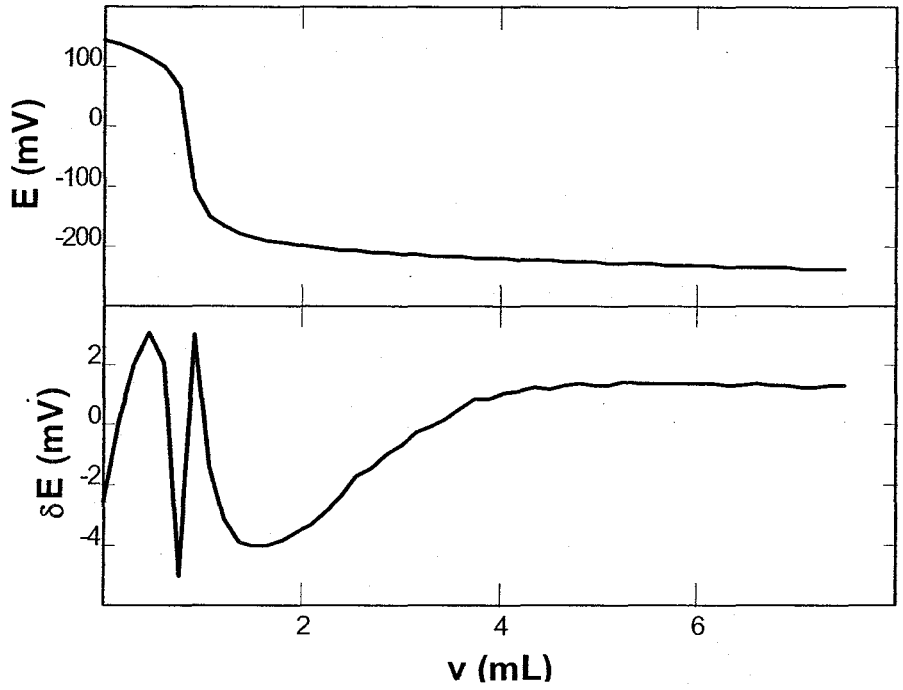

Figure 5.6.2. *E* and *δE* for $H_2\mathbf{L}^{M1}$ (second titration).

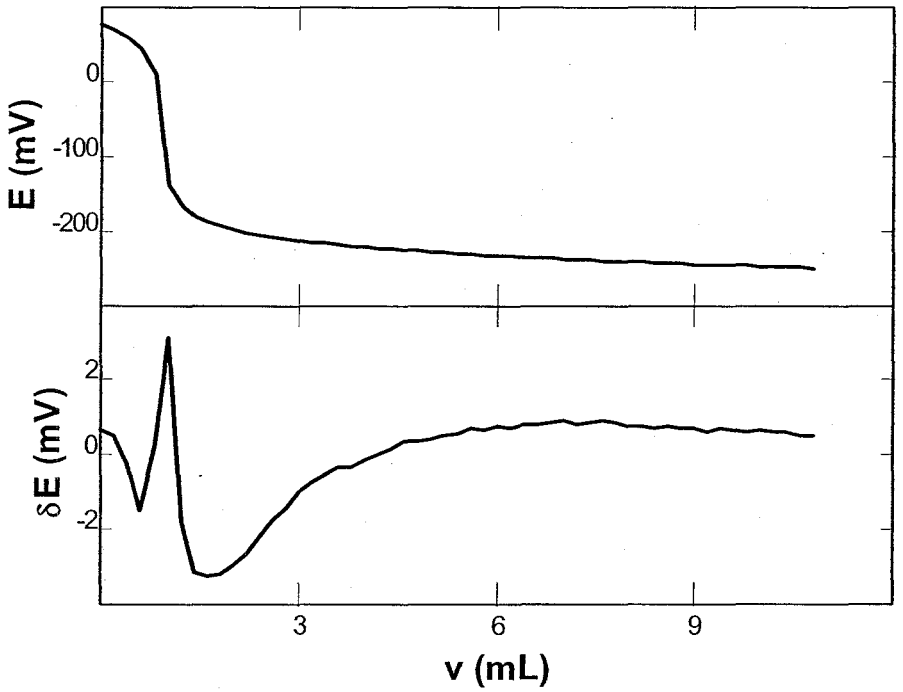

Figure 5.6.3. *E* and *δE* for $H_2\mathbf{L}^{M2}$ (first titration).

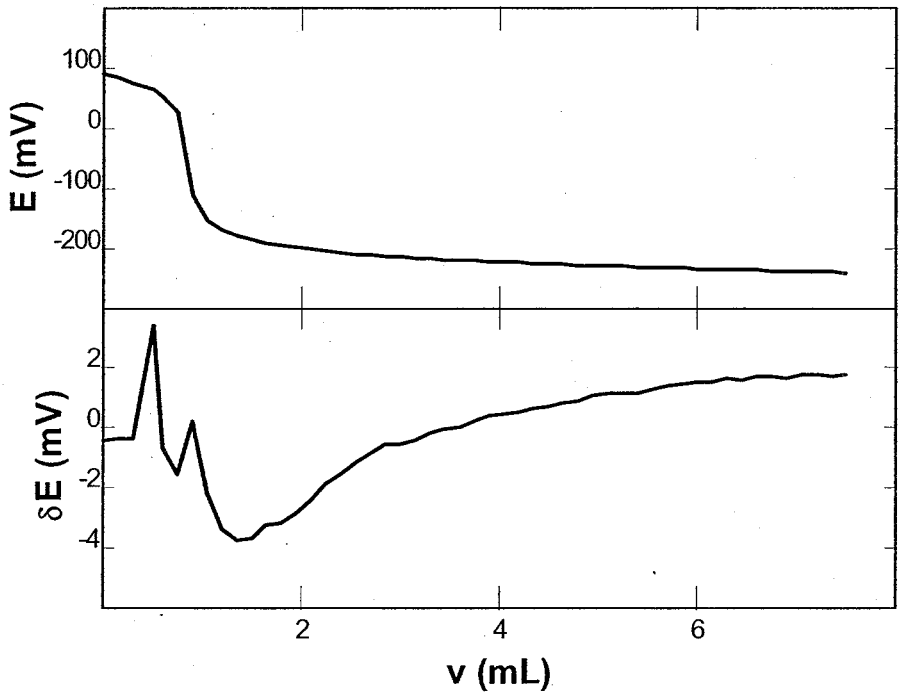

Figure 5.6.4. *E* and *δE* for $H_2\mathbf{L}^{\mathbf{M2}}$ (second titration).